Terms and Conditions of Use of Digitised Theses from Trinity College Library Dublin

Copyright statement

All material supplied by Trinity College Library is protected by copyright (under the Copyright and Related Rights Act, 2000 as amended) and other relevant Intellectual Property Rights. By accessing and using a Digitised Thesis from Trinity College Library you acknowledge that all Intellectual Property Rights in any Works supplied are the sole and exclusive property of the copyright and/or other IPR holder. Specific copyright holders may not be explicitly identified. Use of materials from other sources within a thesis should not be construed as a claim over them.

A non-exclusive, non-transferable licence is hereby granted to those using or reproducing, in whole or in part, the material for valid purposes, providing the copyright owners are acknowledged using the normal conventions. Where specific permission to use material is required, this is identified and such permission must be sought from the copyright holder or agency cited.

Liability statement

By using a Digitised Thesis, I accept that Trinity College Dublin bears no legal responsibility for the accuracy, legality or comprehensiveness of materials contained within the thesis, and that Trinity College Dublin accepts no liability for indirect, consequential, or incidental, damages or losses arising from use of the thesis for whatever reason. Information located in a thesis may be subject to specific use constraints, details of which may not be explicitly described. It is the responsibility of potential and actual users to be aware of such constraints and to abide by them. By making use of material from a digitised thesis, you accept these copyright and disclaimer provisions. Where it is brought to the attention of Trinity College Library that there may be a breach of copyright or other restraint, it is the policy to withdraw or take down access to a thesis while the issue is being resolved.

Access Agreement

By using a Digitised Thesis from Trinity College Library you are bound by the following Terms & Conditions. Please read them carefully.

I have read and I understand the following statement: All material supplied via a Digitised Thesis from Trinity College Library is protected by copyright and other intellectual property rights, and duplication or sale of all or part of any of a thesis is not permitted, except that material may be duplicated by you for your research use or for educational purposes in electronic or print form providing the copyright owners are acknowledged using the normal conventions. You must obtain permission for any other use. Electronic or print copies may not be offered, whether for sale or otherwise to anyone. This copy has been supplied on the understanding that it is copyright material and that no quotation from the thesis may be published without proper acknowledgement.

The One-Dimensional Compression of Fibrous Peat and Other Organic Soils

The One-Dimensional Compression of Fibrous Peat and Other Organic Soils

by

Conleth O'Loughlin

Thesis Submitted to the University of Dublin, Trinity College,

for the Degree of Doctor of Philosophy

October 2001

Declaration

The author hereby declares that this Thesis, in whole or in part, has not been submitted to any other university as an exercise for a degree. Except where reference has been given in the text, it is entirely the author's own work.

The author confirms that the library may lend or copy this Thesis upon request, for academic purposes.

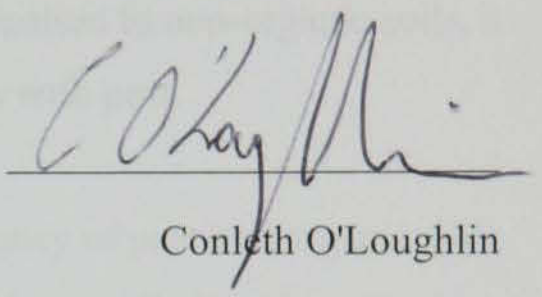

Conleth O'Loughlin

October 2001

Abstract

Geotechnical challenges associated with constructing over peat and organic soils are generally concerned with controlling stability and long term settlement. The use of geosynthetics in this regard has played a significant role in alleviating potential instability, although the problems associated with settlement, and in particular creep settlement, remain.

Despite recent advances in soil improvement techniques, such as thermal precompression and deep *in situ* mixing, preloading remains one of the more popular and effective means of reducing long term settlements in peat, provided the time spans involved can be tolerated.

However, for such projects to be successful, a means of forecasting the rate and magnitude of the coupled consolidation and creep settlements is required. Although several such methods are available, and have been successful in their application to non-organic soils, a number of behavioural non-linearities limit their effectiveness with peat.

The work in this Thesis investigates the time and rate dependency of peat and organic soils when loaded under one-dimensional conditions. Of particular interest is the role and nature of the organic matter. The effect of high load increment ratio (LIR) is assessed, as stress levels well in excess of the relatively low *in situ* stresses in virgin peat deposits are often applied in an attempt to control settlements. A large and comprehensive database of laboratory tests is presented, including Multi Stage Loading (MSL) oedometer tests and Constant Rate of Deformation (CRD) tests. These tests were used as a means of validating constitutive models currently employed in the prediction of one-dimensional compression. A suitable isotache model has been chosen, and its potential in predicting *in situ* behaviour based on laboratory-derived parameters is examined.

Acknowledgements

I would like to express my sincere gratitude to Dr. Barry Lehane, whose supervision and timely interventions were key to the completion of this Thesis. His enthusiasm and support throughout my graduate study was invaluable.

Thanks to the technical staff of the Department of Civil, Structural & Environmental Engineering, in particular to Mr. Martin Carney in the Soils Laboratory for his never ending patience.

Over these past four years, I have had both the pleasure and misfortune of sharing an office with two good friends, Sam and Eddie. Thanks lads for the arguments, laughs and pointless discussions. Thanks also to Arturo Gonzalez for the good old times at CRC. Bread is in the oven!

Special thanks are due to my family, in particular to Marie and Karl, who put me up and put up with me over this past year; thank you both. To my mother and father for their support, prayers and understanding.

I gratefully acknowledge the financial support received from the Department of Education for Northern Ireland, the Geotechnical Society of Ireland, and Trinity College Dublin.

To all who predicted that when you put sixteen tanks on a bog and fill them with water, that they would sink, well I guess you were right! To the few who were just a little curious and got christened on Clara bog, thanks.

And finally, I would like to thank Fiona, who has had to put up with a lot over these past four years. Your support and encouragement has been unwavering, particularly in the last legs. I really appreciate it, as I do you.

Table of Contents

Chapter 1

Introduction

Chapter 1

Introduction

1.1 BACKGROUND AND MOTIVATION

The Irish budgetary adjustment programme of the 1980's and early 1990's resulted in a necessary reduction in the capital expenditure programme for this period. As a result of this curtailment, the start of the 21st century has found Ireland in a position where its infrastructure is seriously inadequate for the current car ownership rates, and is now under severe strain due to the recent rapid economic growth. In order to redress this problem, the Irish National Development Plan 2000-2006 has allocated IR£17.6 billion of the total investment from public, EU and private funds, for economic and social infrastructure development. This figure accounts for 51.6 % of the total available funds, and is a notable 54.9 % annual increase over 1999 figures. A significant portion of this development fund has been allocated for the widening, realignment and reconstruction of deficient sections of existing national roads. Figure 1.1 identifies the routes that are set to benefit from the development strategy for national primary and secondary roads, along with the distribution of Irish peatlands in the form of raised and blanket bogs. Evidently many of the planned routes cross over areas underlain by peat deposits, thus presenting construction challenges for the geotechnical engineer.

For several decades, peat has generally been regarded as one of the most problematic soils in geotechnical engineering, owing to the particularly high *in situ* water content and associated voids ratio prevalent in such soils. Soils with high voids ratio are typically very compressible and are therefore poor foundation materials. To date, the tendency has been to either avoid constructing over peat deposits, or to simply replace the organic material with granular fill. However, the need for an improved infrastructure in Ireland requires engineers to face up to the problems associated with construction over peat.

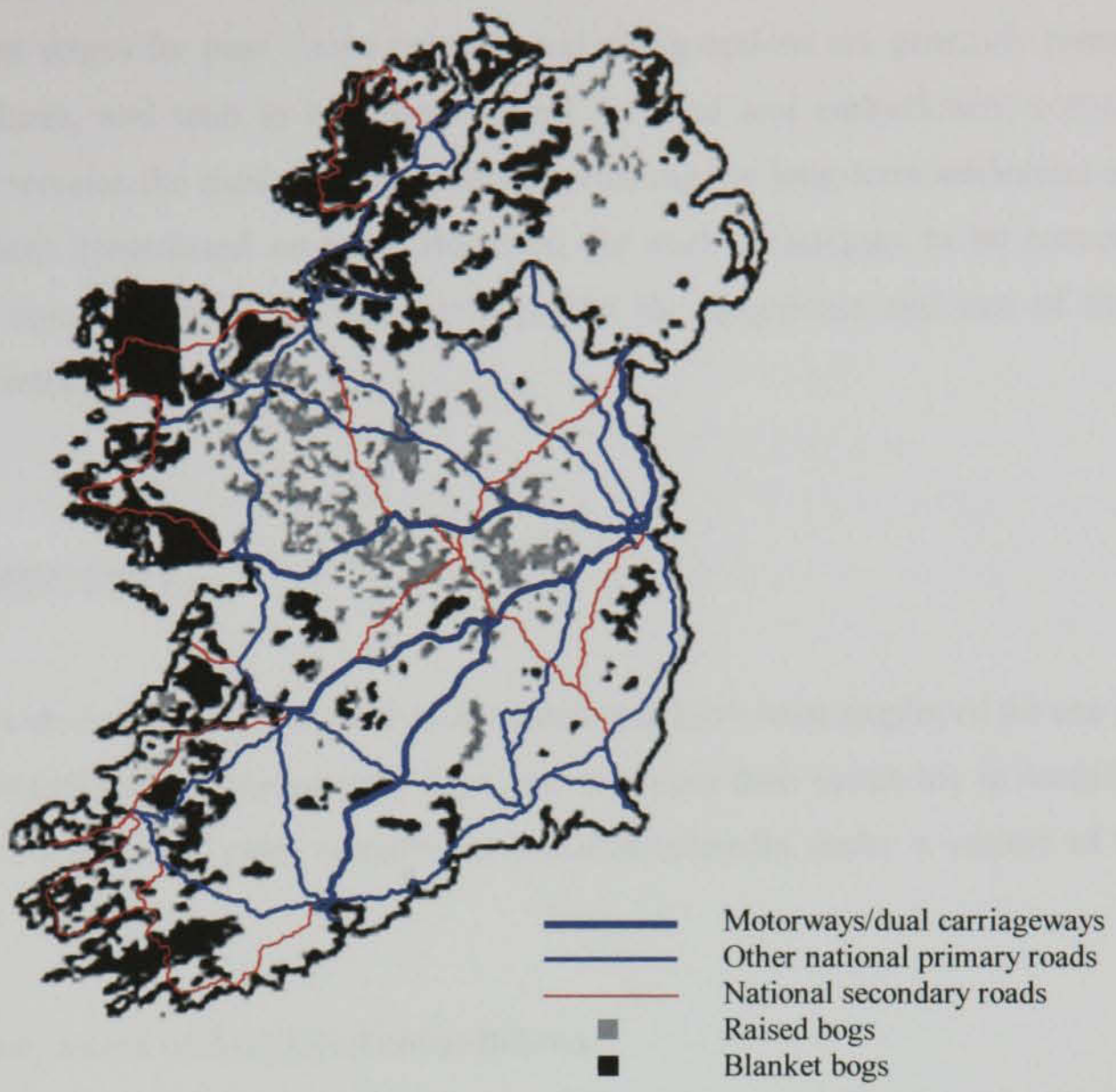

Figure 1.1 National primary and secondary road improvements for 2000 - 2006

A variety of soil improvement methods have been employed for projects involving embankments and roads founded on peats and organic soils:

1. Preloading: shown to be reliable in reducing long-term settlements. Stability of embankments can be enhanced by using stage-construction and geosynthetic reinforcement.
2. Thermal precompression: settlement rates are increased significantly by ground heating; subsequent cooling then reduces the long-term settlements.
3. Deep *in situ* mixing (lime-cement columns): mixing peat with cement (and sometimes lime) to create stabilized columns.
4. Stone columns: sand or compacted gravel filled into water jetted holes in order to increase the strength of fills, increase settlement rates whilst aiding to reduce overall settlement amounts.
5. Piles: generally restricted to founding structures rather than roads and embankments.

Of these methods, thermal precompression and deep *in situ* mixing are still in the development stages for peat. Stone columns and piling options are generally restricted to large structures, and tend to be uneconomical for road and embankment construction. Preloading remains the most popular means of reducing the long-term settlement of roads and structures constructed on peat. However, for such techniques to be successful, a method is required which can accurately predict the magnitude and rate of the time-dependent settlements.

1.2 OBJECTIVES

This Thesis investigates current analytical models that have been employed for use in stage loading and preloading projects with clays, and examines their suitability in modelling the response of a range of peats compressed one-dimensionally under a variety of loading conditions.

The main objectives of this project are as follows:

1. To assess the compressibility characteristics of a range of peats and organic soils, paying particular attention to long-term creep compression.
2. To investigate the role of organic content and state of humification of the organic matter.
3. To identify fundamental differences between the behaviour of peat in compression, compared with other non-organic soils. Consequently, to identify features of a constitutive model that are required to predict the rate and magnitude of settlements under one-dimensional loading conditions.
4. To examine the potential in predicting *in situ* behaviour using a suitable constitutive model together with parameters derived from small-scale laboratory tests.

1.3 THESIS OUTLINE

The structure of the eight chapters contained within this Thesis is outlined here. **Chapter 2** presents an up-to-date and comprehensive review of current knowledge of peat behaviour gained from stage loading and preloading construction on peat, and from associated

laboratory studies. The potential for one-dimensional models (developed mainly for clay) in capturing the highly non-linear nature of peat is also assessed. **Chapter 3** includes a detailed classification of the four main soil groups (poorly humified fibrous peat, well humified fibrous peat, amorphous and silty peat, and an organic clay) considered in this Thesis. Correlations between loss-on-ignition and water content are provided and compared with a database of peats and organic soils, compiled from the literature. Selected results from a relatively large database of Multi Stage Load (MSL) oedometer tests and Constant Rate of Deformation (CRD) tests are presented in **Chapter 4**. Much of the reported data is taken from Clara peat test results, although several other tests are included for comparison. **Chapter 5** initially provides details regarding the subsidence of a road constructed over a raised bog in Clara, Co. Offaly over 150 years ago. The design and implementation of an *in situ* load test on the bog is subsequently described, as are the field measurements collated over a two year period. An interpretation of the experimental data obtained both in the laboratory, and in the field is provided in **Chapter 6**, drawing parallels with previous studies where relevant. The experimental findings are subsequently used to identify the problematic nature of fibrous peat in one-dimensional compression. Formulations are proposed upon which the selection of an appropriate constitutive model for peat is based. In **Chapter 7**, an *isotache* model is selected which is considered to have the highest potential for successful application to peat. The formulation of the model is discretised using finite difference techniques and programmed using Microsoft Visual C++. This program, referred to as CREEP, is then used to predict the stress-strain response due to a variety of one-dimensional loading conditions, both in the laboratory and the field. Finally, **Chapter 8** presents the main conclusions from this Thesis, and makes recommendations for further work.

Chapter 2

Literature Review

Chapter 2

Literature Review

2.1 INTRODUCTION

Geotechnical challenges associated with embankment and road construction over peat and organic soils include potential instability and excessive long term settlement. However, with the recent advances in the use of soil reinforcement, construction has primarily become a problem of controlling settlements (Edil and den Haan, 1994). Although construction over soft soils is generally avoided, the declining availability of more favourable foundation soils has resulted in the necessary development of areas underlain by peaty and organic deposits. A resurging interest in peat and organic soils as foundation materials has been underlined by the formation of ISSMFE Technical Committee on Peat, TC15, in 1985, which was restructured in 1994 to include organic soils in its brief. Although advancements in a number of alternative soil improvements methods, such as deep *in situ* mixing and thermal precompression have been made, the use of preloading remains one of the most common means of reducing long term settlement (Carlsten, 1991; den Haan, 1997). This chapter initially reviews current knowledge gained from stage loading and preloading projects on peat, and from associated laboratory studies. The final section deals with one-dimensional compression models that have mainly been developed for clay, but which, in principle, may equally be applicable to peat and organic soils.

2.2 TIME-DEPENDENT COMPRESSION OF PEAT SOILS

A considerable amount of experimental data from the literature indicates that the long term settlement of peat is continuous. Busiman (1936) showed that the creep settlement of

embankments constructed over peat in Holland continued for more than eighty years. In a similar study at the same meeting, van der Burght (1936) provided data which showed that an embankment founded on peat settled for a period of 91 years. Both Buisman (1936) and van der Burght (1936) concluded that the long term settlement could best be described by a linear relationship between settlement and logarithm of time. Other more recent field studies such as that reported by Lefebvre *et al.* (1984) testify to this relationship. Weber (1969) provided a considerable amount of settlement data for several embankments constructed over peat deposits. The settlement records, which have been maintained for several years, show an essentially linear relationship between settlement and logarithm of time (Figure 2.1). After approximately 15 years, the relative compression of the 7 m layer of high water content peat measured approximately 74%, compared with approximately 23% for the 6 m layer of low water content clayey peat, even though the applied stress level of the latter was 33% higher. This result serves as a good indication of the magnitude of peat settlement associated with even relatively moderate loads.

Laboratory studies of peat have been carried out by a number of workers in various countries, with notable contributions emerging from Canada, USA, Netherlands, Japan, UK and Ireland. A general conclusion which may be drawn from the literature on peat is that the one dimensional compression is due to (i) volume changes associated with the dissipation of excess pore pressures, and (ii) volume changes due to viscous deformations of the soil layer. Although many workers including Šuklje (1957, 1969, 1982), Bjerrum

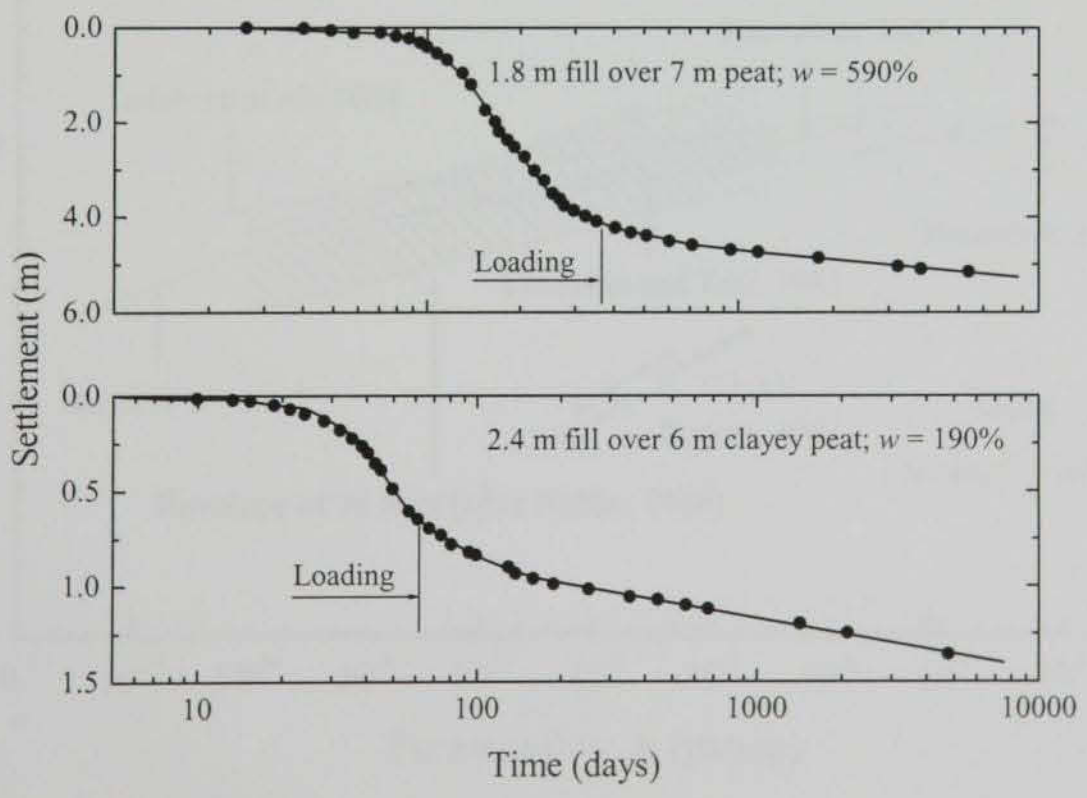

Figure 2.1 Settlement time data for embankments constructed over peat (after Weber, 1969)

(1967), Leroueil *et al.* (1987) and Kim and Leroueil (2001) consider these two time-dependent processes occur simultaneously, it is convenient now to examine their respective processes to separately. The following sections attempt to provide an up-to-date review of the compression behaviour of peat loaded under one-dimensional conditions. Although laboratory and field behaviour are addressed in separate sections, correlations and comparisons are made where possible.

2.2.1 Permeability and consolidation

One of the most notable features of peat is the reduction in permeability with decreasing void ratio and water content (Hobbs, 1986). Carlsten (1991) suggested a vertical permeability in the range 10^{-5} - 10^{-7} m/s for virgin peat, and showed this value reduced by a factor of 1000 at a relative compression ($\Delta H/H_o$) of 50%. This trend agrees well with that reported by Berry and Vickers (1975) for a fibrous peat from the UK. Similar trends have been reported by Dhowian and Edil (1981), Adams (1969) and Miyakawa (1960) and, more recently, by Mesri *et al.* (1997). The decline in permeability is most severe in undisturbed fibrous peat deposits, as the *in situ* undisturbed porosity of these soils is generally very high (Landva and La Rochelle, 1983), thus making the soil readily pervious

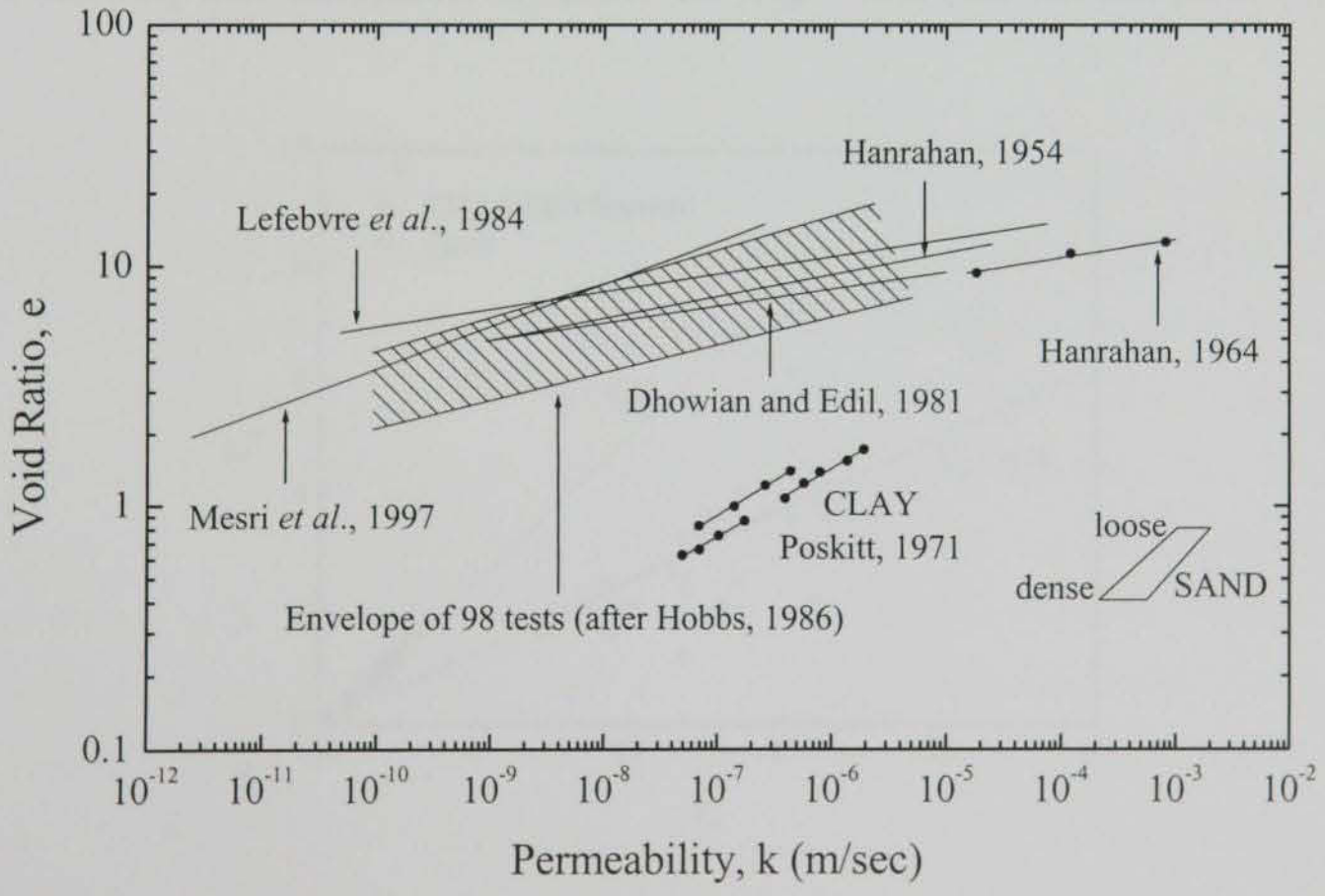

Figure 2.2 Relationship between permeability and void ratio for peat

to flow. Figure 2.2 shows typical variations in the vertical permeability with void ratio. Many of the data in Figure 2.2 are due to Hobbs (1986), who concluded that the permeability was not directly linked to the applied stress, but to the initial void ratio, reflecting the natural state of the soil. Hobbs (1986) proposed Equation 2.1 as a general relationship between void ratio and permeability.

$$k = k_o \left(\frac{e}{e_o} \right)^{11.03} \qquad 2.1$$

This equation, which is based on permeability data presented by Hanrahan (1954), passes approximately through the centre of the shaded envelope in Figure 2.2. A more appropriate fit to other soils can be obtained by varying the limiting values, k_o and e_o, and also by altering the exponent, 11.03.

Mesri *et al.* (1997) showed that current permeability data available for peat can be described by $C_k = e_o/4$, where $C_k = \Delta e/\Delta \log k$ (see Figure 2.3). The corresponding value for soft clays and silts as determined by Tavenas *et al.* (1983) and Mesri *et al.* (1994a) is $C_k = e_o/2$. Considering that initial void ratios in peat are generally much higher than those of clays and silts (e.g. see Figure 2.2), it is evident that this result is an indication of the somewhat different structure in peat soils. Mesri *et al.* (1997) used the data in Figure 2.3 to explain that only the macropores, defined as the large voids between soil particles, act as

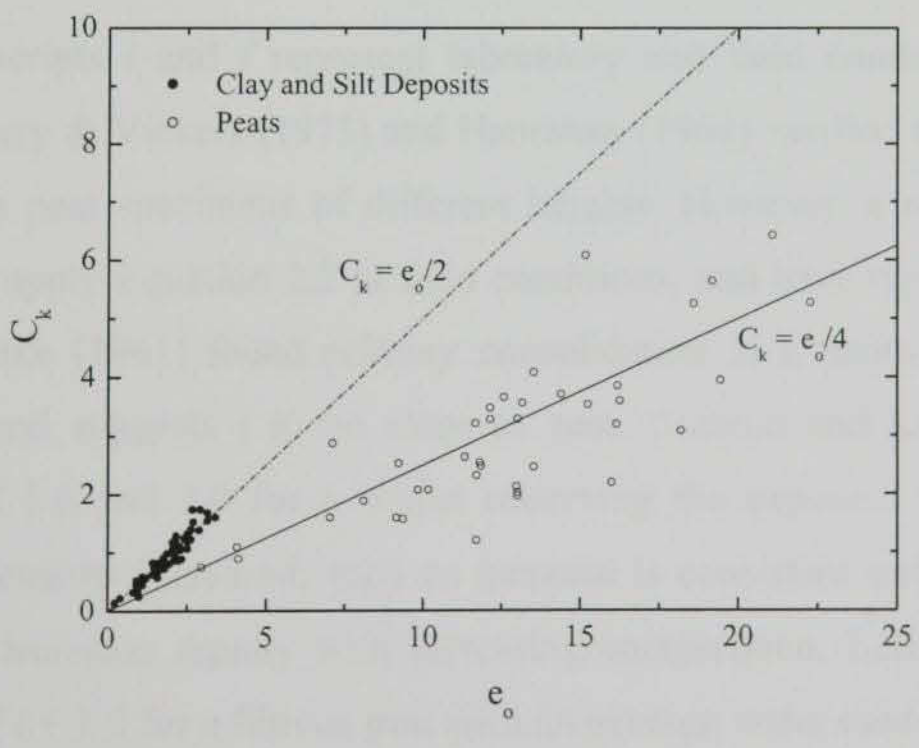

Figure 2.3 Values of C_k for peats as well as soft clay and silt deposits (after Mesri *et al.*, 1997)

flow channels. Both Mesri *et al.* (1997) and Hobbs (1986) compare the permeability of fibrous peat with sodium montmorillonite at a high void ratio, e.g. 20. The corresponding differences in permeability at this high porosity are significant; 10^{-10} m/s for sodium montmorillonite compared with 5×10^{-7} m/s for fibrous peat. It is notable that the quoted permeability of fibrous peat in its natural state, reported by Lefebvre *et al.* (1984), is comparable with that of medium sand. Hobbs (1986) attributes the large variation in permeability to the manner in which water is held in peat. The structure of poorly humified peat consists mainly of relatively large diameter (*ca.* 1 mm) leaf and stem fibres, whereas the soil particles of sodium montmorillonite are flaky and more than 1000 times smaller. The amount of water-bound surface area will obviously be higher in the sodium montmorillonite, thus increasing the likelihood of absorbed water layers coalescing and blocking potential seepage paths. The dissipation of pore water during the consolidation of peat can be considered at macroscopic level. Such reasoning has been the basis for many of the rheological models developed for peat in the 1960's and early 1970's (see § 2.4.1).

There is considerable disagreement surrounding the validity of the commonly used H^2 scaling law which allows the time required for *in situ* consolidation to be estimated using known t_p values (times for consolidation) from laboratory tests and the length of the drainage path, d, in the laboratory and field:

$$\frac{t_f}{t_l} = \left(\frac{d_f}{d_l}\right)^{i=2} \qquad 2.2$$

in which the subscripts l and f represent laboratory and field conditions respectively. Barden (1969), Berry & Vickers (1975) and Hanrahan (1964) verified the use of $i = 2$ for laboratory tests on peat specimens of different heights. However, a number of workers have attempted to apply Equation 2.2 to field conditions, and have reported variations in the exponent i. Lake (1961) found primary consolidation in a Scottish bog peat to be extremely rapid, and suggests i to be close to zero. Samson and La Rochelle (1972) reported values of 1.6 and 2.0 for i, whilst observing the exponent to increase as the applied stress increments increased; such an increase is consistent with the presumption that permeability decreases rapidly with increasing compression. Lefebvre *et al.* (1984) proposed values of $i = 1.1$ for a fibrous peat with an average water content of 1460 %, and $i = 1.5$ for a fibrous peat with an average water content of 860 %.

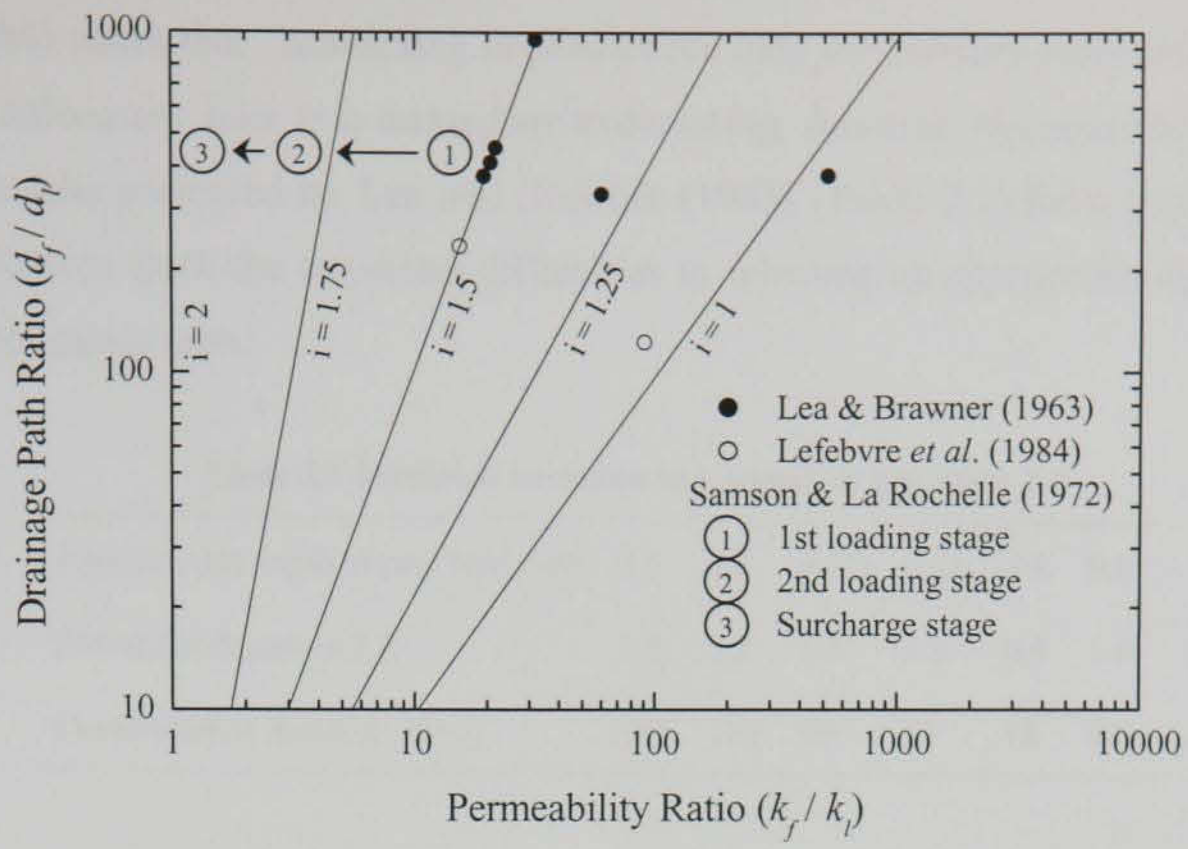

Figure 2.4 Relationship between permeability ratio, k_f/k_l, drainage path ratio, d_f/d_l, and the power i in Equation 2.2 (after Hobbs, 1986)

Hobbs (1986) suggests that the faster field consolidation rates encountered in test fills on peat are generally due to significant variations in the vertical permeability in the field, compared with that observed in the laboratory. Hobbs also raises an interesting point in identifying horizontal drainage effects due to deviations from true one-dimensional behaviour, but suggests that it would be illogical to adjust Equation 2.2 to account for this, as this would require variables to account for the effective radius of the fill and hydraulic anisotropy. Equation 2.2 can be modified to account for differences in the field and laboratory vertical permeability:

$$\frac{t_f}{t_l} = \left(\frac{d_f}{d_l}\right)^{i=2} \frac{k_l}{k_f} \qquad 2.3$$

Hobbs (1986) used Equation 2.3 together with data reported in the literature to form an empirical relationship between the permeability ratio (k_l/k_f), drainage path ratio (d_f/d_l), and the exponent i (see Figure 2.4). Considering Figure 2.4 for an average value of i = 1.5, and a drainage path ratio of approximately 400[1], the permeability ratio (k_l/k_f), is approximately 20. Although horizontal drainage will reduce this value, this approximate measure serves as a useful exercise in accounting for the vast differences in the vertical permeability as

[1] Drainage path ratio based upon a 4 m peat layer with drainage permitted towards the upper boundary, and 10 mm as a typical drainage path length in oedometer tests with drainage towards the top and bottom.

encountered in the laboratory and the field. Despite the apparent merit of Equation 2.3, Hobbs (1986) states that *"attempting to predict the time for primary consolidation in the field from laboratory tests is a hazardous undertaking, however rigorous the underlying theory"*. Results presented by Lea and Brawner (1963) (Table 2.1) for a peat deposit in British Columbia show the important difficulties in selecting an appropriate duration of t_p based on laboratory tests.

Table 2.1 Predicted variation in t_p based on Equation 2.2

Approximate depth of peat layer (m)	3.5	3.8	4.25	4.25	4.8	9.5
Power *i* in Equation 2.2	1.5	1.5	1.5	1.3	0.9	1.5
Consolidation duration (days)	120	174	90	25	10	326

Landva and La Rochelle (1983) reported consolidation durations of three months and less for test fills constructed over a 7 m thick fibrous peat deposit. In contrast, Berry (1983) predicted, on the basis of 24 Rowe cell tests, $t_p \approx 10$ years for a 2.5 m fibrous peat deposit. However, den Haan (1997) suggests that the potential for accurately forecasting the development of settlement and pore pressure dissipation during consolidation is increased if the non-linearity of permeability and anisotropy is accounted for.

2.2.2 Compression – time relationships

Uncertainties associated with the determination of t_p from laboratory $e - \log t$ and $\varepsilon - \log t$ plots further adds to the difficulty in applying Equation 2.2 to *in situ* conditions. Although Hobbs (1986) and Mesri *et al.* (1997) find that in most cases, the end of consolidation can be determined from Casagrande's log t method or Taylor's $\sqrt{t}$ method, Edil and den Haan (1994) conclude that the only reasonable estimations for t_p are those based on pore pressure measurements. The success of graphical construction methods in estimating t_p is linked in particular to the magnitude of the load increment ratio, $\Delta\sigma/\sigma$ (Mesri and Godlewski, 1977; Edil and den Haan, 1994; Edil 1997). Edil (1997) illustrates the effect of $\Delta\sigma/\sigma$ on a fibrous peat from Middleton, USA (see Figure 2.5).

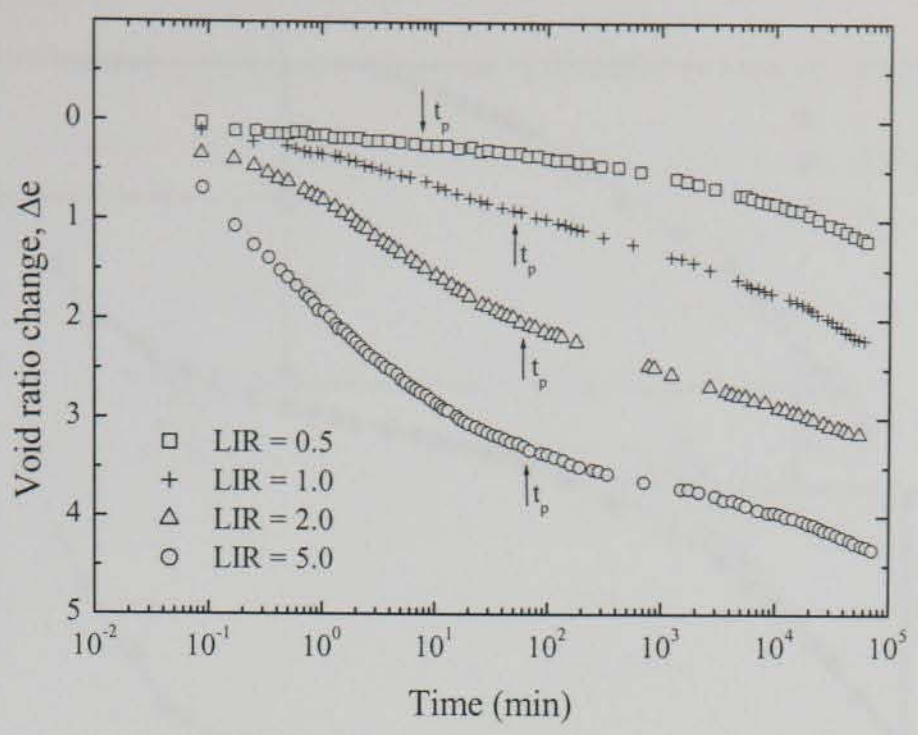

Figure 2.5 Compression time curves for various LIR (after Edil, 1997)

Edil (1997) concludes from Figure 2.5 that the transition from the consolidation phase to the *so-called* secondary phase is difficult to determine for the stress increments involving LIRs less than unity. However, for the LIR = 2.0 and LIR = 5.0 stress increments, the end of primary consolidation is clearly distinguishable from the e – log t curve, with values agreeing well with t_p as determined from pore pressure measurements. In a separate study, Edil *et al.* (1991) showed that Casagrande's method was unsuitable for peat, and that Taylor's method underestimated t_p by a factor of up to 100.

It is also evident from Figure 2.5, that the tangential slope ($C_\alpha = -\partial e/\partial \log t$) gradually increases at $t \gg t_p$. Edil and Dhowian (1979) and Dhowian and Edil (1980) term this increase in C_α with time as *tertiary compression*, which should be interpreted as decreasing strain rate, changing at an increasing rate. Den Haan (1994) provides a clear definition of tertiary compression: *"tertiary compression can be defined as a decrease of slope m in a plot of log strain rate versus log time, after a relatively constant stretch at* $m \approx 1$*"*. A clear illustration of tertiary compression is provided in Figure 2.6, which shows the development of strain and excess pore pressure with time for the first stress increment of a specimen of peat from Portage, USA. Further data due to Dhowian and Edil (1980) for progressive stress increments of an oedometer test on Portage peat are provided in Figure 2.7. There is a clear indication of tertiary compression in the lower stress increments, although the marked steepening of the ε – log t curve becomes less distinguishable as the consolidation stress increases.

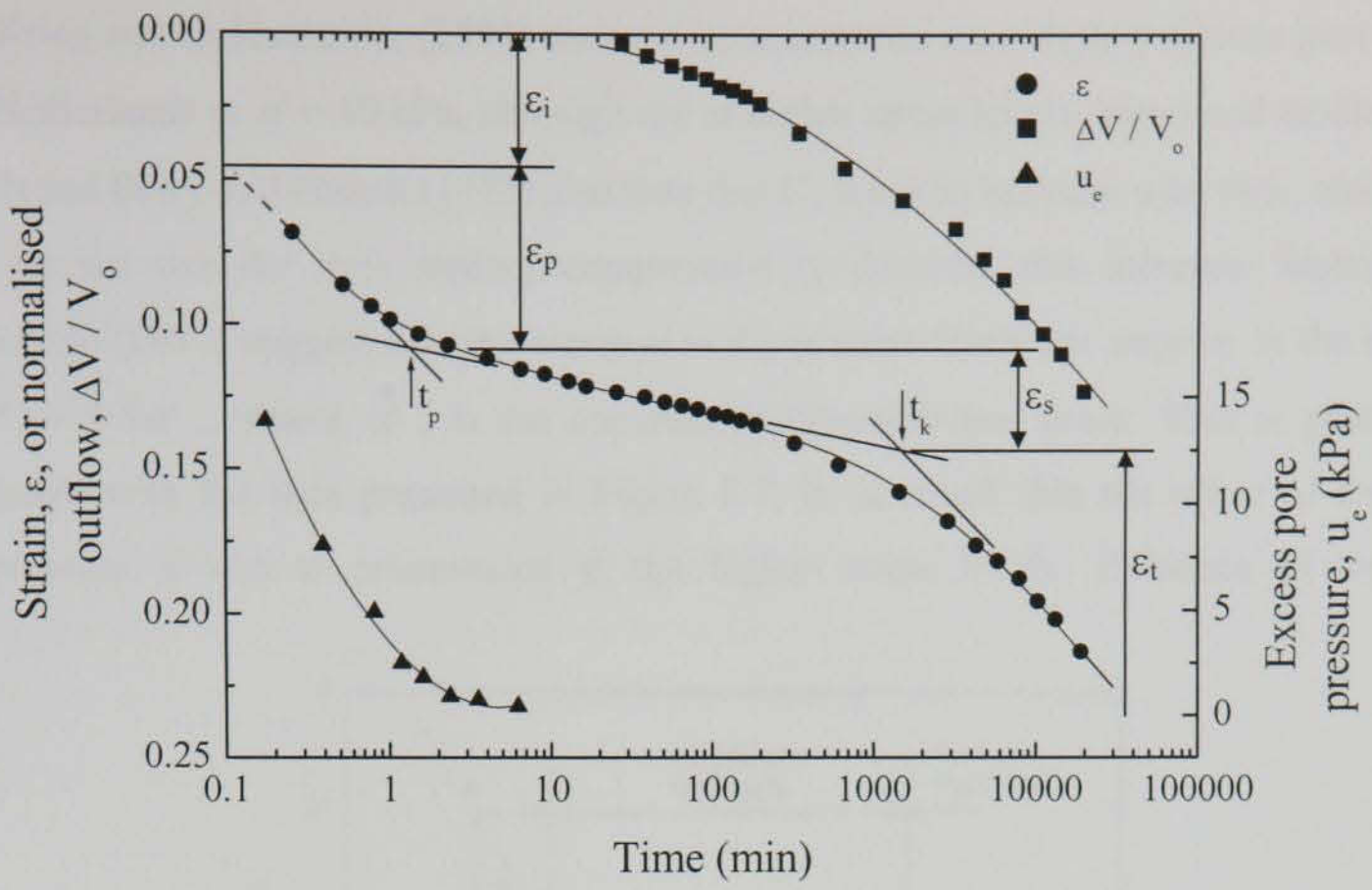

Figure 2.6 Compression curve components for Portage peat; normalised outflow and excess pore pressure are also shown (after Dhowian and Edil, 1980)

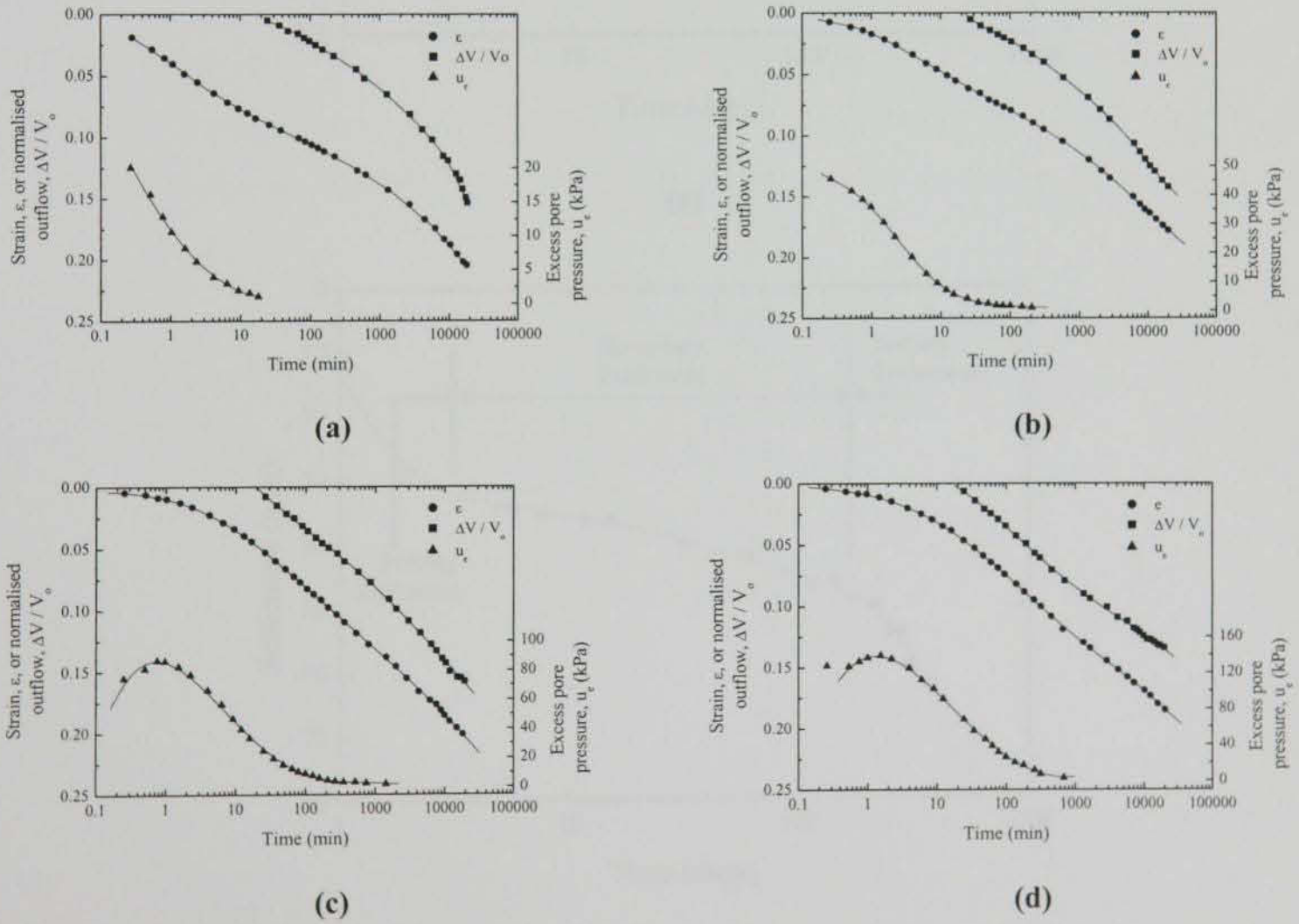

Figure 2.7 Compression data for a Portage peat specimen: (a) 25-50 kPa, (b) 50-100 kPa, (c) 100-200 kPa, (d) 200-400 kPa (after Dhowian and Edil, 1980)

Several other studies have revealed that the slope of the e – log t curve often increases at $t > t_p$. Krieg and Goldscheider (1994) reported its occurrence on a slightly fibrous peat from The Netherlands at $\sigma' = 40$ kPa, although not at higher stress levels. Mesri and Godlewski (1977) and Berry and Poskitt (1972) also note that C_α tends to increase with time, although they do not use the term tertiary compression to describe this increase. Mesri and Godlewski (1977) suggest that the increase in C_α is most likely for stresses in the range $0.5\sigma'_c$ - $1.5\sigma'_c$, where σ'_c is the apparent preconsolidation stress. This is generally consistent with the data presented in Figure 2.7, in so much that the effect of tertiary compression is not as pronounced at the higher stress levels. Evidence of tertiary

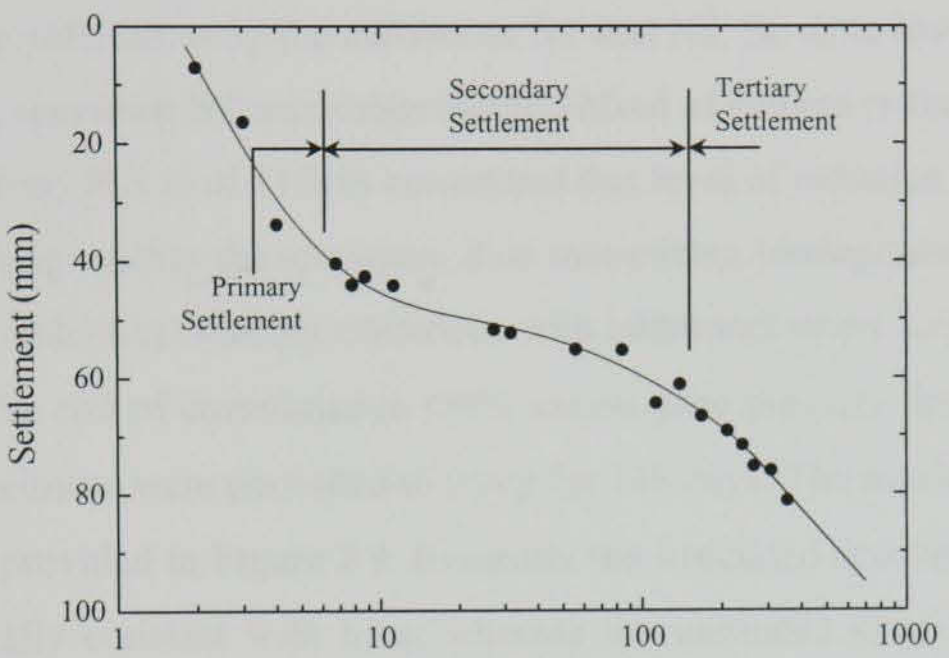

(a)

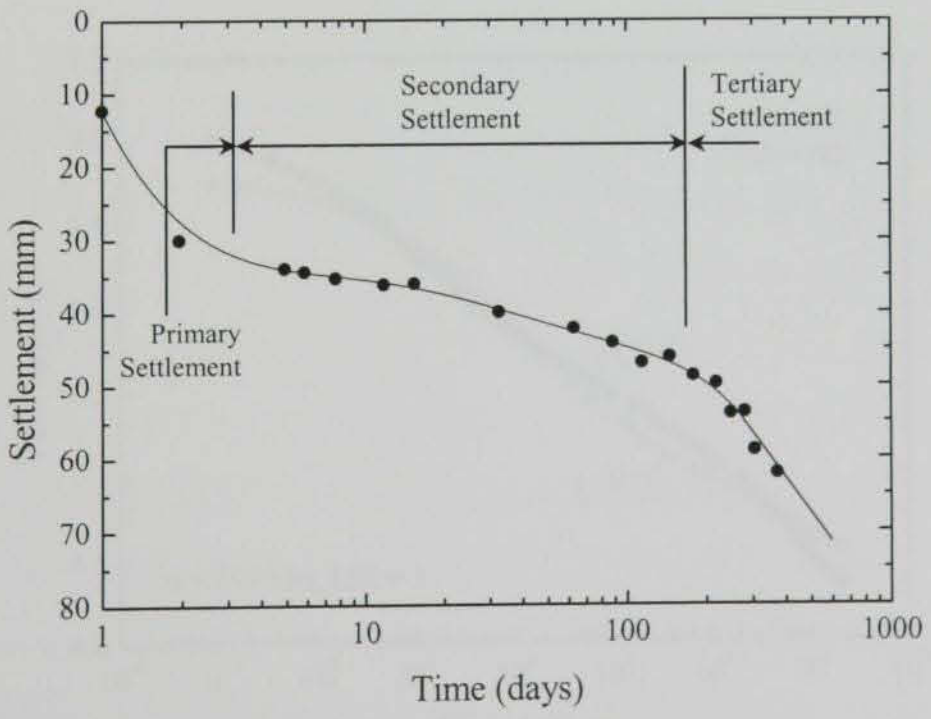

(b)

Figure 2.8 *In situ* settlement-time curves showing tertiary compression for: (a) 3 m embankment, (b) 2 m embankment (after Candler and Chartres, 1988)

compression in the field has been reported by Candler and Chartres (1988) (see Figure 2.8) and by Fox and Edil (1996).

Mesri *et al.* (1997) showed that an increase in C_α with time can be explained by the C_α/C_c concept of compressibility (see § 2.4.2.3). The authors also speculated that biodegradation of peat particles in laboratory conditions may result in a slight increase in compression with time. A study by van der Heijden *et al.* (1994) revealed that biodegradation leads to deformation and decomposition of plant cells. Mesri *et al.* (1997) suggest that the loss of structural integrity of the cells may result in a gradual increase in compression with time. In a discussion to this paper, Fox *et al.* (1999) presented the results of two additional tests on Middleton peat, referred to by the authors as N1 and N2. So as to investigate the effect of biodegradation, specimen N2 was subjected to 2 Mrad of gamma radiation over a 9 hour period prior to testing. Fox *et al.* (1999) considered this level of radiation to be sufficient to kill bacteria and fungi within the specimen, thus minimising biodegradation during creep. Both tests involved identical loading conditions with additional stress increments (LIR = 1) being applied at the end of consolidation (99% excess pore pressure dissipation). At σ' = 198 kPa, both specimens were permitted to creep for 148 days. The resulting e – log t plots for both tests are provided in Figure 2.9. Evidently the irradiated specimen, N2, shows C_α to remain essentially constant with time, whereas the untreated specimen, N1, exhibits tertiary compression, which is consistent with previous laboratory data for Middleton peat (e.g. Dhowian and Edil, 1980; Fox *et al.*, 1992). This result provides significant insight

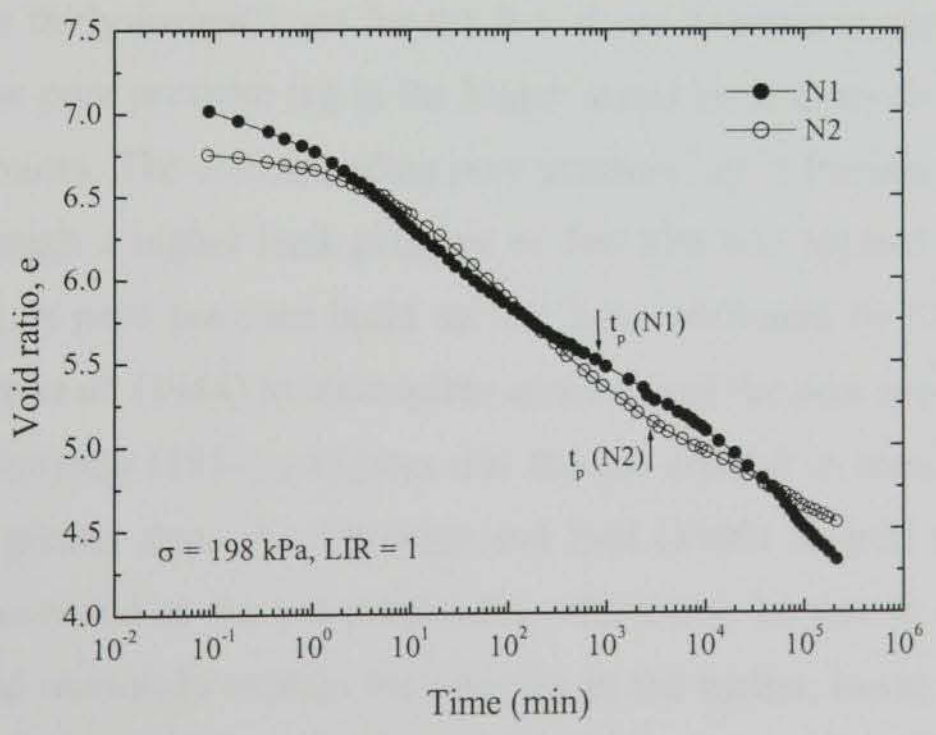

Figure 2.9 e – log t curves for untreated (N1) and irradiated (N2) specimens of Middleton peat (after Fox *et al.*, 1999)

into tertiary compression and may draw into question the results of several previous laboratory studies on peat.

The excess pore pressure data in Figure 2.7 is also of interest. At $\sigma' = 50$ kPa, the consolidation duration, t_p, is approximately 15 minutes (based on 95% excess pore pressure dissipation). The value of t_p is seen to increase with increasing stress level, and hence reducing void ratio, to approximately 270 minutes for $\sigma' = 400$ kPa. This variation in t_p further supports the reduction in permeability with void ratio shown in Figure 2.2. The values of t_p from Figure 2.7 are relatively high compared with values of $t_p < 1$ minute reported by Samson and La Rochelle (1972) and Fox and Edil (1996).

Two other points from Figure 2.7 are worthy of discussion. Firstly, the maximum measured pore pressure is consistently lower than the applied stress increment, and secondly, for $\sigma' = 200$ kPa and $\sigma' = 400$ kPa, this maximum value develops approximately 1 minute after the application of the stress increment. This result is consistent with data reported by Lefebvre *et al.* (1984) for a Canadian fibrous peat (see Figure 2.10). The stress increments in Figure 2.10a and Figure 2.10b involved a back pressure (u_b) of 250 kPa, whereas no back pressure was applied in the stress increments shown in Figure 2.10c and Figure 2.10d. For the stress increments without back pressure, the ratio $\Delta u/\Delta\sigma$ is generally 0.5-0.8 compared with 0.9-1.0 for the stress increments subject to the 250 kPa back pressure. As with the Portage peat data (which involved application of back pressure), a certain amount of time elapses before the pore pressure reaches its maximum value (see Figure 2.7). This is fairly insignificant for the low stress increments, and the use of back pressure reduces the pore pressure lag in the higher stress increments from approximately 75 minutes to 5 minutes. The corresponding pore pressure lag in Portage peat (Figure 2.7) is less severe, although a higher back pressure of 560 kPa was applied in that particular case. The time lag in pore pressure build up has been attributed by Dhowian and Edil (1980) and Lefebvre *et al.* (1984) to incomplete saturation of the peat specimens due to the presence of gas. Hanrahan (1954) estimates that the gas content in some Irish Sphagnum peat bogs may be greater than 5%. Dhowian and Edil (1980) suggest that an increased amount of gas is generated as the test progresses, which may be due to decomposition in the peat. This would obviously explain the time lag in the earlier, lower magnitude stress increments, although it is plausible that the effect of incomplete saturation due to gas may be difficult to examine at low stresses as permeability is already very high in this range, and consolidation therefore extremely rapid. Hobbs (1986) also discusses incomplete

saturation of peat due to gas, suggesting that gas content may be higher in the field than in the laboratory due to sampling disturbance. Hobbs concludes that the presence of gas may contribute to rapid field settlements and recommends that laboratory tests should not be back pressured in order to obtain complete saturation. This recommendation was taken on board for most, but not all, of the laboratory tests described in Chapter 4.

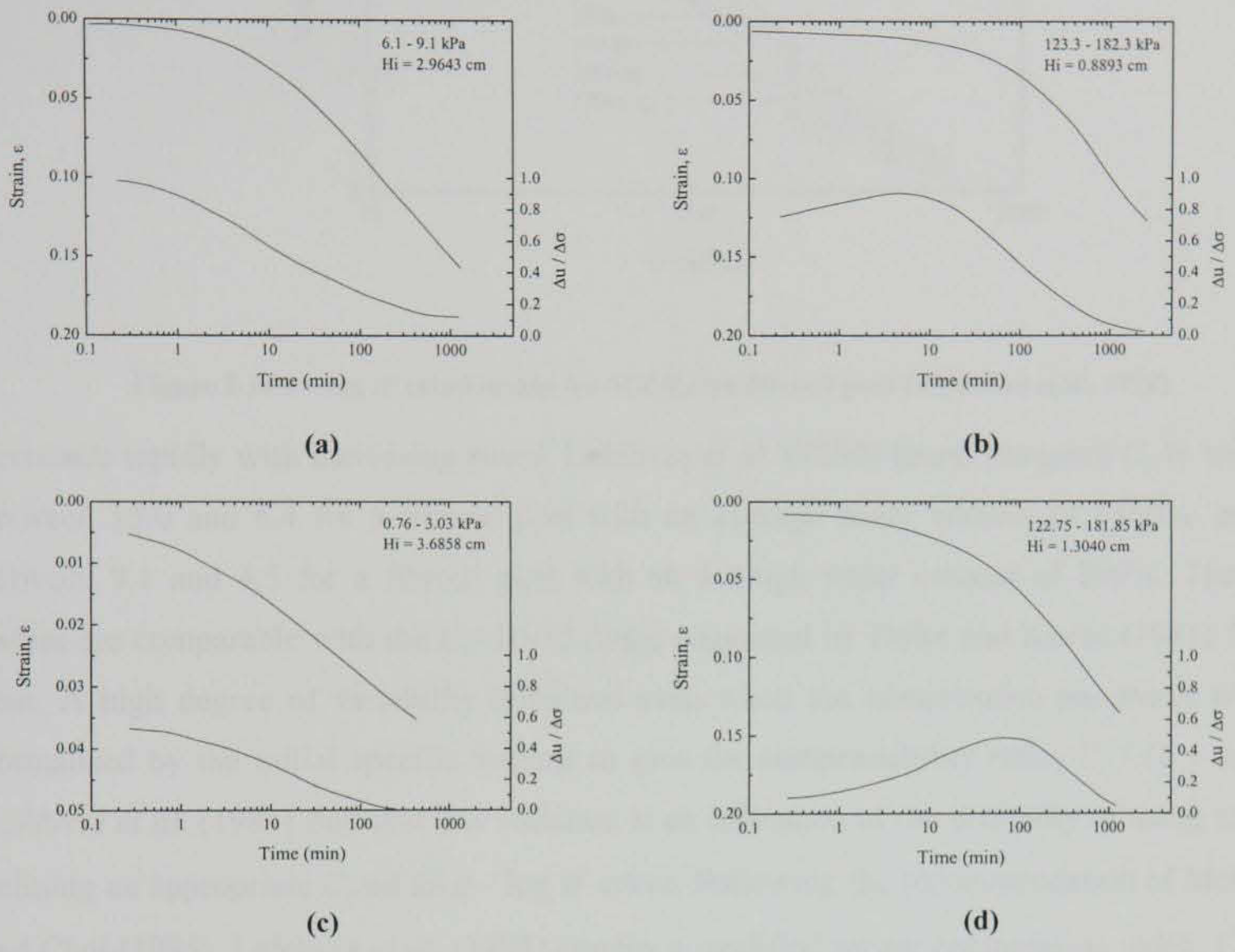

Figure 2.10 Vertical strain and pore pressure versus time for Canadian fibrous peat: (a) 6.1-9.1 kPa, u_b = 250 kPa; (b) 123.3-182.3 kPa, u_b = 250 kPa; (c) 0.76-3.03 kPa;(d) 122.75-181.85 kPa (after Lefebvre *et al.*, 1984)

2.2.3 Compression indices and strain

The conventional means of describing the compressibility of a soil is by way of e – log σ' curves. For many inorganic soils the slope of the virgin curve can be conveniently described by the compression index, C_c = -Δe / Δ log σ'. However, for many soft organic soils and peats, the e – log σ' curve is not linear, but convex (den Haan, 1997). Examples of this non-linearity are given in Barden (1969) and Fox *et al.* (1992) and are shown here in Figure 2.11 and Figure 2.12. Evidently C_c is not a constant parameter in these cases, but

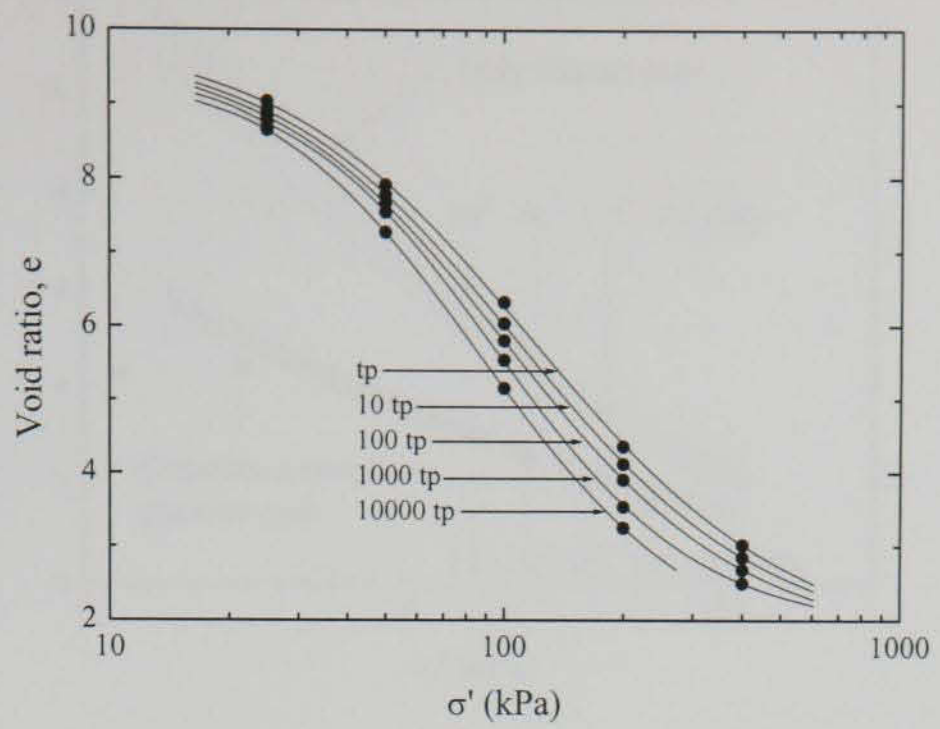

Figure 2.11 e – log σ' relationship for Middleton fibrous peat (after Fox *et al.* 1992)

decreases rapidly with increasing stress. Lefebvre *et al.* (1984) found (tangent) C_c to vary between 15.0 and 6.4 for a fibrous peat with an average water content of 1460%, and between 9.1 and 4.5 for a fibrous peat with an average water content of 860%. These values are comparable with the C_c=10-15 range suggested by Holtz and Kavac (1981) for peat. A high degree of variability remained even when the compression parameter was normalised by the initial specific volume to give the compressibility ratio, C_c / (1 + e_o). Lefebvre *et al.* (1984) find that this variation is an indication of the difficulty of using and defining an appropriate C_c on an e – log σ' curve. Following the recommendation of Mesri and Choi (1985), Lefebvre *et al.* (1984) employ a modified *secant* compression index, C_c', between the preconsolidation stress, σ'_c, and different values of applied effective stress, σ'. They found the variation of C_c' with stress to be small for the lower values of initial void ratio and most significant for high initial void ratios. Lefebvre *et al.* (1984) shows the variation in C_c' with e_o for σ'/σ'_c = 20 (see Figure 2.13). Evidently this notation results in a lower degree of variation as the compression ratio, C_c' / (1 + e_o) remains tolerably constant.

Despite the apparent merit of Figure 2.13, Landva and La Rochelle (1983) express reservation as to the use of any relationship based on the apparent preconsolidation stress, σ'_c. They find that for fibrous, undisturbed bog peats, determination of σ'_c is very difficult, and may be close to zero or even negative if a considerable amount of gas is present. Evidently this affects the functionality of the C_c' - σ'/σ'_c relationship as the ratio, σ'/σ'_c, will be either infinite or unacceptably large. The value of σ'_c, may be considerably higher

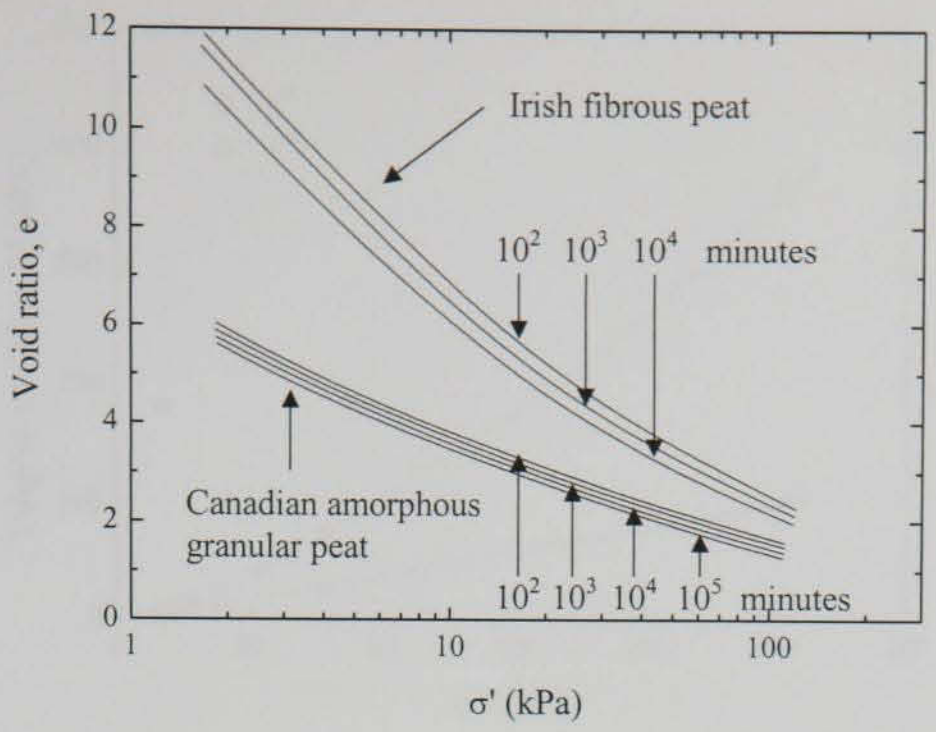

Figure 2.12 e – log σ' relationship for amorphous and fibrous peat at different periods of sustained loading(after Barden, 1969)

in Canadian peat deposits as snow loading may preconsolidate the peat by up to 8 kPa (based on 2 m high snow drift). Lefebvre *et al.* (1984) use similar reasoning to partially explain the 3.2-7.8 kPa range of σ'_c, determined from oedometer tests on fibrous peat from Quebec, Canada. Ling Kah Jai (1997) also identified the difficulties associated with a constant value of C_c, and showed how the conventional formulation may be invalid whenever σ'_c appears to be zero.

Although the e – log σ' relationship is commonly adopted in practice, a number of

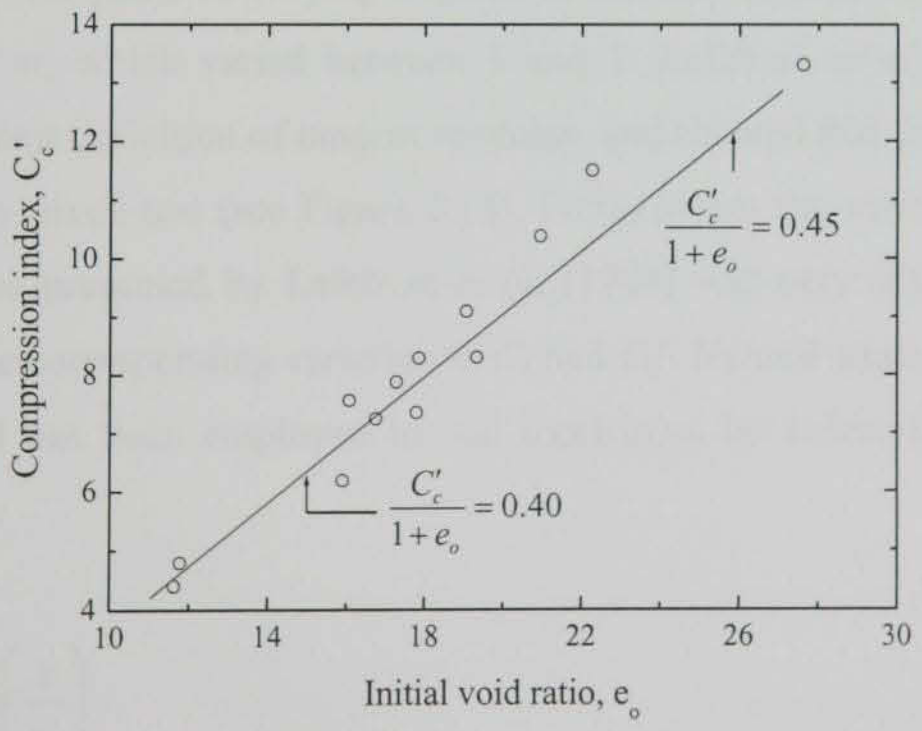

Figure 2.13 Compression index, C_c', versus initial void ratio, e_o, for Canadian fibrous peat at $\sigma'/\sigma'_c = 20$ (after Lefebvre *et al.*,1984)

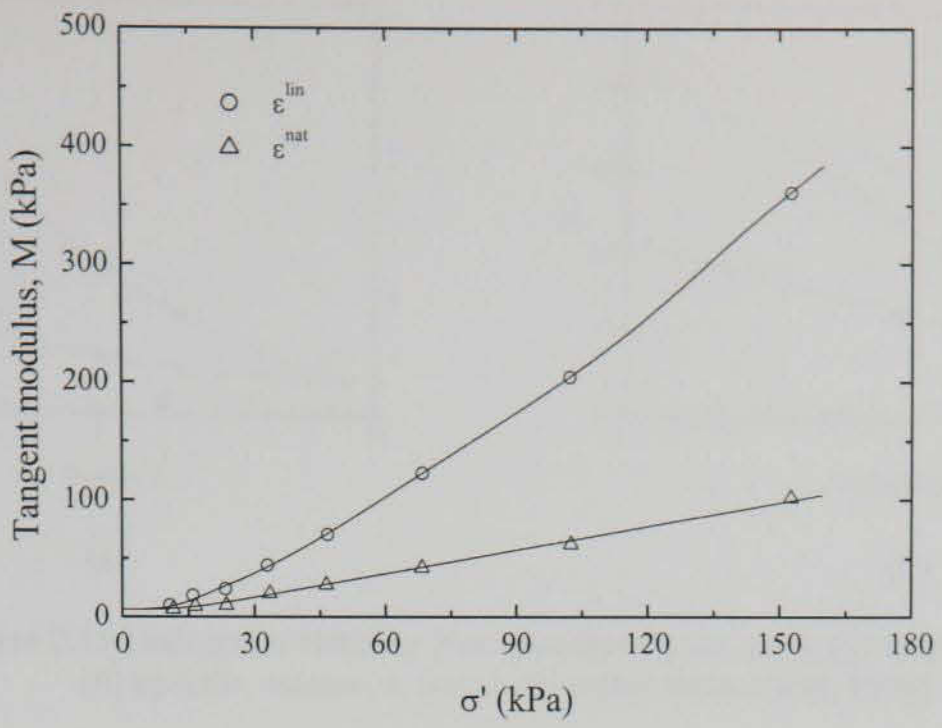

Figure 2.14 Tangent modulus, determined using both natural and linear strain, versus effective stress for Canadian fibrous peat (after Lefebvre *et al.*, 1984)

alternative formulations have been proposed. Hobbs (1986) and Leroueil *et al.* (1985) advocate the use of strain, $\varepsilon = \Delta H/H_o$, instead of void ratio, thus accounting for the inherent variation in initial void ratio of seemingly similar samples. However, as strain may also be defined in this context as $\varepsilon = \Delta e/(1+e_o)$, the non-linearity prevalent in e – log σ' curves for peat will remain.

A number of workers have employed tangent modulus, $M = d\sigma'/d\varepsilon$, as a means of describing the compressibility of peat. Helenelund (1980) showed that the relationship between M and σ' for peats of varying degrees of humification can be described by the modulus number, m, which varied between 5 and 7. Lefebvre *et al.* (1984) employed *natural strain* in their definition of tangent modulus, and showed that this led to a constant value of m for any given test (see Figure 2.14). Furthermore, the variation in m over the entire test database presented by Lefebvre *et al.* (1984) was very slight, and much less significant than the corresponding variation in C_c and C_c'. Natural strain, ε^{nat}, is defined in Equation 2.4, and has been employed in soil mechanics by Juárez-Badillo (1965) and Butterfield (1979).

$$\varepsilon^{nat} = -\int_{v_o}^{v} \frac{dv}{v} = -\ln\left(\frac{v}{v_o}\right) \qquad 2.4$$

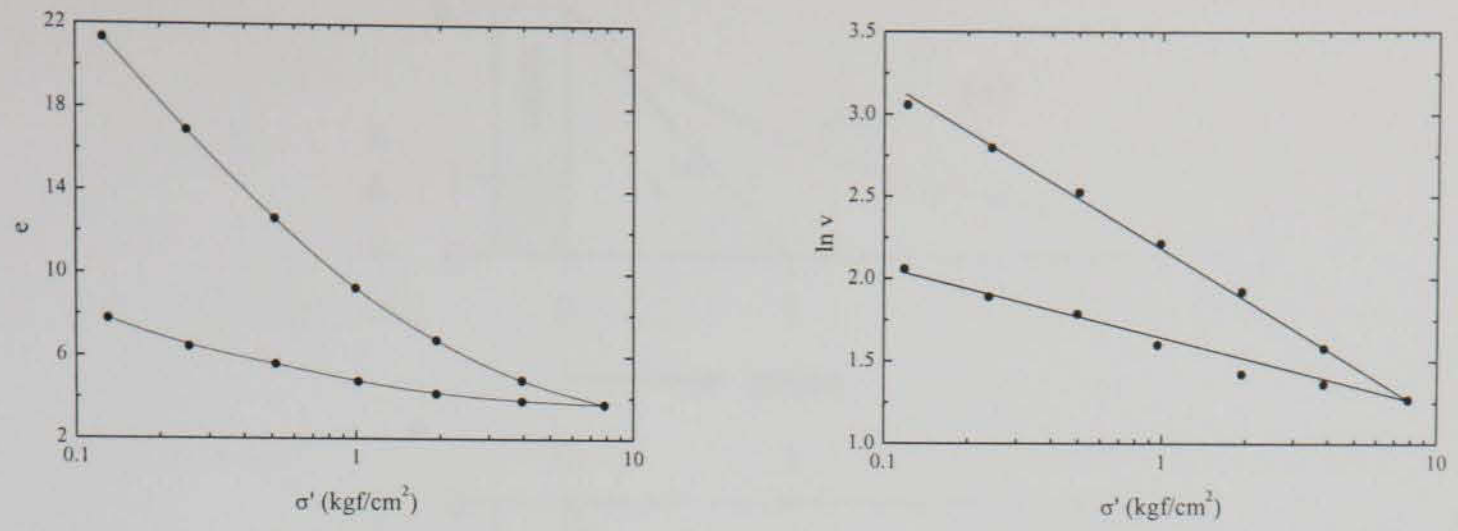

(a) **(b)**

Figure 2.15 Oedometer data for Newfoundland peat using (a) void ratio, *e*, (b) specific volume, *v*, (logscale) (after Butterfield, 1979)

where specific volume, $v = 1+e$. Natural strain is related to conventional strain, hereafter referred to as *linear strain*, ε^{lin}, through Equation 2.5:

$$\varepsilon^{nat} = -\ln\left(1-\varepsilon^{lin}\right) \qquad 2.5$$

Butterfield (1979) showed how linearity could be restored to the virgin stress-strain curve for a number of soils including Newfoundland peat (see Figure 2.15) by using natural strain as a measure of the compression of the soil. In Figure 2.15 $\ln(v)$ replaces ε^{nat}, although it is evident from Equation 2.4 and also from den Haan (1994a) that the two measures of compression are interchangeable in much the same way as e and ε^{lin}. One implication of using natural strain is that it has infinity as its limiting value rather than unity as with linear strain (see Figure 2.16). Although this is necessary to obtain a linear relationship between strain and logarithm of effective stress, values of strain in excess of unity are difficult to interpret, as they are not indicative of relative compression.

Den Haan (1992) showed that a power relationship could be used to describe the virgin compression of a wide range of soils, including peats.

$$\frac{v}{v_1} = \left(\sigma' - \sigma'_s\right)^{-b} \qquad 2.6$$

In Equation 2.6, v_1 is the reference specific volume and σ'_s is used to account for the brittleness of natural clays. For a wide range of soils including peats, σ'_s can be taken as zero, which allows Equation 2.6 to be written as:

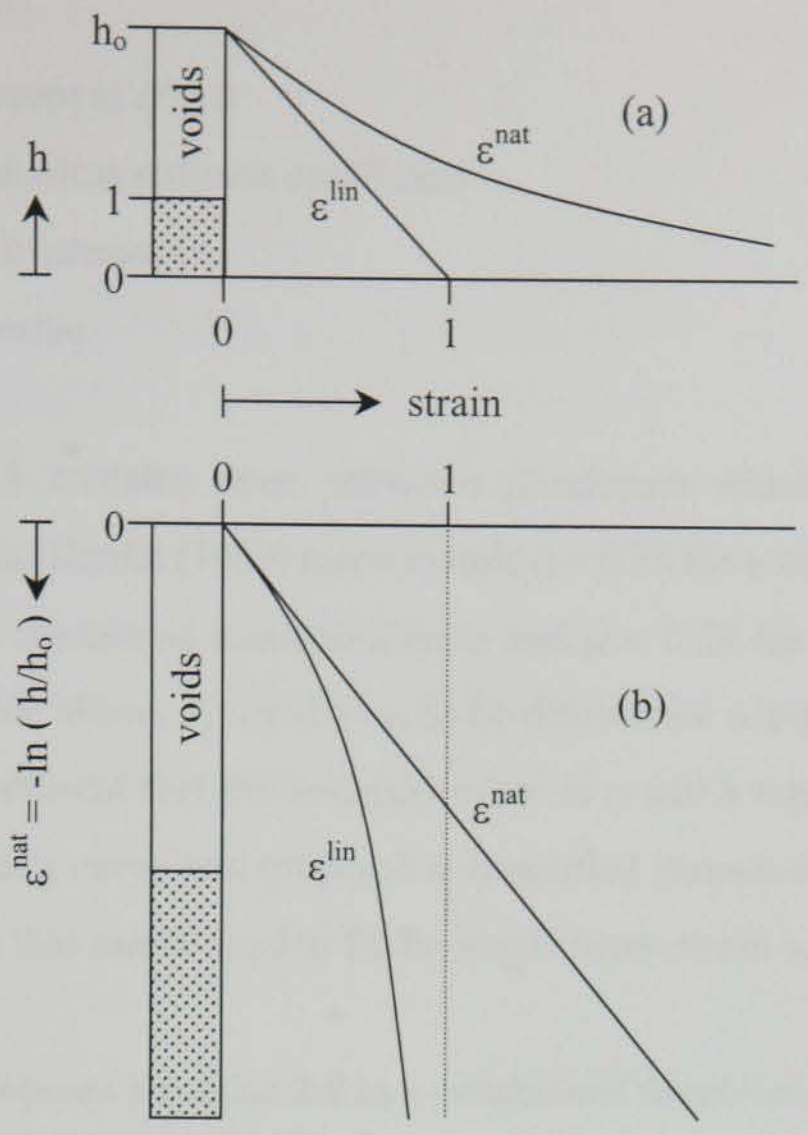

Figure 2.16 Linear and natural strain: (a) as function of sample height, *h*; (b) as function of $-\ln(h/h_o)$ (after den Haan and Edil, 1994)

$$-\ln\left(\frac{v}{v_1}\right) = b\ln(\sigma') \qquad 2.7$$

Equation 2.7 is essentially the natural compression law for soils proposed by Butterfield (1979) and Juárez-Badillo (1965, 1975, 1981a, 1981b), defining a linear relationship between logarithm of natural strain and logarithm of effective stress. A similar formulation, although somewhat different in mathematical structure, was proposed by Meyer and Dereczenik (1994).

Liu and Znidarcic (1991), Lan (1992), Edil and den Haan (1994) and Edil *et al.* (1994) adopt the formulation of Hardin (1989) to describe the relationship between void ratio and effective stress. Hardin's formulation relates the inverse of void ratio to effective stress through:

$$\frac{1}{e} = \frac{1}{e_{int}} + \frac{1}{S_{1-D}}\left(\frac{\sigma'}{\sigma_a}\right)^{\mu} \qquad 2.8$$

where

$1/e_{int}$ is the intercept at $\sigma' = 0$

$S_{1\text{-}D}$ is a dimensionless stiffness coefficient

σ_a is atmospheric pressure

μ is a constant value

Evidently Equation 2.8 contains three unknown parameters which cannot be directly obtained from $e - \sigma'$ data. Hardin (1989) recommends $\mu = 0.35$ for a wide range of cohesive soils, $\mu = 0.5$ for soils containing montmorillonite and $\mu = 0.25$ for a limestone residual clay. This practical guide allows $S_{1\text{-}D}$ and $1/e_{int}$ to be determined using regression analysis. However, Lan (1992) showed that the assumed value of μ had a significant influence on the shape of the resulting curve and proposed a simplified formulation with $\mu = 1$. This results in a formulation that can be used to fit the virgin stress-strain curve only.

Ling Kah Jai (1997) proposes Equation 2.9 as a generalised formulation which can be used for all soil types:

$$(e - e_m)(\sigma' + \sigma'_k)^{b_c} = K_B \qquad 2.9$$

where σ'_k and e_m are asymptotic values of effective stress and void ratio respectively, and K_B is a constant parameter based on an assumed linear relationship between void ratio and the compression index, C_c. Ling Kah Jai (1997) finds that for peat soils, σ'_k and e_m may be conveniently taken as zero to give:

$$\frac{e}{K_B} = \sigma'^{b_c}_k \qquad 2.10$$

Equation 2.10 is essentially a form of the generalised formulation proposed by den Haan (1992):

$$\frac{v - v_\infty}{v_1 - v_\infty} = (\sigma' - \sigma'_s)^{-b} \qquad 2.11$$

in which the specific volume at infinite stress, v_∞=1, and the structure parameter, σ'_s=0. Formulations of the type shown in Equation 2.11 are commonplace, having been adopted

by a number of workers such as Hansen (1969), Garlanger (1972), Christie and Honks (1985) and Jose *et al.* (1990). By assuming v_∞=1, den Haan (1992) obtains Equation 2.7. An interesting characteristic of the various formulations considered in this section is the limiting value as stress becomes infinite. Conventional use of C_c implies infinite negative volume at infinite stress which, due to the high non-linearity of the e – log σ' curves depicted in Figure 2.11 and Figure 2.12, can have severe implications over even moderate stress levels. The natural strain formulation has an asymptotic value of zero volume at infinite stress, whereas Hardin's formulation (Equation 2.8) and that proposed by Ling Kah Jai (1997) has zero voids ratio at infinite stress. Den Haan (1994) concludes that the general consensus is that the asymptote for infinite stress is a slightly negative void ratio, due to partial compression of the soil particles, but with volume greater than zero.

Den Haan and Amir (1994) adopt a revised form of Fokkens (1970) formula, which assumes a unique relationship between the ratio of water to organic content, *w/H*, and effective stress. The revised form due to Den Haan and Amir (1994) is given in Equation 2.12, and has been extrapolated in time to 10^4 days or 27 years, which the authors suggest represents final compression.

$$\frac{w}{N} = 26.7(\sigma')^{-0.437} \qquad 2.12$$

where N is the loss on ignition which, for highly organic content soils, is interchangeable with organic content, H (Skempton and Petley, 1970).

Equation 2.12 is based on the premise that the scatter in plots of water content, or void ratio versus effective stress can be normalized by the organic content. Den Haan and Amir (1994) show, on the basis of 29 oedometer tests on Zegveld Polder peat (Netherlands), that the scatter is indeed reduced, although a unique relationship is not obtained. A similar relationship incorporating both water content and organic content has been proposed by Al-Khafaji and Andersland (1981), whereas an alternative formulation (Equation 2.13), based solely on the natural water content, w_n, has been suggested by Oikawa and Igarahi (1997):

$$e = 2.47\left[1 - \frac{1}{\exp(2.91/\sigma')^{0.39}}\right] w_n^{\,0.85\left[1-1/\exp(1.85/\sigma')^{0.45}\right]} \qquad 2.13$$

2.3 CASE STUDIES OF EMBANKMENTS CONSTRUCTED OVER PEAT DEPOSITS

The settlement records for several case studies relating to *Radforth* peats are summarised in Figure 2.17. The term Radforth is generally reserved for peats with low or insignificant mineral content (Carlsten, 1988). Such peats tend to be encountered in raised bogs, and as such are derived mainly from *Sphagnum* plants, particularly in the upper layer (Hobbs, 1986). Radforth peats are generally very compressible due to a high *in situ* natural water content and associated void ratio (Landva and La Rochelle, 1983). In Figure 2.17, numbers next to individual data points refer to the time in years since the start of construction. The end of primary consolidation *in situ* stress-strain curve of an Irish fen peat, with an organic content of 42.2% is included for comparison. The relative compression of Radforth peats under moderate stress levels is well indicated by Figure 2.17. The range of data serves as a potentially useful means of estimating the settlement of embankments constructed over

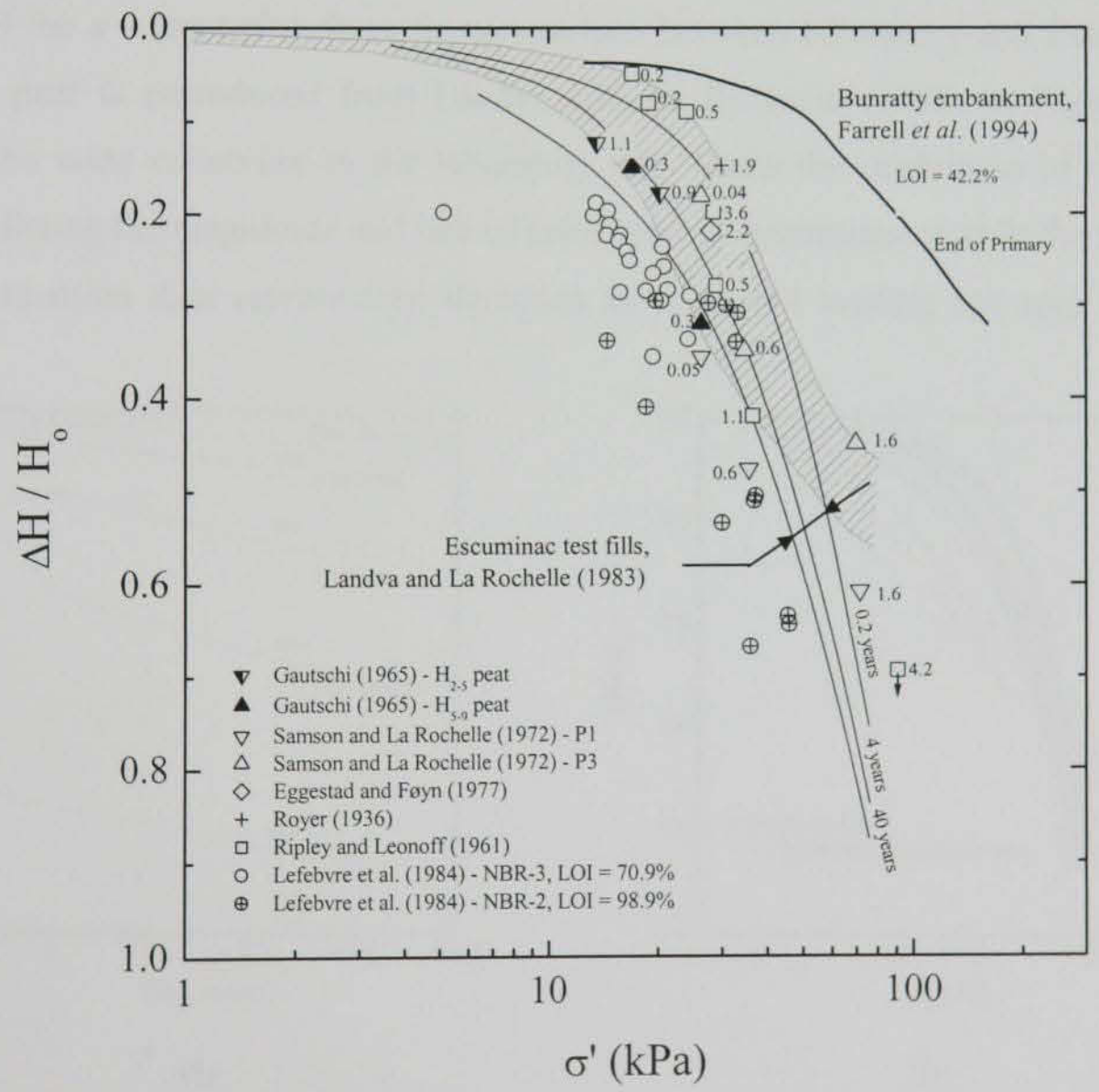

Figure 2.17 Relative compression under various embankments constructed on peat

Radforth peat deposits. However, Landva and La Rochelle (1983) concluded that part of the settlement at $\sigma' \geq 30$ kPa was due to shear deformations, resulting from embankments which were relatively narrow in relation to the depth of the underlying peat layer. They suggest that the shaded region in Figure 2.17 is a more likely limitation to the expected settlement. However, the data presented by Landva and La Rochelle (1983) did not include the end of primary compression data from the NBR-2 and NBR-3 sites in James Bay, Quebec. Evidently these data, which were added to the plot by the author, lie outside the envelope shown in Figure 2.17, even though insignificant lateral strains occurred at the NBR-3 site (Lupien *et al.*, 1981).

The time dependent behaviour of peat is well illustrated by the Escuminac test fills settlement data in Figure 2.18, which show significant compression over a 40 year period. The annotation in the ε – log t relationship ($\varepsilon = \Delta H/H_o$) of Figure 2.18a relates to the initial stress increment followed by the reduction in stress due to settlement and partial submergence of the fill. It is interesting to note the effect that this partial submergence has on the apparent coefficient of creep compression, C_α, as determined from the latter part of the slope of the ε – log t plot. Specific comparison between laboratory and field data for Escuminac peat is reproduced from Landva and La Rochelle (1983) in Figure 2.18b. Evidently the wide variability in the laboratory data limits the usefulness of oedometer tests in predicting the magnitude and rate of settlement of Escuminac peat in the field. The *in situ* stress-strain data representing durations of sustained loading are seen to merge

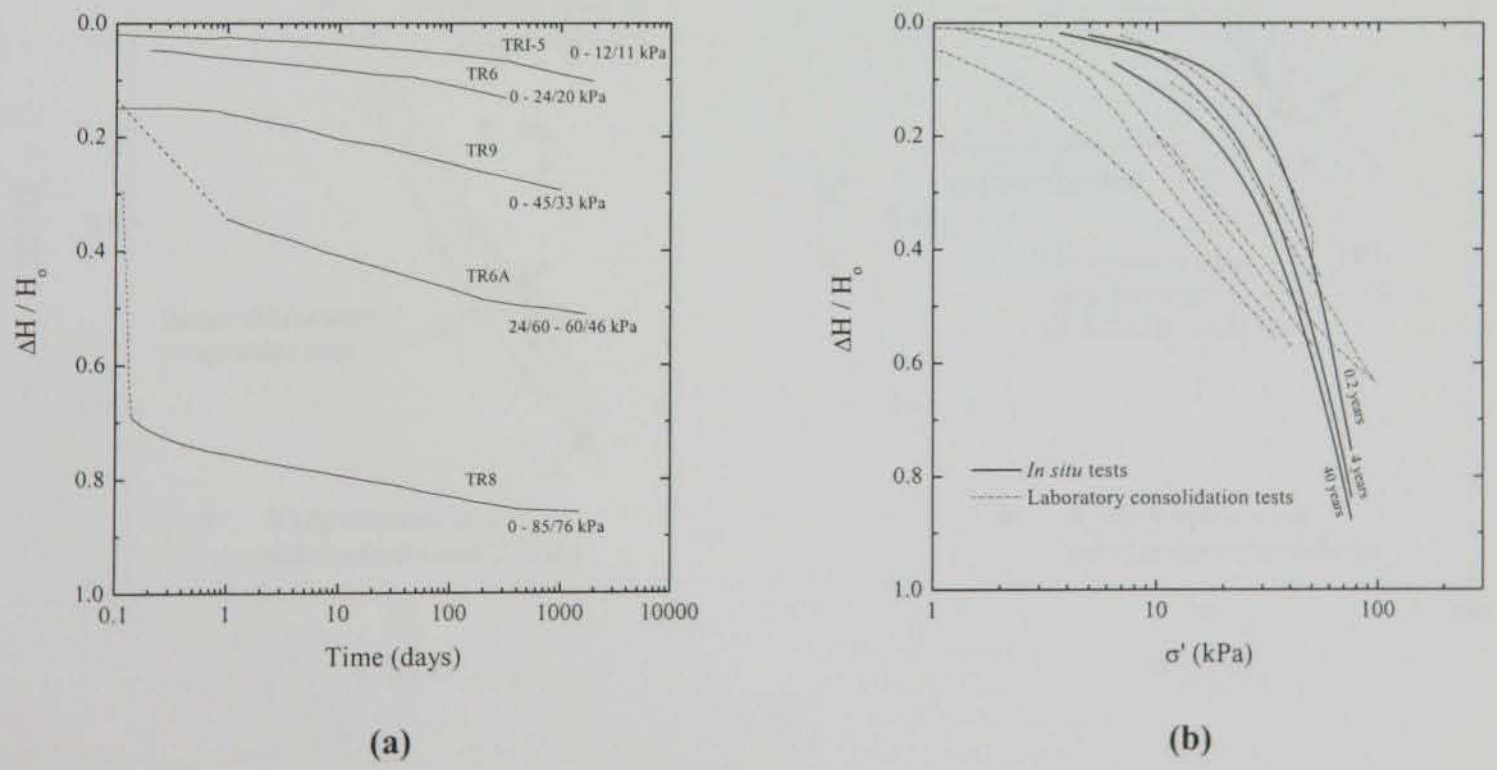

Figure 2.18 Performance of Escuminac test fills constructed over Radforth peat: (a) relative compression versus time, (b) relative compression versus effective stress (after Landva and La Rochelle, 1983)

together with increasing stress level. Although this observation is consistent with the laboratory data reported by Barden (1969) for Irish fibrous peat and Fox *et al.* (1992) for Middleton fibrous peat (see Figure 2.11 and Figure 2.12), it should be remembered that the shape of the stress-strain curves may be influenced by the shear deformations associated with $\sigma' \geq 30$ kPa.

Lefebvre *et al.* (1984) had mixed success in correlating field and laboratory data for James Bay peat, Quebec. Test fills were constructed over two peat deposits, namely NBR-2 and NBR-3. The peat at NBR-2 had an average *in situ* water content of 1460% and organic content of 99%, whereas that at NBR-3 had an average *in situ* water content of 860% and organic content of 71%. The lower water content at NBR-3 has been attributed by Lefebvre *et al.* (1984) to the observed circulation of water, which may have resulted in the deposition of mineral particles within the peat. Comparison of laboratory and field data for NBR-2 peat is provided in Figure 2.19a and for NBR-3 peat in Figure 2.19b. In Figure 2.19, the range of 24 hour laboratory data is shown together with the average compression curve derived from these data. The *in situ* data of Figure 2.19 relates to the end of primary consolidation as determined from the slope of the field settlement versus log time curve. For the peat at NBR-3, *in situ* data are seen to fall within the band defined by the laboratory tests, with the majority of the data showing good agreement with the laboratory

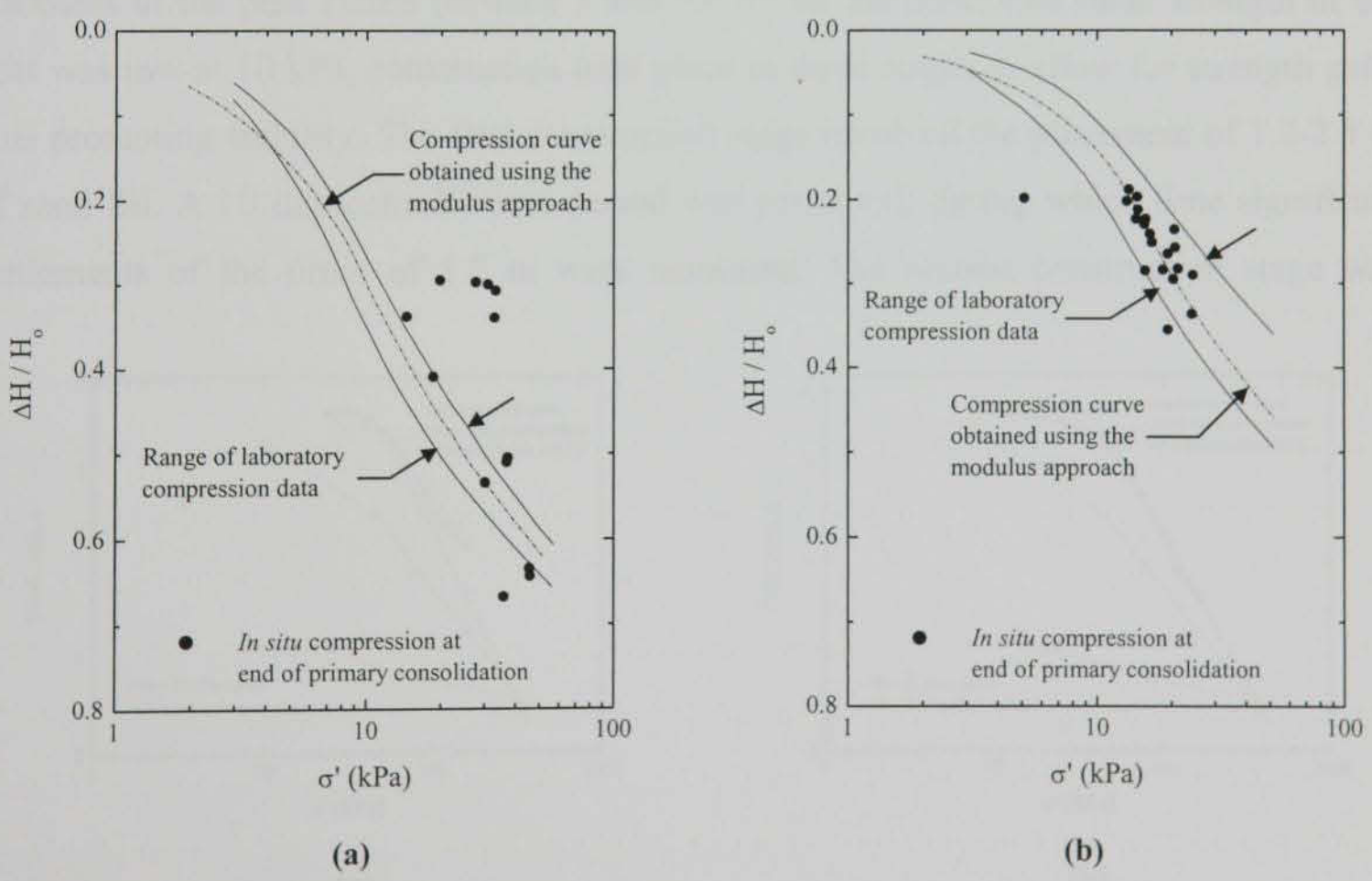

Figure 2.19 Comparison of *in situ* and laboratory compression for Canadian fibrous peat: (a) NBR-2, average water content = 1460%, (b) NBR-3, average water content = 860% (after Lefebvre *et al.*, 1984)

measured compression curve. At NBR-2 however, the field compression data shows considerable scatter and tends to lie outside the band of laboratory data. Lefebvre *et al.* (1984) attributed this high degree of scatter for the field data at NBR-2 to significant lateral spreading of the fill during construction. Lupien *et al.* (1981) estimated that this heave resulted in lateral strains of the order of 18-65%.

Farrell (1997) described the application of relatively simple geotechnical principles to a preloading design involving staged construction of 11 m high embankments. Farrell *et al.* (1994) and Farrell (1997) showed that good correlation can be made between laboratory and *in situ* data when the laboratory e – log σ' curve is corrected for sample disturbance using the method suggested by Schmertmann (1953). Figure 2.20 presents two *in situ* and laboratory e – log σ' curves for a fen peat with an organic content of 42.2%. Evidently the agreement between laboratory and field results is better in Figure 2.20b. It is also worth noting that the *in situ* e – log σ' relationship depicted in Figure 2.20a is non-linear.

Samson and La Rochelle (1972) describe the construction of an expressway over a peat deposit in Canada. The peat is typical of the Radforth peats considered previously, in that the average organic content is 91%. The compressibility of this peat is reflected in the high initial water content of 890%. Along the length of the proposed carriageway the original thickness of the peat varied between 3 and 5.8 m. As the undrained shear strength of the peat was low at 10 kPa, construction took place in three stages to allow for strength gain, thus promoting stability. The first construction stage involved the placement of 1.2-2.5 m of sand fill. A 10 day consolidation period was permitted, during which time significant settlements of the order of 1.2 m were measured. The second construction stage was

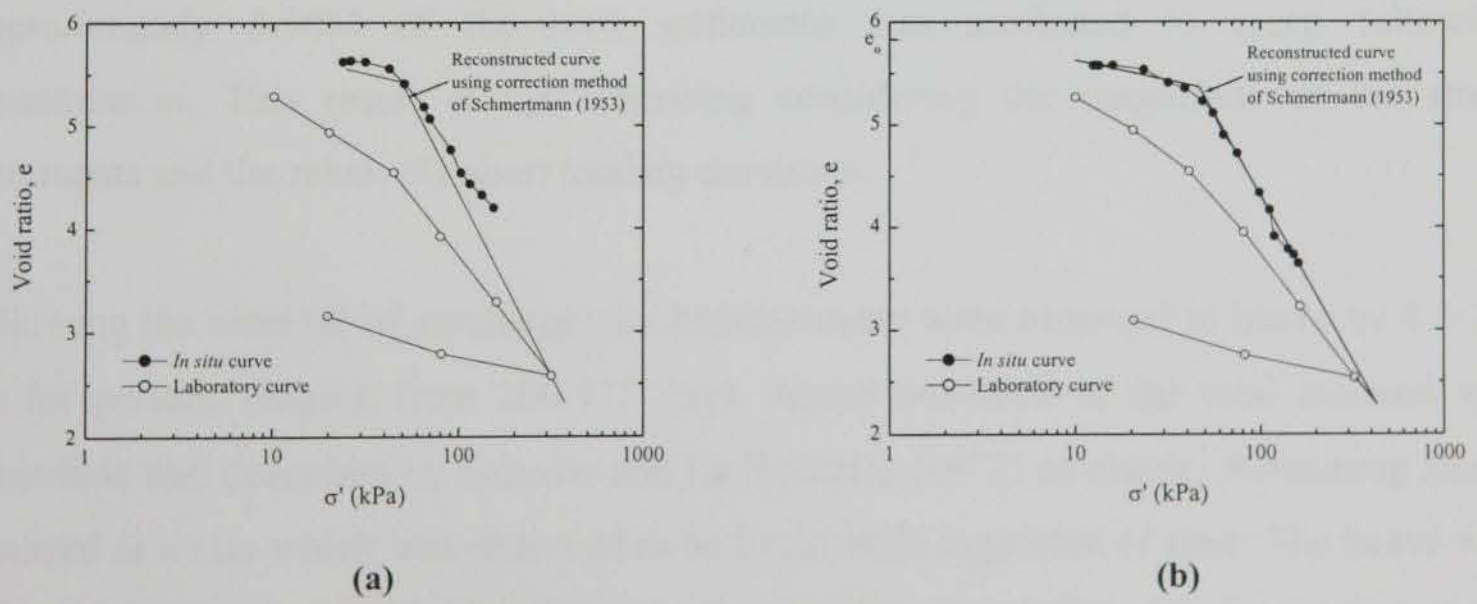

Figure 2.20 Comparison of *in situ* and laboratory e – log σ' relationships for Irish fen peat (a) Farrell (1997), (b) Farrell *et al.* (1994)

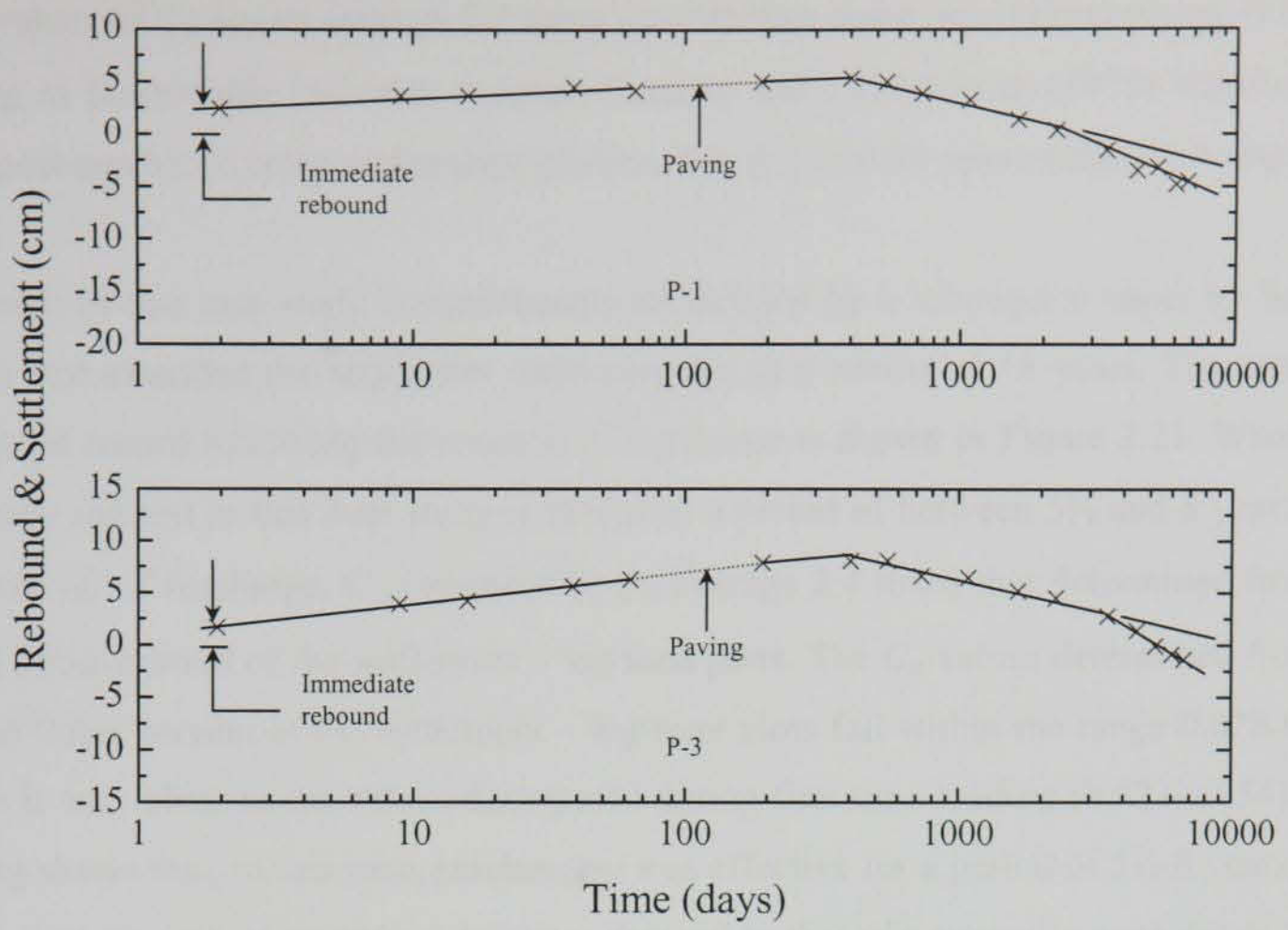

Figure 2.21 Rebound and settlement versus logarithm of time curves for an expressway built over peat (after Samson, 1985)

completed in 0.3 m lifts, bringing the embankments to total thicknesses of 2.5-3.3 m. Finally, after approximately 6 months, the embankments were raised to their maximum height of 3.6-5.8 m, including the temporary surcharge of 1.0-1.5 m of sand fill. This surcharge represented about 50% of the final design effective stress. After a period of approximately 12 months the surcharge was removed, and the road completed within a further 3 months. At the end of the 12 month surcharging period, the total settlement varied between 1.4 to 3.3 m, corresponding to 40-60% of the original thickness of the peat. Approximately 5-10% of the total settlement was attributed to creep following consolidation. This result is not surprising considering the magnitude of the stress increments and the relatively short loading durations.

Following the removal of surcharge, the embankments were observed to heave by 4.3-7.9 cm for periods ranging from 200-475 days. About one-third of the total rebound was immediate and described by Samson and La Rochelle (1972) as elastic. Remaining heave occurred at a rate which was observed to be linear with logarithm of time. The heave was followed by a slow rate of creep compression, corresponding to an average creep coefficient, C_α = 0.007-0.032. In this instance, C_α is defined in terms of strain referenced

to the thickness of the peat at the assumed end of consolidation. It is of interest to note that these values of C_α are on average 2.2 times smaller than those determined during first time loading at comparable effective stresses. Samson and La Rochelle (1972) reported that these post-surcharge creep settlements continued at this rate for approximately 4 years.

The merit of this case study is significantly heightened by a subsequent paper by Samson (1985) that extended the settlement measurements to a period of 18 years. The complete settlement record following the removal of surcharge is shown in Figure 2.21. What is of particular interest in this case study is that after a period of between 5½ and 8 years after the removal of surcharge, C_α increased by on average 2.4 times that determined from the initial linear section of the settlement – log time plots. The C_α values determined from the second linear section of the settlement – log time plots fall within the range 0.028-0.073, which is very close to the values determined during first time loading (0.022-0.054). This finding shows that, in this case, surcharging was effective for a period of 5½-8 years, after which time the rate of settlement became identical to that of a normally consolidated peat. It was estimated that the effect of the temporary surcharge was to reduce overall post-

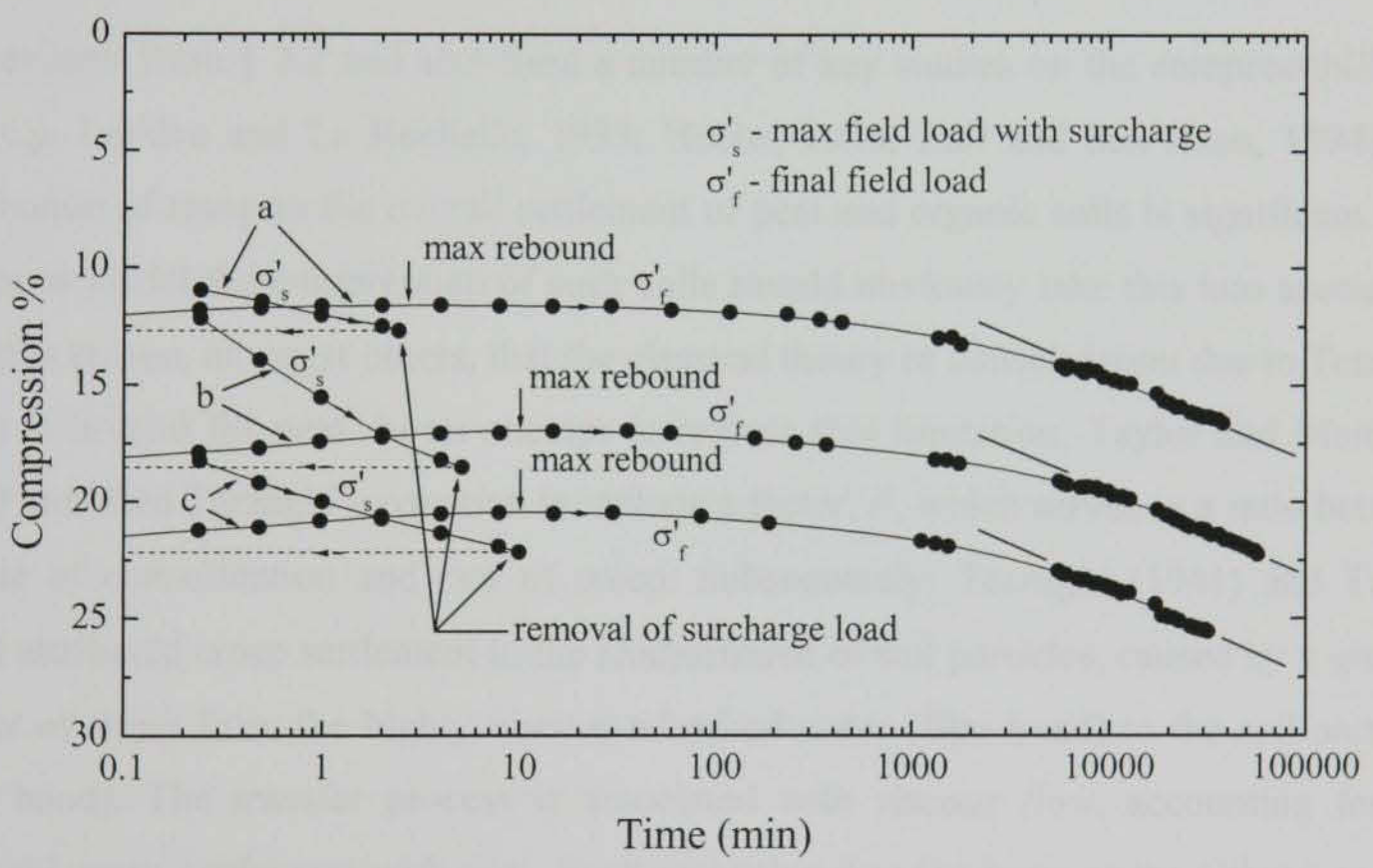

Test Nº	Initial water content	σ'_s (kPa)	σ'_f (kPa)	max rebound
a	424%	69	46	1.26%
b	475%	69	46	1.95%
c	526%	70	45	2.32%

Figure 2.22 Rebound and long-term compression curves for preconsolidated peat samples (after Samson, 1985)

construction settlements by about 65%.

Samson (1985) attempted to mimic the *in situ* loading conditions in the laboratory, by means of oedometer tests on samples retrieved from beneath the embankment before the removal of surcharge. Specimens were reconsolidated to the *in situ* stress of 69 kPa, before one-third of the applied load was removed. The peat specimens were permitted to rebound and subsequently compress at the lower, over consolidated stress of 49 kPa. The results of the laboratory tests are provided in Figure 2.22, where it can be seen that rebound took place within a few minutes, after which time the peat slowly recompressed until such time as the slope of the settlement – log time plot became linear. Samson (1985) showed that the creep coefficient, C_α, determined from this plot was virtually identical to that obtained from *standard* oedometer loading at an equivalent stress level. Furthermore, good agreement was obtained between laboratory and *in situ* creep settlement observations.

2.4 ONE-DIMENSIONAL COMPRESSION MODELS

As is evident from § 2.2 and also from a number of key studies on the compressibility of peat (e.g. Landva and La Rochelle, 1983; Hobbs, 1986; Edil and den Haan, 1994), the contribution of creep to the overall settlement of peat and organic soils is significant. Any attempt to model the compression of such soils should obviously take this into account. It is for this reason, amongst others, that the classical theory of consolidation due to Terzaghi (1923) is invalid for peat. In an attempt to redress this limitation, Taylor and Merchant (1940) modified Terzaghi's equation to include a factor, F, which serves as a ratio between the rate of consolidation and rate of creep. Subsequently, Terzaghi (1941) and Taylor (1942) attributed creep settlement to the readjustment of soil particles, caused by a gradual transfer of stress from the highly viscous adsorbed water (film bond) to the soil particles (grain bond). The transfer process is associated with *viscous flow*, accounting for the continued creep settlement with time. Such reasoning was the basis of the Gibson and Lo (1961) rheological model. Other rheological models were subsequently employed to build constitutive equations describing one-dimensional compression during the consolidation phase, and thereafter at constant effective stress. As explained by Imai (1995), these rheological models have not been widely used, as the underlying concepts are difficult to relate to familiar parameters such as C_c and C_α.

The pioneering work of Bjerrum (1967) represented a significant advancement in the understanding of soil viscosity and its influence over the stress-strain response of highly sensitive clay. Bjerrum's (1967) work prompted a resurgence in the development of one-dimensional constitutive models such as that proposed by Garlanger (1972) and Christie and Tonks (1985). The advent of advanced testing methods, in particular the Constant Rate of Deformation test, played a significant role in furthering the understanding of strain rate in laterally constrained compression.

Leroueil *et al.* (1985) estimated that at the time of writing, more than 25 different models had been developed for one-dimensional compression. Since then, many more models have been proposed, although a general consensus still has not been reached as to the most appropriate means of modelling the stress-strain response of soils under one-dimensional loading conditions. Although the majority of these models have been developed for clay, they are in principle equally valid for peat, although they may require certain modifications to account for the non-linearities observed in § 2.2. The aim of this section is not to provide a comprehensive review of all of these models, but to highlight the key advancements which have been made in one-dimensional constitutive modelling, and to describe in some detail a few of the more widely used approaches.

2.4.1 Rheological models

Many of the currently available rheological models have been developed in the UK in the 1960s and early 1970s. Some, such as that proposed by Berry and Poskitt (1972), have been specifically aimed at peat soils, whereas other more general frameworks such as Gibson and Lo (1961) and Barden (1968) are equally valid for clays. In rheology, elastic, plastic and viscous components of strain are generally treated separately, and represented by springs, sliders and dash-pots. The following sections review two such models that have been employed in predicting the consolidation and creep settlement of peat.

2.4.1.1 Gibson and Lo (1961)

Gibson and Lo (1961) developed a rheological model in which the structural viscosity of the soil skeleton was assumed to be linear. The theory can be represented by a top spring connected in series to a Kelvin element and dash-pot (see Figure 2.23a). Upon a stress

increment, the top spring, representing primary consolidation, will compress instantly, whereas the compression of the Kelvin element, representing creep, will be retarded by the presence of the dash-pot. For large values of time, the time-dependent strain, $\varepsilon(t)$, may be expressed as:

$$\varepsilon(t) = \Delta\sigma\left[a + b\left(1 - e^{-\lambda/bt}\right)\right], \quad t > t_a \qquad 2.14$$

where a, b and λ/b are empirical parameters that implicitly govern consolidation, creep and creep rate respectively and t_a is the time after which the applied stress increment becomes fully effective. Edil and Dhowian (1979) showed how these parameters could be conveniently determined from field and oedometer data. Edil (1982) and Edil and Mochtar (1984) used the model to predict the settlement of peat in the laboratory and field. As the model is only really applicable when effective stress is constant ($t > t_a$), the model fails to predict the consolidation phase accurately (Lan, 1992). In addition, Edil and Mochtar (1984) found the creep compression parameters, b and λ/b to be highly non-linear. The same authors also encountered significantly differing rates between the field and laboratory and were forced to present correction graphs in order to use laboratory determined parameters for *in situ* settlement predictions.

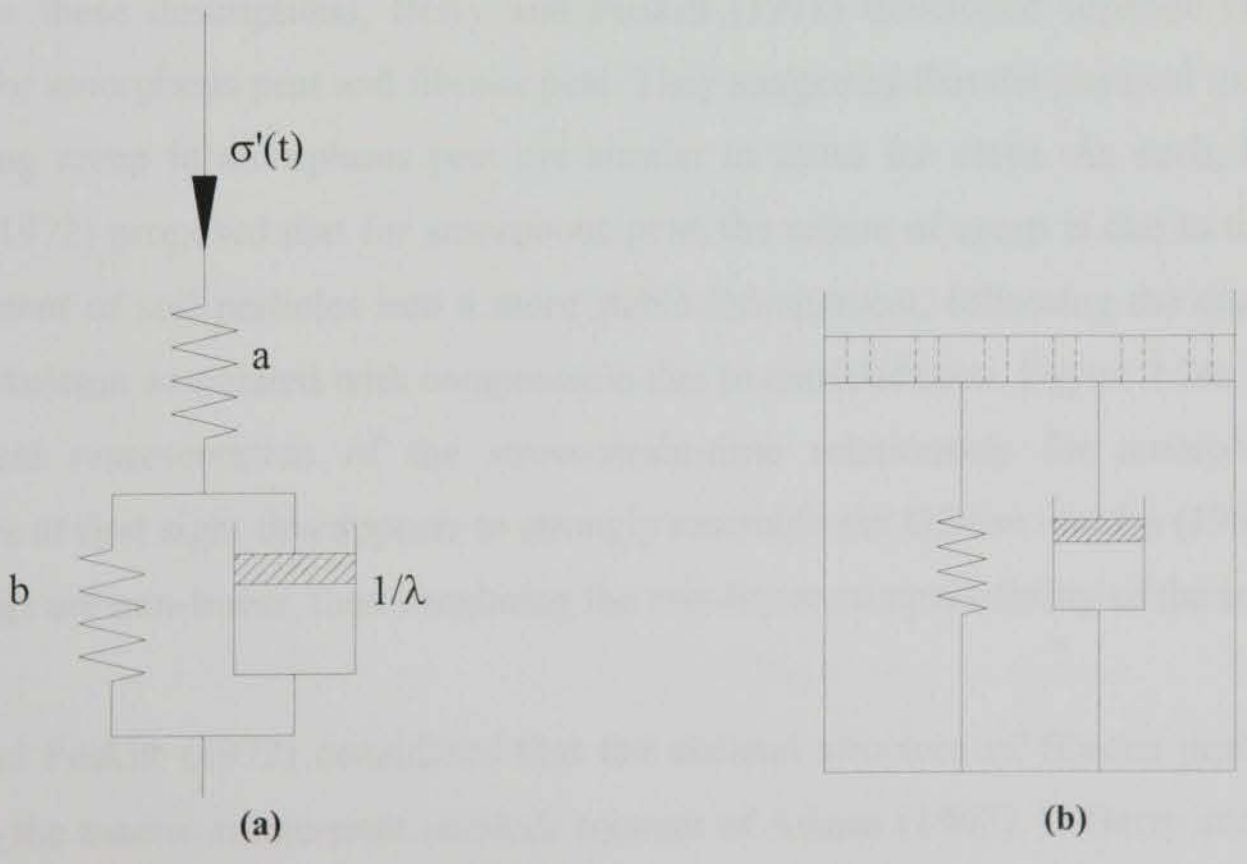

Figure 2.23 Rheological representation of:
(a) Gibson and Lo (1961) model, (b) Barden (1968) model

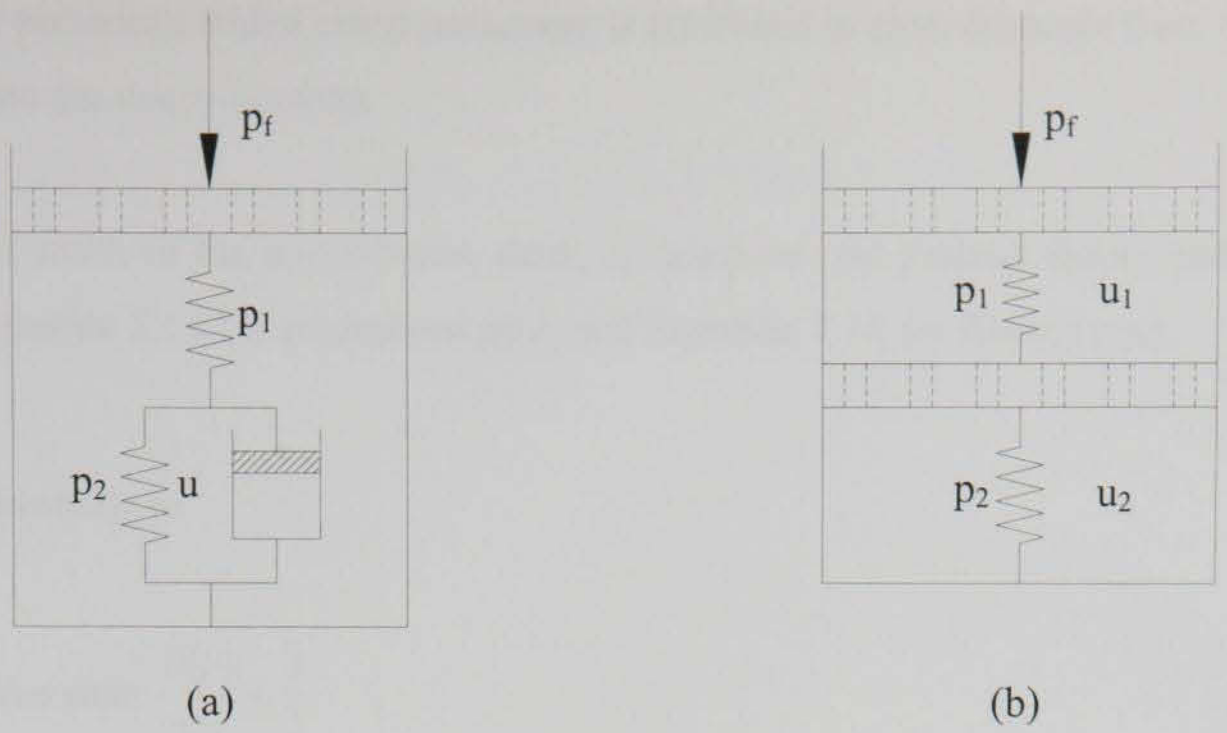

Figure 2.24 Rheological representation of the Berry and Poskitt (1972) theory for: (a) amorphous-granular peat, (b) fibrous peat (after Berry and Poskitt, 1972)

2.4.1.2 Berry and Poskitt (1972)

MacFarlane and Radforth (1965) broadly categorise peat as either amorphous or fibrous. The soil particles in amorphous peat are mainly colloidal in size, and the pore water is absorbed around the grain structure. In contrast, fibrous peat has an essentially open structure, with enclosed secondary structures of mainly non-woody fine fibrous material. The water in fibrous peat tends to exist as *free water* rather than viscous adsorbed water. Based on these descriptions, Berry and Poskitt (1972) developed separate rheological models for amorphous peat and fibrous peat. They suggested that the physical mechanisms controlling creep in amorphous peat are similar to those for clays. As such, Berry and Poskitt (1972) proposed that for amorphous peat, the nature of creep is due to the gradual readjustment of soil particles into a more stable arrangement, following the disruption of the soil skeleton associated with compression due to consolidation. Figure 2.24a shows the rheological representation of the stress-strain-time relationship for amorphous peat. Although, at first sight this appears to strongly resemble the Gibson and Lo (1961) theory, the springs are non-linear, thus simulating the non-linear compressibility of the soil.

Berry and Poskitt (1972) considered that the skeletal structure of fibrous peat could be based on the macro- micro-pore network concept of Adams (1963). In Berry and Poskitt's (1972) rheological model for fibrous peat (see Figure 2.24b), the consolidation process is considered to be due to drainage from the macro-network (i.e. the dissipation of the excess

pore water pressure), whilst creep settlement is attributed to slow drainage from the macro-network into the micro-network.

The rate of strain of the micro-pores, $d\varepsilon/dt$, is based on rate process theory and takes the form of Equation 2.15 for amorphous peat, and Equation 2.16 for fibrous peat.

$$\frac{d\varepsilon}{dt} = \beta(e)\sinh\alpha(e)\sigma \qquad 2.15$$

$$\frac{d\varepsilon}{dt} = A(e)\Delta\sigma\sinh\left[\frac{B(e)}{\Delta\sigma}u_2\right] \qquad 2.16$$

where the terms α, β and A are specified functions of void ratio, σ is stress and u_2 the micro-pore pressure. The models have been verified by Berry and Poskitt (1972) for laboratory tests on fibrous and amorphous peat, and Berry (1983) provides an assessment of the macro- micro-pore theory for preloading design. However, Landva and Pheeney (1980) dispute the micro-pore concept on account of the observed relatively large openings in the intact cellular structure of fibrous peat.

Berre and Iversen (1972) used the Gibson and Lo (1961) model to predict the strain and pore pressure response of a marine postglacial clay from Drammen, Norway. They showed that sensible predictions were only obtained at large values of time, which is consistent with the findings of Lan (1992). The authors also compared experimental results with Barden's (1968) rheological model (see Figure 2.23b). Predictions obtained using Barden's (1968) theory were seen to be an improvement over the Gibson and Lo (1961) theory, although the model failed to accurately predict the pore pressure response. Berre and Iversen (1972) concluded that Barden's (1968) theory could be improved if a top spring was introduced into the rheological model.

Additional rheological models, such as those proposed by Christensen and Wu (1964) and Szymanski (1982) have been proposed for one-dimensional compression. Lechowicz *et al.* (1984) showed that a form of the latter model could be used to accurately predict peat settlement. Lan (1992) suggested that many of the currently available rheological models could not be used for peat, as the commonly made assumption that C_α is constant is not valid for peat.

2.4.2 Elastic visco-plastic models

According to Leroueil *et al.* (1985), almost all the published theories for one-dimensional compression can be represented by the following equations, where R represents a function and the dot signifies the time differential:

$$R(\sigma', e) = 0 \qquad 2.17$$

$$R(\sigma', e, t) = 0 \qquad 2.18$$

$$R(\sigma', e, \dot{\sigma}', e) = 0 \qquad 2.19$$

$$R(\sigma', e, e) = 0 \qquad 2.20$$

Although compression is described in Equations 2.17-2.20 by void ratio, e, the dependency of strain on change in void ratio infers that linear strain, ε^{lin}, or natural strain, ε^{nat}, may be interchanged with e in the above equations. Equation 2.17 represents models in which the stress-strain state is assumed to be both unique and independent of stress history and aging (e.g. such as assumed by Terzaghi's 1923 consolidation theory). Although Equation 2.17 is widely used in practice, earlier work such as that of Buisman (1936), showed that Equation 2.17 is invalid for most soils, as void ratio continues to decrease under constant effective stress. A number of theories have been proposed which compensate for the limitations of Equation 2.17 by considering the time-dependency of soils. Models such as those described by Equation 2.17 are also time-dependent, in that the consolidation process takes place over a finite time scale, although in the present context, time-dependency refers to changes in volume without corresponding changes in effective stress. Bjerrum (1967), Garlanger (1972) and Hansen (1969) have proposed theories employing Equation 2.18, in which void ratio, or strain is a function of effective stress and time. However, these models present difficulties in selecting an appropriate origin for time, particularly when laboratory studies are used as a basis for predicting *in situ* behaviour. A number of workers such as Šuklje (1956), Hawley and Borrin (1973) and Leroueil *et al.* (1985), have overcome this difficulty by proposing models corresponding to Equation 2.19 and Equation 2.20, in which time (Equation 2.18) is replaced with rate of change of void ratio, or strain rate. Equation 2.19 and Equation 2.20 form the basis of current *elastic visco-plastic* theory, although the particular relationship proposed by each model tends to differ. One such difference is in the interpretation of strain rate. Some modellers, such as Leroueil *et al.*

(1985) and Imai and Tang (1992) advocate the use of *total* strain rate, whereas others, such as den Haan (1996) and Yin and Graham (1994, 1996) propose that strain rate should be interpreted as *creep* strain rate. The latter group usually postulate an appropriate relationship between *direct* or *instant* strain rate (sometimes also referred to as *elastic* strain rate), effective stress and effective stress rate (den Haan, 1995). It is in this way that the process of consolidation is modelled. Total strain rate is then taken as the sum of creep strain rate and direct strain rate, where the latter tends to zero as the effective stress rate reduces due to the dissipation of excess pore pressures during consolidation.

It is not proposed in this section to provide a comprehensive review of all of the theories proposed for one-dimensional compression. Rather, an attempt has been made to present an overview of the principles that have been employed in the past, and to link this with reported experimental data where possible. In addition, some of the more widely accepted theories are described in some detail.

2.4.2.1 Bjerrum's instant and delayed compression

Bjerrum's (1967) concepts of *instant* and *delayed* compression have provided the framework upon which the majority of current constitutive one-dimensional compression models are based. In his Rankine Lecture, Bjerrum (1967) used instant compression to describe strains associated with increases in effective stress. Although Bjerrum coined

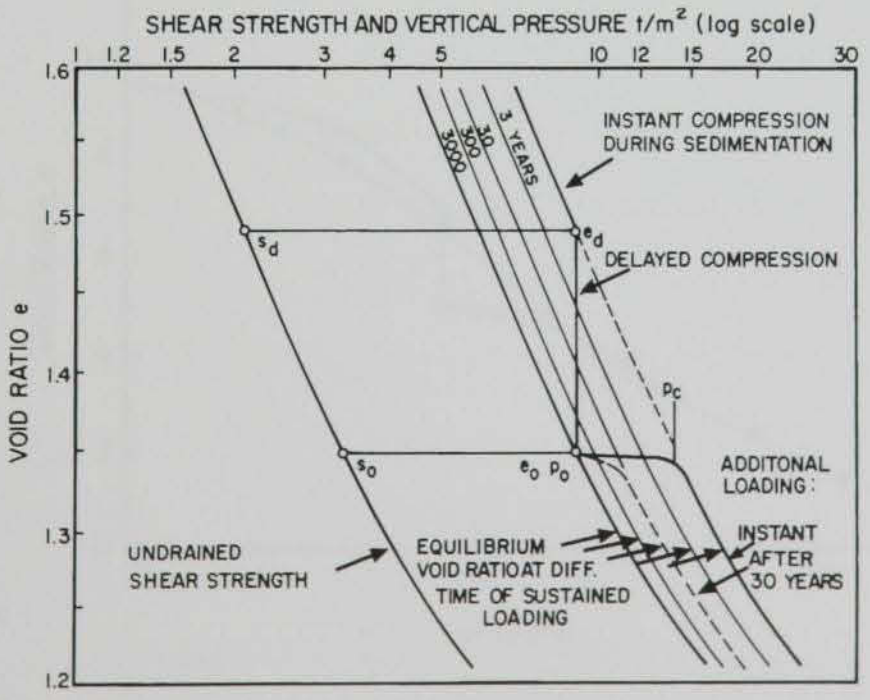

Figure 2.25 Bjerrum's time line conceptual model (after Bjerrum, 1967)

these strains as instant, he recognised that the finite permeability of soil would cause a certain degree of time-dependency. The term, delayed compression, was employed by Bjerrum to explain volume changes at constant effective stress. Bjerrum proposed that this process could be described by a series of parallel time lines in e – log σ' space, where each line represents equal periods of sustained loading. This *time-line* theory is shown in Figure 2.25. Bjerrum used the time-line concept to explain how clays strengthen and develop reserve resistance against compression. The main contribution of Bjerrum (1967) was in explaining how soils sometimes exhibit overconsolidation after aging. Referring to Figure 2.25, it can be seen that if a soil is permitted to creep at a constant effective stress from a void ratio, e_d, to e_o, the state point will move from the instant time line to a time line of, in this case, 3000 years. Upon an increase in stress, the state path moves to the right to join the instant time line, thus creating an increased preconsolidation stress, p_o. Although this has been shown experimentally by a number of workers for clays (Samson *et al.* 1981, Leroueil *et al.* 1985), only a few cases have been reported for peat. The result of one such study (Matsuo, 1998) is considered here in brief.

Two oedometer tests on Momijiyama (Japan) fibrous peat were incrementally loaded using a LIR=1. At a stress level of 78.5 kPa the sample represented by the open symbols in Figure 2.26 was permitted to creep for 445 days, before being reloaded in stress increments of 20-40 kPa. Evidently, the preconsolidation stress increases to approximately 200 kPa, after creeping for over one year at 78.5 kPa. Beyond 200 kPa, the peat exhibits normally

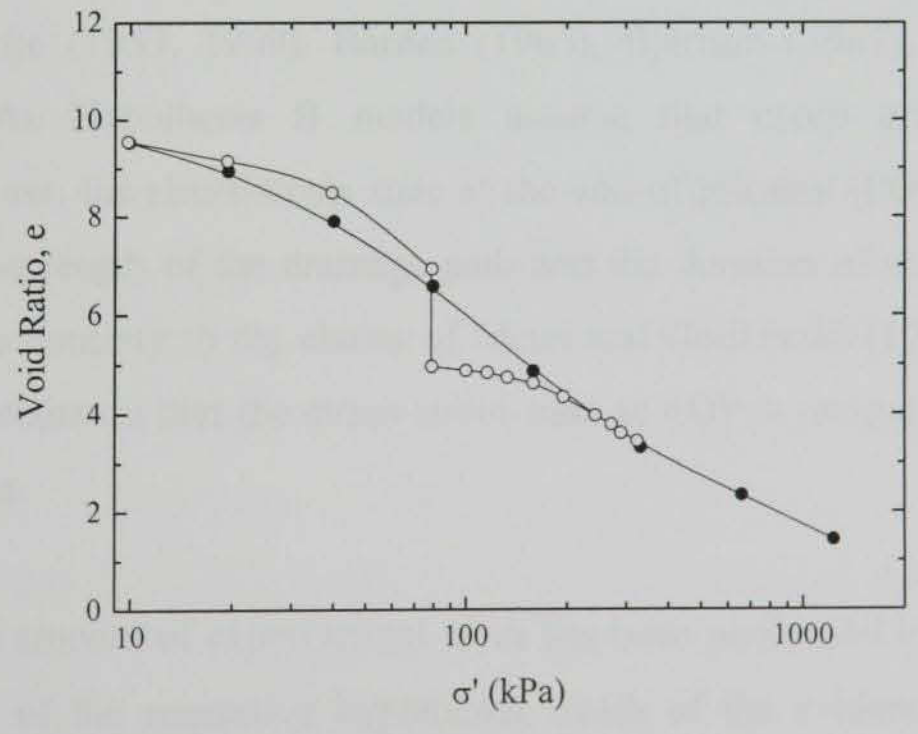

Figure 2.26 Development of a *quasi-preconsolidation* stress after aging (after Matsuo 1998)

consolidated behaviour, joining the measured e – log σ' relationship of the other sample.

Many of Bjerrum's concepts, and in particular the instant time line, are vague and are either difficult to understand (Imai, 1995), or implement (Christie and Tonks, 1985). Despite this, the work of Bjerrum (1967) is recognised as a major contribution towards a thorough understanding of the time dependency of soil compression, and is the basis for the majority of current one-dimensional constitutive models (Imai, 1995).

2.4.2.2 Hypothesis A versus Hypothesis B

Models employed for one-dimensional straining conditions generally treat consolidation and creep compression as either separate or continuous processes. This division has led to two extreme theories, namely Hypothesis A and Hypothesis B (Ladd *et al.*, 1977; Jamiolkowski *et al.*, 1985). Hypothesis A separates strains arising from the dissipation of excess pore pressures from those due to creep, whereas Hypothesis B assumes that creep occurs both at constant effective stress and during consolidation. Models belonging to the Hypothesis A category include proposals by Leonards (1972), Ladd *et al.* (1977), Mesri and Godlewski (1977) and Mesri and Choi (1985). In their simplest form such models generally assume a Terzaghi-style solution for the consolidation process, and employ a creep coefficient such as C_α, to model continuing settlements at constant effective stress. Separation of consolidation and creep is arbitrary, although in most cases the time corresponding to 90 or 95% consolidation is assumed. Hypothesis B models include those suggested by Šuklje (1957, 1969), Barden (1965), Bjerrum (1967), and Leroueil and Kabbaj (1987). As Hypothesis B models assume that creep acts throughout the consolidation process, the stress-strain state at the end of primary (EOP) consolidation is dependent upon the length of the drainage path and the duration of excess pore pressure dissipation. This is contrary to the claims of Mesri and Godlewski (1977) and Mesri and Choi (1985) who maintain that the stress-strain state at EOP is unique irrespective of the drainage conditions.

Although a certain amount of experimental work has been performed in an effort to prove or disprove either of the respective hypotheses, much of the evidence is unconvincing (Leroueil *et al.* 1985). For example, the well-known oedometer tests on Drammen clay

specimens of different heights (Berre and Iversen, 1972) which have been used to validate Hypothesis B have also been used by Leonards (1977) in support of Hypothesis A.

Mesri and Choi (1985) conclude on the basis of oedometer tests on both thin and thick clay layers that the EOP stress-strain relationship is indeed unique, whilst Mesri (1995) suggests that the uniqueness principle be accepted on the basis of the excellent agreement obtained between measured and predicted results for ten case histories of embankments constructed on soft clays.

Based on the results of confined compression tests on Middleton peat samples of different heights, Edil *et al.* (1991) suggested that Hypothesis A may be invalid, and that the laboratory EOP stress-strain should not be used to predict *in situ* behaviour. Recognising that laboratory tests are possibly unsuitable to test the EOP concept (Leroueil *et al.*, 1985), Kabbaj *et al.* (1988) compared the behaviour of four test embankments with the results of laboratory tests. They concluded on the basis of their study, that the EOP concept is not valid as the laboratory EOP stress-strain curve tended to underestimate the *in situ* strains. Leroueil (1996) showed using results obtained from consolidating specimens connected in series, that the stress-strain curve depends on the location relative to the drainage boundary. As the *in situ* drainage path is generally much higher than that of specimens tested in the laboratory, Leroueil (1996) concludes that the laboratory EOP stress-strain path cannot be identical to that *in situ*.

2.4.2.3 Mesri's C_α/C_c approach

The C_α/C_c concept, as described in Mesri and Godlewski (1977), suggests that *"there is a unique relationship between* $C_\alpha = \partial e/\partial \log t$ *and* $C_c = \partial e/\partial \log \sigma'$ *that holds true at all combinations of time, effective stress, and void ratio."* The C_α/C_c ratio can then be used along with the EOP $e - \log \sigma'$ curve to completely define creep behaviour at any value of σ' in compression and recompression (Mesri *et al.* 1997). It should be noted that in this context, the C_α/C_c and EOP concept usually infers that creep does not take place during consolidation, although according to Mesri *et al.* (1990) this is not a fundamental requirement. Mesri *et al.* (1990) show mathematically how a unique EOP stress-strain relationship can still allow for creep deformations during consolidation, although their arguments were challenged and subsequently rejected by Yin and Graham (1990). The

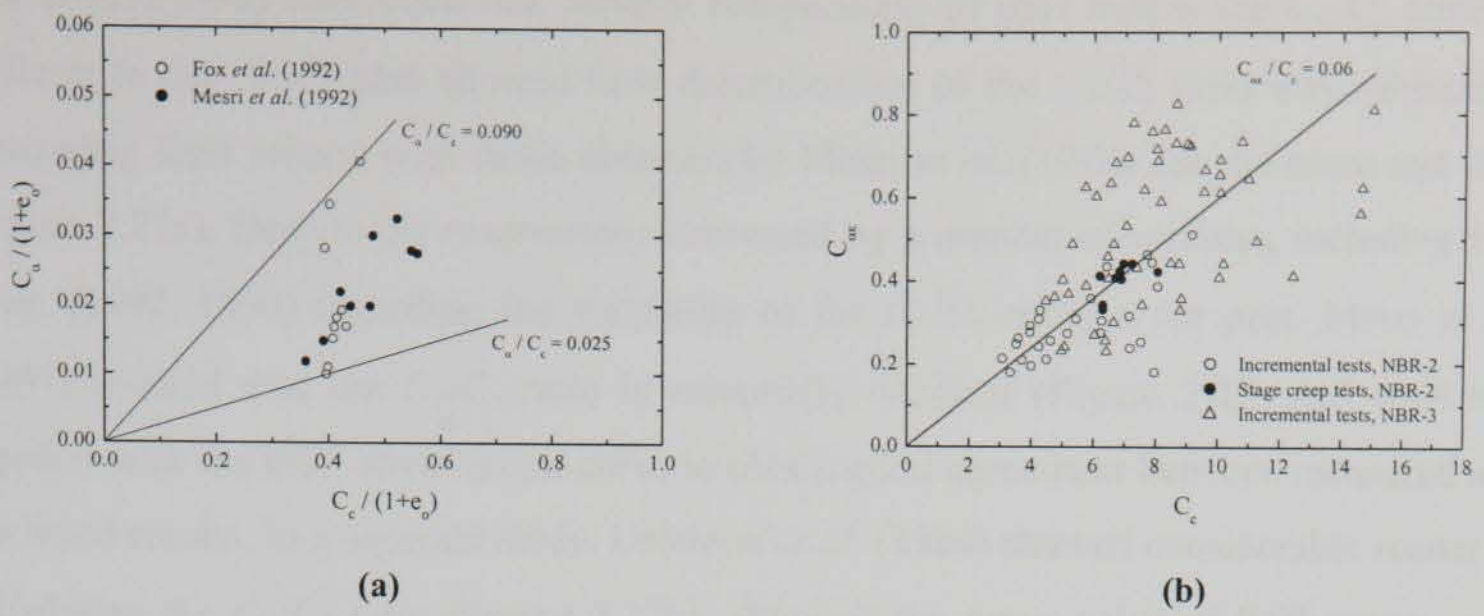

Figure 2.27 Relationship between (a) $C_\alpha/(1+e_o)$ and $C_c/(1+e_o)$ for Middleton fibrous peat (after Fox *et al.* 1992) (b) C_α and C_c for Canadian fibrous peat (after Lefebvre *et al.* 1984)

C_α/C_c and EOP concept, which has been associated with Mesri for many years, is dealt with in numerous publications including Mesri and Godlewski (1977), Mesri and Castro (1987), Mesri (1987) and Mesri *et al.* (1997).

Mesri and Godlewski (1977) propose that values of C_c should be determined from the EOP compression curve and paired with C_α values determined from the first log cycle of secondary compression. However, it is well recognized that the time taken for primary consolidation in compressible materials such as peat and organic soils is difficult to determine using conventional graphical techniques due to the absence of the inflection point, which distinguishes the EOP compression phase (Edil and den Haan, 1994; Fox *et al.*, 1999). EOP can be determined accurately when excess pore pressures are measured, but this is seldom the case in standard oedometer tests. Mesri and Godlewski (1977), stated that although the EOP e – log σ' curve is usually used to define C_c, any e – log σ' curve during secondary compression with corresponding values of C_α, may be used to calculate the C_α/C_c ratios. Mesri *et al.* (1997) and Lefebvre *et al.* (1984) showed that the uniqueness of C_α/C_c values between respective samples are improved when normalized by the initial specific volume, v_o ($v_o = 1+ e_o$).

The correct interpretation of the C_α/C_c concept has been dealt with in various publications over the years by Mesri and his co-workers. In brief, Mesri and his co-workers have found it necessary to re-iterate on many occasions that correct interpretation of the C_α/C_c concept requires the *correct* pairing of C_α and C_c values.

Fox *et al.* (1992) concluded that tertiary compression of peat makes the C_α/C_c concept difficult to use. They also showed how determination of the C_α/C_c ratio was subjective, comparing their results with those obtained by Mesri *et al.* (1994) for the same test data (Figure 2.27a). Despite the reservations expressed by a number of workers, including Fox *et al.* (1992, 1994) regarding the suitability of the C_α/C_c concept for peat, Mesri *et al.* (1997) showed that the C_α/C_c ratio is essentially constant (Figure 2.28) and used this together with the EOP stress-strain curve to obtain good agreement between measured and predicted results. In a separate study, Lefebvre *et al.* (1984) showed considerable scatter in calculating the C_α/C_c ratio (Figure 2.27b), although the mean value of 0.06 agrees well with the 0.052 value suggested by Mesri *et al.* (1997). According to Mesri *et al.* (1997), current reliable data suggest that $C_\alpha/C_c = 0.06 \pm 0.01$ for peat.

Yin and Graham (1990) suggest that Mesri and Choi's (1984) theory is not fully general, and cannot be used in an analysis of constant rate of deformation tests or relaxation tests. They also imply that as the method suggested by Mesri and Choi (1984) for calculating the apparent preconsolidation arising from aging is empirical, the model is not well equipped to handle strain rate effects arising from different loading conditions.

Mesri (1986) explained how the unique EOP and associated C_α/C_c concept could be employed to describe the postsurcharge creep settlement case study reported by Samson (1985); see § 2.3. According to Mesri *et al.* (1997), the merit of this method is that it can

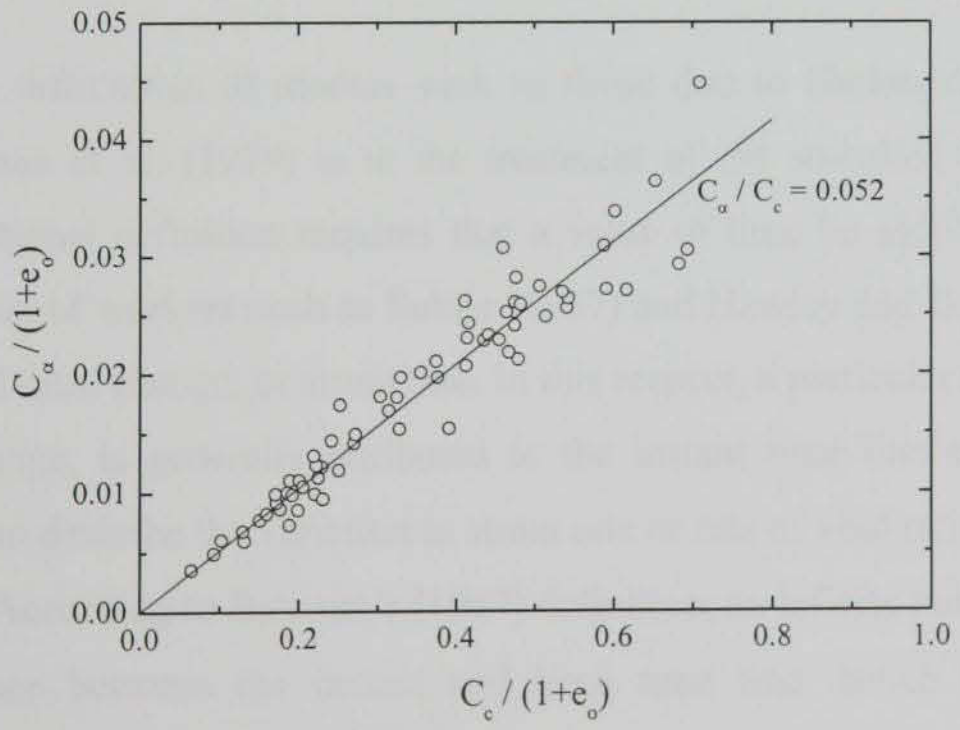

Figure 2.28 Relationship between $C_\alpha/(1+e_o)$ and $C_c/(1+e_o)$ for Middleton fibrous peat (after Mesri *et al.* 1997)

describe the commonly encountered steepening of creep curves (plotted as e –log t), thus doing away with the need for the tertiary compression concept described and reported in detail by Edil and Dhowian (1979), Dhowian and Edil (1980), Fox *et al.* (1992).

2.4.2.4 Elastic Visco-Plastic theory

Current elastic visco-plastic theory is generally based on Bjerrum's (1967) time-line concept. Garlanger (1972) was the first to provide a mathematical framework for Bjerrum's work, proposing that the e-σ'-t relationship could be formulated as:

$$-\frac{\partial e}{\partial t} = \alpha \frac{e}{\sigma'}\left(\frac{\partial \sigma'}{\partial t}\right) + c\frac{e}{t_1}\left(\frac{e}{e_o}\right)^{1/c}\left(\frac{\sigma'}{\sigma'_c}\right)^{b/c} \qquad 2.21$$

where α assumed different values for $\sigma' < \sigma'_c$ and $\sigma' > \sigma'_c$ and b, c and t_1, are constants. One drawback of Garlanger's model is that a specific value of time must be attributed to t_1, from which point creep is assumed to act. It follows that Garlanger's model belongs to the Hypothesis A category, as if creep was permitted to occur throughout the consolidation process, t_1=0, making Equation 2.21 invalid. Despite this, Garlanger (1972) showed the model to be remarkably accurate in predicting both pore pressure and strain responses for laboratory tests on Drammen clay (Norway) as reported by Berre and Iversen (1972). Reasonable agreement was also obtained between measured and predicted settlements for several buildings in Drammen.

One of the main difficulties of models such as those due to Garlanger (1972), Hansen (1969) and Magnan *et al.* (1979) is in the treatment of the so-called instant time line. Although conventional definition requires that a value of time be ascribed to the instant time line, a number of workers such as Šuklje (1957) and Hawley and Borin (1973) prefer to use rate of void ratio change, or strain rate. In this respect, a particular strain rate, or rate of void ratio change, is generally attributed to the instant time line and a constitutive equation defined to describe the variation in strain rate or rate of void ratio change between successive lines. According to Bjerrum's (1967) definition, an infinite number of time lines exist in e-σ' space between the instant and limit time line, hence the mathematical treatment of these time lines is continuous rather than discrete. In Hawley and Borin's (1973) model the instant time line is defined as having $de/dt = \infty$, and the limit time line with $de/dt = 0$.

Šuklje's (1957) used the term *isotache* to describe lines of constant rate of void ratio change. Subsequently, several models, such as that previously mentioned due to Hawley and Borin (1973), and others such as Edil *et al.* (1994), den Haan and Edil (1994), den Haan (1996), Yin and Graham (1994, 1996), Leroueil *et al.* (1985), and Kim and Leroueil (2001) propose models which employ the isotache principle or variations thereof. One thing that these models have in common is the assumption that a unique relationship exists between void ratio (or strain), effective stress and rate of change of void ratio (or rate of strain). This principle has been verified experimentally by several studies, including the notable work of Graham *et al.* (1983) and Leroueil *et al.* (1985). Figure 2.29 shows the results of a deformation rate controlled compression test on Belfast clay reported by Graham *et al.* (1983). This test involved stepped changes in the deformation rate and periods of stress relaxation. Figure 2.29 testifies to the isotache principle as intermittent changes in the deformation rate correspond to a unique e-σ' path. Similar results were reported by Leroueil *et al.* (1985) for Batiscan clay (Canada). An important implication of the isotache principle is that the apparent preconsolidation stress, σ'_c, is dependent on strain rate. Experimental evidence of this has been provided for clays by a number of workers including Samson *et al.* (1981) (see Figure 2.30) and Leroueil *et al.* (1985).

Fewer studies have been performed on peat in this regard, with the work of Edil *et al.* (1994), den Haan and Edil (1994), den Haan (1996, 1997) being notable exceptions. Comparisons of different tests: Constant Rate of Deformation (CRD), Single Load

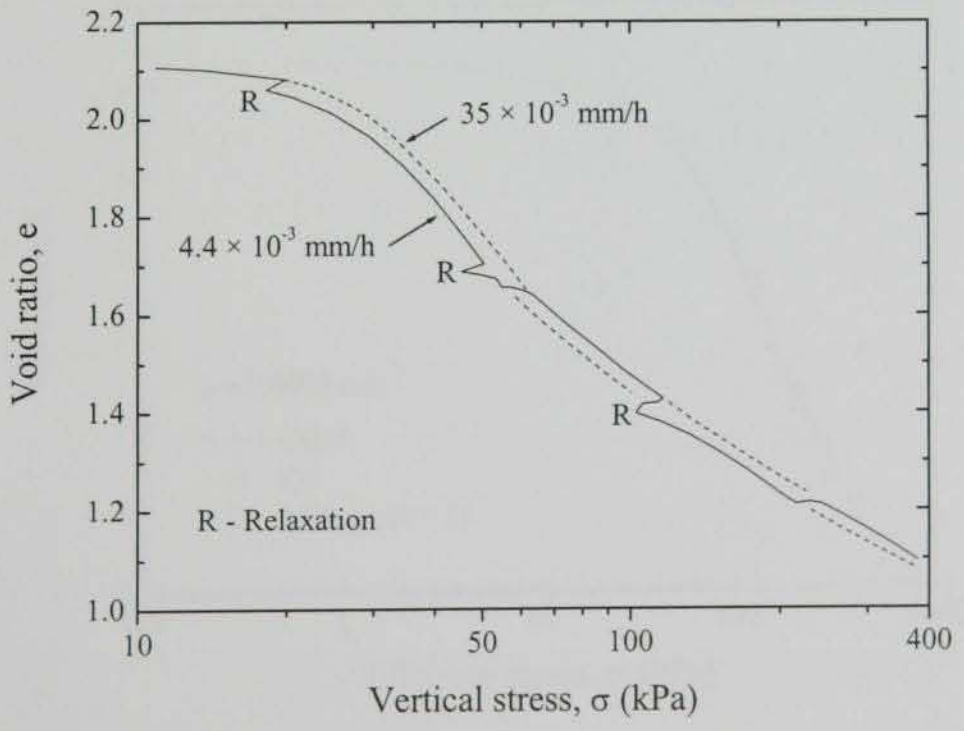

Figure 2.29 Step-changed deformation rates in controlled deformation rate test on Belfast clay (after Graham *et al.* 1983)

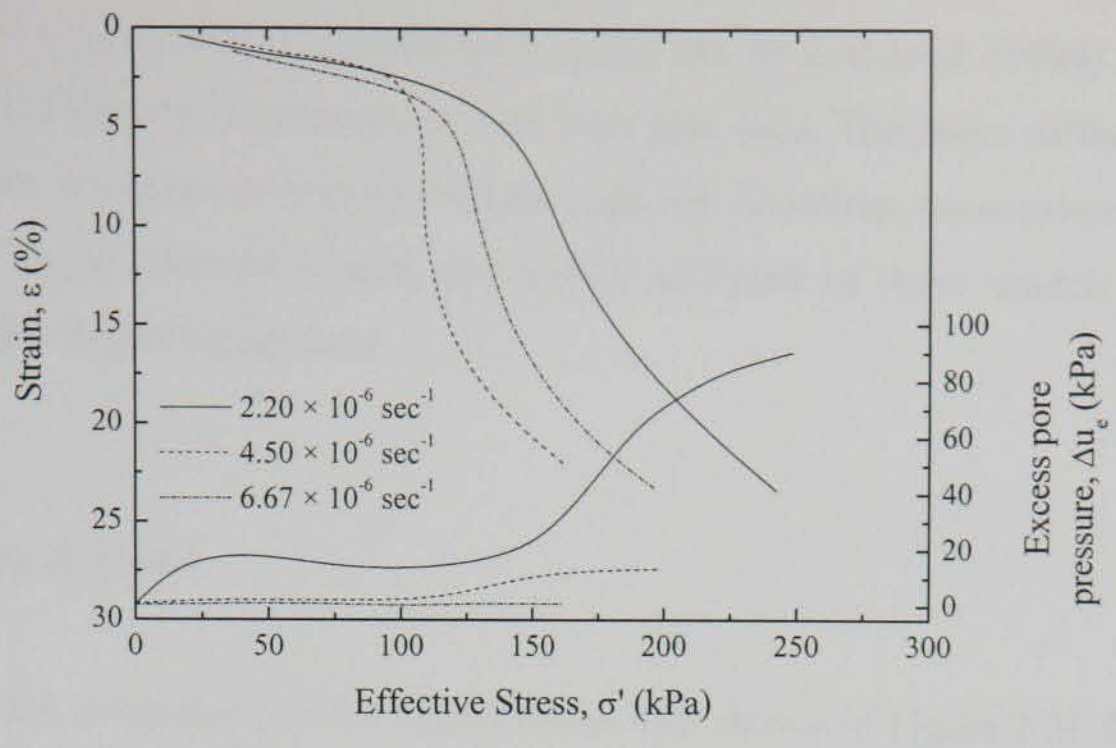

Figure 2.30 Constant rate of deformation tests on St. Césaire (after Samson *et al.* 1981)

Constant Stress (CS) and Multi Stage Load (MSL), on Middleton fibrous peat reported by Edil *et al.* (1994) are reproduced here in Figure 2.31. The test data, which correspond to a void ratio rate change of 0.0005 min^{-1}, show an essentially unique relationship between void ratio, effective stress and rate of change of void ratio.

On the basis of experimental evidence such as that shown in Figure 2.29 and Figure 2.31, several theories have been proposed to account for the rate-dependency of soils in one-

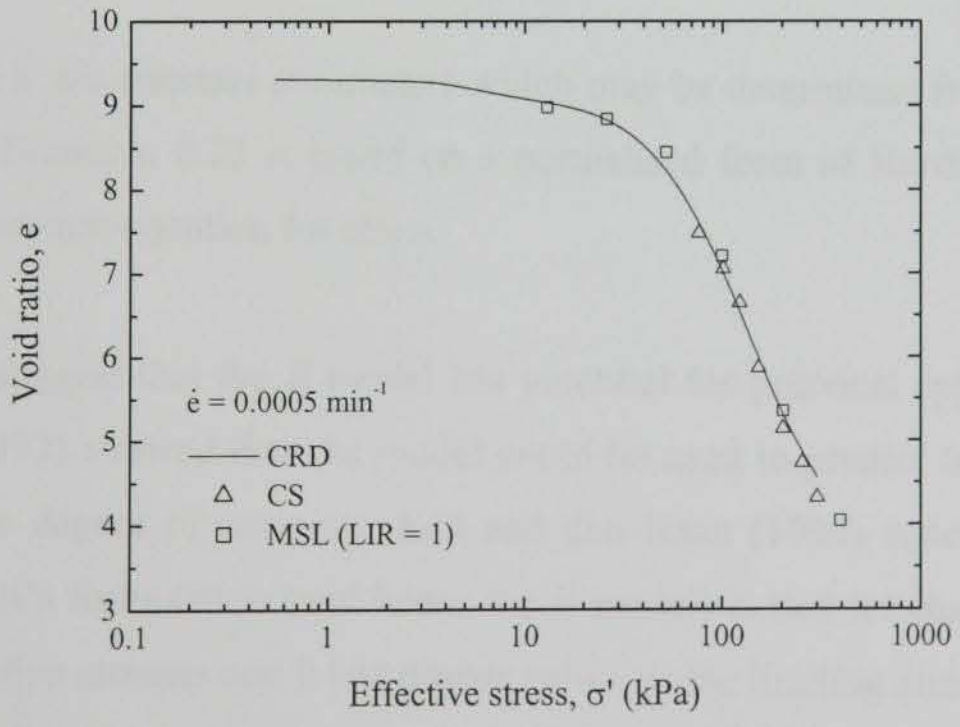

Figure 2.31 Comparison of $\sigma' - e - \dot{e}$ relationship for CRD, CS and MSL tests on Middleton fibrous peat (after Edil *et al.* 1994)

dimensional straining conditions. Although the majority of these models have been developed for clays, a few exceptions such as that due to Edil *et al.* (1994) and den Haan and Edil (1994) have been proposed for use with peat soils. The major difference with the latter is in their provision for coping with the high non-linearities encountered in peat soils. Some of the more commonly used and widely accepted of these models will now be examined in the following sections.

2.4.2.5 The B Model

Prompted by the uniqueness of the experimental data shown in Figure 2.31 for Middleton peat, Edil *et al.* (1994) proposed that the one-dimensional compression of peat could be modelled by a unique relationship between effective stress, void ratio and rate of change of void ratio. The authors stipulated that this relationship held true only in the virgin stress range, and suggested that currently available experimental evidence for peat was insufficient to categorically rule out the importance of the rate of effective stress change.

Edil *et al.* (1994) assumed a semi-logarithmic relationship between rate of change of void ratio $(\dot{e})$ and effective stress, which may be formulated as:

$$\ln(\dot{e}) = A + B\ln\left(\frac{\sigma'}{D}\right) - B\ln\left(\frac{e_o}{e} - \frac{1}{E}\right) \qquad 2.22$$

where A, B, D and E are constant parameters which may be determined from compression tests (Lan, 1992). Equation 2.22 is based on a normalised form of Hardin's (1989) one-dimensional compression equation for clays.

Edil *et al.* (1994) suggest that the B model has potential for practical applications in the laboratory. Lan (1992) showed that the model could be used to predict *in situ* behaviour within a reasonable degree of accuracy. Edil and den Haan (1994) stated that the main advantage of Hardin's formulation (and hence the B model) is that it behaves well over a large range of effective stresses and it has proper values at the limiting stresses of zero and infinity. However, den Haan (1994) showed Hardin's formulation to be unsuccessful in linearising stress-strain data for peats, and consequently concluded that the B model had limited scope for peat.

2.4.2.6 *The C_σ Model*

Combining concepts presented in Edil *et al.* (1994) and Fox and Edil (1994), Edil and den Haan (1994) propose a more analytically rigorous model which they have coined the C_σ model. This model accounts for straining due to changes in stress, temperature and time. Edil *et al.* (1994) propose a unique linear relationship between log $\dot{e}$ and σ', and define a *stress coefficient of creep*, C_σ:

$$C_\sigma = \frac{d\ln(\dot{e})}{d\sigma'} \qquad 2.23$$

A thermal coefficient of creep, C_T is defined by Fox and Edil (1994) as:

$$C_T = \frac{\ln \dot{e}_2 - \ln \dot{e}_1}{T_2 - T_1} \qquad 2.24$$

Although this parameter was considered essentially constant for Middleton peat (Fox and Edil, 1994) it is included in the formulation in light of the lack of data on other (peat) soils.

Combining these concepts, Fox (1992) and Edil & den Haan (1994) proposed the following relationship for the one-dimensional compression of peat:

$$\dot{e} = -a_v\dot{\sigma}' - C_f \exp(C_T T)\sinh(C_\sigma \sigma') \qquad 2.25$$

where a_v is the coefficient of compressibility, and C_f is the *fabric coefficient of peat*, which is a non-linear function of void ratio, and is partially dependent on fibre orientation (Edil and den Haan, 1994). According to Fox and Edil (1994), C_f is difficult to characterise, as it is sensitive to variations in the *peat fabric*. Den Haan (1994) suggests that the uncertainty associated with C_f restricts the usefulness of Equation 2.25.

Equation 2.22 and Equation 2.25 may be combined with Darcy flow and the continuity equation according to finite strain consolidation theory (Gibson *et al.* 1967) to predict settlements during consolidation and at constant effective stress. One notable difference between the *B* model and C_σ model is that the latter obtains total strain rate or total void ratio rate as the sum of creep and consolidation rates, whereas the *B* model combines both rates in a single expression. This may possibly account for the poor predictions obtained

from the *B* model during consolidation (Lan, 1992; Edil *et al.*, 1994). However, Edil and den Haan (1994) suggest that this is not a critical weakness, as the contribution of *creep settlement* in Equation 2.22 and Equation 2.25 is the dominant factor.

2.4.2.7 EVP Model

The *EVP* model, as proposed by Yin and Graham (1989, 1994, 1996) possesses many of the features characteristic of current elastic visco-plastic models. The *EVP* model is essentially an extension of the time line concept (Bjerrum, 1967). However the *EVP* model employs the isotache principle described previously, and a more rigorous treatment of Bjerrum's (1967) instant time line is provided.

The *EVP* model assumes that in the normally consolidated region, the creep strain rate for a given stress and strain state is unique and that, at a given creep strain rate, there is a linear relationship between strain and the logarithm of effective stress, and a linear relationship between strain and the logarithm of creep strain rate. The stress-strain-strain rate relationship assumed by the *EVP* model is summarised in Figure 2.32, and particular characteristics of the model are now described briefly.

An Instant Time Line (Figure 2.32) is defined in stress-strain space along which strains are elastic and recoverable. Graham and Yin (2001) show how the instant time line differs from the conventional normal consolidation line (NCL). The NCL is the line that governs

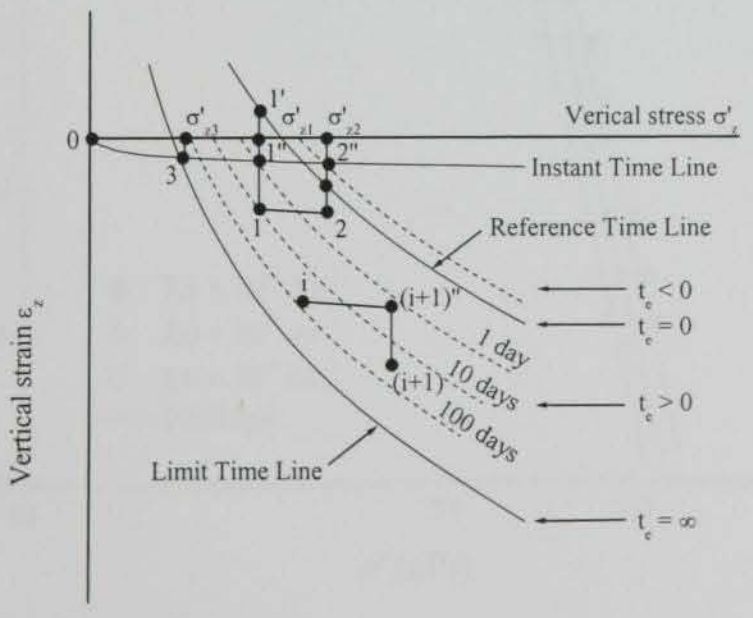

Figure 2.32 Schematic diagram of Elastic Visco-Plastic (EVP) model (after Yin and Graham, 1994)

the magnitude of strain changes associated with increases in effective stress. However, as can be seen from Figure 2.33, increases in strain associated with corresponding increases in effective stress are strain rate dependent. Therefore the NCL is not a true *elastic line*. Yin and Graham (1994) and Graham and Yin (2001) reserve the definition of the instant time line for elasticity, and use this idea to justify Equation 2.26:

$$\dot{\varepsilon} = \dot{\varepsilon}^{e} + \dot{\varepsilon}^{vp} \qquad 2.26$$

In Equation 2.26, the superscript, *e*, denotes elastic and *vp* denotes visco-plastic. According to Graham and Yin (2001), the separation of total strain rate into elastic strain rate and visco-plastic strain rate is not arbitrary, but is based on the assumption that strains arising from stress increases will contain a certain amount of viscous, creep strains. The trends exhibited in Figure 2.33 justify this assumption.

The choice of how best to define instant or elastic strains is generally left to the discretion of the analyst as such strains can never actually be measured directly (den Haan, 1996). The *EVP* model formulates instant strain rate as:

$$\dot{\varepsilon}^{e} = \frac{\kappa}{v_o}\frac{1}{\sigma'}\frac{d\sigma'}{dt} \qquad 2.27$$

where κ/v_o is a material parameter which describes the elastic stiffness of the soil.

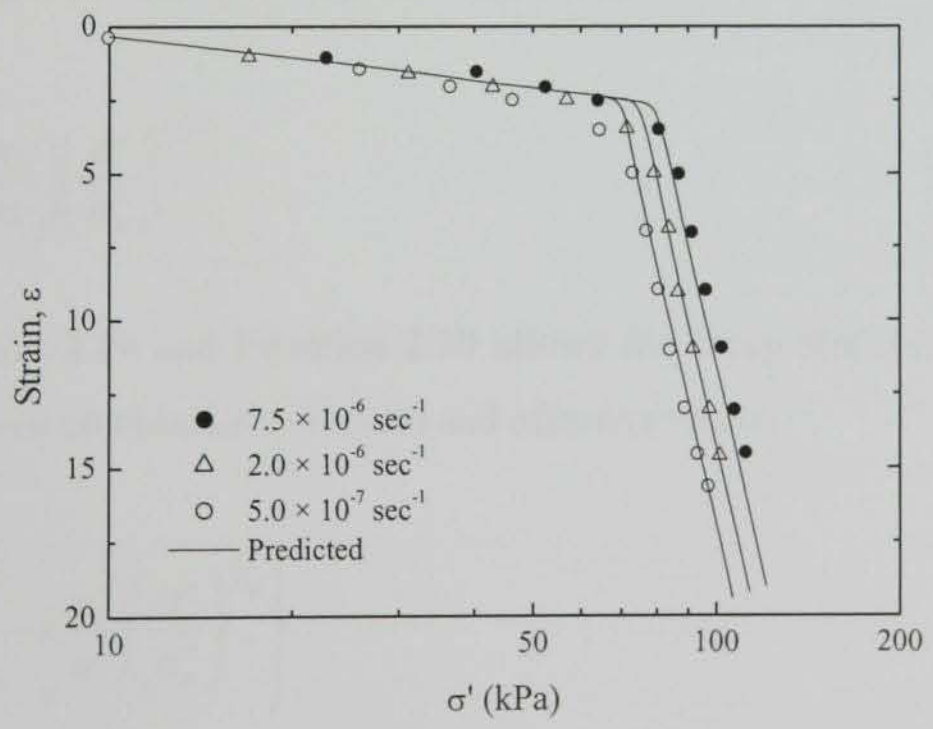

Figure 2.33 Modelling rate-dependency of stress-strain relationship for Bäckebol clay using the EVP model (after Yin and Graham, 1989)

The *EVP* model chooses to scale creep strain rates by introducing a term referred to as equivalent time, t_e. Time lines, which were defined by Bjerrum (1967) as lines equal to periods of sustained loading, are reinterpreted by the *EVP* model as lines with equal values of equivalent time, t_e, and constant creep strain rates. They are parallel in stress-strain space and the creep strain rate of any particular line is controlled by the creep coefficient ψ/v_o. The relationship between strain, effective stress and equivalent time for the *EVP* model is given by:

$$\varepsilon = \frac{\lambda}{v_o}\ln\left(\frac{\sigma'}{\sigma'_o}\right) + \frac{\psi}{v_o}\ln\left(\frac{t_o + t_e}{t_o}\right) \qquad 2.28$$

where σ'_o is the effective stress at zero strain on the *EVP* model's Reference Time Line (RTL, defined with $t_e = 0$), λ/v_o is the slope of lines of constant creep strain rate, ψ/v_o is the coefficient of creep compression, v_o is the initial specific volume and t_o is a constant used to define the creep strain rate on the RTL.

Creep strain rate may be determined by differentiating the second term on the right hand side of Equation 2.28:

$$\dot{\varepsilon}^{vp} = \frac{\psi}{v_o}\frac{1}{t_o + t_e} \qquad 2.29$$

Rewriting Equation 2.28 in terms of equivalent time, t_e leads to:

$$t_e = -t_o + t_o \exp\left(\varepsilon\frac{v_o}{\psi}\right)\left(\frac{\sigma'}{\sigma'_o}\right)^{-\lambda/\psi} \qquad 2.30$$

Combining Equation 2.29 and Equation 2.30 allows the creep strain rate to be uniquely defined for any given combination of strain and effective stress:

$$\frac{d\varepsilon^{vp}}{dt} = \frac{\psi}{v_o}\frac{1}{t_o}\left\{\exp\left(-\varepsilon\frac{v_o}{\psi}\right)\left(\frac{\sigma'}{\sigma'_o}\right)^{\lambda/\psi}\right\} \qquad 2.31$$

Combining Equations 2.26, 2.27 and 2.29 yields a general equation which may be solved for any one-dimensional loading condition:

$$\frac{d\varepsilon^{vp}}{dt} = \frac{\kappa}{v_o}\frac{1}{\sigma'_o}\left(\frac{d\sigma'}{dt}\right) + \frac{\psi}{v_o}\frac{1}{t_o}\left\{\exp\left(-\varepsilon\frac{v_o}{\psi}\right)\left(\frac{\sigma'}{\sigma'_o}\right)^{\lambda/\psi}\right\} \qquad 2.32$$

The rate of change of effective stress, $d\sigma'/dt$, may be incorporated into a chosen theory of consolidation. Yin and Graham (1996) employ the standard Terzaghi consolidation theory, whereas others such as Nash and Ryde (2001) adopt the finite strain theory of Gibson *et al.* (1967). Equation 2.32 can be readily solved for one-dimensional conditions using finite difference techniques.

The limit time line defined by the *EVP* model (see Figure 2.32) represents the eventual termination of creep strains. However, the *EVP* model described here adopts a semi-logarithmic function to scale creep strains, which implies that straining will continue indefinitely. This assumption is invalid as the laws of conservation of mass demand that volume cannot be destroyed, and oedometer data presented by Berre and Iversen (1972) and Dhowian and Edil (1980) show creep strains to eventually terminate. Yin (1999) proposed an alternative fitting function, which incorporates a limiting value of strain. However, the long term *in situ* creep settlements reported by Buisman (1936) and Weber (1969) indicate that incorporation of such a function is unnecessary for most practical applications.

Figure 2.33 shows the successful application of the EVP model to constant rate of deformation tests on Bäckebol clay. The model is seen to cope well with the varying rates of deformation, which within the context of the *EVP* model as described here, may be interpreted as rates of strain. Yin and Graham (1996) showed how the model could be used to predict the strain and pore pressure response of the oedometer tests on Drammen clay reported by Berre and Iversen (1972). The authors showed the *EVP* model to provide better predictions than both the Gibson and Lo (1961) model and Barden's (1968) model. Zhu and Yin (1999) incorporated the one-dimensional *EVP* model into a finite element application, and subsequently used their model to predict the development of pore pressure in the foundation of the Berthierville test embankment in Canada. Nash and Ryde (1999, 2001) incorporated the *EVP* theory into the one-dimensional consolidation theory for vertical and radial flow, and showed their BRISCON model to be successful in modelling the effects of surcharge. Elsewhere, Nash and Ryde (2000) discussed the implications of modifying the isotaches in the *EVP* model so that they were described by (i) natural strain, and, (ii) the power law proposed by den Haan (1992) (see Equation 2.6).

2.5 VARIABILITY OF PEAT IN COMPRESSION

Another topic which has not been considered in the previous sections, but which is certainly worthy of discussion, is the variability and inhomogeneous nature of peat deposits. As a general rule, peat deposits have significant spatial variability to the degree that it is difficult to obtain representative samples for testing unless several samples are taken (Magnan, 1994). Edil and den Haan (1994) suggest that this is one of the main reasons why laboratory results provide only a crude estimation of *in situ* behaviour. Landva and La Rochelle (1983) exemplified this by considering the construction of a road embankment over an apparently homogeneous Sphagnum peat deposit. Although the construction methods were the same throughout the length of the road, the total settlement varied between 0.3 and 3.0 m. The authors concluded that, in this case, predictions of *in situ* settlements based on the results of laboratory tests would be futile. Landva and La Rochelle (1983) suggest that empirical relationships based on inexpensive classification tests may be a more feasible option in some cases. Perrin (1973) showed that the recorded strains from 21 oedometer tests on a black peat from Borgoin, France under a stress of 57 kPa ranged from 5 to 40%. Similar experiences were reported by Hanrahan (1954), who showed considerable differences in the measured 24 hour compression curves of laboratory specimens, sampled from the same general location. Although the variability can often be attributed to changes in properties such as organic content, porosity and water content, Fox (1992) reported that in many cases, intrinsic differences in the rate of creep compression could not be accounted for.

To date, engineers remain undecided about how best to cope with these problems. In some respects, the trend has been to move away from sophisticated theories such as those described in § 2.4.2, relying more on experience and empirical relationships derived from classification data. An alternative approach is to use test fills in conjunction with observational methods such as that described by Asaoka (1978). Based on the predicted settlements from such methods, direct adjustments can be made to the preloading design in the early stages of construction. However, the success of such methods in peat is as yet unconfirmed. Cartier *et al.* (1989) reported a reasonable prediction of the consolidation settlement of a test embankment on peat using Asaoka's (1978) method, whereas Edil *et al.* (1991) applied the same method to several case studies involving both clay and peat, and questioned its applicability to peat settlement.

Regardless of the predictive method employed for peat settlement, the natural variability of peat deposits is a serious issue, and one that must be considered in any serious analysis (den Haan, 1997).

2.6 SUMMARY AND CONCLUSIONS

This chapter contains an up-to-date and comprehensive review of current knowledge of peat behaviour under one-dimensional loading conditions. Emphasis has been placed on describing the high non-linearity of peat by considering mainly fibrous, compressible peat. Other soils such as fen peat, which is typically classified as amorphous, may not exhibit the characteristics described here to the same degree.

Some of the main conclusions which can be drawn from this chapter are summarised as follows:

1. Peat is an extremely compressible material and problematic soil, with an initial voids ratio often in excess of 20. Relative compression of the order 70-90% is commonplace, even under moderate stress levels.

2. A major contribution of the measured settlement is due to creep, which in the laboratory and *in situ* case studies considered here, continues for long periods of time.

3. Creep settlement at constant effective stress can often be described by a linear relationship between settlement and logarithm of time.

4. Tertiary compression, which is where the slope of the creep curve (e – log t) steepens, can, in some cases, occur, but its effect tends to be less pronounced at higher stress levels.

5. Consolidation in peat is generally extremely rapid, particularly at high void ratios. The presence of gas in peat influences the measured pore pressure response in laboratory tests; particularly if a back pressure is not used. No evidence of similar phenomena in field cases has been provided. The consolidation duration increases

as void ratios decrease, reflecting the strong dependence of permeability on void ratio.

6. The H^2 scaling law may not be valid for peat.

7. The apparent preconsolidation stress, σ'_c, is difficult to determine in undisturbed peat and is strongly rate dependent. Consequently, predictions based on the conventional use of C_c and σ'_c may be questionable.

8. The e – log σ' relationship for peat is highly non-linear; a number of alternative formulations have been proposed to account for this. Natural strain appears to be the most promising in this regard.

9. Evidence suggesting that laboratory tests can be used to predict *in situ* behaviour is conflicting.

10. Preloading and surcharging as a construction method appears to have merit in reducing long term settlements, although the time span over which these settlements are controlled is limited.

11. Rheological models have been proposed to account for the limitations of Terzaghi's (1923) theory and variations thereof. The main merit of these models lies in their contribution to the overall understanding of consolidation and creep settlement.

12. Currently available models employed for one-dimensional compression generally assume void ratio or strain to be a function of effective stress and time or effective stress and rate of change of void ratio. In some cases, the rate of change of effective stress is also considered.

13. Proposed theories generally fall within two categories; Hypothesis A and Hypothesis B. Hypothesis A models separate strains due to consolidation from strains due to creep, whereas Hypothesis B models assume that creep acts at all values of time and effective stress. Although experimental evidence suggests that Hypothesis A is incorrect, its application is relatively simple and the results are often convincing. Hypothesis A is widely used in practice.

14. The constancy of C_α/C_c, proposed by Mesri and Godlewski (1977) has been used, mainly by Mesri and his co-workers to obtain successful predictions of the creep settlement of peat. Several other attempts to derive *constant* C_α/C_c ratios for peat have been unsuccessful.

15. Many models have been suggested on the basis of Bjerrum's (1967) time-line concept. More recently the time-line theory has been replaced with the isotache principle, which redefines time-lines as lines with constant rates of strain or void ratio change. These models overcome previous difficulties associated with attributing a value of time to the instant time line.

16. One such isotache model, namely the *EVP* model (Yin and Graham, 1989, 1994, 1996) has been described in detail. Several other similar models have been proposed and shown to be successful in their application (Christie and Tonks, 1985; Leroueil *et al.* 1985; Szavits-Nossan, 1988; Imai, 1989; Imai and Tang, 1992; Edil and den Haan, 1994, den Haan 1996, Niemunis and Krieg, 1996; Stolle *et al.*, 1997, 1999; Kim and Leroueil, 2001). There are two main approaches within these isotache models. The first, advocated by Leroueil *et al.* (1985), Imai and Tang (1992), Niemunis and Krieg (1996) and Kim and Leroueil (2001) assumes a unique relationship between effective stress, strain and *total* strain rate. The second includes models proposed by Szavits-Nossan (1988), den Haan and Edil (1994), den Haan (1996) and Yin and Graham (1989, 1994, 1996), and assumes a unique relationship between effective stress, strain and *creep* strain rate. The latter group of models generally presume a relationship between strain, effective stress and rate of effective stress, and incorporate this into the existing effective stress, strain and *creep* strain rate formulation. Leroueil *et al.* (1985) omit rate of effective stress from their model as they claim that it has little bearing on the relationship between effective stress, strain and strain rate. However, other workers such as Fox (1992) suggest that the rate of effective stress is an important quantity and should be formulated.

Chapter 3

Description of soils

Chapter 3

Description of soils

3.1 INTRODUCTION

One of the main aims of this research project as outlined in Chapter 1, was to examine the compressibility characteristics of peat, and to determine whether or not constitutive models which have been successfully employed to model the behaviour of clays, could also be applied to peat. To this end, the author decided to concentrate on a peat which showed very little resemblance (in terms of geotechnical properties and behaviour) to mineral soils.

Peats encountered in the raised bogs of the Irish midlands tend to possess geotechnical properties that are not typical of many non-organic soils. Amongst the most obvious of these properties include an unusually high natural water content and associated *in situ* void ratio, low strength and poor bearing capacity. It was envisaged that a comprehensive study of such an *extreme* peat would provide better insight and understanding into the nature of other, more typical peats and viscous clays.

The research described here is mainly focused on a fibrous peat from Clara, Co. Offaly. The involvement of TCD in the joint Irish-Dutch study of Clara bog influenced the author's decision to obtain peat samples from this location. However, in an attempt to put the findings of the experimental work on Clara peat into context, a number of other soils have also been considered. To a certain extent, selection was based on sample availability, although considerable effort was made to ensure that the chosen soils provided representative information from a wide range of organic soils. A fibrous peat from Ballydermot bog, Co. Offaly was selected, as this soil is a variation on the highly compressible, virgin peat which is typical of that encountered in the Irish midlands. Much

of the classification data and testing of Ballydermot peat is due to Hebib (2001), and his work is acknowledged here. Peat from Cork has also been considered, albeit to a much lesser extent. As part of the TCD research into pile behaviour in soft clay, McCabe (2002) performed several oedometer tests and classification tests on an organic clay from Belfast. Results from the classification data reported by McCabe (2002) are included here.

3.2 SITE DESCRIPTIONS

The location of the four sites from which the soil samples were retrieved is shown in Figure 3.1. Both Clara bog and Ballydermot bog are located in Co. Offaly in the Irish midlands. The peat encountered in the upper layers of both bogs is derived from *Sphagnum* mosses and is typically fibrous, although that in Clara bog is younger and less humified than that in Ballydermot bog. According to Kelly (1993), the depth of the peat layer in Clara varies from less than 1 m at the bog boundary to over 10 m in the central regions of Clara Bog West and over 9 m in the central regions of Clara Bog East (see § 5.2.2, Figure 5.4). The upper layer of young, poorly humified Sphagnum peat is underlain by older, well humfied Sphagnum peat, which, in turn, is underlain by a layer of fen peat. At the sampling location in Clara bog, the stratigraphy beneath the peat layer is stiff lacustrine clay, poorly graded post-glacial till and carboniferous limestone bedrock.

Extensive peat extraction has taken place in Ballydermot bog for over 50 years (Hebib, 2001). The associated drainage has caused a marked reduction in the depth of the peat

Figure 3.1 Map of Ireland showing the sampling sites relative to Dublin

layer, from 7 to 4 m. The stratigraphy of Ballydermot bog has been reported by Hebib (2001) to be old Sphagnum peat underlain by reed swamp peat, shell marl and finally boulder clay.

The site conditions in Cork comprises 3-4.5 m of very recently placed fill, followed by a 3-4 m layer of amorphous peat, 1.5 m of silty peat and then a layer of sandy gravel. Pockets of grit, together with some relatively large wood chips were encountered within the upper peat layer.

Samples of Belfast organic clay were retrieved from a site close to the Belfast City Airport. Permission for testing by TCD was obtained from the Department of the Environment for Northern Ireland. The stratigraphy of the site is 1.4 m of topsoil underlain by 7.5m of soft very lightly overconsolidated marine clay underlain by loose-medium dense sand.

3.3 SAMPLING METHODS

The effects of disturbance caused by sampling and specimen preparation in peat has been well documented by a number of workers including Landva *et al.* (1983) and Hillis and Brawner (1961). The latter state that it is improbable that even apparently undisturbed peat samples are representative of *in situ* material by the time that the specimen reaches the testing apparatus. They attribute this to:

1. Presence of gas, which causes the peat sample to lose shape and volume upon stress relief
2. Reduction in moisture content on extrusion and preparation
3. Structure disturbance caused by the walls of the sampling tube as it is pushed into the soil

Although a number of new *undisturbed samplers* (e.g. SGI sampler, University of New Brunswick sampler) have been developed for use with soft soils such as peat, common practise generally relies on either piston samplers or standard U100 sampling tubes. In an attempt to obtain peat samples at depth from Clara bog, the author used U100 sampling tubes. Two main problems were encountered:

1. Inability of the thin-walled sampling tube to cut through the fibres in the peat
2. Loss of sampled peat as the tube is extracted

The first of these problems was the most common and difficult to remedy. As the peat entered the base of the sampling tube, a plug formed which appeared to compress the underlying peat as the tube was advanced. Although rotating the tube as it was advanced helped to alleviate this problem, a comparison of the length of the retrieved sample and length of the sampling tube indicated that significant compression had occurred. The second problem may be attributed to the high water content and low cohesive strength of the peat. Often about half the length of the peat sample would fall from the base of the tube as it was extracted. Excavating around the buried tube and blocking the base by hand solved this problem, although this entailed much additional work in difficult conditions.

A number of workers including Hobbs (1986), Lefebvre *et al.* (1984) and Karlsrud *et al.* (1996) have advocated the use of block sampling. As the dimensions of typical block samples are much larger than the diameter of standard sampling tubes, the relative disturbance is reduced considerably. Hand-carved block samples were retrieved from Clara bog from depths of between 500 and 750 mm. The sampling procedure involved the following steps:

1. Hand excavation of a pit
2. Removal of the upper layer of peat from the exposed vertical face
3. Carving block samples from the exposed vertical face using a hand saw
4. Trimming the samples to fit the sealed plastic containers

These steps are illustrated in Figure 3.2a – Figure 3.2c.

Hebib (2001) described a novel method that was employed to obtain $1m^3$ block samples of Ballydermot peat. Samples were taken from a vertical face, 2.5 m high, using a custom-made block sampler (see Figure 3.2d), which was attached to the lifting arm of a tracked excavator. The sampler was fabricated from a steel box which had three faces removed. Each of the remaining exposed faces had sharpened edges so as to minimise disturbance during sampling. Retrieved samples were wrapped in polythene so as to prevent loss of moisture, and placed in wooden boxes for transportation to the laboratory.

As samples of Cork peat and Belfast organic clay were retrieved from depth, fixed head thin wall piston sampling methods were used.

(a)

(b)

(c)

(d)

Figure 3.2 Sampling methods in peat:
(a) Clara, hand excavated pit; (b) Clara, removal of superfluous peat;
(c) Clara, trimmed block sample; (d) Ballydermot, recovering 1 m^3 peat block sample

3.4 CLASSIFICATION OF PEAT AND ORGANIC SOILS

The most popular classification system used by engineers to categorise peats is the von Post system (1922), which was originally devised for horticultural, agricultural, and forestry requirements in Sweden. Although Hobbs (1986) provided an English translation and extension to the von Post classification system, few of the classifying groups are actually used in practice. Geotechnical engineers general identify peat soils according to the degree of humification, using von Post humification values ranging from H_1 for intact young peat, to H_{10} for completely decomposed peat. Variations and extensions of the von Post system, such as that proposed by Hobbs (1986) now include categories for organic

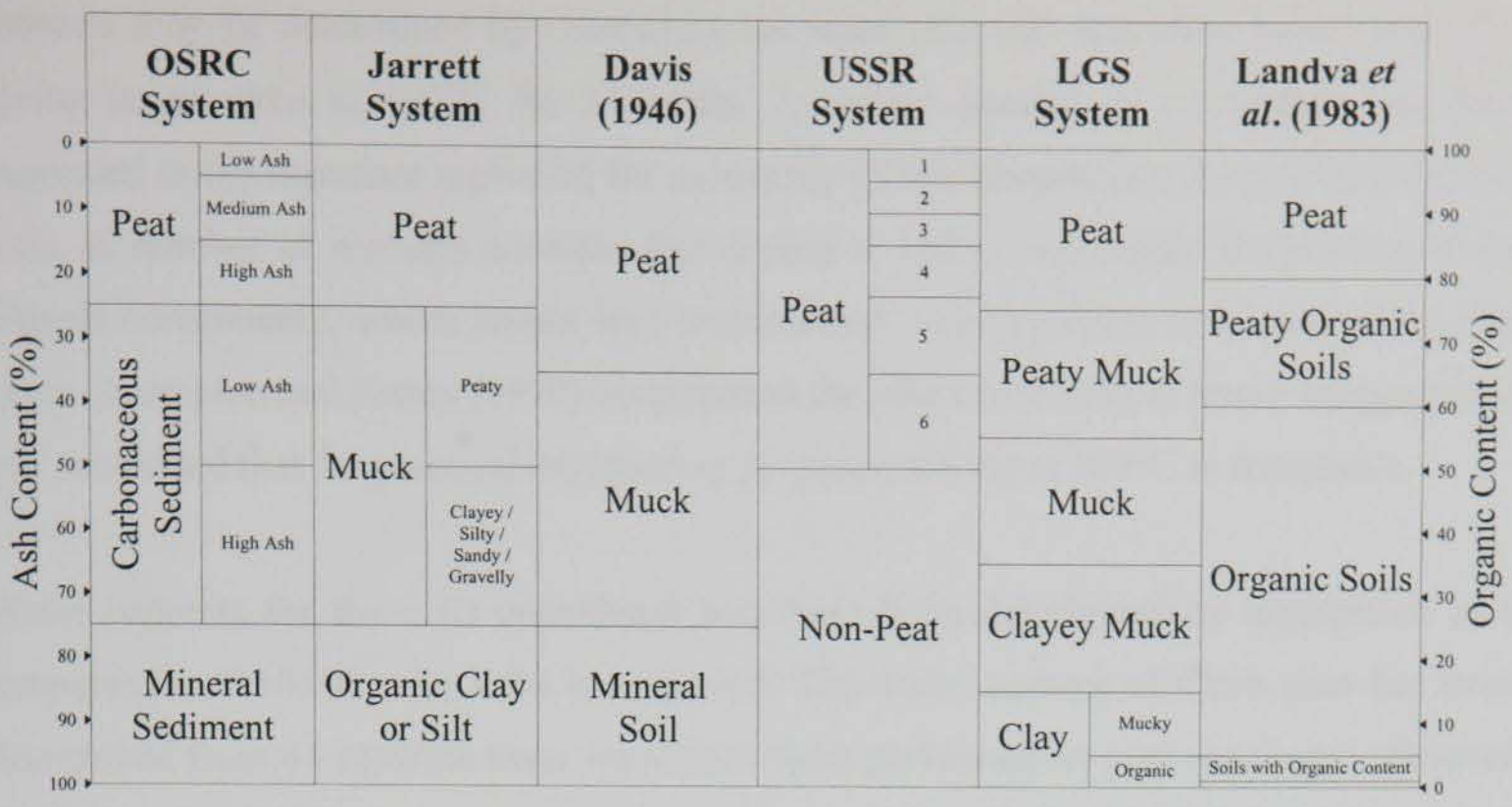

Figure 3.3 Comparison of classification systems used for the categorisation of peat and organic soil: Organic Sediments Research Centre (OSRC), Jarrett System, Davis system, USSR system, Louisiana Geological Survey (LGS) System and Landva *et al.* (1983) system (after Andrejko *et al.*, 1983)

content, as determined using ashing techniques. Andrejko *et al.* (1983) and Landva *et al.* (1983) list 12 different systems that use organic content as a means of classifying peat and organic soils. A comparison of 6 different systems summarised in Figure 3.3 shows that peats are defined as the soils with the highest organic content, organic clays as the soils with the lowest organic content, with a range of so-called *mucks* and variations thereof in between. It is evident from Figure 3.3 that the threshold organic contents that separate the various soils types vary depending on the classification system adopted. For instance, a soil with an organic content of 50% would be termed a peat according to the Russian classification, muck according to LGS classification and an organic soil according to the classification system proposed by Landva *et al.* (1983). It is evident, therefore, that defining a soil by organic content alone is insufficient; other factors such as natural water content, structure, degree of humification, nature of organic content and specific gravity also need to be considered. The following sections provide details regarding the classification tests performed on the four soil types considered here.

3.4.1 Water content

The water content of soils, particularly peat, is an important geotechnical property as this is directly linked to the initial void ratio, and hence compressibility of the soil. Water

contents may be determined by comparing the mass of a soil specimen before and after drying in an oven at 105°C for 24 hours. A certain amount of reservation has been expressed in the literature regarding the suitability of this temperature for peat and organic soils. A number of workers consider that drying at 105°C will result in charring of the organic constituents, which would lead to measured water contents in excess of the true value. Skempton and Petley (1970) investigated the effect of drying at lower temperatures, and concluded that for practical engineering purposes, drying at 105°C is acceptable.

Water contents for the soils considered here have been determined by application of a temperature of 105°C over a 24 hour period. The water content of Clara peat has been determined from 64 separate tests; these tests were performed on peat specimens retrieved from a number of block samples, all of which were located within 1 m of the ground level. The results of the water content tests are summarised in Figure 3.4, which shows that although a high degree of variability exists in the measured values, the majority of the results fall between 1300% and 1500%. The average water content from the 64 tests is 1407%. Although the variation in measured values exceeds 750 percentage points, the degree of variability is much less severe for peat specimens located within the same block sample (approximately 200%).

A limited number of water content tests were performed on Ballydermot peat by the author; the results were relatively consistent, ranging between 810% and 935% with a

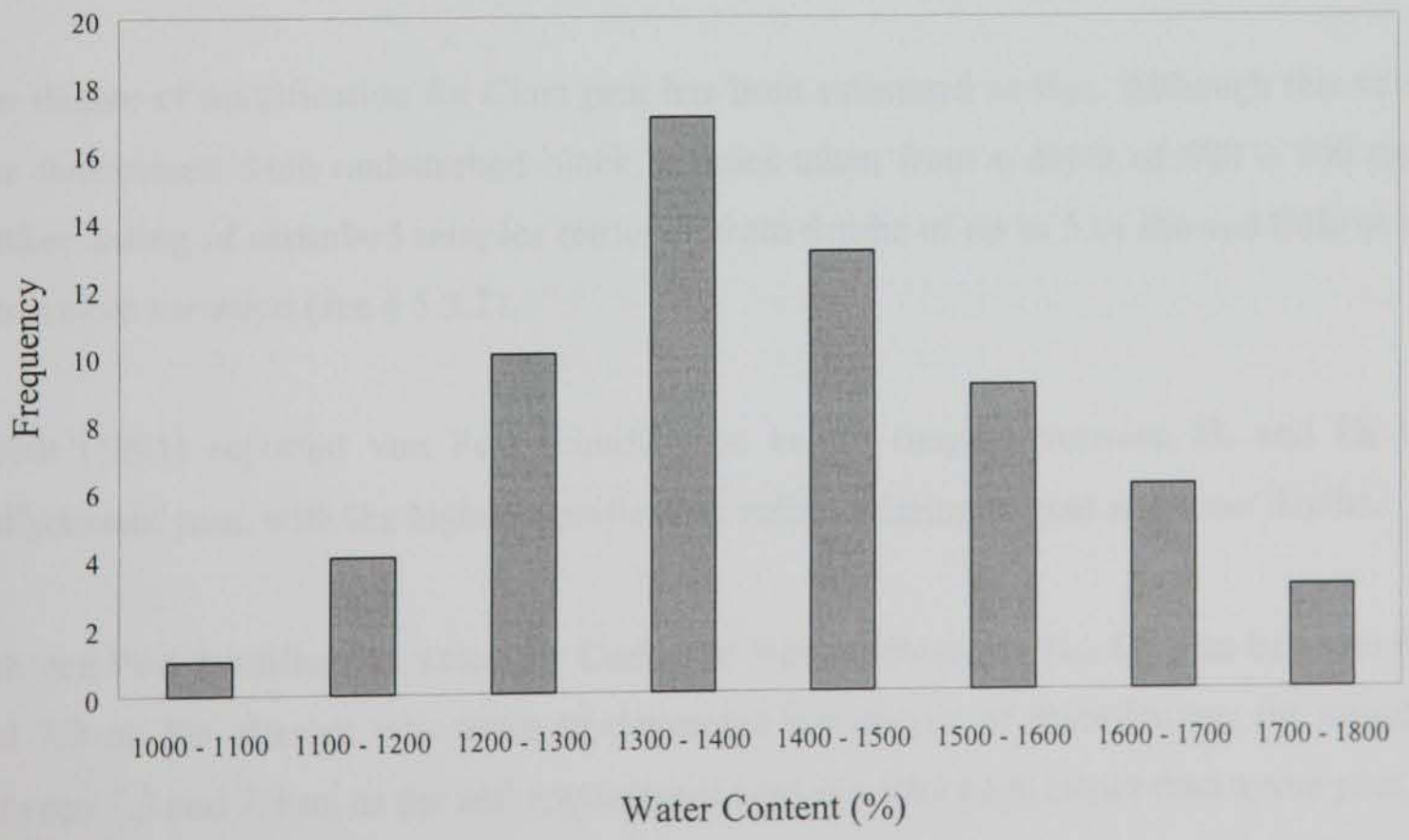

Figure 3.4 Results of water content tests on Clara peat

mean value of 865%. These values are in good agreement with Hebib (2001) who reported values in the range 750% – 950%.

The results of the water contents performed on Cork peat vary significantly with depth. Between 6.2 m and 7.5 m, the average water content is 447%, compared with 208% for depths between 7.5 and 7.9 m.

McCabe (2002) performed numerous water content tests on Belfast organic clay; the measured values varied from approximately 15% at a depth of 0.2 m to a maximum value of 70% at a depth of 5 m. The average water content for the range of depths considered here (3.0 – 7.0 m) is approximately 60%.

3.4.2 Degree of Humification

The *squeeze test* is the standard method for determining the degree of humification according to the von Post scale. This simple test requires that a small sample of peat be squeezed in the hand. A visual inspection of the colour and form of the expelled fluid (or peat), together with the nature and structure of the remaining residue is then used to categorise the degree of humification on a 10-point scale. Although this method is quite subjective, it serves as a simple, quick and useful means of describing the state of decomposition of the peat.

The degree of humification for Clara peat has been estimated as $H_{2\text{-}3}$. Although this value was determined from undisturbed block samples taken from a depth of 500 – 700 mm, further testing of disturbed samples retrieved from depths of up to 5 m showed little or no discernible variation (see § 5.3.2).

Hebib (2001) reported von Post humification values ranging between H_6 and H_9 for Ballydermot peat, with the higher humification values relating to peat at greater depths.

The von Post humification value for Cork peat was estimated as H_{10} for peat between 6.2 and 7.0 m. No attempt was made to determine the degree of humification for samples between 7.3 and 7.9 m, as the soil encountered here is a silty peat, rather than a *true* peat.

3.4.3 Organic Content

Organic content is an important quantity as it provides a good indication of how likely the soil conforms to the problematic behaviour of pure peat. A number of wet ashing techniques involving chemical analysis are available for the determination of organic content, although such methods are generally only successful in soils with relatively small amounts of organic matter (Hobbs, 1986). A more common and useful method is to burn a small soil specimen in a furnace after drying at 105°C for 24 hours (BS1377). Comparison of the measured mass before and after burning yields the ignition loss or ash content. Much debate surrounds the choice of ignition temperature and duration of burning, although correction factors are available for temperatures in excess of 450°C (Hobbs, 1986). Good experience has been obtained in TCD with the recommendation of Arman (1971), who proposed an ignition temperature of 450°C, and a burning duration of 5 hours.

The organic content has been defined by Hobbs (1986) as *"the pure, ash-free, vegetable matter and any residual organic compounds from the process of decomposition"*. This definition implies that the organic content may be calculated simply by subtracting the ignition loss from 1.0, or 100 if the ignition loss is expressed as a percentage rather than a ratio. Although it is recognised that mineral compounds present in the soil may lose mass during burning, the above definition suffices for most engineering purposes.

Organic contents have been determined for the soils considered here using the procedure previously described. A total of 37 separate loss-on-ignition tests were performed on Clara peat sample trimmings. In an effort to homogenise the peat, the dried specimens were ground using a mortar and pestle and passed through a 1.18 mm grading sieve. This procedure was repeated until no soil was retained on the sieve. The results of the loss-on-ignition tests showed little scatter, with organic contents falling within the narrow range of 97.26% – 98.97%. The average organic content is 98.1%.

Hebib (2001) reported organic contents for Ballydermot peat ranging from 98% for peat near the original ground level, to 94% for peat at a depth of 2.5m. A limited number of loss-on-ignition tests performed by the author on Ballydermot peat gave practically constant results, with an average organic content of 98.6%.

The results of loss-on-ignition tests performed on Cork peat taken from an average depth of 6.6m gave an average organic content of 79.5%, compared with 32.2% for the silty peat at an average depth of 7.6m.

McCabe (2002) reported an average organic content of 11.0% for Belfast organic clay.

3.4.4 Specific Gravity, G_s

According to den Haan (1997) and Hobbs (1986), the specific gravity of organic soils is strongly dependent upon the amount and type of organic constituents. This property is therefore much more variable in peat and organic soils than it is in mineral soils. The author combined all available G_s data to produce Figure 3.5, which shows the correlation between loss-on-ignition and specific gravity.

Specific gravity may be determined in the laboratory by comparing the mass of a volume of kerosene, with the mass of the same volume of an oven-dried peat/kerosene mixture. However, the measured values from specific gravity tests on Clara peat varied by up to 0.4, which is much higher that the allowable tolerance of 0.05 recommended by Hobbs (1986). The data in Figure 3.5 show that similar scatter exists for other soils with almost 100% organic matter. The variance may be attributed to the type of the organic matter predominant in the soil, though this is unlikely, as a high degree of variability still exists within each soil group. Landva *et al.* (1983) encountered similar scatter in their relationship between ash content and specific gravity. They suggest that the wide range of scatter is due to:

1. Incomplete saturation of the organic matter in the specific gravity test (i.e. presence of gas in the kerosene/peat mixture)
2. Inaccurate determination of the ash content

The data in Figure 3.5 are seen to be quite well fitted by the following equation, which was first proposed by Skempton and Petley (1970):

$$\frac{1}{G_s} = \frac{1-C(1-N)}{G_{s,organic}} + \frac{C(1-N)}{G_{s,mineral}} \qquad 3.1$$

where:

G_s = Specific gravity

$G_{s,\,organic}$ = Specific gravity of organic material

$G_{s,\,mineral}$ = Specific gravity of mineral material

N = Loss-on-ignition expressed as a ratio

C = Correction factor

The correction factor, C, compensates for the loss of mineral matter for furnace temperatures exceeding 450°C. Skempton and Petley (1970) suggest C = 1.04 for a temperature of 550°C, whereas Arman (1971) recommends a temperature of 450°C and a correction factor of 1.0. Equation 3.1 is plotted in Figure 3.5 for these two correction factors and $G_{s,\,organic}$ = 1.4 and $G_{s,\,mineral}$ = 2.7. It is evident from Figure 3.5 that C may be taken as unity for peat and for soils with organic contents greater than 30-40%. The degree of correlation is obviously dependent upon the separate specific gravities of the organic and mineral matter, although the respective values of 1.4 and 2.7 are seen to provide a reasonable fit. These limiting values of 1.4 and 2.7 were first proposed by Skempton and Petley (1970), and later advocated and adopted by a number of workers including Hobbs (1986), Farrell (1997) and Nichol and Farmer (1998).

Determination of specific gravity for the peat soils considered here is based upon Equation

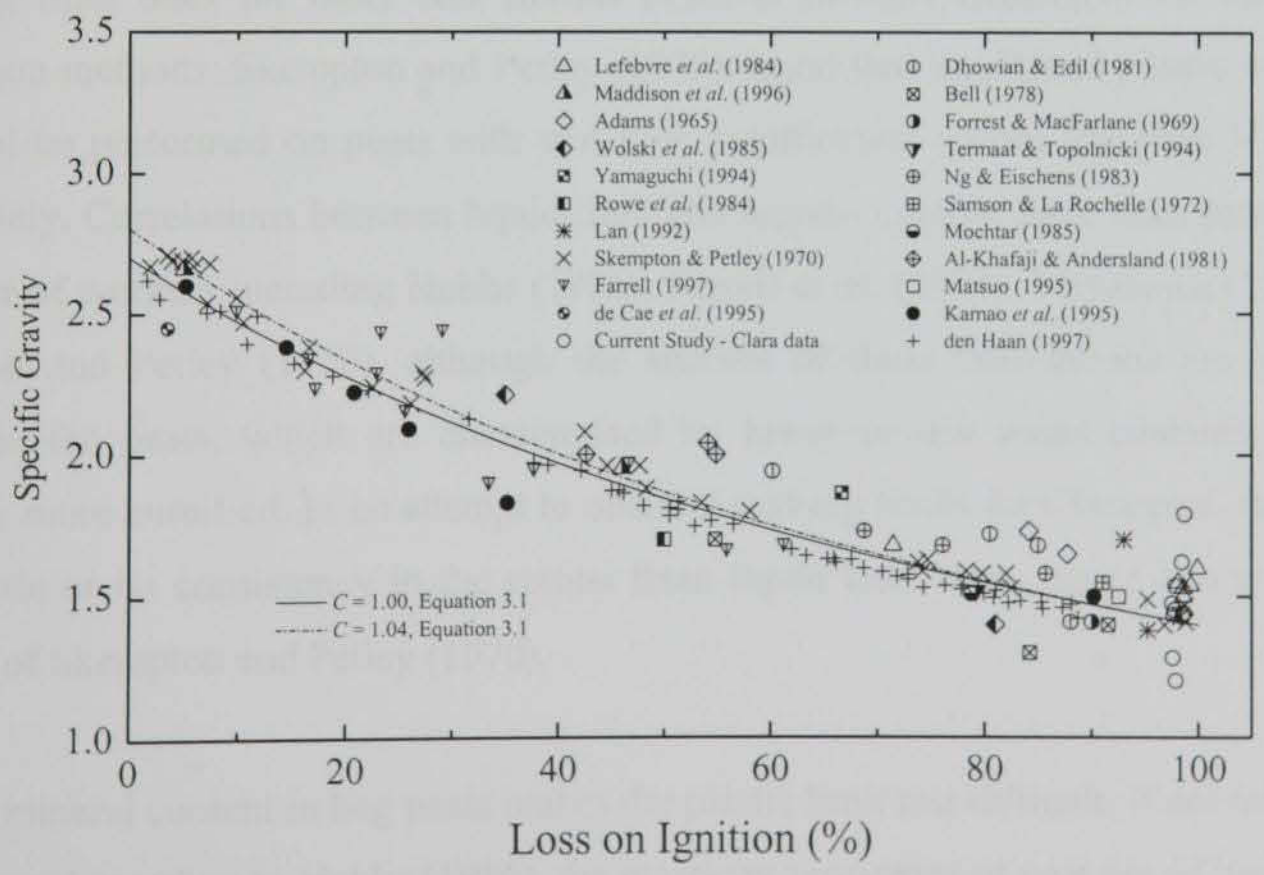

Figure 3.5 Correlation of specific gravity with loss-on-ignition

3.1. Using the organic contents given in § 3.4.3, the following values of specific gravity have been calculated:

- Clara peat - $G_s = 1.41$
- Ballydermot peat - $G_s = 1.41$
- Cork peat - $G_s = 1.55$; Cork silty peat - $G_s = 2.08$

The specific gravity results for Belfast organic clay are reasonably consistent with a mean value of 2.65. The corresponding specific gravity according to Equation 3.1 is 2.45. This value, which is based on an ignition loss of 11% (see § 3.4.3), is significantly lower than the measured result and suggests that a correction factor of unity in Equation 3.1 is not valid for soils of relatively low organic content. Similar findings were reported by Hobbs (1986) who stated that the error in assuming $C = 1.0$ was greater for soils of low organic content. The measured value of 2.65 is considered more reliable in this case, and has been assumed in this study.

3.4.5 Atterberg Limits

Although Atterberg limits are commonly reported for mineral soils, the fibrous nature of peat often makes liquid and plastic limit tests difficult to perform. Den Haan (1997) states that although the tests are impossible to perform on very fibrous peat, the success of Atterberg limit tests for other less fibrous peats is strongly dependent on the sample preparation methods. Skempton and Petley (1970) found that liquid and plastic limit tests could not be performed on peats with von Post humification values less than H_3 and H_5 respectively. Correlations between liquid limit and organic content have been proposed by a number of workers including Hobbs (1986), Farrell *et al.* (1994), Miyakawa (1960) and Skempton and Petley (1970), although the success of these correlations are generally limited to fen peats, which are characterised by lower *in situ* water contents, and are generally more humified. In an attempt to obtain Atterberg limits for Clara peat, the author found little or no consistency in the results from liquid limit tests, hence confirming the findings of Skempton and Petley (1970).

The low mineral content in bog peats makes the plastic limit test difficult, if not impossible to perform. According to Hobbs (1986), the plasticity properties of peat are of limited use, as the results, where obtainable, provide little information regarding the behaviour of peat.

As previously stated, no consistent value for the liquid limit of Clara peat could be obtained. Hebib (2001) encountered similar difficulties with Ballydermot peat, quoting a 4 mm difference in cone penetration for a peat sample at a constant water content. However, liquid and plastic limits were obtainable for Cork peat. An average liquid limit, w_L of 690% and plastic limit, w_P of 561% were measured for peat at an average depth of 6.6 compared with w_L = 317% and w_P = 208% for the silty peat at an average depth of 7.6m. According to McCabe (2002), the average Atterberg limits for Belfast organic clay are w_L = 65% and w_P = 30% between depths of 3 and 6 m.

3.4.6 Bulk Density

The bulk density (γ_b) may be determined directly by considering the mass of a known volume of soil. Bulk densities were calculated for the soils considered here by measuring the mass of cylindrical oedometer samples.

The measured values are summarised as follows:

- Clara peat - γ_b = 0.98 – 1.02 Mg/m^3
- Ballydermot peat - γ_b = 1.10 – 1.15 Mg/m^3 (Hebib, 2001)
- Cork peat - γ_b = 1.02 Mg/m^3; Cork silty peat - γ_b = 1.18 Mg/m^3
- Belfast organic clay - γ_b = 1.64 – 1.77 Mg/m^3

The degree of saturation (S_r) is directly linked to the specific gravity and bulk density of the soil. Calculated S_r values ranged from approximately 95% to in excess of 100%. The lower values, which generally relate to the 'pure' peat samples, may be attributed to the presence of gas. Hanrahan (1954) reports that the gas content in Irish bog peats often exceeds 5%.

3.4.7 Scanning Electron Microscopy Analysis

In order to develop a visual appreciation of the soils, their microstructure was examined using a Hitachi S-3500 N Variable Pressure Scanning Electron Microscope (VPSEM). The VPSEM uses a relatively new development in microscopy, in that the specimen chamber is not operated under a vacuum, but at a relatively low pressure, generally between 20 and 30

Pa. The presence of air molecules within the specimen chamber helps to dissipate the build up of charge on the surface of the specimen. The advantage of this is that specimens no longer have to be coated with a conducting material (usually a very fine layer of gold) before examination. The soils were prepared for examination by oven drying at 105°C for 24 hours. Specimens were fractured in their natural state before drying so as to minimise particle disturbance. Following the recommendation of Mitchell (1976), the dried, fractured surface was treated with a gentle blast of hydrogen to ensure that the surface was representative of the undisturbed fabric and structure of the soil.

(a)

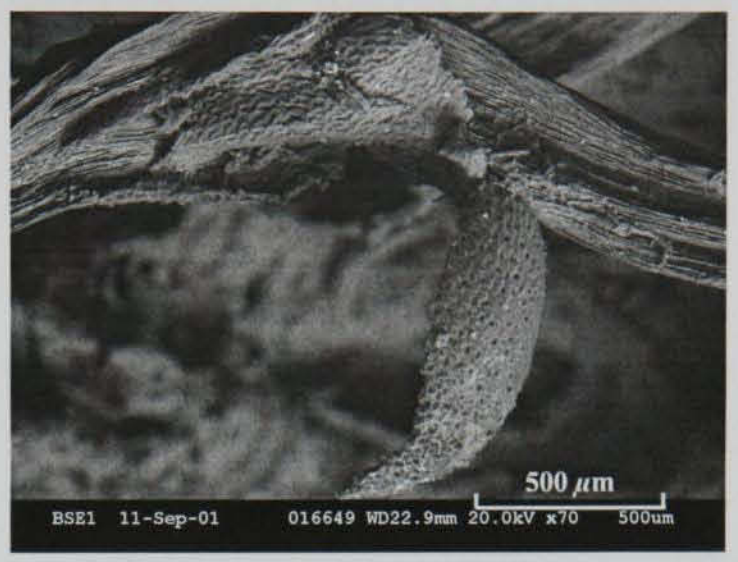

(b)

(c)

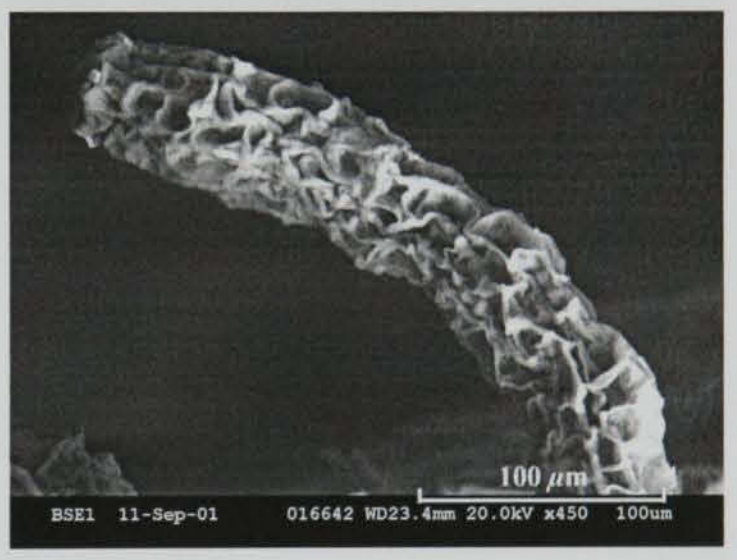

(d)

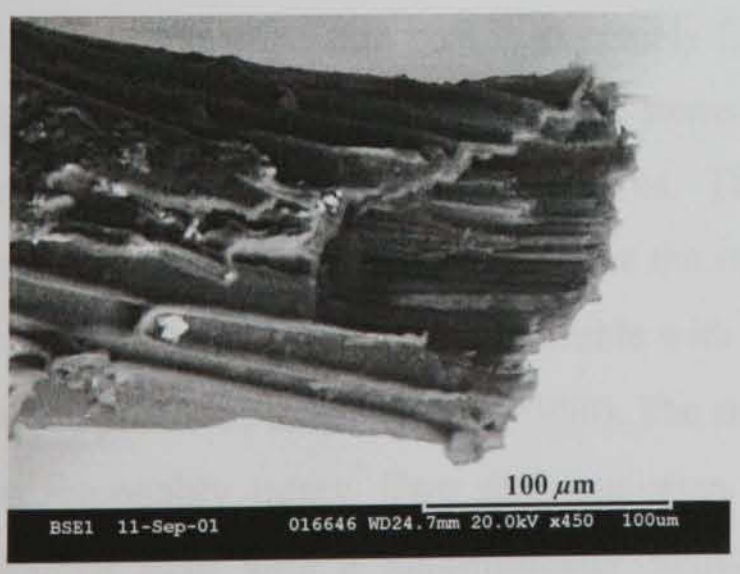

(e)

(f)

Figure 3.6 SEM images of Clara peat

Although it is recognised that oven drying may induce undesirable capillary stresses in the peat (Landva and Pheeney, 1980), and between soil particles (Mitchell 1976), these effects are not considered severe enough to cause significant disturbance.

(a)

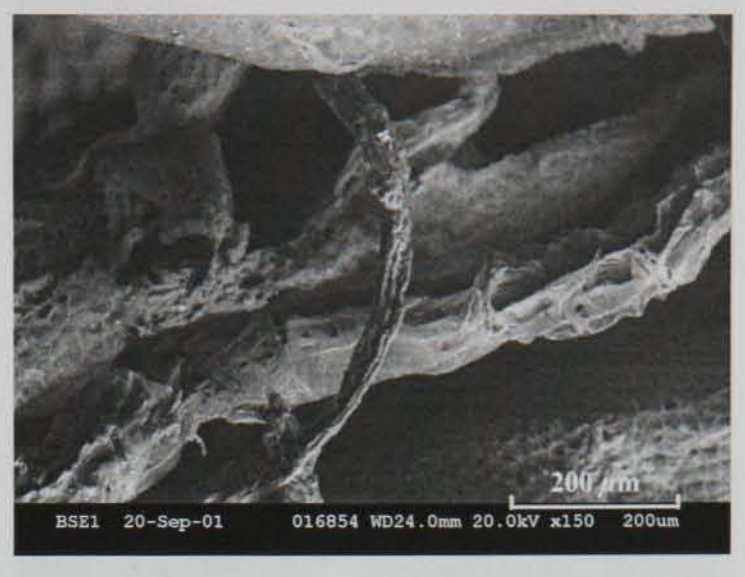

(b)

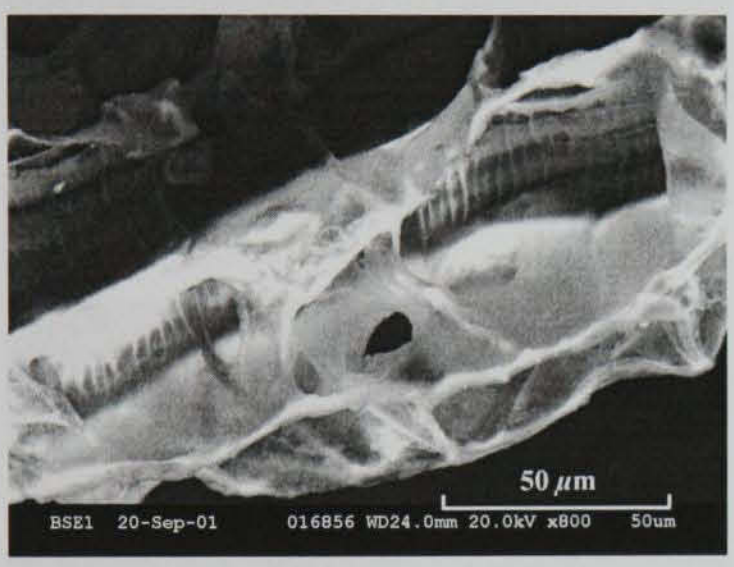

(c)

(d)

Figure 3.7 SEM images of Ballydermot peat

Figure 3.6 shows typical SEM images of Clara peat. Images such as those shown in Figure 3.6a indicate that Clara peat is extremely fibrous. All images suggest relatively large pore spaces, at macroscopic level between stems and leaves, and at microscopic level within the open and perforated plant structures. The thickness of the individual fibres varies considerably; values determined from the images in Figure 3.6 range from between 20 and 140 μm. These values are comparable with the 20-500 μm range reported for a Sphagnum stem by Landva and Pheeney (1980). The state of the individual stems and leaves appear to be reasonably intact. Two different stem types are identifiable; Figure 3.6c shows an isolated stem with a longitudinally ribbed wall structure, whereas Figure 3.6d shows another isolated stem with a more irregular and perforated structure, although this may be

(a)

(b)

(c)

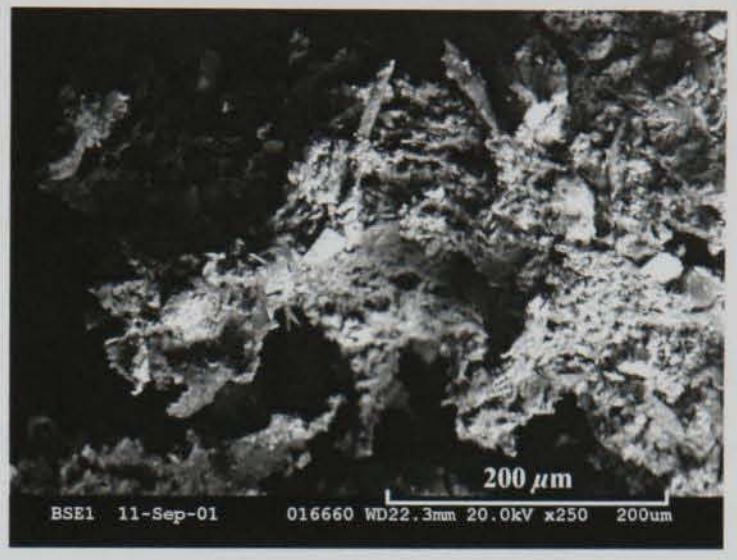

(d)

(e)

(f)

Figure 3.8 SEM images of: Cork peat (a) – (d), Cork silty peat (e) – (f)

due to partial humification. An open ended stem in shown in Figure 3.6e; the stem is seen to be approximately cylindrical and hollow. Intermittent specks such as those shown on the stems in Figure 3.6a and Figure 3.6c are possibly mineral particles as they are much lighter in colour and therefore much denser. SEM images of Ballydermot peat are provided in Figure 3.7. The fibres are comparable in dimension to that of Clara peat, although the actual stems appear to be more humified. This is well illustrated in Figure 3.7c, which is a magnified view of a stem in Figure 3.7b. The walls of the stem are at least partially desiccated, leaving an open framework of cell walls. Landva and Pheeney (1980) use

similar images of a H_{3-5} Sphagnum peat to identify stages in the humification process. Despite the apparent humification of the stems, the bundle of Sphagnum leaves shown in Figure 3.7d appear to be relatively intact, although separated from the stems. Figure 3.7a supports the premise that the stems are hollow in structure.

Unlike the SEM images of Clara and Ballydermot peat, the state of the organic matter for Cork peat (Figure 3.8a – Figure 3.8d) suggests that this soil is amorphous or granular. Individual stems and leaves are difficult to identify, indicating that the peat is well humified. Any *probable* organic matter such as that shown in Figure 3.8a and Figure 3.8b suggest a woven structure. No easily identifiable organic matter is observed in the images of Cork silty peat (Figure 3.8e, Figure 3.8f), although the soil appears to be composed of large quantities of diatoms and other microfossils.

The SEM images of Belfast organic clay (Figure 3.9) provide no visual evidence of organic matter, although like Cork silty peat, the soil appears to consist of relatively large quantities of diatoms that are often fragmented. Other unidentified microfossils are evident from the images; the structure of many of these fossils are similar to those encountered in

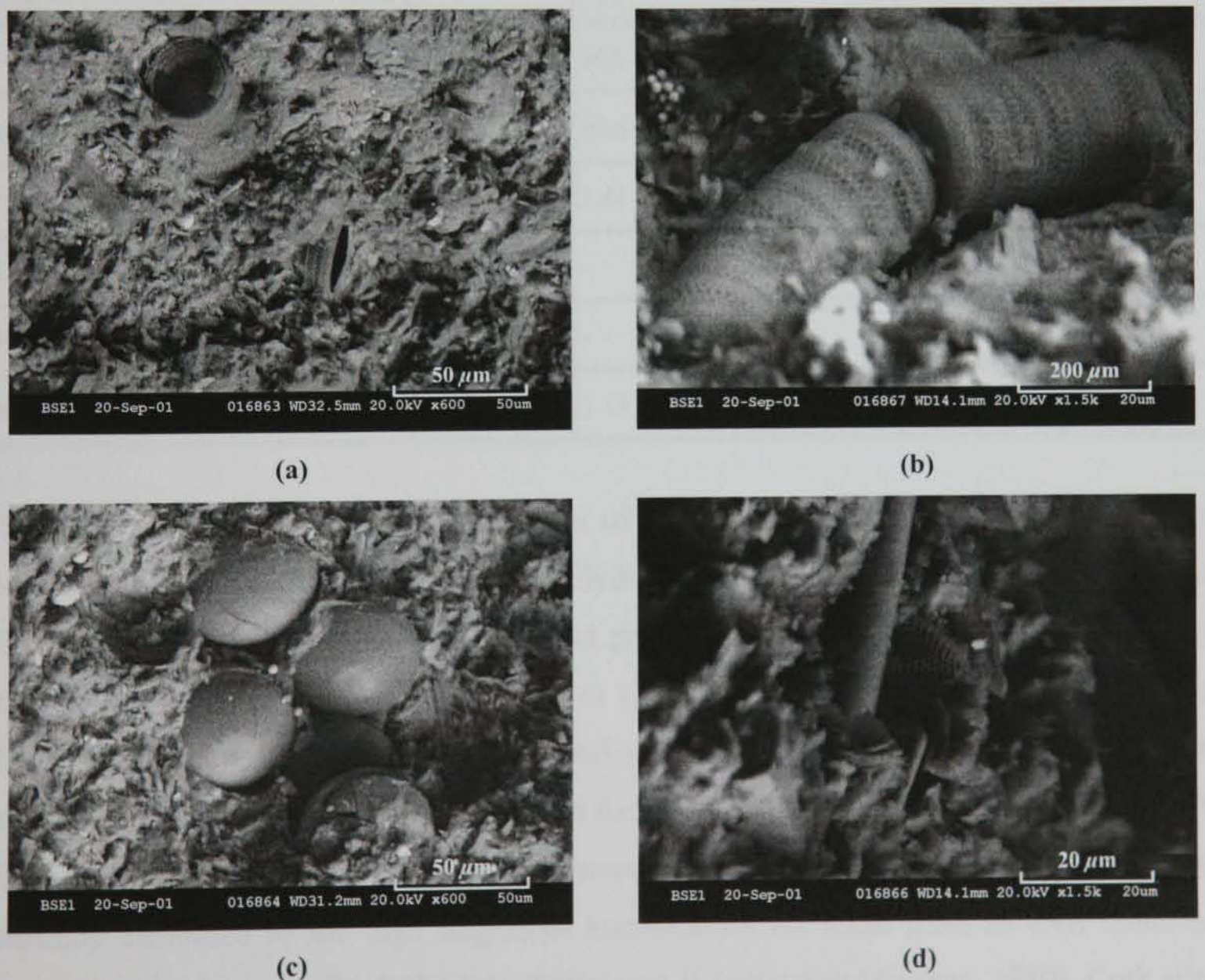

Figure 3.9 SEM images of Belfast organic clay

Mexico City clay, as reported by Mesri *et al.* (1975).

3.5 DISCUSSION

The classification data reported for the four soil groups considered in this study encompasses a wide range of geotechnical properties. It is evident that the peat soils are predominated by organic matter, which is recognised as having a significant bearing on the natural water content and specific gravity of the soil (Hobbs, 1986). The average geotechnical classification properties for each soil are summarised in Table 3.1.

Table 3.1 Average geotechnical classification properties of peats and organic clay

	Clara	Ballydermot	Cork		Belfast
Sampling Depth (m)	0.5 – 0.75	0.5 – 2.5	6.2 – 7.5	7.5 – 7.9	3.0 – 7.0
Description	Fibrous peat	Fibrous peat	Amorphous peat	Silty peat	Organic clay
Degree of Humification ($H_1 - H_{10}$)	H_{2-3}	H_{6-9}	H_{10}	-	-
Natural Water Content (%)	1407	865	447	208	60
Organic Content (%)	98.1	98.6	79.5	32.2	11.0
Specific Gravity	1.41	1.41	1.55	2.08	2.65
Liquid Limit (%)	-	-	690	317	65
Plastic Limit (%)	-	-	561	208	30
Bulk Density ($Mg/m^{3)}$	1.02	1.13	1.02	1.18	1.71

The SEM images provide ample evidence of organic matter in the form of Sphagnum leaves and stems for both Clara and Ballydermot peat. The apparent structure of the Sphagnum stems suggests that Ballydermot peat is more humified than Clara peat. This conclusion is based largely on the images and humification descriptions provided by Landva and Pheeney (1980) in their extensive work on the fabric and structure of peat soils. Evidence of organic matter is limited for Cork peat, and practically non-existent for Cork silty peat despite the relatively high measured organic contents. This may be at least partially attributed to the high degree of humification for Cork peat, as well humified organic matter is generally difficult to distinguish (Landva and Pheeney, 1980). Cork silty

peat and Belfast organic clay contain high quantities of siliceous-based microfossils, including diatoms. Diatoms are unicellular algae with silica based cell walls, which are generally highly structured. Although no evidence of *plant-based* organic matter was encountered in the SEM images of Belfast organic clay, it is suggested that the measured organic content of 11% may be at least partially due to the remains of diatom organics and other microorganisms. Similar reasoning was used by Mesri *et al.* (1975) to explain the *authentic* organic content of Mexico City clay (5-10%). The SEM images of the diatoms and siliceous shells show the surfaces to be finely perforated. Such perforations are capable of holding relatively large quantities of water (Mesri *et al.*, 1975), which will obviously contribute to the overall measured water content of Cork silty peat and Belfast organic clay.

Loss-on-ignition has been plotted on Figure 3.10 against water content for a wide range of soils, including the peats and organic clay considered here (see Figure 3.10). The full line fitted to the data reported for the Irish soils is seen to provide a reasonable correlation for the entire data. Relationships proposed by MacFarlane and Rutka (1961) and Miyakawa (1960) are also shown for comparison. It is apparent that the water content is strongly dependent upon the amount of organic matter present, up to an approximate threshold loss-on-ignition value of 80%. A high degree of scatter between loss-on-ignition and water content exists for soils with higher organic contents; this variance is likely to be due to the

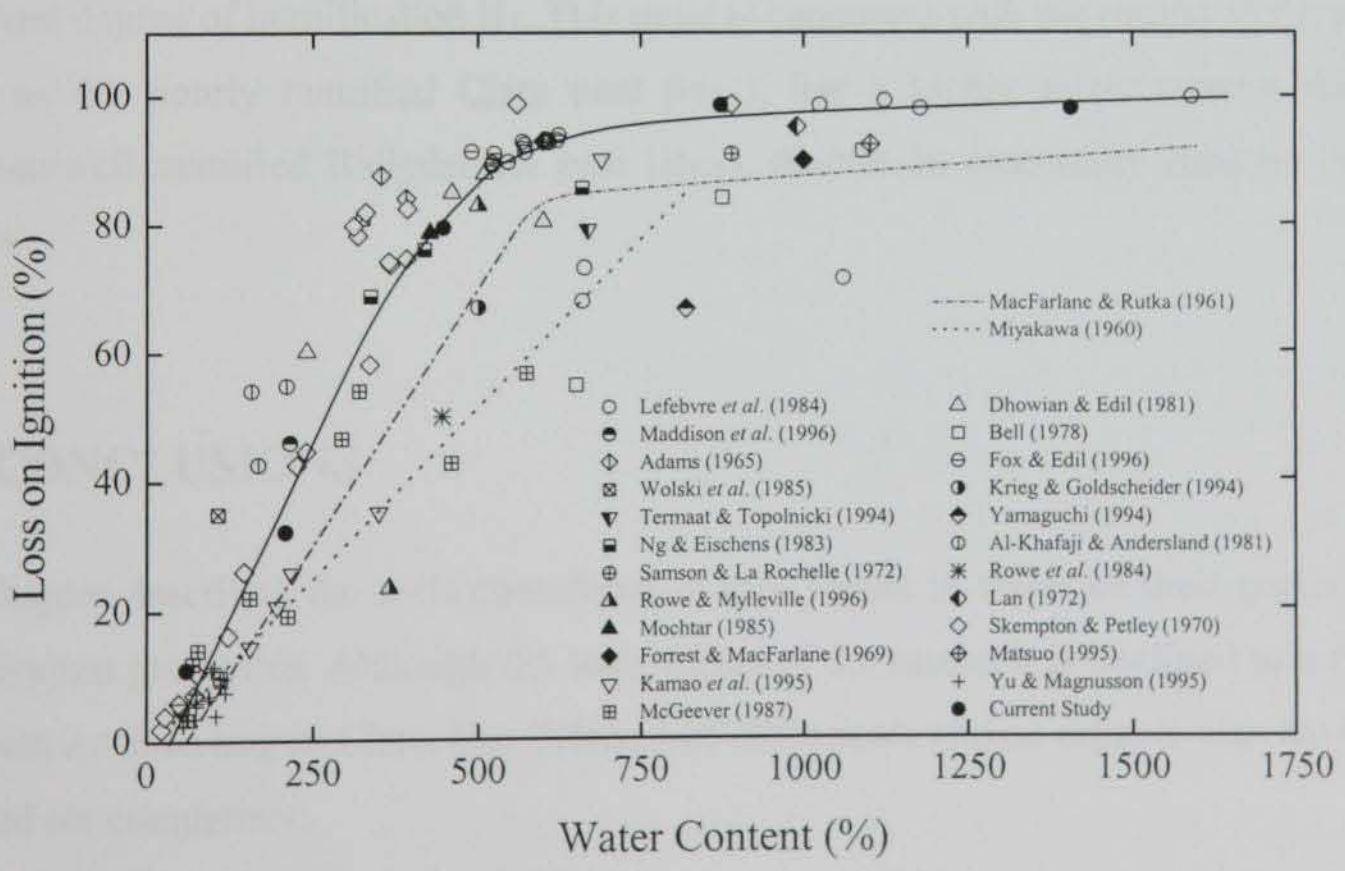

Figure 3.10 Correlation of water content with loss-on-ignition

degree of humification of the organic matter. Similar reasoning has been used by Hobbs (1986) to explain the wide range of scatter encountered in the plot of loss-on-ignition against water content presented by Sandroni *et al.* (1984). The poor correlation between loss-on-ignition and water content for highly organic soils, shown here and elsewhere (Landva *et al.*, 1983; Sandroni *et al.*, 1984), illustrates the shortcomings in the numerous classification systems that categorise peat and organic soils based solely on organic content. It is notable that the threshold loss-on-ignition of 80% observed here is the organic content that is commonly used to distinguish between peat and organic soils (see Figure 3.3).

The soils with loss-on-ignition values greater than 80% tend to largely (but not exclusively) correspond to peat soils which are classified as fibrous or poorly humified. For instance, the fibrous peat data reported by Lefebvre *et al.* (1984) is plotted on Figure 3.10 at water contents typically larger than 1000%. The degree of humification for the higher water content data points was estimated by Lefebvre *et al.* (1984) as H_{2-3}. The data points at lower water contents and loss-on-ignition values relate to a separate peat deposit in which a well defined transverse flow of water resulted in the migration of a relatively large percentage of mineral matter. In contrast, many of the data points that were derived from data reported by Skempton and Petley (1970), correspond to peat at a high or moderate stage of humification. Peat with water contents in the range 150 – 300% was reported as H_{8-9}, 300 – 400% as H_{5-7}, with one isolated data point at a water content of 890% and degree of humification H_3. This trend is consistent with the results of the current study, as the poorly humified Clara peat (H_{2-3}), has a higher water content than the moderate/well humified Ballydermot peat (H_{6-9}), despite an essentially constant organic content.

3.6 CONCLUSIONS

This chapter described the soils considered in this Thesis in terms of their geotechnical classification properties. Although the main thrust of the research is confined to a fibrous peat from a raised bog in Clara, Co. Offaly, two other peats and an organic clay have been included for comparison.

1. Classification data has been obtained using standardised techniques, although the recommended procedure for specific gravity (BS 1377) gave results for Clara peat which were considered too variable to be reliable. A simple formulation due to Skempton and Petley (1970) has been demonstrated to fit the observed dependency between loss-on-ignition and specific gravity quite well, particularly at a loss-on-ignition greater than approximately 30%. The data has been fitted to a wide range of data sourced from the literature.

2. SEM images indicate that Ballydermot peat is more humified than Clara peat, as the walls of certain Sphagnum stems appear to be partially desiccated. Intact organic matter is not easily distinguishable for Cork peat, suggesting that this peat represents an increased stage of humification over both Ballydermot peat and Clara peat. These findings are reflected in the results of the von Post humification test.

3. A correlation between loss-on-ignition and water content for the soils considered here and for several other referenced soils has been presented in Figure 3.10. The water content is seen to be dependent upon the presence of organic matter up to an approximate threshold loss-on-ignition of 80%. Beyond this value, water contents vary considerably, even for one given loss-on-ignition value. Landva and Pheeney (1980) discuss the dependence of water content on the stage of humification of the soil. They concluded that well humified peats are likely to have lower water contents than poorly humified peats, as much of the water in the latter is contained within the *intact* organics at cellular level. Similar consistencies were found in the data presented in Figure 3.10, as the poorly humified peat tended to correspond to higher water contents.

4. It is apparent that, although both Clara and Ballydermot peat are classified as fibrous, they are essentially different. The state of humification is the fundamental reason for the disparity. This property, although seldom reported in the literature, allows peat soils to be easily distinguishable, and may be more easily interpreted than classification terms such as fibrous or amorphous. Amorphous or granular peat is often used to describe peat soils with a von Post classification of $H_{7\text{-}10}$ (Jarrett, 1997). According to this method, Ballydermot peat would be classified as amorphous, although the SEM images show this peat to be fibrous. Landva and Pheeney (1980) suggest that proper identification of peats should be based on the

degree of humification and water content. The findings of the work presented here support this recommendation.

Chapter 4

Laboratory testing of peat and organic soils

Chapter 4

Laboratory testing of peat and organic soils

4.1 INTRODUCTION

A number of workers including Edil and den Haan (1994), Landva *et al.* (1983) and Fox *et al.* (1992) argue that conventional analytical methods are inappropriate for peat, as these soils exhibit unusual compressibility characteristics that bear little or no resemblance to that of mineral soils. Other investigators such as Farrell (1997, 2001), Carlsten (1991) and Mesri *et al.* (1997) have successfully predicted field and laboratory behaviour using mainly traditional geotechnical concepts. The lack of general agreement amongst engineers about how best to cope with embankments and roads constructed over peat deposits is an on-going problem. To this end, the author, during the course of the research described in this Thesis, initiated a programme of laboratory and field experimental work with the aim of obtaining a better understanding of the fundamental behaviour of peat soils loaded under one-dimensional conditions.

The specific aims of the laboratory experimental programme are as follows:

1. Examination of the contribution and nature of creep compression through oedometer tests involving a large load increment duration (LID)
2. Investigation of the effects of a load increment ratio (LIR) greater than unity
3. Assessment of the influence of rate selection and rate changes in tests performed at constant rates of deformation
4. Provide a basis for validating constitutive and empirical theories aimed at predicting the one-dimensional compression of clay and peat soils
5. Examination of the role of organic content and humification state in observed behaviour

As the *in situ* stresses in peat deposits are generally much lower than those imposed by even relatively modest structures, the research interest is largely confined to virgin, or normally consolidated behaviour. However, the effects of unloading and *pre-yield* behaviour are examined, albeit to a much lesser extent. The consolidation of peat, understood here to refer solely to compression due to the dissipation of excess pore water pressure, is also investigated, although to a lesser degree than creep compression.

As discussed in Chapter 3, the major concentration of the research, and hence laboratory tests, have been confined to Clara peat, as this soil possesses many of the geotechnical properties and characteristics which bear little resemblance to non-organic, mineral soils. However, a limited amount of experimental data obtained from tests on the other soils described in Chapter 3 is included for comparison.

4.2 TESTING PLAN

A total of 48 one-dimensional tests have been performed as part of this study. In order to easily distinguish between the tests, the naming convention described by Table 4.1 has been adopted. In Table 4.1, MSL refers to Multi Stage Load tests performed in the standard oedometer apparatus, whereas CRD refers to Constant Rate of Deformation tests. CRD tests are often referred to in the literature as Constant Rate of Strain (CRS) tests (Wissa *et al.* 1971, Leroueil *et al.* 1985). However, such terminology implies a specific definition of strain (Lee, 1981). Although the conventional definition of strain ($\varepsilon = \Delta H/H_o$) is generally interchangeable with deformation rate, a number of workers including Juárez-Badillo (1965), Butterfield (1979), Lefebvre *et al.* (1984), den Haan (1992, 1996), Nash and Ryde (2000), prefer the use of *natural strain* ($\varepsilon = -\ln(H/H_o)$). Since constant rate of deformation

Table 4.1 Naming convention for oedometer and CRD tests

Source	Oedometer	CRD tests	Example
Clara	CL_MSL	CL_CRD	CL_CRD_06
Ballydermot	BD_MSL	BD_CRD	BD_MSL_02
Cork	CK_MSL	-	CK_MSL_03
Belfast	BF_MSL	-	BF_MSL_04

is not synonymous with constant rate of natural strain, the term CRD is deemed more appropriate and has been adopted here.

Specific details of the tests performed are summarised in Tables 4.2 to 4.6. Tests performed by Dr. Samir Hebib on Ballydermot peat and by Mr. Bryan McCabe on Belfast organic clay are marked accordingly. CRD tests are described by the imposed rate of strain, r, where strain assumes its conventional definition, $\varepsilon = \Delta H/H_o$.

Table 4.2 Clara peat MSL oedometer test descriptions

Test Number	w : (%)	e_0	σ'_0 : (kPa)	σ'_f: (kPa)	LIR	LID : (days)
CL_MSL_01	1825.27	24.74	5.0	320.0	1.0	1
CL_MSL_02	1829.96	25.65	5.0	320.0	1.0	1
CL_MSL_03	2138.17	31.93	5.0	320.0	1.0	1
CL_MSL_04	2028.42	31.84	1.0	512.0	1.0	1
CL_MSL_05	1950.20	28.81	1.4	340.2	2.0	1 - 60
CL_MSL_06	1368.60	18.81	2.0	200.0	1.0 - 4.0	7 - 200
CL_MSL_07	1432.22	20.11	2.0	250.0	0.5 - 7.0	7 - 200
CL_MSL_08	1296.86	19.49	4.0	150.0	0.5 - 9.0	105 - 200
CL_MSL_09	1574.95	22.09	20.35	468.1	1.2 - 3.3	7 - 13
CL_MSL_10	1481.14	19.94	27.14	515.58	1.1 - 2.0	7 -13
CL_MSL_11	1602.82	23.65	48.0	1202.0	0.4 - 8.0	7 - 13
CL_MSL_12	1575.08	22.69	25.0	431.0	0.25 - 4.8	7 -13
CL_MSL_13	1472.11	20.76	33.7	803.0	0.4 - 4.3	7 - 13
CL_MSL_14	1348.81	19.11	5.44	710.0	1.0	1 - 6
CL_MSL_15	1115.47	17.76	6.25	800.0	1.0	1 - 6
CL_MSL_16	1095.68	16.09	5.0	640.0	1.0	1 - 4
CL_MSL_17	1087.52	16.57	6.25	800.0	1.0	1 - 6
CL_MSL_18	1126.37	15.64	3.0	600.0	0.5 - 5.7	1 - 8
CL_MSL_19	1202.34	16.89	30.0	480.0	1.0	1
CL_MSL_20	1549.72	21.77	30.0	240.0	0.25 - 3.0	0.06 - 4.6
CL_MSL_21	1496.31	21.03	30.0	300.0	0.25 - 3.0	0.05 - 0.3
CL_MSL_22	1274.82	19.41	5.0	8.0	0.6	105 - 150

Table 4.3 Clara peat CRD test descriptions

Test Number	w : (%)	e_0	σ'_f: (kPa)	r : ($sec^{-1} \times 10^{-6}$)
CL_CRD_01	1347.46	19.13	285.3	1.08
CL_CRD_02	1247.87	18.28	605.3	1.19-5.43
CL_CRD_03	1066.99	15.65	611.2	0.22-1.25
CL_CRD_04	1519.25	22.05	559.1	8.33
CL_CRD_05	1616.21	23.42	54.6	0.08-0.83
CL_CRD_06	1296.06	19.32	580.9	0.33-3.98
CL_CRD_07	1369.56	19.65	567.8	8.33
CL_CRD_08	1596.88	23.44	207.2	0.83-8.33
CL_CRD_09	1738.12	25.06	550.6	2.5-25

Table 4.5 Ballydermot peat MSL oedometer test descriptions

Test Number	w : (%)	e_0	σ'_0: (kPa)	σ'_f: (kPa)	LIR	LID : (days)
BD_MSL_01[†]	816.48	12.37	5	395	0.33-1.25	1-2
BD_MSL_02[†]	839.19	13.14	5	395	0.33-1.25	1-2
BD_MSL_03[†]	831.84	12.49	5	160	1	1
BD_MSL_04[†]	657.34	9.86	10	20	1	37-39
BD_MSL_05	738.46	11.08	6.25	601	0.47-3.8	0.75-8
BD_MSL_06	808.67	11.95	6.25	889	1.85-3.33	0.75-8
BD_CRD_01	1039.70	15.93	0	309.5	1	0.6-3

[†] Test performed by Dr. Samir Hebib

Table 4.4 Cork peat/silty peat MSL oedometer test descriptions

Test Number	w : (%)	e_0	σ'_0: (kPa)	σ'_f: (kPa)	LIR	LID : (days)
CK_MSL_01	220.72	4.67	12.5	400	1	1-3
CK_MSL_02	455.64	7.44	12.5	400	1	1-3
CK_MSL_03	418.26	6.98	12.5	600	1-11	0.1-23

Table 4.6 Belfast organic clay MSL oedometer test descriptions

Test Number	w : (%)	e_o	σ'_o: (kPa)	σ'_f: (kPa)	LIR	LID : (days)
BF_MSL_01†	-	1.47	12.5	800	1	1
BF_MSL_02†	47.90	1.79	6.25	400	1	1-4.5
BF_MSL_03†	70.13	1.69	6.25	800	1	1-3
BF_MSL_04†	70.28	1.77	6.25	800	1	1-5
BF_MSL_05†	58.34	1.40	6.25	800	1	1-3
BF_MSL_06†	52.84	1.29	6.25	800	1	1-10
BF_MSL_07	55.75	1.42	6.25	1200	0.4-4.7	0.75-7

† Test performed by Mr. Bryan McCabe

4.3 SPECIMEN PREPARATION

Due to the fibrous and compressible nature of the peat soils, particular care had to be taken in trimming and preparing the specimens for testing. In the case of Clara peat, relatively large fibres and wood remnants impaired the quality of the specimen; such specimens were discarded, as they were considered unrepresentative of the peat sample. Specimens of Clara peat were retrieved from the block samples using a sharp serrated knife. The undesirable compression caused by pushing an oedometer ring into the soil was avoided by using the ring as a template to mark the circumference of the specimen. Specimens could then be retrieved from the sample by cutting away the excess material, and advancing the oedometer ring as trimming progressed. Protruding fine fibres were trimmed at the level of the oedometer ring, and superficial voids filled with sample trimmings in accordance with the recommendations of Head (1982). Figure 4.1 shows the steps involved in the specimen preparation process. The fibrous nature of Clara peat is apparent from the sample trimmings shown in Figure 4.1a.

4.4 OEDOMETER TEST RESULTS

One of the main aims of this experimental programme was to assess the nature and contribution of creep settlement of peat. Hobbs (1986) states that for peat, creep under oedometric conditions is the dominant process governing settlement, with consolidation

(a) (b)

Figure 4.1 Preparing a specimen of Clara peat for testing: (a) removing excess peat whilst advancing the oedometer ring, (b) trimming the specimen to the height of the oedometer ring

merely distorting the shape of the eventual linear ε - log t curve. The creep of peat has been assessed by way of oedometer tests involving stress increments that were in some instances maintained for several months. Although a number of standard oedometer tests (LIR=1, LID=24 hours) have been performed, the majority of oedometer tests involve LIRs in the range 0.25-11. The relevance of LIR>>1 is particularly relevant to peat deposits, as stress increments well in excess of the relatively low in-situ stress are often applied in an attempt to reduce long-term settlement.

The oedometer tests were performed in Wykeham-Farrance loading frames, with specimen diameters of 75.0, 76.2 and 100 mm and heights of either 19.05 or 20.0 mm. Drainage was permitted towards both the top and bottom of the specimen, with the exception of three tests which were performed in Rowe Cells, with pore pressures monitored at the base of the specimen.

4.4.1 Evolution of deformation and pore pressure with time

In a study of the compressibility characteristics of soils loaded under oedometric conditions, Leonards and Girault (1961) identified three separate compression – time curves (Figure 4.2):

1. Type I: Classic S-shaped curve, with a clearly defined transition from consolidation phase to sole creep compression phase (LIR=1)

2. Type II: Similar to Type I, but with a gradual increase in the slope (with log t axis) of the creep portion of the curve (LIR<0.5)
3. Type III: No discernible transition point from the consolidation phase to the creep only compression phase; the slope of curve (with log t axis) gradually increases to a constant value (LIR<0.5)

These three types of compression curves have been observed by a number of workers including Barden (1969), Mesri and Godlewski (1977) and den Haan (1996). Consequently, an attempt has been made to identify the e – log t plots considered here by the appropriate Leonards and Girault curve.

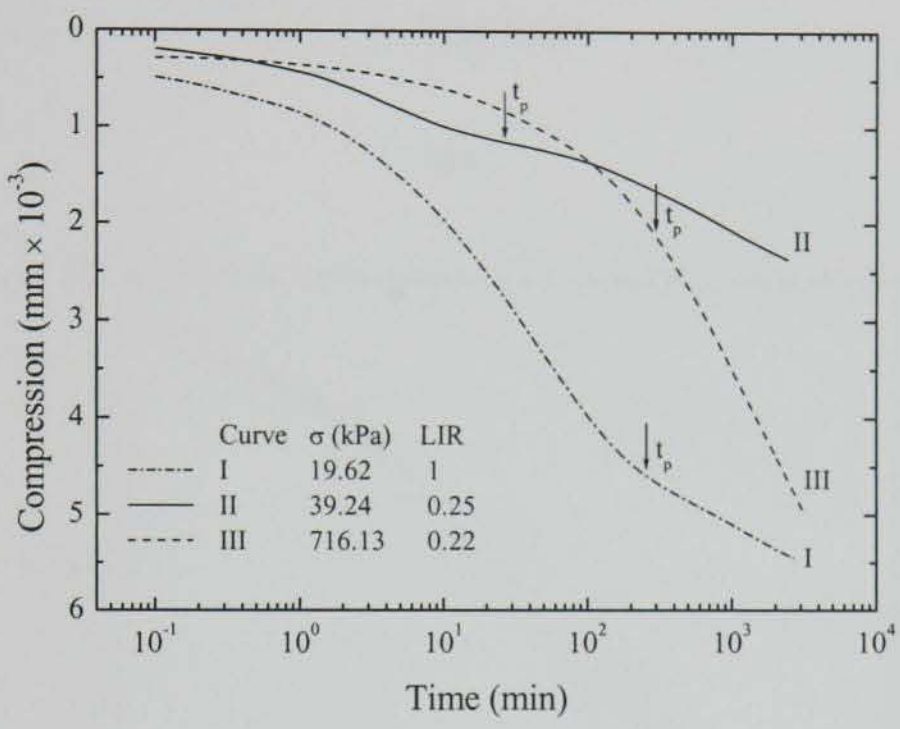

Figure 4.2 Compression – time relationships for Mexico City clay (after Leonards and Girault, 1961)

4.4.1.1 Clara peat

Two typical e – log t curves for Clara peat are provided in Figure 4.3. The data were measured during normally consolidated stress increments of CL_MSL_01, involving a LIR=1 and LID=24 hours. Both curves are typical of the Type I curve, although the reduction in void ratio is larger for the 20-40 kPa stress increment. In the absence of pore water pressure measurements, graphical construction is often used in e – log t plots to estimate the duration of consolidation, t_p. Taylor's method estimates t_p at 90% excess pore pressure dissipation from the initial portion of the e - $\sqrt{t}$ curve, whereas Casagrande construction relies on the commonly observed inflection point in laboratory e - log t plots to determine the point of *complete* excess pore water pressure dissipation. End of primary

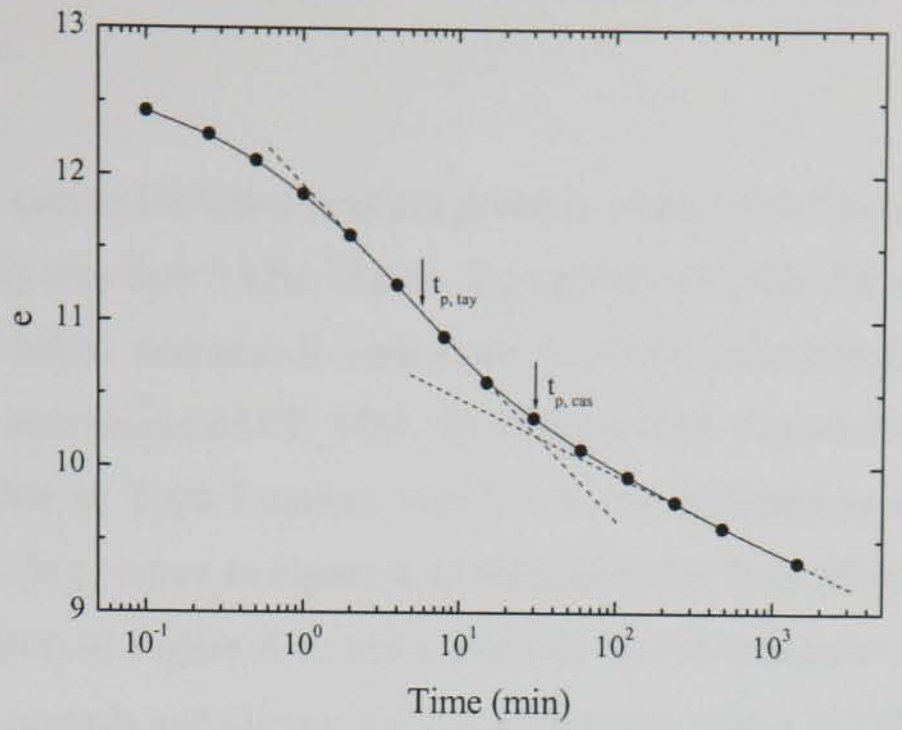

(a)

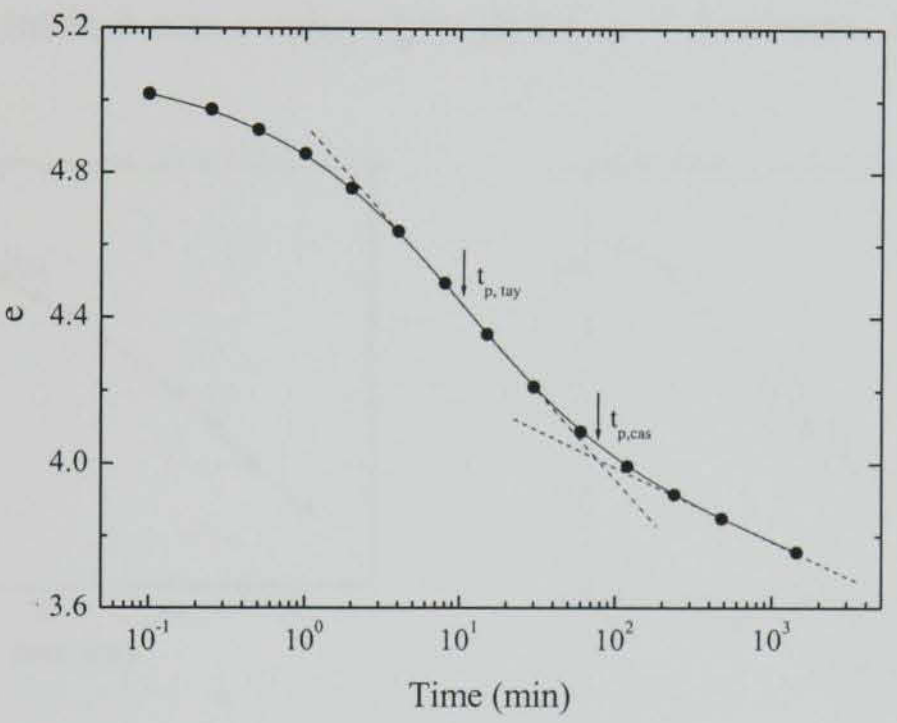

(b)

Figure 4.3 Typical *e* – log *t* plots for Clara peat:
(a) CL_MSL_01, 20-40 kPa; (b) CL_MSL_01, 160-320 kPa

consolidation as estimated using Taylor's root time method and Casagrande's log time method are denoted by $t_{p,tay}$ and $t_{p,cas}$ respectively.

Casagrande construction gave $t_{p,cas}$ = 31 minutes for the 20-40 kPa stress increment and 78 minutes for the 160-320 kPa stress increment. Taylor's method produced significantly lower values for both stress increments; $t_{p,tay}$ = 6 minutes for the 20-40 kPa stress increment and 11 minutes for the 160-320 kPa stress increment. Comparison of the two stress increments shows that t_p is lower for the 20-40 kPa stress increment. This finding is

reflected in the shape of the e – log t plot, which steepens more rapidly than the 160-320 kPa stress increment.

Additional e – log t curves for Clara peat are given in Figure 4.4. These data relate to low stress levels, typically less than 5 kPa. The e – log t plots of Figure 4.4 are characterised by a much more rapid initial decrease in void ratio than that encountered in the 20-40 and 160-320 kPa stress increments of CL_MSL_01 (Figure 4.3). Figure 4.4b and Figure 4.4d are clearly identifiable as Type I curves, which is to be expected as the LIR is 1 and 2 respectively. The e – log t curve in Figure 4.4a resembles the Type III plot shown in Figure 4.2, whereas the curve in Figure 4.4c bears little or no resemblance to any of the three curves defined by Leonards and Girault (1961). In the case of the 1-2 kPa stress increment of CL_MSL_04 (Figure 4.4a) and the 0-5 kPa stress increment of CL_MSL_03 (Figure 4.4c) $t_{p,cas}$ was unobtainable, as the transition compression phases are unidentifiable. However, Taylor's method was employed to give $t_{p,tay}$ = 5 minutes. Intersection points

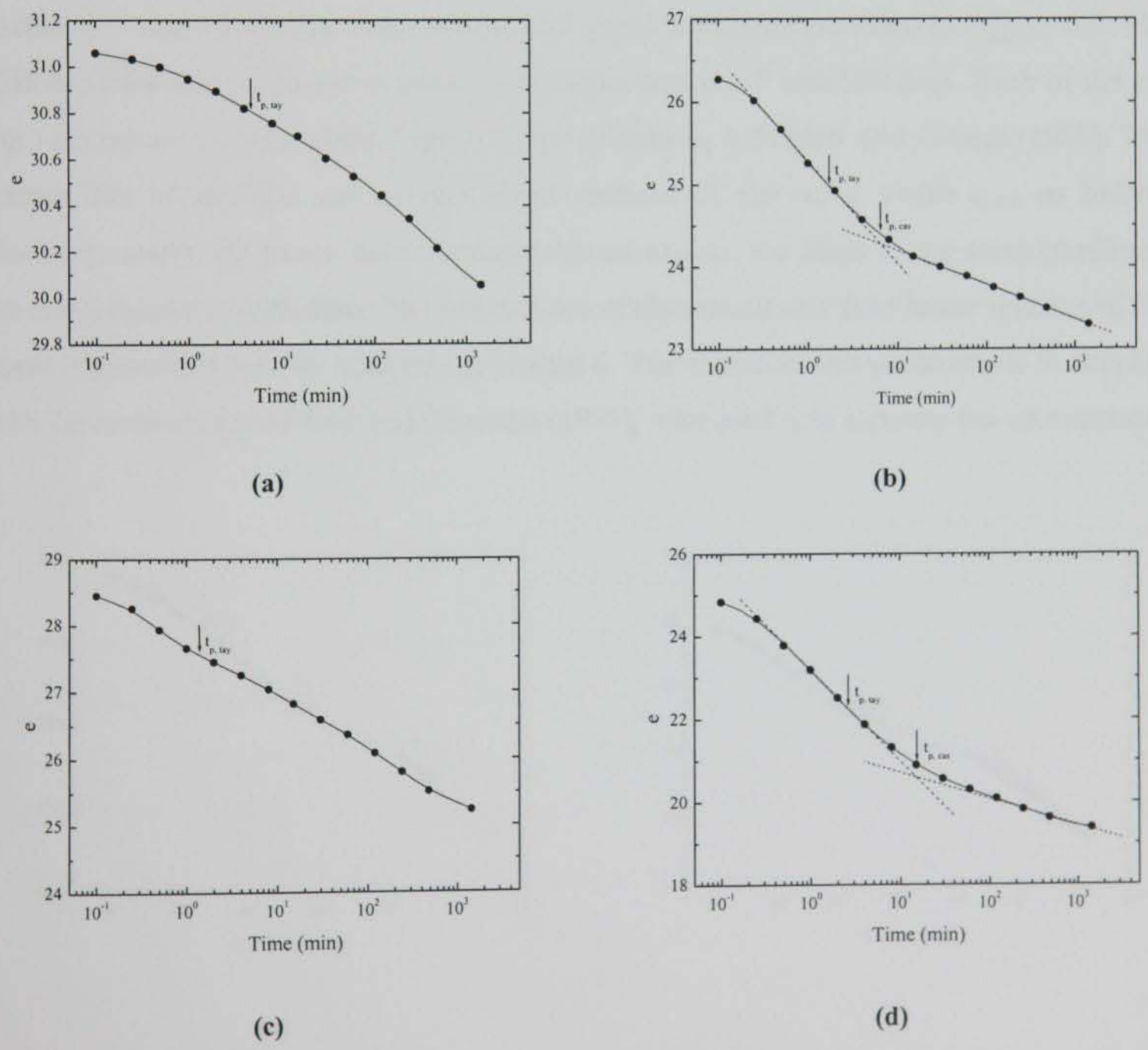

Figure 4.4 Various e – log t curves at low stress levels for Clara peat: (a) CL_MSL_04, 1-2 kPa; (b) CL_MSL_05, 1.4-4 kPa; (c) CL_MSL_03, 0-5 kPa; (d) CL_MSL_02, 0-5 kPa

were easily produced for the high LIR stress increments of Figure 4.4b and Figure 4.4d; graphical construction yielded $t_{p,cas}$ = 6.5 minutes for the 1.4-4 kPa stress increment of CL_MSL_05 and $t_{p,cas}$ = 15 minutes for the 0-5 kPa stress increment of CL_MSL_02. Corresponding values using Taylor's method are $t_{p,tay}$ = 1.7 minutes and 2.6 minutes for CL_MSL_05 and CL_MSL_02 respectively. As before, Casagrande's method produces higher t_p values than Taylor's method. The duration of consolidation determined in this manner is much shorter than that estimated for the higher stress levels (20-40 kPa, 160-320 kPa) of CL_MSL_01.

Following the period of primary consolidation, an approximately linear relationship between e and log t can be observed in the stress increments shown in Figure 4.3 and Figure 4.4. However, the LID for each of the stress increments considered above is relatively low at 24 hours. Consequently, the contribution and nature of creep compression will now be investigated by considering tests in which the LID>>24 hours.

Further e – log t plots for Clara peat at low stress levels are provided in Figure 4.5. The LID involved with these stress increments varies between 7 and 150 days. Each of the e – log t curves are typical of the Type II curve defined by Leonards and Girault (1961). The intersection of the first and second linear sections of the curve yields $t_{p,cas}$ as before. However, unlike the stress increments considered to date, the slope of the creep portion of the curve increases with time. The intersection of the second and third linear sections of the curve is described here by a parameter termed t_k. The choice of this parameter is in keeping with the terminology of Edil and Dhowian (1979), who used t_k to separate the conventional

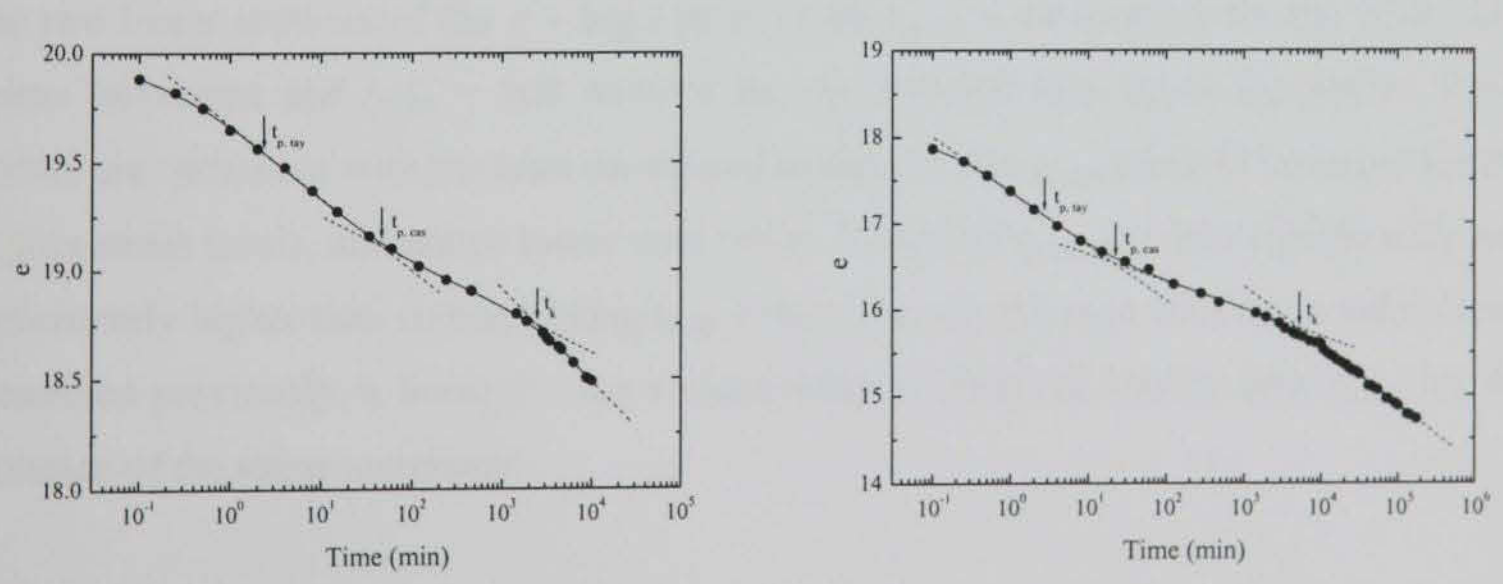

Figure 4.5 e – log t curves for Clara peat at low stresses with high LID: (a) CL_MSL_07, 0-2 kPa; (b) CL_MSL_06, 2-5 kPa

creep portion of the e – log t curve from the *tertiary* portion of the e – log t curve. Graphical construction gave $t_{p,cas}$ = 47 minutes and t_k = 1.7 days for the 0-2 kPa stress increment of CL_MSL_07 (Figure 4.5a) and $t_{p,cas}$ = 22 minutes and t_k = 3.6 days for the 2-5 kPa stress increment of CL_MSL_06 (Figure 4.5b). The slope of the tertiary creep curve ($t > t_k$) remains approximately constant for the duration of each stress increment shown in Figure 4.5.

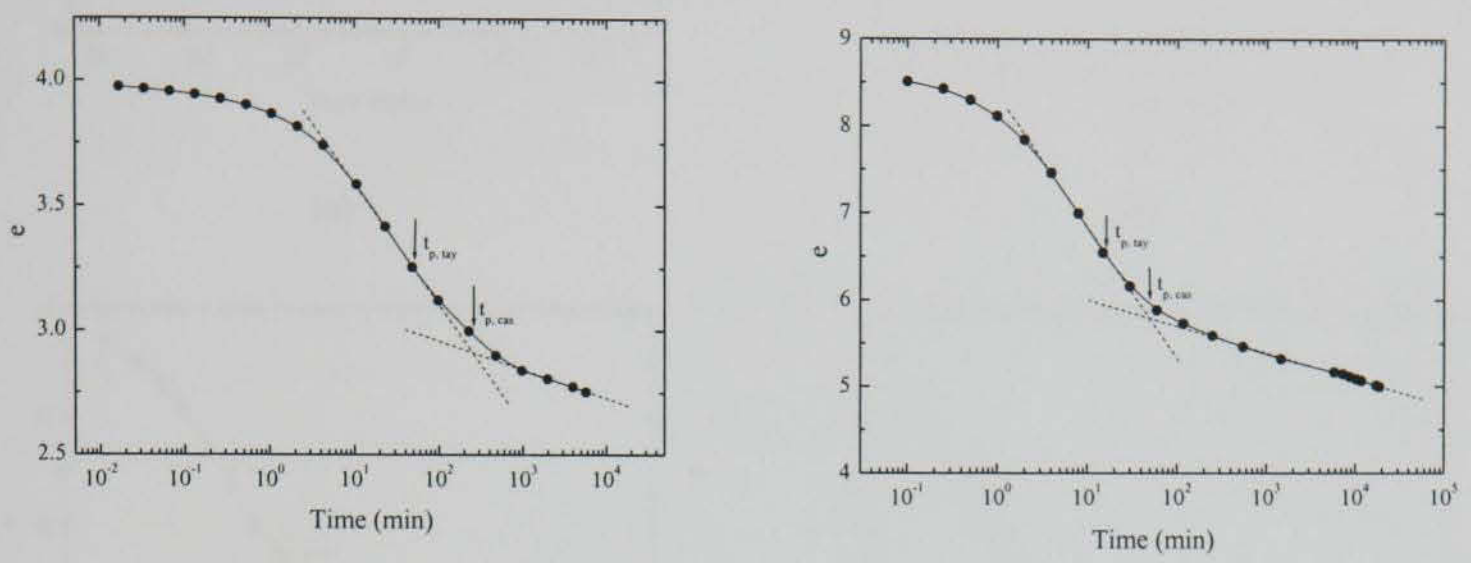

Figure 4.6 e – log t curves for Clara peat:
(a) CL_MSL_15, 200-400 kPa (LIR=1); (b) CL_MSL_10, 27-81 kPa (LIR = 2)

Figure 4.6 shows e – log t curves corresponding to the 200-400 kPa stress increment of CL_MSL_15 (Figure 4.6a) and the 27-81 kPa stress increment of CL_MSL_10 (Figure 4.6b). The 200-400 kPa increment (LIR=1) was maintained for approximately 4 days, whereas the 27-81 kPa increment (LIR=2) was maintained for approximately 13 days. As both plots conform to the Type I curve, $t_{p,cas}$ can be readily determined. The intersection of the two linear sections of the e – log t plots yields $t_{p,cas}$ = 44 minutes for the 27-81 kPa stress increment and $t_{p,cas}$ = 260 minutes for the 200-400 kPa stress increment. These values are consistent with the tests considered to date, in that $t_{p,cas}$ tends to be larger for the higher stress levels, and hence lower void ratios. Values of $t_{p,cas}$ are also significantly and consistently higher than corresponding $t_{p,tay}$ values. As was the case with the *standard* tests described previously, a linear e – log t relationship is observed shortly after $t_{p,cas}$ for the duration of the stress increment.

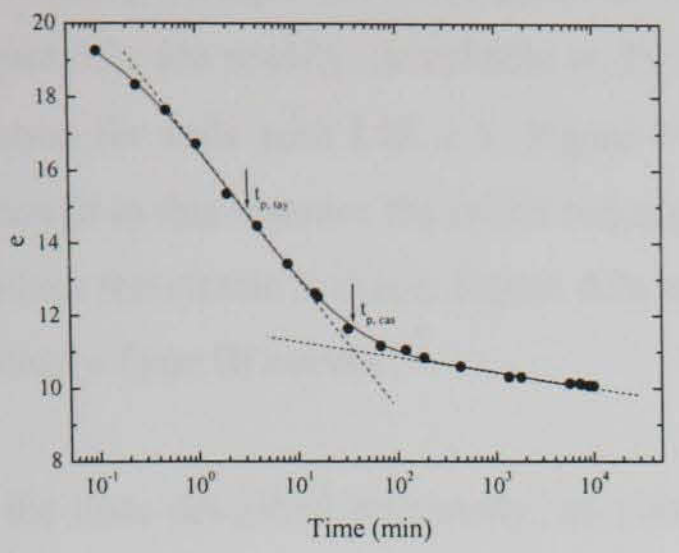

(a)

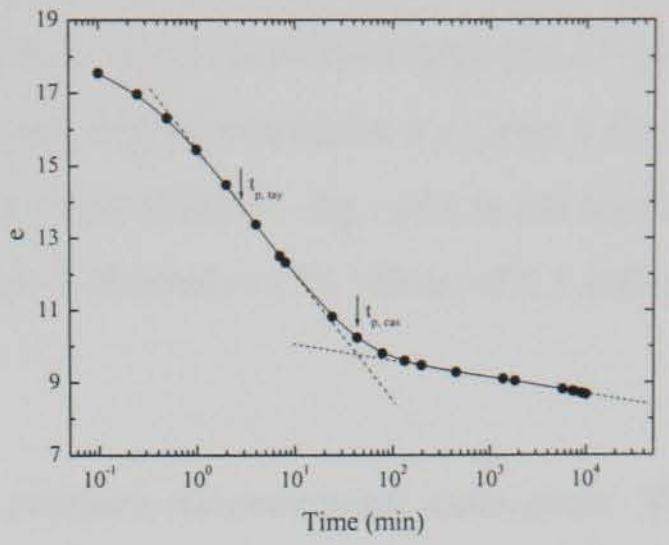

(b)

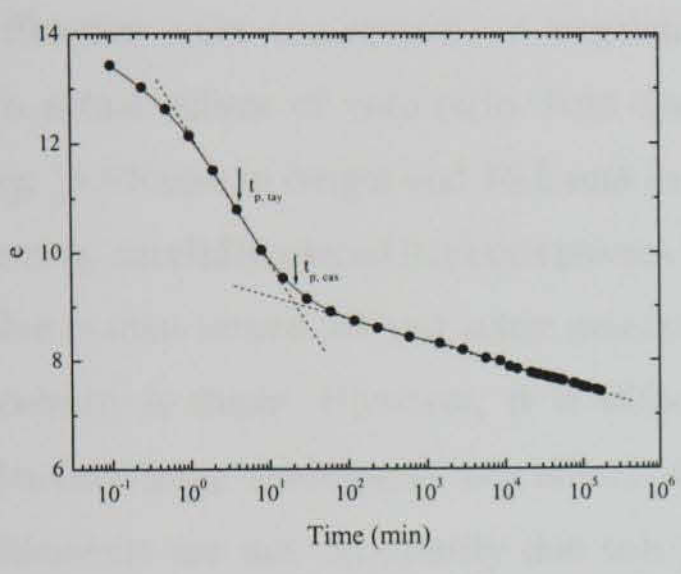

(c)

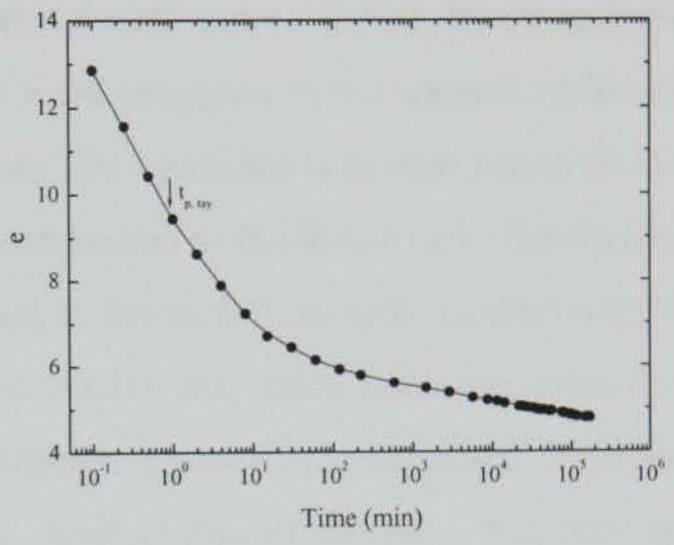

(d)

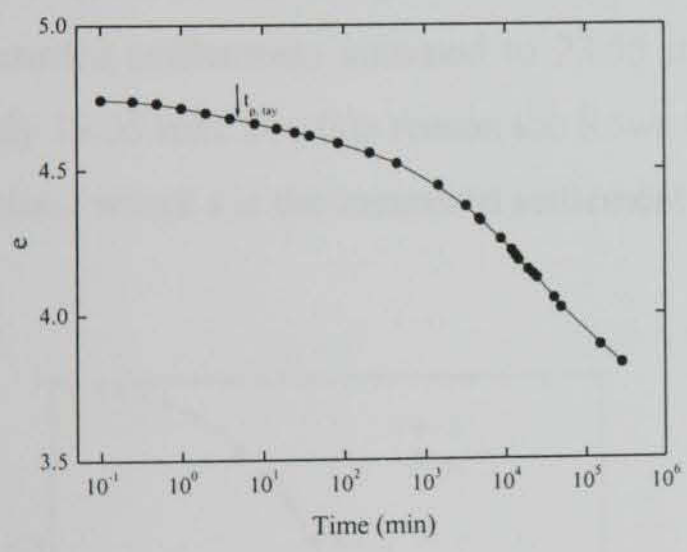

(e)

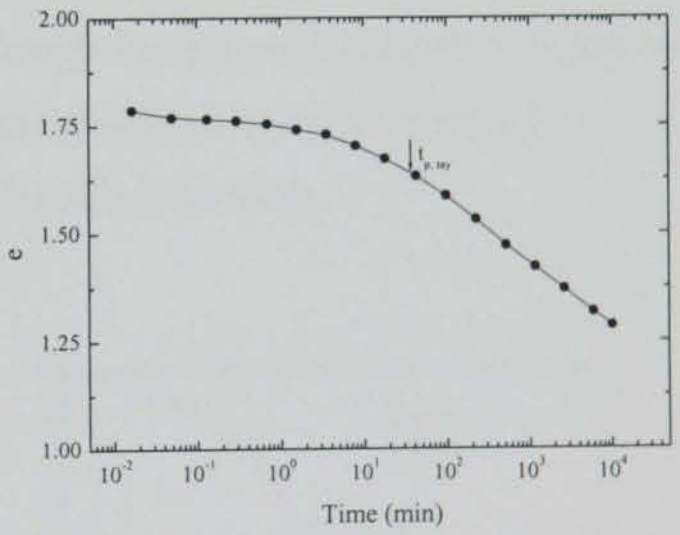

(f)

Figure 4.7 *e* – log *t* curves for stress increments of Clara peat involving high LIDs and various LIRs: (a) CL_MSL_09, 0-20 kPa (LIR=20); (b) CL_MSL_10, 0-27 kPa (LIR=27); (c) CL_MSL_07, 6-50 kPa (LIR=7.3); (d) CL_MSL_08, 10-100 kPa (LIR=9); (e) CL_MSL_08, 100-150 kPa (LIR=0.5); (f) CL_MSL_18, 400-600 kPa (LIR=0.5)

Additional e – log t data for stress increments at various stress levels, involving various LIRs and prolonged LIDs are given in Figure 4.7. The curves depicted in Figure 4.7a – Figure 4.7c are readily identifiable as Type I curves, which is consistent with the e – log t relation for soils with LIR ≥ 1. Figure 4.7d to some degree resembles the Type I curve, although in this instance the initial reduction in the slope of the e – log t plot is too rapid to produce the classic *S*-shape. Figure 4.7e and Figure 4.7f involve LIR values of 0.5 and are typically Type III curves.

In the tests described previously, no pore water pressure measurements were made. The results of two Rowe cell tests on Clara peat are now presented.

Difficulties were encountered in translating observed settlements during Rowe cell tests into actual values of void ratio. Peat specimens were prepared in a standard oedometer ring, 19.05 mm in height and 76.2 mm in diameter. The specimen was then removed from the ring, carefully placed between porous stones and placed in the Rowe cell. The drainage valve is then turned off and water pressure applied to the bellofram until contact with the specimen is made. However, it is difficult to establish the exact point of contact, as relatively large settlements are observed even though drainage is prevented. Measured settlements are not necessarily due solely to the compression of the peat, but may also incur movement of the bellofram relative to the surface of the peat specimen. These *bedding* errors can be quite severe, as is exemplified by Test CL_MSL_19 in which the recorded settlements summed to 23.55 mm, although the trimmed specimen height was only 19.05 mm. For this reason the Rowe cell tests considered here are presented as s – log t plots, where s is the measured settlement for each stress increment.

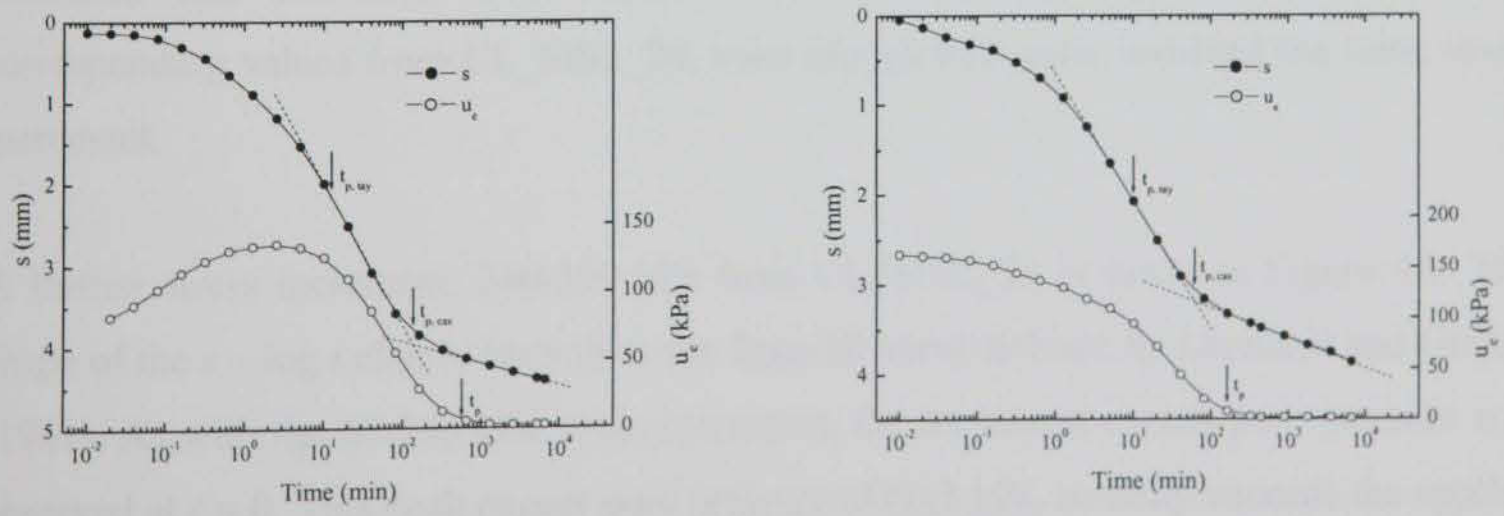

Figure 4.8 s – log t and u_e – log t data for (a) CL_MSL_20, 60-240 kPa, (b) CL_MSL_21, 60-240 kPa

Figure 4.8a shows settlement and pore pressure data plotted against logarithm of time for the 60-240 kPa stress increment of CL_MSL_20. This stress increment, which corresponds to a LIR of 3, is characterised by a well-defined inflection point which delineates the end of primary consolidation. The shape of the s – log t plot resembles the Type I curve defined by Leonards and Girault (1961). Although the increase in total stress was 180 kPa, the maximum recorded excess pore pressure was 135.7 kPa. This increase in pore pressure corresponds to approximately 75% of the total stress increase. It is also noteworthy that the peak pore pressure occurred 2.5 minutes after the stress increment was applied and the drainage valve opened. Marked on Figure 4.7 is the consolidation duration t_p, which is defined here, and by Edil *et al.* (1991) as the time taken for the measured pore pressure at the base of the specimen to decrease to 5% of its peak value. Also shown on Figure 4.7 are the times $t_{p,cas}$ and $t_{p,tay}$ as defined earlier. The duration of primary consolidation for the 60-240 kPa stress increment of CL_MSL_20 has been estimated as 13 minutes using Taylor's method, and 136 minutes using Casagrande's method. Both of these methods are significantly lower than the measured value of t_p = 572 minutes.

A similar stress increment (60-240 kPa) from CL_MSL_21 is provided in Figure 4.7b. This test differed from CL_MSL_20 in that a back pressure of 50 kPa was applied. Unlike CL_MSL_20, there was no time lag for the pore pressure to reach a maximum value. The peak value of 177.5 kPa which was observed at t = 0, corresponds to 98.6% of the increase in total stress (180 kPa). As before, the end of primary consolidation as estimated using conventional graphical procedures and actual pore pressure measurements are shown. In this instance, $t_{p,tay}$ = 10 minutes, $t_{p,cas}$ = 62 minutes and t_p = 160 minutes. This trend is consistent with that of CL_MSL_20, in that both graphical construction methods underestimate t_p, with Taylor's root time method proving to be least accurate. Both measured and estimated consolidation durations are significantly lower than the corresponding values from CL_MSL_20, even though both tests involved the same stress increment.

A further stress increment, 240-300 kPa from CL_MSL_21 is given in Figure 4.9. The shape of the s – log t clearly resembles the Type III curve defined by Leonards and Girault (1961). As with the 60-240 kPa stress increment, the maximum excess pore pressure was observed at t = 0. This peak excess pore pressure of 66.3 kPa, actually exceeds the applied total stress increase of 60 kPa. However, the actual magnitude of the applied stress increment could well exceed the target value of 300 kPa, as the accuracy is largely

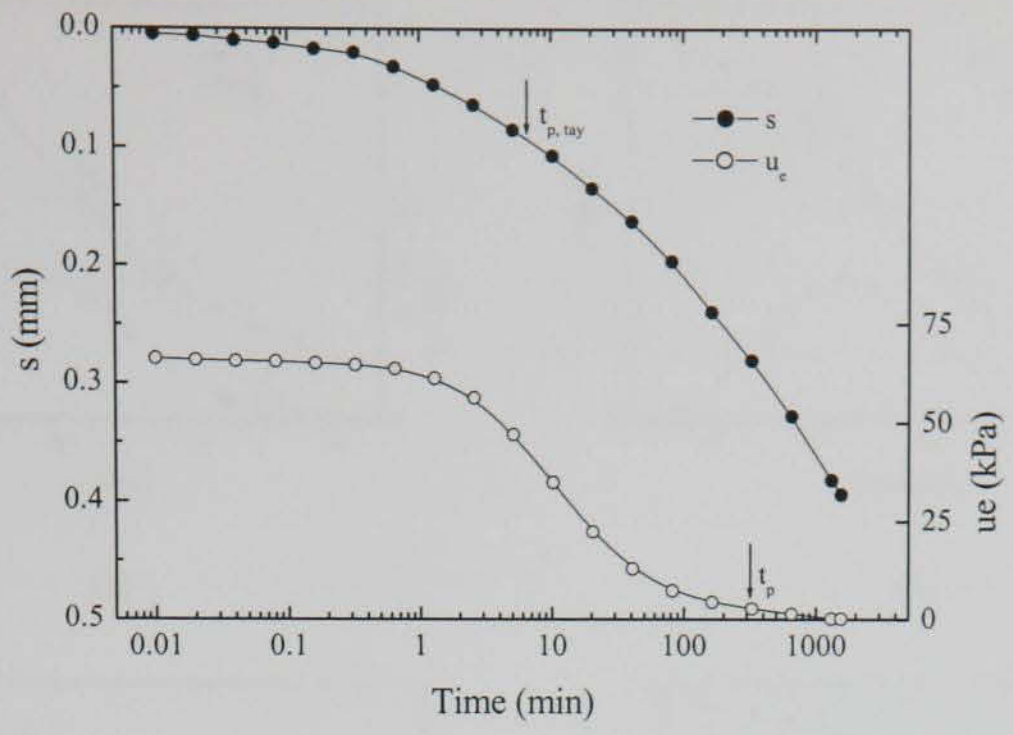

Figure 4.9 s – log t and u_e – log t data for CL_MSL_21, 240-300 kPa

controlled by the resolution of the analogue display used in this test. As the inflection point which approximates the end of primary consolidation in Casagrande's construction method was not observed, $t_{p,cas}$ could not be determined. This is consistent with the stress increments of CL_MSL_08 and CL_MSL_18 (Figure 4.7e and Figure 4.7f respectively) which involved a LIR = 0.5. However, $t_{p,tay}$ in this instance has been estimated as 6.5 minutes. The end of consolidation has been determined from pore pressure measurements as 315 minutes, which is significantly higher than that determined using Taylor's method.

4.4.1.2 Ballydermot peat

Selected stress increments from three tests performed on Ballydermot peat are shown in Figure 4.10. Although BD_CRD_01 was performed in the CRD apparatus, two successive constant stress increments (35-70 kPa, 75-150 kPa) were also applied, following intermittent periods of constant rates of deformation. Figure 4.10a and Figure 4.10b shows s – log t and u_e – log t for the 35-70 kPa and 75-150 kPa stress increments of BD_CRD_01. In both stress increments a considerable amount of time elapses before the excess pore pressure reaches its peak value. Similar behaviour was observed during the 60-240 kPa stress increment of CL_MSL_20, although the time lag involved with BD_CRD_01 is notably larger (6-16 minutes compared with 2.5 minutes). The maximum measured excess pore pressure was considerably lower than the corresponding increase in stress for both increments; 39% for the 35-70 kPa stress increment and 36% for the 75-150

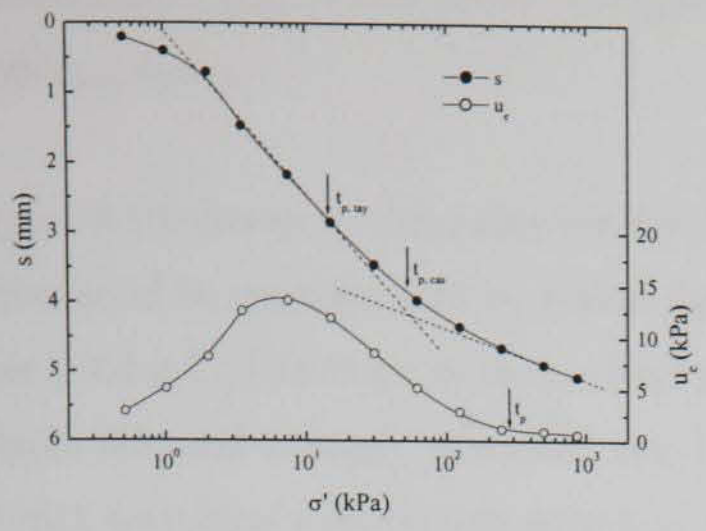

(a)

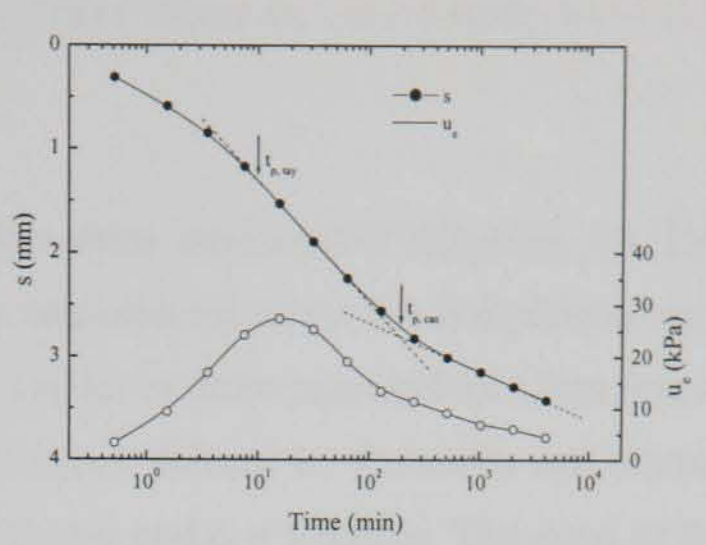

(b)

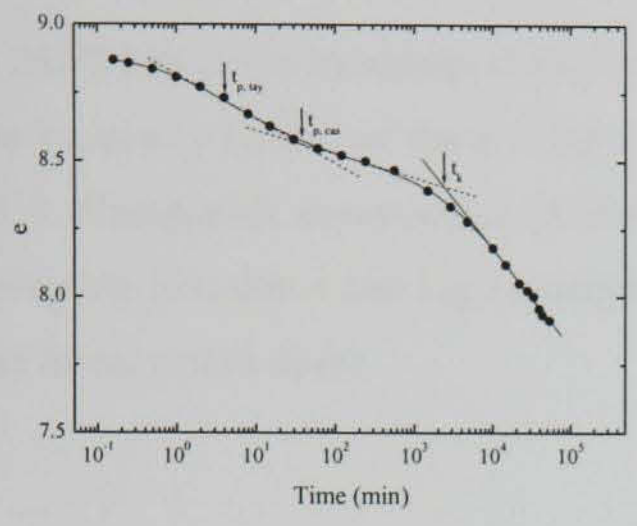

(c)

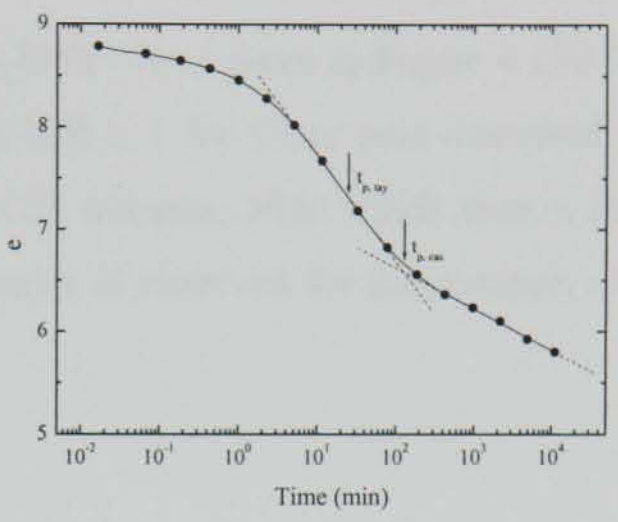

(d)

Figure 4.10 Various Ballydermot peat stress increments: (a) BD_CRD_01, 35-70 kPa; (b) BD_CRD_01, 75-150 kPa; (c) BD_MSL_04, 10-20 kPa; (d) BD_MSL_06, 25-72 kPa

kPa stress increment. As was the case with CL_MSL_20, no back pressure was applied during this test. In the case of the 35-70 kPa stress increment (Figure 4.10a), the excess pore pressure reduces to an approximately constant value of 1 kPa. The end of consolidation, t_p, has been assumed at this point, even though this value is still larger than 5% of the *apparent* peak excess pore pressure. Excess pore pressures reduce more gradually in the 75-150 kPa stress increment (Figure 4.10b), with residual values greater than 4 kPa after 3 days. No satisfactory estimation of the consolidation duration could be obtained in this case.

Both s – log t plots are typical of the Type I curve, with a well-defined point of inflection which has been used to estimate the duration of consolidation, $t_{p,cas}$ using graphical construction. As was the case with CL_MSL_20 and CL_MSL_21, Casagrande's method underestimates t_p determined from pore pressure measurements. The time taken for 90%

consolidation, $t_{p,tay}$, is also shown on Figure 4.10. These values are considerably lower than both $t_{p,cas}$ and t_p.

Figure 4.10c shows e – log t data for the 10-20 kPa stress increment of BD_MSL_04. This stress level is considered to be within the over consolidated range for Ballydermot peat (see § 4.4.2.2). The shape of the e – log t plot is similar to those provided for Clara peat in Figure 4.5, and strongly resembles the Type II curve defined by Leonards and Girault (1961). Graphical construction gave $t_{p,cas}$ = 38 minutes and t_k = 1.6 days. The slope of the assumed creep curve ($t > t_p$) increases gradually with time to a constant value at 4.5 days.

The 25-72 kPa stress increment (LIR=1.88) of BD_MSL_06 is given in Figure 4.10d. This Type I curve is typical of the e – log t plots with LIR > 1 for Clara peat described in § 4.4.1.1. Casagrande construction yielded $t_{p,cas}$ = 129 minutes, after which time a linear relationship between e and log t emerges; the linearity is observed for the duration of the stress increment (8 days).

4.4.1.3 Cork peat

Tests were performed on Cork peat in an attempt to provide comparisons for Clara peat with a less organic, more humified peat. Stress increments from two tests, CK_MSL_01 and CK_MSL_03 are provided in Figure 4.11. CK_MSL_01 relates to a silty peat with an organic content of 32.2% and water content of 208%, whereas CK_MSL_03 relates to a peat with an organic content of 79.5% and a water content of 447%. The transition

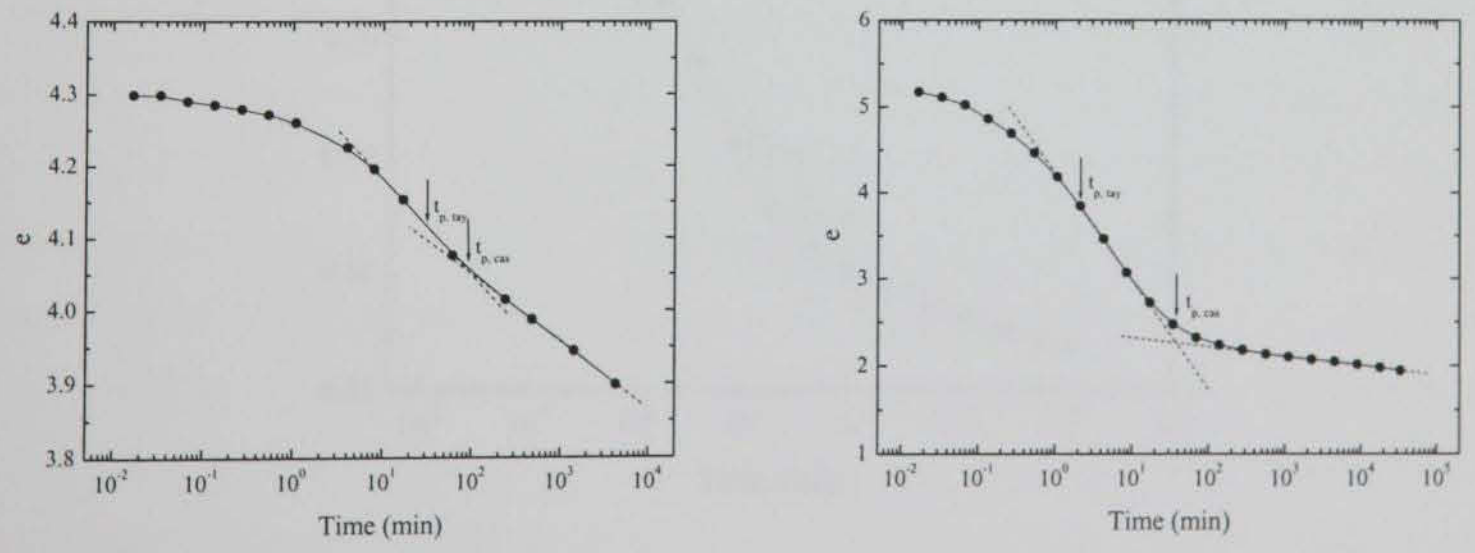

(a) **(b)**

Figure 4.11 e – log t data for Cork peat: (a) CK_MSL_01, 25-50 kPa; (b) CK_MSL_03, 50-600 kPa

between the compression stages of the 25-50 kPa stress increment (CK_MSL_01, see Figure 4.10a) is not as well defined as that for Clara and Ballydermot peat. The 50-600 kPa stress increment of CK_MSL_03 is similar to those obtained for the other high LIR stress increments cases considered in § 4.4.1.1. Casagrande construction yielded $t_{p,cas}$ = 38 minutes, after which time the e – log t plot becomes linear for the duration of the stress increment (23 days).

4.4.1.4 Belfast organic clay

It is generally understood that organic content contributes significantly to creep settlement

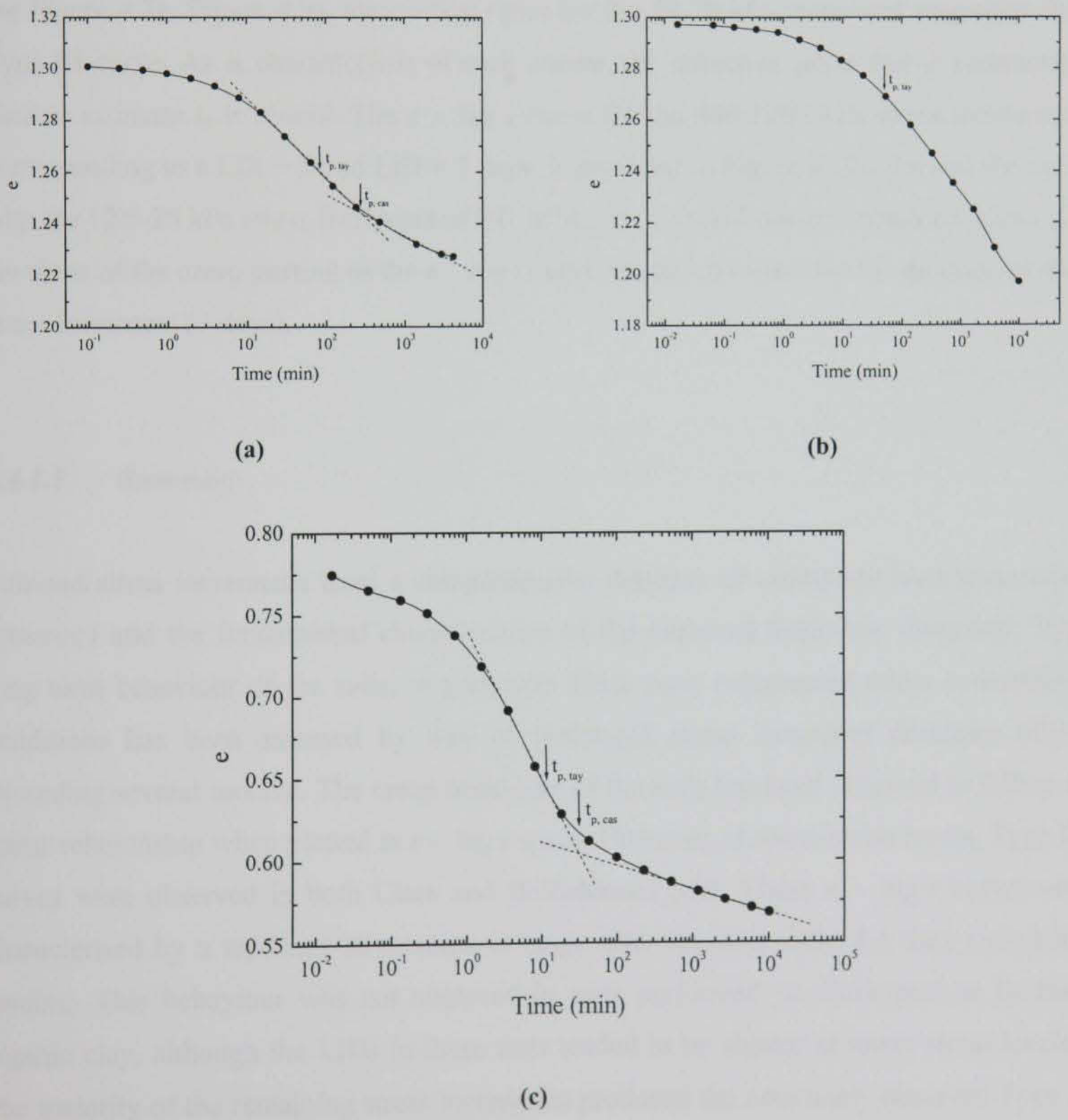

Figure 4.12 e – log t data for Belfast organic clay:
(a) BF_MSL_05, 12.5-25 kPa (b) BF_MSL_07, 50-70 kPa (c) BF_MSL_07, 400-1200 kPa

(Mesri 1973, Mesri *et al.* 1997, O'Loughlin and Lehane 2001). For this reason, the creep characteristics of an organic clay have been assessed. Included in this section are selected results from oedometer tests performed on Belfast organic clay. As before, the influence of prolonged LID and high LIR are examined.

The e – log t relation for the 12.5-25 kPa stress increment of BF_MSL_05 is given in Figure 4.12. As is evident from § 4.4.2.4, this increment is well within the over consolidated stress range. It is apparent from Figure 4.12a that a Type I curve is obtained. However, the creep portion of the e – log t plot tends to reduce in slope at larger values of time. The effect of variable LIR for Belfast organic clay is also shown in Figure 4.12. Both stress increments, 50-70 kPa (Figure 4.12b) and 400-1200 kPa (Figure 4.12c), were obtained from BF_MSL_07. As was the case with corresponding tests on Clara peat (e.g. see Figure 4.7e, Figure 4.9), the e – log t plot for the 50-70 kPa increment resembles the Type III curve. As is characteristic of such curves, the inflection point that is commonly used to estimate t_p is absent. The e – log t curve for the 400-1200 kPa stress increment, corresponding to a LIR = 2 and LID = 7 days, is provided in Figure 4.12c. As was the case with the 12.5-25 kPa stress increment of BF_MSL_05, a Type I curve is obtained, although the slope of the creep portion of the e – log t curve remains constant for the duration of the stress increment (7 days).

4.4.1.5 Summary

Selected stress increments from a comprehensive database of oedometer tests have been presented and the fundamental characteristics of the observed behaviour discussed. The long term behaviour of the soils, in particular Clara peat, compressed under oedometric conditions has been assessed by way of prolonged stress increment durations often exceeding several months. The creep behaviour of the soils has been observed to follow a linear relationship when plotted in e – log t space. However, at lower stress levels, Type II curves were observed in both Clara and Ballydermot peat. These e – log t curves are characterised by a tendency to increase in slope after approximately 2-4 days sustained loading. This behaviour was not observed in tests performed on Cork peat or Belfast organic clay, although the LIDs in these tests tended to be shorter at lower stress levels. The majority of the remaining stress increments produced the commonly observed Type I

curve as defined by Leonards and Girault (1961). Stress increments involving a LIR < 1 resulted in Type III curves, with no clearly defined reversal of slope as with Type I plots.

The end of primary consolidation has been estimated for each stress increment using Taylor's root time method, and where possible, Casagrande's log time method. The latter was only possible for Type I and Type III curves, with a more pronounced demarcation observable in tests with LIR >> 1. In all cases, Taylor's method produced lower values of t_p, with the ratio $t_{p,tay}/t_{p,cas}$ falling between 5-40%.

A limited amount of tests involving pore pressure measurements were performed on Clara and Ballydermot peat. The results of these tests, although being hampered, to some extent, by incomplete sample saturation and poor pore pressure transducer response time, indicated that neither the Casagrande or Taylor methods produced accurate estimates of t_p as determined from measured pore pressure data. Taylor's method resulted in gross inaccuracies, with errors consistently exceeding 95%. The 60-80% error observed with Casagrande's method is less severe but still very significant.

In the tests involving pore pressure measurements, a time lag in the pore pressure response was observed. However, no delay was observed in CL_MSL_21, which was performed under a back pressure of 50 kPa. In the tests in which a back pressure was not applied (CL_MSL_01, BD_CRD_01) the maximum excess pore pressure only reached 35-40% of the applied stress increment for Ballydermot peat, and 75% for Clara peat.

Although the graphical construction methods have been demonstrated to be erroneous, a general trend is discernible, in that the consolidation duration is longer for the higher stress levels and lower void ratios.

4.4.2 Void ratio – effective stress relationship

The relationship between void ratio and effective stress is generally reported in terms of either end of primary (EOP) or 24 hour consolidation data (Burland, 1989). As standard oedometer tests seldom involve pore pressure measurements, graphical construction techniques such as Casagrande's log time method or Tayor's root time method are commonly employed to determine the consolidation duration, and subsequently the EOP e

– log σ' curve. However, as shown in § 4.4.1, and elsewhere by Edil *et al.* (1991), such graphical analytical methods can be seriously erroneous. Consequently, the e – log σ' relationships presented here are reported in terms of 24 hour compression.

This section presents and compares the relationship between measured compression and effective stress.

4.4.2.1 Clara peat

A typical e – log σ' curve for Clara peat is provided in Figure 4.13. This test (CL_MSL_04) involved a wide range of stress levels, from 1 kPa to 512 kPa. The LIR was 1, and the LID 24 hours. The conventional empirical construction method indicates that the apparent preconsolidation stress, σ'_c, is approximately 3 kPa. Beyond this value, the plot is characterised by an increase in curvature, followed by a linear section up to approximately 25 kPa. It is useful to determine the range of linearity of the e – log σ' curve in the virgin stress range. This is conveniently expressed in terms of the ratio, σ'_{lin} / σ'_c, where σ'_{lin} is the limiting value of effective stress beyond which the e – log σ' relationship becomes non-linear. As determined from CL_MSL_04, σ'_{lin} = 25 kPa, resulting in σ'_{lin} / σ'_c = 8.3 for Clara peat. The e – log σ' curve becomes highly non-linear at stresses greater than 25 kPa. The compressibility of the soil is reflected in the measured overall reduction in void ratio, Δe, of 30.

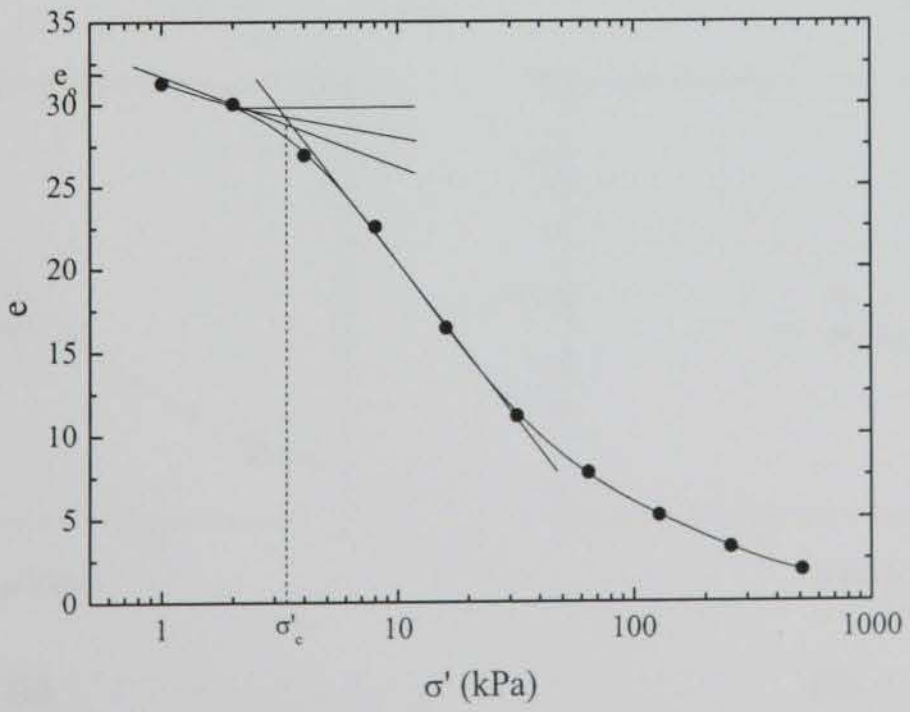

Figure 4.13 Typical e – log σ' relationship for Clara peat: CL_MSL_04

Tests CL_MSL_14 to CL_MSL_17 inclusive involve a LIR = 1, with LIDs ranging from between 1 and 6 days. The purpose of these tests was to examine the influence of unloading and subsequent reloading at moderate stress levels (40-50 kPa). Further unloading took place at higher stresses (640-800 kPa). The specimens were permitted to swell for between 1 and 6 days during these unloading sequences.

The results of two of these tests are shown in e – log σ' format in Figure 4.14. As with CL_MSL_04, the e – log σ' relationship is highly non-linear for both tests. However, unlike CL_MSL_04, no apparent preconsolidation stress is determinable from first time loading. The initial stress increment of CL_MSL_16 and CL_MSL_17 is 5 kPa and 6.25 kPa respectively. These values are higher than σ'_c = 3 kPa, as determined from CL_MSL_04, and explains why an initial virgin e – log σ' relationship is observed in Figure 4.14.

The unload-reload loops in Figure 4.14 are typical of that observed in mineral soils. Only a slight decrease in void ratio is observed after reloading to the previous maximum stress (40 kPa, CLMSL_16; 50 kPa, CL_MSL_17). The effect of the unload-reload loop causes only a slight disturbance to the measured stress-strain relationship, with the soil state rejoining the initial e – log σ' curve shortly after the previous maximum stress is exceeded.

Figure 4.15 shows the e – log t response of the peat during unloading for both CL_MSL_14 and CL_MSL_15. In this discussion, the first stress decrement is defined as

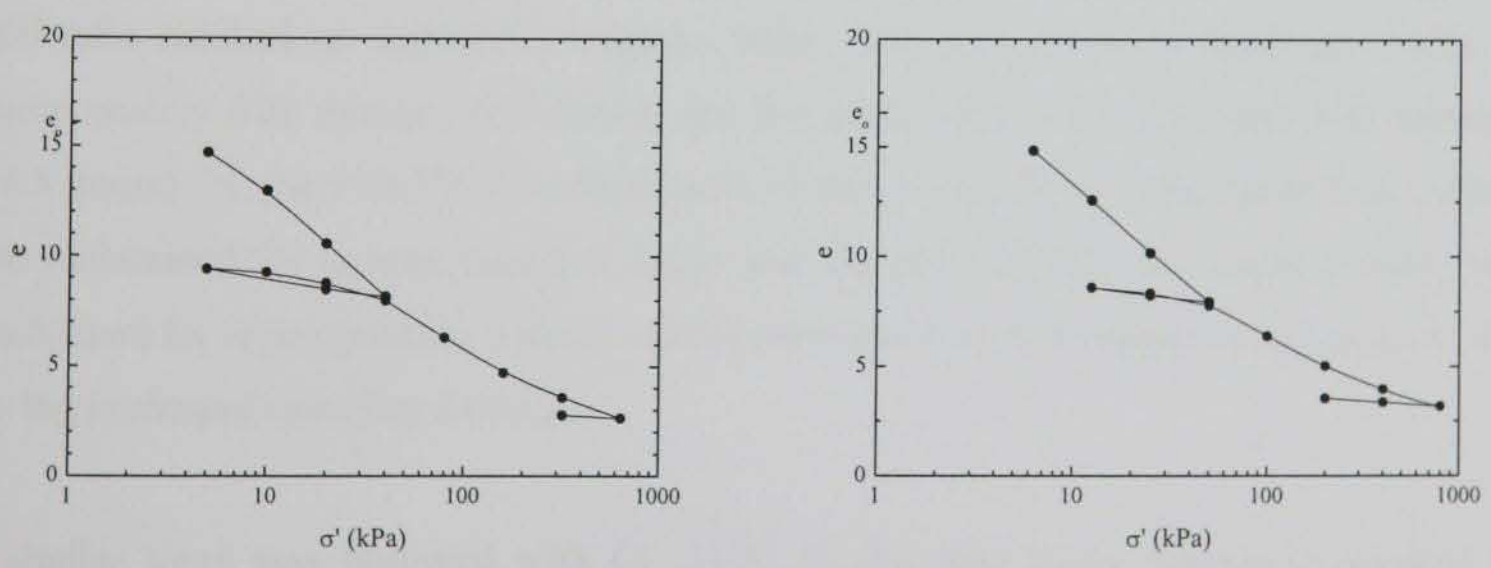

Figure 4.14 Effect of unloading and subsequent reloading on the measured e – log σ' relationship for Clara peat: (a) CL_MSL_16, (b) CL_MSL_17

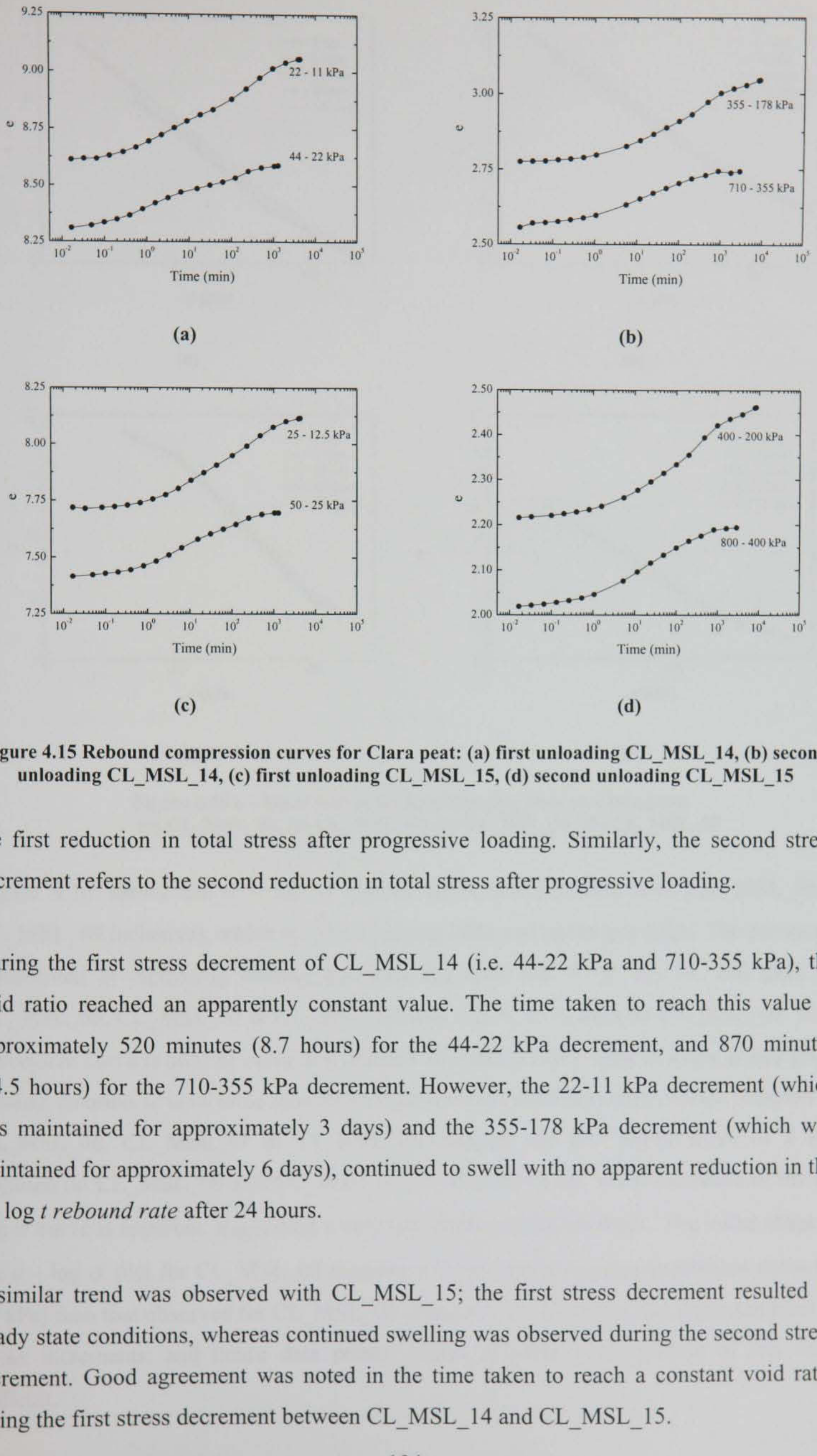

Figure 4.15 Rebound compression curves for Clara peat: (a) first unloading CL_MSL_14, (b) second unloading CL_MSL_14, (c) first unloading CL_MSL_15, (d) second unloading CL_MSL_15

the first reduction in total stress after progressive loading. Similarly, the second stress decrement refers to the second reduction in total stress after progressive loading.

During the first stress decrement of CL_MSL_14 (i.e. 44-22 kPa and 710-355 kPa), the void ratio reached an apparently constant value. The time taken to reach this value is approximately 520 minutes (8.7 hours) for the 44-22 kPa decrement, and 870 minutes (14.5 hours) for the 710-355 kPa decrement. However, the 22-11 kPa decrement (which was maintained for approximately 3 days) and the 355-178 kPa decrement (which was maintained for approximately 6 days), continued to swell with no apparent reduction in the $e - \log t$ *rebound rate* after 24 hours.

A similar trend was observed with CL_MSL_15; the first stress decrement resulted in steady state conditions, whereas continued swelling was observed during the second stress decrement. Good agreement was noted in the time taken to reach a constant void ratio during the first stress decrement between CL_MSL_14 and CL_MSL_15.

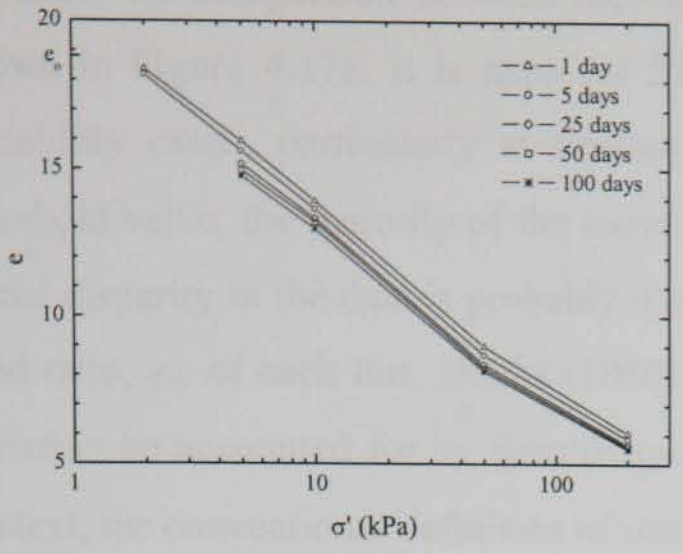

(a)

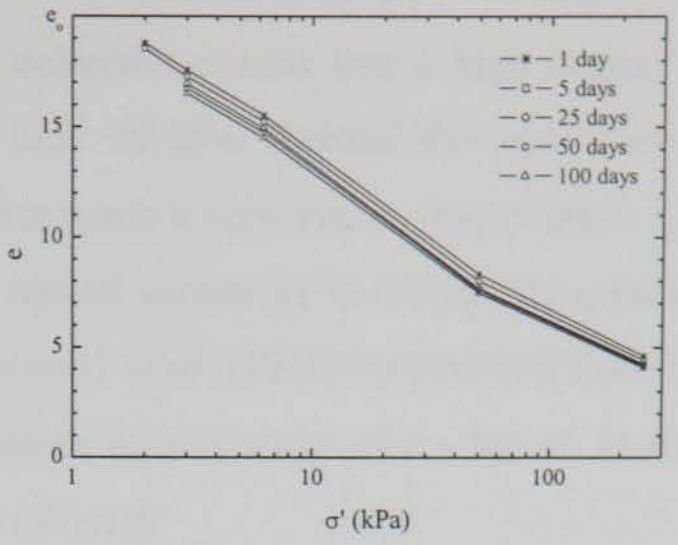

(b)

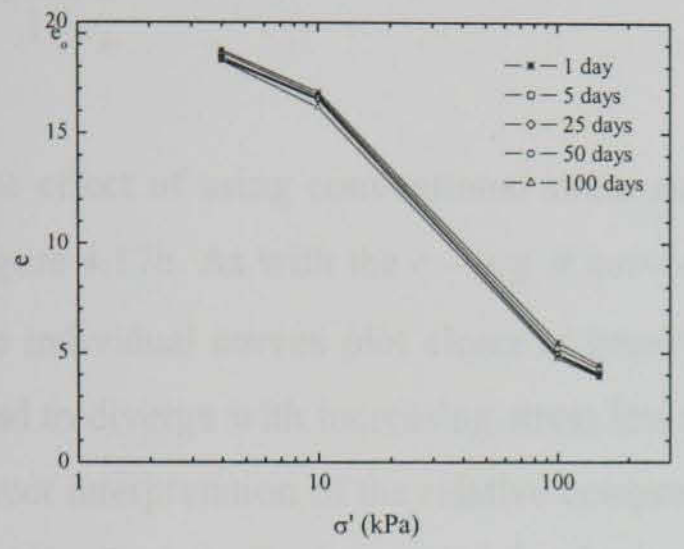

(c)

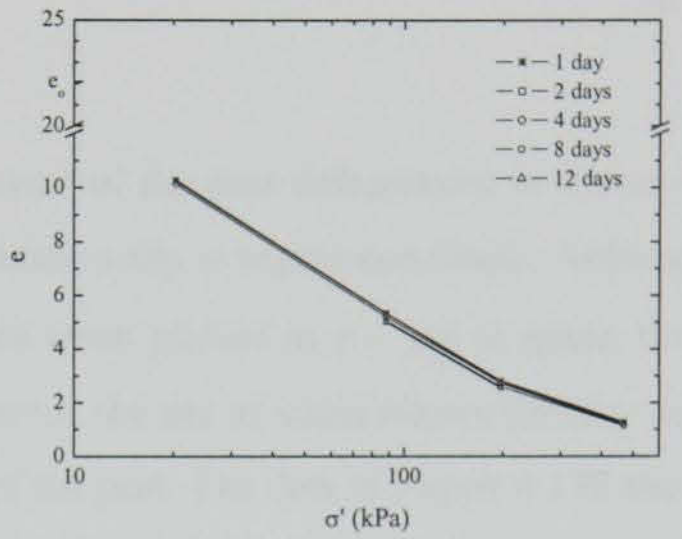

(d)

Figure 4.16 e – log σ' curves for long duration tests on Clara peat: (a) CL_MSL_06, (b) CL_MSL_07, (c) CL_MSL_08, (d) CL_MSL_09

Figure 4.16 shows the e – log σ' curves for 4 non-standard tests (CL_MSL_06 – CL_MSL_09 inclusive), which involved varying LIRs and prolonged LIDs. The curves are represented at increasing loading durations for each test; 1, 5, 25, 50, 100 days for CL_MSL_06, CL_MSL_07 & CL_MSL_08, and 1, 2, 4, 8, 12 days for CL_MSL_09. Each successive curve is seen to occur at a reduced void ratio. The e – log σ' curve at any given loading duration is seen to be non-linear even over the moderate stress levels imposed on CL_MSL_06, CL_MSL_07 & CL_MSL_08. Despite the low initial stress of 2 kPa imposed on CL_MSL_06 and CL_MSL_07, no increase in the initial curvature of the e – log σ' curve is apparent, suggesting a very low preconsolidation stress. The initial shape of the e – log σ' plot for CL_MSL_08 suggests a higher apparent preconsolidation stress (4-10 kPa) than that observed for CL_MSL_04 (Figure 4.13). However, the limited number of stress increments, and hence data points, makes accurate determination of this value difficult.

To allow for comparison between the various e – log σ' curves, several test results are shown in Figure 4.17a. It is apparent from the collective results that a high degree of variability exists, particularly at stresses lower than 20 kPa. Beyond this approximate threshold value, the majority of the curves merge towards a common e – log σ' state. The initial disparity in the data is probably due to the natural variability in the initial measured void ratio, e_o, of each test. Hobbs (1986) and Leroueil *et al.* (1985) recommend that this variation be accounted for by describing compression data in terms of ε – log σ'. In this context, the conventional definition of strain, ε, is adopted:

$$\varepsilon = \frac{\Delta e}{1 + e_o} \qquad 4.1$$

The effect of using conventional strain as a measure of the peat deformation is shown in Figure 4.17b. As with the e – log σ' curves, the relationship is highly non-linear. Although the individual curves plot closer at lower stresses when plotted in ε – log σ' space, they tend to diverge with increasing stress level. However, the use of strain allows for easy and direct interpretation of the relative compression of the peat. The data in Figure 4.17b show that the final strain at stress levels of approximately 300-800 kPa generally falls within 80-95%.

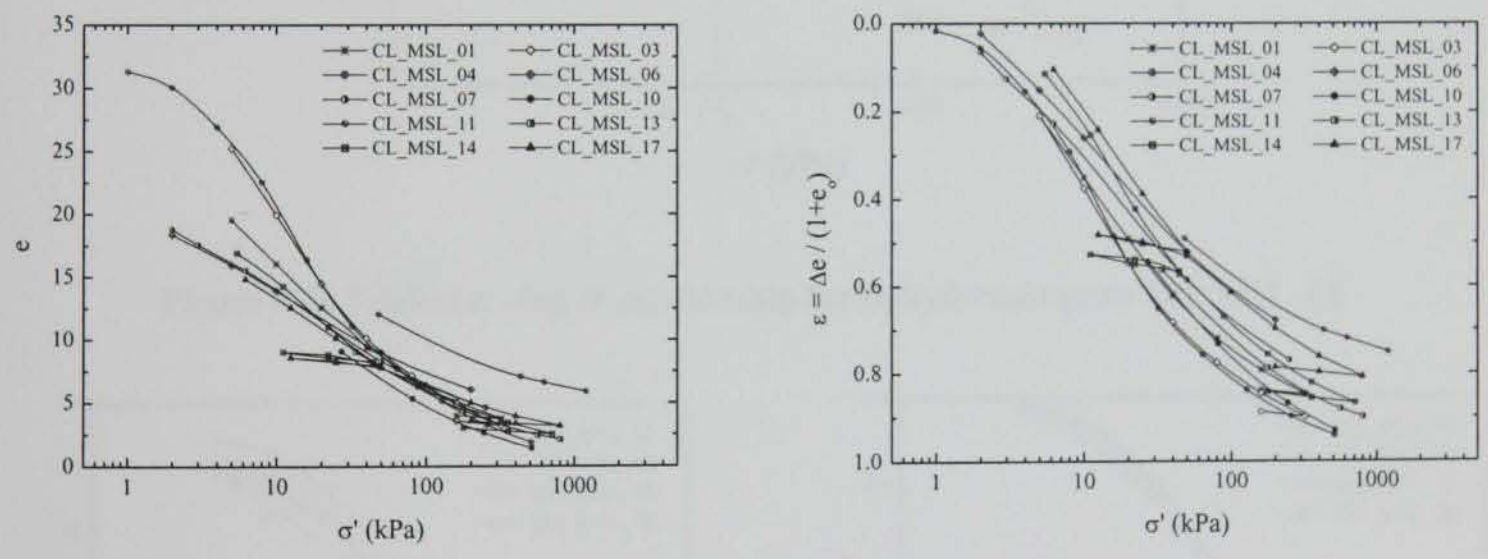

Figure 4.17 Comparison of measured 24 hour (a) e – log σ' (b) ε – log σ' data for Clara peat

4.4.2.2 *Ballydermot peat*

The relationship between void ratio and logarithm of effective stress for BD_MSL_02 is given in Figure 4.18. The preconsolidation stress, σ'_c, in this case has been estimated as 17 kPa, which agrees well with σ'_c = 15 kPa, as reported by Hebib (2001). The virgin e – log σ' curve remains linear up to σ'_{lin} = 80 kPa, resulting in σ'_{lin} / σ'_c = 4.7. As with Clara peat, the e – log σ' curve eventually follows a non-linear relationship.

Comparisons between the 24 hour e – log σ' curves for Ballydermot peat are shown in Figure 4.19. As with Clara peat, both void ratio, e, and strain, ε, are employed as a measure of the soil compression. The variation in the plots is much less severe for the limited

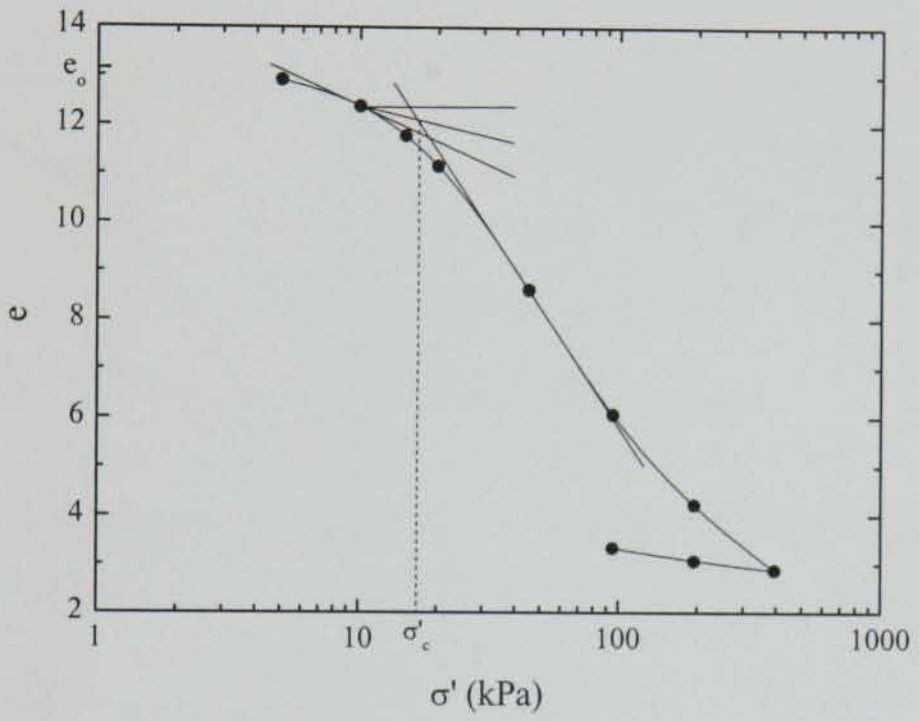

Figure 4.18 Typical e – log σ' relationship for Ballydermot peat: BD_MSL_02

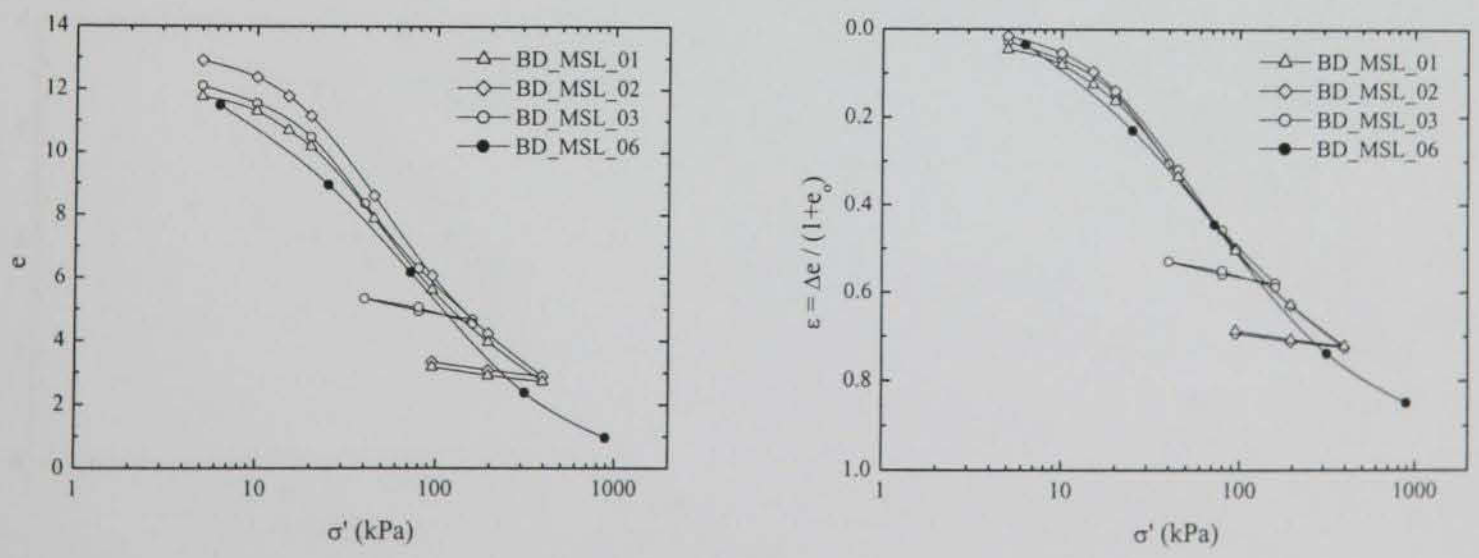

Figure 4.19 Comparison of measured 24 hour (a) e – log σ' (b) ε – log σ' data for Ballydermot peat

amount of data available for Ballydermot peat. Unlike the Clara test results, the overall agreement between the respective tests appears to be increase slightly whenever strain is used to describe the soil compression. The final strain, corresponding to a stress level of 400 kPa is approximately 70%; the higher stress level of approximately 900 kPa in BD_MSL_06 resulted in a final strain of approximately 85%.

4.4.2.3 Cork peat

The limited amount of test data from Cork peat is presented in Figure 4.20 and Figure 4.21. As before, graphical construction methods have been employed to estimate σ'_c. This resulted in σ'_c = 48 kPa for Cork silty peat (CK_MSL_01, Figure 4.20a), and σ'_c = 36 kPa

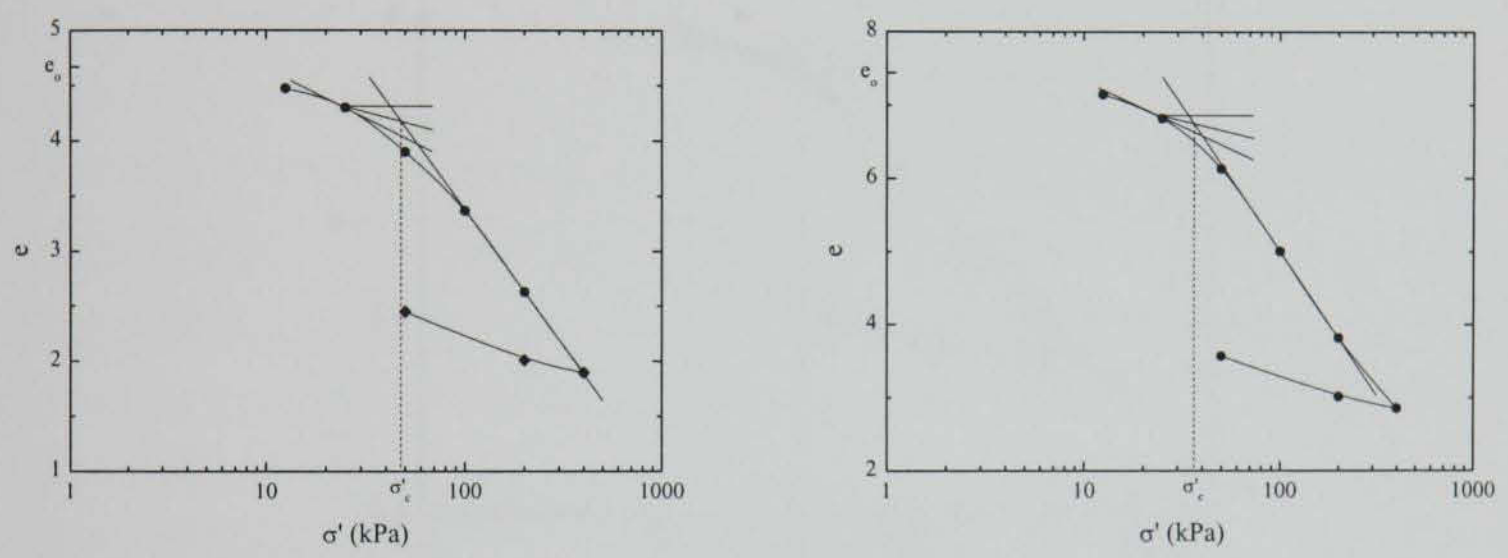

Figure 4.20 Typical e – log σ' relationships for:
(a) Cork silty peat: CK_MSL_01, (b) Cork peat: CK_MSL_02

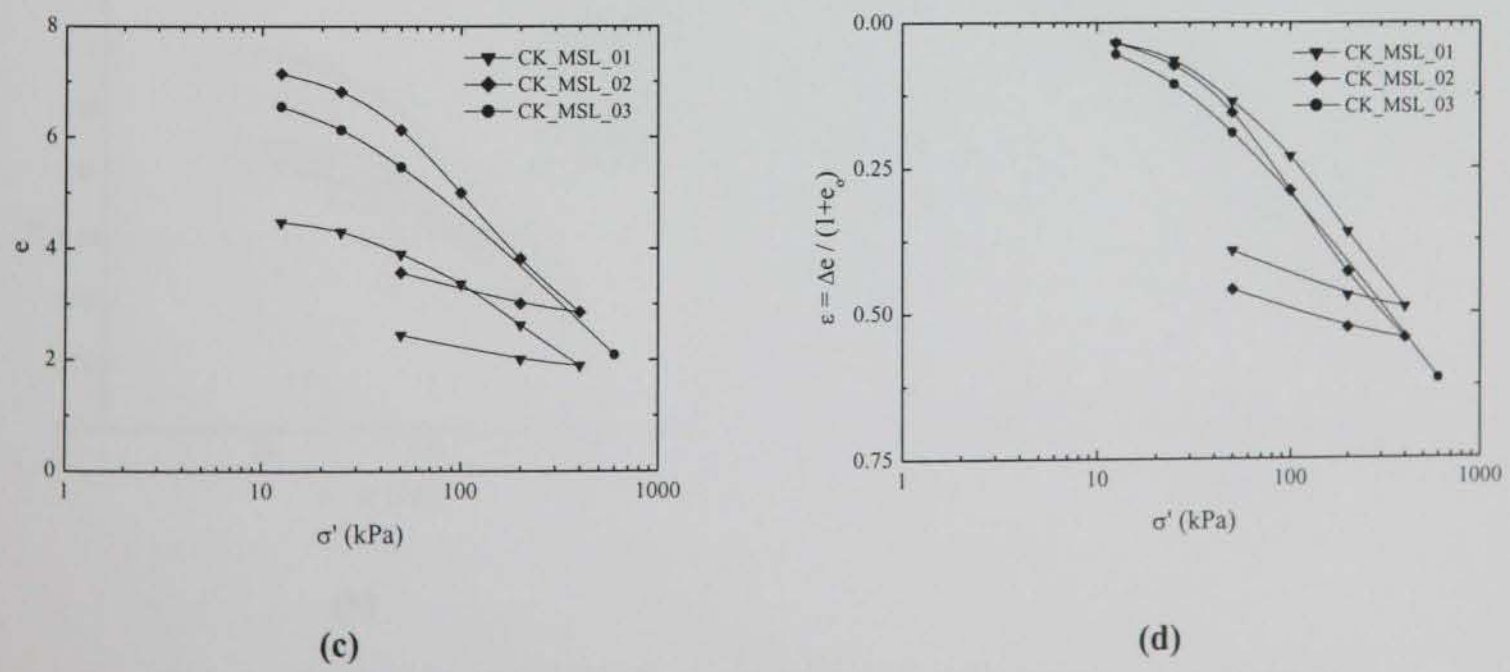

Figure 4.21 Comparison of measured 24 hour (a) e – log σ' (b) ε – log σ' data for Cork peat

for Cork peat (CK_MSL_02, Figure 4.20b). The virgin sections of the e – log σ' curve remained linear up to the maximum stress of 400 kPa for CL_MSL_01, whereas slight concavity is apparent beyond 200 kPa for CL_MSL_02, resulting in $\sigma'_{lin} / \sigma'_c = 5.5$. Figure 4.21a compares the separate e – log σ' curves. It is apparent that Cork silty peat (CK_MSL_01) is less compressible; this is reflected further in the corresponding ε – log σ' plot in Figure 4.21b.

4.4.2.4 Belfast organic clay

A typical e – log σ' curve for Belfast organic clay is provided in Figure 4.22. The data,

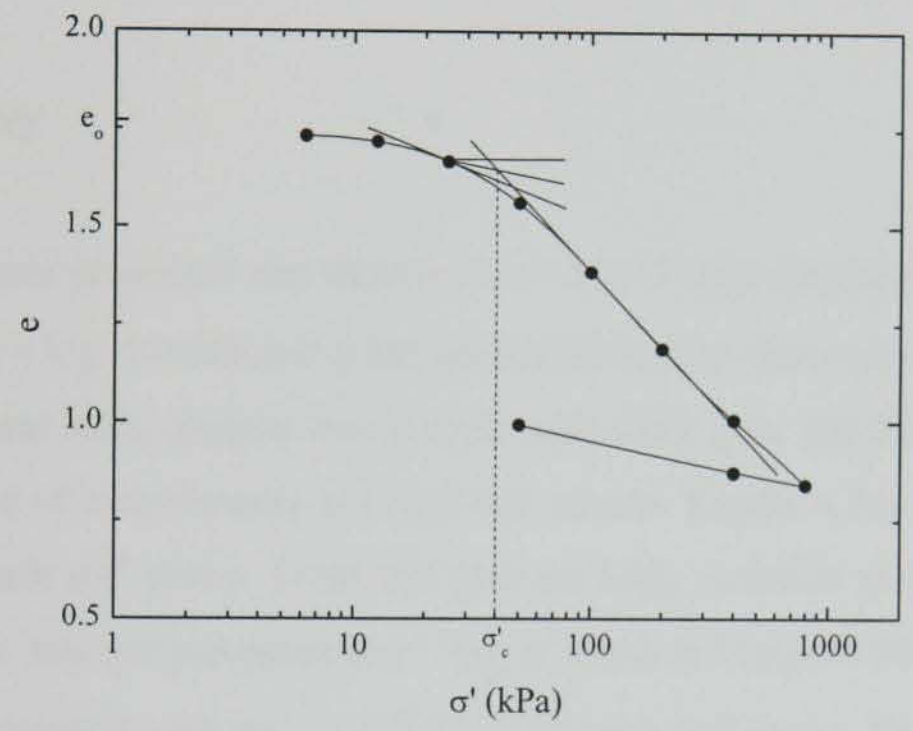

Figure 4.22 Typical 24 hour e – log σ' relationship for Belfast organic clay: BF_MSL_04

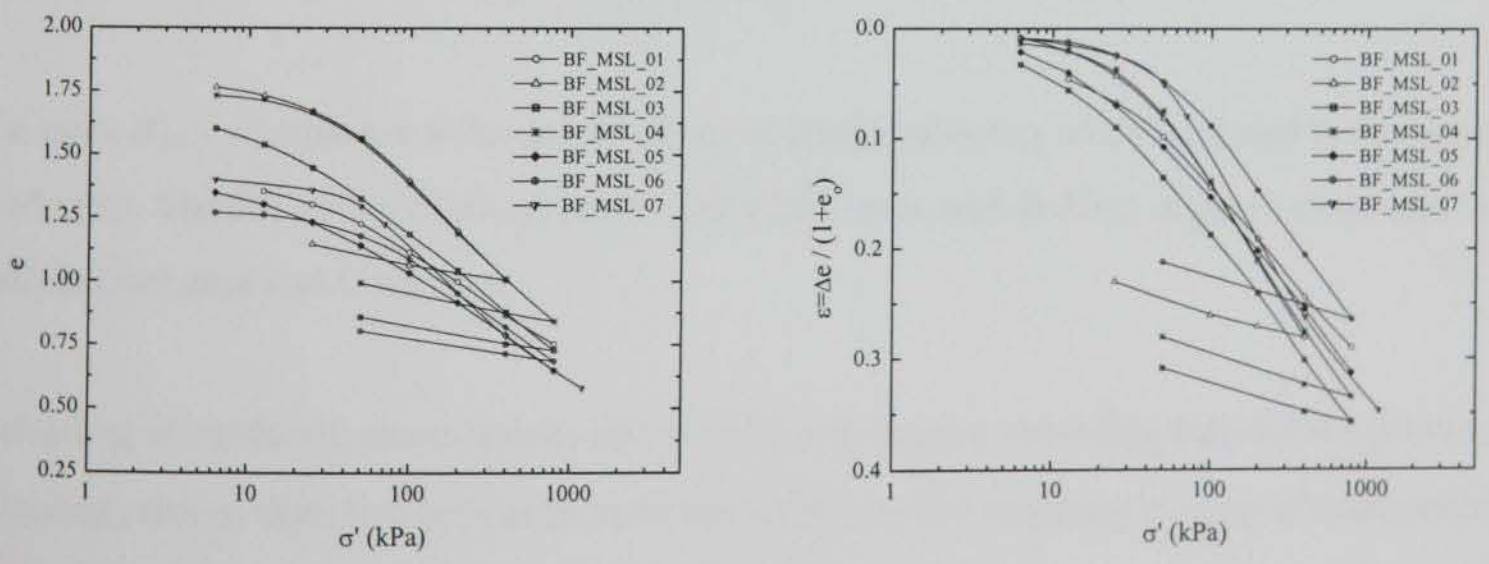

(b) **(c)**

Figure 4.23 Comparison of 24 compression data for Belfast organic clay using (a) void ratio, e (b) strain, ε

which were derived from BF_MSL_04, indicates that the virgin e – log σ' relationship remains linear up to approximately 340 kPa. Graphical construction methods yield $\sigma'_c = 40$ kPa, resulting in $\sigma'_{lin} / \sigma'_c = 8.5$. The test data are characterised by lower void ratios than those encountered in the peat soils. Figure 4.23a and Figure 4.23b allows the compression data for all the tests to be readily compared. The test curves tend to be relatively well spaced, with an approximately constant preconsolidation stress. Overall, the virgin e – log σ' relationship is only slightly non-linear. BF_MSL_01 and BF_MSL_04 follow a relatively unique relationship, whereas the remaining tests show no apparent common e – log σ' relationship. Evidently the variations in the initial void ratio between tests has a direct bearing on the final e – log σ' state. Plotting the same data in ε – log σ' space has an adverse effect, as the resulting curves tend to diverge with increasing stress.

4.4.2.5 Summary

The previous sections presented and described e – log σ' data for the soils considered. A highly non-linear e – log σ' relationship has been observed for the more compressible Clara and Ballydermot peat soils. Similar trends exist with Cork peat and Belfast organic clay, although the degree of non-linearity is much less severe. Figure 4.24a compares selected test results from each soil group. From this plot the high variation in initial void ratio is apparent. The same data are presented in ε – log σ' space in Figure 4.24b. The variation in σ'_c is seen to be consistent with the overall strain of each soil group. Not surprisingly, this trend is also linked to the initial void ratio, with the larger measured strains corresponding to the soils with lower e_o and higher σ'_c values.

The ratio $\sigma'_{lin} / \sigma'_c$ appears to be independent of compressibility of the soil and hence initial void ratio. Similar ratios were observed for Clara peat and Belfast organic clay, and for Ballydermot peat and Cork peat.

Unloading at moderate stress levels, followed by subsequent reloading beyond the previous maximum stress, does not appear to have any effect on the resulting e – log σ' relationship for Clara peat. However, the swelling of the peat specimens was monitored for 1 day during the first stress decrement, and between 3 and 6 days during the second stress decrement. Steady state conditions were reached in less than 15 hours for the first stress

decrement, whereas no tendency to reach a constant steady state (as determined from e – log t data) was observed during the second stress decrement, even after 6 days. Relatively similar trends were observed in all four tests (CL_MSL_14 – CL_MSL_17 inclusive).

The results of tests on Clara peat involving LIDs in excess of 100 days have been presented in e – log σ' at increasing durations of sustained loading. Successive curves plotted at lower values of void ratio, indicating the time dependency of Clara peat. Similar methodology could not be applied to the other soil groups, as tests with high LID tended to be confined to one or two stress increments.

4.5 CRD TEST

The CRD test was first proposed by Hamilton and Crawford (1959) as a convenient and rapid means of determining the preconsolidation stress, σ'_c, and void ratio-effective stress relationship. Two main advantages of the CRD test over the conventional MSL oedometer test have contributed to its growing acceptance and widespread use:

1. Reduced testing time: for standard tests, the test duration may be reduced from 7 – 10 days to less than 1 day
2. Higher resolution of the measured stress-strain curve: stress-strain relationships derived from MSL oedometer tests are often based on a limited number of data points

In addition, CRD tests are more easily automated that MSL oedometer tests, as the latter

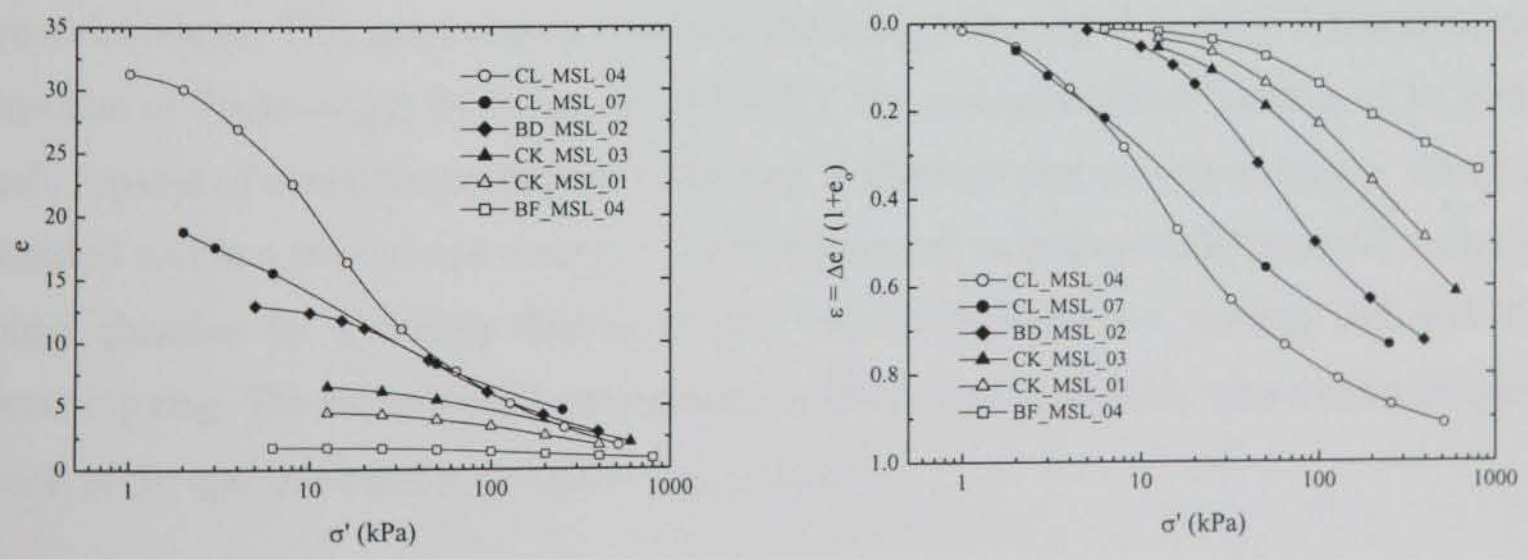

Figure 4.24 Comparison of 24 hour e – log σ' curves for the various soil types using: (a) void ratio, e (b) strain, ε

generally requires the application of additional dead loads every 24 hours.

However, the popularity of the CRD test has been influenced by the disagreements surrounding the selection of an appropriate rate of deformation (Sheahan and Watters, 1997). Most of the proposed selection guidelines are based on the ratio of excess pore pressure at the base of the specimen to the total stress increment (u_e/σ). Smith and Wahls (1965) recommend that the imposed rate of deformation results in $u_e/\sigma \leq 0.5$, whereas Wissa *et al.* (1971) advocate the use of a deformation rate slow enough to yield $u_e/\sigma \leq 0.05$. In a later study, Gorman *et al.* (1978) concluded that the chosen rate of deformation rate should be high enough to cause $u_e \geq 7$ kPa, whilst ensuring that $u_e/\sigma \leq 0.3 - 0.5$.

Various investigations, such as that of Graham *et al.* (1983) and Leroueil *et al.* (1985), into the influence of deformation rate in CRD tests, have played a significant role in the understanding and interpretation of time and rate effects on the measured stress-strain response of soft clays. Despite the relative abundance of CRD experimental data on clays in the literature, few CRD data are available for peat. The research programme described in this chapter therefore includes several CRD tests on Clara peat (see Table 4.3). The main aim of the CRD tests is to examine the deformation rate dependency on the measured stress-strain response.

4.5.1 Description of CRD apparatus

CRD tests have been carried out at TCD using a Wykeham Farrance WF26050 consolidometer. This apparatus is based on the design developed at MIT (Massachusetts Institute of Technology) by Wissa *et al.* (1971). The consolidometer consists of an inner cell, capable of containing a specimen 100 mm in diameter and 20 mm in height, which is situated within a triaxial cell chamer. The specimen cell is hydraulically isolated from the outer chamber by a rolling diaphragm seal located between the loading cap and the retaining ring. The experimental arrangement is shown in Figure 4.25, with a more detailed view of the specimen cell provided in Figure 4.26b.

Initial testing showed this arrangement to be unsuitable for compressible soils such as fibrous peat. The author proposed a series of modifications that were implemented by Wykeham Farrance and TCD. The first change was to increase the maximum stroke of the

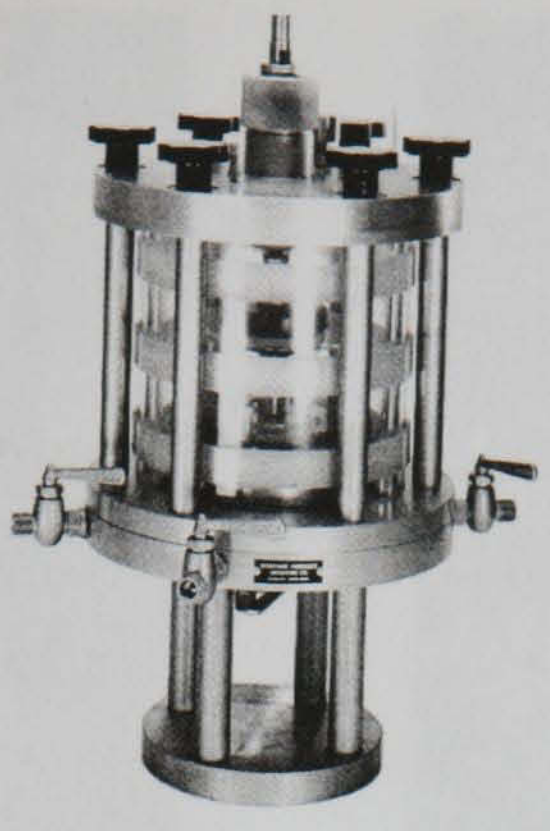

Figure 4.25 Wykeham Farrance WF26050 consolidometer

loading cap of the specimen cell. Initially this was restricted to 14 mm, or a strain of 70%. However, as is evident from the test results described in § 4.4.2, strains of up to 95% at moderate stresses are commonplace in peat. The modified specimen cell allowed for a maximum stroke of 19 mm, or 95% strain.

Secondly, the outer chamber was removed. This was deemed beneficial as the absence of the cell allowed for complete control over the docking of the specimen, and any necessary adjustments such as slight tilting of the loading cap during the initial stages of testing.

The third and final modification was the removal of the back pressure controller. This was particularly necessary in CRD tests involving intermittent incremental stress increments similar to those in MSL oedometer tests. In these cases, the GDS 3MPa/200 cc pressure/volume controllers failed to respond quickly enough to the large volume changes associated with stepped stress increments. This resulted in a build up of back pressure and hence reduction in effective stress on the specimen. Removal of the back pressure controller alleviated this problem.

The newly adapted CRD testing arrangement is shown in Figure 4.26. The index for the annotation in Figure 4.26 is as follows:

1. Specimen cell
2. Stresses measured by load cell of 5 kN capacity (equivalent total stress of 640 kPa)

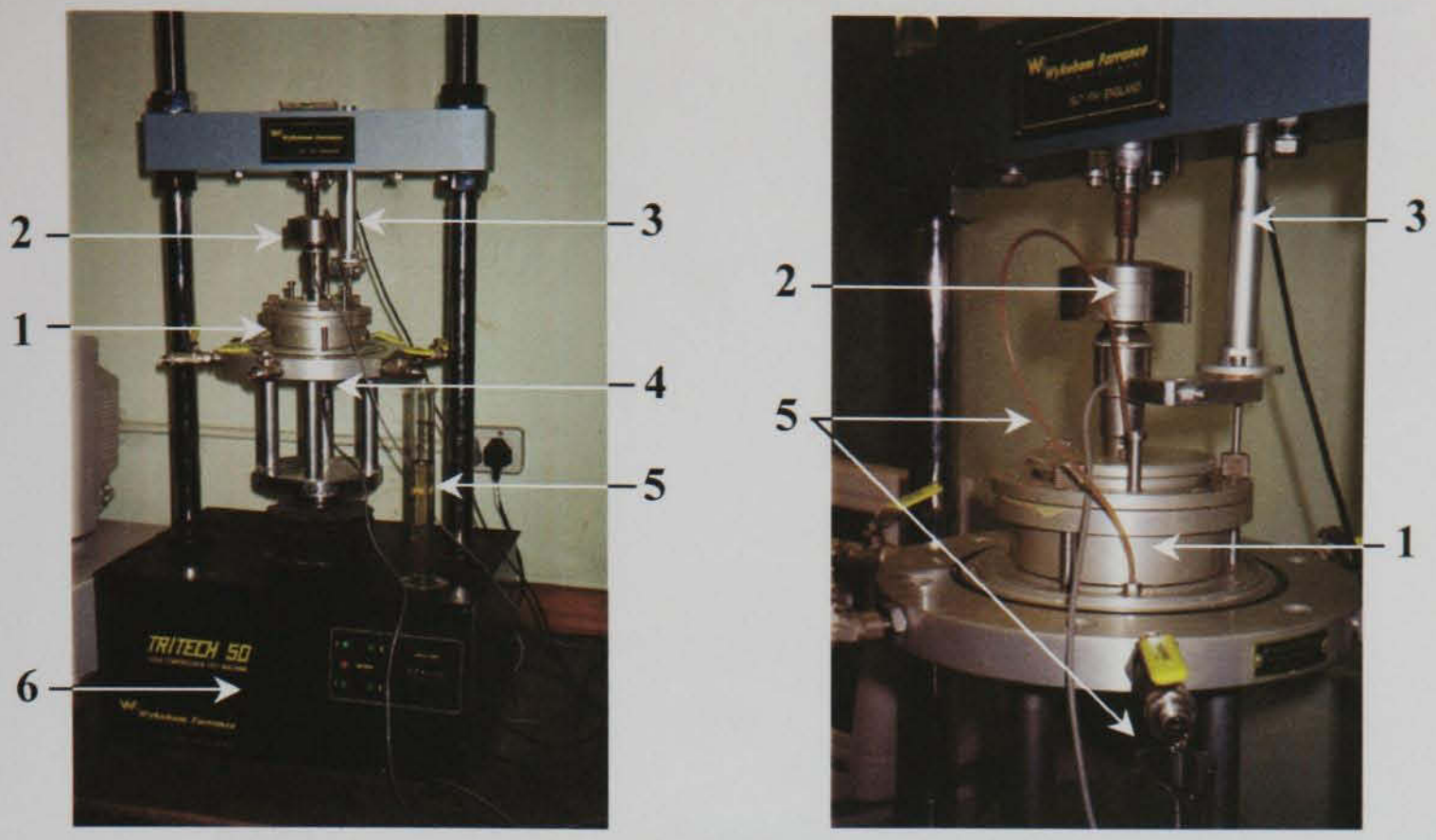

Figure 4.26 Modified CRD apparatus used in TCD

3. Settlement measured by means of a standard LVDT (Linear Variable Differential Transformer) displacement transducer, mounted on the base of the load cell
4. Drainage from the top of the specimen into a standard volume measurement cylinder
5. Pore pressures measured at the base of the specimen
6. Wykeham Farrance Tritech 50 kN loading frame

Settlement, axial force and pore pressure data are logged via an 8-channel GDS data acquisition pad. The rate of deformation may be preset on the loading frame, or controlled by the data acquisition and control software, GDSLAB. A logging frequency of either 30 or 60 seconds was generally adopted to provide high resolution stress-strain data.

4.5.2 Test Results

Numerous CRD tests were performed on Clara peat, although many had to be interrupted and discarded due to severe tilting of the loading cap. Despite efforts to ensure that the loading cap remained parallel to the specimen cell, tilting remained a common problem, particularly with the original experimental arrangement, which included the outer cell chamber. Even slight tilts resulted in the loading cap eventually becoming lodged within

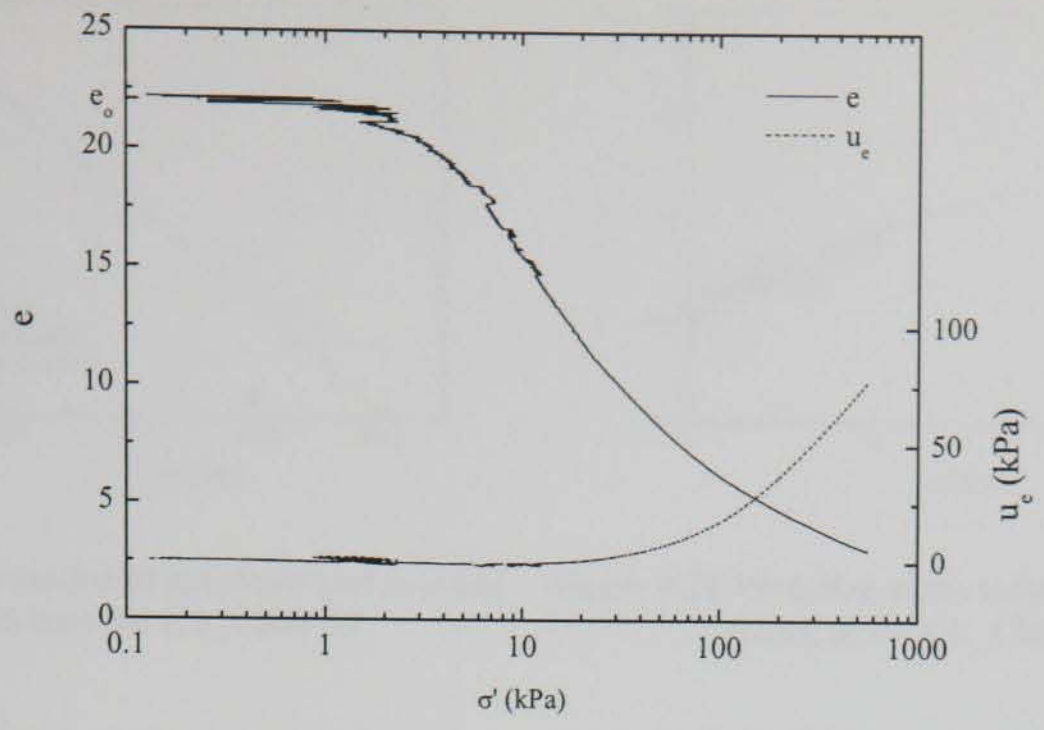

Figure 4.27 Measured e – log σ' and u_e – log σ' data for CL_CRD_04

the specimen cell. A total of nine successful CRD tests have been included in the experimental programme described in this chapter. Many of the tests, such as CL_CRD_05 and CL_CRD_06 involved stepped changes in the deformation rate, resulting in prolonged test durations, often exceeding three weeks.

The measured e – log σ' response of CL_CRD_04 is provided in Figure 4.27. Although the deformation rate for this test was set at 0.01 mm/min, or strain rate, $r = 8.33 \times 10^{-6}$ sec^{-1}, the actual measured rate of deformation actually decreased a little over the course of the test. In a number of the CRD tests, the axial force, and hence specimen stress, was measured using an external proving ring and not the load cell shown in Figure 4.26. The measured reduction in r during CL_CRD_04 was considered to be due to increasing deformation of the proving ring as the soil specimen stiffens. This is illustrated in Figure 4.28, which shows the deformation of the proving ring and soil specimen with time. Also shown in Figure 4.28 is the total deformation, calculated by summing the proving ring and soil specimen deformations. It is evident from Figure 4.28 that the total deformation rate remains constant during the course of the test, whereas the deformation rate of the soil specimen reduces from an initial rate of 0.01 mm/min to a minimum average rate at the end of the test of 0.004 mm/min.

The e – log σ' relationship of CL_CRD_04 (Figure 4.27) is characterised by an apparent preconsolidation stress, σ'_c, of approximately 2 kPa. This value is difficult to determine as considerable fluctuations in the data have been recorded at low stresses. Also shown in

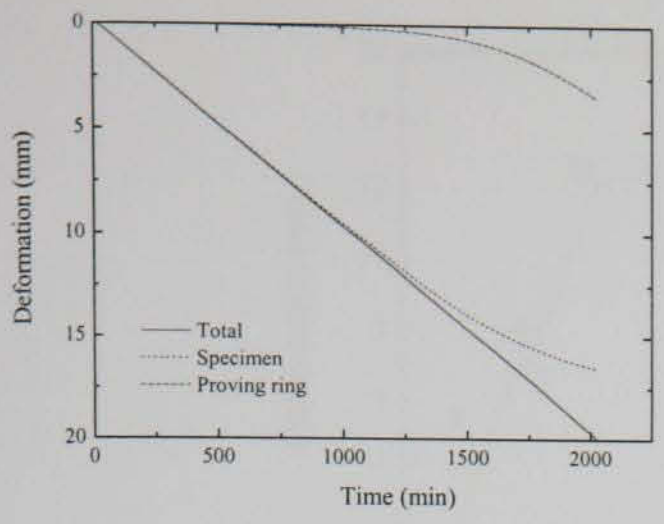

Figure 4.28 Deformation of specimen and proving ring with time for CL_CRD_04

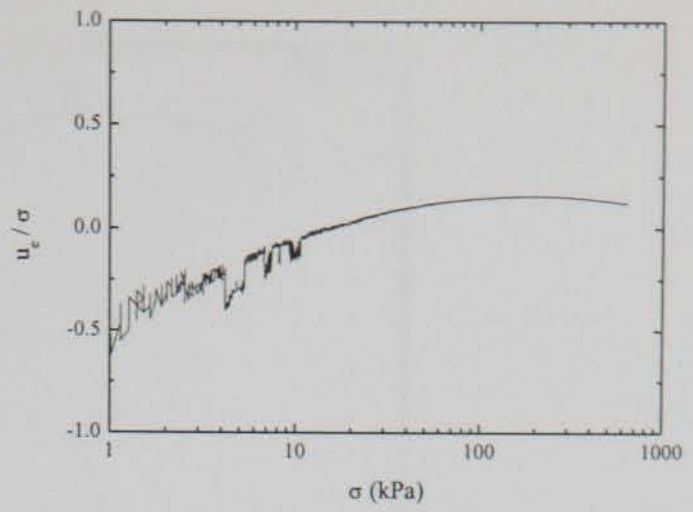

Figure 4.29 Variation of the ratio, u_e/σ, with total stress, σ, for CL_CRD_04

Figure 4.27 is the excess pore pressure, u_e, measured at the base of the specimen. A maximum value of u_e = 75 kPa is recorded at the maximum permissible total stress, σ = 636.5 kPa. The variation of the ratio, u_e/σ, with total stress, σ, is shown in Figure 4.29. This ratio initially assumes negative values, as the measured pore pressure fluctuated around ±1.5 kPa at low stress values. Beyond approximately 15 kPa, u_e/σ becomes positive, with values never exceeding 0.16. This value is within the tolerable range recommended by ASTM D4186. It is also interesting to note that the maximum value of u_e/σ occurs at σ=200kPa and not at the maximum stress, σ = 636.5 kPa.

Test CL_CRD_06 involved loading and unloading at constant rates of deformation, and stepped changes in the imposed rate of deformation. This test was set to load at intermittent deformation rates of ±0.005 mm/min and ±0.0005 mm/min. However, as was the case with CL_CRD_04, the deformation of the proving ring caused these rates to decrease slightly as the soil stiffened. The measured deformation of the specimen with time is shown in Figure 4.30; the annotation shown in described below:

A-B deformation rate = 0.00478 mm/min; $r = 3.98 \times 10^{-6}$ sec^{-1}

B-C deformation rate = -0.00458 mm/min; $r = -3.82 \times 10^{-6}$ sec^{-1}

C-D deformation rate = 0.00454 mm/min; $r = 3.78 \times 10^{-6}$ sec^{-1}

D-E deformation rate = 0.00040 mm/min; $r = 0.33 \times 10^{-6}$ sec^{-1}

E-F deformation rate = -0.00028 mm/min; $r = -0.23 \times 10^{-6}$ sec^{-1}

F-G deformation rate = 0.00223 mm/min; $r = 1.86 \times 10^{-6}$ sec^{-1}

Figure 4.31 shows the effect of the imposed rates of deformation on the measured $e - \log\sigma'$ relationship. To allow for ease of interpretation, the points at which the deformation rate

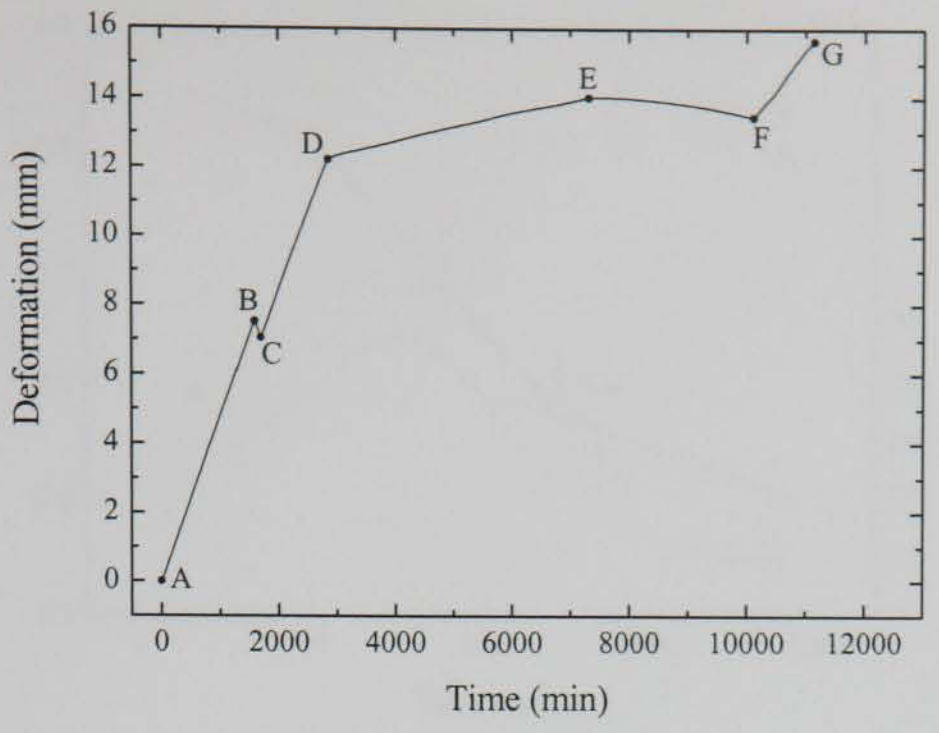

Figure 4.30 Stepped changes in the deformation rate of CL_CRD_06

were changed (A-G, Figure 4.30) are included in Figure 4.31. The apparent preconsolidation stress in this test is slightly higher than CL_CRD_04, at approximately 5 kPa. Upon unloading, and subsequent reloading, the $e - \sigma'$ state rejoins the virgin loading curve. No distortion to the resultant curve is evident. At point D, the deformation rate is reduced ten-fold, causing a decrease in the effective stress, despite an associated decrease in pore pressure. The e – log σ' relationship is consequently shifted to the left of the original relationship. Unloading from point E, and subsequent reloading from point F at the higher rate of 0.00223 mm/min, causes the e – σ' state to seemingly rejoin the e – log σ' path that would have been observed had no deformation rate changes been imposed.

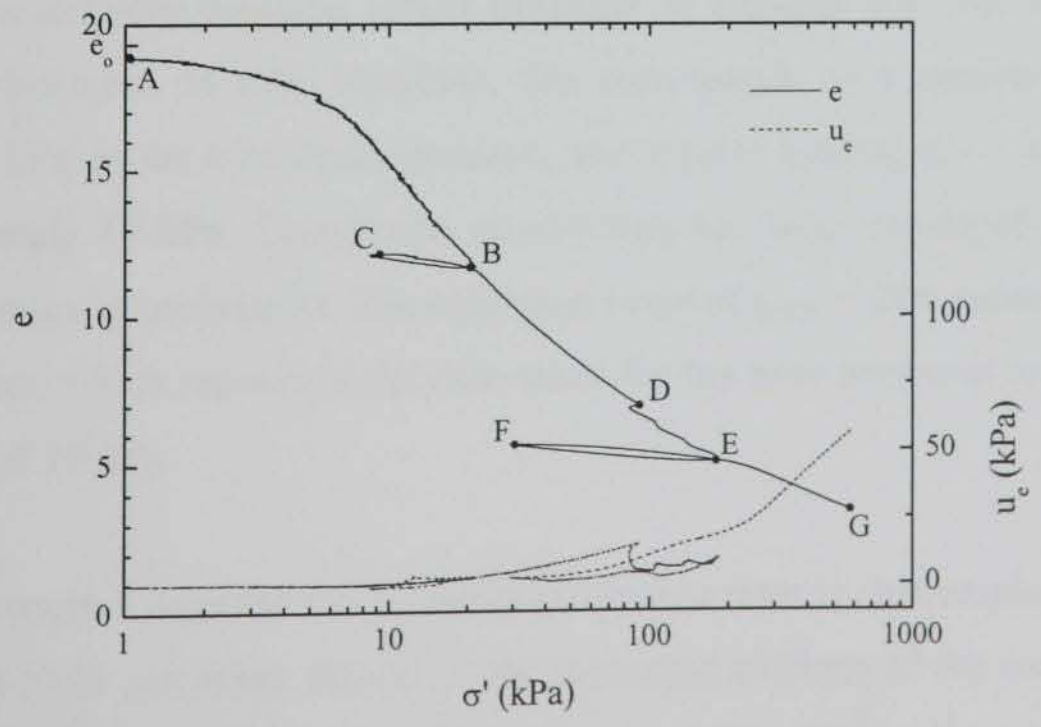

Figure 4.31 Measured e – log σ' and u_e – log σ' data for CL_CRD_06

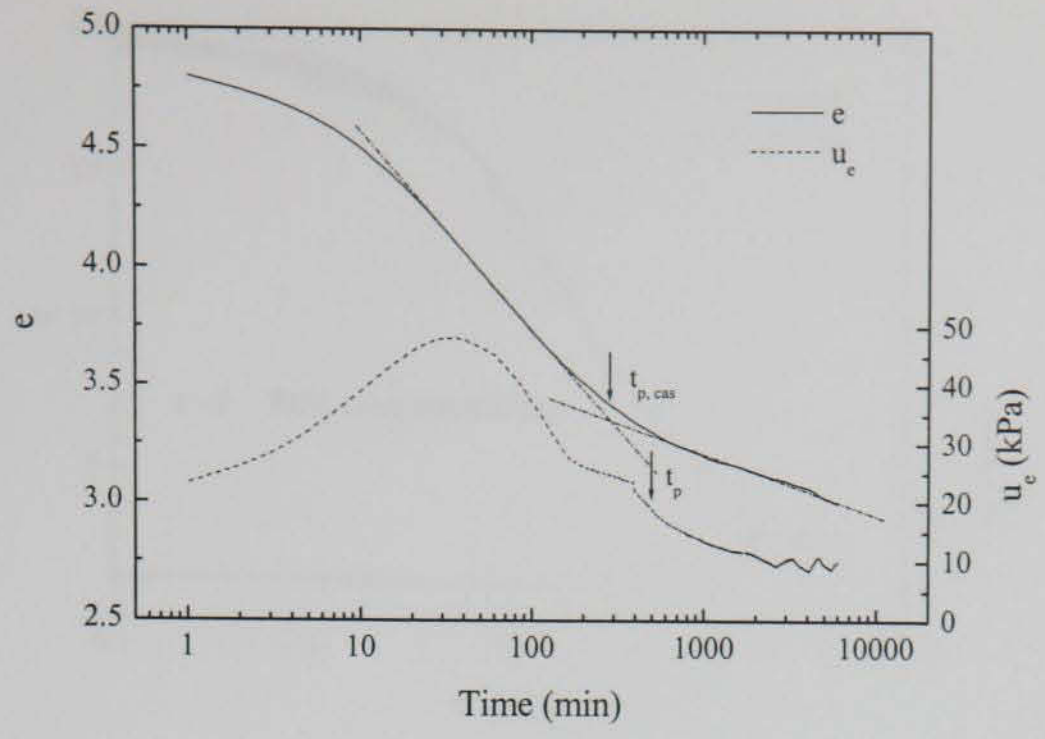

Figure 4.32 e – log t and u_e – log t data for the constant stress increment (100-172 kPa) of CL_CRD_07

However, as the e – log σ' relationship is highly non-linear, it is difficult to determine the effect, if any, of the final increase in deformation rate.

CL_CRD_07 involved an initial constant rate of deformation of 0.01 mm/min ($r = 8.33 \times 10^{-6}$ sec^{-1}), which was maintained up to $\sigma' = 100$ kPa. At this stage, the test was interrupted, and the loading frame set to a target total stress of 172 kPa. This stress increment, which corresponds to a LIR = 0.72, was maintained for approximately 4 days. The observed e – log t and u_e – log t relationships corresponding to this stress increment are shown in Figure 4.32. As was the case with CL_MSL_20 (Figure 4.8), and BD_CRD_01 (Figure 4.10a, Figure 4.10b), a time lag was observed before the pore pressure reached its peak value. The maximum recorded pore pressure, which occurred 30 minutes after the stress increment was applied, measured 48 kPa. However, this corresponds to a maximum *excess* pore pressure of 29 kPa, as the initial pore pressure, due to prior loading at $r = 8.33 \times 10^{-6}$ sec^{-1}, was approximately 19 kPa. Casagrande construction has been employed to estimate the duration of primary consolidation. The estimated value of $t_{p,cas} = 284$ minutes is lower than $t_p = 495$ minutes, which represents the time taken for the pore pressures to decrease to the original value of 19 kPa.

After approximately 4 days the rate of deformation was reset to that employed for the first part of the test (0.01 mm/min). However, the increased stiffness of the soil resulted in an average rate of deformation of 0.0038 mm/min, or $r = 3.15 \times 10^{-6}$ sec^{-1}.

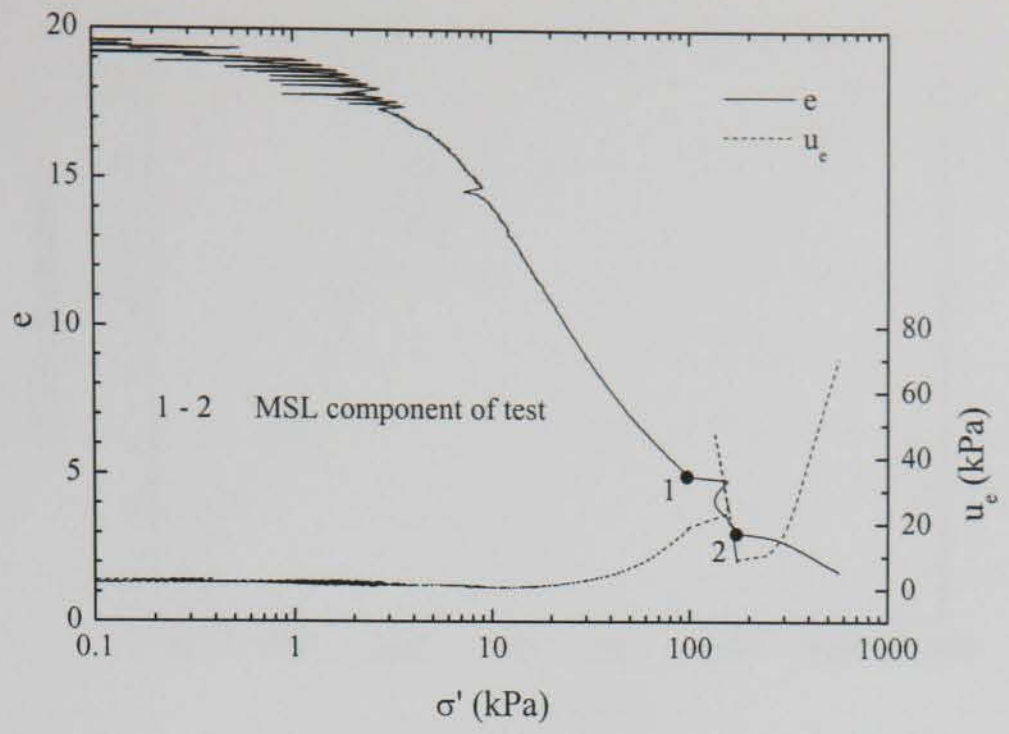

Figure 4.33 Measured e – log σ' and u_e – log σ' data for CL_CRD_07

Figure 4.33 shows the e – log σ' relationship for the entire loading sequence of CL_CRD_07. Upon application of the 100-172 kPa stress increment, the effective stress increases to 156 kPa. This increase is due to the time-lag in pore pressure. As the pore pressure begins to increase, the effective stress reduces to a minimum value of 134 kPa; this value corresponds to a loading time of 30 minutes, at which point the pore pressure reaches the maximum value of 48 kPa in Figure 4.32. As the pore pressure dissipates, the effective stress increases towards 172 kPa. The creep observed in Figure 4.32 causes a further reduction in void ratio at this constant effective stress. Reloading at a constant rate of deformation from this point results in an apparent preconsolidation stress, σ'_c, = 250 kPa. This value is approximately 80 kPa higher than the maximum applied stress of 172 kPa. Beyond 250 kPa, *normal* virgin loading is observed.

In the CRD tests previously described, the use of the proving ring resulted in measured deformation rates that were lower than intended. So as to investigate the effect of this reduction, tests CL_CRD_08 and CL_CRD_09 were performed using the load cell shown in Figure 4.26. The results of CL_CRD_08 are described here. The imposed deformation with time is shown in Figure 4.34, and summarised below:

A-B deformation rate = 0.01 mm/min; $r = 8.33 \times 10^{-6}$ sec^{-1}

B-C deformation rate = -0.01 mm/min; $r = -8.33 \times 10^{-6}$ sec^{-1}

C-D deformation rate = 0.10 mm/min; $r = 83.33 \times 10^{-6}$ sec^{-1}

D-E deformation rate = 0.001 mm/min; $r = 0.83 \times 10^{-6}$ sec^{-1}

E-F deformation rate = 0.01 mm/min; $r = 8.33 \times 10^{-6}$ sec^{-1}

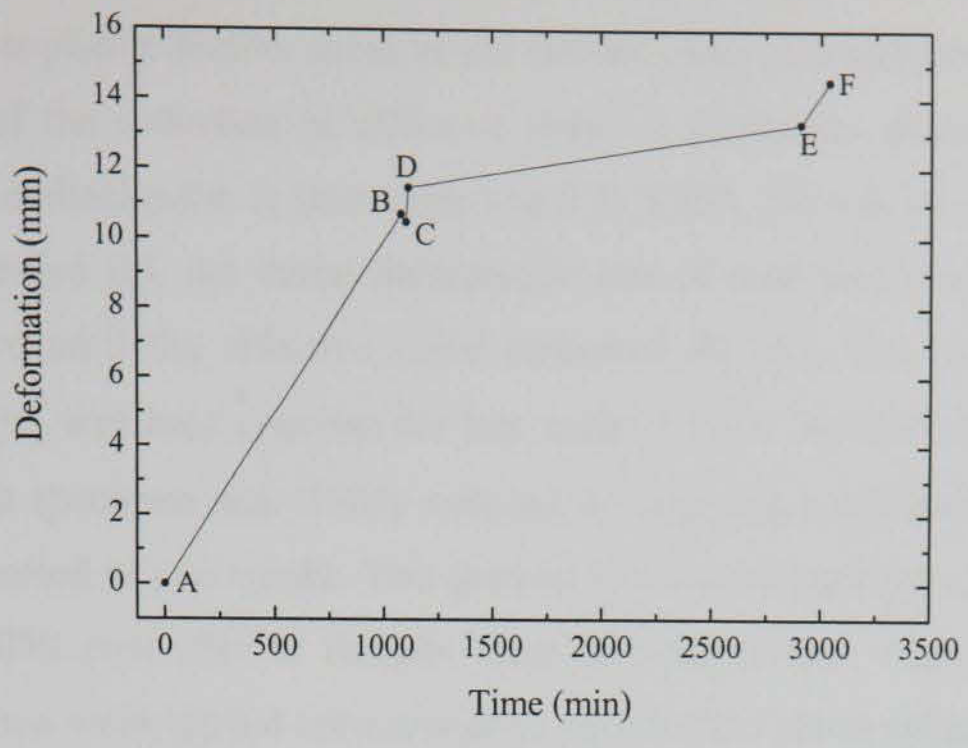

Figure 4.34 Stepped changes in the deformation rate of CL_CRD_08

Examination of Figure 4.34 reveals that there was no measurable reduction in the target rates of deformation (e.g. compare E-F with A-B).

The measured e – log σ' relationship corresponding to the loading sequence described above is shown in Figure 4.35. As with CL_CRD_06, the changes in deformation rate, denoted by A-F, are shown. It is evident from Figure 4.35 that decreases in the deformation rate result in a decrease in the measured pore pressure and effective stress. Increases in the deformation rate, such as C-D, shift the e – log σ' relationship to the right.

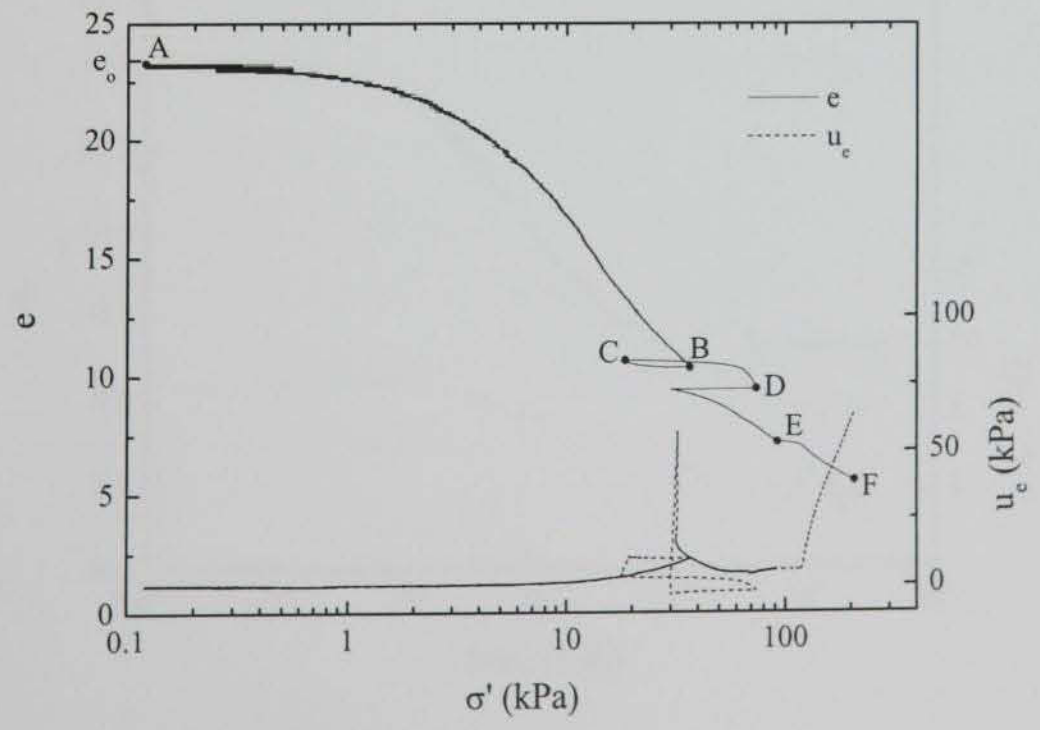

Figure 4.35 Measured e – log σ' and u_e – log σ' data for CL_CRD_08

Settlements of embankments constructed over peat deposits are often excessive, causing reductions in the applied effective stress as the embankment becomes partially submerged. The magnitude of the reduction in effective stress is obviously directly related to the settlement of the embankment. A laboratory test (CL_CRD_09) was devised which would simulate a submerged fill. An initial deformation rate of 0.03 mm/min ($r = 25.0 \times 10^{-6}$ sec^{-1}) was applied until the effective stress measured 40 kPa. The corresponding total stress, $\sigma = 46$ kPa, was held constant for just under 3 days. At this stage, the effective stress on the peat specimen was slowly reduced by applying a gradual increase in back pressure over a period of two weeks. This gradual increase in back pressure was achieved by setting the GDS controller to linearly ramp to a maximum value of 20 kPa. This increase, over a two week period corresponds to an effective stress reduction of 20 kPa at 1.43 kPa per day. The actual reduction in effective stress due to the settlement of an embankment is more likely to be linear with logarithm of time, as this is a better approximation to the observed *in situ* settlements. However, a linear reduction in effective stress was considered to be adequate for the purposes of the experiment.

Figure 4.36 shows the e – log t and u_e – log t response to the constant effective stress, followed by the reducing effective stress. The pore pressure at the beginning of this stage of the test measured approximately 7 kPa. The resulting Type I (Leonards and Girault, 1961) curve is a result of the dissipation of this relatively low excess pore pressure. After approximately 500 minutes the e – log t relationship becomes linear. This creep curve is typical of that observed in the MSL oedometer tests described in § 4.4.1. The reduction in

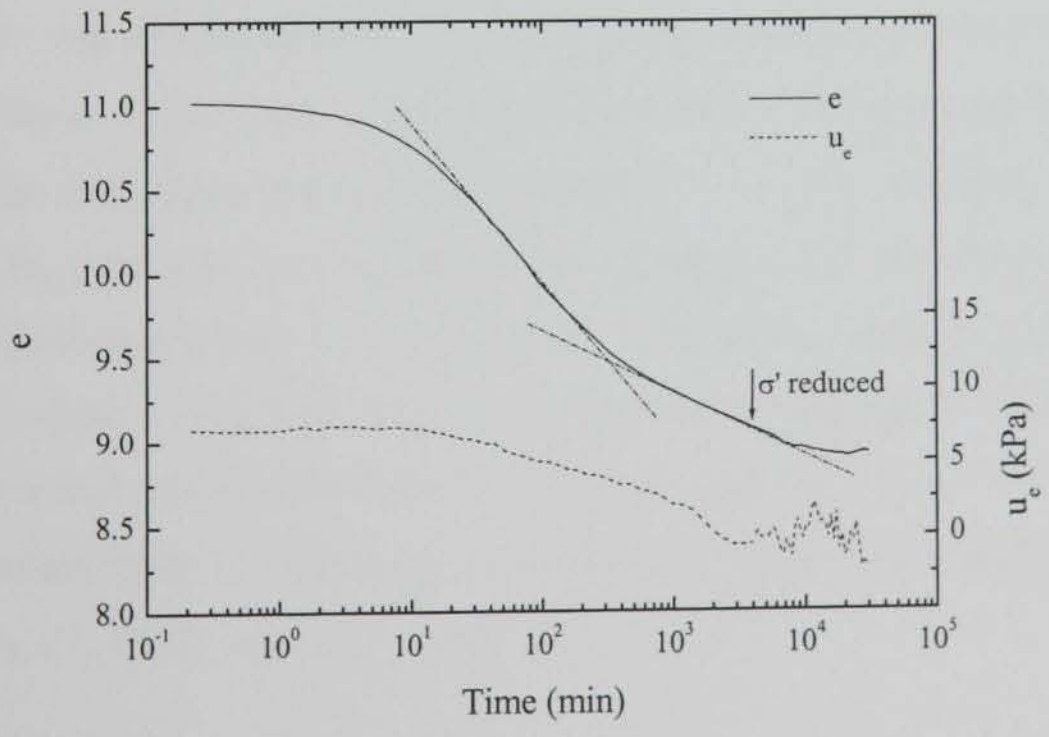

Figure 4.36 e – log t and u_e – log t data for CL_CRD_09, during the period of constant stress and reducing effective stress

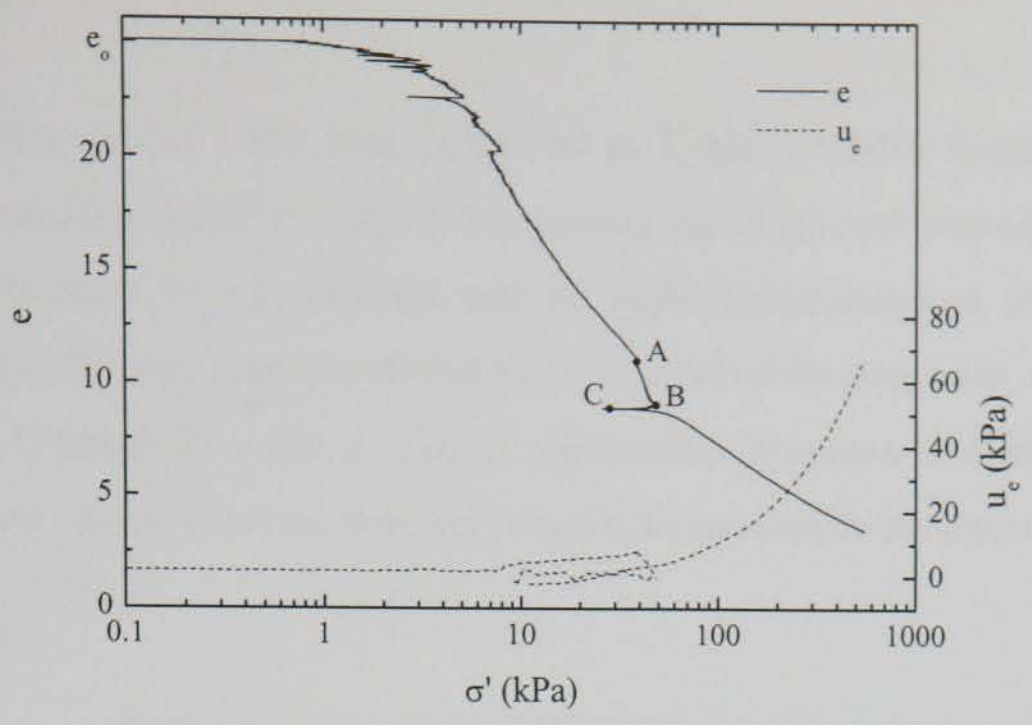

Figure 4.37 Measured e – log σ' and u_e – log σ' data for CL_CRD_09

typical of that observed in the MSL oedometer tests described in § 4.4.1. The reduction in effective stress is marked on Figure 4.36 at approximately 3 days. At this point the excess pore pressure had dissipated, resulting in $\sigma' = 46$ kPa. The reduction in effective stress has no measurable effect for approximately 3 days, by which stage $\sigma' = 42$ kPa. Between 3 and 12 days, the slope of the e – log t curve reduces considerably as the effective stress continues to reduce. After approximately 12 days ($\sigma' = 29$ kPa) the sample begins to swell slightly, resulting in a slight increase in void ratio. At the end of the 2 week reduction in effective stress, $\sigma' = 26$ kPa. This stress level was maintained for a further 4 days before loading at a constant rate of deformation of 0.003 mm/min ($r = 2.5 \times 10^{-6}$ sec^{-1}).

The resulting e – log σ' relationship from this loading sequence is shown in Figure 4.37. The portion of the e – log σ' curve marked A-B on Figure 4.37 represents the 3 day period during which the total stress remained constant at $\sigma = 46$ kPa. However, as is apparent from Figure 4.36, pore pressures dissipated during this period, resulting in the observed increase in effective stress from A-B in Figure 4.37. The period of reducing effective stress is marked B-C, where a very small decrease in void ratio is apparent. Loading from Point C involved a constant rate of deformation of 0.003 mm/min ($r = 2.5 \times 10^{-6}$ sec^{-1}), causing the e – log σ' relationship to shift to the right, similar to that which was observed during reload periods in CL_CRD_06 and CL_CRD_08.

4.5.3 Summary

The results of five of the CRD tests described in Table 4.3 have been presented and described. The measured CRD e – log σ' relationship for Clara peat was seen to be highly non-linear. Reductions in the imposed rate of deformation resulted in a subsequent decrease in the excess pore pressure measured at the base of the specimen, and decrease in effective stress. Consequently, the e – log σ' relationship appeared to shift to the left. An increase in the rate of deformation, however, caused an increase in the excess pore pressure

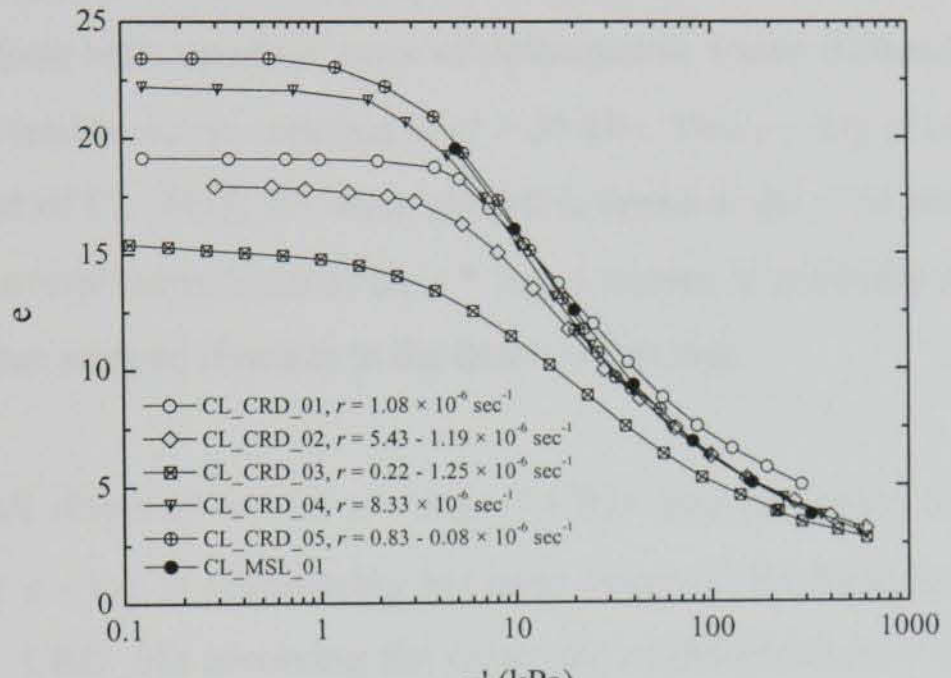

(a)

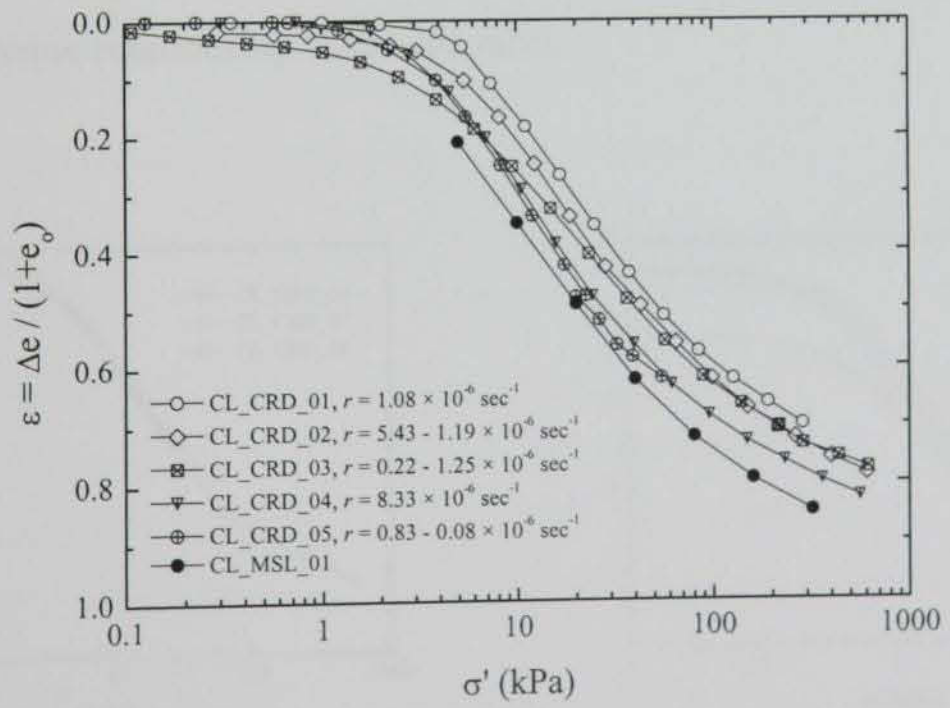

(b)

Figure 4.38 Comparison of CRD results for Clara peat: (a) e – log σ', (b) ε– log σ'

and effective stress, resulting in an apparent shift to the right of the measured e – log σ' relationship. The long-term effect of stepped changes in the deformation rate is often difficult to determine as the observed e – log σ' relationship is highly non-linear.

Figure 4.38 compares measured e – log σ' and ε – log σ' data for several of the CRD tests, and for a standard MSL oedometer test, CL_MSL_01. Although the use of strain compensates for the variation in initial void ratio, the ε – log σ' data at higher stress levels indicates a significant degree of disparity, similar to that observed for the MSL oedometer tests on Clara peat (see Figure 4.17). A tolerably consistent trend is observed for three of the CRD tests (CL_CRD_02, CL_CRD_04, CL_CRD_05) when plotted in e – log σ' space. Although these tests involved rates of deformation which differed by factors of up to 100, the curves tend to merge together at $\sigma' > 20$ kPa. This e – log σ' relationship is also consistent with that of CL_MSL_01 when plotted in terms of the void ratio, e. It is notable however, that the overall separation of the e – log σ' curves is generally much greater than that anticipated from stepped changes in the deformation rate.

Despite the overall disparity in the ε – log σ' CRD data presented in Figure 4.38, an acceptably unique ε – log σ' relationship has been observed for three tests (CL_CRD_04, CL_CRD_07, CL_CRD_08) involving the same rate of deformation, $r = 8.33 \times 10^{-6}$ sec^{-1} (Figure 4.39a). Although changes in the deformation rate occurred during these tests, only the ε – log σ' data corresponding to $r = 8.33 \times 10^{-6}$ sec^{-1} is shown. The equivalent e – log σ' curves are shown in Figure 4.39b. Evidently the use of strain in this instance is seen to provide a more unique relationship than void ratio.

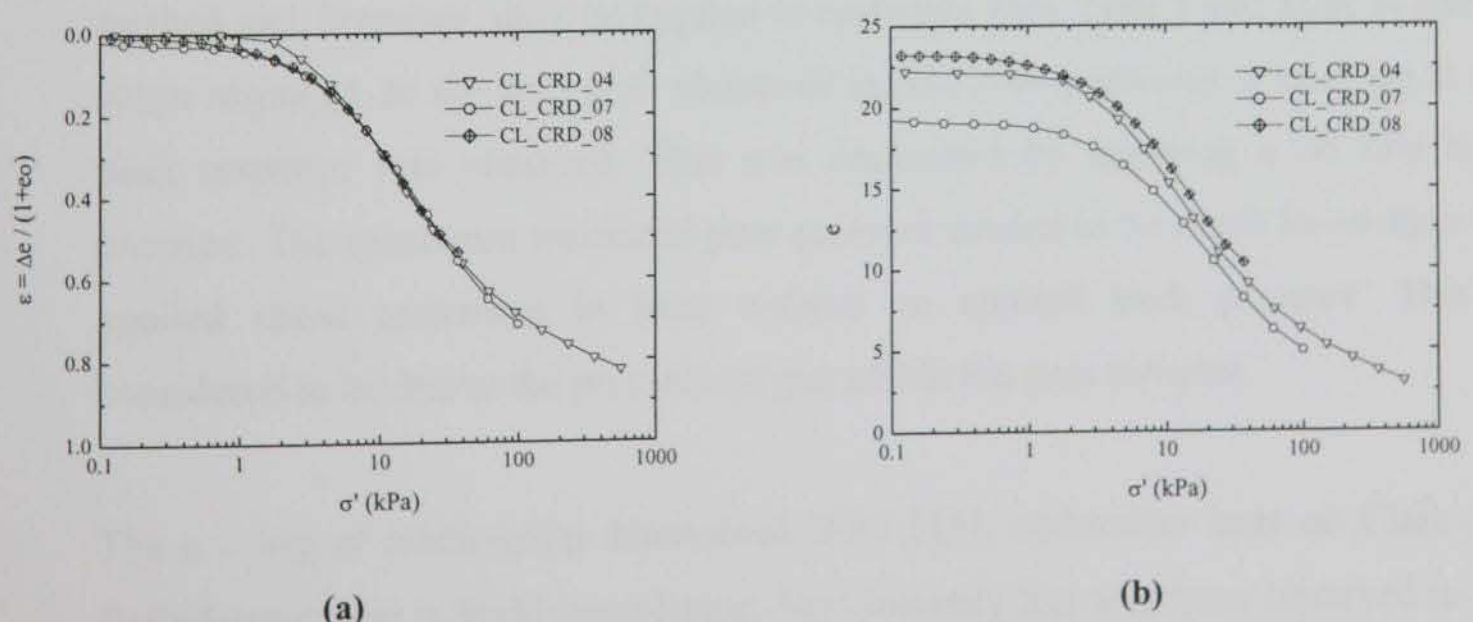

(a) (b)

Figure 4.39 Comparison of CRD results at $r = 8.33 \times 10^{-6}$ sec^{-1}: (a) e – log σ', (b) ε – log σ'

4.6 CONCLUSIONS

Selected test results from a relatively large database of MSL oedometer and CRD laboratory tests have been presented using conventional notation and format. The results of all the tests described in Table 4.2 – Table 4.6 are provided in Appendix A. The conclusions that can be drawn from the work described in this chapter are summarised below:

1. Observed settlement of the soils considered here is due to consolidation and creep. The creep behaviour of the soils appears to follow a linear relationship when plotted in e – log t space.

2. The majority of the stress increments could be identified by the compression curves defined by Leonards and Girault (1961). Stress increment with a LIR $\geq$ 1.0 generally correspond to the Type I curve, whereas stress increments with a LIR < 1.0 resemble the Type III curve. For Clara and Ballydermot peat, stress levels close to or lower than the apparent preconsolidation stress, resulted in an e – log t curve which increases in slope after 24 hours sustained loading. These curves are Type II curves and have been described using the parameter, t_k, defined by Edil and Dhowian (1970) as the intersection of the secondary and tertiary compression curves.

3. A limited number of tests involving pore pressure measurements showed that Taylor's graphical construction method, and to a lesser extent, Casagrande's method, consistently underestimate the consolidation duration, t_p. Casagrande's method can, however, only be applied to materials with Type I and Type II stress-strain response. In the tests with measured excess pore pressures, a time lag in the peak response was observed. This was eradicated by applying a 50 kPa back pressure. The maximum measured pore pressure tended to be much lower than the applied stress increment in tests without an applied back pressure. This is considered to be due to the presence of gas within the peat samples.

4. The e – log σ' relationship determined from MSL oedometer tests on Clara and Ballydermot peat is highly non-linear. Non-linearity has also been observed in e – log σ' data obtained from CRD tests on Clara peat. Similar trends were noted for

Cork peat and Belfast organic clay, although the degree of non-linearity is much less severe.

5. The measured swelling or rebound of Clara peat during unloading was completed in less than 15 hours for the first stress decrement, whereas no appreciable rate of reduction (as determined from e – log t data) was observed during the second stress decrement, even after 6 days.

6. Long duration tests on Clara peat have been presented as a series of *constant loading duration* e – log σ' curves. The curves, ranging in loading duration from 1 – 100 days, plot at successive reductions in void ratio. Although the curves are initially parallel, they tend to converge at higher stress levels.

7. Three CRD tests on Clara peat involving a deformation rate corresponding to $r = 8.33 \times 10^{-6}$ sec^{-1}, show consistency when plotted in terms of strain and not void ratio.

8. Individual CRD test results show that reductions in the imposed rate of deformation shift the e – log σ' curve to the left, whereas an increase in the rate of deformation cause the measured e – log σ' relationship to shift to the right.

9. The results of CRD tests on Clara peat indicate that the natural variation between measured e – log σ' curves at comparable rates of deformation, is much higher than the separation resulting from stepped changes in deformation rate.

Chapter 5

In situ load test on fibrous peat

Chapter 5

In situ load test on fibrous peat

5.1 INTRODUCTION

The design of preloading schemes is often based on data interpreted from standard laboratory tests. The relative success of such projects is largely dependent upon the assumption that compression parameters determined from small-scale oedometer tests can be either directly or indirectly employed to predict full-scale field behaviour. The relative merit and validity of this assumption has received due attention in recent years (Edil, 1983; Farrell, 1997; Carlsten, 1991; Kabbaj *et al.*, 1988). Problems associated with the correlation of laboratory and field observations are often attributed to scale effects and to the variability of apparently similar samples (Magnan 1994, Edil 1994), although the merit of the chosen constitutive model in describing the highly non-linear nature of peat is also of fundamental importance. In order to supplement the experimental data obtained in the laboratory, a full-scale field test was initiated in 1998. Permission was obtained from the National Parks and Wildlife Service (NPWS) to perform the field test in Clara bog (see Figure 5.1), close to where the samples used for laboratory testing were obtained.

This chapter initially provides details regarding the subsidence of a road constructed on Clara bog over 150 years ago. The design, implementation and observations of the field test in the bog is subsequently described.

The field experiment described in this chapter is used subsequently to compare the compressibility characteristics of fibrous peat as measured in the laboratory and the field, and to obtain verification of current constitutive models for *in situ* tests on fibrous peat, using model parameters obtained from laboratory tests.

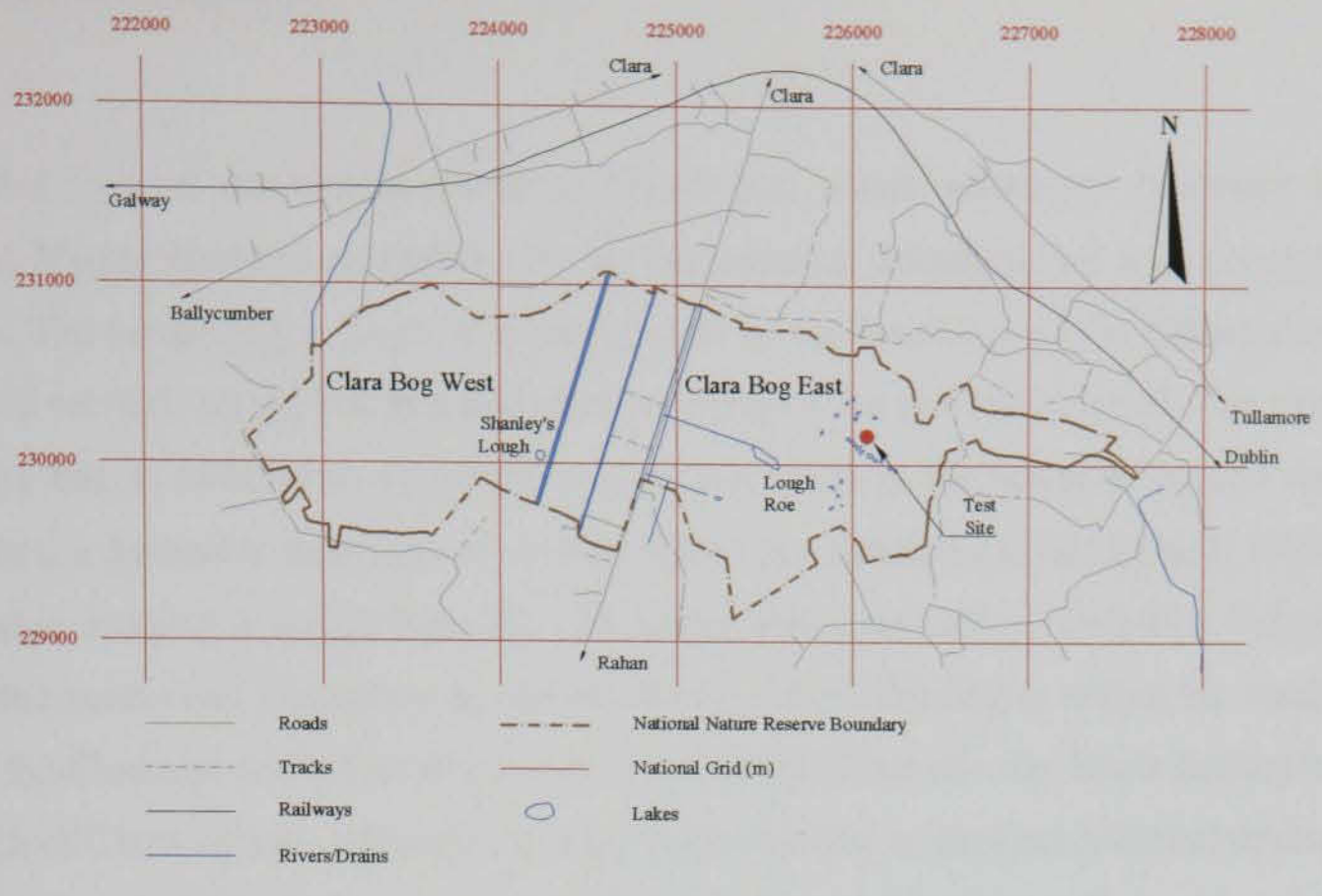

Figure 5.1 Map of Clara bog with details of local infrastructure and geographical features

5.2 CLARA BOG

Clara bog is situated approximately 9 km north west of Tullamore and 2 km south of Clara town, Co. Offaly. The bog encompasses an area of approximately 665 ha including cut-away sections (Kelly, 1993). A large percentage of the bog (approximately 460 ha) was purchased by the NPWS in 1986, who declared the area as a National Nature Reserve. Due to the rapid and almost complete loss of natural peatlands in Western Europe, Clara bog is recognised by several hydrological and ecological bodies at both national and international level as an important heritage site. Although there are no intact raised bogs remaining in Ireland (Bellamy, 1986; Cross, 1990), Clara bog is arguably the best remaining example of an undisturbed raised bog in Western Europe. The bog is of particular hydrological interest, due to the presence of *soak* systems, which are complexes of pools or small lakes that are formed as a result of the internal drainage structure of the bog. The nature of soaks tends to promote vegetation types that are generally not encountered in disturbed peatlands. It is for this reason that Clara bog has received such widespread international attention.

5.2.1 Site Description

A detailed map of the bog is shown in Figure 5.1, which shows the boundary of the National Nature Reserve in relation to the surrounding infrastructure and geographical features. The actual bog is larger than that shown by the boundary of the Nature Reserve, as several sections on the western and southern margins are privately owned. The extent of the entire bog is difficult to determine as peat extraction in the privately owned sections has caused a perimeter recession of several metres per annum (van der Schaaf, 1999). An esker ridge, ranging in height from 10 – 25 metres above the surrounding area, bounds the bog to the north (van Tatenhove & van der Meer, 1990). The bog is within the catchment area of the Clodiagh and Silver Rivers which run south of the site; the River Brosna runs to the north of Clara village, although the esker ridge is likely to prevent potential drainage in this direction. Relatively large cut-away sections bound the bog to the west and to the south; these areas are typically drier than the central regions of the bog and are forested in places. A road, which runs in a North-South direction between Rahan and Clara, splits the bog into two approximately equal sections, herein referred to as Clara Bog West and Clara Bog East (see Figure 5.1).

Drainage in Clara Bog East has taken place through a series of open surface drains, approximately 0.5 m deep and running parallel at 15 m intervals (see Figure 5.2). These drains, which were installed by Bord na Mona in the early 1980's in preparation for a peat extraction program for the bog, were subsequently blocked in 1987 by NPWS when they purchased the site.

5.2.2 Formation and Stratigraphy

Clara bog lies in a region underlain mainly by Lower Carboniferous strata bedrock, which is composed of three principle limestone types; lower limestone, middle (calp) limestone and an upper limestone (Kelly, 1993). The limestone bedrock is overlain by a layer of poorly graded glacial deposits, which are mainly composed of limestone tills, morainic sands and gravels (Kelly, 1993). The bog developed during the early Holocene period (10000 years ago to present day) in a small, depressed basin which was a part of a large post-glacial lake, known as Lough Borra (Kelly, 1993; Orr & McEnaney 1994). Due to the low permeability and hence poor drainage of the underlying calcareous boulder clay, water

Figure 5.2 View of Clara Bog East showing surface drains and bog lake

accumulated relatively quickly in the basin, creating a lake. Initially, sedges and reeds developed inwards from the perimeter of the lake, causing the lake to become shallower as the remains of the vegetation began to accumulate. Fen vegetation then began to infill the lake, depositing layers of dark fen peat as they advanced. As the depth of fen peat grew, plants at the surface became more cut off from the mineral-rich water below. The nutrient-demanding fen plants were then replaced by *Sphagnum* mosses, which are able to survive on the limited supply of nutrients present in rainfall. The formation of Sphagnum peat accelerated due to the drainage barrier provided by the underlying fen peat, and a climatic change which took place about 4000 years ago, resulting in increased humidity and rainfall levels. As there was an increased abundance of rainfall, and poor drainage, the Sphagnum mosses became permanently waterlogged causing the bog to grow upwards so as to create the typical raised dome shape (Kelly, 1993).

As part of their extensive study of the stratigraphy of Clara bog, Bloetjes and van der Meer (1992), presented borehole data for the entire bog. The author subsequently developed contoured surface profile and peat thickness maps (see Figure 5.3 and Figure 5.4), which were generated from the data using cubic interpolation techniques. From Figure 5.4 it can be seen that the depth of the peat layer varies from between 3 and 5 m at the boundary of

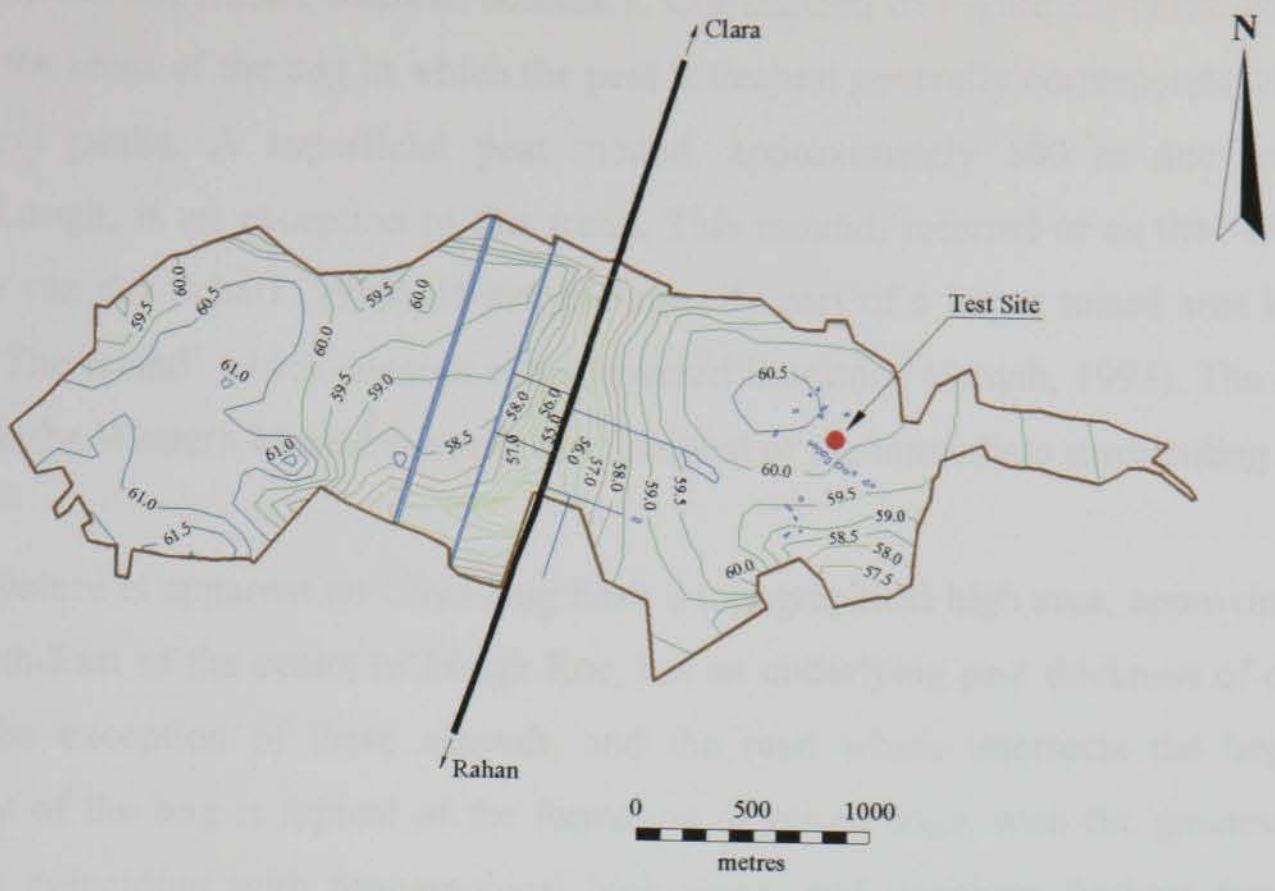

Figure 5.3 Surface contour map of Clara bog

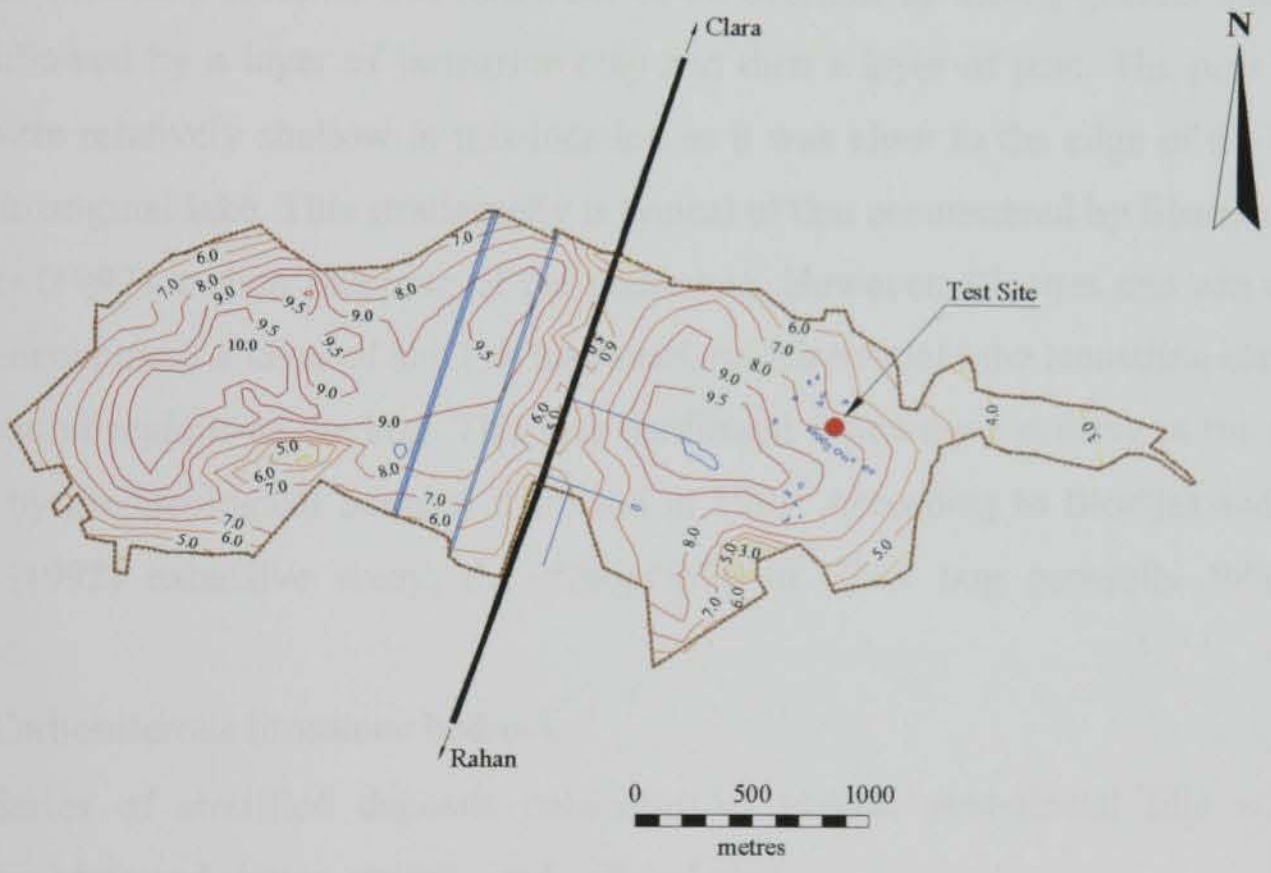

Figure 5.4 Total peat thickness contour map of Clara bog

the Nature Reserve to over 10 m in the centre of Clara Bog West, and over 9 m in the centre of Clara Bog East. Kelly (1993) reported peat thicknesses varying from less than 1m to 10 m, although the shallower areas are believed to correspond to the actual bog

boundary and not the Nature Reserve boundary. Comparison of Figure 5.3 and Figure 5.4 shows that the areas of the bog in which the peat is deepest generally corresponds with the topographical peaks. A superficial peat mound, approximately 500 m due west of Shanley's Lough, is an exception to this trend. This mound, referred to as the 'Western Mound' by van der Schaff (1999), is morphologically part of a larger raised area known locally as 'The Island' which consists of till covered limestone (Smyth, 1993). The 4-5 m peat layer at the Western Mound is much less than that of the immediate surrounding area.

A similar feature is apparent on Clara Bog East; a topographical high area, approximately 200 m South-East of the centre of Lough Roe, has an underlying peat thickness of only 3 m. With the exception of these *mounds*, and the road which intersects the bog, the stratigraphy of the bog is typical of the formation of raised bogs, with the greatest peat thicknesses coinciding with topographical high areas, and positions furthest from the original lakeshore.

Data interpreted by Flynn (1990) from a borehole log close to the northern edge of Clara Bog East showed Carboniferous limestone to be overlain by sands, gravels and boulder clays, followed by a layer of lacustrine clay and then a layer of peat. The peat and clay layers were relatively shallow in this location as it was close to the edge of the bog, and hence the original lake. This stratigraphy is typical of that encountered by Bloetjes and van der Meer (1992) in their mapping of the entire bog. However, Bloetjes and van der Meer (1992) encountered a layer of shell or lake marl, which overlaid the lacustrine clay mainly in the central regions of the bog. This was confirmed following a drilling in the centre of the bog by the Geological Society of Ireland in 1991. According to Bloetjes and van der Meer's (1992) extensive study, the stratigraphy in Clara bog generally follows this sequence:

- Carboniferous limestone bedrock
- Series of stratified deposits consisting of several post-glacial tills with large boulders and stones, gravel, sand, silt and clay
- Thick layers of stiff lacustrine clay
- Shell or lake marl (mainly confined to the centre of the bog)
- Fen peat
- Strongly humified sphagnum peat
- Poorly humified sphagnum peat

5.2.3 Clara-Rahan Road

The Clara-Rahan road, which is shown in Figure 5.5, is believed to have been constructed in the mid 1800's as an access for peat (turf) extraction. The road has been estimated to have subsided by at least 6 m by Samuels (1992), and between 8 and 9 m by van der Schaff (1999). The current condition of the road indicates the severity of the subsidence; differential settlements caused by the inhomogeneous nature of the underlying peat have resulted in an uneven surface, with extensive potholes and large cracks clearly visible. It is quite probable that the state of the road surface has necessitated extensive repair and resurfacing over the years, as settlement rates for roads constructed over thick peat deposits generally significantly exceed the rate at which the pavement thickness increases from standard resurfacing and maintenance (Nichol and Farmer, 1998). Large drainage channels were constructed on both sides of the road shortly after construction work started. Samuels (1992) proposed that these drainage channels were necessary to alleviate flooding, due to the excessive settlement of the road during consolidation. This however, has induced drainage towards the road, which has the effect of increasing the effective stress in the soil above the decreasing water table level, which combined with the increase in surcharge caused by the road repairs, causes increased consolidation settlement and continued creep settlement.

Figure 5.5 Clara-Rahan road looking to the North, and Clara village

Similar experiences were reported by Allen (1969) for a reclamation site in the East Anglian fens (UK), where gravity drainage caused a peat layer to reduce from 6.7 m to 3.4 m over an 84 year period. Nichol and Farmer (1998) also described similar problems for approximately 100 m of a carriageway built over a relatively thick upland bog in Wales. They partly attributed the uneven and undulating surface of the problematic section to the presence of nearby scrub willows, which have contributed to the road subsidence by extraction of peat moisture from beneath the road surface. The potential for damage to bog roads caused by external drainage has long since been recognised in Ireland, considering that a law was passed in 1851 which forbade the extraction of peat within 9 m of the road centre (Farrell, 1997).

The subsidence of the road is believed to be the main reason for the interruption of the raised dome profile evident in the western and eastern sections of the bog (Bell, 1991; van der Schaff, 1999). This is evident from the contoured surface profile of the bog shown in Figure 5.3. The contours are generally much closer together in the proximity of the road, indicating that the surface gradients are steepest in these regions, and that the road is currently considerably lower than the central areas of Clara Bog West and Clara Bog East.

Two transects (cross-section) of the bog, which intersect the location of the chosen test site (see Figure 5.1) are shown in Figure 5.6 and Figure 5.7. These transects were generated from the contour maps shown in Figure 5.3 and Figure 5.4, which are based upon the borehole data presented in Bloetjes and van der Meer (1992). Their data were obtained from disturbed samples retrieved using a Hiller borer on an irregular grid with sampling locations spaced between 200 and 300 m. The potential for accurate interpolation on such a coarse grid is questionable although the results prove useful if interpreted as a gross stratigraphy of the entire bog. The West-East transect (Figure 5.6), shows that there is a marked reduction in the depth of peat in the proximity of the Clara-Rahan road which bisects the bog. The majority of the compression appears to have taken place in the upper layer of poorly humified sphagnum peat. This is to be expected as poorly humified sphagnum peat generally exists at higher *in-situ* water contents, and hence higher *in-situ* void ratios, than the underlying layers of less compressible humified and fen (transition) peat (Hobbs, 1986). Further verification for this can be obtained from the various transects shown in Figure 5.8. These transects show the profile of the bog in a West-East direction, at 100 m intervals along the length of the Clara-Rahan road. It is evident from the profiles that the construction of the road has resulted in significant compression within the peat

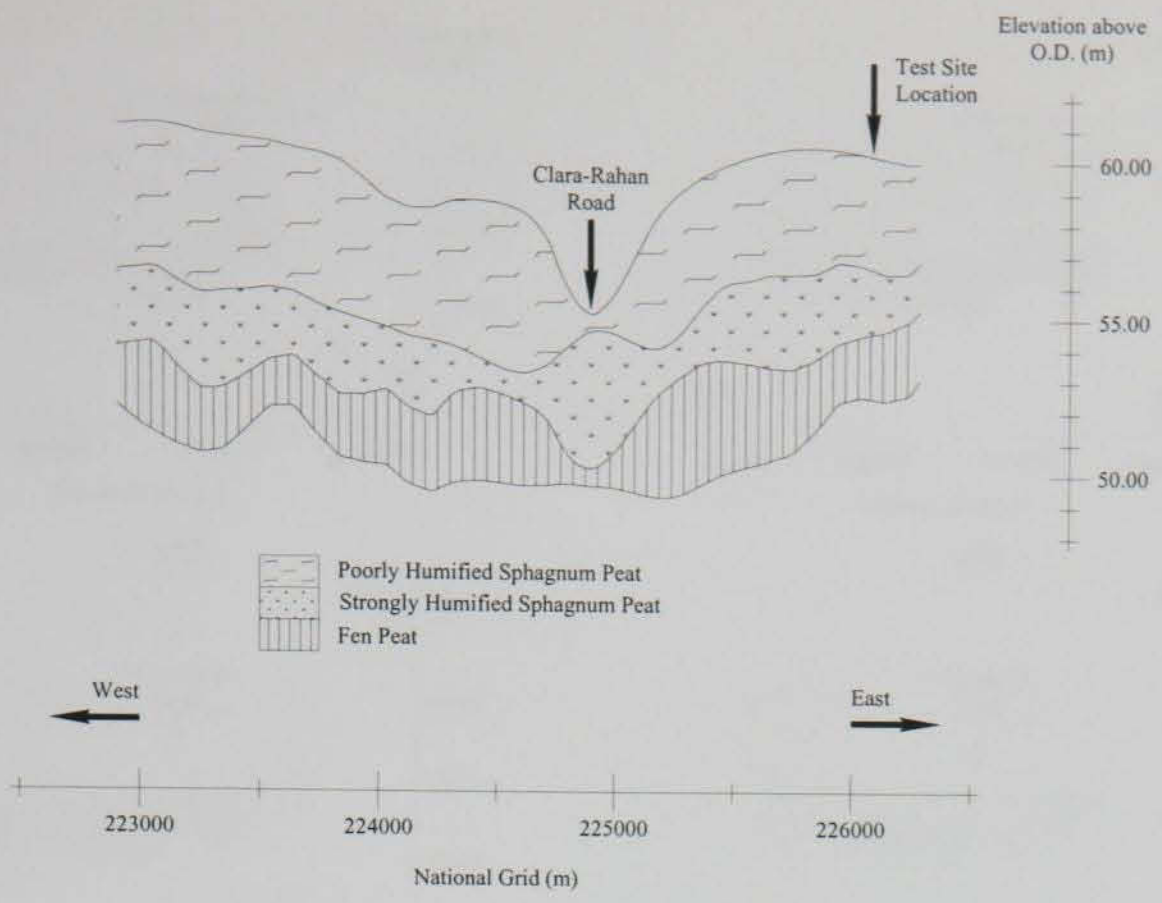

Figure 5.6 West-East transect of Clara bog

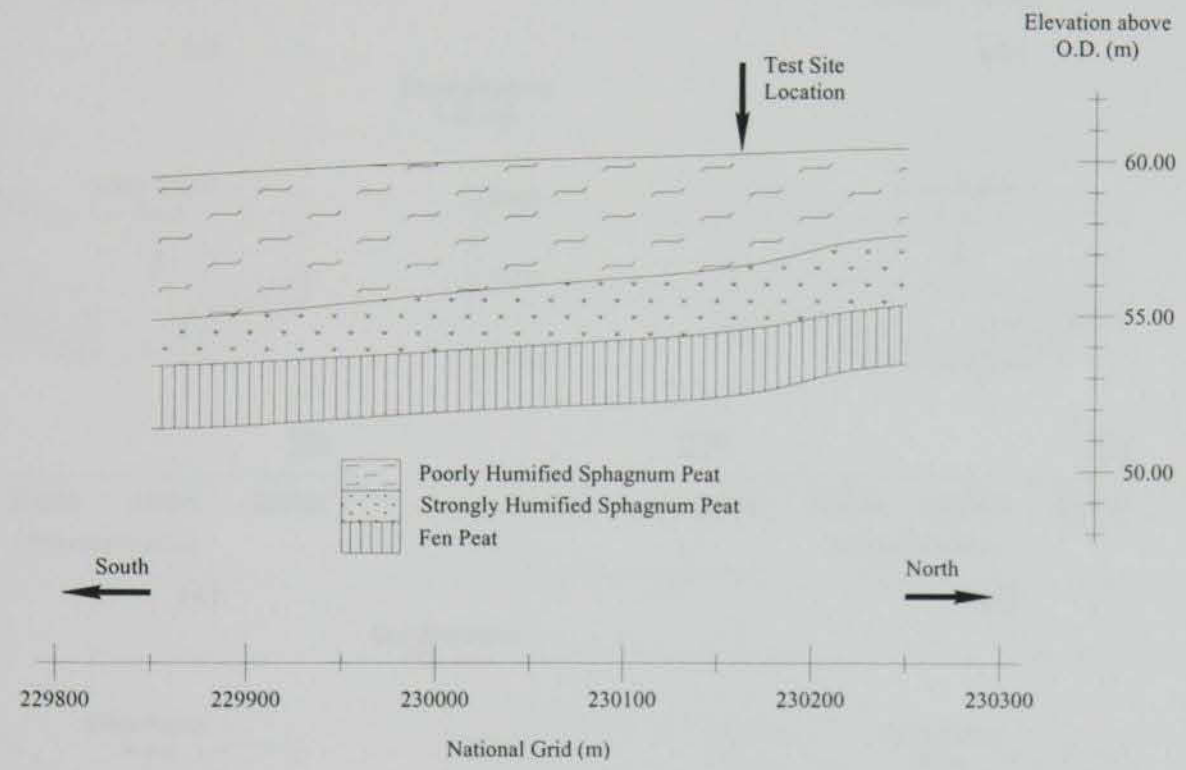

Figure 5.7 South-North transect of Clara bog

layer, and that the majority of the compression has taken place in the upper layer of poorly humified sphagnum peat. With the exception of Figure 5.8e and Figure 5.8f, the humified sphagnum and fen peat generally follow the undulating profile of the underlying mineral soil. It should be noted that these exceptions, which all relate to the same general locality, coincide with the profiles with the highest settlements, and that the discrepancy is due to an apparent increase in the thickness of the strongly humified peat layer. The apparently shallow depth of poorly humified peat in these instances may be attributed to the increased settlement and hence drainage at these locations. Furthermore, the interface between the

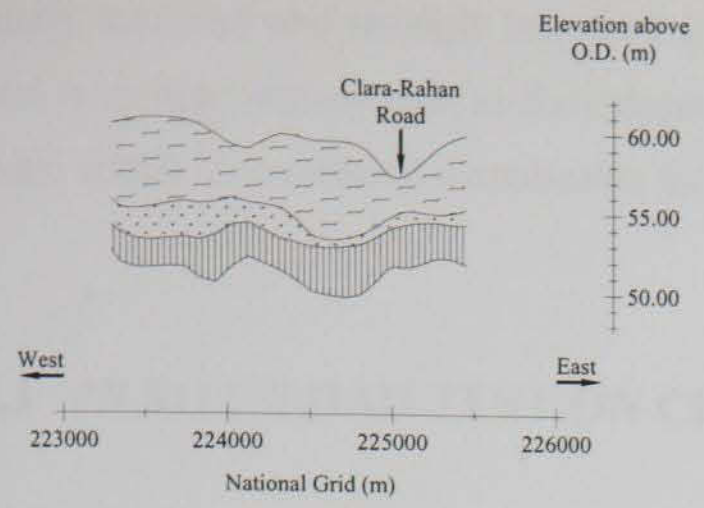

(a)

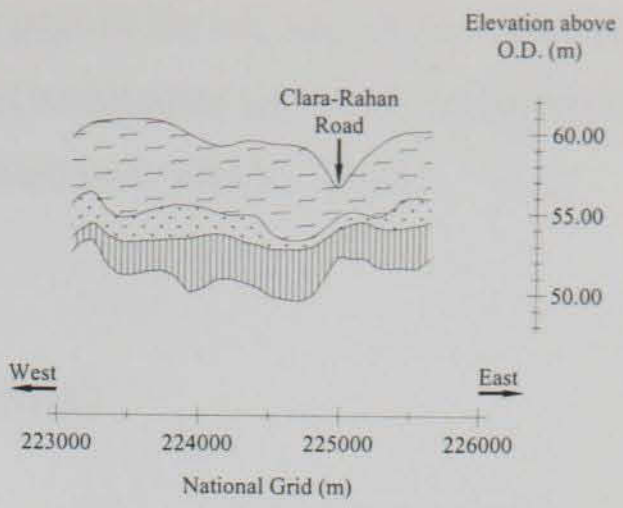

(b)

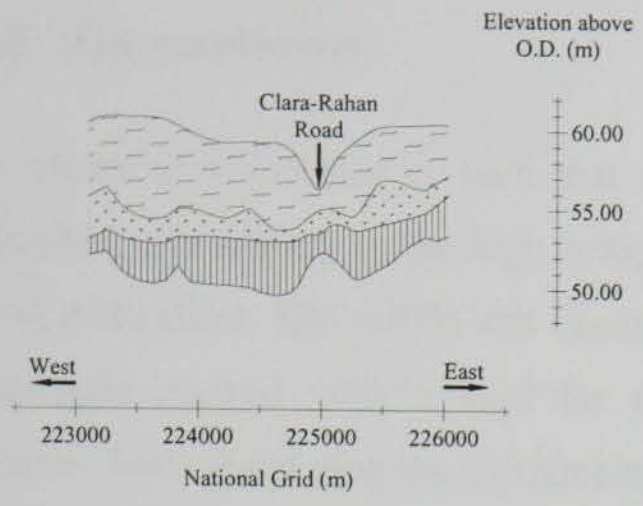

(c)

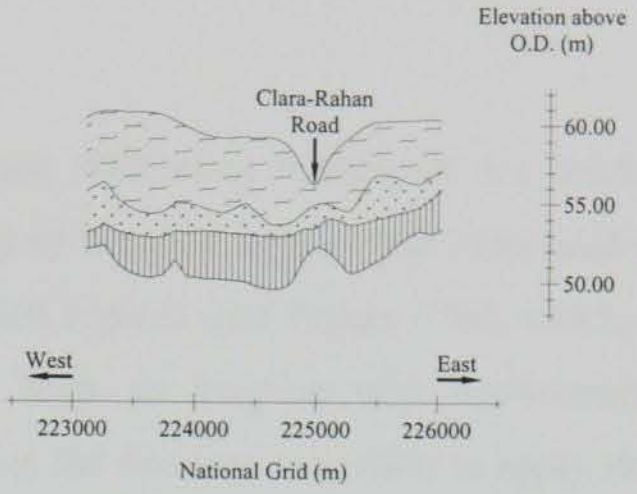

(d)

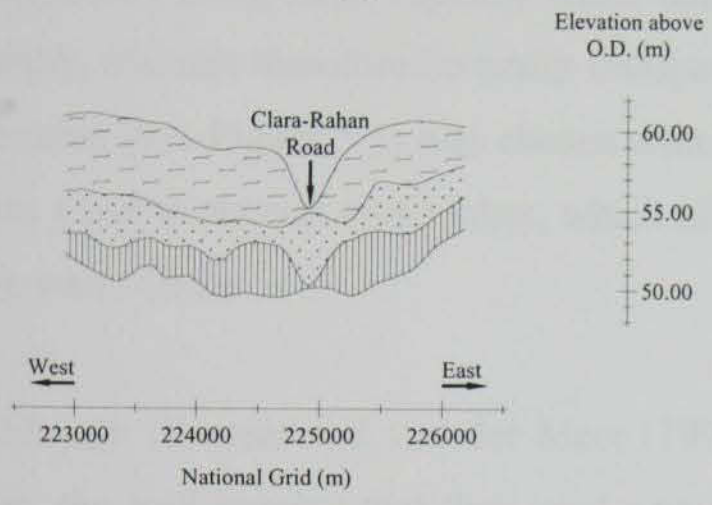

(e)

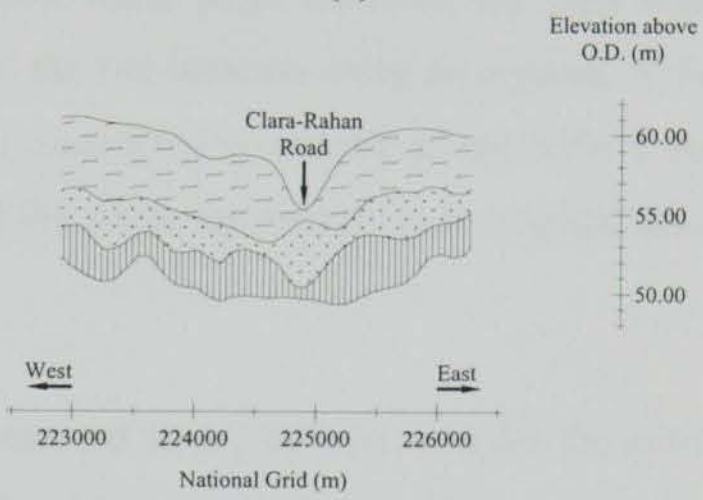

(f)

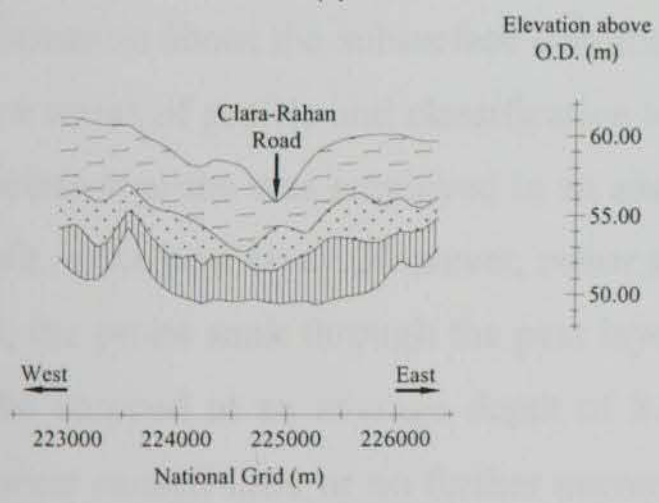

(g)

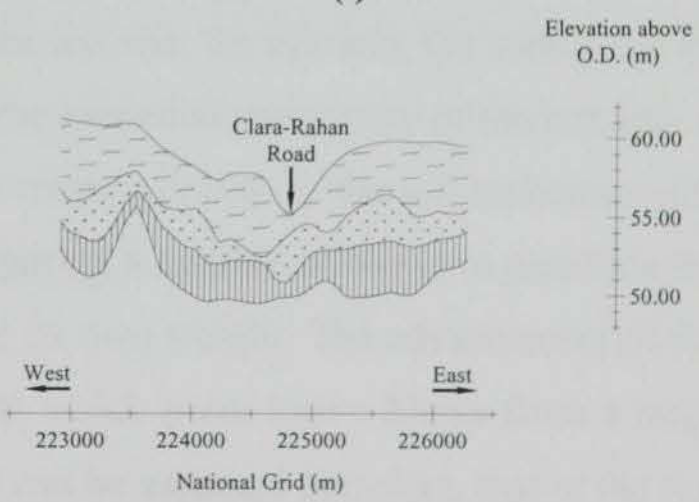

(h)

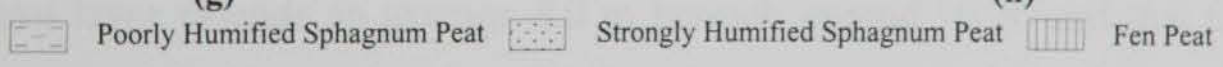

Figure 5.8 Various West-East transects of Clara Bog at Northings: (a) 230650 m (b) 230550 m (c) 230450 m (d) 230350 m (e) 230250 m (f) 230150 m (g) 230050 m (h) 229950 m

poorly humified and strongly humified sphagnum peat in the vicinity of the Clara-Rahan road is an approximate one, as the categorisation is based upon the von Post classification scale, which is considered inapplicable for compressed peat (Hobbs, 1986).

5.3 *IN SITU* LOAD TEST ON CLARA BOG

5.3.1 Site conditions

The nature of Clara bog is such that conventional preloading techniques are rendered unfeasible, due mainly to the high compressibility of the peat deposit and associated site access difficulties. Site traffic was limited to a small argocat (see Figure 5.9c), which is a lightweight tracked vehicle used for traversing bogs. In keeping with environmental concerns, and considering the topography of the bog, the decision was made to apply stress increments using large capacity water tanks. These water tanks are relatively light when empty, and can therefore be easily transported to the site location using an argocat. A site location (see Figure 5.1) was chosen which was considered acceptable to the NPWS, and was close to several small lakes, which allowed the stress increments to be applied using the water tanks.

Although Bloetjes and van der Meer (1992) presented stratigraphical data for the entire bog, the grid spacing that they used was considered too coarse to provide representative information about the subsurface conditions at the test site. To this end, the author carried out a series of profile and classification tests in the immediate proximity of the test site. A Macintosh probe was employed in an attempt to create a profile of the soil resistance with depth in the peat layer. However, rather than requiring a number of blows to penetrate the soil, the probe sank through the peat layer under its own weight. The advancement of the probe stopped at an average depth of 8.0 m[1], at which point heavy blows from a large hammer caused little or no further movement. It can be assumed therefore, that at the test site, the peat layer extends an average 8.0 m beneath ground level, and that the peat is underlain by a much stiffer material, which, based on Bloetjes and van der Meer's data, is most likely to be Lacustrine clay. Examination of Figure 5.4 shows the total peat depth at

[1] averaged from 4 separate soundings over an 8 x 4 m grid

(a)

(b)

(c)

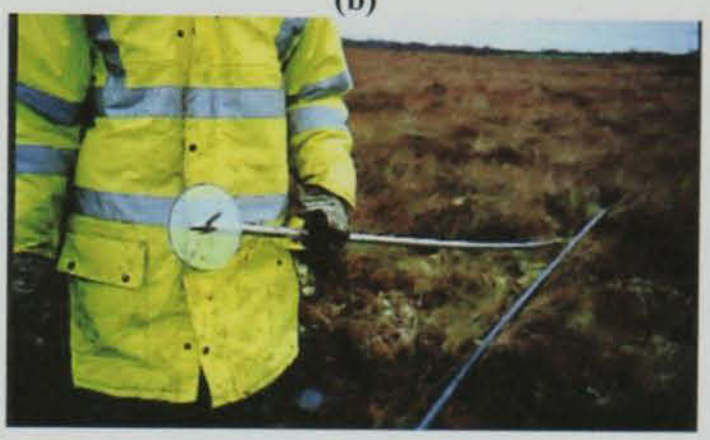

(d)

(e)

(f)

Figure 5.9 (a) Hand-augering holes for settlement plates (b) Inserting benchmarks (c) Placing railway sleepers (d) Settlement plate (e) Test site before the tanks were positioned (f) Test site conditions, March 1999

the chosen test site to be close to 8 m, which is consistent with the findings from the probe tests.

5.3.2 Peat classification

As discussed in § 3.3, undisturbed samples could only be obtained by carving block samples from a hand-excavated pit. However, disturbed samples were obtained from various depths within the peat layer using a *Vertex Soil Sampler*. Although the Hiller sampler is usually used for obtaining peat cores, the Vertex sampler had the advantage of

being able to control the depth from which the peat is retrieved, and limiting disturbance and mixing of the sample. Samples were obtained at two different locations from between 2.0 and 6.0 m depth; no samples could be retrieved from 1.0 – 2.0 m, as the peat would not enter the sampling tube. Bloetjes and van der Meer (1992) experienced similar problems when using a Hiller sampler on Clara bog. The samples were sealed in plastic bags and brought back to the laboratory for classification. These classification tests included ignition loss, water content and von Post humification. All samples registered between 2 and 3 on the von Post humification scale, identifying the peat as a poorly humified fibrous peat. The amount of coarse fibres identifiable in the samples seemed to be slightly reduced in the samples retrieved from depth, which would suggest that the peat encountered at greater depths was older and more decomposed. This observation however, was not reflected in the degree of humification according to the von Post scale. The peat cores provided no evidence to the existence of a layer of strongly humified peat or fen peat within the first 6 metres. This conflicts with the stratification data provided in Figure 5.6 and Figure 5.7, which suggests that a layer of strongly humified peat exists 3.5 m below ground level. The undulating nature of the peat layers, and the coarseness of the sampling grid employed by Bloetjes and van der Meer (1992), evidently have affected the accuracy of Figure 5.6 and Figure 5.7.

The results of the water content and ignition loss tests are shown in Figure 5.10, where it is clear than the water content is extremely variable, ranging from 700% to 2500%. Similar scatter in the water content of Clara peat was observed by Samuels (1992), who reported water contents ranging from 950% to 3910%. The variability in the loss in ignition is much less severe, with values falling within the narrow bracket of 96.4% to 98.6%. *In situ* vane tests were also performed at various depths within the peat layer; results varied slightly between 9 kPa and 12 kPa, with the majority measuring 10 kPa. These results are summarized in Figure 5.11 together with *in situ* vane test results cited by Orr & McEnaney (1994) for three locations in Clara Bog West, approximately 250 metres to the west of the Clara-Rahan road. The vane test results reported herein are generally higher than those recorded by Orr and McEnaney (1994), although the latter showed a high degree of spatial variability, attributed by the authors to variations in the depth of the acrotelm, and the degree of humification. However, the results reported here are in good agreement with the typical undrained shear strength value of 10 kPa suggested by Rodgers (1997) for an Irish peat of high moisture content (*ca.* 1000% – 1500%).

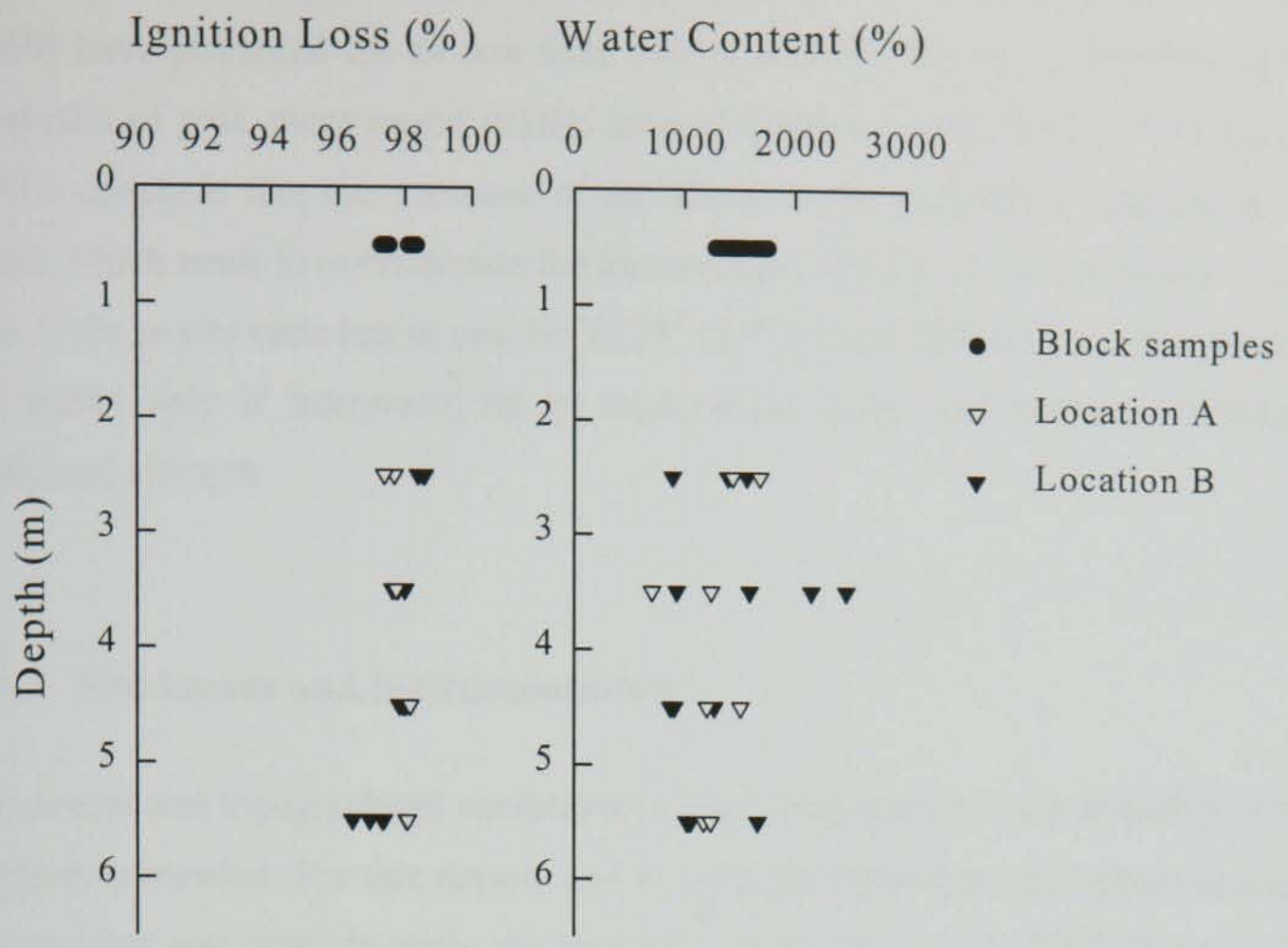

Figure 5.10: Ignition loss and water content values at the test site location

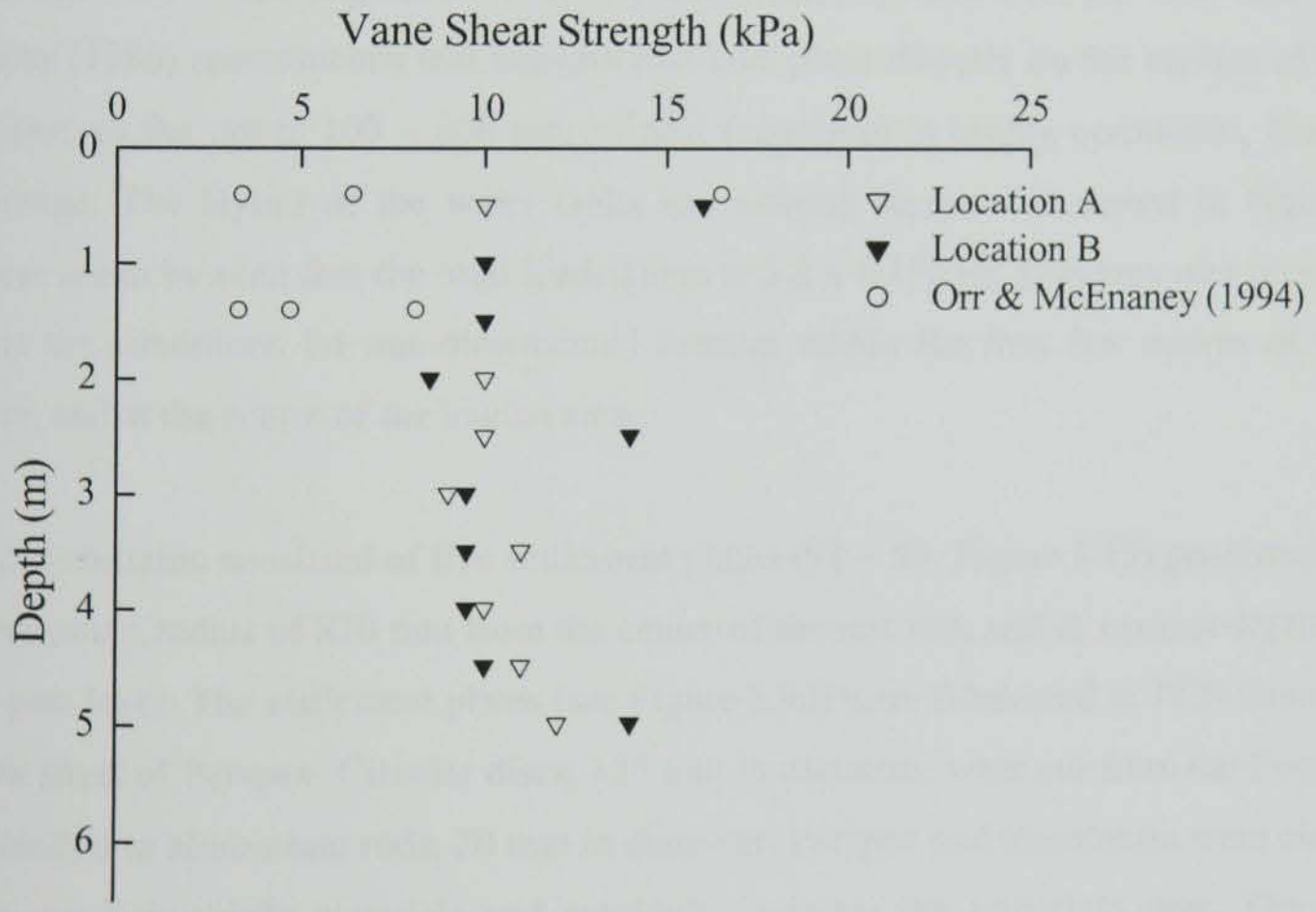

Figure 5.11 *In situ* vane test results at the test site location

Average undrained shear strength values of 10 kPa were also reported by Samson & La Rochelle (1972) and Lefebvre *et al.* (1984) for two separate Canadian fibrous peat deposits with material properties comparable to those in Clara. Controversy exists surrounding the

suitability of the vane test for peat. Although Bell (1978), Hanrahan (1964) and McFarlane (1960) have promoted the *in situ* vane test as a useful means of determining the shear properties of peat, more recent studies such as Landva (1980), Edil (1997) and den Haan (1997) conclude that the presence of the fibres in the peat has a reinforcing or tensile effect, which tends to overestimate the true strength of the peat. An extensive review of the role of the *in situ* vane test in peat by TC15[2] (1997) concluded that *in situ* vane test results are useful only if interpreted as an engineering index, and not as a measure of the undrained strength.

5.3.3 Site layout and instrumentation

The access and topographical conditions in Clara bog restricted the available construction methods somewhat. For this reason, and to keep the environmental impact to a minimum, the decision was made to apply the load increments using cubic 1000 litre capacity water tanks arranged on a platform of wooden railway sleepers. The practice for field tests on mineral soils is to remove the upper topsoil and to construct the embankment directly on a drainage mat, which is placed on the excavated surface. However, for field tests on peat, Hobbs (1986) recommends that construction take place directly on the surface of the peat deposit, as the upper 100 – 600 mm of peat (acrotlem) is highly permeable, thus aiding drainage. The layout of the water tanks and railway sleepers is shown in Figure 5.12, where it can be seen that the total loaded area is 5.2 x 4.175 m. This area was presumed to meet the conditions for one-dimensional loading within the first few metres of the peat layer, and at the centre of the loaded area.

Instrumentation consisted of five settlement plates (S1 – S5, Figure 5.12) positioned within a maximum radius of 870 mm from the centre of the test site, and at various depths within the peat layer. The settlement plates (see Figure 5.9d) were fabricated in TCD from a 5 mm thick sheet of Perspex. Circular discs, 125 mm in diameter, were cut from the Perspex and connected to aluminium rods, 20 mm in diameter. Perspex and aluminium were chosen, as they are lightweight materials and wouldn't compress the underlain peat. The original design specified that the settlement plates be positioned at 500 mm, 1000 mm, 2000 mm, 3000 mm and 4000 mm. The settlement plates were to be positioned in holes augered to the diameter of the settlement plate (125 mm). Plastic casing was initially proposed as a

[2] ISSMFE Technical Committee on Peat, initiated in 1985

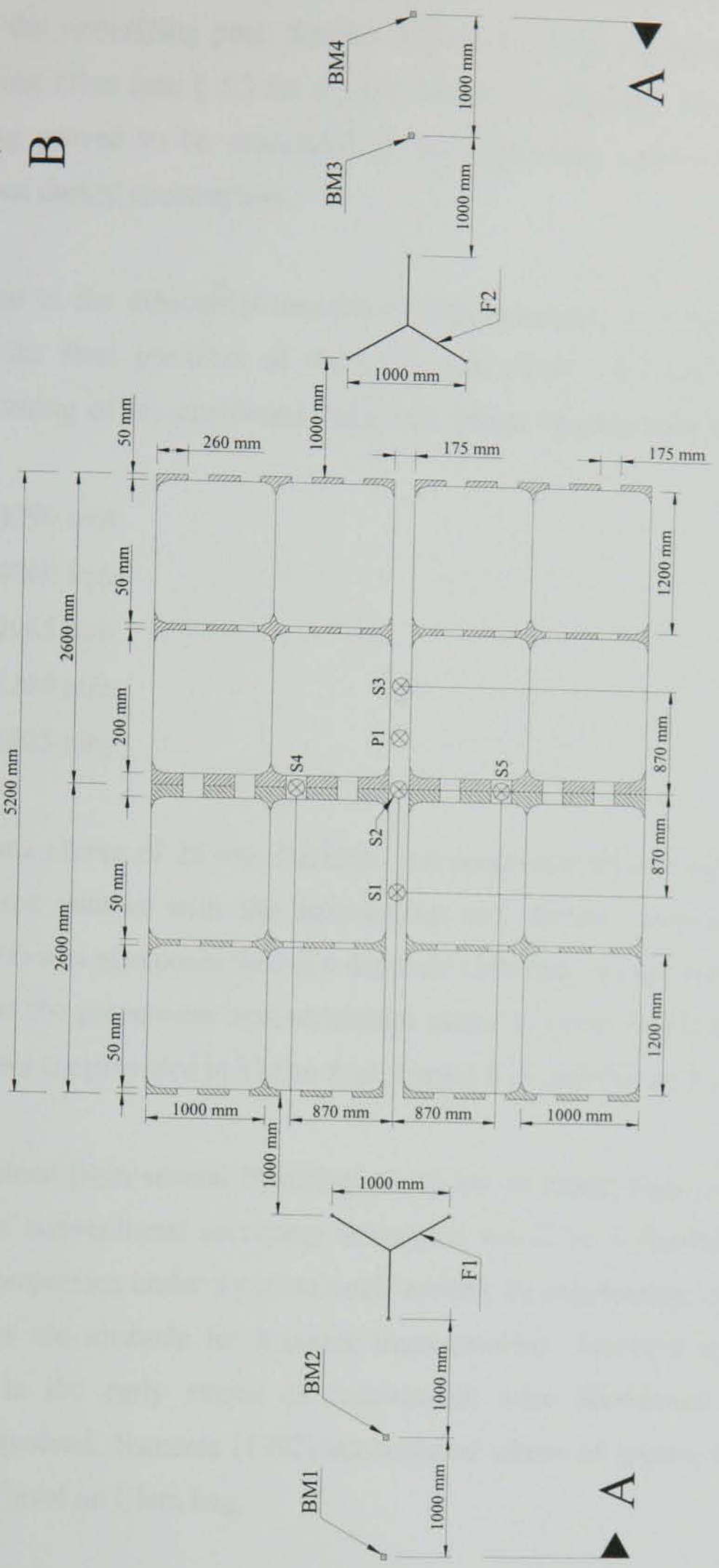

Figure 5.12: Plan view of the site layout

means of ensuring that the excavated holes remained open until the settlement plates were in the correct position. However, a preliminary test on the bog, which involved pushing a thin walled plastic pipe, 150 mm in diameter, through the peat was unsuccessful, as a plug

formed at the base of the open-ended pipe. Further advancement of the pipe simply compressed the underlying peat. Similar difficulties were experienced with thin-walled U100 sampling tubes (see § 3.3 for a more detailed discussion). Further tests without the aid of casing proved to be successful as the high water table ensured that the holes remained open during construction.

However, due to the difficulties associated with accurately controlling the depth of the hand-auger, the final positions of the settlement plates were not exactly as intended. Careful measuring of the positioned settlement plates showed their depths below ground level to be:

- S1 – 3790 mm
- S2 – 4060 mm
- S3 – 2065 mm
- S4 – 1360 mm
- S5 – 1025 mm

An outer plastic sleeve of 25 mm diameter was positioned around each of the settlement rods to prevent contact with the surrounding soil during compression. A standpipe piezometer (P1) was also positioned at a depth of 2500 mm. A plan view of the site layout, with details of the piezometer and settlement plates is given in Figure 5.12. Additional schematic views are provided in Figure 5.13, Figure 5.14 and Figure 5.15.

Experience gained from several hydrological studies in raised bogs in Ireland convinced the author that conventional surveying techniques would be unfeasible in Clara. As the peat readily compresses under a person's self-weight, an engineering tripod and surveying level would be too unstable for accurate measurements. Attempts to use a tripod and dumpy level in the early stages of construction were abandoned due to the large inaccuracies involved. Samuels (1992) encountered errors of greater than 75 mm when using a dumpy level on Clara bog.

An alternative and novel arrangement was designed, whereby movement of the settlement plates could be measured relative to a datum wire positioned at a fixed height above the test site. The wire used was 1.3 mm diameter stranded *Bowden* wire, which is pre-tensioned and sold commercially as throttle and accelerator cables. This datum wire is suspended and tensioned from supports F1 and F2 (see Figure 5.12-Figure 5.14). Each

support was fixed by means of three 32 mm diameter steel bars, which were driven into the underlying mineral soil in a triangular arrangement. Potential movement of the datum wire can be monitored relative to independent benchmarks (BM1 – BM4, Figure 5.12-Figure 5.14). These wooden benchmarks are also lodged into the Lacustrine clay beneath the peat layer.

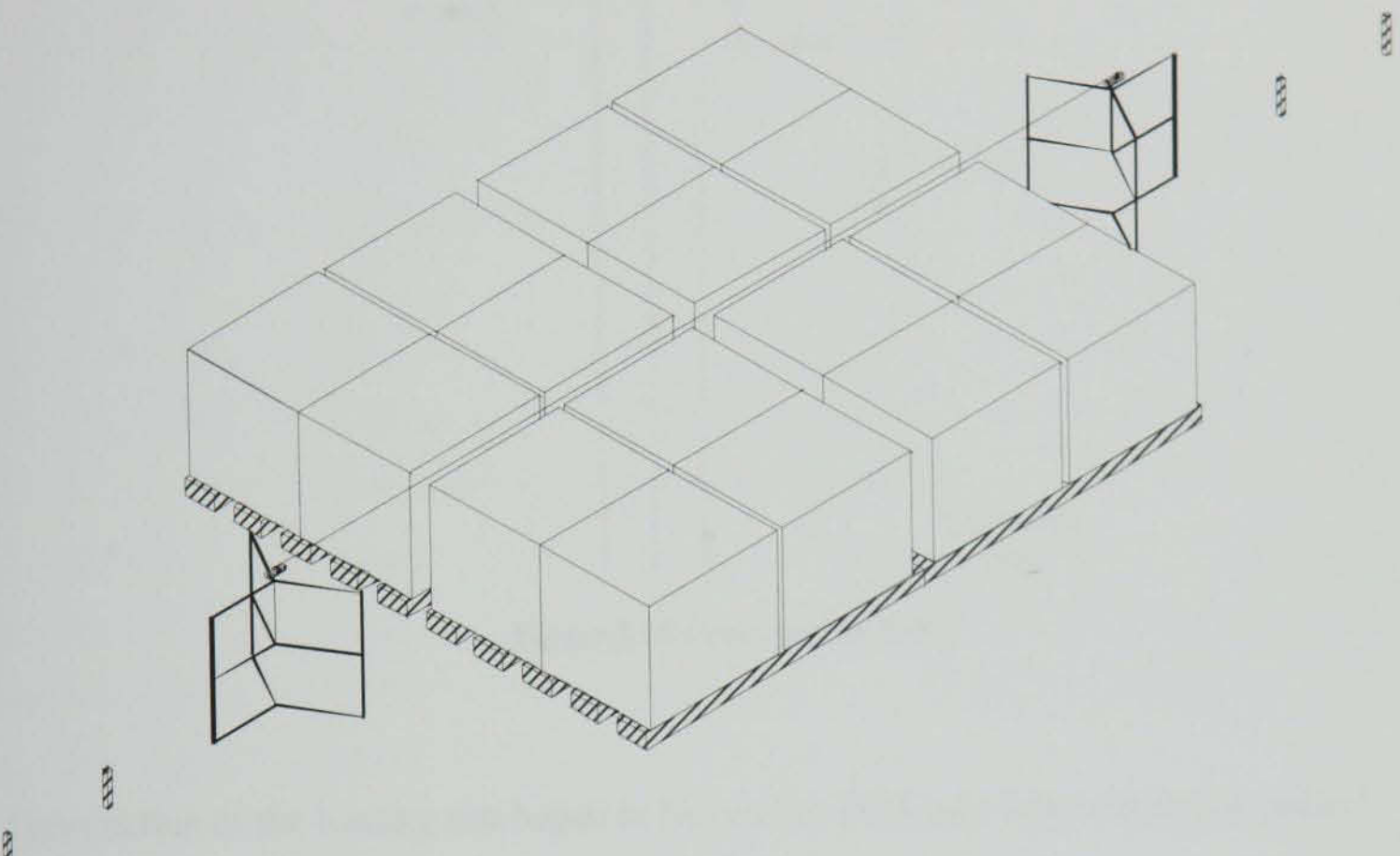

Figure 5.13 Isometric view of the layout

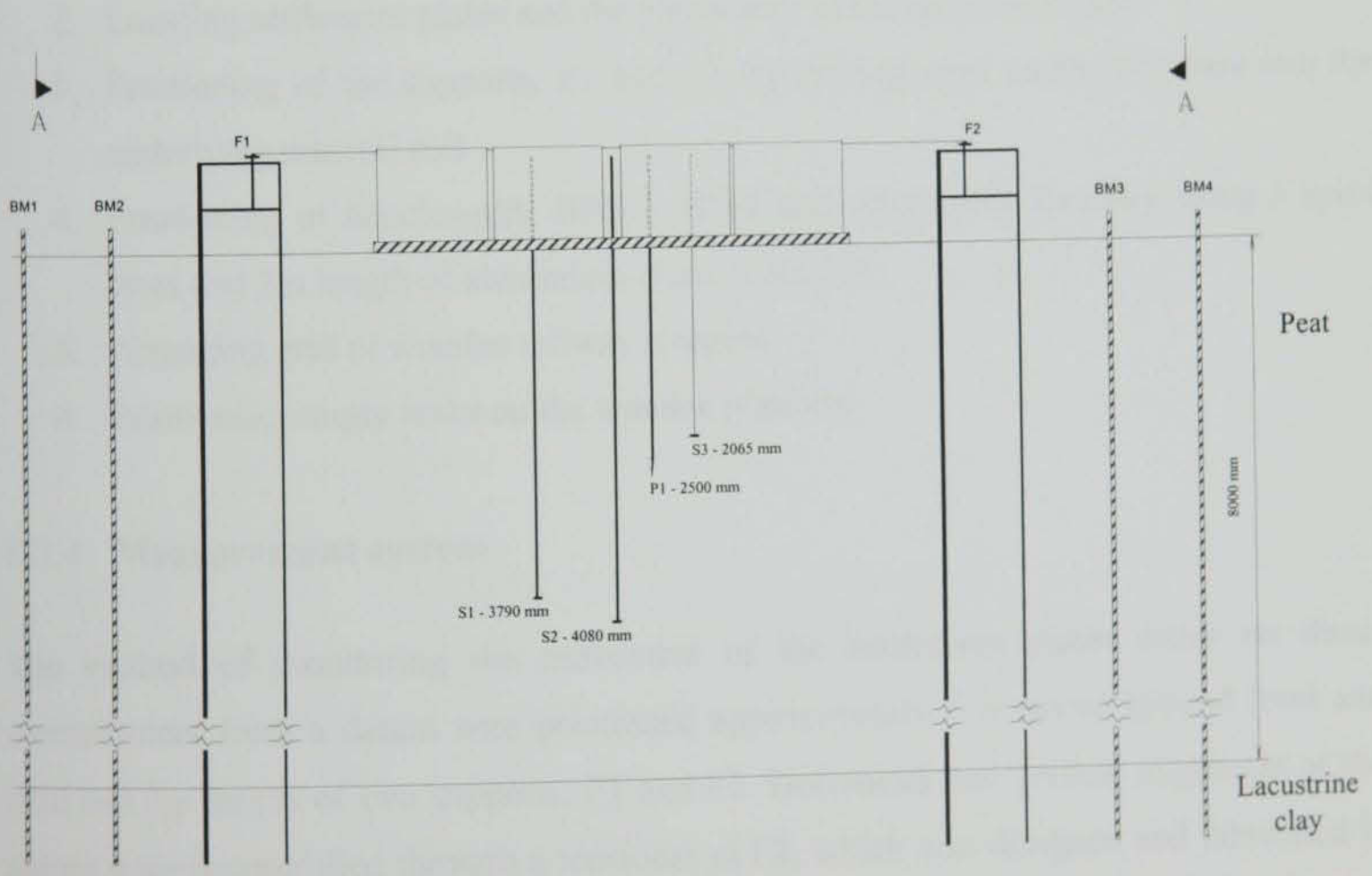

Figure 5.14 Cross-section A-A

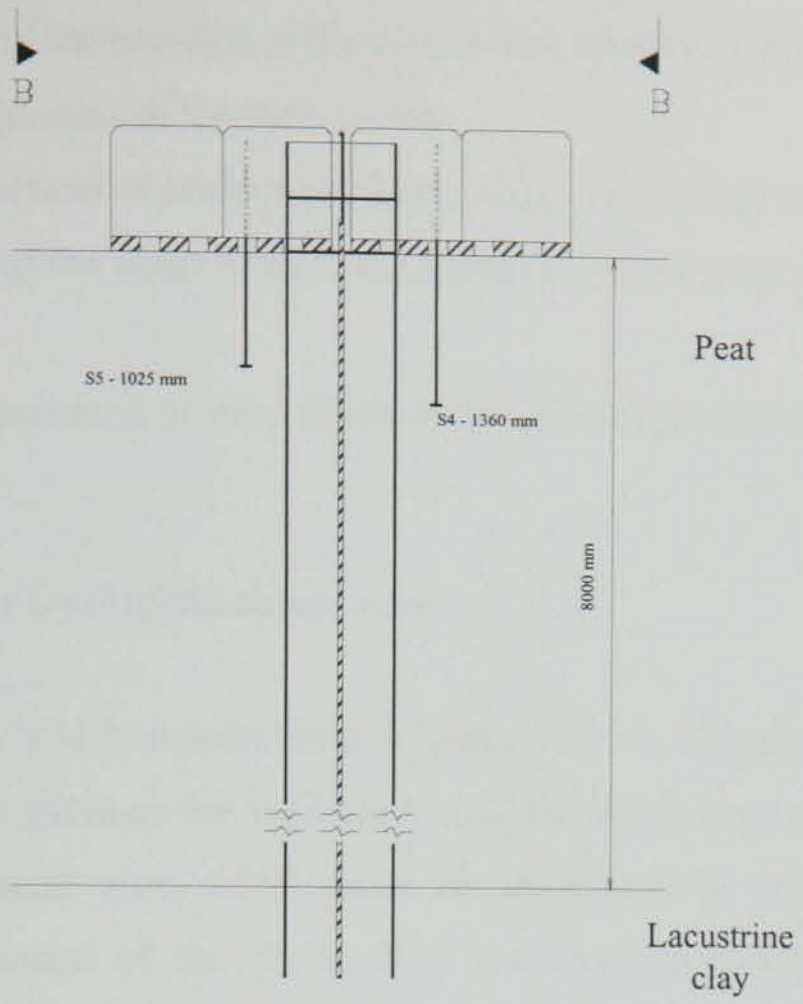

Figure 5.15 Cross-section B-B

Construction of the loading test began in November 1998, and followed this sequence:

1. Hand-augering holes for the settlement plates
2. Locating settlement plates and the piezometer at the required depths
3. Positioning of the supports, F1 and F2, by driving steel connecting bars into the underlying mineral soil
4. Positioning of benchmarks, BM1 – BM4 and subsequent levelling using a spirit level and 2m length of aluminium channel section
5. Arranging grid of wooden railway sleepers
6. Positioning empty tanks on the wooden platform

5.3.4 Measurement system

The method of monitoring the movement of the settlement plates relies on direct measurement from a datum wire positioned approximately 1 m above ground level and held taut by means of two supports, F1 and F2. Horizontal and vertical alignment of the datum wire is controlled through a tensioner at F2, which was designed and fabricated in TCD.

Each set of field measurement encompasses the following steps:

1. Measurement of the position of the datum wire relative to benchmarks
2. Horizontal alignment of the datum wire
3. Direct measurement of settlement plates using a spirit level and measuring tape
4. Measurement of the water level in the standpipe piezometer using a dip meter

The above steps are discussed in more detail in the following sections.

5.3.4.1 Checking the level of the datum wire

As the datum wire is held horizontal over a span of 7.2 m, considerable tension exists in the wire, which exerts strain on the supports F1 and F2. Such strain will invariably result in movement of the datum wire, which must be monitored in order to obtain accurate measurements. Movement of the datum wire is measured relative to the independent benchmarks, BM1 – BM4. A channel section of aluminium, 2 m in length is laid along the tops of the benchmark pairs (BM1-BM2 and BM3-BM4), and the level verified using a spirit level (see Figure 5.16a, Figure 5.16b). The level of the datum wire at each support is then checked relative to the corresponding pair of benchmarks using a laser light mounted on a horizontal base. The laser light is the type sold commercially for use as a pointer in projected presentations. It emits a narrow beam of light, which is visible up to a distance of 100 m. Adjustable vertical feet on the mount control the alignment of the projected beam. The mount was calibrated in TCD laboratories to ensure that a horizontal beam was obtained. The mount and laser light unit is placed on the aluminium section and the height of the datum wire measured using a standard tape measure (see Figure 5.16c).

5.3.4.2 Levelling of the datum wire

As measurements are made directly between the datum wire and the tops of the settlement plates, it is important to ensure that there is no sag in the datum wire. A simple, yet effective means was devised to check for this.

Initially, a measurement was made at the centre of the test site between the datum wire and the aluminium section of the adjustable datum (see Figure 5.16e and § 5.3.4.3 for details). The tension in the wire was increased at F2, and a subsequent measurement made. This

process was repeated until no apparent difference in consecutive measurements was noted. At this stage, the wire was considered to be horizontal. Typically, a sag of 4 – 10 mm existed in the wire between site visits. As the tension increase in the datum wire could potentially adjust the height of the datum wire at supports F1 and F2, the steps described in the previous section are then repeated.

(a)

(b)

(c)

(d)

(e)

(f)

(g)

Figure 5.16 (a) & (b) Checking the level of the benchmarks (c) Measuring the height of the datum line relative to the benchmarks (d) Filling the tanks to capacity for the second stress increment (e) Adjustable datum (f) Checking settlement plate readings (g) Test site conditions, November 2000

5.3.4.3 Measuring the level of the settlement plates

After the steps listed in § 5.3.4.1 and § 5.3.4.2 have been completed, the top of each settlement rod is measured relative to the datum wire using a standard tape measure. This is a simple procedure for settlement plates S4, S2 and S5 as they are directly under the wire, but for S1 and S3 an alternative means was required. To this end, an *adjustable datum* was designed, which would allow a straight aluminium section to be levelled horizontally, and raised or lowered to the height of the datum wire. Measurements between the outlying settlement rods and the top of the aluminium section can then be made.

Details of the adjustable datum (see Figure 5.16e), which is positioned close to the centre of the test site, are provided in Figure 5.17 and Figure 5.18. The horizontal level of the aluminium section (4) is checked using a spirit level, and controlled by adjusting the levelling bolts (2) at the base of the adjustable datum. The height may be adjusted so that it matches that of the datum wire. The aluminium section can be rotated through 360° so that it is in direct alignment with the settlement rod.

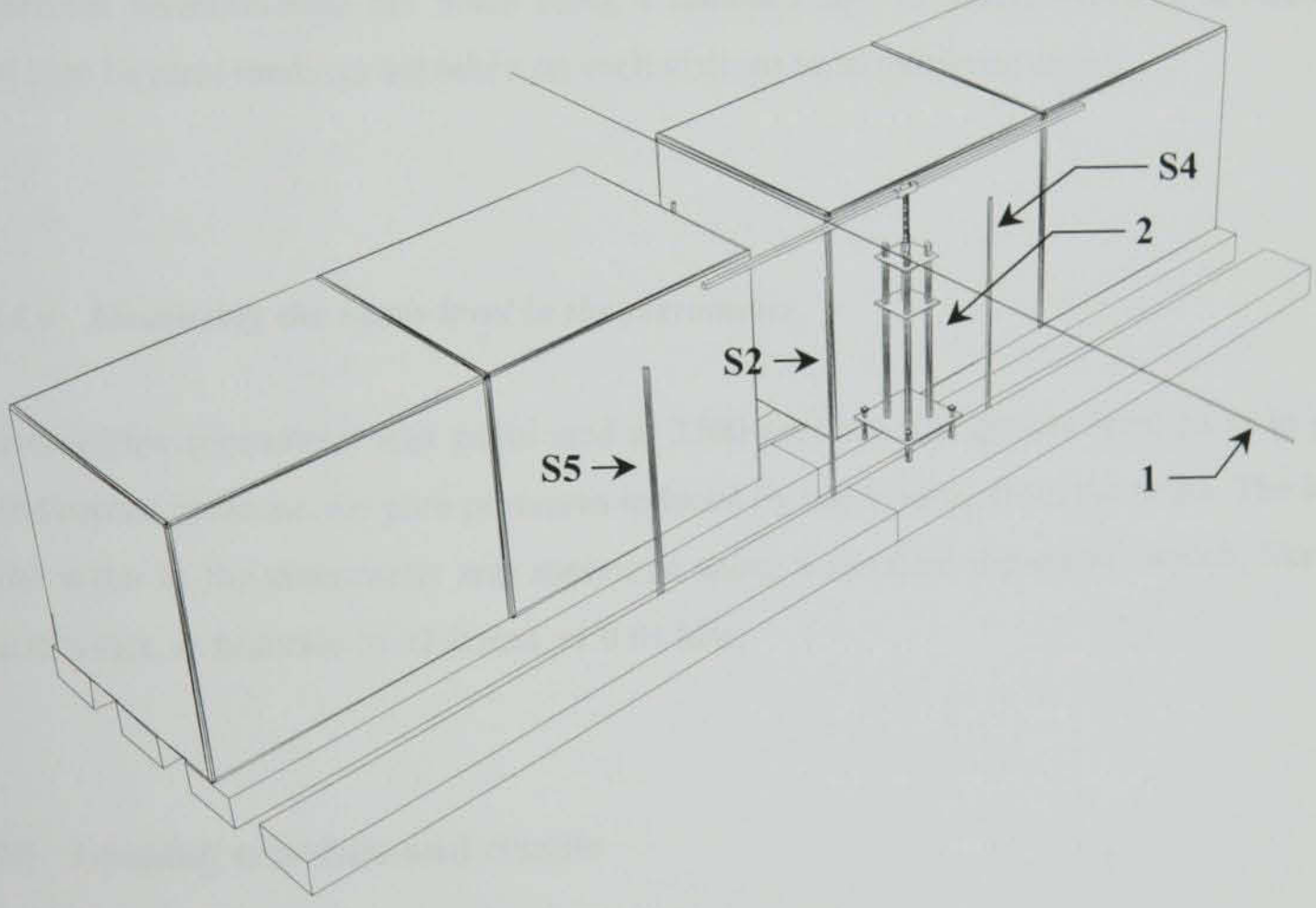

Figure 5.17 Schematic view of the measuring system: (1) datum wire (2) adjustable datum

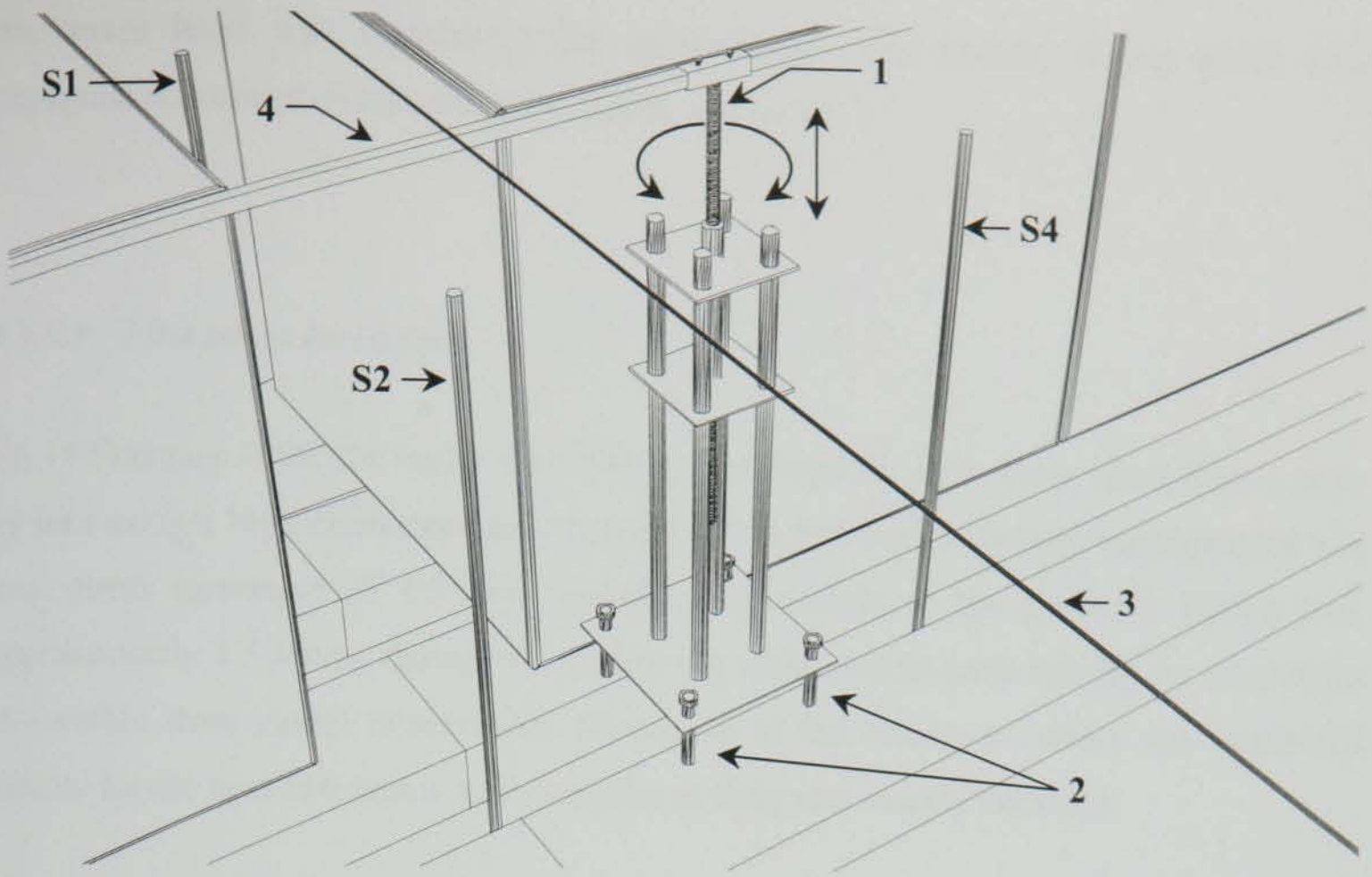

Figure 5.18 Detail of adjustable datum: (1) Vertical adjustment (2) Levelling bolts (3) Datum wire (4) Aluminium section

Settlement measurements are made using a standard tape measure, which is accurate to ±1.0 mm. Several readings are taken on each visit, so as to minimise errors.

5.3.4.4 Measuring the water level in the piezometer

The standpipe piezometer was positioned at 2500 mm beneath ground level so as to give an indication of the excess pore pressures induced by the loading from the tanks. The level of the water in the piezometer was measured using a standard dip-meter, which, like the tape measure, is accurate to ±1.0 mm, or 0.01 kPa.

5.3.5 Loading schedule and results

The weight of each railway sleeper is approximately 70 kg, which, considering the number of sleepers, and the loaded area, corresponds to a nominal stress of 0.6 kPa. The weight of the empty plastic tanks and their aluminium cages was considered to be insignificant. This

low stress level was maintained for approximately one month, during which time negligible movement of the settlement plates was noted.

5.3.5.1 First stress increment

On 15 February 1999, the tanks were filled to half-capacity with water taken from a near-by lake using a high discharge-capacity pump. This first load increment corresponded to a total stress increment of 4.3 kPa (including the weight of the sleepers). Filling took approximately 1.5 hours, during which time the tanks settled quite rapidly, by an amount discernible from casual observation. Movement of the settlement plates was monitored closely for the next few hours, and thereafter at daily and weekly intervals.

As the total stress concentration is greater in the centre of the loaded area, larger settlements occurred here. This resulted in a ground surface that deformed in a concave manner, which tended to tilt the water tanks towards the centre of the site. Within four days the severity of the tilt was such that settlement plates S1 and S3 became lodged between the tanks, preventing further movement. The situation was alleviated by prising the tanks apart with a lever, and placing timber spacing blocks between the tanks. This problem was not encountered in the perpendicular direction (S4 – S5), as the spacing was larger here to allow for access.

The piezometer appeared to register an increase of approximately 0.235 kPa upon application of the first stress increment. Subsequent readings remained virtually unchanged for the duration of this stress increment.

The performance of the settlement plates, S1, S2, S3 and S5 are shown in Figure 5.19. Measurements taken from S4 showed little or no movement, despite its position at 1360 mm beneath ground level. The data in Figure 5.19 shows that for the plates located closer to the original level of the ground surface, large settlements occurred within the first 2 hours, although periodic measurements could not be taken during this time as the fill was in progress. Furthermore, as expected, the settlement plates at deeper locations moved less than those positioned higher.

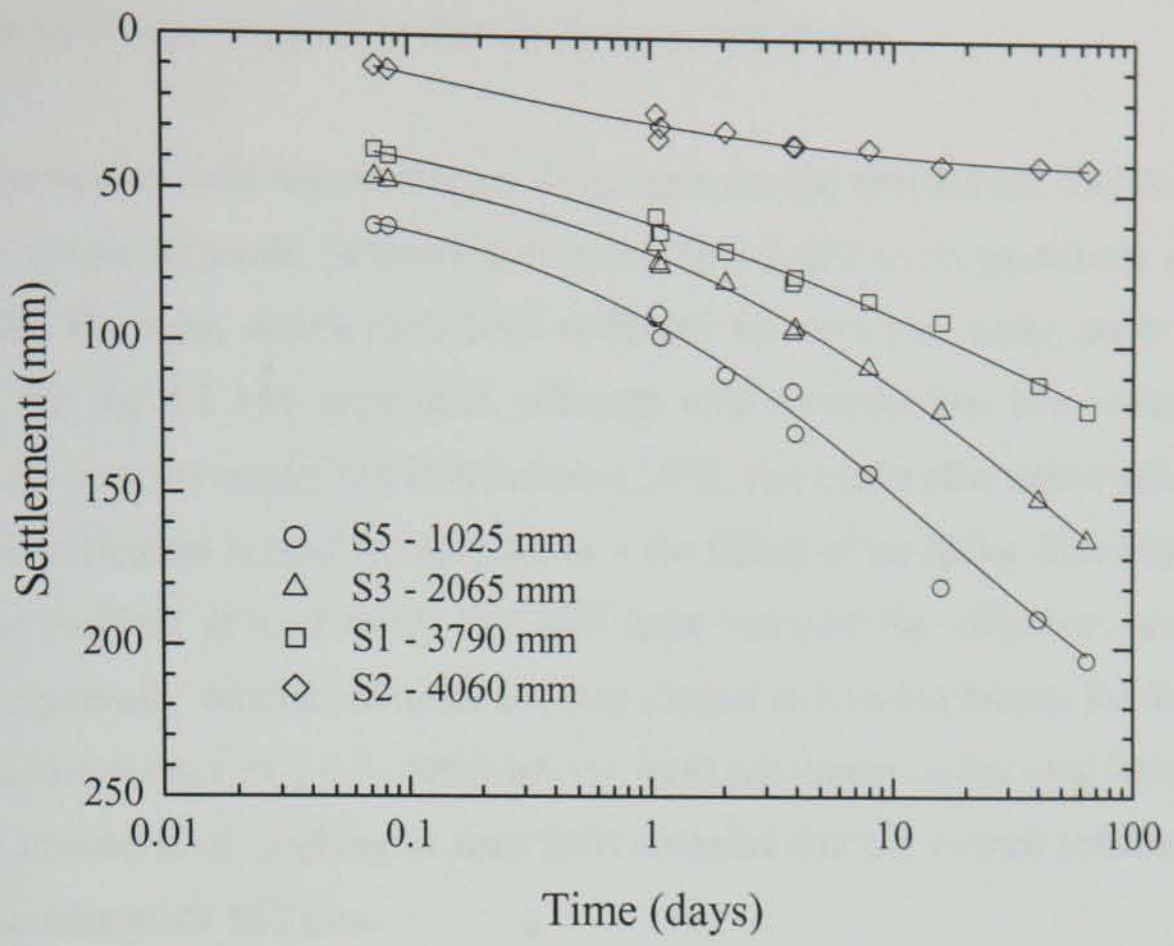

Figure 5.19 Performance of settlement plates with time for the first stress increment

5.3.5.2 Second stress increment

The first stress application was maintained for just over two months, after which time the tanks were filled to capacity (see Figure 5.16d), giving a total stress of 7.9 kPa. This second stress application registered a further, slightly higher increase in the measured pore pressure (0.285 kPa), which remained unchanged for approximately 10 days. The pore pressure response is considered unreliable, as the instantaneous measured increases in pore pressure are much lower than the corresponding applied stress increments. This may be due to smear effects developing around the tip of the piezometer cone, which could impair the performance of the piezometer. Edil and Den Hann (1994) also discuss the difficulty in determining the end of primary consolidation from piezometer measurements. They point out that excess pore pressures often remain high due to the ineffectiveness of the piezometers, and that excess pore pressures can be induced as the tip of the piezometer settles. Samson and La Rochelle (1972) had similar experiences with non-effective piezometers in a fibrous peat deposit in Canada.

As was the case with the 4.3 kPa stress increment, settlement plate S4 failed to respond to the increase in surcharge, suggesting that the Perspex disc broke.

Daily and then weekly field measurements were made for the first month, and thereafter at progressively longer intervals. Settlement data for the 7.9 kPa stress increment are shown in Figure 5.20. The data, which have been collected for over two years, show a similar trend to that for the 4.3 kPa increment, although with considerably less scatter. Figure 5.16g shows the test site conditions in November 2000, two years after construction began. The excessive settlement is readily apparent, as is the tilting of the tanks. The water table is clearly at the original ground level; this will have reduced the effective stress of the footing, as the partially submerged tanks are now subject to buoyant forces. Implications of this are discussed further in § 6.5. Although the total settlement of the peat layer was not monitored at ground level, probing in June 2001 revealed that the overall settlement of the tanks was approximately 860 mm.

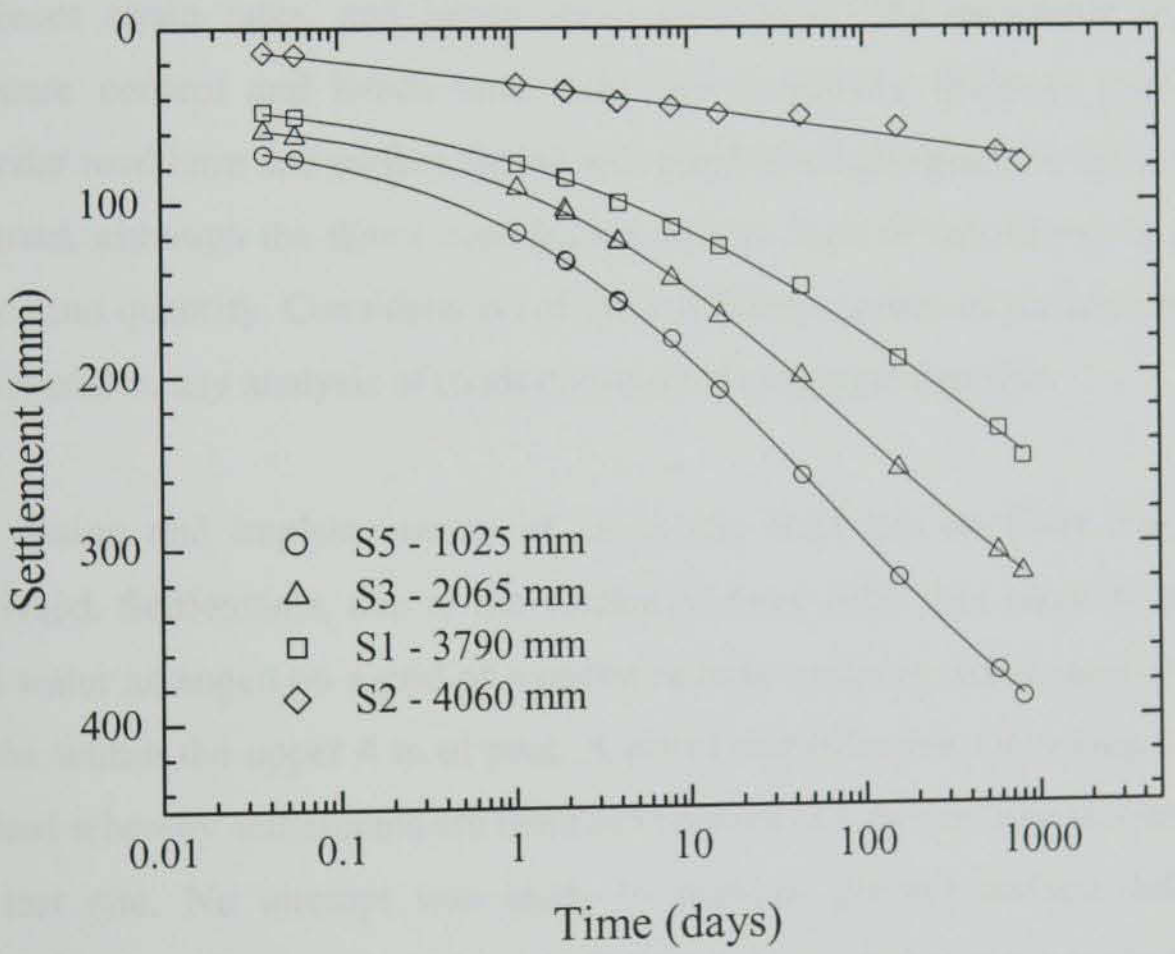

Figure 5.20 Performance of settlement plates with time for the second stress increment

5.4 SUMMARY AND CONCLUSIONS

This chapter reviewed the performance of a road constructed over Clara bog in the 1800s and provided construction details and settlement records for an *in situ* loading test on the bog. The main findings and notable points from this chapter are discussed below.

1. The settlement of the road over two centuries has been excessive and is still continuing. It is highly probable that the road was constructed over what was once the highest part of the bog, but is now considerably lower, due to subsidence. Stratigraphical transects generated from borehole data show the settlement of the road to be mainly confined to the upper layer of poorly humified sphagnum peat. Settlements have been complicated not only by the continuing creep settlement, but also by the drainage caused by two large surface drains running alongside either side of the road. The effect of these drains has been to increase the effective stress in the peat above the water table, which in itself is continuing to lower. Increases in effective stress will have caused additional consolidation settlement, which increases strain rates, and hence creep settlement. The inevitable reduction in moisture content and hence void ratio due to gravity drainage caused by the granular road base and surface drains will also have contributed to the settlement of the road, although the direct contribution of this form of subsidence is difficult to assess and quantify. Consideration of these different causes of settlement should be considered in any analysis of roads constructed over peat deposits.

2. The design and implementation of an *in situ* load test on Clara bog has been described. Settlements, due to the surcharge from 1000 litre capacity tanks filled with water arranged on a grid of wooden railway sleepers, are measured at various depths within the upper 4 m of peat. A novel and effective measuring system was devised whereby settlements are recorded relative to a datum wire suspended above the test site. No attempt was made to monitor ground surface deformations, although a probing test carried out in June 2001 revealed that the tanks had settled by approximately 860 mm in just over two years. A standpipe piezometer positioned at a depth of 2500 mm failed to operate properly. Partial submergence of the tanks will have reduced the effective stress at ground level, although the implications of this have not been considered here (see § 6.5). The low stresses involved in the field test are comparable with those associated with rural roads

constructed over bogs in Ireland. Construction and maintenance options are limited in these cases as the pavement thickness required to withstand the loads imposed by local traffic and agricultural vehicles invariably causes settlements which are considered excessive (Farrell, 1997). The results of the field test can therefore be considered as a practical and useful case study for practising geotechnical engineers.

Chapter 6

Interpretation and discussion of experimental results

Chapter 6

Interpretation and Discussion of Experimental Results

6.1 INTRODUCTION

The results of the experimental programme considered in this Thesis have been described in detail in Chapters 4 and 5. However, thus far no attempt has been made to interpret these data in a manner which may form the basis of useful relationships, or a useful constitutive model. This chapter aims to formulate various aspects of the measured data, with a view towards identifying features of a constitutive model which are required to predict the magnitude and rate of settlements under one-dimensional *in situ* conditions. In brief, the following aspects are considered in some detail:

1. Suitable formulations which may be used to describe the response of peat under first-time (or virgin) loading
2. Aspects of long-term creep behaviour both in the overconsolidated and virgin stress region
3. Isotache principle for peat
4. In situ test

6.2 FORMULATION OF VIRGIN STRESS-COMPRESSION CURVES

6.2.1 Application of compression index, C_c

The conventional method of formulating virgin stress-strain data for soils is through the compression index, C_c. The premise of this method is that plotting effective stress on a

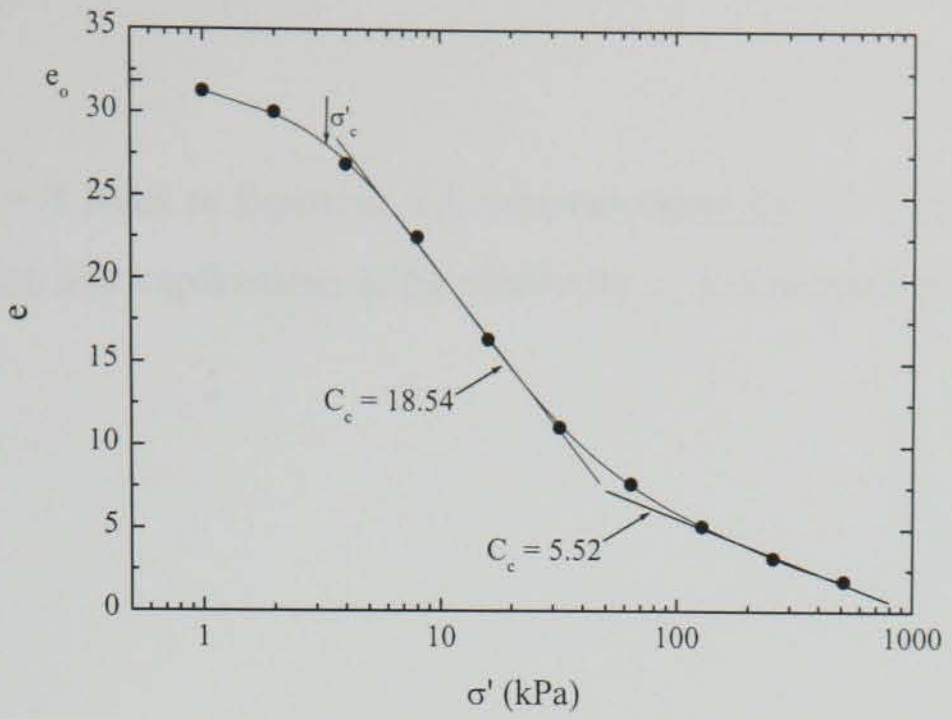

Figure 6.1 Determining C_c from e – log σ' data of CL_MSL_04

semi-logarithmic scale will linearise e - σ' data. However, as can be seen from § 4.4.2, peat stiffens more rapidly than can be linearised on e – log σ' scales. This is particularly evident on Figure 6.1, which shows an attempt to describe the compression of Clara peat using C_c. Fitting the initial and final portions of the e – log σ' curve results in a decrease in C_c, from 18.5 to 5.5. These values are comparable with the 15 – 4.5 range reported by Lefebvre *et al.* (1984) for a poorly humified fibrous peat with similar properties to Clara peat. This result, together with the non-linear e – log σ' relationships observed for Ballydermot peat and Cork peat suggest that the merit of employing C_c as a compression index is limited. Although C_c remains tolerably constant for Cork silty peat and Belfast organic clay, the parameter is obviously not applicable to all soils, particularly those with a higher initial voids ratio (for example, 5-6). There thus appears to be sufficient justification for adopting an alternative approach.

6.2.2 Use of power function

The generalised power function proposed by den Haan (1992) is reproduced here in Equation 6.1. Den Haan (1992) showed that the structure parameter, σ'_s, in Equation 6.1 could be conveniently taken as zero for a wide range of soils including peats. Two separate virgin compression functions can be obtained from Equation 6.1, depending on the limiting values of specific volume at infinite stress, v_∞.

$$\frac{v - v_\infty}{v_1 - v_\infty} = (\sigma' - \sigma'_s)^{-b} \qquad 6.1$$

Assuming that $v_\infty = 1$ leads to Equation 6.2, whereas choosing $v_\infty = 0$ produces Equation 6.3. The justification and implications of the choice for v_∞ is discussed in § 2.2.3.

$$\frac{e}{e_1} = (\sigma')^{-b} \qquad 6.2$$

$$\frac{v}{v_1} = (\sigma')^{-b} \qquad 6.3$$

The parameters, e_1 and b can be determined from linear regression by rewriting Equation 6.2 as:

$$\ln(e) = \ln(e_1) - b\ln(\sigma') \qquad 6.4$$

The same approach can be adopted for Equation 6.3 to give v_1 and b.

Figure 6.2 shows e - σ' data for CL_MSL_02 fitted by Equation 6.2 and Equation 6.3. Evidently, both functions provide a good fit to the measured data. A further example is provided in Figure 6.3a. In this case the test (CL_MSL_04) involved an initial stress of 1

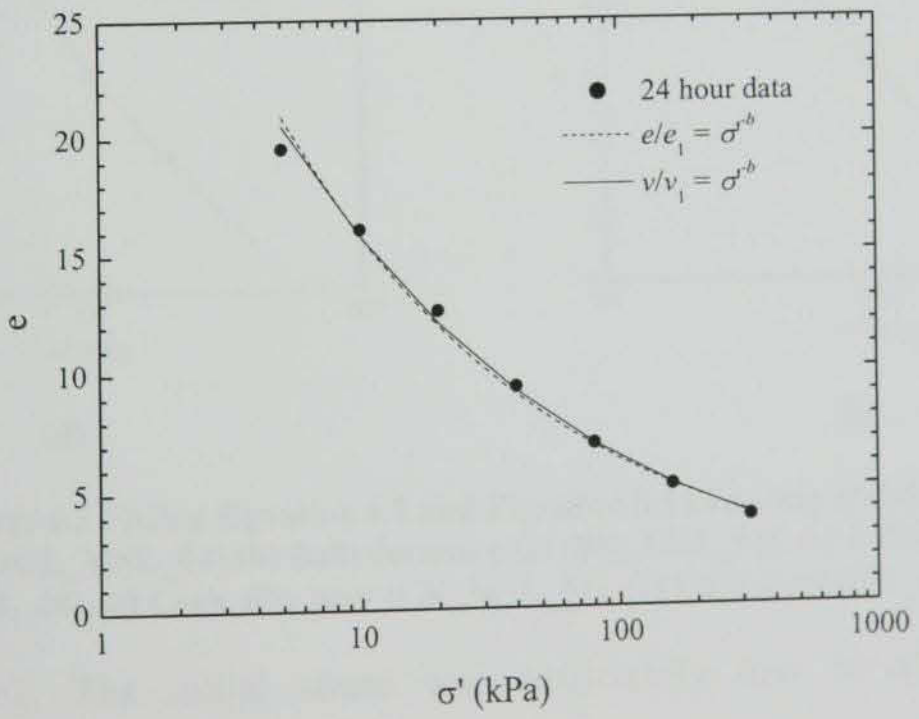

Figure 6.2 Fitting Equation 6.2 and Equation 6.3 to e – log σ' data of CL_MSL_01

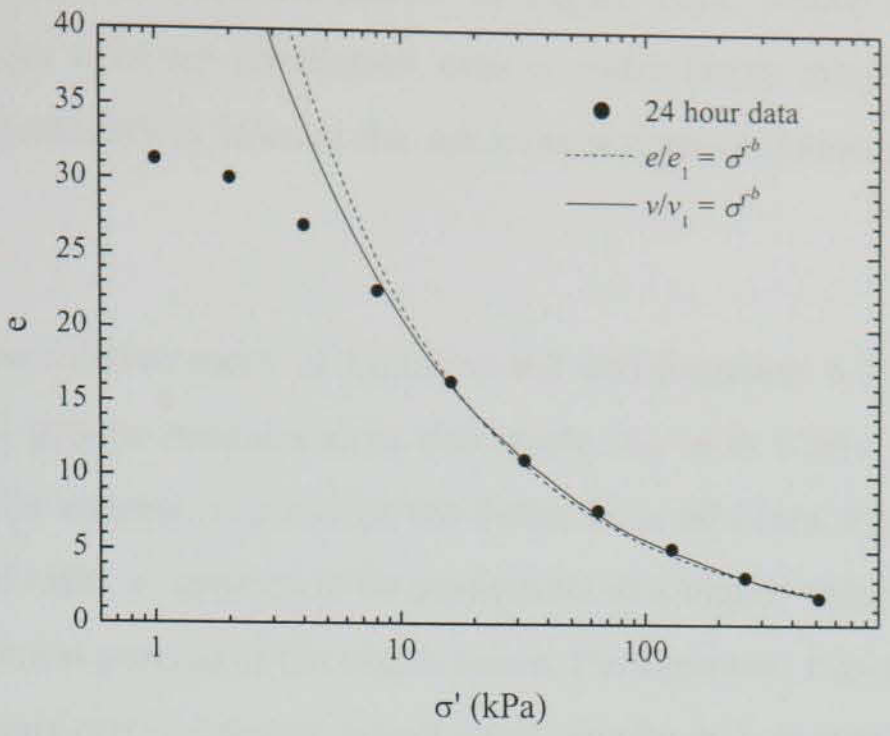

(a)

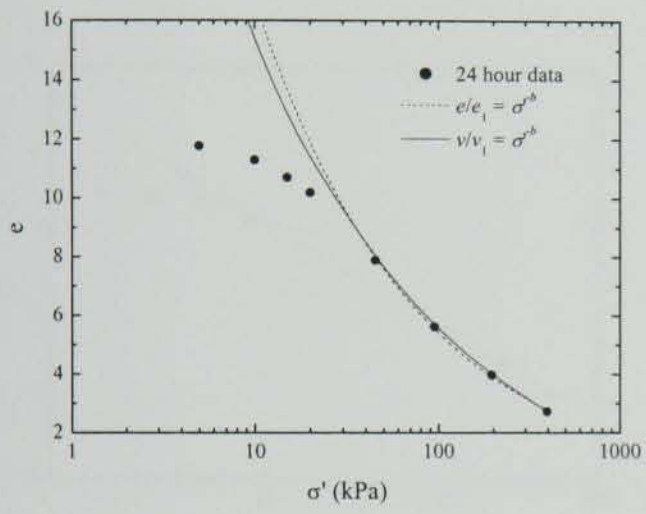

(b)

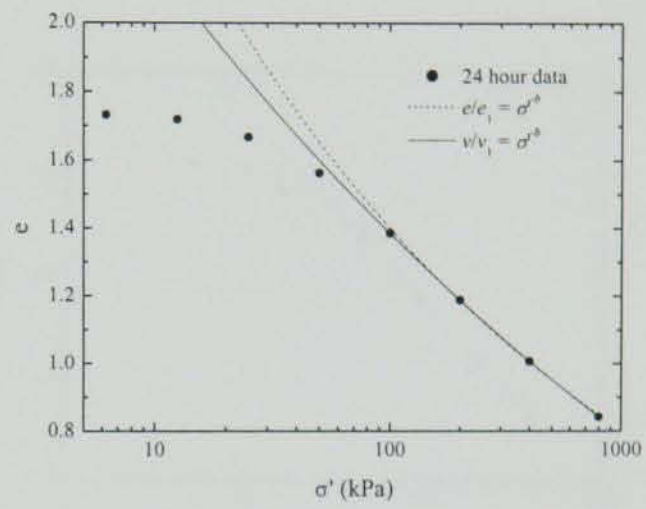

(c)

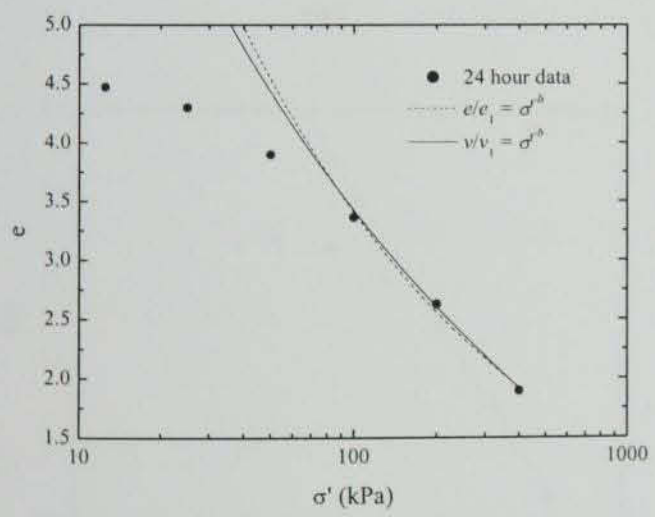

(d)

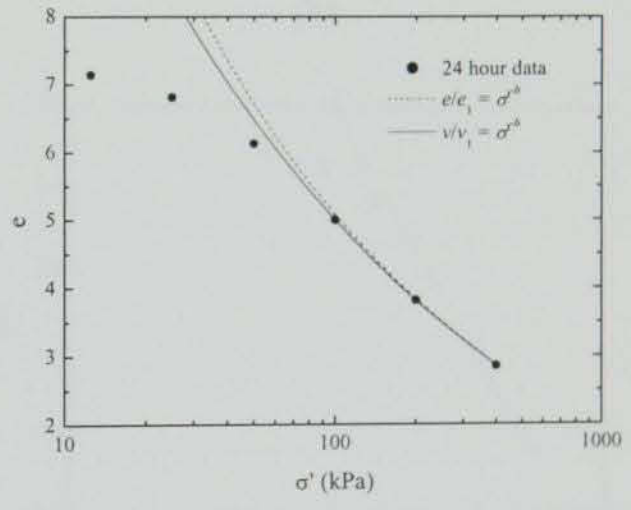

(e)

Figure 6.3 Fitting Equation 6.2 and Equation 6.3 to e – log σ' data of: (a) Clara peat (CL_MSL_04),(b) Ballydermot peat (BD_MSL_01), (c) Belfast organic clay (BF_MSL_04),(d) Cork silty peat (CK_MSL_01), (e) Cork peat (CK_MSL_02)

kPa and a LIR=1. The initial stress was sufficiently low to allow the apparent preconsolidation stress to be observed. In this case the parameters from Equation 6.2 and Equation 6.3 were determined from the virgin stress-strain curve only. The fitted equations

together with the measured data are shown in Figure 6.3a, where it can be seen that Equation 6.3 provides a better correlation over a wider stress range. In particular, the stress-strain curve immediately beyond the apparent preconsolidation stress is fitted quite well.

Figure 6.3 shows the relative merit of Equation 6.2 and Equation 6.3 in fitting the e - σ' data for all the soil groups considered in this study. As with Clara peat, Equation 6.3, which utilises specific volume, v, provides the better fit in all cases. Equation 6.2 which is cast in terms of void ratio, e, appears to be asymptotic at a higher value of stress, resulting in a poor fit to the initial portion of the virgin curve. Furthermore, Equation 6.2 tends to be more convex in the mid-stress interval, which again, results in a slightly poorer fit.

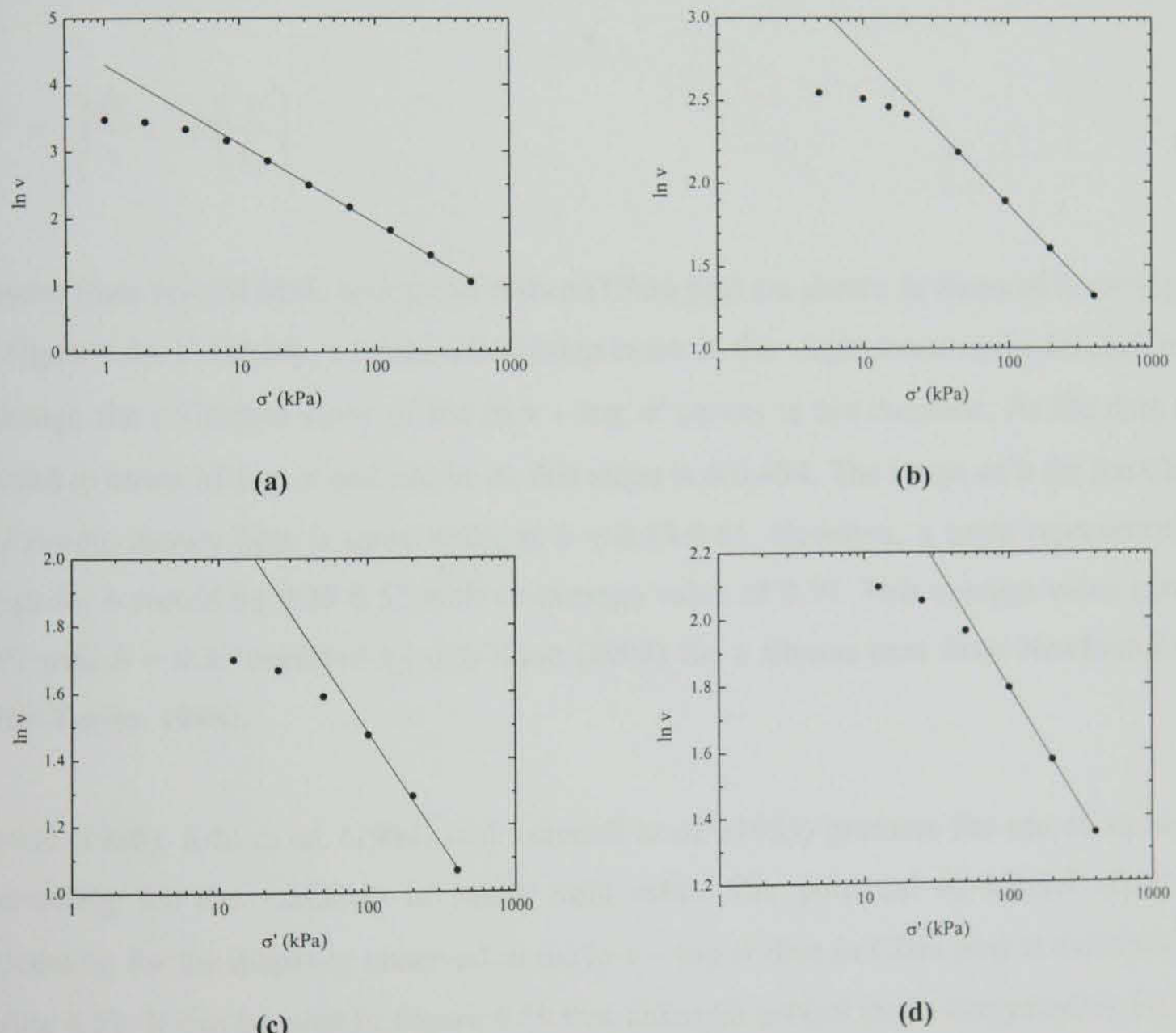

Figure 6.4 Fitting Equation 6.5 to (a) Clara peat (CL_MSL_04), (b) Ballydermot peat (BD_MSL_01), (c) Cork silty peat (CK_MSL_01) (d) Cork peat (CK_MSL-02)

6.2.3 Natural strain-natural logarithmic stress representation

Although Equation 6.3 provides a good fit to the virgin e - $\log\sigma'$ curve, the plotted relationship is still highly non-linear for the more compressible Clara and Ballydermot peat. As expected, linearity can be restored to the virgin compression curve by expressing Equation 6.3 in natural logarithmic form:

$$\ln(v) = \ln(v_1) - b\ln(\sigma') \qquad 6.5$$

Figure 6.4 shows the merit of using Equation 6.5; void ratio on the y-axis is replaced by ln v, resulting in a linear relationship in the virgin stress range. Natural strain is interchangeable with ln v in much the same way as linear strain is with void ratio, e. The definition of natural strain is given in Equation 6.6:

$$\varepsilon^{nat} = -\int_{v_o}^{v}\frac{dv}{v} = -\ln\left(\frac{v}{v_o}\right) \qquad 6.6$$

Results from several MSL oedometer tests on Clara peat are shown in terms of ln v – log σ' in Figure 6.5a. Evidently, a linear relationship exists in the virgin stress range for each test, although the collective slope of the ln v – log σ' curves is not constant. As the data are plotted in terms of log σ' and not ln σ', this slope is b/0.434. The range of b for the Clara test results shown here is quite wide, at b = 0.15-0.61. However, a more representative range for b would be 0.25-0.52 with an average value of 0.39. This average value agrees well with b = 0.39 reported by den Haan (1992) for a fibrous peat from Newfoundland (after Taylor, 1948).

Hobbs (1986), Edil *et al.* (1994) and Leroueil *et al.* (1985) promote the use of strain in accounting for the variation in initial void ratio. The potential of natural strain in accounting for the disparity observed in the ln v – log σ' data in Clara peat is examined in Figure 6.5b. It can be seen in Figure 6.5b that although natural strain compensates for the initial disparity in the curves, at higher stresses the curves tend to diverge. This suggests that despite the natural variability in the ln v – log σ' data, specific volume leads to a more unique relationship over natural strain.

The same exercise was repeated for Ballydermot peat and the results summarised in Figure 6.6. In this case, the relationship is reasonably consistent for both specific volume and natural strain, although the use of natural strain tends to lead to less divergence between the respective tests.

Figure 6.7 compares Belfast organic clay test results in terms of natural strain (Figure 6.7a) and specific volume (Figure 6.7b). As with Clara and Ballydermot peat, the data are linear in the virgin stress range. However, the spacing of the curves is considerable when plotted in terms of both specific volume and natural strain. This variation is primarily due to

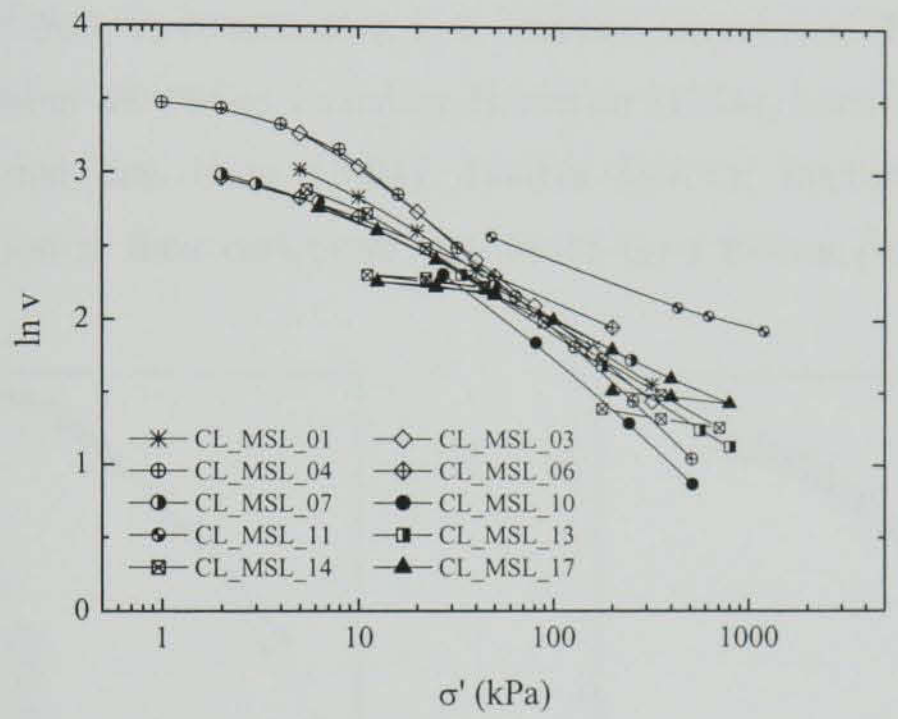

(a)

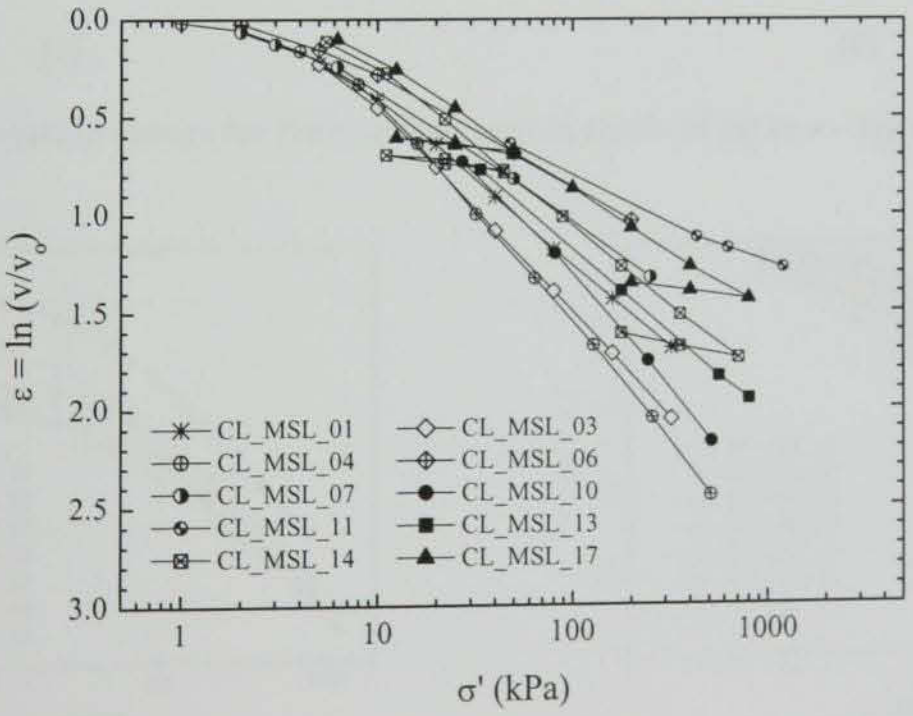

(b)

Figure 6.5 Compression curves for Clara peat in terms of (a) ln v – log σ', (b) ε^{nat} – log σ'

inherent differences between samples. For example, the clay fraction and plasticity index of the samples generally increased with depth; sampling disturbance is also considered to be a significant contributing factor. These effects are considered in greater detail in McCabe (2002).

6.2.4 Uniqueness / variability of compression curves

The variability in the normal compression curves for what would be considered 'identical' samples of Clara peat is considerably larger than that of the block samples of Ballydermot peat. Variability of peat in compression is a common occurrence. This topic has been addressed in a number of studies including Hanrahan (1954), Landva and La Rochelle (1983) and Edil and den Haan (1994). Landva and La Rochelle (1983) showed considerable variation in their oedometer test results for a fibrous peat from Escuminac

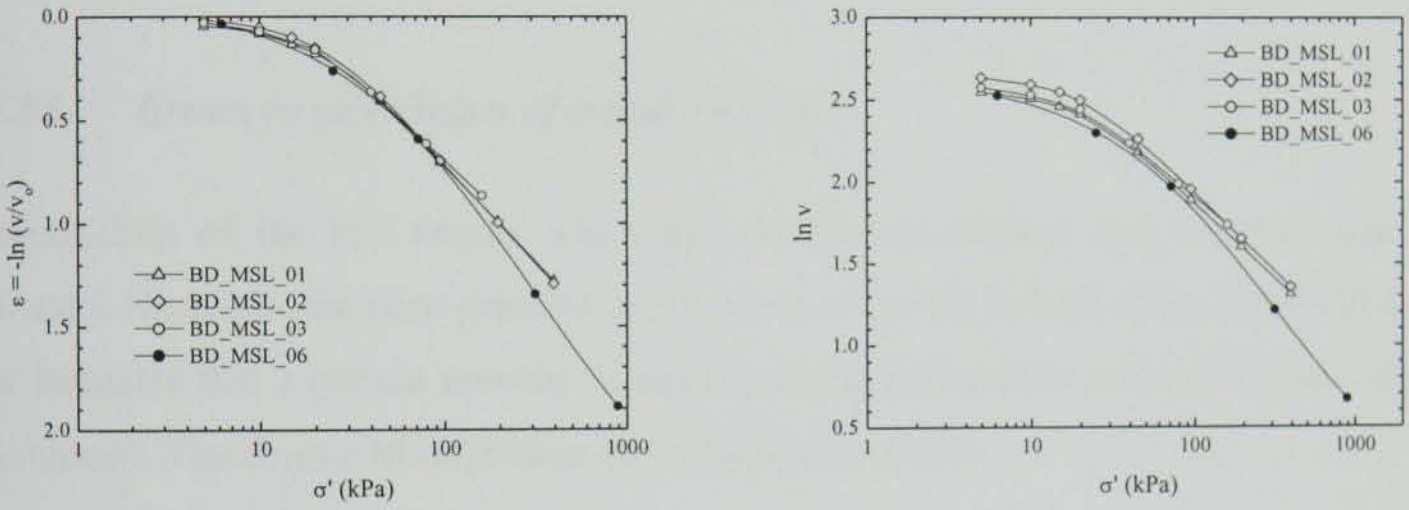

(a) (b)

Figure 6.6 Compression curves for Ballydermot peat in terms of (a) ln v – log σ', (b) ε^{nat} – log σ'

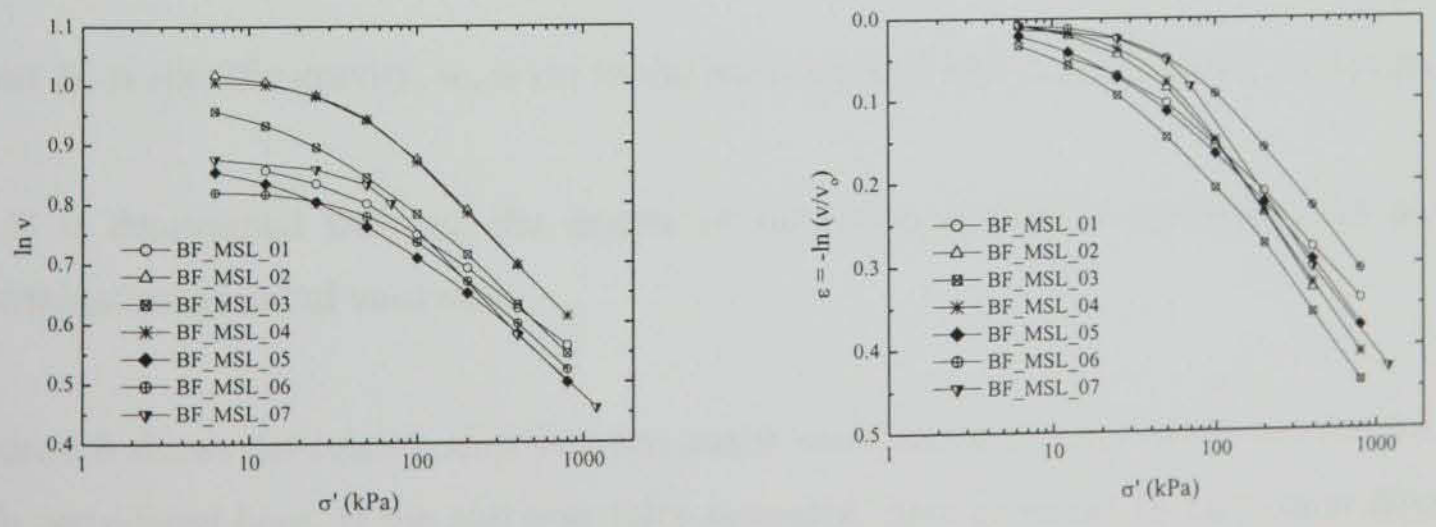

(a) (b)

Figure 6.7 Compression curves for Belfast organic clay in terms of (a) ln v – log σ', (b) ε^{nat} – log σ'

(see Figure 2.18b). Although this is often attributed to natural variation in initial void ratio, interpreting the test data reported here in terms of strain did not lessen the disparity. In the case of Clara peat, normalising the results with respect to initial void ratio actually worsened the correlation. Another factor that is often considered in this respect is sampling disturbance. This may indeed contribute to undesirable precompression of the peat specimens prior to testing, although the effects should be minimal considering that Clara peat specimens were taken from block samples, and that care was taken during specimen preparation. Sampling disturbance is a factor for the Belfast organic clay as tube-sampling methods were employed. Evidently, some other factor(s) are present which influence the compressibility of the peat specimens. One such factor may be the presence of roots, woody remnants or large fibres in the test specimens (Edil, 1994). Another factor may be slight variance in the specific gravity of the peat, although this was shown in § 3.4.4 (Figure 3.5), to be strongly dependent on organic content, which for Clara peat showed negligible variance (see § 3.4.3).

6.2.4.1 Errors in calculation of initial void ratio

Interpretation of the test results was made on the assumption that the peat was fully saturated. However, the pore pressure lag that was observed in both Clara and Ballydermot peat indicates that a certain amount of gas is present in the peat, making the peat slightly unsaturated. The degree of saturation, S_r, is calculated from:

$$S_r = \frac{w_o G_s}{e_o} \qquad 6.7$$

where G_s is specific gravity, w_o is the initial water content and e_o is the initial void ratio.

As S_r is determined from e_o, the degree of saturation cannot be accounted for in the determination of initial void ratio.

Figure 6.8 shows the relationship between initial void ratio and initial water content for the soils considered here. If the soil was fully saturated, then e_o could be calculated directly from the initial water content, w_o, and the determined specific gravity, G_s (Equation 6.7). Evidently this would result in a linear relationship depending on the specific gravity of the

soil. However, Figure 6.8 shows this not to be the case. The lines representing S_r = 100% and S_r = 95% bracket the majority of the data points for Clara and Ballydermot peat. These lines represent Equation 6.7 for G_s = 1.41, which is the average specific gravity adopted in this study for both Clara and Ballydermot peat. Evidently the scatter in the Clara data is greater than in the Ballydermot data, which is well fitted by S_r = 95%. Much of the Clara data fall within the S_r = 95% and S_r = 100% lines. Examining the range of data at any given water content quantifies the error in the calculated values of initial void ratio. For example, at w_o = 1100%, the variation in e_o is 15.65-17.82, whereas at w_o = 2000%, the variation in e_o is 28.20-31.51. The high degree of correlation observed with Ballydermot peat may partially explain the lack of scatter in Figure 6.6.

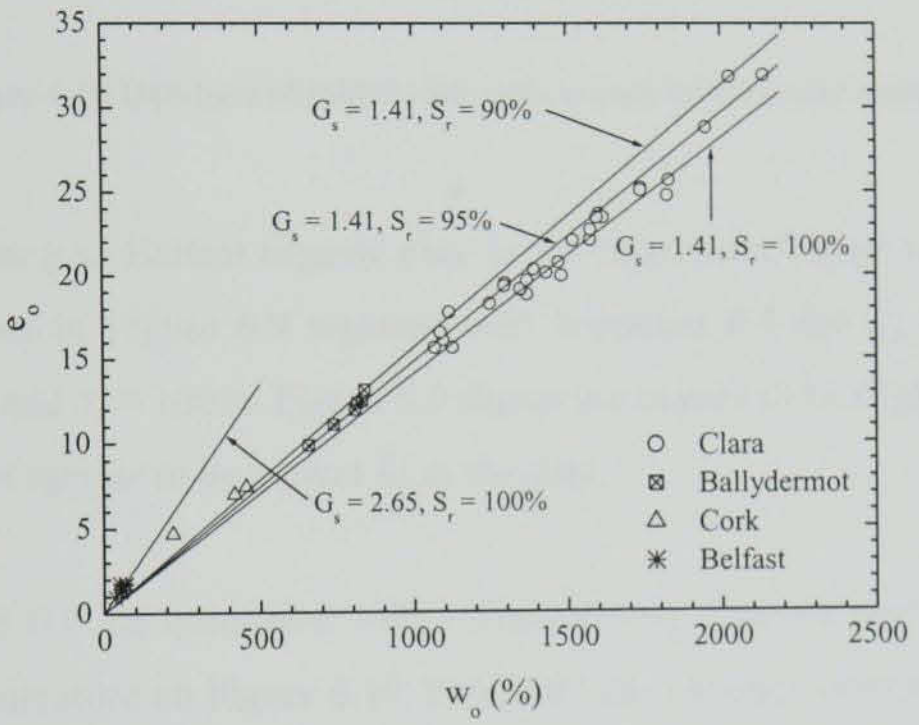

Figure 6.8 Initial void ratio versus initial water content

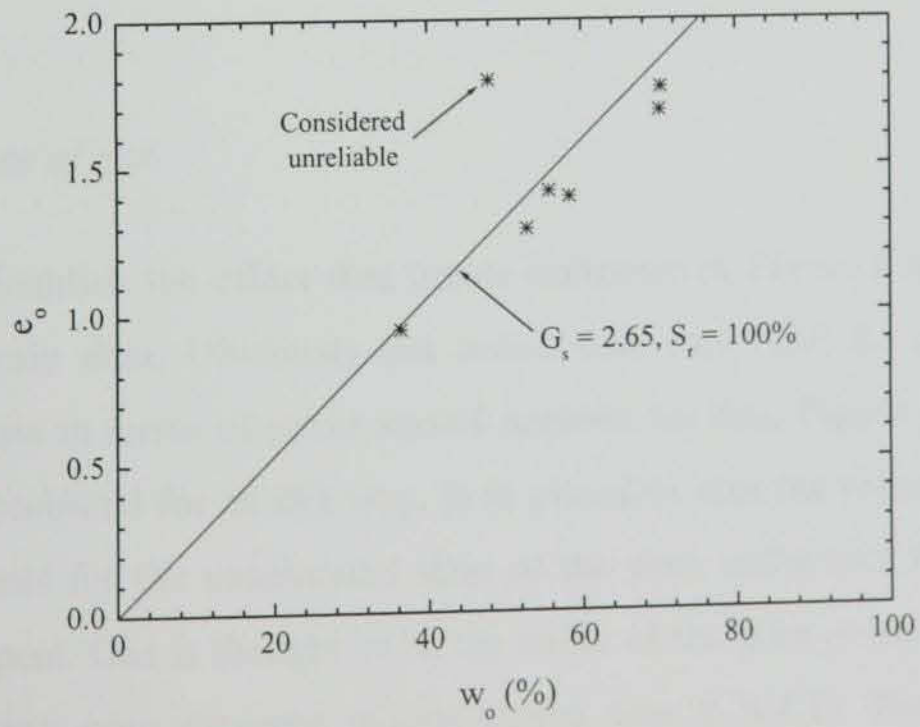

Figure 6.9 Initial void ratio versus initial water content for Belfast organic clay

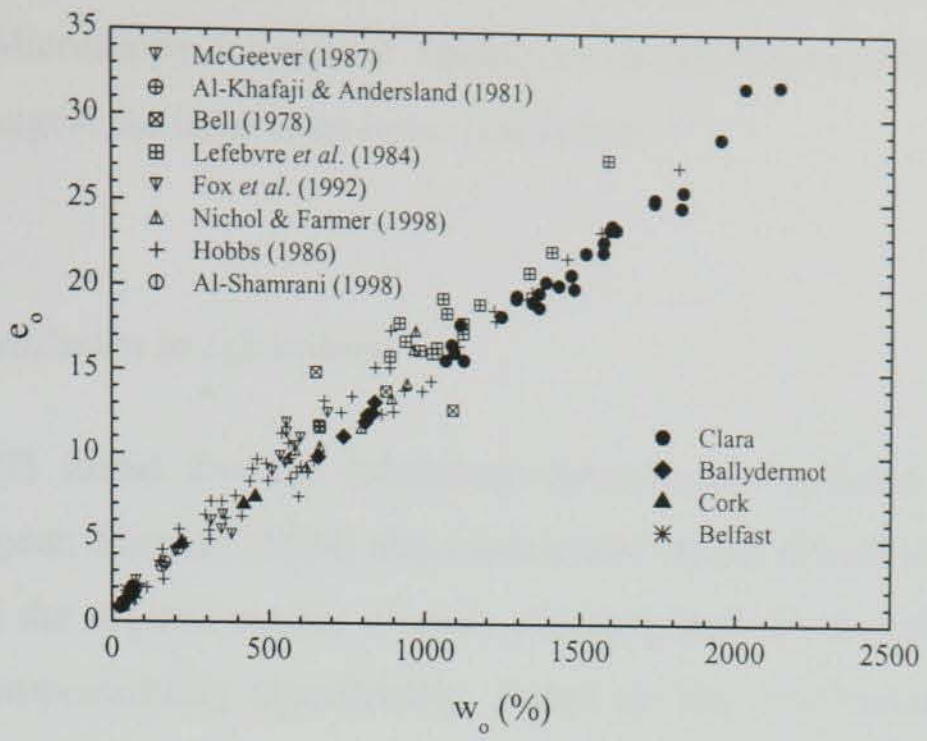

Figure 6.10 Database of initial void ratio versus initial water content

As the data pertaining to Belfast organic clay is not clear from Figure 6.8, it is shown on more suitable scales in Figure 6.9 together with Equation 6.7 for G_s = 2.65 (measured value, see § 3.4.4) and S_r = 100%. Figure 6.9 shows the scatter to be slight, although the G_s = 2.65 line does not appear to be a good fit to the data.

The data in Figure 6.8 are compared with corresponding data for peat and organic soils sourced from the literature on Figure 6.10. Evidently the variance does not just exist in the data reported here. For example, the data points due to Lefebvre *et al.* (1984) show considerable scatter.

6.2.4.2 Presence of gas

It is difficult to establish the effect that trends indicated in Figure 6.8 may have on the resulting stress-strain data. Obviously the initial void ratio will be different, although normalising the data in terms of strain should account for this. Figure 6.5 shows that the variation is not accounted for in this way. It is plausible that the presence of gas, which presumably accounts for the unsaturated state of the peat, influences the compressibility characteristics of peat. Gas is thought to be the cause of the pore pressure lag observed in MSL tests involving pore pressure measurements (see § 4.4.1). Presumably this will influence the compressibility characteristics of the peat, depending on whether the gas is

dissolved in the pore water and/or trapped within the cellular structure of the organic matter. Electron Microscopy images of Sphagnum stems reported by Landva and La Rochelle (1983) suggest the latter is an important factor.

6.2.4.3 Biodegradation in laboratory

Mesri *et al.* (1997) found that the laboratory environment induced humification and biodegradation of peat. Magnan (1994) also commented on the effects of the chemical and biological state of the organic matter of peat, claiming that the humification process is likely to affect compressibility significantly. Based on the conclusions of Mesri *et al.* (1997) and Magnan (1994), it is plausible to suggest that the process of humification and/or structural degradation may influence the measured compression of the peat specimens. Many of the tests involved have high LIDs, of the order of several months. If humification is a time-dependent process as Magnan (1994) suggests, then these tests may be particularly susceptible to compressibility variations.

Various explanations have been suggested in the foregoing to explain the disparity in the measured stress-strain data. In the author's experience, the most obvious and likely explanation is the inhomogeneous nature of fibrous peat. The presence of fibres is likely to reinforce the soil structure, as is evident from the vane test results reported by Landva and Pheeney (1980). During specimen preparation, it was observed that the concentration of mainly fine fibrous material varied significantly within each block sample. It is not surprising therefore, that the compression of separate peat samples differs, even when the specimens are taken from the same general vicinity of the block sample. Fox (1992) introduces the term *fabric coefficient of creep*, C_f, to account for variations within the peat fabric. However, this parameter is difficult to quantify and as such is limited in its application (den Haan, 1994).

6.2.4.4 General temperature effects

Temperature effects are well known to contribute to variations in the void ratio of inorganic clays (Gray, 1936; Mitchell, 1969; Leroueil, 1994). Recently, Fox (1992), Fox and Edil (1994, 1996) and Hansen (1996) investigated the effects of temperature variation on the measured settlement of peat. Although these latter studies were aimed at

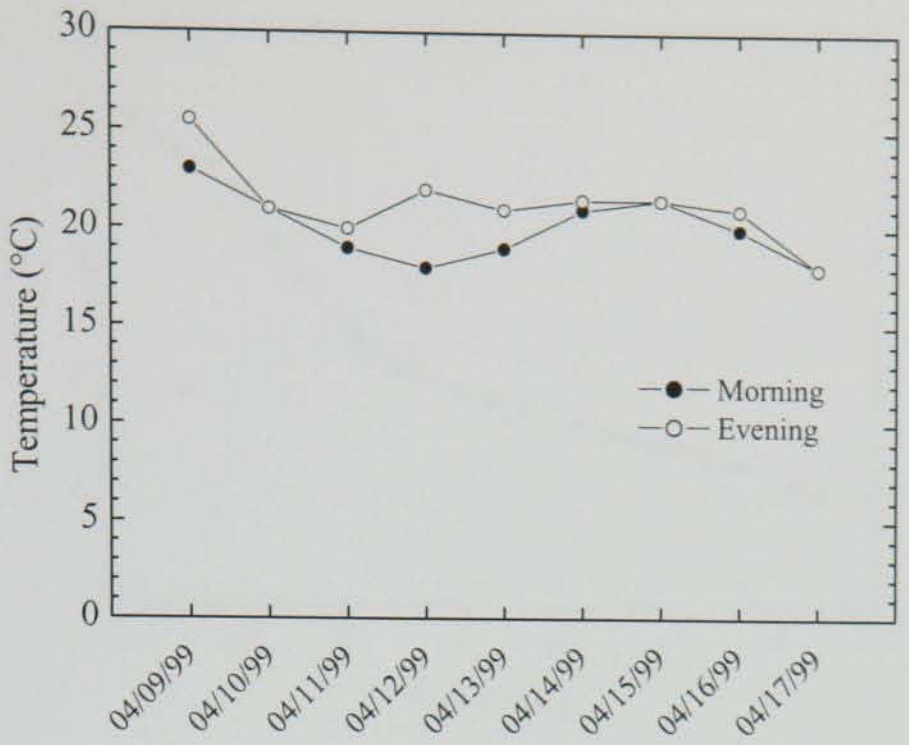

Figure 6.11 Temperature variations in the TCD laboratory over a nine day period

accelerating laboratory and *in situ* settlement rates, the results can to some extent be used to assess the possible effects that slight variations in ambient temperature may have on laboratory tests. Fox (1992) and Fox and Edil (1996) noted a sharp increase in excess pore pressure and creep coefficient, C_α, after a rapid increase in soil temperature. However, the imposed temperature differences involved with these studies were generally of the order 10-50°C. Figure 6.11 shows the variation in temperature over a nine day period in the TCD laboratory. Measurements were made twice a day, at approximately 8:30 in the morning and 5:30 in the evening. The average temperature is approximately 20°C, with typical variations of ± 2°C. Although these measurements did not include probable minimums during the night, the variation is much less than that involved in the study of Fox and Edil (1996), and as a result is likely to have minimal effect on measured settlements.

Figure 6.12 shows the 50-250 kPa stress increment of CL_MSL_07, which was maintained for over 6 months. The long-term creep settlement is evidently linear with logarithm of time, indicating that the nominal variation in the temperature of the TCD laboratory has little effect in peat. However, laboratory temperatures are still much higher than those *in situ*, and this marked increase in temperature may accelerate humification of the organic matter in peat (Mesri *et al.*, 1997).

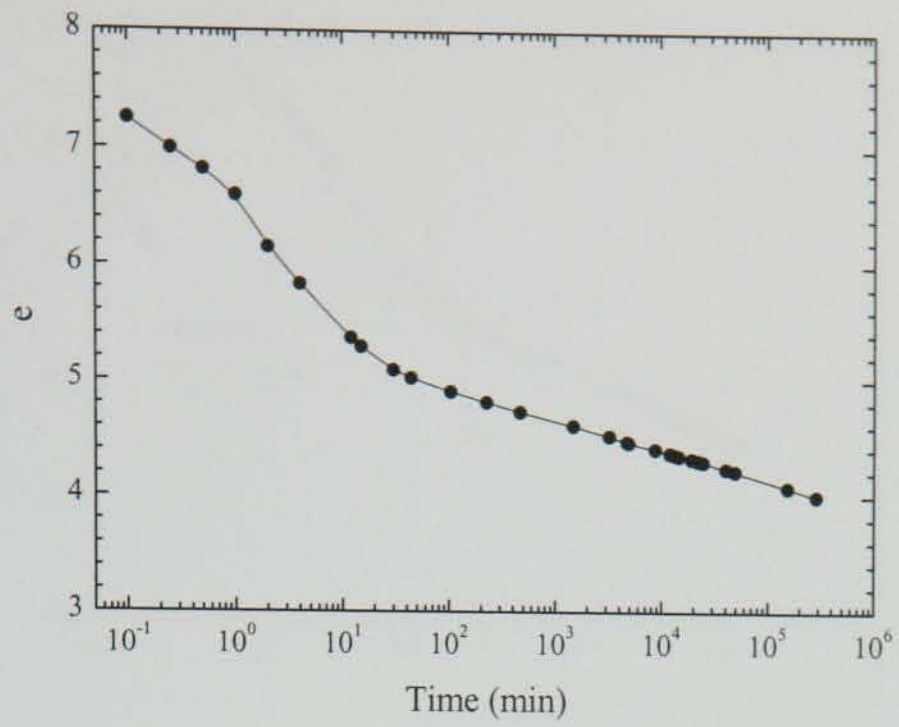

Figure 6.12 50-250 kPa stress increment of CL_MSL_07

6.3 FORMULATION OF COMPRESSION-TIME CURVES

6.3.1 The importance of creep in organic soils

The contribution of creep to the overall settlement of peat and organic soils is well known to be significant (Hobbs, 1986; Fox and Edil, 1996). Although the actual magnitude of creep settlement is often calculated from the end of consolidation, creep is generally understood as a continuous process, occurring during consolidation and at constant effective stress. Based on this assumption, which is generally referred to as Hypothesis B (see § 2.4.2.2), an appreciation of the *total* creep settlement for any given stress increment can be gained by considering Figure 6.13. The compression under this 10-50 kPa stress increment (CL_MSL_06) is in terms of the conventional definition of strain, $\varepsilon = \Delta e/(1+e_o)$, where e_o is the void ratio at the start of the stress increment. Hobbs (1986) defines a notational creep curve by extrapolating the measured creep curve (at constant effective stress) back towards zero time. Hobbs (1986) argues that in an infinitely permeable soil, the strain would follow the notational creep curve A'-B shown in Figure 6.13.

Such reasoning is based upon the assumption that the applied stress increment would cause an instantaneous increase in strain, ε_{inst}, followed by time dependent creep. However, due to the impermeable nature of soil, excess pore pressures associated with the stress increment are dissipated slowly, causing the ε - log t curve to follow the A-B path in

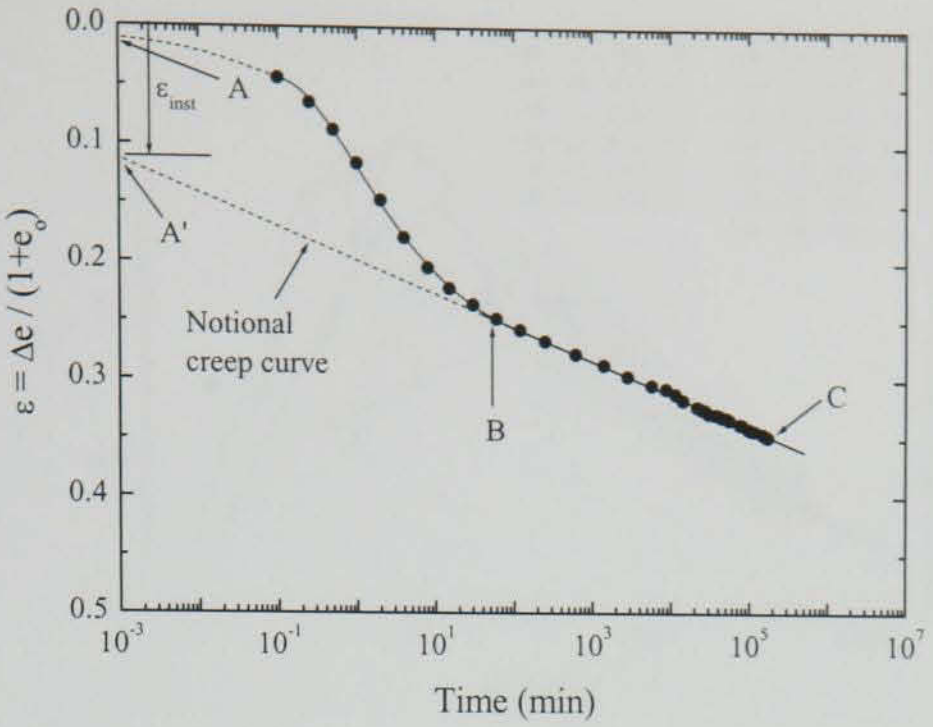

Figure 6.13 Strain *vs* log time for the 50-250 kPa stress increment of CL_MSL_07

Figure 6.13 (measured data). However, as $t = 0$ cannot be defined on a logarithmic scale, the magnitude of ε_{inst} is dependent upon the chosen origin of time. Nonetheless, if ε_{inst} is assumed to occur over a very short period of time, then the creep settlement, described in Figure 6.13 by A'-C, will be much greater than B-C, which is the assumption of Hypothesis A. Although schematic in nature, it is felt that the representation on Figure 6.13 provides a good indication of the dominant effects of creep on the settlement of peat soils.

6.3.2 Creep coefficient of compression, C_α

The creep coefficient of compression, C_α, has been determined from the linear portion of the $e - \log t$ curve according to Equation 6.8:

$$C_\alpha = -\frac{\Delta e}{\Delta \log t} \qquad 6.8$$

The variation in C_α with stress level is shown in Figure 6.14 for Clara peat, and in Figure 6.15 for Ballydermot peat, Cork peat and Belfast organic clay. The C_α data in each case tend to increase in magnitude to a maximum value, well past the apparent preconsolidation stress before starting to decrease again. This trend is C_α is commonly observed (Mesri and Godlewski, 1977; Graham *et al.* 1983; Leroueil *et al.*, 1985). However, due to the low

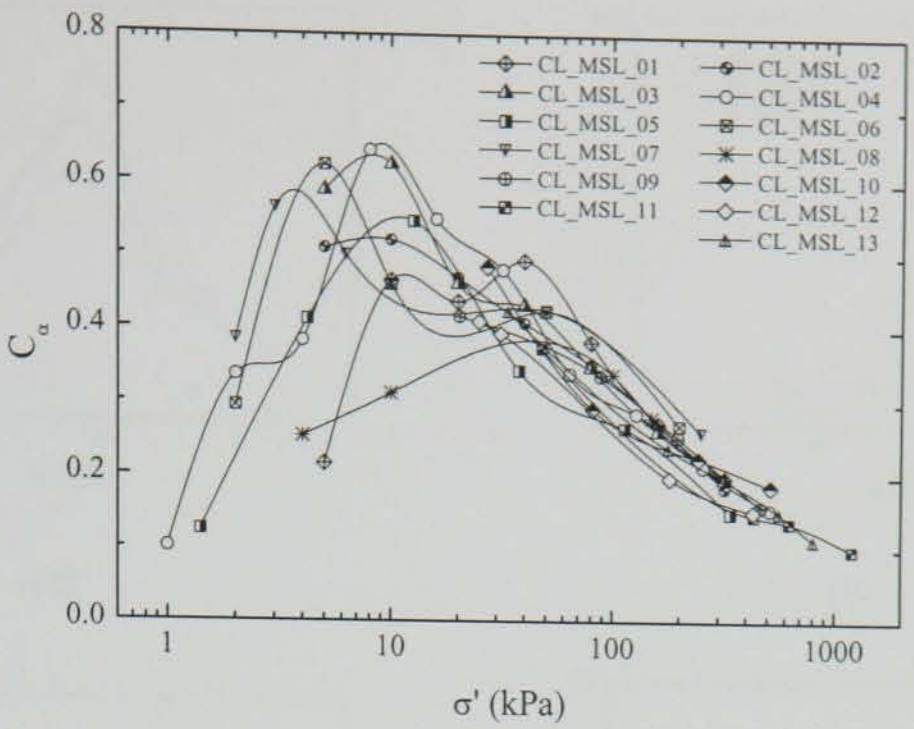

Figure 6.14 Variation in C_α with stress for Clara peat

preconsolidation stress of Clara peat, the initial increase in C_α is not well defined, although a clearly identifiable reduction in C_α exists with increasing stress. The magnitude of C_α varies between 0.1 and 0.65 for Clara peat. The trend is however, well exemplified by Figure 6.15a which shows the variation in C_α with stress for Ballydermot peat. In this case, C_α values increase steadily to a maximum value in the range σ' = 50-100 kPa before decreasing. The range of measured C_α values varies between 0.05 and 0.6 for Ballydermot peat. Figure 6.15b shows corresponding data for Belfast organic clay. Again the typical increase and subsequent decrease in C_α is observed. BF_MSL_06 was stiffer and siltier than the other two samples and is the probable reason for its lower values of C_α The C_α values for Cork peat and Cork silty peat are shown in Figure 6.15c and Figure 6.15d respectively. Although the data have been determined from a single test in each case, the variation in C_α with stress level is consistent with the trend observed in Ballydermot peat and Belfast organic clay. C_α typically ranges between 0.02 and 0.25 for Cork silty peat, and between 0.03 and 0.3 for Cork peat. In summary it is evident that the value of C_α on any one sample can vary by a factor of more than 10 and depends on the stress level.

It is interesting to note the relationship between organic content and typical C_α values. For all the soils considered, C_α increases with increasing organic content, which is consistent with the observations of Landva and La Rochelle (1983) and Mesri *et al.* (1997). Clara and Ballydermot peat have organic contents of 98.1% and 98.6% respectively, and this is reflected in an essentially consistent range of C_α for these soils (≈ 0.05-0.65). The C_α

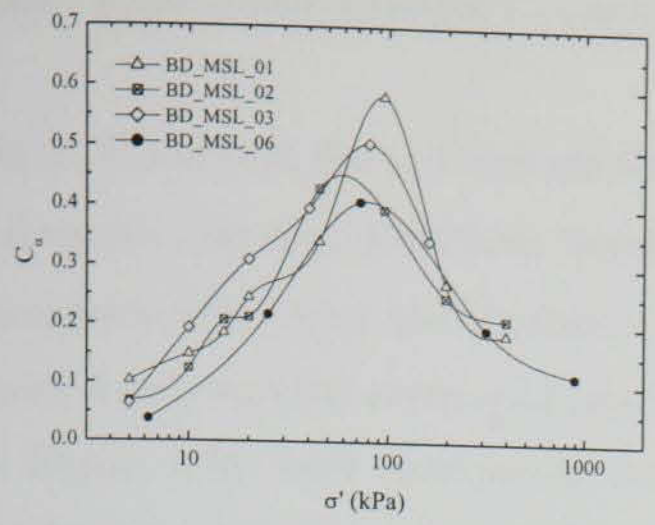

(a)

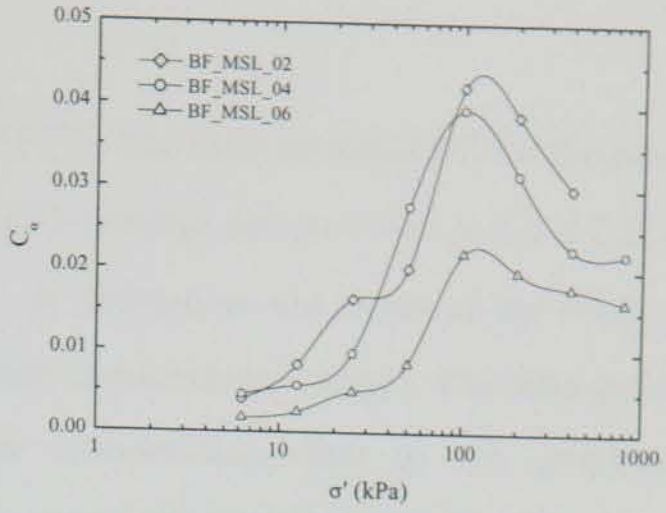

(b)

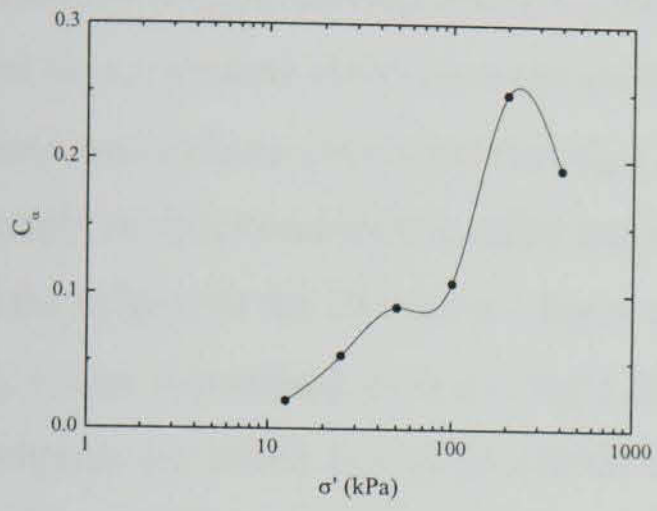

(c)

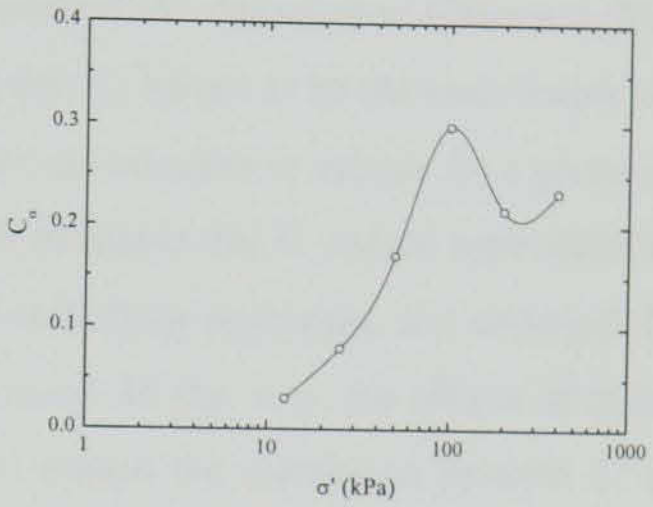

(d)

Figure 6.15 Variation in C_α with stress for: (a) Ballydermot peat, (b) Belfast organic clay, (c) Cork silty peat, (d) Cork peat

values for Belfast organic clay are much lower, which is consistent with the much lower organic content of 11%. The relationship between organic content and C_α also holds for Cork peat (organic content of 79.5%) and Cork silty peat (organic content of 32.2%).

C_α evidently also depends on the initial water content and consequently initial void ratio. However, as is shown in Figure 3.10, the dependence of initial water content on organic content only holds up to an approximate threshold organic content of 80% (see § 3.5). For soils with organic contents in excess of 80%, the water content depends more on soil structure and the degree of humification. It follows therefore, that C_α only depends on the initial water content up to a certain threshold value, after which the dependence is either considerably less or non-existent. Figure 6.14 and Figure 6.15a support this conclusion.

6.3.3 Relationship between C_α and C_c

The C_α/C_c concept, due to Mesri and Godlewski (1977), has been investigated for the peats and organic clay considered here. Details of the C_α/C_c concept are provided in § 2.4.2.3. In accordance with Mesri and Godlewski (1977), C_c is defined as the slope of the e-log σ' curve, during both the overconsolidated and normally consolidated ranges. The data points in Figure 6.16 were determined from 24-hour compression data as the graphical construction methods used in § 4.4.1 to estimate t_p were considered unreliable. Mesri and Godlewski (1977) state that any compression curve after EOP can be used to calculate C_c values, so long as corresponding C_α ratios are assumed. As discussed in Chapter 2, Mesri and his co-workers claim incorrect pairing of C_c and C_α values to be the main reason why many studies have concluded that C_α/C_c ratios are not constant or unique for a given soil. In light of this, considerable effort has been made to ensure that C_c values were calculated at the *tangent* to the 24-hour e – log σ' curve for each stress increment, and corresponding C_α values determined from e – log t data at 24 hours. In this way, the effects of tertiary compression, which Fox *et al.* (1992) claimed to worsen the correlation between C_c and C_α, are significantly reduced, if not completely removed. Following the recommendations of Mesri *et al.* (1997) and Lefebvre *et al.* (1984), C_α and C_c values have been normalised by the initial specific volume, v_o ($v_o = 1 + e_o$), where e_o is the initial void ratio. Figure 6.16 shows that the range of C_α/C_c ratios for the database of organic soils considered in this Thesis lie within the range 0.02 – 0.08. The mean values for the C_α/C_c ratios and the associated coefficients of determination (r^2) are summarized in Table 6.1 for each soil group. To aid clarity, the C_α/C_c relationship for each soil group is shown separately in Figure 6.17.

Table 6.1 Mean C_α/C_c ratios

Soil group	Number of data points used	C_α/C_c	r^2
Clara	72	0.042	0.579
Ballydermot	24	0.051	0.853
Cork	11	0.063	0.898
Belfast	39	0.047	0.684

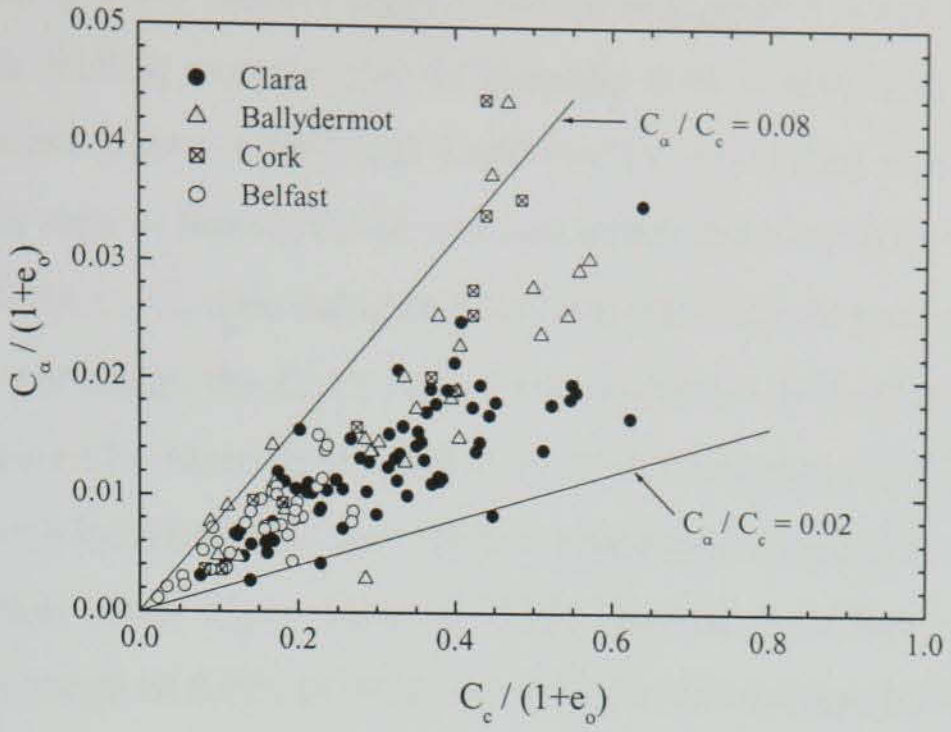

Figure 6.16 C_α - C_c relationship for organic soil database

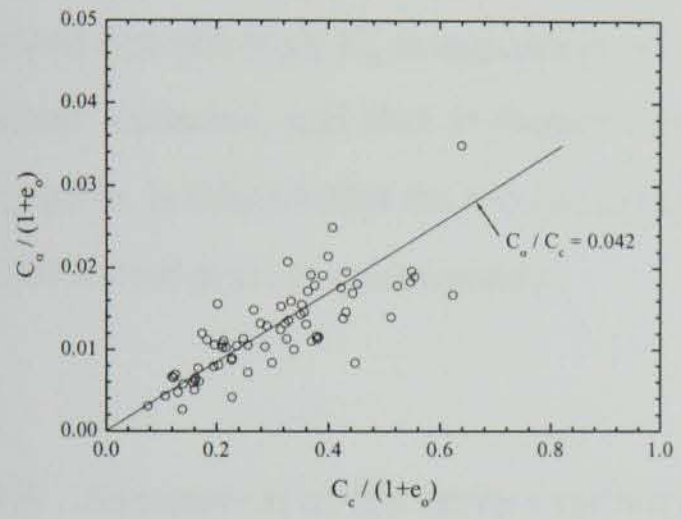

(a)

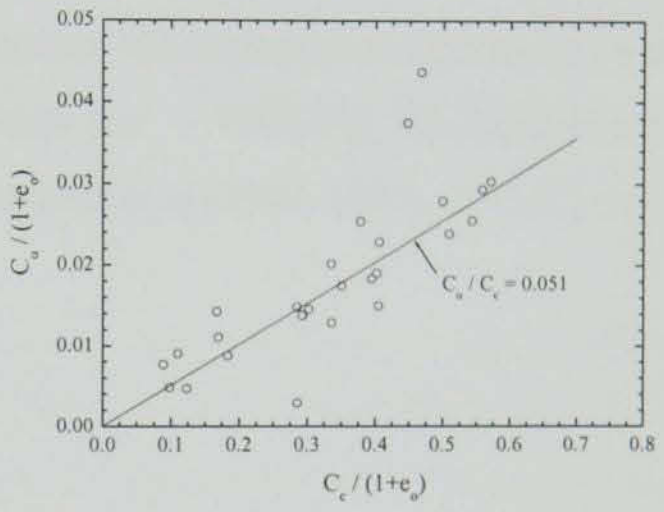

(b)

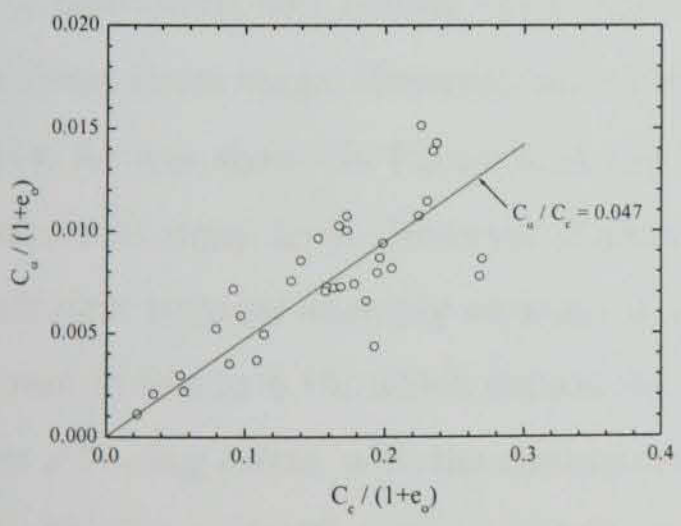

(c)

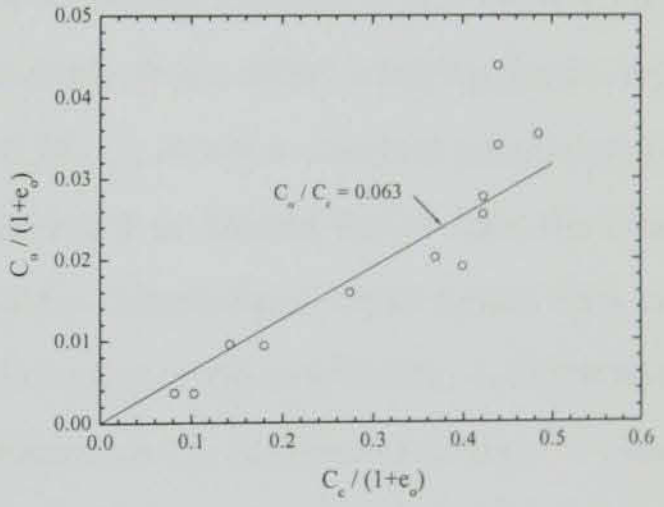

(d)

Figure 6.17 Relationship between C_α and *Cc* for: (a) Clara peat, (b) Ballydermot peat, (c) Belfast organic clay, (d) Cork peat

The results in Figure 6.17 show that there is an obvious relationship between C_α and C_c, although the relatively low r^2 values suggest that the relationship is not unique. The C_α/C_c ratios obtained for Belfast organic clay is typically 0.05 ± 0.01 and within the range reported by Mesri and Castro (1987) and Ladd (1971). According to Mesri *et al.* (1994, 1997), reliable data suggest that C_α/C_c for peat lies within the range 0.06 ± 0.01. This range is compatible with the C_α/C_c ratio calculated for both Ballydermot peat and Cork peat, but not Clara peat. In particular, the C_α/C_c ratio for Ballydermot peat ($C_\alpha/C_c = 0.051$) agrees well with that reported by Mesri *et al.* (1997) for Middleton peat ($C_\alpha/C_c = 0.052$), which, although slightly less humified, has geotechnical properties comparable with Ballydermot peat. The somewhat lower C_α/C_c ratio of 0.042 derived for Clara peat is, however, consistent with the range of 0.028 to 0.062 reported for fibrous peat by Dhowian and Edil (1980). The lower C_α/C_c ratio for Clara peat is to be expected, considering that the range of C_α values is consistent with that of Ballydermot peat, and that the higher initial water content and associated initial void ratio will result in higher values of C_c. Hobbs (1986) showed that although C_α is dependent on water content, the dependence decreases as water content increases, and that at higher water contents (*ca.* > 1000 %), the dependence is negligible. It follows that the recommendation by Mesri *et al* (1994, 1997), of $C_\alpha/C_c = 0.06 \pm 0.01$ for *all* peats is questionable.

6.3.4 Assessment of the creep coefficient *c*

§ 6.2 considered how natural strain could be used to restore linearity to $\varepsilon - \log \sigma'$ data in the virgin stress range. However, no reference was made to the effect it has on the $\varepsilon - \log t$ curve. As was shown in Figure 6.14 and Figure 6.15, C_α is not a constant parameter, but varies with stress level. However if strain is interpreted as natural strain, then the creep coefficient remains tolerably constant in the normally consolidated stress range. This can be seen in Figure 6.18, which depicts the variation in the creep coefficient, c, determined from $\varepsilon^{nat} - \log t$ data, with the corresponding variation in C_α determined from $\varepsilon^{lin} - \log t$ data. The creep coefficients, c and C_α, have been normalised by the maximum value in each case to allow for ease of comparison. Data points are shown from 10 kPa as this is the approximate stress level above which a linear $\varepsilon^{nat} - \log \sigma'$ relationship has been observed for Clara peat (for example, see Figure 6.5). Figure 6.18 shows that although c tends to increase slightly with σ' at lower stresses, the variation is much less than the corresponding

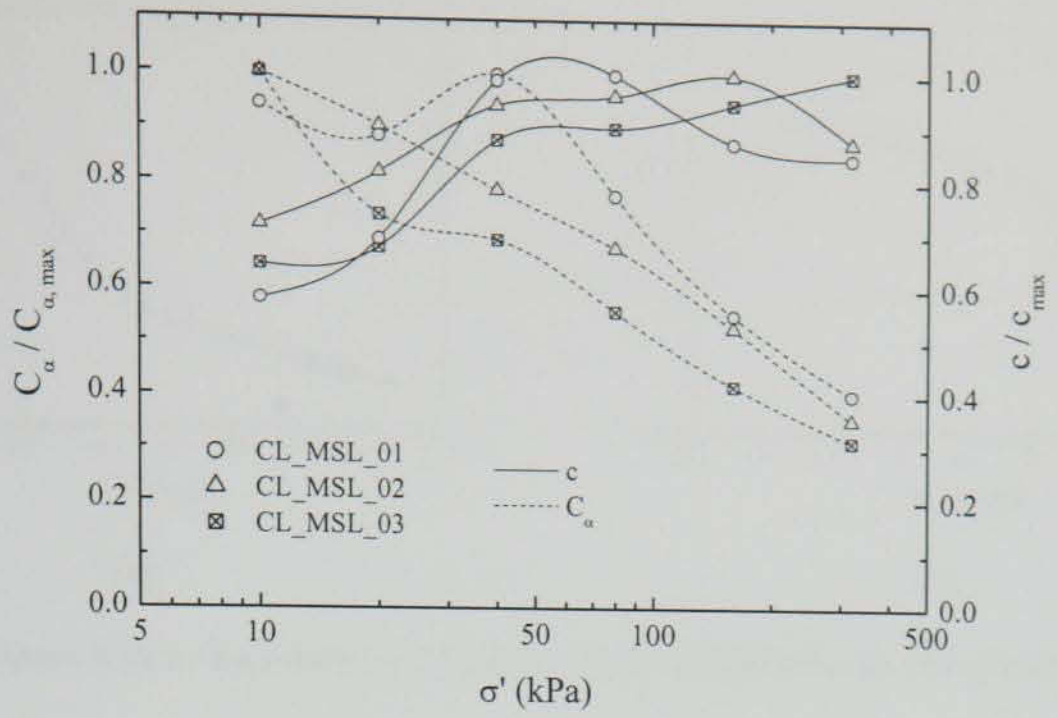

Figure 6.18 Variation in the creep coefficients, C_α and c for Clara peat

range in C_α. Furthermore, c is tolerably constant at stresses of 40 kPa and above, whereas C_α reduces considerably in this stress range.

6.3.5 Apparent tertiary compression due to stress history

Although the long term creep settlement has generally been observed to follow a linear relationship with logarithm of time (for example, see Figure 4.7), certain stress increments in Clara peat and Ballydermot peat exhibited tertiary compression, which is defined as an increase in the slope of the ε - log t curve after a period of constant C_α. Tertiary compression was only observed at stress levels in the vicinity of the apparent preconsolidation stress in Clara peat and Ballydermot peat, although these were the only soils involving high LID at relatively low stress levels.

Figure 6.20 shows measured strain data from two stress increments of CL_MSL_08; 10-100 kPa (Figure 6.20a) and 100-150 kPa (Figure 6.20b). Tertiary compression was not observed in these stress increments, which were maintained for 120 days and 200 days for the 100 and 150 kPa stress increments respectively. As such, the creep coefficient, c, could be determined with a high degree of confidence. For both stress increments, c = 0.024. However, an early stress increment (4-10 kPa) of CL_MSL_08 exhibited tertiary compression. The measured data from this stress increment is shown in Figure 6.19. The end of consolidation has been estimated using Casagrande's method and is marked $t_{p.cas}$ in

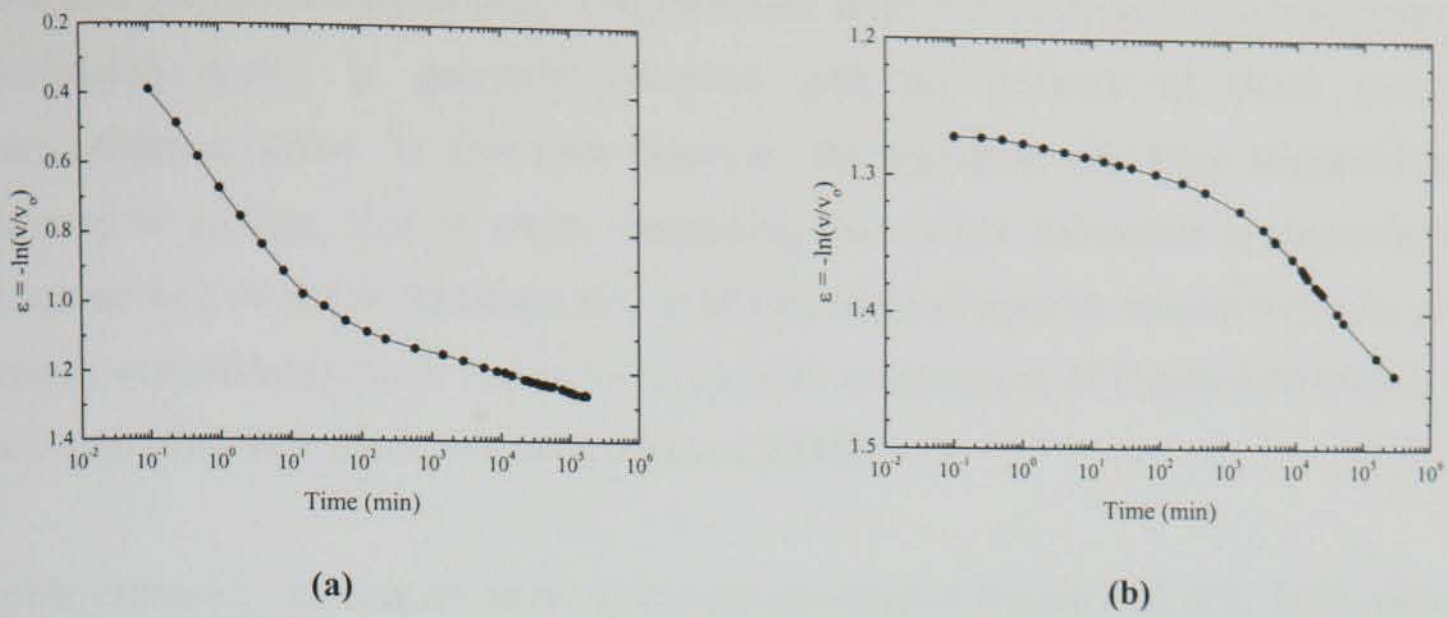

Figure 6.20 ε - log t data for CL_MSL_08 (a) 10-100 kPa (b) 100-150 kPa

Figure 6.19. After $t_{p,cas}$, the slope of the ε - log t curve becomes linear for a short period of time with $c = 0.003$ (A-B). The slope of the ε - log t curve increases to $c = 0.006$ after 100 minutes and continues to creep at this rate for 50 days. At this point a sudden increase in the slope of the ε - log t curve was measured. This increase corresponds to $c = 0.028$, which represents an almost five-fold increase in creep strain rate. Creep straining continues at this increased rate for the remainder of the stress increment (additional 55 days).

This stress increment is particularly interesting because the creep coefficient, $c = 0.028$, corresponding to section C-D (see Figure 6.19) is of the same approximate order as that determined for the 100 and 150 kPa stress increments ($c = 0.024$). Essentially, the peat has stopped exhibiting overconsolidated behaviour, and has quite suddenly started to behave

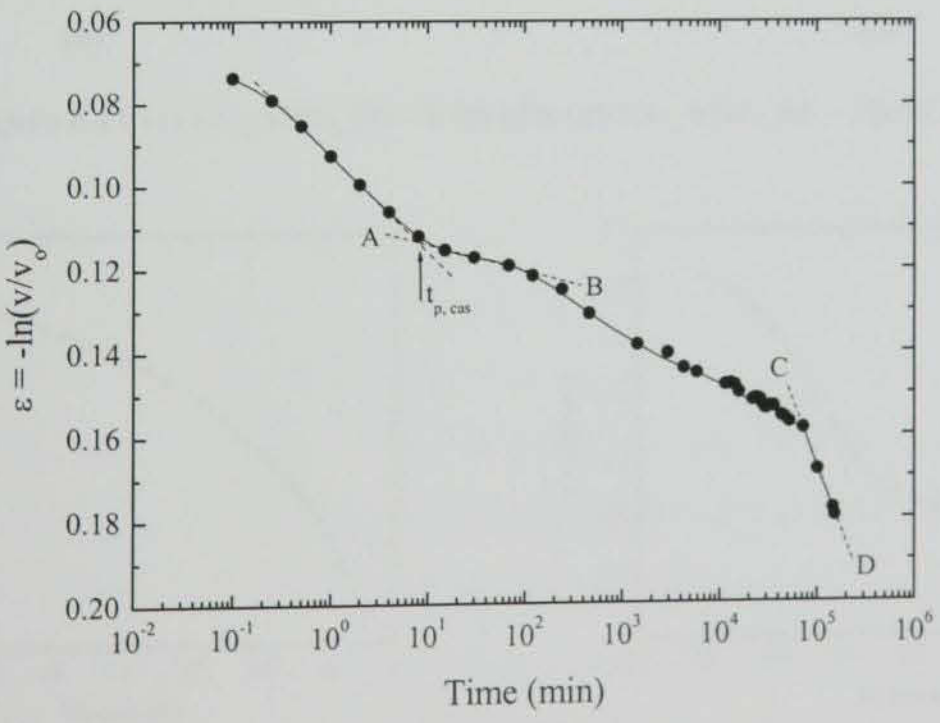

Figure 6.19 Illustration of tertiary compression for the 4-10 kPa stress increment of CL_MSL_08

like a normally consolidated peat. The transition from the overconsolidated to normally consolidated region is generally observed with an increase in stress past the preconsolidation stress. In this case however, the transition has been triggered by a reduction in volume, due to creep, suggesting that *virgin behaviour* is dependent on volume as well as stress. Although the 10 kPa stress level may be considered to be in the normally consolidated stress region for Clara peat, examination of Figure 6.4a reveals that *true* virgin behaviour exists beyond a stress of 10 kPa.

Further examples showing an increase in c are provided in Figure 6.21 (CL_MSL_06) and Figure 6.22 (CL_MSL_07). The final slope (C-D) of the ε - log t curve for the 5-10 kPa stress increment of CL_MSL_06 (Figure 6.21a) corresponds to c = 0.024, which is considerably in excess of c = 0.004 as determined from the first linear section of the ε - log t curve after $t_{p,cas}$ (A-B). As with CL_MSL_08, this final value of c (0.024) is in good agreement with c = 0.019 as determined from the next stress increment (10-50 kPa, see

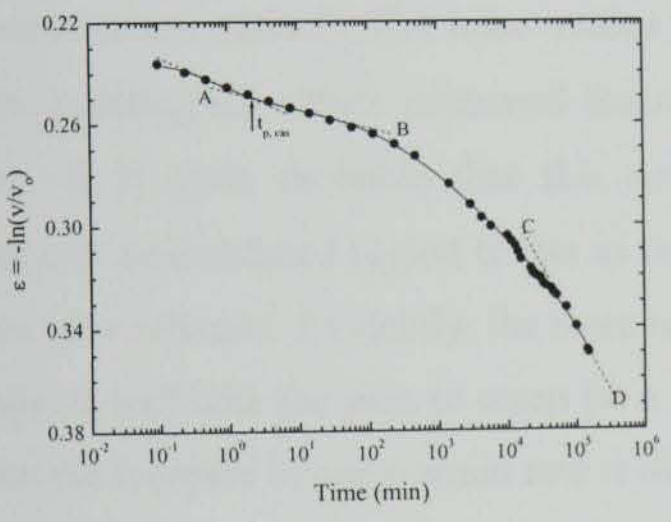

(a)

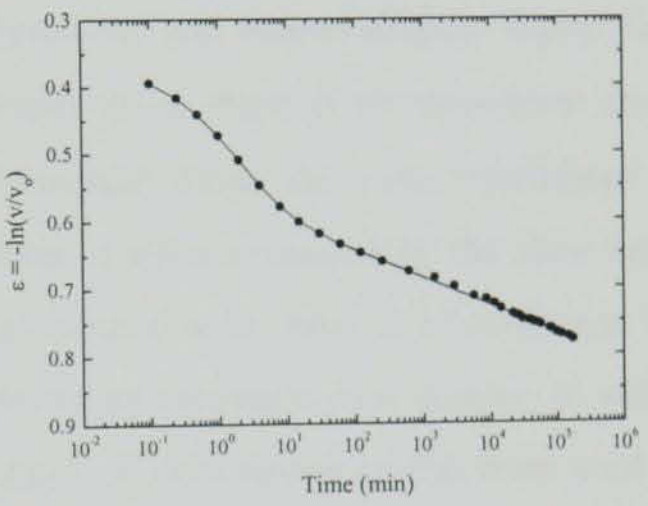

(b)

Figure 6.21 (a) CL_MSL_06 – 5-10 kPa (b) CL_MSL_06 – 10-50 kPa

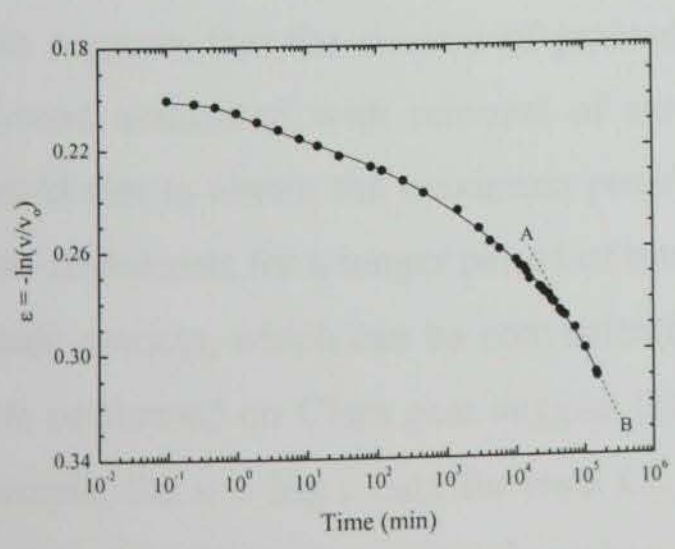

(a)

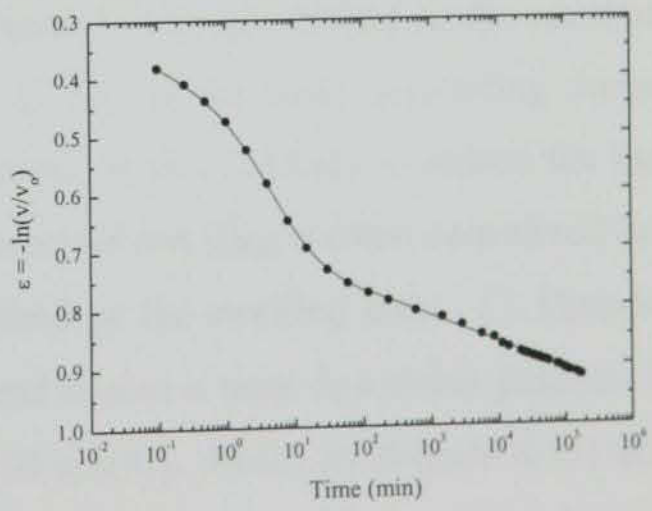

(b)

Figure 6.22 (a) CL_MSL_07 – 3-6 kPa (b) CL_MSL_07 – 6-50 kPa

Figure 6.21b). A similar trend can be observed in CL_MSL_07 (Figure 6.22). As the inflection point which is required to estimate $t_{p,cas}$ is not observed in the 3-6 kPa stress increment (Figure 6.22a), an initial value of c could not be accurately determined. However, the shape of the ε - log t curve indicates that c increases steadily with time, reaching a final value of 0.025 after approximately 25 days. This value agrees well with c = 0.019, as determined from the 6-50 kPa stress increment of this test (Figure 6.22b). One notable difference with these two tests (CL_MSL_06 and CL_MSL_07) is that the increase in c is gradual, whereas with CL_MSL_08 the increase is sudden.

The above description of an increase in the slope of the ε - log t curve is similar to observations reported by Samson (1985). In this case study (see § 2.3 for details) a peat deposit was preloaded to a stress of 69 kPa. After a period of time, approximately one-third of the surcharge stress was removed. Thereafter heave was observed for one year, followed by a very low rate of creep. However, at times ranging between 5½ and 8 years, a sudden increase in the creep coefficient, C_α, from 0.007-0.032 to 0.028-0.073 was noted at all measurements stations. The latter values are comparable, and indeed slightly higher than corresponding C_α values measured during the construction stage at an equivalent stress level. It is quite probable that this apparent transition from the overconsolidated to normally consolidated region is due to the reduction in volume caused by the slow creep rates after rebound. Evidently, the more rebound associated with removal of surcharge, the longer it will take the peat to creep (at a slow rate) to its *minimum past volume*, at which point the increase in creep strain rate is likely to occur. Similar reasoning has been used by Lefebvre (1986) to explain the accelerated creep settlement rates reported by Samson (1985).

This suggests that the success of preloading projects is strongly linked to the maximum rebound associated with removal of surcharge. If this is the case, preloading projects should aim to obtain the maximum possible rebound, as this is likely to reduce the long-term settlements for a longer period of time. Rebound, or swelling is often considered as an elastic process, which can be conveniently described by the swelling index, C_s. However, tests performed on Clara peat suggest that rebound is also a time dependent process. For example, the e – log t data for tests CL_MSL_14 and CL_MSL_15 (Figure 4.15) show continued swelling at an approximately constant rate (on a logarithmic time scale) for up to 6 days. In summary, the probable link between maximum rebound and subsequent delay in normally consolidated creep settlement requires further investigation.

The idea that the virgin stress range is controlled by volume rather stress is plausible, if not likely, for soils that have been preloaded. However, Clara peat is a young, virgin soil that can only have experienced minimal past stresses. As the bulk density is close to the density of water (see § 3.4.6), the overburden stress must be close to zero. However, the drainage scheme in Clara bog which was initiated by Bord na Mona in the early 1980's may have caused an increase in the overburden stress. As these drains were approximately 0.5 m deep, the maximum probable overburden stress would be 5 kPa. Blocking of these drains in 1987 by NPWS returned the water table to close to ground level. This overburden stress is likely to have caused a minimum previous specific volume, through drainage induced consolidation and creep. This assessment, though admittedly approximate, may explain the indication of a minimum specific volume in the MSL oedometer tests, which in turn, explains the transition into the normally consolidated region for tests CL_MSL_06, CL_MSL_07 and CL_MSL_08.

If this hypothesis is accepted, then it may be used to explain the *in situ* tertiary compression described by Fox and Edil (1996). As part of their investigation into the thermal precompression of peat, Fox and Edil (1996) described a test fill over an unheated fibrous peat deposit (Middleton). Construction took place in two lifts corresponding to stress increments of 18 kPa and 42 kPa. Measured settlement data indicate that the slope of the ε - log t curve increased after consolidation (determined from pore pressure data). However, as the stress levels involved are less than, or close to the apparent preconsolidation stress for Middleton peat (25-50 kPa, Lan 1992, ≈40 kPa, Fox 1992, 25-40 kPa, Edil *et al.* 1994; 30-40 kPa, Mesri *et al.* 1997) based on the foregoing conclusion, it is not surprising that the creep curve increased in slope towards the minimum past specific volume.

6.4 ISOTACHE CONCEPT

The rate dependency of clays has been formulated in a number of one-dimensional constitutive models using the *isotache* concept. Isotaches are defined by Šuklje (1957) as lines in stress-strain space along which the *creep* strain rate is constant. At constant effective stress these isotaches are also lines of constant *total* strain rate, although a number of studies (Leroueil *et al.*, 1985; Imai and Tang, 1992; and Kim and Leroueil, 2001) suggest that the distinction between total and creep strain rates is unnecessary. The

laboratory data presented in Chapter 5 have been interpreted in terms of strain rates so as to allow for verification of the isotache principle for peats.

6.4.1 MSL oedometer tests

Figure 6.23 shows the stress, strain, strain-rate relationship for Ballydermot peat (BD_MSL_01). Both conventional and natural strain have been used to quantify the compression. As expected, a linear relationship between strain and logarithm of stress is obtained only when strain is interpreted as natural strain. Evidently the lines are tolerably parallel and linear in the virgin stress range. Parallel and linear isotaches do not occur in the overconsolidated region. However, this is to be expected as the coefficient of creep compression, c, is not constant in the overconsolidated region (den Haan, 1996).

The stress, strain, strain-rate relationship for Clara peat (CL_MSL_16) is shown on Figure 6.25. As has been indicated earlier (§ 6.2), normally consolidated behaviour in Clara peat is generally observed beyond $\sigma' \approx 10$ kPa. The effect of unloading from σ' =40 kPa and subsequent reloading on the isotaches diminishes as soon as the previous maximum stress has been exceeded (40 kPa), when isotaches are again parallel and linear. The question of whether isotaches remain unique when defined as lines of constant total strain rate can be addressed by examining Figure 6.24, which shows the stress, strain, strain-rate relationship for CL_MSL_13. As the initial stress (33.65 kPa) in this test is relatively large, the

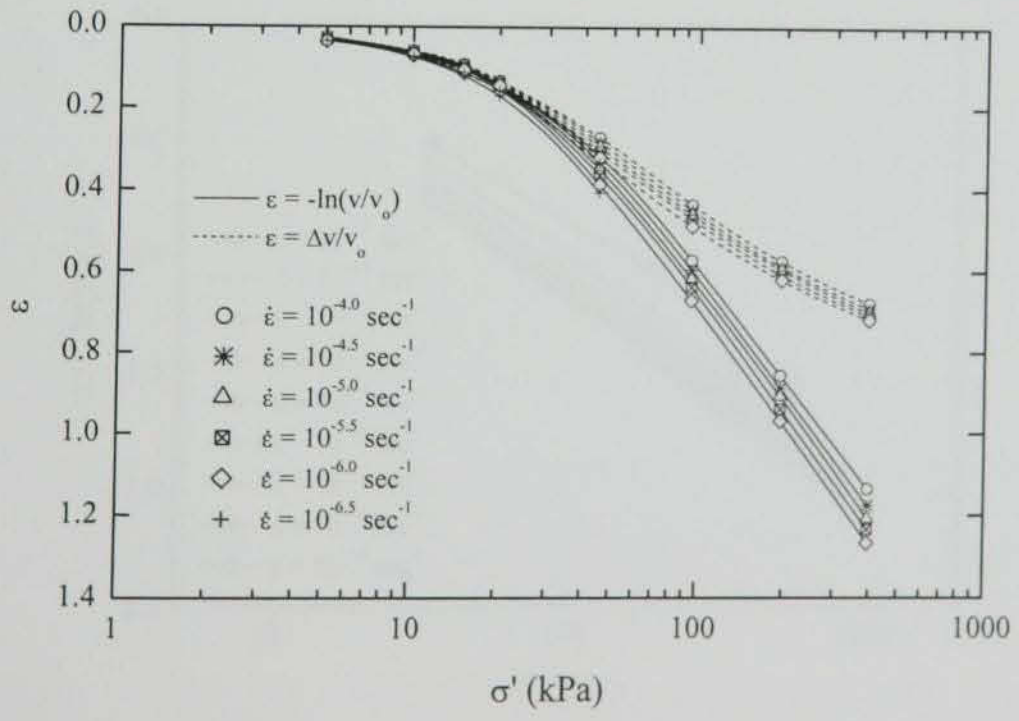

Figure 6.23 Stress, strain, strain-rate relationship for Ballydermot peat (BD_MSL_01)

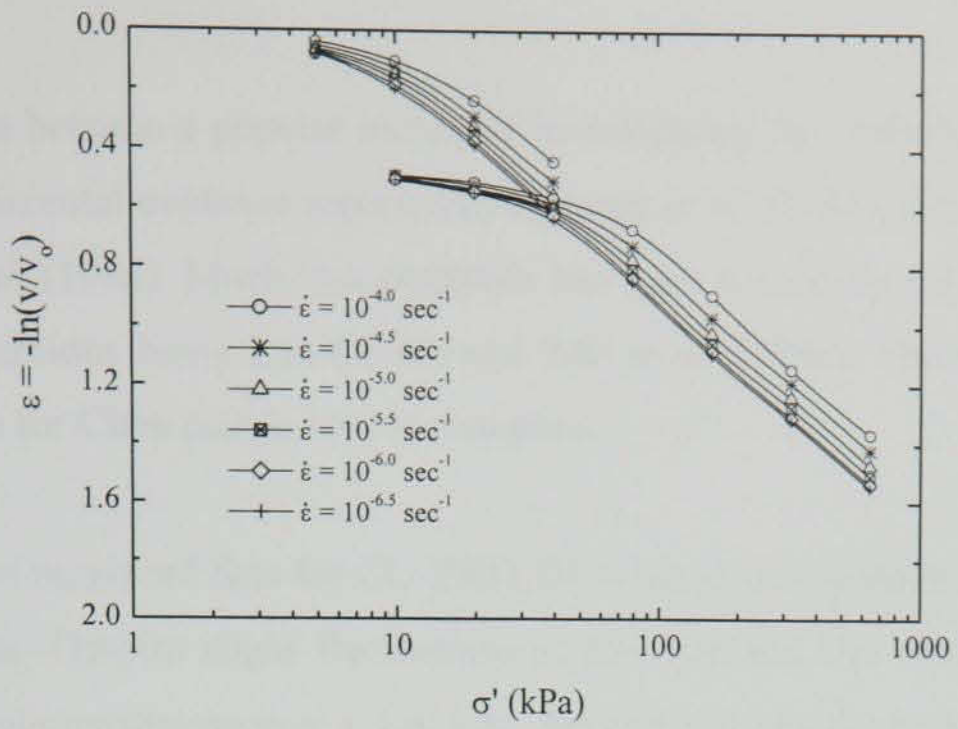

Figure 6.25 Stress, strain, strain-rate relationship for Clara peat (CL_MSL_16)

isotaches are linear and parallel, with no initial distortion as was the case with CL_MSL_16 (Figure 6.25). However, the final stress increment, (563-803 kPa) shows sharp tilting of the isotaches at faster strain rates. This is considered to be due to the very low LIR (0.43), which has distorted the linearity of the isotaches during consolidation.

However, as the effective stresses become constant, (when $d\varepsilon^{lin}/dt<10^{-5}$ sec^{-1}) linear and parallel isotaches are once again observed. Evidently the relationship between stress, strain and strain rate is only unique in this instance when strain rate is interpreted as *creep* strain rate and not *total* strain rate.

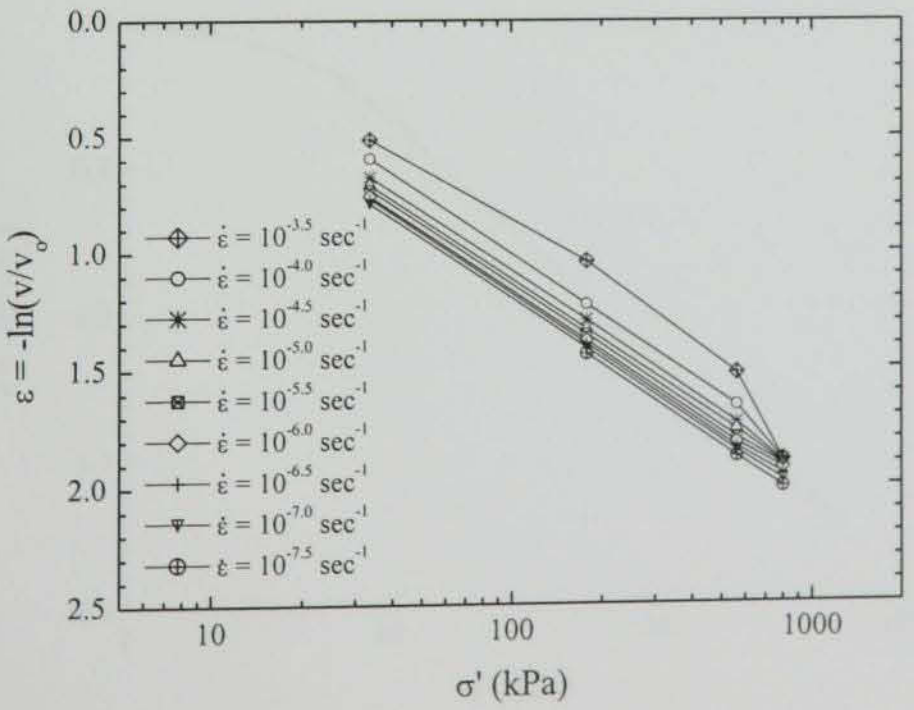

Figure 6.24 Effect of LIR on the stress, strain, strain-rate relationship for Clara peat (CL_MSL_13)

6.4.2 CRD tests

The CRD test has become a popular means of investigating the isotache concept for soft clays, with experimental evidence reported by Samson *et al.* (1981), Graham *et al.* (1983) and Leroueil *et al.* (1985). Much less emphasis has been placed on CRD testing of peat, with notable exceptions being Lan (1992) and Edil *et al.* (1994). The uniqueness of the isotache principle for Clara peat is now investigated.

Figure 6.26 shows measured data for CL_CRD_04 in terms of natural strain and logarithm of effective stress. Despite slight fluctuations at low stresses, the stress-strain response follows a linear relationship up to $\sigma' \approx 100$ kPa. Beyond 100 kPa the measured stress-strain relationship moves to the right, which, according to the isotache principle, corresponds to a higher rate of strain. This result is not surprising considering that the imposed rate of deformation is constant, which in turn infers a constant rate of strain when strain is defined as linear strain, $\varepsilon^{lin} = \Delta v/v_o$. Rates of both linear and natural strain are defined in terms of specific volume in Equation 6.9:

$$\varepsilon^{nat} = -\ln\left(\frac{v}{v_o}\right) \qquad \Rightarrow \frac{d\varepsilon^{nat}}{dt} = -\frac{1}{v}\left(\frac{dv}{dt}\right)$$

$$\varepsilon^{lin} = 1 - \frac{v}{v_o} \qquad \Rightarrow \frac{d\varepsilon^{lin}}{dt} = -\frac{1}{v_o}\left(\frac{dv}{dt}\right) \qquad 6.9$$

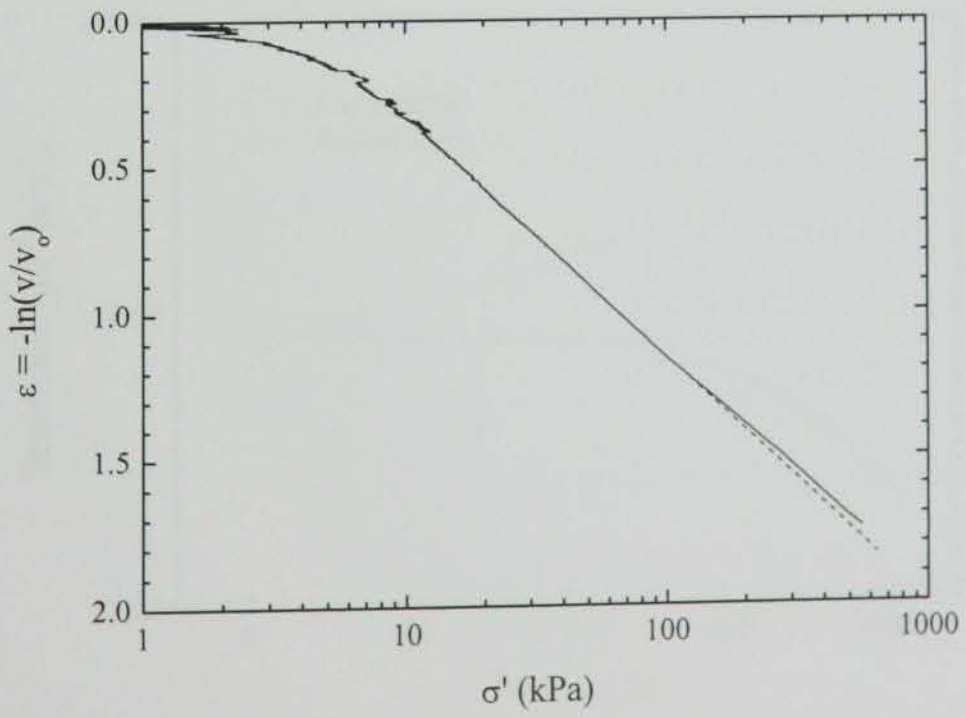

Figure 6.26 Stress, strain, strain-rate relationship from CRD testing of Clara peat (CL_CRD_04)

Substituting for dv/dt in Equation 6.9 gives:

$$\frac{d\varepsilon^{nat}}{dt} = \frac{v_o}{v}\frac{d\varepsilon^{lin}}{dt} \qquad 6.10$$

The rate of deformation, and hence linear strain rate, is controlled by the loading frame and in this test (CL_CRD_04) is set to a constant value of 0.01 mm/min ($d\varepsilon^{lin}/dt = 8.33 \times 10^{-6}$ sec^{-1}). However, as the term v_o/v increases with stress, the rate of natural strain, $d\varepsilon^{nat}/dt$, will always be greater than the corresponding rate of linear strain, $d\varepsilon^{lin}/dt$. In accordance with the isotache principle, this explains why the stress-strain path gradually moves to the right, corresponding to a higher rate of natural strain. However, this is complicated further by the reduction in deformation rate due to partial deformation of the relatively flexible external proving ring (see Figure 4.28). The problems associated with the use of an external proving ring in CRD tests have been raised briefly by Mesri and Feng (1986) and Lan (1992). Figure 4.28 clearly illustrates that the deformation rate, and hence linear strain rate of the specimen is reducing with time. However, it is uncertain if this will also cause a reduction in natural strain rate, considering that natural strain rate is continually increasing (Equation 6.10).

Figure 6.27 shows the variation in both linear strain rate and natural strain rate for CL_CRD_04 with time. As expected, natural strain rate is always greater than linear strain rate. The rate of linear strain rate begins to decrease after approximately 1000 minutes

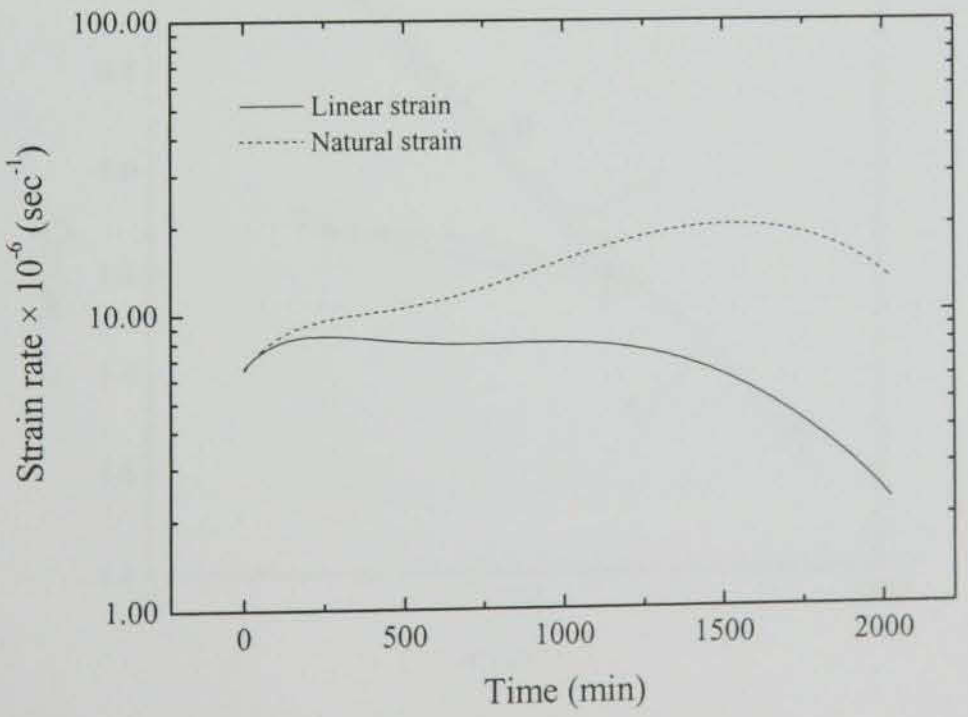

Figure 6.27 Variation in strain rate (linear and natural) with time for CL_CRD_04

although natural strain rate continues to increase until approximately 1500 minutes. At this point, the deformation of the proving ring evidently causes a faster reduction in linear strain, than that implied by Equation 6.10. The reduction in natural strain rate is less significant, and does not appear to be sufficient to cause any discernible variation in the stress-strain path on Figure 6.26.

Figure 6.28 shows the stress-strain relationship for CL_CRD_06, which involved loading and unloading at constant rates of deformation, and stepped changes in the deformation rate. The annotation in Figure 6.28 is the same as that described in § 4.5.2 and Figure 4.30.

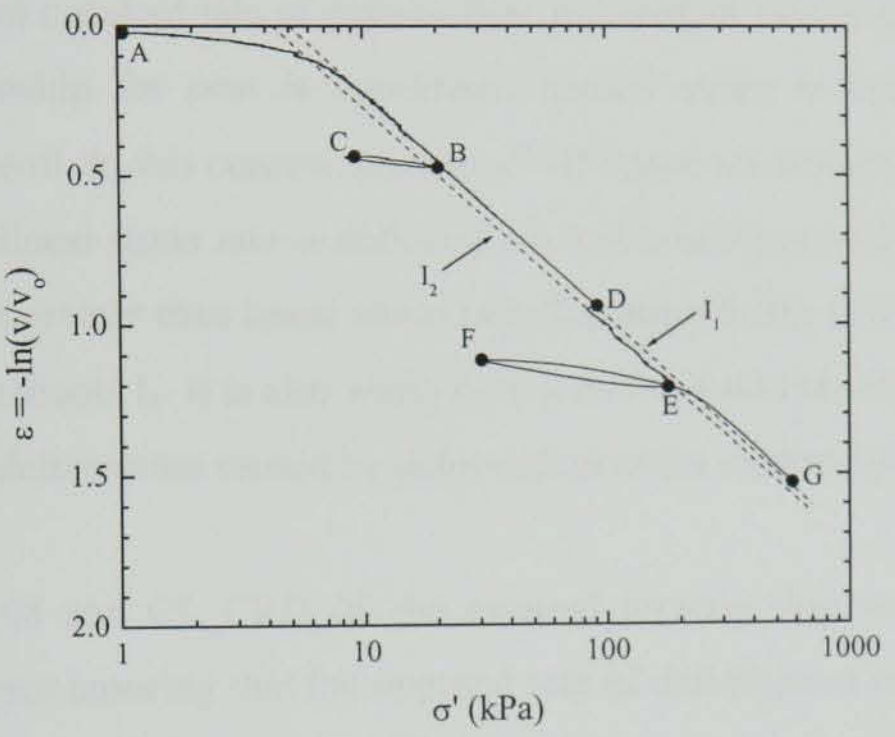

(a)

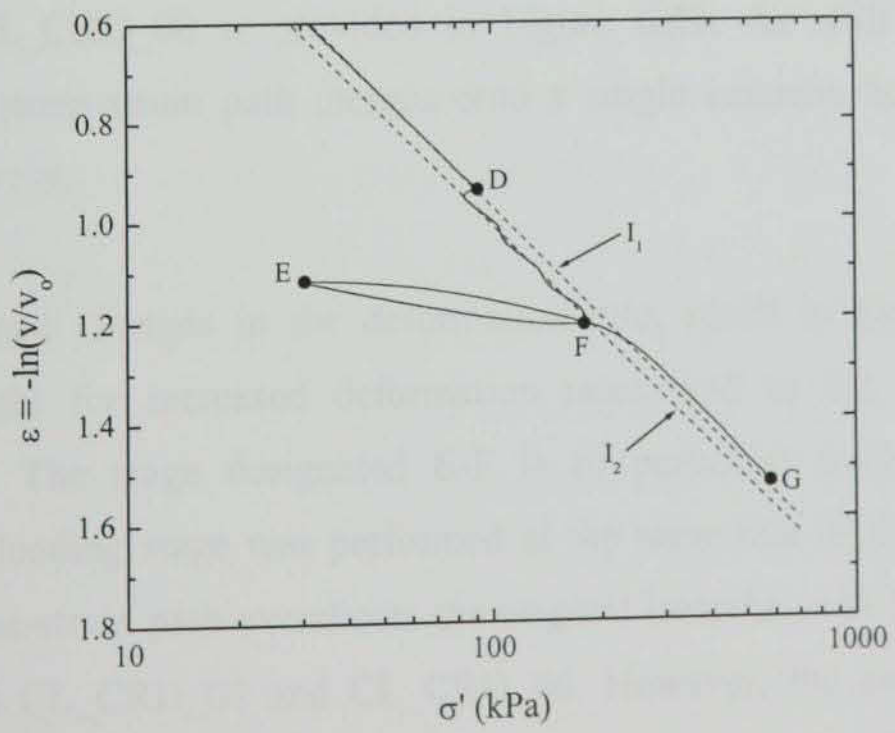

(b)

Figure 6.28 Stress-strain relationship for CL_CRD_06

The stress-strain relationship is linear in the virgin stress range to point B, and appears to follow a unique isotache, herein referred to as I_1.

After unloading and subsequent reloading, the stress-strain state rejoins and follows I_1 to point D. The deformation rate was then reduced 10-fold, and the stress-strain path shifts to the left, joining isotache I_2, which corresponds to a lower strain rate. Deformation continues along I_2 to E, at which point the specimen was unloaded to F. The deformation rate was then increased 10-fold and the specimen reloaded to point G. In this latter portion of the test (F-G), the stress-strain state appears to *overshoot* I_1, which is the isotache unique for that rate of deformation. However, as with CL_CRD_04, the isotaches shown in Figure 6.28 relate to lines of constant rate of deformation, or constant rate of *linear* strain. As the stress-strain relationship for peat is non-linear, natural strain is used to describe the compression of the soil. In this context, lines in ε^{nat}-σ' space are isotaches of creep *natural strain* rate, and not linear strain rate as defined by I_1 and I_2 in Figure 6.28. Considering that natural strain rate is greater than linear strain rate (Equation 6.10), it is not surprising that the ε^{nat}-σ' state overshoots I_1. It is also worth noting that this *overshoot* takes place despite the reduced rate of deformation caused by deformation of the external proving ring.

In tests CL_CRD_08 and CL_CRD_09 the external proving ring was replaced with a stiffer load cell, hence ensuring that the imposed rate of deformation remained essentially constant. The effects of the reduced rate of deformation are now assessed by comparing the ε^{nat}-σ' data of CL_CRD_04 and CL_CRD_06 with CL_CRD_08. The measured ε^{nat} - logσ' relationship for CL_CRD_08 is provided in Figure 6.29. As with CL_CRD_04 and CL_CRD_06, the stress-strain path merges onto a single isotache beyond the apparent preconsolidation stress.

As expected, stepped changes in the deformation rate, result in the stress-strain path shifting to the right for increased deformation rates, and to the left for decreased deformation rates. The stage designated E-F is of particular interest to the present discussion as this loading stage was performed at the same rate of deformation as A-B. Evidently, the stress-strain path overshoots the original isotache, which is consistent with Equation 6.10 and CL_CRD_04 and CL_CRD_06. However, the amount of overshoot does not appear to be much greater than that of CL_CRD_04 and CL_CRD_06, which suggests that the reduction in strain rate due to deformation of the proving ring in these tests had little effect.

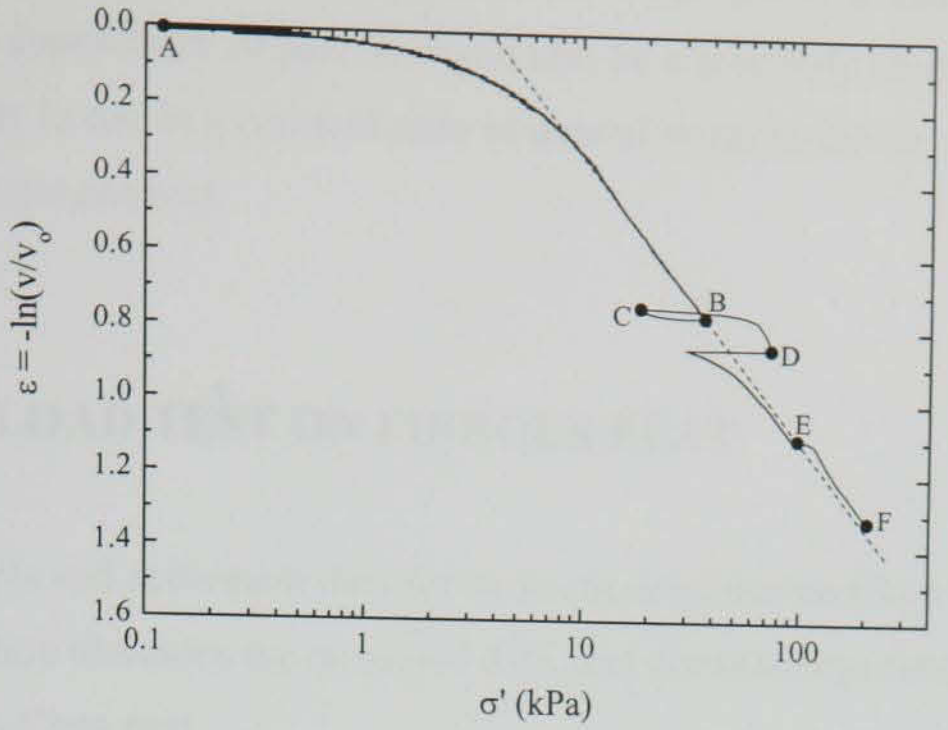

(a)

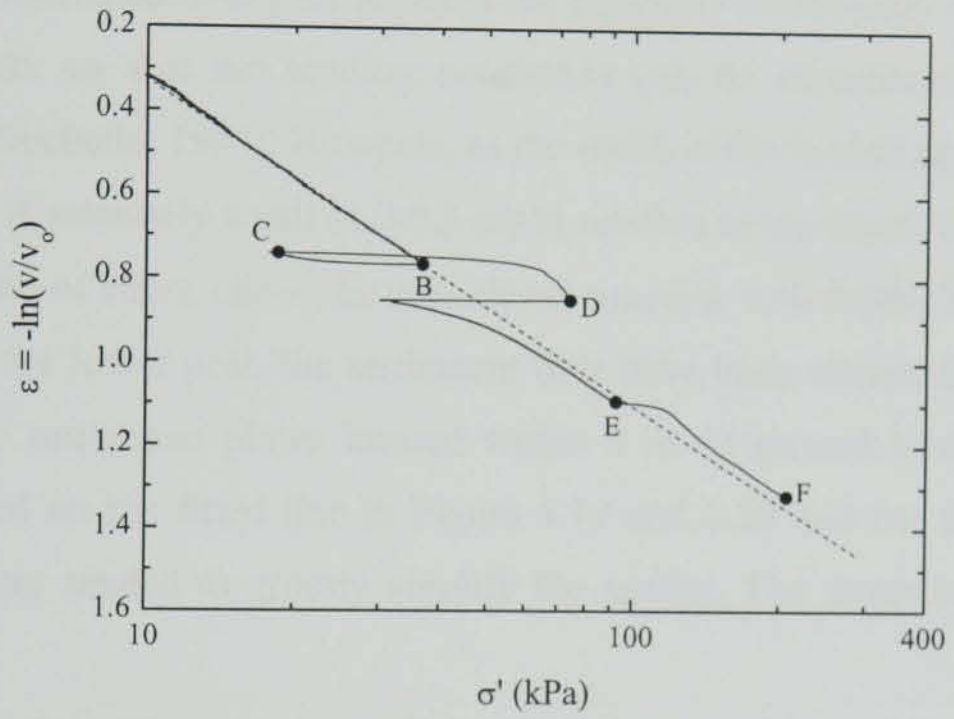

(b)

Figure 6.29 Stress-strain relationship for CL_CRD_08

Several factors have been mentioned in the foregoing, which complicate verification of the isotache principle for peat using the CRD test. One such complication is the adverse reduction in strain rate due to deformation of the proving ring. Results from CL_CRD_08 suggest that this effect has little bearing on measured data, although interpretation of the test results requires an assumption on the imposed rate of deformation. The main complication however, is as a result of an imposed rate of linear strain and not of natural strain. This causes the rate of natural strain to continually increase throughout the test, by an amount determinable by Equation 6.10. Consequently, true natural strain isotaches cannot be defined as the natural strain rate is continuously changing. This point must be considered when using CRD data as a means of determining parameters for *isotache-type*

constitutive models. Despite these drawbacks, the CRD test is a convenient means of assessing the rate dependency of peat. It would also be a relatively simple matter to allow the CRD apparatus to run in a constant state of natural strain mode (in which the velocity reduces as the test progresses).

6.5 IN SITU LOAD TEST ON FIBROUS PEAT

Construction details and settlement data for an *in situ* load test on Clara bog are provided in § 5.3. This section discusses the measured data, and draws comparisons with associated laboratory tests on Clara peat.

Embankments constructed over peat deposits are generally sufficiently wide in relation to the depth of peat, so that the loading conditions can be considered one-dimensional (Landva and La Rochelle, 1983). However, as the width of the loaded area (in the load test considered here) is relatively small (4.2-5.2 m) in relation to the depth of the peat layer (8 m), the distribution of stress cannot be considered constant with depth. To compensate for lateral strains in the lower peat, the settlement data have been interpreted as strains mid-way between the settlement plates located within 4 m of ground level. The calculated strains were based on the fitted line in Figure 5.19 and 5.20 and not the measured data points, as the latter tended to grossly amplify the scatter. The strain profiles are herein referred to as:

- $S_{1\text{-}3}$ for a point midway between S1 and S3
- $S_{3\text{-}5}$ for a point midway between S3 and S5

6.5.1 Application of first stress increment

Figure 6.30 shows the development of strain with time for the first stress increment (4.3 kPa). The strain at $S_{3\text{-}5}$ is greater than that at $S_{1\text{-}3}$, which is to be expected, considering that vertical stresses reduce with depth. After approximately 30 days, the strain at $S_{3\text{-}5}$ tends to level off, whereas at $S_{1\text{-}3}$ an approximately constant slope in ε - log t space is observed. The reason for this variance is uncertain. It can be seen from Figure 5.19 that both S3 and S5 continue to settle, although the strain tending towards a constant value indicates that the distance between the plates is not changing. Obviously this may be due to errors within the

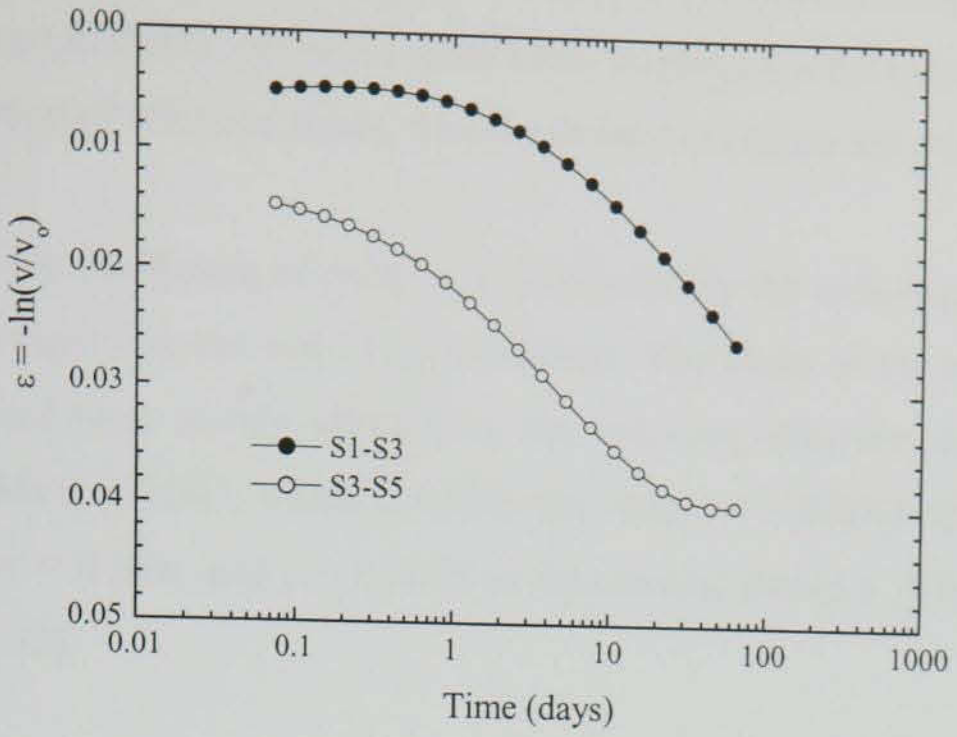

Figure 6.30 Strain profiles $S_{1\text{-}3}$ and $S_{3\text{-}5}$ during the first stress increment

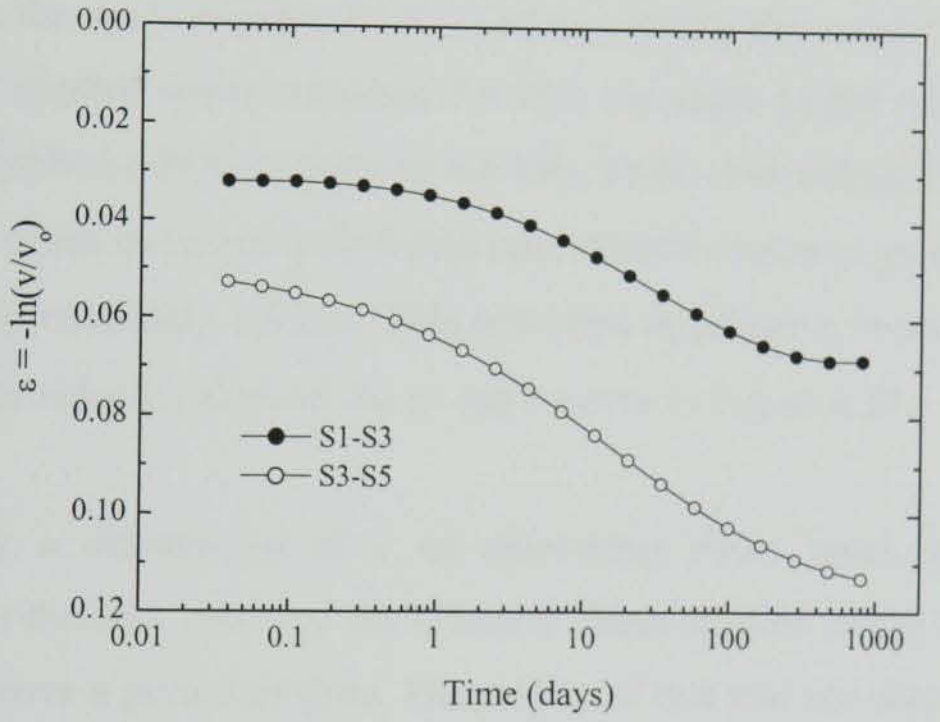

Figure 6.31 Strain profiles at $S_{1\text{-}3}$ and $S_{3\text{-}5}$ during the second stress increment

measurement system, for example, overmeasurement of S3. Field observations indicate that the partial submergence of the load resulted in a reduction in effective stress at ground level, from 4.3 kPa at the start of the test, to approximately 3 kPa at the end of this increment. The effect most probably explains why the strains tend to become constant at $S_{3\text{-}5}$.

The S-shaped strain profile at $S_{3\text{-}5}$ in Figure 6.30 suggests the end of consolidation at between 20 and 30 days. However, considering the proximity of $S_{3\text{-}5}$ to the drainage boundary, and that virgin fibrous peat generally has a very high initial permeability

(Dhowian and Edil, 1980; Hobbs, 1986), 20-30 days is considered to be well in excess of the true primary consolidation period. A more likely explanation for the apparent inflection point is the reduction of effective stress, which will tend to reduce the coefficient of creep.

Determination of the coefficient of creep, c, is hampered by the reducing effective stresses and uncertainties regarding the end of consolidation. The slope of the strain profile, $S_{1\text{-}3}$, appears to have not been unduly affected by the reducing effective stress. The average slope of $S_{1\text{-}3}$, yields $c = 0.007$, which is within the range; $c = 0.0065$ as determined from CL_MSL_04 at $\sigma' = 4$ kPa, and $c = 0.0075$ as determined from CL_MSL_05 at $\sigma' = 4.2$ kPa (see Figure 6.32).

6.5.2 Application of second stress increment

Figure 6.31 shows the strain profiles for $S_{1\text{-}3}$ and $S_{3\text{-}5}$ during the second stress increment. Although the total applied stress measured 7.9 kPa, the slight initial submergence of the load reduced the applied effective stress to 6.6 kPa. Field observations indicate that over the duration of the stress increment (≈800 days) the effective stress at ground level reduced from 6.6 kPa to approximately 1.5 kPa. This reduction in effective stress is considered to be the reason for the reducing slope of the ε - log t curves in Figure 6.31.

In order to verify a dependence of c on decreasing stress level, a laboratory test (CL_CRD_09) was devised, whereby the effective stress applied to the peat sample was reduced gradually over a period of time. The results of this test are described in § 4.5.2, Figure 4.36, and clearly show that the creep rate reduces significantly with decreasing effective stress. The test data are reproduced here in Figure 6.33 in terms of natural strain to allow for determination of c. The section A-B, corresponds to $c = 0.015$, which is typical of that encountered in Clara peat in the normally consolidated region. No variation in c is discernible until the effective stress reduces from 46kPa by approximately 9% to 42 kPa. Between 42 and 26 kPa c remains fairly constant, at 0.006. This value is about 2.5 times smaller than along A-B, and remains essentially constant despite a 43% reduction in effective stress. It is also worth noting that this c value of 0.006 is within the range of those determined from the two laboratory tests conducted in the overconsolidated stress range (see Figure 6.32), and is closely comparable to that estimated for the first stress increment of the field test ($S_{1\text{-}3}$, $c = 0.007$).

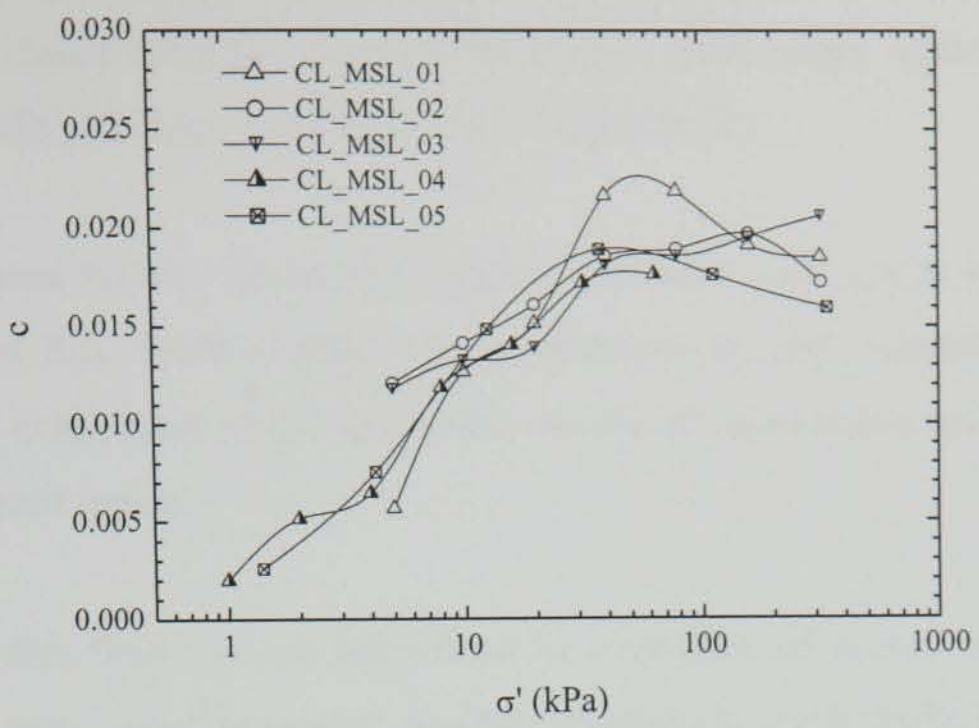

Figure 6.32 Variation in *c* determined from laboratory tests with stress level

The average value of c at $S_{3\text{-}5}$ for the second stress increment is 0.01 between 10 and 60 days. This is consistent with the observation that c increases with stress level in the overconsolidated stress range (Figure 6.32). The *in situ* value of $c = 0.01$ agrees well with that determined from CL_MSL_04 and CL_MSL_05 (Figure 6.32) for the initial stress of 6.6 kPa. However, over this time scale (10-60 days), the applied effective stress is considered to have reduced from 6.6 kPa to an average value of 4.2 kPa. The laboratory value of c for the latter stress level is approximately 0.0065, which is comparable with the *in situ* value measured at about the same stress level in the first load increment in the field

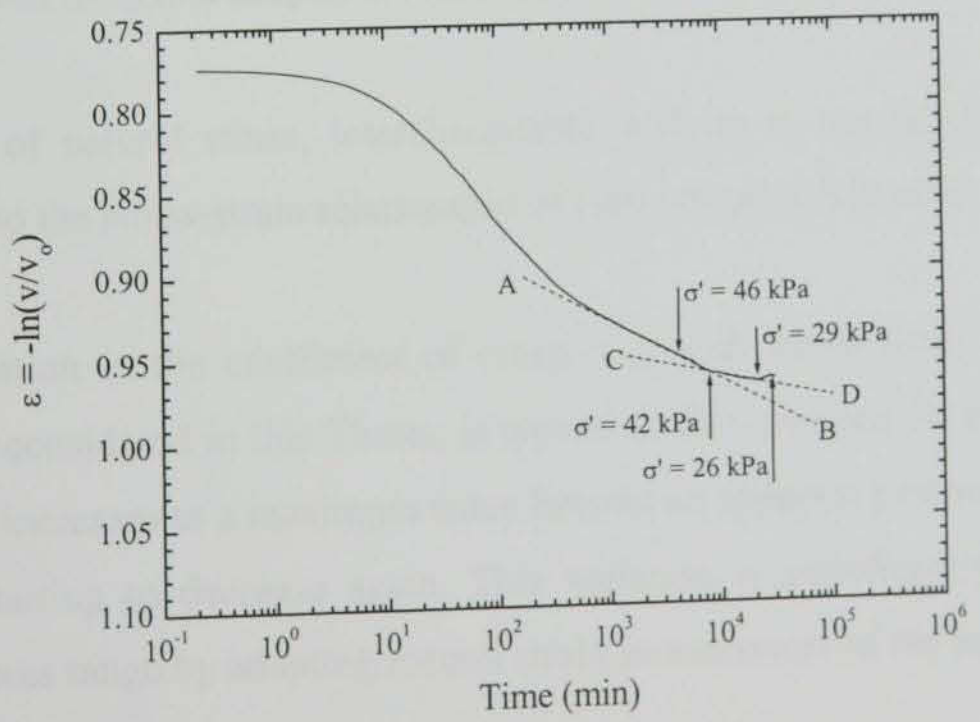

Figure 6.33 Reduction in *c* with decreasing effective stress (CL_CRD_09)

test. After 800 days submergence causes the effective stress to reduce to 1.5 kPa, at which point the *in situ* value of c for $S_{3\text{-}5}$ is 0.003-0.004. This range agrees well with the laboratory value of c at a stress level of 1.5 kPa (Figure 6.32).

Values of c inferred for $S_{1\text{-}3}$ during the second increment were typically 50% less than those inferred for $S_{3\text{-}5}$. Such a trend was presumably, in part, related to the reduced effective stresses at the level of $S_{1\text{-}3}$ and to the non-linear relationship between c and σ' in the overconsolidated region.

The findings of this field test are influenced by a number of factors, such as reducing effective stress, non one-dimensional loading conditions, particularly for $S_{1\text{-}3}$, and the physical difficulties associated with accurately measuring creep rates after extended periods of loading. Despite these limitations, the results are indicative of the extremely high compressibility of fibrous peat, even under very moderate loading.

6.6 SUMMARY AND CONCLUSIONS

The experimental results described in Chapters 4 and 5 have been interpreted with a view towards identifying a suitable constitutive one-dimensional compression model for peats. Several behavioural non-linearities have been identified and formulated where possible. Other features have been interpreted and quantifiably assessed. Some of the key points and conclusions derived from this chapter are summarised as follows:

1. The use of natural strain, interchangeable with ln v, has been used to restore linearity to the stress-strain relationship of very compressible soils.

2. The variation in the coefficient of creep, C_α, with stress level indicated by the database considered in this Thesis, is typical of that reported for peats and organic soils; C_α increases to a maximum value beyond an apparent preconsolidation stress, before starting to decrease again. This variation is significantly reduced in the virgin stress range by adopting natural strain as a measure of the soil compression.

3. Although, ln v produces an essentially linear relationship between strain and logarithm of stress, a degree of disparity still exists within respective tests on Clara

peat and Belfast organic clay. The latter is attributed to the effects of sampling disturbance and to significant variations within the samples tested. However, the variability of Clara peat is a consistent feature for seemingly similar samples. This variability could not be accounted for by normalising by the initial specific volume, and factors such as the following three were identified as significant:

- Gas content, resulting in incomplete saturation
- Variations in the concentration of fibres within the peat specimens
- Accelerated humification due to laboratory conditions

4. C_α depends strongly on the organic content, but a correlation between C_α and initial water content is only valid up to a maximum organic content of 80%.

5. C_α/C_c ratios have been determined, and generally fall within the range of ratios suggested by Ladd (1971), Mesri and Castro (1987) and Mesri *et al.* (1997). An exception to this is Clara peat, which has a C_α/C_c ratio of 0.042. A single C_α/C_c ratio cannot define the creep compression of *all* peat soils.

6. Tertiary compression, which is characterised by the steepening of ε - log t curves, observable at constant effective stress, can be explained by the transition from an overconsolidated to a normally consolidated state; this transition point is best determined at the point at which the previous minimum volume is reached.

7. It is suggested that the success of preloading projects is linked to the amount of rebound obtainable after removal of surcharge, as the soil will take longer to creep towards its *minimum past specific volume*, at which point the increase in creep strain rate to the normally consolidated rate is likely to occur.

8. The isotache concept is considered valid for peat if natural strain and natural strain rate are adopted. A unique relationship has been observed between stress, strain and strain rate, but only when strain rate is interpreted as creep natural strain rate.

9. CRD tests have been performed on Clara peat to verify the isotache principle. The CRD test is only partially suitable in this regard, as the imposed rate of deformation infers a constant rate of linear strain and not natural strain. It has been shown that for increasing compression, natural strain rate will always be higher that linear

strain rate. Hence in CRD tests, the stress-strain state is continuously moving towards isotaches corresponding to higher rates of natural strain. This was observed at higher stresses when the difference between linear strain rate and natural strain rate is appreciable.

10. The performance of the load test on Clara bog, described in Chapter 5, has been assessed. Comparisons of the coefficient of creep, c, with laboratory tests at an equivalent stress level show good agreement. However, determination of the *in situ* values of c is hampered somewhat by the reduction in effective stress due to the submergence of the load.

Chapter 7

Modelling one-dimensional compression of fibrous peat

Chapter 7

Modelling one-dimensional compression of fibrous peat

7.1 INTRODUCTION

Although the author initially employed the *EVP* model (Yin and Graham; 1989, 1994, 1996) to predict the time-dependent compression of fibrous peat, such was the extent of modifications required that alternative constitutive models were considered. The modifications made to the *EVP* model are described in O'Loughlin and Lehane (2001a, 2001b). These papers are included for reference in Appendix B.

From the currently available constitutive models, the *abc* model (den Haan and Edil, 1994; den Haan, 1996) is considered to have the highest potential for successful application to peat. This model incorporates many of the features stated in the conclusions to Chapter 6, which are considered essential for realistic modelling.

This chapter initially describes the essential features of the *abc* model, and shows how the formulation may be incorporated into computer code. The second section of this chapter assesses the potential of the *abc* model for use with fibrous peat, by comparing the predicted stress-strain response with that measured in laboratory tests under a variety of loading conditions. Finally, the model is used to predict the settlement of a test embankment constructed over a fibrous peat deposit in the James Bay area, Canada.

7.2 *abc* MODEL

The *abc* model is essentially similar to the *EVP* model, in that both assume a unique relationship between strain, effective stress and creep strain rate. However, O'Loughlin

and Lehane (2001a) showed that the *EVP* model often grossly over-predicts settlements in fibrous peat. The main reason for these inaccuracies is that the *EVP* model employs the conventional definition of strain ($\varepsilon = \Delta H/H_o$) as a measure of the soil deformation. O'Loughlin and Lehane (2001a) highlighted several other key factors, such as the assumption that the permeability, k, remains constant and the assumption that settlements are small compared with the depth of the soil layer. These shortcomings prompted the author to consider the *abc* model, which possesses many of the features essential for successful application to fibrous peat. Elements of the *abc* model, such as the parameters b and c, and the power formulation in Equation 6.5 have already been described in the previous chapters. However, these terms and formulations are redefined here for ease of reference.

7.2.1 Stress, strain, creep-strain formulation

Den Haan (1992) proposed that the following power relationship could be used to describe the virgin compression of a wide range of soils.

$$\frac{v - v_\infty}{v_1 - v_\infty} = \left(\sigma' - \sigma'_s\right)^{-b} \qquad 7.1$$

In Equation 7.1, the parameter σ'_s is used to account for the brittle nature of a range of natural clays, by shifting the vertical asymptote of the power curve from $\sigma' = 0$ to $\sigma' = \sigma'_s$. v_1 is a reference specific volume at an effective stress of unity. Den Haan (1992) showed that for a wide variety of soils including peats, remoulded clays and granular soils, optimal fits could be obtained by taking $\sigma'_s = 0$. Existing power formulations such as those preferred by Garlanger (1972), Christie & Tonks (1985) and Mesri *et al.* (1975), do non include the structure parameter σ'_s, and generally assume that $v_\infty = 1$, which has the effect of reducing Equation 7.1 to:

$$\frac{e}{e_1} = \sigma'^{-b} \qquad 7.2$$

Formulations such as that described by Equation 7.2 infer that at infinite stress the voids would completely collapse, justifying the choice of $v_\infty = 1$. However, other workers such as

Juárez-Badillo (1981a) and Hardin (1989) believe that the correct limiting value at an infinite stress level should be zero volume, as the solids are likely to compress before the voids completely reduce to zero. For non-brittle soils such as peat, adopting the latter argument in Equation 7.1, leads to:

$$\frac{v}{v_1} = \sigma'^{-b} \qquad 7.3$$

The success of both formulations in fitting the virgin stress-strain curve of the soils considered in this Thesis is compared in Figure 6.2 and 6.3. Evidently Equation 7.3 provides the optimal fit. Although the argument of limiting values of volume at infinite stress appear to bear little practical significance, the improved correlation justifies the argument, and also the use of Equation 7.3.

As the structure parameter, σ'_s, can be taken as zero for a wide range of soils, the power function defined by Equation 7.1 can be reduced to a logarithmic function:

$$\ln v = \ln v_1 - b \ln \sigma' \qquad 7.4$$

It is obvious from Figure 6.1 that the e – log σ' relationship for peat is highly non-linear and impossible to characterize by a single value of C_c. However, as is shown on Figure 6.4, if the data are re-plotted in terms of ln v, then a linear relationship is obtained in the virgin stress range. The use of ln v is interchangeable with natural strain, which differs from conventional, linear strain in definition. Natural strain, ε^{nat}, is measured incrementally with respect to the current specific volume, v:

$$\varepsilon^{nat} = -\int_{v_o}^{v} \frac{dv}{v} = -\ln\left(\frac{v}{v_o}\right) \qquad 7.5$$

The conventional linear strain, ε^{lin}, is defined as the change in volume with respect to the initial or reference specific volume, v_o.

$$\varepsilon^{lin} = -\frac{\Delta v}{v_o} \qquad 7.6$$

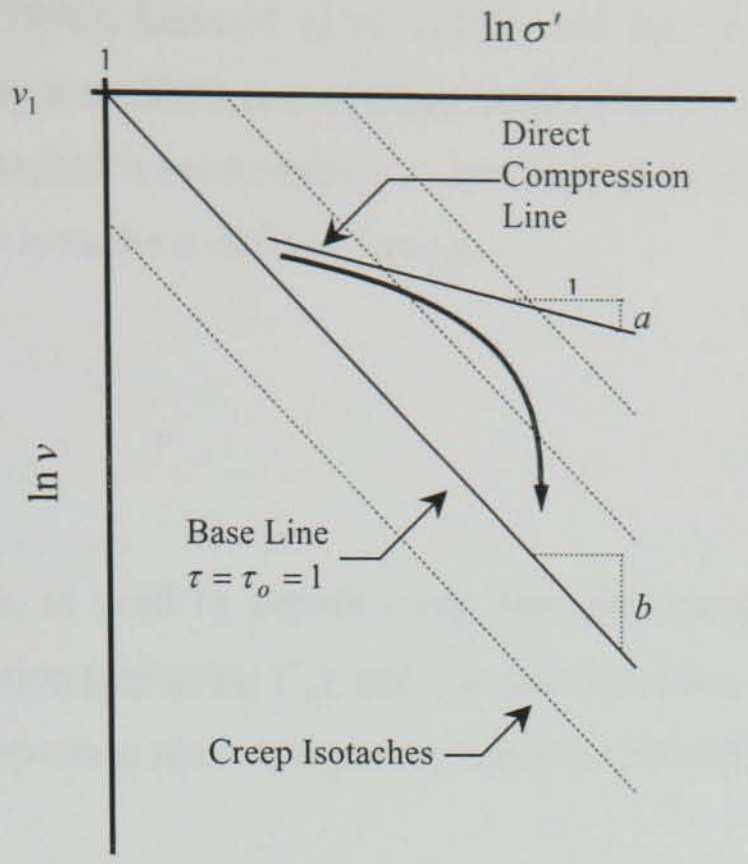

Figure 7.1 Stress, strain, creep-strain-rate relationship adopted by the *abc* model

where v_o is the reference specific volume. Both measures of compression are related in a simple manner by:

$$\varepsilon^{nat} = -\ln\left(1 - \varepsilon^{lin}\right) \qquad 7.7$$

Natural strain has been preferred in the past by Juárez-Badillo (1981a, 1981b), Butterfield (1979) and Lefebvre *et al.* (1984), as it is much more successful in linearising ε - log σ' data for soft soils such as peat.

Although Equation 7.1 has been used in § 6.2.2 to fit data measured after 24-hour compression, the *abc* model adopts natural strain rate, rather than time as a means of describing the viscous behaviour of the soil. The benefits of rate over time have been dealt with in numerous publications including Leroueil *et al.* (1985) and Imai (1995). In brief, many of the models which employ time in the formulation (Bjerrum, 1967; Garlanger, 1972; Magnan *et al.*, 1979), encounter difficulties in assigning a particular value of time to the instant time line which is employed in these models.

The *abc* model adopts the isotache concept coined by Šuklje (1957), defining a unique relationship between effective stress, natural strain, and rate of natural strain. This relationship is described on Figure 7.1 by a family of isotaches, each representing a unique value of natural strain rate. Unlike seemingly similar models such as those proposed by

Niemunis and Krieg (1996), Leroueil *et al.* (1985) and Kim & Leroueil (2001), these isotaches are defined by a constant rate of creep strain rate and not total strain rate. The separation of these isotaches is controlled by c, and their slope described by b. The creep strain rate on any given isotache is defined through:

$$\frac{d\varepsilon_s}{dt} = \frac{c}{\tau} \qquad 7.8$$

where the subscript, s, is used to denote creep (secular) compression, c is the creep coefficient of compression (replacing C_α), and τ is *intrinsic time*, which is adopted by the *abc* model to scale creep strain rates. Integrating Equation 7.8 with respect to time:

$$\int_{\varepsilon_{s,o}}^{\varepsilon_s} d\varepsilon_s = \int_{t_o}^{t} \frac{c}{\tau} dt$$

$$\varepsilon_s - \varepsilon_{s,o} = c \ln\left(\frac{\tau}{\tau_o}\right) \qquad 7.9$$

The subscript, o, in Equation 7.9 refers to an origin of time and creep strain rate at constant effective stress. Equation 7.9 assumes a linear relationship between creep strain and the natural logarithm of intrinsic time. Den Haan and Edil (1994) showed that at large values of laboratory loading time (typically 24 hours), intrinsic time, τ, and loading time, t, are essentially interchangeable. This implies that the parameter, c, can be determined directly from ε - ln t data, provided that t is sufficiently large to result in a linear relationship between measured strain and the natural logarithm of time.

Equation 7.4 is extended to account for the rate dependent strain described by Equation 7.9:

$$-\ln\left(\frac{v}{v_1}\right) = b \ln \sigma' + c \ln\left(\frac{\tau}{\tau_o}\right) \qquad 7.10$$

The isotaches in Figure 7.1 are described by Equation 7.10, where τ_o is a reference value of intrinsic time, fixed at 1 day on the base or reference line. Equation 7.10 defines a unique relationship between natural strain, effective stress and rate of natural strain. The origin of strain in this instance is v_1, which can be determined by extrapolating the base line (with τ_o

= 1 day) back to an effective stress of unity. It should be noted that Equation 7.10 is only proposed to be valid in the virgin stress range, as the development of isotaches in the overconsolidated region are neither parallel nor linear.

Equation 7.10 describes the development of creep strain rates as a unique function of effective stress and strain. These strain rates are assumed to be valid at constant effective stress and during consolidation. However, during consolidation total strain rate is assumed to be due to the combination of creep strain rate and (direct) strain rates arising from increases in effective stress. The assumed relationship between direct strain rate ($d\varepsilon_d/dt$) and rate of effective stress is:

$$\frac{d\varepsilon_d}{dt} = \frac{a}{\sigma'}\frac{d\sigma'}{dt} \qquad 7.11$$

where a is similar, but not identical to the elastic compression index, κ/v, from critical state soil mechanics.

Combining Equation 7.8 with Equation 7.11 gives the total strain rate for any given stress-strain state in the virgin stress range:

$$\frac{d\varepsilon}{dt} = \frac{a}{\sigma'}\frac{d\sigma'}{dt} + \frac{c}{\tau} \qquad 7.12$$

7.2.2 Finite strain consolidation equation

Gibson *et al.* (1967) showed how the standard consolidation equation could be modified so as to allow for a moving boundary. Figure 7.2 shows the Langragian coordinate system that they adopted, which does not require the commonly made assumption that strains must be small in comparison with the thickness of the soil layer. The *abc* model makes use of this finite strain consolidation theory by incorporating Equation 7.12 into the *finite strain* consolidation equation. The following derivation (Equation 7.13 – Equation 7.21) is taken from den Haan (1996).

If the soil element in Figure 7.2 deforms from dz_o to dz and the state of the soil element is described by v_o and v respectively, then:

$$\frac{dz}{dz_o} = \frac{v}{v_o} \tag{7.13}$$

Darcy's law may be expressed as:

$$q = -\frac{\partial}{\partial z}\left[k\frac{\partial}{\partial z}\left(\frac{u_e}{\gamma_w}\right)\right] \tag{7.14}$$

where q is the rate of outflow, k is the permeability and u_e is the excess pore water pressure. Using the relationship in Equation 7.13, Equation 7.14 may be written as:

$$q = -\frac{1}{\gamma_w}\frac{v_o}{v}\frac{\partial}{\partial z_o}\left(k\frac{v_o}{v}\frac{\partial u_e}{\partial z_o}\right) \tag{7.15}$$

Terzaghi's effective stress equation can be applied to saturated soils:

$$\sigma = \sigma' + u_w \tag{7.16}$$

where the pore water pressure u_w, is defined as the sum of the hydrostatic pore water pressure u_s, and the excess pore water pressure u_e:

$$\sigma = \sigma' + u_e + u_s \tag{7.17}$$

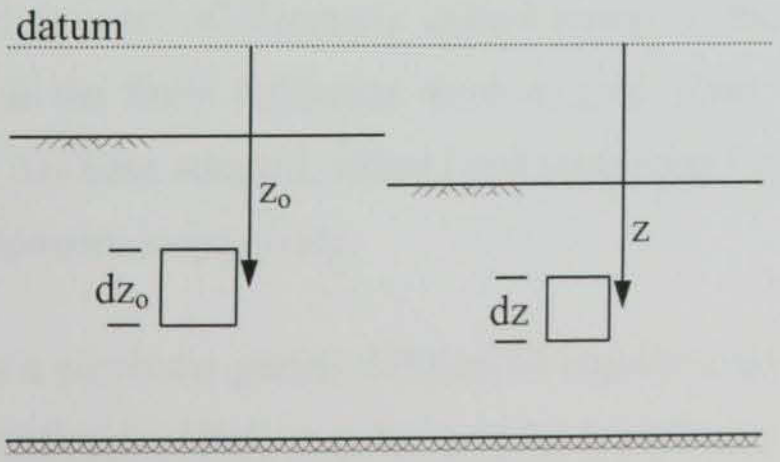

Figure 7.2 Langragian coordinate system adopted by the *abc* model

The gradient of hydrostatic pressure when subtracted from the gradient of total pressure (unit weight of solids, γ_s) give the effective unit weight ($\gamma_s - \gamma_w$) and hence:

$$\frac{\partial}{\partial z_o}(\sigma - u_s) = \frac{\gamma_s - \gamma_w}{v_o} \qquad 7.18$$

Combining Equations 7.15, 7.17 and 7.18 yields:

$$\begin{aligned} q &= -\frac{1}{\gamma_w}\frac{v_o}{v}\frac{\partial}{\partial z_o}\left[k\frac{v_o}{v}\left(\frac{\gamma_s - \gamma_w}{v_o} - \frac{\partial \sigma'}{\partial z_o}\right)\right] \\ &= \frac{1}{\gamma_w}\frac{v_o}{v}\frac{\partial}{\partial z_o}\left(k\frac{v_o}{v}\frac{\partial \sigma'}{\partial z_o}\right) - \frac{\gamma_s - \gamma_w}{\gamma_w}\frac{v_o}{v}\frac{\partial}{\partial z_o}\left(\frac{k}{v}\right) \end{aligned} \qquad 7.19$$

The rate of outflow, q, can be equated to the total rate of deformation which is equal to the sum of direct compression rate and creep strain rate:

$$q = \frac{\partial \varepsilon}{\partial t} = \frac{\partial \varepsilon_d}{\partial t} + \frac{\partial \varepsilon_s}{\partial t} \qquad 7.20$$

From Equations 7.19 and 7.12,

$$\frac{d\sigma'}{dt} = \frac{\sigma'}{a}\left[\frac{1}{\gamma_w}\frac{v_o}{v}\frac{\partial}{\partial z}\left\{k\frac{v_o}{v}\frac{\partial \sigma'}{\partial z}\right\} - \frac{\gamma_s - \gamma_w}{\gamma_w}\frac{v_o}{v}\frac{\partial}{\partial z}\left(\frac{k}{v}\right) - \frac{c}{\tau}\right] \qquad 7.21$$

Numerical methods such as the *finite difference method* are commonly employed for solving coupled consolidation and creep problems under oedometric conditions. The finite difference method can be used to represent the time and space derivatives in Equation 7.21 by algebraic equations derived from Taylor's series expansions. These algebraic equations can then be applied to a set of discretely spaced points in the space and time domain, usually referred to as the finite difference *mesh* or *grid*. Here, the finite difference grid shown in Figure 7.3 has been adopted, where i and j represent the finite difference nodes in the space and time domains respectively.

As Equation 7.21 is a parabolic partial differential equation, the combined method finite difference technique (Özişik, 1994) may be used by introducing the coefficient θ to yield

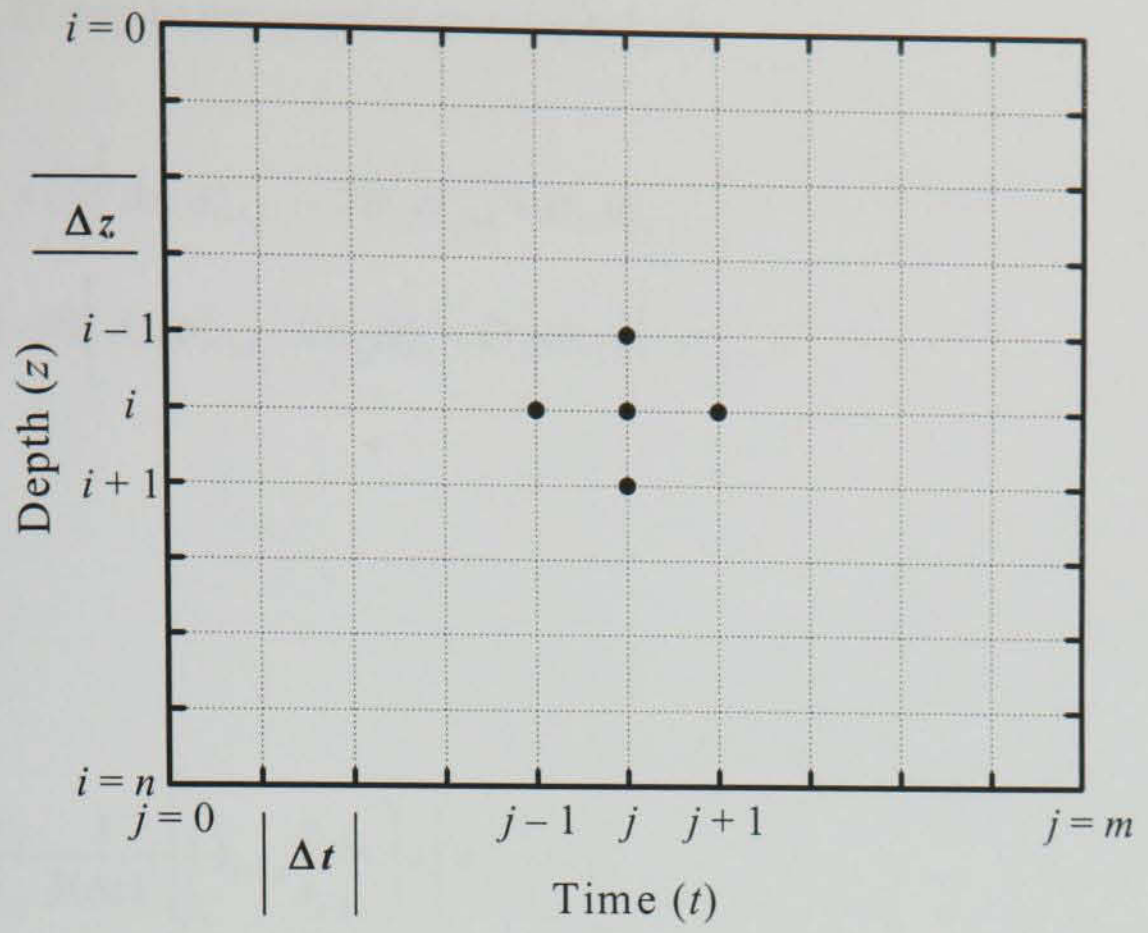

Figure 7.3 Finite difference grid

an explicit ($\theta = 0$), implicit ($\theta = 1$), or semi-implicit ($\theta = ½$) type solution. The combined finite difference approximation of Equation 7.21 may be expressed as:

$$\frac{\sigma'_{i,j+1}-\sigma'_{i,j}}{\Delta t}=\frac{\sigma'_{i,j}}{a}\left[\frac{1}{\gamma_w}\frac{v_{i,o}}{v_{i,j}}\theta\left\{\left(\left(k\frac{v_o}{v}\right)_{i-1/2}\frac{\sigma'_{i-1,j+1}-\sigma'_{i,j+1}}{(\Delta z)^2}\right)+\left(\left(k\frac{v_o}{v}\right)_{i+1/2}\frac{\sigma'_{i+1,j+1}-\sigma'_{i,j+1}}{(\Delta z)^2}\right)\right\}\right]$$
$$+\frac{\sigma'_{i,j}}{a}\left[\frac{1}{\gamma_w}\frac{v_{i,o}}{v_{i,j}}(1-\theta)\left\{\left(\left(k\frac{v_o}{v}\right)_{i-\frac{1}{2}}\frac{\sigma'_{i-1,j}-\sigma'_{i,j}}{(\Delta z)^2}\right)+\left(\left(k\frac{v_o}{v}\right)_{i+\frac{1}{2}}\frac{\sigma'_{i+1,j}-\sigma'_{i,j}}{(\Delta z)^2}\right)\right\}\right] \qquad 7.22$$
$$-\frac{\sigma'_{i,j}}{a}\left[\frac{\gamma_s-\gamma_w}{\gamma_w}\frac{v_{i,o}}{v_{i,j}}\frac{1}{2\Delta z}\left\{\left(\frac{k}{v}\right)_{i+1,j}-\left(\frac{k}{v}\right)_{i-1,j}\right\}-\frac{c}{\tau_{i,j}}\right]$$

For laboratory conditions, the author has found that the explicit method necessitates extremely small time steps to ensure numerical stability. Although the implicit method is unconditionally numerically stable, the finite difference approximation for $d\sigma'/dt$ is only accurate to the first order. A more computationally efficient semi-implicit scheme has been developed by Crank and Nicolson (1947), which is both numerically stable and accurate to the second order for both the time derivative, $d\sigma'/dt$ and the space derivative, $d/dz\{k\ v_o/v\ d\sigma'/dz\}$. As this method is unconditionally stable, the time step does not necessarily need to remain constant, but may increase as the solution progresses.

Equation 7.22 may be expressed more compactly as:

$$\sigma'_{i,j+1} = \sigma'_{i,j} + r\theta\left[A_{i,j}\,\sigma'_{i-1,j+1} - 2B_{i,j}\sigma'_{i,j+1} + D_{i,j}\sigma'_{i+1,j+1}\right] + r(1-\theta)\left[A_{i,j}\,\sigma'_{i-1,j} - 2B_{i,j}\sigma'_{i,j} + D_{i,j}\sigma'_{i+1,j}\right] - rG_{i,j} \qquad 7.23$$

where:

$$r = \Delta t\frac{\sigma'_{i,j}}{a} \qquad 7.24a$$

$$A_{i,j} = \frac{1}{\gamma_w}\frac{v_{i,o}}{v_{i,j}}\frac{1}{2(\Delta z)^2}\left[\left(k_{i-1,j}\frac{v_{i-1,o}}{v_{i-1,j}}\right) + \left(k_{i,j}\frac{v_{i,o}}{v_{i,j}}\right)\right] \qquad 7.24b$$

$$D_{i,j} = \frac{1}{\gamma_w}\frac{v_{i,o}}{v_{i,j}}\frac{1}{2(\Delta z)^2}\left[\left(k_{i+1,j}\frac{v_{i+1,o}}{v_{i+1,j}}\right) + \left(k_{i,j}\frac{v_{i,o}}{v_{i,j}}\right)\right] \qquad 7.24c$$

$$G_{i,j} = \frac{\gamma_s - \gamma_w}{\gamma_w}\frac{v_{i,o}}{v_{i,j}}\frac{1}{2\Delta z}\left[\left(\frac{k_{i+1,j}}{v_{i+1,j}}\right) - \left(\frac{k_{i-1,j}}{v_{i-1,j}}\right)\right] + \frac{c}{\tau_{i,j}} \qquad 7.24d$$

$$B_{i,j} = \frac{1}{2}\left(A_{i,j} + D_{i,j}\right) \qquad 7.24e$$

Rearranging Equation 7.23 so that the unknown effective stress terms are on the left hand side yields:

$$\begin{aligned} &-r\theta A_{i,j}\sigma'_{i-1,j+1} + (1 + 2r\theta B_{i,j})\sigma'_{i,j+1} - r\theta D_{i,j}\sigma'_{i+1,j+1} \\ &= (1-\theta)rA_{i,j}\sigma'_{i-1,j} + \left[1 - 2rB_{i,j}(1-\theta)\right]\sigma'_{i,j} + (1-\theta)rD_{i,j}\sigma'_{i+1,j} - rG_{i,j} \end{aligned} \qquad 7.25$$

Dividing across by r gives:

$$\begin{aligned} &-\theta A_{i,j}\sigma'_{i-1,j+1} + \left(\frac{1}{r} + 2\theta B_{i,j}\right)\sigma'_{i,j+1} - \theta D_{i,j}\sigma'_{i+1,j+1} \\ &= (1-\theta)A_{i,j}\sigma'_{i-1,j} + \left[\frac{1}{r} - 2B_{i,j}(1-\theta)\right]\sigma'_{i,j} + (1-\theta)D_{i,j}\sigma'_{i+1,j} - G_{i,j} \end{aligned} \qquad 7.26$$

Equation 7.26 may be expressed in matrix form as: $[A]\{\sigma'\}_{j+1}=\{c\}_j$ where $[A]$ is *tridiagonal*, i.e. a matrix with nonzero elements only on the main diagonal and the two diagonals adjacent to the main diagonal.

$$\begin{bmatrix} b_{1,j} & d_{1,j} & & & & & \\ a_{2,j} & b_{2,j} & d_{2,j} & & & & \\ & & \ddots & & & & \\ & & a_{i,j} & b_{i,j} & d_{i,j} & & \\ & & & & \ddots & & \\ & & & & a_{n-1,j} & b_{n-1,j} & d_{n-1,j} \\ & & & & & a_{n,j} & b_{n,j} \end{bmatrix} \begin{bmatrix} \sigma'_{1,j+1} \\ \sigma'_{2,j+1} \\ \vdots \\ \sigma'_{i,j+1} \\ \vdots \\ \sigma'_{n-1,j+1} \\ \sigma'_{n,j+1} \end{bmatrix} = \begin{bmatrix} c_{1,j} \\ c_{2,j} \\ \vdots \\ c_{i,j} \\ \vdots \\ c_{n-1,j} \\ c_{n,j} \end{bmatrix} \qquad 7.27$$

where:

$$\{a\}_j = -\theta \begin{bmatrix} 0 \\ A_{2,j} \\ \vdots \\ A_{i,j} \\ \vdots \\ A_{n-1,j} \\ a_n \end{bmatrix}, \quad \{b\}_j = \begin{bmatrix} b_1 \\ 1/r + 2\theta B_{2,j} \\ \vdots \\ 1/r + 2\theta B_{i,j} \\ \vdots \\ 1/r + 2\theta B_{n-1,j} \\ b_n \end{bmatrix}, \quad \{d\}_j = -\theta \begin{bmatrix} d_1 \\ D_{2,j} \\ \vdots \\ D_{i,j} \\ \vdots \\ D_{n-1,j} \\ 0 \end{bmatrix}$$

$$\{c\}_j = \begin{bmatrix} c_1 \\ (1-\theta)A_{2,j}\sigma'_{1,j} + \left[\frac{1}{r} - 2B_{2,j}(1-\theta)\right]\sigma'_{2,j} + (1-\theta)D_{2,j}\sigma'_{3,j} - G_{2,j} \\ \vdots \\ (1-\theta)A_{i,j}\sigma'_{i-1,j} + \left[\frac{1}{r} - 2B_{i,j}(1-\theta)\right]\sigma'_{i,j} + (1-\theta)D_{i,j}\sigma'_{i+1,j} - G_{i,j} \\ \vdots \\ (1-\theta)A_{n-1,j}\sigma'_{n-2,j} + \left[\frac{1}{r} - 2B_{n-1,j}(1-\theta)\right]\sigma'_{n-1,j} + (1-\theta)D_{n-1,j}\sigma'_{n,j} - G_{n-1,j} \\ c_n \end{bmatrix} \qquad 7.28$$

a_n, d_1, c_1 and c_n are special cases, dependant upon the boundary conditions. In the case of a half-closed layer with a free-draining upper boundary (i=1) and an impermeable lower boundary (i=n):

$$a_n = 2, \quad b_1 = 1, \quad b_n = \frac{1}{r} + 2\theta B_{n,j}, \quad d_1 = 0, \quad c_1 = 0,$$

$$c_n = 2(1-\theta)A_{n-1,j}\sigma'_{n-2,j} + \left[\frac{1}{r} - 2B_{n-1,j}(1-\theta)\right]\sigma'_{n-1,j} - G_{n-1,j} \qquad 7.29$$

In the case of an open layer with both boundaries free-draining:

$$a_n = 0, \quad d_1 = 0, \quad c_1 = 0, \quad c_n = 0 \qquad 7.30$$

The corresponding change in strain may be determined by integrating Equation 7.12 with respect to time:

$$\int_{\varepsilon_{i,j}}^{\varepsilon_{i,j+1}} \frac{d\varepsilon}{dt} dt = a \int_{\sigma'_{i,j}}^{\sigma'_{i,j+1}} \frac{d\sigma'}{\sigma' dt} dt + c \int_{\tau_{i,j}}^{\tau_{i,j+1}} \frac{dt}{\tau} \qquad 7.31$$

or,

$$\varepsilon_{i,j+1} = \varepsilon_{i,j} + a \ln\left(\frac{\sigma'_{i,j+1}}{\sigma'_{i,j}}\right) + c \ln\left(\frac{\tau_{i,j+1}}{\tau_{i,j}}\right) \qquad 7.32$$

Equation 7.27 can be efficiently solved for problems involving MSL loading conditions using a tri-diagonal matrix algorithm such as that described by Thomas (1949). The solution of Equation 7.27 yields the effective stress, $\sigma'_{i,j+1}$, which can then be input into Equation 7.32 to calculate the strain, $\varepsilon_{i,j+1}$. A more suitable formulation can be obtained for CRD loading conditions by rewriting Equation 7.12 as:

$$\frac{d\varepsilon}{dt} = \frac{a}{\sigma'}\left(\frac{d\sigma}{dt} - \frac{du}{dt}\right) + \frac{c}{\tau} \qquad 7.33$$

In this context, $d\varepsilon/dt$ is the rate of deformation or rate of linear strain, which is linked to the rate of natural strain through Equation 6.10. If CRD tests involve deformation rates that are typical of those measured after excess pore water pressures have dissipated in MSL tests, then the rate of pore pressure dissipation, du/dt, is effectively equal to zero. This assumption infers that there is no variation in the strain or effective stress distribution

throughout the specimen thickness, which allows the finite difference approximation of Equation 7.33 to be written as:

$$\left(\varepsilon_{j+1}-\varepsilon_{j}\right)-a\left(\frac{\sigma_{j+1}-\sigma_{j}}{\sigma_{j+1}}\right)-c\frac{\Delta t}{\tau_{j+1}}=0 \qquad 7.34$$

where ε_{j+1} and ε_j are linear strains, which can be translated into natural strain through Equation 7.7. As the deformation rate is controlled in CRD tests, ε_{j+1} and ε_j are known, so the only unknown quantity is the stress, σ_{j+1}, which can be determined using optimisation techniques such as the simplex method or Powell's (1964) method.

Equations 7.27 and 7.32 have been implemented in a dedicated software application called CREEP, which was developed by the author using Microsoft Visual C++ 6.0. A typical user interface from CREEP is shown in Figure 7.4.

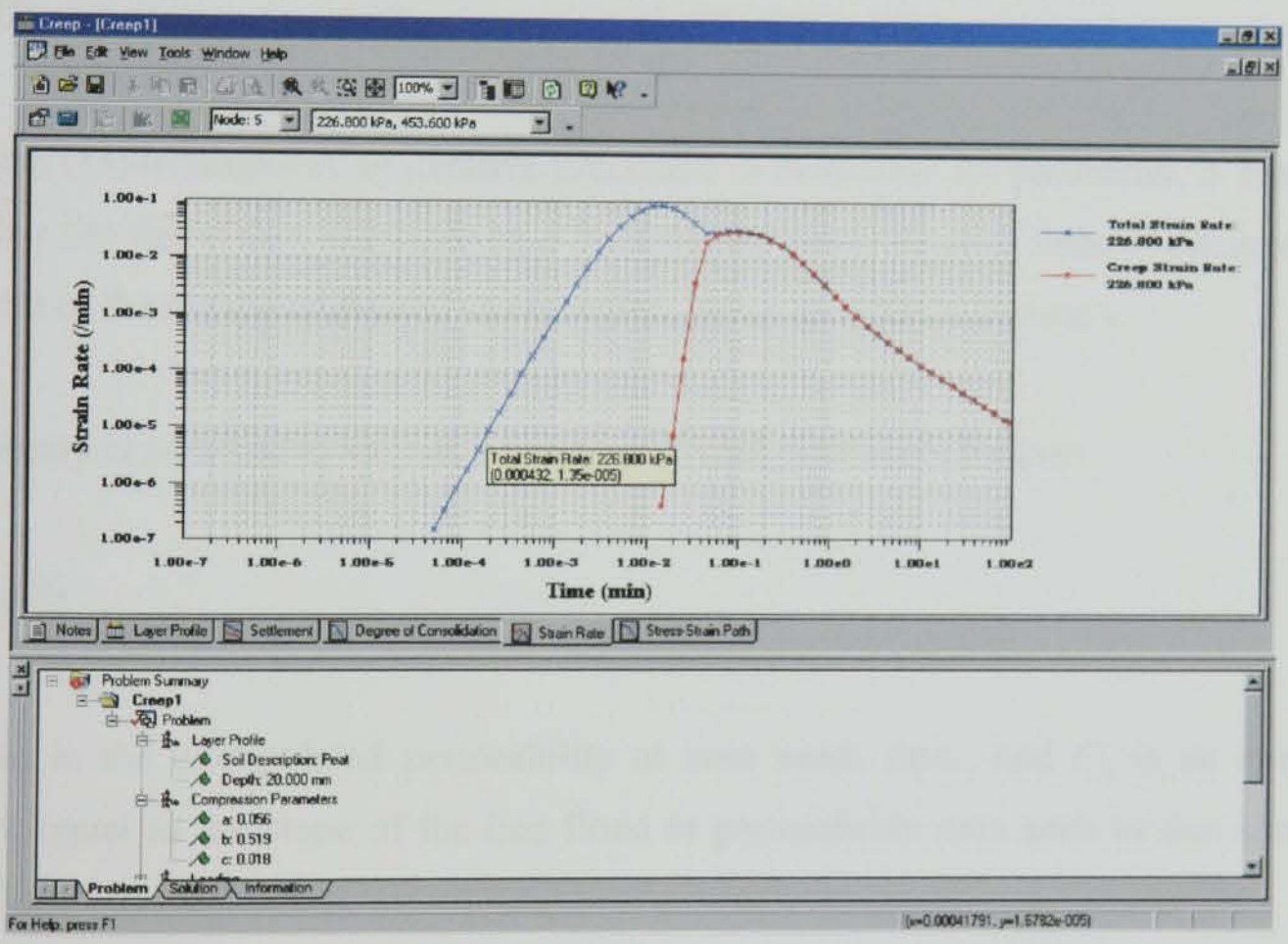

Figure 7.4 Typical user interface from CREEP

7.3 Application of model to laboratory tests on Clara peat

The suitability of the *abc* model in describing the stress-strain response of fibrous peat has been assessed by comparing predictions obtained from CREEP with measured data. Model

parameters have been determined from CL_MSL_01 and applied to the following tests: CL_MSL_01, CL_MSL_02, CL_MSL_07, CL_MSL_12, CL_MSL_13 and CL_CRD_06. The predicted strain profiles from these tests are presented and subsequently discussed.

7.3.1 Determining model parameters

In this section determination of the model parameters is briefly described. Compression data are interpreted in terms of ln v or natural strain, and lines of constant creep strain rate constructed in ln v – ln σ' space. The slope of these lines in the virgin stress range yields the parameter, b. The parameter c can be determined from ln v – ln t plots for each load increment at constant effective stress. An average value of c is then assumed, and used to define the creep strain rate on the base line at τ = 1 day (Equation 7.12). Although Equation 7.12 is expressed in terms of intrinsic time, τ, the author finds that t and τ are generally interchangeable after 1 day loading. This line is extrapolated back to the ln v axis at an effective stress of unity (ln $\sigma' = 0$) to yield the parameter v_1.

Den Haan (1996) proposes an iterative procedure to determine the parameter, a. However, the author has found that, determining a from the *minimum* slope of lines of constant creep strain rate in the overconsolidated stress region, gives acceptable accuracy.

Permeability is assumed to vary as a function of void ratio according to:

$$k = k_o 10^{e/C_k} \tag{7.35}$$

where k_o is the extrapolated permeability at zero voids ratio, and C_k is an empirical constant, equal to the slope of the line fitted to permeability data such as that shown in Figure 7.5.

In this study, the unit weight of the soil has been omitted from the formulation as it leads to a buoyant unit weight, which in peat, is close to zero. This allows $G_{i,j}$ in Equation 7.24b to be simplified to:

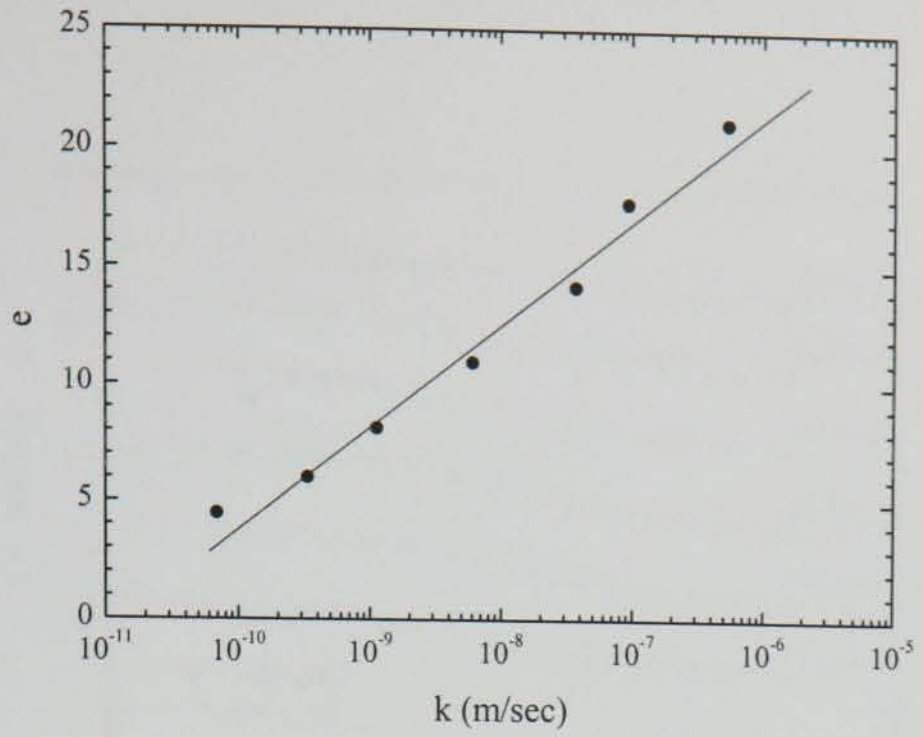

Figure 7.5 Variation in permeability with void ratio for CL_MSL_01

$$G_{i,j} = \frac{c}{\tau_{i,j}} \qquad 7.36$$

The *abc* model parameters have been determined in accordance with the procedure previously outlined, and are listed in Table 7.1.

Table 7.1 *abc* model parameters determined from CL_MSL_01

a	b	c	v_1	C_k	k_o (m/sec)
0.040	0.373	0.020	40.556	4.385	1.383×10^{-11}

The initial specific volume, as measured for each test, is also included as an input parameter for respective tests.

7.3.2 Modelling laboratory tests

The parameters listed in Table 7.1 have been input to CREEP to obtain predicted strains for the virgin stress increments of the following MSL oedometer tests: CL_MSL_01, CL_MSL_02, CL_MSL_07, CL_MSL_12, CL_MSL_13. One CRD test, CL_CRD_06 is also considered.

The predicted strains for the tests considered are provided in Figure 7.6 through to Figure 7.7.

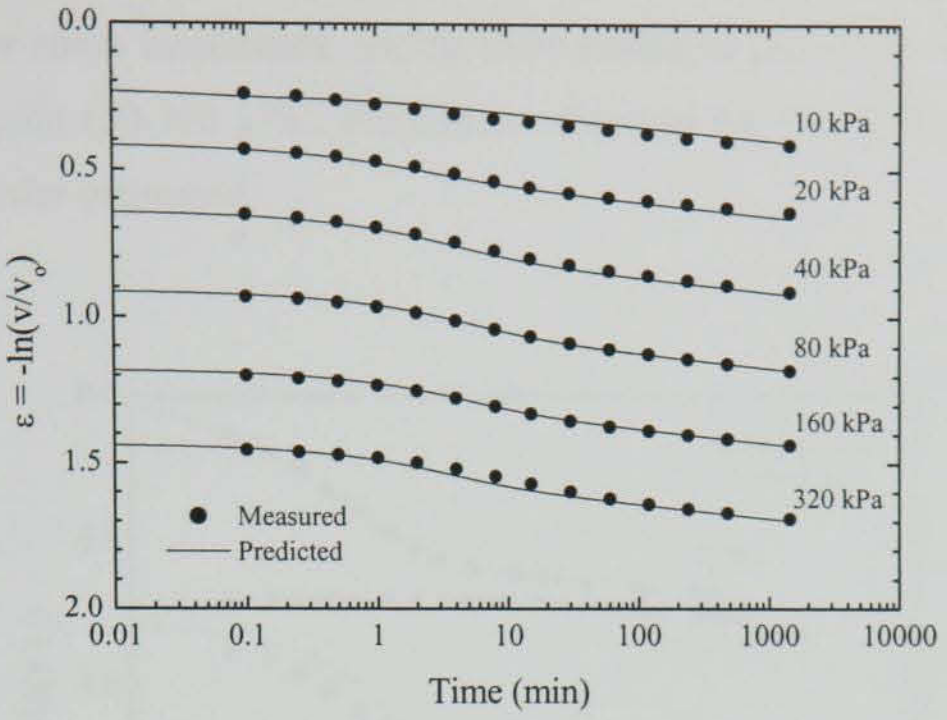

Figure 7.6 Measured and predicted strain profiles for CL_MSL_01

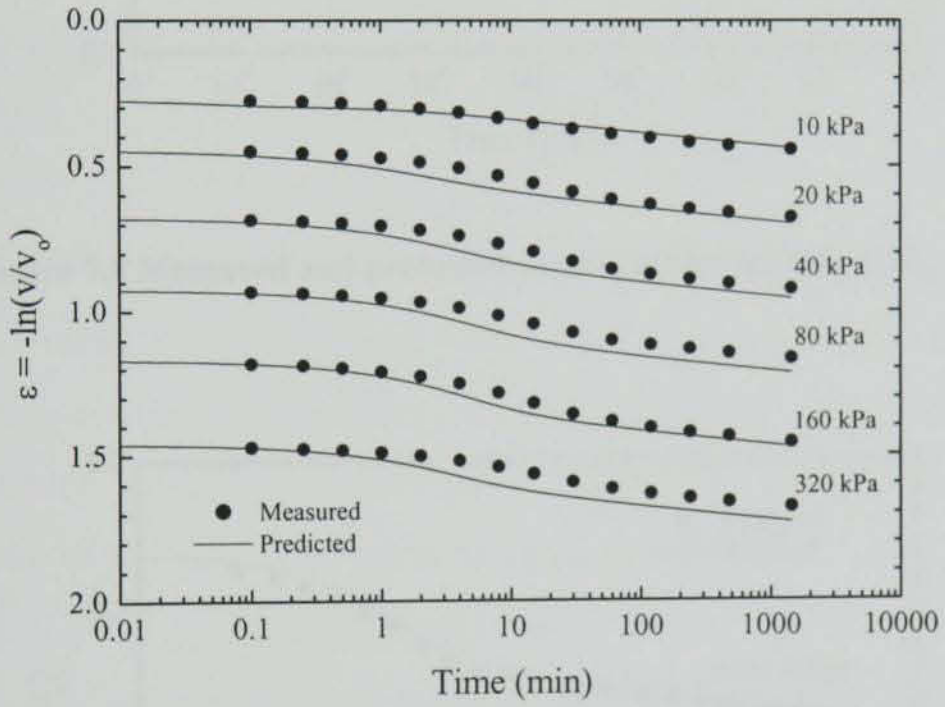

Figure 7.7 Measured and predicted strain profiles for CL_MSL_02

Figure 7.6 compares measured and predicted strains for CL_MSL_01. As the parameters have been determined from this test, the good agreement obtained is expected. Good agreement was also obtained between measured and predicted strains for CK_MSL_02 (Figure 7.7), which like CL_MSL_01 is a 'standard' test, with a LIR=1, and LID=1 day.

The relative merit of the *abc* model in capturing the effects of high LIR and LID are assessed in Figure 7.8 – Figure 7.12. Evidently, the agreement between predicted and

measured data is good for CL_MSL_12 (Figure 7.8), despite the slight over-prediction of the final stress increment (181.25-431.25 kPa). A similar trend is apparent in CL_MSL_07 (Figure 7.9), in that acceptable agreement is obtained between measured and calculated data for the *earlier* stress increments, and an over-estimated prediction is obtained for the final stress increment (50-250 kPa). Predictions obtained for CL_MSL_13 (Figure 7.10) are consistently under-estimated.

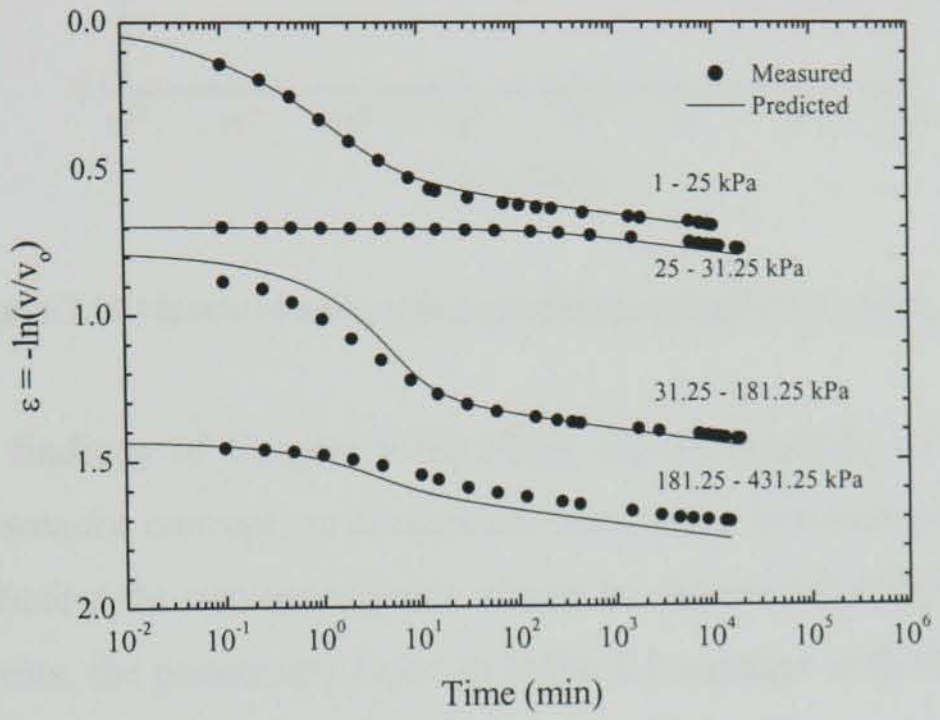

Figure 7.8 Measured and predicted strain profiles for CL_MSL_12

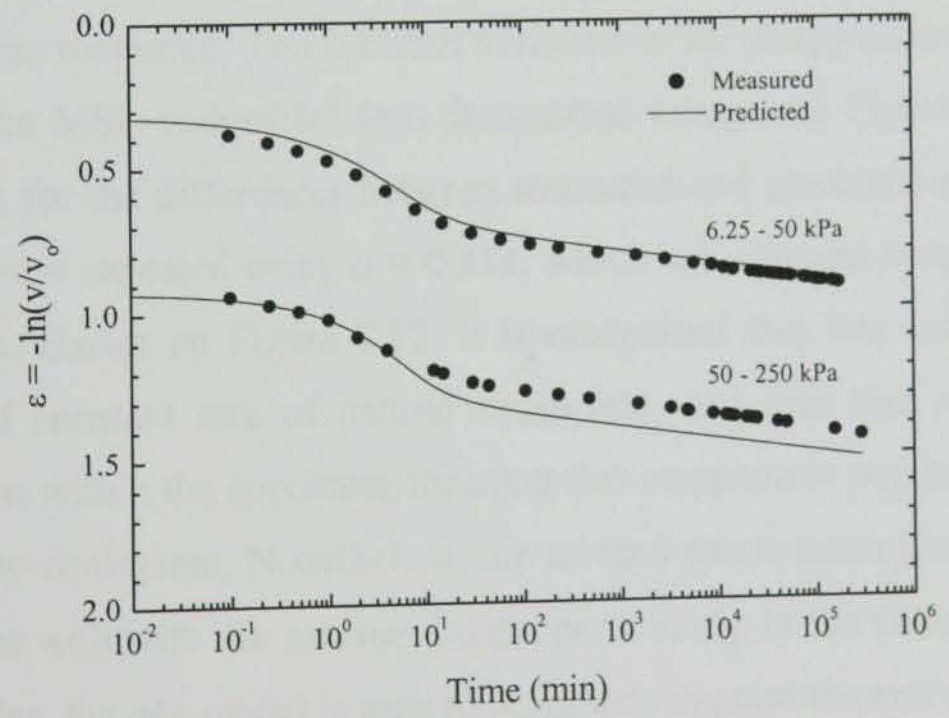

Figure 7.9 Measured and predicted strain profiles for CL_MSL_07

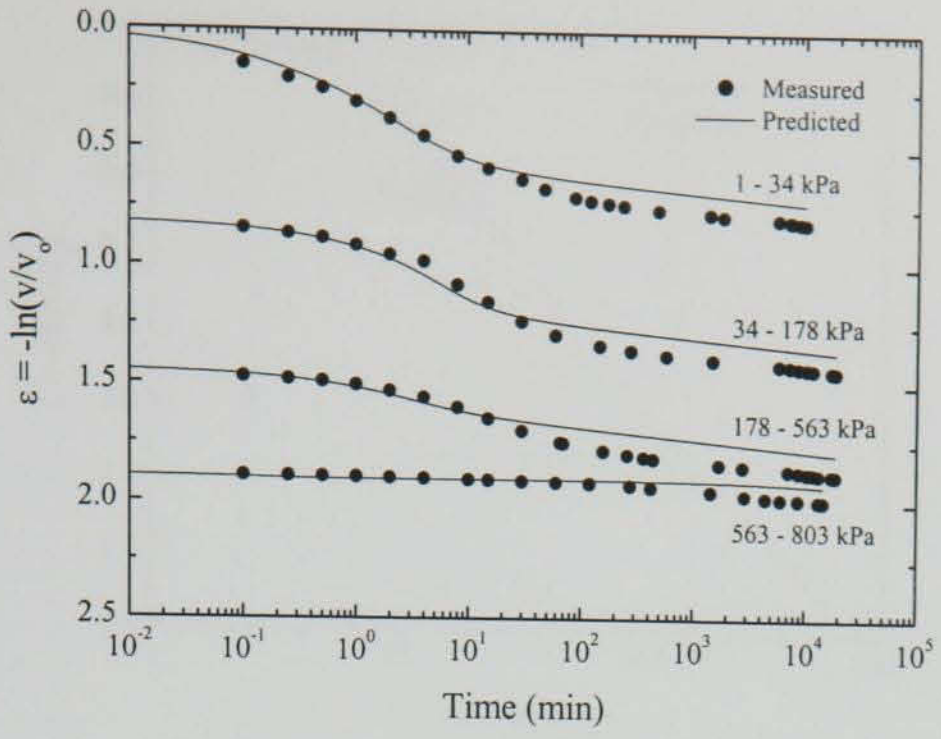

Figure 7.10 Measured and predicted strain profiles for CL_MSL_13

Withstanding the findings of Chapter 6 regarding the unsuitability of the CRD test for investigating the isotache concept, an attempt has been made to investigate the merit of the *abc* model in predicting the rate dependence of peat as observed in CRD tests. As with the MSL oedometer tests, the parameters listed in Table 7.1 together with the measured initial specific volume for CL_CRD_06 (see Table 4.3) have been used in the analysis. Predictions are provided in Figure 7.12, where it can be seen that the *abc* model predicts the strain rate dependent preconsolidation stress quite well during the initial loading stage. However, as loading continues, the *abc* model predicts a response that is somewhat stiffer than that which was measured. The inherent variation in the compression parameter, b, as is evident from the MSL oedometer tests formulated using b in Figure 6.5, is the most likely explanation for the differences between measured and predicted data. The analysis for CL_CRD_06 was repeated using $b = 0.319$, which was derived from the slope of the *apparent* isotache, shown on Figure 7.12. It is recognised that this value of b does not represent lines of constant rate of natural strain rate, and also that some excess pore pressures will exist within the specimen, meaning that creep strain rate and total strain rate are not necessarily equivalent. Nonetheless, the revised stress-strain prediction shown on Figure 7.12 agrees well with the measured data, particularly in the normally consolidated region. In particular, the *abc* model is seen to accurately capture the rate dependence of the stress-strain path measured during CL_CRD_06.

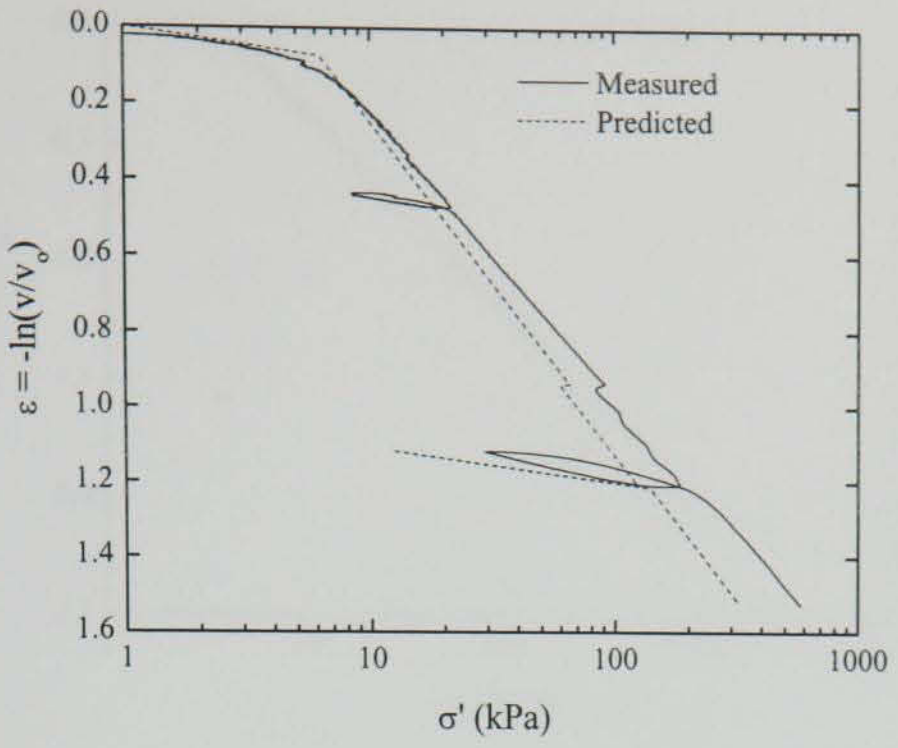

Figure 7.11 Measured and calculated stress-strain response for CL_CRD_06

The sensitivity of c can be easily assessed by considering a hypothetical CRD test in which c is permitted to vary. This has been done using the parameters in Table 7.1, an average rate of linear strain of 4×10^{-6} sec^{-1} and three values of c: 0.01, 0.02 and 0.04. The corresponding calculated stress-strain paths are shown on Figure 7.13. Evidently the stress-strain paths are dependent upon the chosen value of c, although the variance is not overly significant within a practical stress range (< 100 kPa). It is also noteworthy that the stress-strain paths are not parallel. The rate of deformation and hence rate of linear strain is constant, which from Equation 6.10 results in an increasing rate of natural strain. This explains the divergence of the stress-strain paths in Figure 7.13.

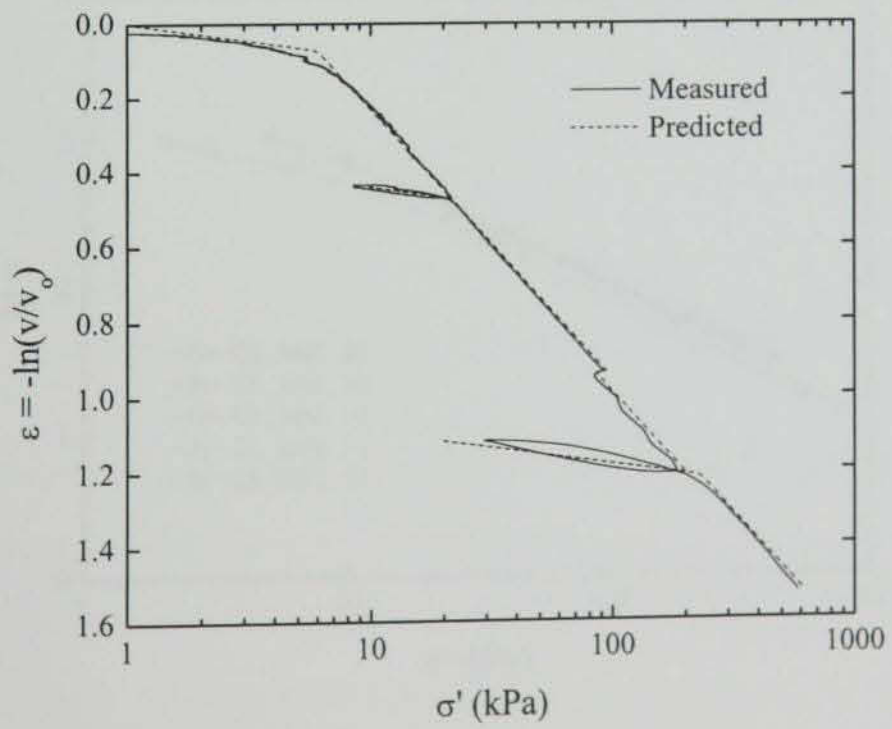

Figure 7.12 Measured and predicted stress-strain response for CL_CRD_06 using the parameters listed in Table 7.1

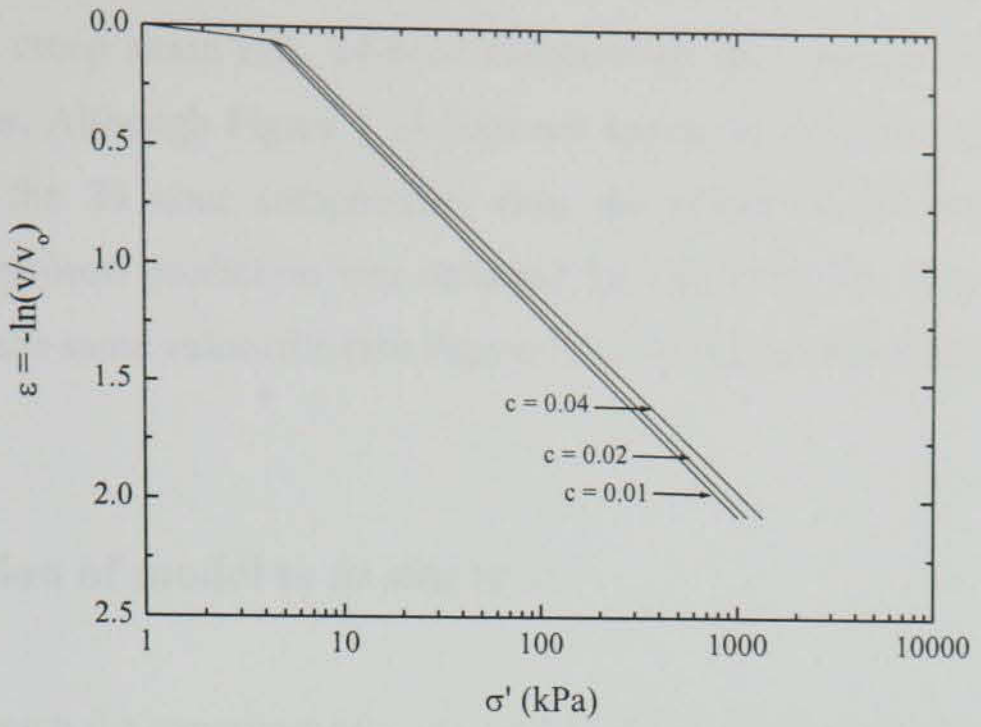

Figure 7.13 The effect of varying c on CRD stress-strain response

A good indication of the merit of the parameter *c* can be obtained from Figure 7.6. As was shown on Figure 6.18, *c* tends to vary slightly with stress level. However, this variance is not reflected in the predictions obtained for CL_MSL_01 (Figure 7.6), which encompassed a relatively wide range of stresses.

The calculated predictions are however relatively sensitive to the chosen value of v_1. The 24 hour compression ln v – log σ' plots for the tests considered in Figure 7.6 to 7.11 are

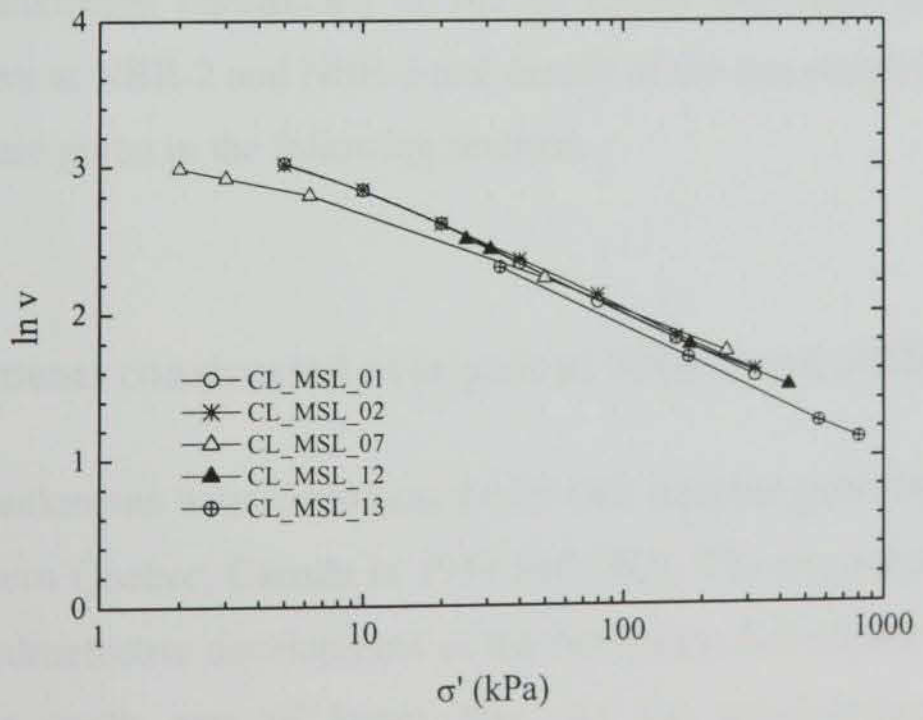

Figure 7.14 ln v – log σ' relationship for tests on Clara peat

shown in Figure 7.14. Den Haan (1996) claims that although b is defined as the slope of lines of constant creep strain rate, 24-hour compression data generally suffices for most practical purposes. Although Figure 7.14 does not appear to indicate significant variation in the slope of the 24 hour compression data, the effect on the predicted strains is significant. The poorest prediction was obtained for CL_MSL_13, (Figure 7.10), which, although having the same value of b (see Figure 7.14), evidently has a lower value of v_1.

7.4 Application of model to *in situ* tests

As indicated through the experimental work, and in the analysis of the field test, Clara peat is slightly overconsolidated. The *abc* model is not suitable for predicting settlement rates and magnitudes in the overconsolidated region, as the parallel system of isotaches does not hold here. This is an unfortunate finding considering the level of work involved not only with the field test, but also with the associated laboratory programme. Permission was sought to increase the load so as to move into the normally consolidated region, but was not granted.

In an effort to obtain *in situ* verification for the *abc* model, the author reviewed several case studies involving embankment construction over peat deposits. Several of these case studies are either described or referred to in Chapter 2. However, many of these projects did not incorporate a detailed laboratory study. An exception to this was the NBR-2 and NBR-3 test embankments constructed in the St James Bay area in Canada. A brief summary of the peat at NBR-2 and NBR-3 and details of the test embankments constructed at these locations are given in the following sections.

7.4.1 Embankments constructed over peat at NBR-2 and NBR-3, James Bay

A number of embankments were constructed over two separate peat deposits in the James Bay area in Northern Quebec, Canada in 1979 and 1980. The programme was initiated in response to the hydroelectric development of the Nottaway, Broadback and Rupert rivers, which run to the south east of James Bay. As the development necessitated the construction of many kilometres of road over poorly drained fibrous peat deposits, and considering the scarcity of free draining granular material in the James Bay area, a number

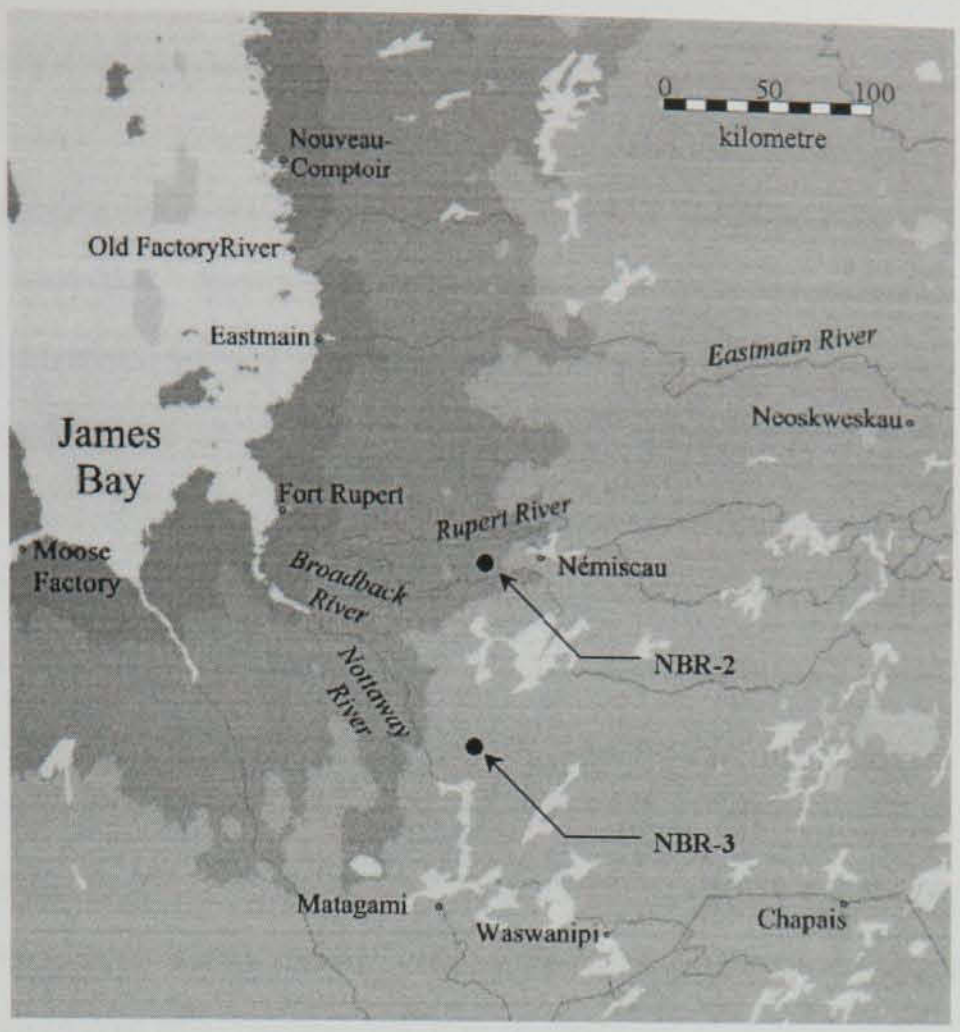

Figure 7.15 Map of Quebce, Canada, showing the location of the NBR-2 and NBR-3 test sites

of till embankments were built using various construction techniques. Two test sites were chosen, NBR-2 and NBR-3, which are located, respectively, approximately 238 and 148 km north of Matagami (see Figure 7.15). The performance of the embankments has been documented by Lupien *et al.* (1981) and Lupien *et al.* (1983). Although the peat at NBR-2 has similar geotechnical properties to that at Clara, significant lateral heave was observed during embankment construction. Consequently, the NBR-3 site is considered to be a more suitable case study for assessing the potential of the *abc* model for *in situ* loading conditions.

7.4.1.1 NBR- 3 Site Description

The two NBR sites were named after the three rivers that run through the area (Nottaway, Broadback and Rupert). The topography of the NBR-3 site is slightly inclined, with a maximum slope of 2%. Surface conditions are generally wet, with the water table at ground level. At the embankment locations the peat layer varies in thickness between 2.5 and 2.9 m.

7.4.1.2 *Geotechnical properties*

Undisturbed block samples were retrieved from various depths using a modified version of the Sherbrooke sampler developed by Lefebvre and Poulin (1979). Laboratory classification and identification tests were performed on the retrieved samples, including von Post humification, water content, and loss-on-ignition. Water content profiles are provided for both the NBR-2 and NBR-3 locations in Figure 7.16. The data points in Figure 7.16 represent the average water content at depth, and the error bars indicate the range of measured values. Measured water contents are on average 860% at NBR-3.

According to the von Post humification scale, the peat at NBR-3 is poorly humified, with average values ranging from H_2 to H_4. Fibre content tests were not reported for NBR-3 peat, although the visual presence of intact fibres, and the low degree of humification suggests that this peat can also be classified as fibrous.

At each site the peat layer overlies a clay deposit with a stiff weathered crust. *In situ* vane shear strengths in the clay layer vary from approximately 100 kPa in the weathered crust, to a minium value of 30 kPa in the underlying clay. Figure 7.17 presents the average and

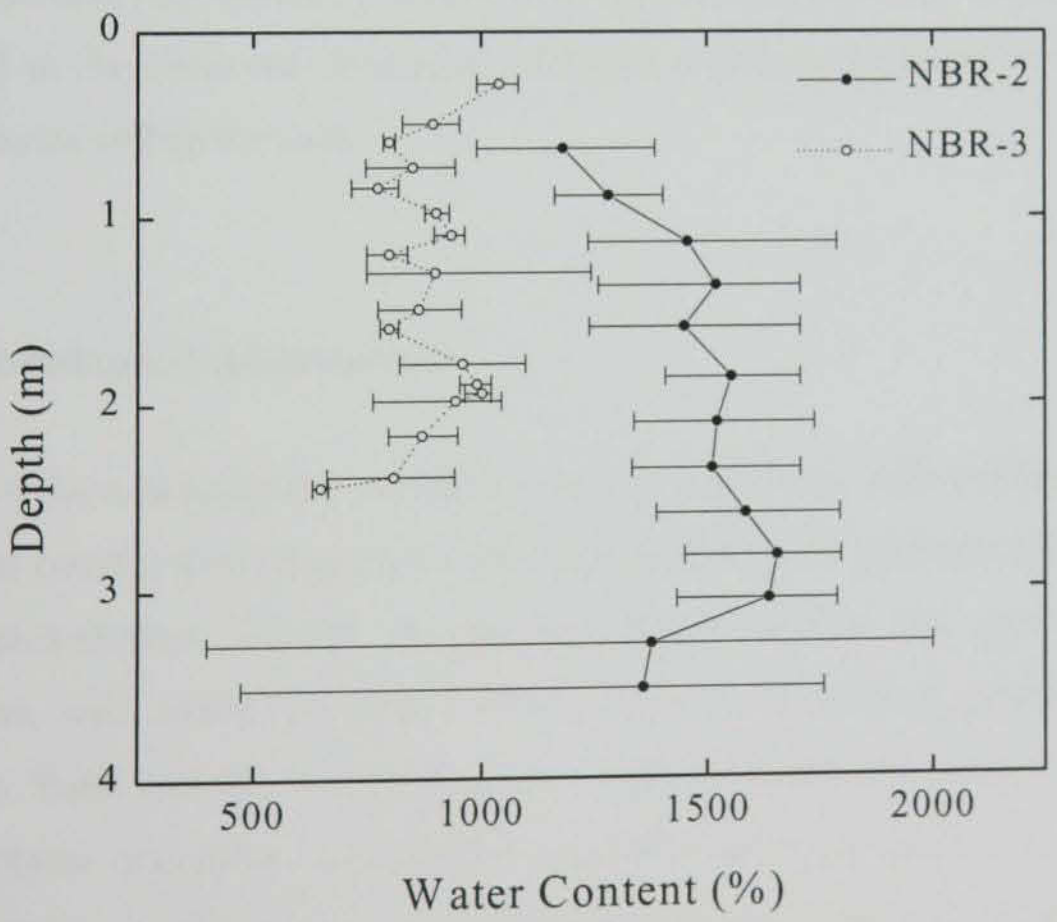

Figure 7.16 Water content profiles for the NBR-2 and NBR-3 sites

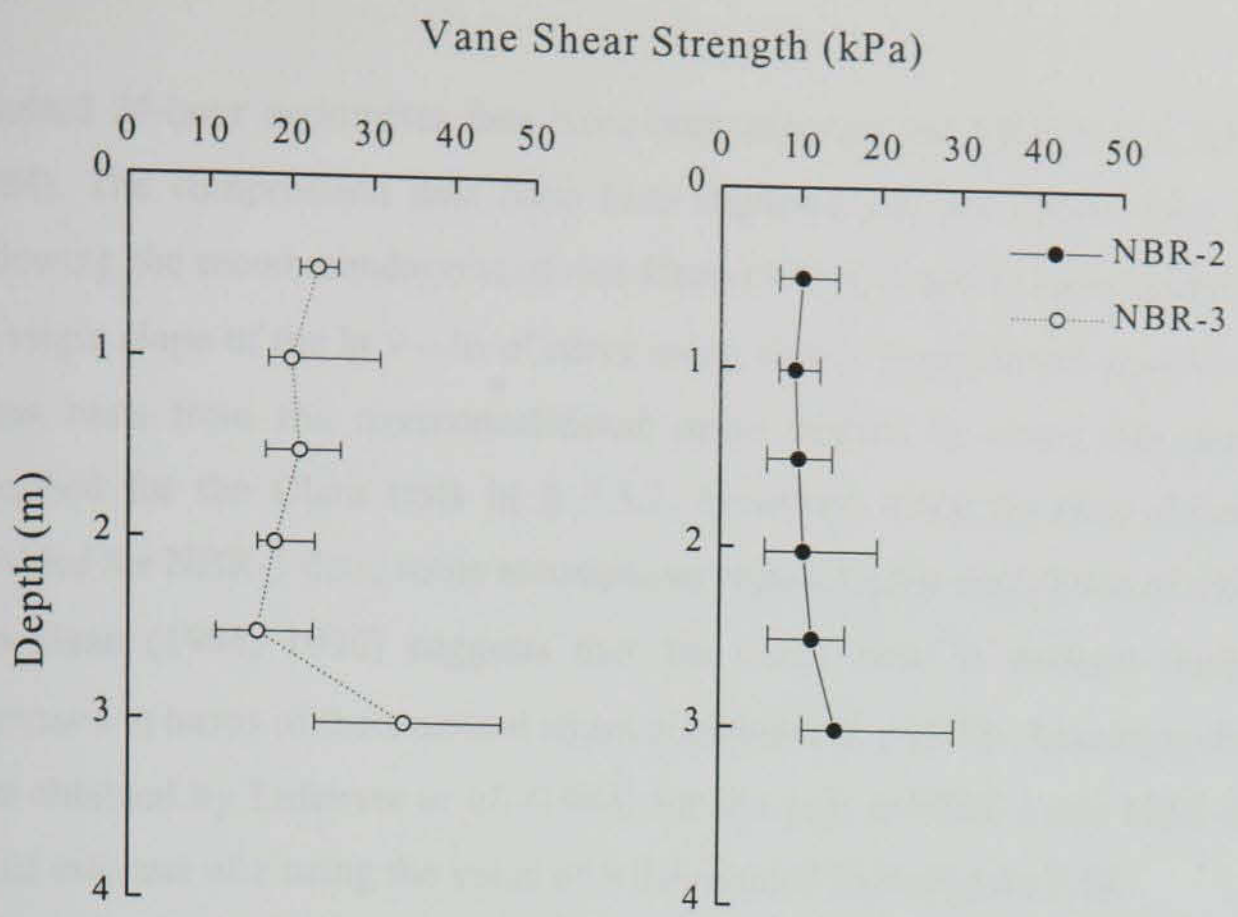

Figure 7.17 Vane shear strength profiles for the NBR-2 and NBR-3 sites

range of *in situ* vane test results for the peat at NBR-3 (20 kPa).

The loss-on-ignition values for the peat at NBR-3 measure, on average, 70%. This value is considered as relatively low for a fibrous peat deposit, and has been attributed by Lefebvre *et al.* (1984) to the observed circulation of water, which could result in the deposition of mineral particles within the peat.

7.4.2 Embankment construction

The length of the embankments varied between 30 and 40 m, with widths decreasing from 15 to 10 m as construction progressed. The instrumentation at each test section consisted of standpipe piezometers located at various depths within the peat layer and till embankments, and settlement plates which were positioned at ground level prior to construction. Each test fill had at least two lines of instrumentation, consisting of two settlement plates and three piezometers, one of which was placed in the fill. Lateral displacements were estimated by comparing the distance between instrumentation lines before and after construction.

7.4.3 *abc* model predictions

Standard 24-hour oedometer data have been reported for NBR-3 peat by Lefebvre *et al.* (1984). The compression data have been digitised and are shown here on Figure 7.18. Following the recommendations of den Haan (1996), b and v_1 have been determined from the virgin slope of the ln v – ln σ' curve using simple regressional analysis. The parameter a has been from the overconsolidated stress region, in much the same way as was described for the Clara tests in § 7.3.2. However, since no time dependent data was provided for NBR-3 data, some assumptions regarding the magnitude of c have been made. Den Haan (1994, 1996) suggests that the C_α/C_c ratio is perhaps more unique when expressed in terms of their natural strain counterparts, c and b. Assuming the C_α/C_c ratio of 0.06 obtained by Lefebvre *et al.* (1984) for the peat at NBR-2 and NBR-3, allows for an initial estimate of c using the value of b determined from Figure 7.18.

Permeability tests on NBR-3 peat were also reported by Lefebvre *et al.* (1984). The permeability data, which are shown on Figure 7.19 have been interpreted in terms of e – log k, so as to allows for determination of the empirical parameters k_o and C_k. Evidently, a considerable degree of scatter exists between the respective tests in Figure 7.19, although as an initial estimate, the 0.47 m test data have been assumed.

Predictions for an instrumented section at NBR-3 (test fill D, section 8D) were obtained using CREEP in conjunction with the parameters listed in Table 7.2. The average depth of

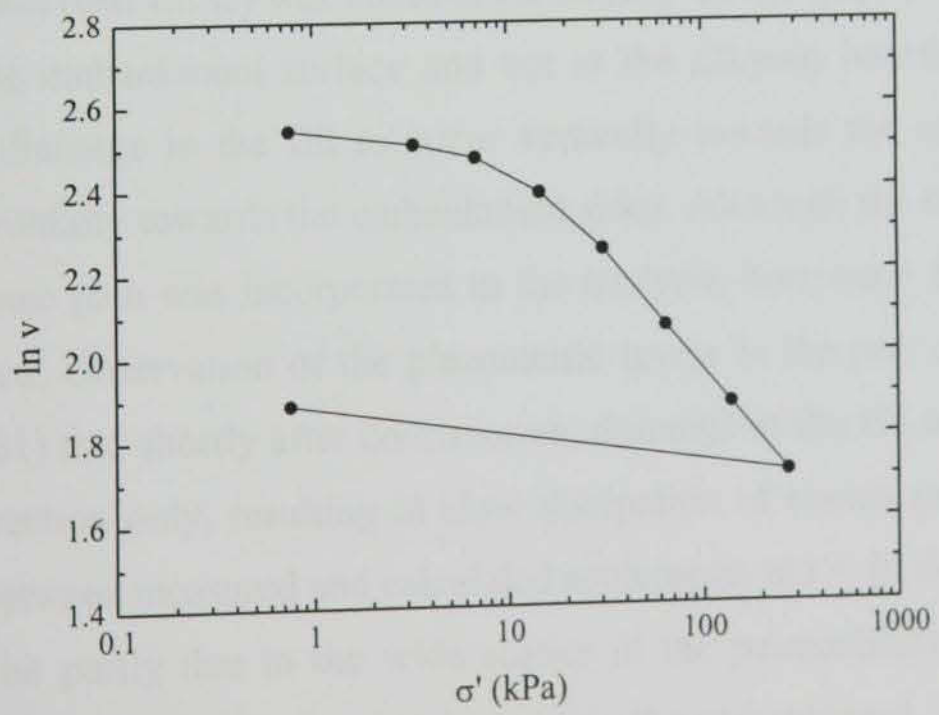

Figure 7.18 ln v – log σ' data from NBR-3

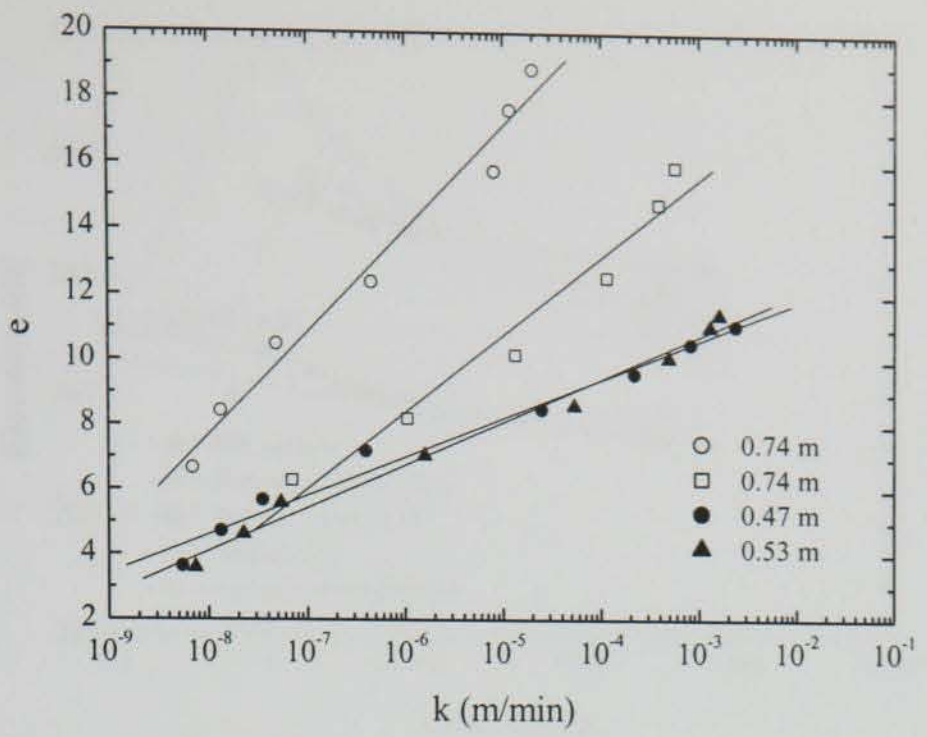

Figure 7.19 e – log *k* relationship for the peat at NBR-3

peat at this point is 2.65 m. The effect of partial submergence, and subsequent reduction of effective stress of the fill was considered by updating the effective stress of the embankment as the solution progresses. The predicted ground level settlement is compared with measured data on Figure 7.20. Evidently the agreement between the measured data and the predicted settlements is poor. However, Lefebvre *et al.* (1984) noted that the *in situ* rate of creep compression was at least twice as high as that measured in the laboratory. Repeating the analysis with c updated to reflect the observations of Lefebvre *et al.* (1984) gives a more accurate prediction of the measured settlements. The revised predictions, which are provided on Figure 7.21 were obtained using $c = 0.03$.

As this embankment (test fill D) was constructed directly on the peat surface, the drainage boundary is at the embankment surface and not at the till/peat interface. Lupien *et al.* (1981) expected drainage in the fill to occur vertically towards the upper embankment surface, and horizontally towards the embankment sides. Although the increased length of the *vertical* drainage path was incorporated in the analysis, horizontal drainage in the fill was not considered. Observation of the piezometric levels in the peat and fill convinced Lupien *et al.* (1981) that shortly after construction, drainage in the fill was taking place in the horizontal direction only, resulting in slow dissipation of excess pore pressures. The poor agreement between measured and calculated settlements at $t < 10$ days on Figure 7.21 is considered to be partly due to the wide scatter in the permeability data depicted on Figure 7.19, and partly due to the retarded drainage in the embankment.

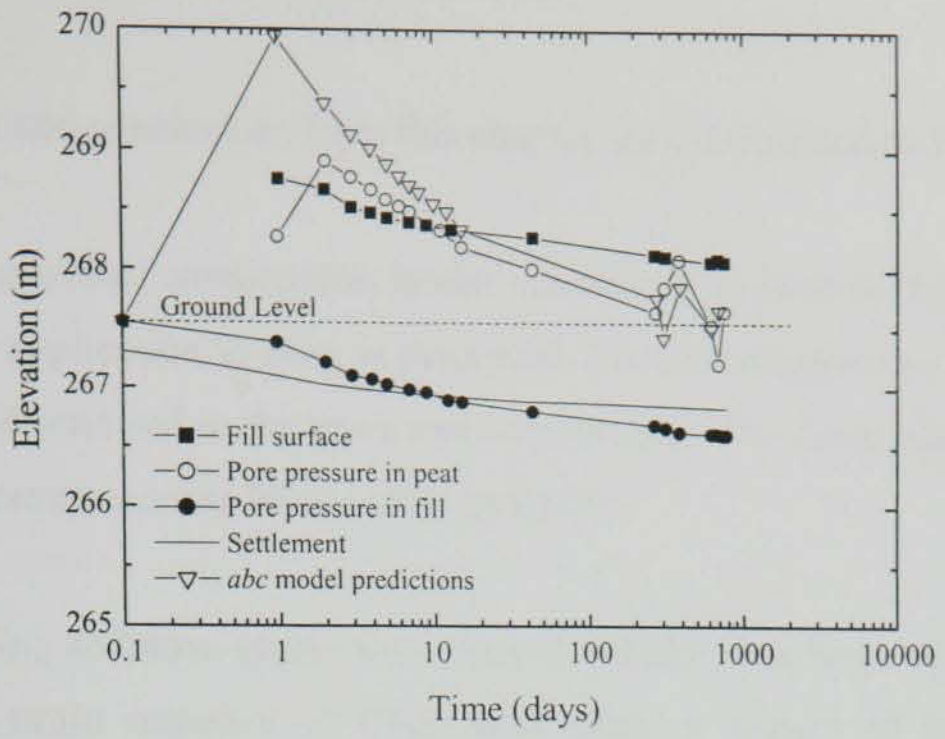

Figure 7.20 Comparison of measured and predicted settlements using the abc model and the parameters listed in Table 7.2

Table 7.2 *abc* model parameters assumed for the peat at NBR-3

a	*b*	*c*	v_1	C_k	k_o (m/sec)
0.025	0.256	0.015	22.900	1.337	1.731×10^{-13}

Evidently differences between *in situ* and laboratory determined parameters (such as *c*) will have a significant bearing on the relative success of the *abc* model. These scale effects are well known (e.g. see Lea and Brawner, 1963), and act as an obstacle in applying laboratory derived compressibility data to *in situ* conditions.

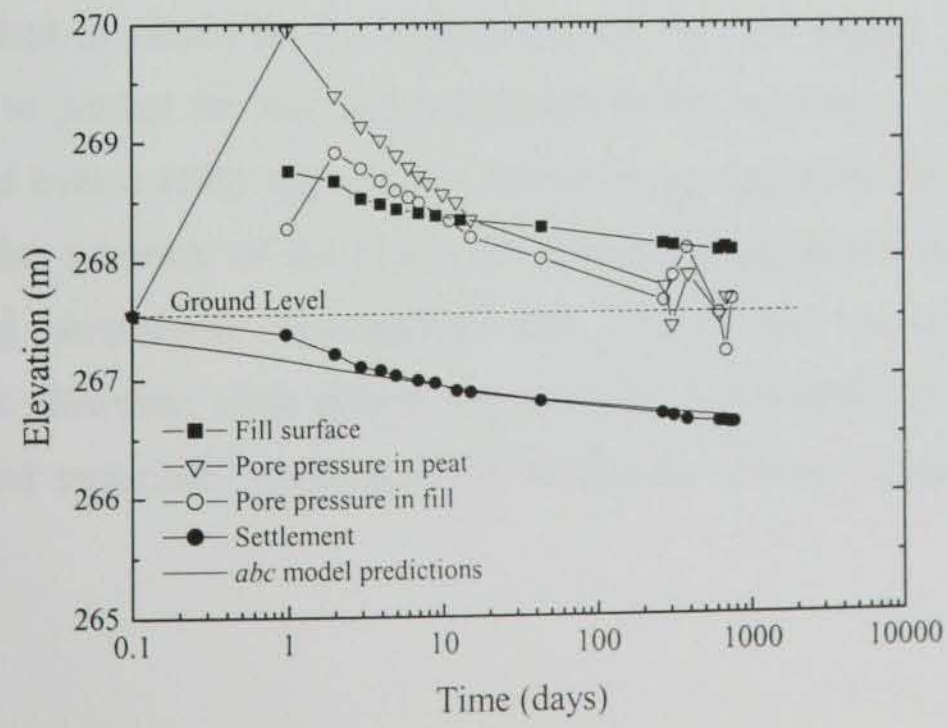

Figure 7.21 Revised predictions for test embankment at NBR-3

7.5 SUMMARY AND CONCLUSIONS

The main findings and conclusions from this chapter are summarised as follows:

1. A one-dimensional compression model, considered to have the highest potential for successful application to peat, is presented. The formulation has been described in detail and discretised in the space and time domain. The discretised formulation has been programmed using Microsoft Visual C++.

2. The resulting software application, termed CREEP, has been employed to predict the stress-strain response of Clara peat under a variety of laboratory loading conditions.

3. The model parameters determined from a 'base test', have been shown to be applicable to several other tests, although the quality of the predictions was not always maintained. Poor quality predictions have been attributed to sensitivity in the model parameter, v_1.

4. No attempt has been made to model the field test described in Chapter 5, as Clara peat is slightly overconsolidated. The *abc* model is not suitable for overconsolidated behaviour as the isotaches in this region are neither parallel nor linear.

5. In an attempt to obtain *in situ* verification for the *abc* model, CREEP has been employed to predict the rate and magnitude of the settlement of an embankment constructed over a relatively shallow fibrous peat deposit in the James Bay area, Canada. The accuracy of the predicted settlements is promising considering the number of simplifying assumptions that were made in determining model parameters. However, scale effects appear to be an important factor, and one that hampers the successful application of laboratory derived parameters to *in situ* conditions.

Chapter 8

Conclusions

Chapter 8

Conclusions

8.1 Classification of organic soils

Standard (and some non-standard) classification tests have been conducted on the five soils considered for this Thesis. These soils, which are Clara Peat, Ballydermot peat, Cork peat, Cork silty peat and Belfast organic clay, have organic contents varying from 11% to 98% . Notable observations made concerning these classification tests (and assisted by classification data reported in the literature) are as follows:

1. A simple formulation proposed by Skempton and Petley (1970) has been demonstrated to fit the measured relationship between loss-on-ignition and specific gravity for these and many other soils, particularly for loss-on-ignition values in excess of 30%.

2. Natural water contents in organic soils can only be related directly to the quantity of organic matter up to an approximate threshold loss-on-ignition of 80%. Above this threshold value, the water content tends to be controlled to a significant extent by the degree of humification. At the same loss-on-ignition, fibrous peats (such as Clara peat) exhibit higher water contents than peats at an increased stage of humification (such as Ballydermot peat) due to water contained within the *intact* organics of fibrous peats at cellular level.

3. SEM images show that both Clara and Ballydermot peats may be classified as fibrous, but that the latter is more humified. The degree of humification, although rarely reported in the literature, is shown to have a critical effect on the mechanical

characteristics and should be incorporated in the standard classification system for organic soils.

4. The standard procedure for determining specific gravity (BS 1377) gave widely variable results for Clara peat and is not recommended for fibrous peat.

8.2 Laboratory test programme

The Thesis presents test results from a comprehensive series of MSL oedometer and CRD laboratory tests performed by the author. General conclusions drawn from these tests are as follows:

1. Settlements in one-dimensional compression are due to a combination of one-dimensional consolidation and creep. The creep behaviour of the soils at constant effective stress broadly follows a linear relationship when plotted in terms of strain, ε, or void ratio, e, against the logarithm of time, log t.

2. The compression-time curves dependence on the load increment ratio (LIR) was found to be compatible with the Type I and Type III curves defined by Leonards and Girault (1961). Type II curves (i.e. when e – log t curves increase in slope after 24 hours sustained loading) were observed for Clara and Ballydermot peat when stress levels were close to or lower than the apparent preconsolidation stress.

3. A limited number of tests involved pore pressure measurements. Acceptable pore pressure responses (in terms of response time) were only observed in samples in which a backpressure was applied. However, even in these instances, maximum recorded pore pressures were lower than the applied stress increment. Similar difficulties have been reported in the literature and are attributed to the presence of gas in organic soils.

4. The tests incorporating pore pressure measurements showed that the Taylor graphical construction method, and to a lesser extent Casagrandes's method, consistently under-estimate the consolidation duration, t_p. Although Casagrande's

method was more accurate than Taylor's method, the former could only be used for Type I and Type II stress increments.

5. The e – log σ' relationship of very compressible materials such as Clara peat and Ballydermot peat is highly non-linear, but is approximately linear in less compressible organic soils such as Belfast organic clay.

6. Swelling following an appreciable reduction in effective stress in oedometer samples of Clara peat leads to a linear increase in e with log t for a period in excess of 6 days.

7. The results of CRD tests on Clara peat indicate that the natural variation between measured e – log σ' curves at comparable rates of deformation, is much higher than the separation resulting from stepped changes in deformation rate. Individual CRD test results show that reductions in the imposed rate of deformation shift the e – log σ' curve to the left, whereas an increase in the rate of deformation cause the measured e – log σ' relationship to shift to the right.

8.3 Interpreted experimental results

The experimental results described in Chapters 4 and 5 have been interpreted with a view towards identifying a suitable constitutive one-dimensional compression model for peats. Some of the key points and conclusions derived from these chapters are as follows:

1. The use of natural strain, interchangeable with ln v, has been used to restore linearity to the stress-strain relationship of very compressible soils.

2. The variation in the coefficient of creep, C_α, with organic content and stress level indicated by the database of laboratory tests conducted for this Thesis is typical of that reported for peats and organic soils. C_α increases to a maximum value beyond an apparent preconsolidation stress, before starting to decrease again. This variation is significantly reduced in the virgin stress range by adopting natural strain as a measure of the soil compression (i.e. use of the creep coefficient, c).

3. Although, ln v produces an essentially linear and unique relationship between strain and logarithm of effective stress, a significant and consistent degree of disparity was found for the tests on Clara peat, which could not be accounted for by normalising by the initial specific volume. Factors such as the presence of gas, variations in the concentration of fibres and accelerated humification in the laboratory were muted as possible reasons for the disparity.

4. C_α/C_c ratios have been determined, and generally fall within the range of ratios suggested by Ladd (1971), Mesri and Castro (1987) and Mesri *et al.* (1997). An exception to this is Clara peat, which has a C_α/C_c ratio of 0.042. It follows that a single C_α/C_c ratio cannot define the creep compression of *all* peat soils.

5. Tertiary compression, which is characterised by the steepening of ε - log t curves, observable at constant effective stress, can be explained by the transition from an overconsolidated to a normally consolidated state; this transition point is best determined at the point at which the previous minimum volume is reached.

6. It is suggested that the success of preloading projects is linked to the amount of rebound obtainable after removal of surcharge. This is because the soil will take longer to creep towards its *minimum past specific volume*, at which point the increase in creep strain rate to the normally consolidated rate is likely to occur.

7. The isotache concept is considered valid for peat, if natural strain and natural strain rate are adopted. A unique relationship has been observed between stress, strain and strain rate, but only when strain rate is interpreted as natural *creep* strain rate.

8. CRD tests have been performed on Clara peat to verify the isotache principle. The CRD test was found to be only partially suitable in this regard, as the imposed rate of deformation infers a constant rate of linear strain and not natural strain. It is shown that, for increasing compression in a CRD test on peat, the stress-strain state moves towards isotaches corresponding to higher rates of natural strain (but a constant rate of linear strain) at high strain levels. The use of an external proving ring should be avoided in CRD tests, as it lowers the imposed rate of deformation of the *specimen*.

9. Comparisons of the coefficient of creep, c, determined from the *in situ* test performed at Clara with those determined in laboratory tests at an equivalent stress level show good agreement. However, determination of the *in situ* values of c was hampered somewhat by the reduction in the applied effective stress that took place due to the submergence of the loading tanks.

8.4 Modelling the one-dimensional compression of fibrous peat

1. On the basis of the observations made from the experimental work in this Thesis, the *abc* model proposed by den Haan and Edil (1994) and den Haan (1996) was adjudged to be the most suitable for describing the one-dimensional compression of peat. The formulation of the *abc* model has been discretised using the combined method finite difference technique and programmed using Microsoft Visual C++.

2. The Thesis has described the determination of the abc model parameters and subsequently uses these in conjunction with CREEP to predict the stress-strain response of Clara peat under a variety of virgin loading conditions in the laboratory. In general, the predicted strains agree reasonably well with measured data for a wide range of load increment ratios and loading durations. However, the inherent variability of the b and v_l parameters of the peat and the sensitivity of the predictions to these parameters combine to give predictions, in some cases, which are significantly in error. Predictions are shown to be relatively insensitive to parameters a and c of the *abc* model.

3. The model parameters determined from laboratory tests, unfortunately, could not be used with CREEP to obtain predictions for the *in situ* load test described in Chapter 5 because of the unanticipated overconsolidation of the *in situ* peat. Therefore, in an attempt to obtain verification of the *abc* model for *in situ* conditions, CREEP was used to obtain surface settlement predictions for a test embankment constructed over a relatively shallow fibrous peat deposit in the James Bay area, Canada. The accuracy of the predicted settlements is promising considering the number of limiting assumptions that were made in determining model parameters. However, scale effects appear to be significant, and may hamper the successful application of laboratory derived parameters to *in situ* conditions.

8.5 Recommendations for further work

1. The isotache principle appears to be valid for peat, provided that strain and strain rate are interpreted as natural strain and natural strain rate respectively. However, this is not the case in the overconsolidated region. Further work is required to formulate the transition of the isotaches from the overconsolidated to virgin stress range. Such formulation should also consider tertiary compression effects in this transition region.

2. The effects of unloading in the laboratory appear to be more time (or rate dependent) that expected. Further investigation of the rate dependency of peat soils in the overconsolidated stress range would certainly be beneficial, considering that Clàra peat is slightly overconsolidated, yet obviously highly compressible and strain rate dependent.

3. The CRD test could be improved to allow for constant rates of *natural* strain, thus permitting a fuller interpretation of CRD test data with regard to the isotache concept.

References

References

Adams, J.I. (1963). A comparison of field and laboratory measurement in peat. *Proc. 9th Muskeg Res. Conf. Ontario Hydro Res. Q.* 15, 1-7.

Adams, J.I. (1965). The engineering behaviour of a Canadian muskeg. *Proc. 6th Int. Conf. Soil Mech. Fdn. Engr.,*1, 3-7.

Al-Khafaji, A.W.N. & Andersland, O.B. (1981). Compressibility and strength of decomposing fibre-clay soils. *Géotechnique,*31, 4, 497-508.

Allen, A.S. (1969). Geological settings of subsidence. *Reviews in Engineering Geology,* 2, 305-342.

Andrejko, M.J., Fiene, F. & Cohen, A.D. (1983). Comparison of ashing techniques for determination of the inorganic content of peats. *Testing of peats and organic soils,* ASTM STP 820, 5-20.

Arman, A. (1971). Discussion to "Ignition loss and other properties of peats and clays from Avonmouth, King's Lynn and Cranberry Moss". *Géotechnique*, 21, 418-421.

Asaoka, A. (1978). Observational procedure of settlement prediction. *Soils Fdns.*, 18(4), 87-101.

Barden, L. (1968). Primary and secondary consolidation of clay and peat. *Géotechnique,* 18, 1-24.

Barden, L. (1969). Time dependent deformation of normally consolidated clays and peats. *Proc. J. Engr. Div. ASCE,* SM1, 1-31.

Bell, F.G. (1978). Roads on peat. *Civil Engineering*, 45-53.

Bell, J. (1991). A study of the environmental effects of a bog road, Clara, Co. Offaly, Ireland. M.Sc. Thesis, Imperial College London, England.

Bellamy, D. (1986). The wild boglands. Bellamy's Ireland. Facts on File Publications.

Berre, T. & Iversen, K. (1972). Oedometer tests with different specimen heights on a clay exhibiting large secondary compression. *Géotechnique*, 22, 1, 53-70.

Berry, P.L. & Poskitt, T.J. (1972). The consolidation of peat. *Géotechnique*, 18, 27-52.

Berry, P.L. & Vickers, B. (1975). Consolidation of fibrous peat. *J. Geotech. Engr. Div. ASCE,* 101, GT8, 741-753.

Berry, P.L. (1983). Application of consolidation theory for peat to the design of a reclamation schedule by preloading. *Q. J. Engr. Geol.,* 16, 103-112.

Bjerrum, L. (1967). Engineering geology of Norwegian normally-consolidated marine clays as related to settlements of buildings. *Géotechnique*, 17, 81-118.

Bloetjes, O.A.J. & van der Meer, J.J.M. (1992). A preliminary stratigraphical description of peat development on Clara bog. Fysisch Geografisch en Bodemkundig Laboratorium, Universiteit van Amsterdam, The Netherlands.

Buisman, A.S.K. (1936). Results of long duration settlement tests, *Proc. 1st Int. Conf. Soil Mech. Fdn. Engr.,* Cambridge, Mass., 1, 51.

Burland, J.B. (1989) On the compressibility and shear strength of natural clays. *Géotechnique*, 40, 3, 327-378.

Butterfield, R. (1979). A natural compression law for soils (an advance on *e*-log *p'*). *Géotechnique*, 29, 4, 469-480.

Candler, C.J. & Chartres, F.R.D. (1988). Settlement measurement and analysis of three trial embankments on soft peaty ground. *Proc. 2nd Baltic Conf. Soil Mech. Fdn. Engr.*, Tallinn, 1, 268-272.

Carlsten, P. (1991). Embankment on soft organic soil using the preloading technique. *Proc. 10th Eur. Conf. Soil Mech. Fdn. Engr.,* Florence, 1, 359-362.

Cartier, G.A., Allayes, M., Londez & Ropers, F. (1989). Secondary settlement of peat during a load test. *Proc. 12th Int. Conf. Soil Mech. Fdn. Engr.*, Rio Janeiro, 3, 1721-1722.

Christensen, R.W. & Wu, T.H. (1964). Analysis of clay deformation as a rate process. *J. Soil Mech. Fdn. Div. ASCE*, 91, SM5, 4481, 15-35.

Christie, I.F. & Tonks, D.M. (1985). Developments in the time lines theory of consolidation. *Proc. 11th Int. Conf. Soil Mech. Fdn. Engr.,* 2, 423-426.

Crank, J. & Nicolson, P. (1947). A practical method for numerical evaluation of solutions of partial differential equations. *Proc. Camb. Phil. Soc.* 43, 50-67.

Cross, J.R. (1990). The raised bogs of Ireland: their ecology, status and conservation. Report to the Minister of State at the Department of Finance, Stationery Office, Dublin.

de Cea, J.C., Diez, J.A. & Olalla, C. (1995). Geotechnical properties of the sediment deposits in the Proserpina reservoir (Merida). *Proc. Compression and Consolidation of Clayey Soils, Hiroshima,* 1, 255-260.

den Haan, E.J. & Edil, T.B. (1994). Secondary and tertiary compression of peat. *Advances in understanding and modelling the mechanical behaviour of peat,* Balkema, Rotterdam, 49-60.

den Haan, E.J. & El Amir, L.S.F. (1994). A simple formula for final settlement of surface loads on peat. *Advances in understanding and modelling the mechanical behaviour of peat,* Balkema, Rotterdam, 35-48.

den Haan, E.J. (1992). The formulation of virgin compression of soils. *Géotechnique,* 3, 465-483.

den Haan, E.J. (1994). Stress-independent parameters for primary and secondary compression. *Proc. 13th Int. Conf. Soil Mech. Fdn. Engr.,* New Delhi, 1, 65-70.

den Haan, E.J. (1994a). General Report Session 1: One-dimensional behaviour. *Advances in Understanding and Modelling the Mechanical Behaviour of Peat,* Balkema, Rotterdam, 95-130.

den Haan, E.J. (1994b). Summary of session 1: One-dimensional behaviour. *Advances in Understanding and Modelling the Mechanical Behaviour of Peat,* Balkema, Rotterdam, 131-140.

den Haan, E.J. (1995). Some remarks on consolidation theory. *Proc. Compression and Consolidation of Clayey Soils,* Hiroshima, 2, 1087-1090.

den Haan, E.J. (1996). A compression model for non-brittle soft clays and peat. *Géotechnique*, 46, 1, 1-16.

den Haan, E.J. (1997). An overview of the mechanical behaviour of peats and organic soils and some appropriate construction techniques. *Conf. on Recent Advances in Soft Soil Engr.*, Sarawak, 17-45.

Dhowian, A.W. & Edil, T.B. (1980). Consolidation behaviour of peats. *Geotech. Test. J.*, 3, 105-114.

Edil, T. B. (1994). General report session 3: Immediate issues in engineering practise. *Advances in understanding and modelling the mechanical behaviour of peat*, Balkema, Rotterdam, 403-413.

Edil, T.B. & Dhowian, A.W. (1979). Analysis of long-term compression of peats. *Geotech. Engr. South East Asian Soc. Soil Engr.*, 10, 159-178.

Edil, T.B. & Mochtar, N.E. (1984). Prediction of peat settlement. *Proc. Symp. Sedimentation Consolidation Models, ASCE*, San Francisco, 411-424.

Edil, T.B. (1982). Use of preloading for construction on peat. *Proc. 13th Minnesota Conf. Soil Mech. Fdn. Engr.,* St. Paul, Minnesota, 125-140.

Edil, T.B. (1983). Improvement of peat: a case history. *Proc. 8th Eur. Conf. Soil Mech. Fdn. Engr.,* Helsinki, 2, 739-744.

Edil, T.B. (1997). Construction over peats and organic soils. *Proc. Conf. on Recent Advances in Soft Soil Engr.*, Kuching, Sarawak, 85-108.

Edil, T.B., & den Haan, E.J. (1994). Settlement of peat and organic soils. *ASCE Geot. Spec. Publ.*, 40, 2, 1543-1572.

Edil, T.B., Fox, P.J. & Lan, L.T. (1991). End-of-primary consolidation of peat. *Proc. 10th Eur. Conf. Soil Mech. Fdn. Engr.*, Florence, 1, 65-68.

Edil, T.B., Fox, P.J. & Lan, L.T. (1991). Observational procedure for settlement of peat. *Proc. Geocoast Conf.*, Yokohama, 2, 165-170.

Edil, T.B., Fox, P.J. & Lan, L.T. (1994). Stress-induced one-dimensional creep of peat. *Advances in understanding and modelling the mechanical behaviour of peat*, Balkema, Rotterdam, 3-18.

Eggestad, A. & Føyn, T., (1977). Vaeg-och vatten-byggaren (*J. Swedish Soc. Civ. Engrs.*), 23, 8-9, 44-45.

Farrell, E.R. (1997). Some experiences in the design and performance of roads and road embankments on organic soils and peats. *Proc. Conf. on Recent Advances in Soft Soil Engr.*, Kuching, Sarawak, 66-84.

Farrell, E.R. (2001). Comparison of laboratory predictions versus field performance. *Problematic Soils: one-day symposium of East Midlands Geotechnical Group*, (in press).

Farrell, E.R., O'Neill, C. & Morris, A. (1994). Changes in the mechanical properties of soils with variations in organic content. *Advances in understanding and modelling the mechanical behaviour of peat,* Balkema, Rotterdam, 19-25.

Flynn, R.M. (1990). Clara bog: a hydrological study. M.Sc. Thesis, University of Birmingham, England.

Fokkens, B. (1970). Berekening van de samendrukking van veenlagen uit het gehalte aan organische stof en water. (Computation of the compression of peat from the content of organic matter and water.) *De Ingenieur, Bouw- en Waterbouwkunde* 3, B23-B28.

Forrest, J.B. & MacFarlane, I.C. (1969). Field studies of response of peat to plate loading. *J. Soil Mech. Fdn. Engr. Div., ASCE,* 95, SM4, 949-967.

Fox, P. J. (1992). An analysis of one-dimensional creep behaviour of peat. Ph.D. Thesis, University of Wisconsin, USA.

Fox, P. J., Roy-Chowdhury, N., Edil, T.B., Juarez-Badillo, E. & Mesri, G. (1999). Secondary compression of peat with or without surcharging; discussions and reply. *J. Geotech. Geoenv. Engr.*, 160-165.

Fox, P.J. & Edil, T.B. (1994). Micromechanics model for peat compression. *Advances in understanding and modelling the mechanical behaviour of peat*, Balkema, Rotterdam, 159-166.

Fox, P.J. & Edil, T.B. (1996). Effects of stress and temperature on secondary compression of peat. *Can. Geotech J.*, 33, 405-415.

Fox, P.J., Edil, T.B. & Lan, L.T. (1992). C_α/C_c concept applied to compression of peat. *J. Geot. Engr. Div. ASCE*, 118, GT8, 1256-1263.

Fox, P.J., Edil, T.B. & Lan, L.T. (1994). Closure to C_α/C_c concept applied to compression of peat. *J. Geotech. Engrg., ASCE*, 120(4), 767-770.

Garlanger, J.E. (1972). Consolidation of soils exhibiting creep under constant effective stress. *Géotechnique,* 22, 1, 71-78.

Gautschi, M.A. (1965). Torf als baugrund (Peat as foundation soil), *Research summary report,* Norwegian Geotechnical Institute, Oslo.

Gibson, R.E. & Lo, K.-Y. (1961). A theory of consolidation for soils exhibiting secondary compression. Norwegian Geotechnical Institute Publication 41, 1-16.

Gibson, R.E., England, G.L. & Hussey, M.J.L. (1967). The theory of one-dimensional consolidation of saturated clays. 1. Finite non-linear consolidation of thin homogeneous layers. *Géotechnique,* 17, 261-273.

Gorman, C.T., Hopkins, T.C., Deen, R.C. & Drnevich, V.P. (1978). Constant rate-of-strain and controlled-gradient consolidation testing. *Geotech. Test. J.*, 1, 3-15.

Graham, J. & Yin, J.-H. (2001). On the time-dependant stress-strain behaviour of soft soils. *Proc. 3rd Int. Conf. on Soft Soil Engr.,* Hong Kong, (in press).

Graham, J., Crooks, J.H.A. & Bell, A.L. (1983). Time effects on the stress-strain behaviour of natural soft clays. *Géotechnique,* 33, 3, 327-340.

Gray, H. (1936). Progress report on the consolidation of fine-grained soils. *Proc. 1st Int. Conf. Soil Mech. Fdn. Engr.*, Cambridge, 2, 138-141.

Hamilton, J.G. & Crawford, C.B. (2001). Improved determination of preconsolidation pressure of a sensitive clay. *Papers on soils*, ASTM STP 254, 254-270.

Hanrahan, E.T. (1954). An investigation into some physical properties of peat. *Géotechnique,* 4, 108-123.

Hanrahan, E.T. (1964). A road failure on peat. *Géotechnique,* 14, 185-202.

Hansen, B. (1969). A mathematical model for creep phenomena in clay. Proc. Speciality Session No.12, "Advances in consolidation theory for clays", *Proc. 7th Int. Conf. Soil Mech. Fdn. Engr.*, Mexico.

Hardin, B.O. (1989). One-dimensional strain in normally consolidated cohesive soils. *J. Geotech. Engr., ASCE*, 115, 5, 689-710.

Hawley, J.G. & Borrin, D.L. (1973). A unified theory for the consolidation of clays. *Proc. 8th Int. Conf. Soil Mech. Fnd. Engr.,* Moscow, 1, 191-196.

Head, K.H. (1982) Manual of soil laboratory testing, Vol.2: Permeability, shear strength and compressibility tests.

Hebib, S., (2001). Experimental investigation of the stabilisation of Irish peat, Ph.D. Thesis, Trinity College Dublin, Ireland.

Helenelund, K.V. (1980). Geotechnical behaviour and properties of Finnish peats, *Valtion Teknillen Tutkimuskeskus,* VTT symp. 8, reprint, 85-107.

Hillis, S.F. & Brawner, C.O. (1961). The compressibility of peat with reference to major highway construction in British Columbia. *Proc. 7th Muskeg Research. Conf.,* Ottawa, 204-227.

Hobbs, N.B. (1986). Mire morphology and the properties and behaviour of some British and foreign peats. *Quart. J. Engr. Geol.,* 19, 7-80.

Holtz, R.D. & Kovacs, W.D. (1981). An introduction to geotechnical engineering. Prentice-Hall, Inc., Englewood Cliffs, N.J.

Imai, G. & Tang, X.Y. (1992). A constitutive equation of one-dimensional consolidation derived from interconnected tests. *Soils Fnds.,* 32, 2, 8396.

Imai, G. (1989). A unified theory of one-dimensional consolidation with creep. *Proc. 12th Int. Conf. Soil Mech. Fnd. Engr.*, 1, 57-60.

Imai, G. (1995). Analytical examinations of the foundations to formulate consolidation phenomena with inherent time-dependence. *Proc. Compression and Consolidation of Clayey Soils,* Hiroshima, 2, 891-935.

Jamiolkowski, M., Ladd, C.C., Germaine, J.T. & Lancellotta, R. (1985). New developments in field and laboratory testing of soils: general report. *Proc. 11th Int. Conf. Soil Mech. Fdn. Engr.,* San Francisco, 1, 57-153.

Jarrett, P.M. (1997). Recent developments in design and construction on peat and organic soils. *Proc. Conf. on Recent Advances in Soft Soil Engr.* Kuching, Sarawak, 1-16.

Jose, B.T., Sridharan, A. & Abraham, B.M. (1989). Log-log method for determination of preconsolidation pressure, *Geotech. Test. J. Am. Soc. Test. Mat.*, 12, 3, 230-237.

Juarez-Badillo, E. (1965). Compressibility of soils. *Proc. 5th Symp. Behaviour of Soil under Stress*, 1, A2, 1-35.

Juarez-Badillo, E. (1975). Constitutive relationships for soils. S*ymp. Recent Developments and Soil Behaviours and the App. to Geotech. Structures.* Kensington, Australia. The University of New South Wales.

Juarez-Badillo, E. (1981a). General compressibility equation for soils. *Proc. 10th Int. Conf. Soil Mech.* Stockholm 1, 171-178.

Juarez-Badillo, E. (1981b). Discussion on "A natural compression law for soils (an advance on *e*-log *p*')". *Géotechnique,* 31, 4, 567.

Kabbaj, M., Tavenas, F. & Leroueil, S. (1988). *In situ* and laboratory stress-strain relationships. *Géotechnique,* 38, 1, 83-100.

Kamoa, S. Yamada, K., Satoh, F. & Aita, K. (1995). Characteristics of long-term resettlement of soft ground after removal of the preload. *Proc. Compression and Consolidation of Clayey Soils,* Hiroshima, 1, 75-78.

Karlsrud, K., Lunne, T. & Brattlien, K.(1996). Improved CPTU interpretations based on block samples, *XIIth Northern Geotech. Conf. (NGM)*, Rykjavik, 1, 195-201.

Kelly, M.L. (1993). Hydrology, hydrochemistry and vegetation of two raised bogs in Co. Offaly. Ph.D. Thesis, Trinity College Dublin, Ireland.

Kim, Y. T. & Leroueil, S., (2001). Modelling of the viscoplastic behaviour of clays during consolidation: application to Berthierville clay in both laboratory and field conditions, *Can. Geotech. J.*, 38, 484-497.

Krieg, S. & Goldscheider, M. (1994). Some results concerning the development of K_o during one-dimensional creep of peat. *Advances in understanding and modelling the mechanical behaviour of peat*, Balkema, Rotterdam, 71-75.

Ladd, C.C. (1971). Settlement analysis for cohesive soils. *Research Report R71-2*, MIT, Cambridge, Massachussetts.

Ladd, C.C., Foott, R., Ishihara, K., Schlosser, F. & Poulus, H.G. (1977). Stress-deformation and strength characteristics. *Proc 9th Int. Conf. on Soil Mech. Fdn. Engr.* Tokyo, 1, 421-494.

Lake, J.R. (1961). Investigations of the problems of constructing roads on peat in Scotland. *Proc. 7th Muskeg Conference,* Ottawa.

Lan, L.T. (1992). A model for one-dimensional compression of peat. Ph.D. Thesis, University of Wisconsin, USA.

Landva, A.O. & La Rochelle, P. (1983). Compressibility of Radforth Peats. *Testing of peats and organic soils*, ASTM STP 820, 157-191.

Landva, A.O. & Pheeney, P.E., (1980). Peat fabric and structure. *Can. Geotech. J.*, 416-435.

Landva, A.O., Korpijaakko, E.O. & Pheeney, P.E. (1983). Geotechnical classification of peats and organic soils. *Testing of peats and organic soils*, ASTM STP 820, 37-51.

Landva, A.O., Pheeney, P.E. & Mersereau, D. E. (1983). Undisturbed sampling of peat. *Testing of peats and organic soils*, ASTM STP 820, 141-156.

Landva, A.V. (1980). Vane testing in peat. *Can. Geotech. J.*, 17, 1, 1-19.

Lea, N.D. & Brawner, C.O. (1963). Highway design and construction over peat deposits in Lower British Columbia. *Highway Research Record No. 7,* Washington.

Lee, K. (1981). Consolidation with constant rate of deformation. *Géotechnique*, 31, 2, 215-229.

Lefebvre, G. (1986) Discussion of "Post-construction settlement of an expressway built on peat by precompression". *Can. Geotech. J.*, 23.

Lefebvre, G., Langlois, P., Lupien, C. & Lavalle, J.G. (1984). Laboratory testing and *in situ* behaviour of peat as embankment foundation. *Can. Geotech. J.,* 21, 2, 322-337.

Leonards, G.A. (1972). Discussion on shallow foundations. Proc. Speciality Conf., Performance of earth and earth-supported structures, Purdue Univ., 3:159-180.

Leonards, G.A. (1977). *Proc. 9th Int Conf. Soil Mech. Fnd. Engr.,* Tokyo, 3, 384-386.

Leonards, G.A. & Girault, P. (1961). A study of one-dimensional consolidation test. *Proc. 5th Int. Conf. Soil Mech. Fnd. Engr.,* Paris, 1, 213-218.

Leroueil, S. & Kabbaj, M. (1987). Discussion of "Settlements analysis of embankments on soft clays," *J. Geotech. Engr., ASCE*, 113(9), 1067-1070.

Leroueil, S. (1994). Compressibility of clays: fundamental and practical aspects. *Vertical and horizontal deformations of foundations and embankments. ASCE Geotech. Spec. Publ.*, 40, 1, 57-76.

Leroueil, S. (1996). Compressibility of clay: fundamental and practical aspects. *J. Geotech. Engr., ASCE*, 122, 534-543.

Leroueil, S., Kabbaj, M., Tavenas, F. & Bouchard, R. (1985). Closure to stress-strain-strain rate relations for the compressibility of sensitive natural clays. *Géotechnique*, 35, 2, 159-180.

Ling Kah Jai, Ir., (1997). Stress-void ratio relationship and peat, *Conf. on Recent Advances in Soft Soil Engr.,* Kuching, Sarawak.

Liu, J. -C. & Znidavcic, D. (1991). Modelling one-dimensional compression characteristics of soil. *J. Geotech. Engr.*, ASCE, 117(1), 162-169.

Lupien, C., Lefebvre, G., Rosenberg, P. & Lavallee, J.-G. (1981). Observations during construction of till embankments on peat foundation. *34th Can. Geotech. Conf.,* Fredericton, New Brunswick.

MacFarlane, I.C. & Radforth, N.W. (1965). A study of the physical behaviour of peat derivatives under compression. *Proc. 10th Muskeg Res. Conf. NRC,* 159-164.

MacFarlane, I.C. (1960). An evaluation of road performance over muskeg in Northern Ontario. *Proc. 6th Muskeg Res. Conf.,* Ottawa., 67, 38-48.

MacFarlane, I.C. & Rutka A. (1961). Highway research board bulletin, 316, 32-43.

Maddison, J.D., Jones, D.B., Bell, A.L. & Jenner, C.G. (1996). Design and performance of an embankment supported using low strength geogrids and vibro concrete columns. *Geosynthetics: applications, Design and Construction,* Balkema, 325-332.

Magnan, J.P. (1994). Construction on peat: State of the art in France. *Advances in understanding and modelling the mechanical behaviour of peat,* Balkema, Rotterdam, 369-380.

Magnan, J.P., Baghery, S., Brucy, M. & Tavenas, F. (1979). Etude numérique de la consolidation unidimensionnelle en tenant compte des variations de la perméabilité et de la compressibilité du sol, du fluage et de la non-saturation. *Bull. Liaison Lab. Ponts et Chaussés,* 103, 83-94.

Matsuo, K (1998). Influence of aging to the peat compressibility. *Proc. Int. Symp. on problematic soils,* Balkema, Rotterdam, 21-24.

Matsuo, K. (1995). Secondary consolidation behaviour of peat. *Proc. Compression and Consolidation of Clayey Soils*, Hiroshima, 1, 129-134.

McCabe, B. (2002) An experimental investigation into pile group behaviour in soft clays. Ph.D. Thesis, Trinity College Dublin, Ireland.

McGeever, J. (1987). The strength parameters of an organic soil, M.Sc. Thesis, Trinity College Dublin, Ireland.

Mesri, G. & Castro, A. (1987). The C_α/C_c concept and K_o during secondary compression. *J. Geotech. Engr., ASCE*, 113(3), 230-247.

Mesri, G. & Choi, Y. K. (1984). Discussion on time effects of the stress-strain behaviour of natural soft clays. *Géotechnique* 34, 3, 439-464.

Mesri, G. & Choi, Y.K. (1985). Settlement analysis of embankments on soft clays. *J. Geotech. Engr. Div., ASCE,* 111, GT4, 441-464.

Mesri, G. & Feng, T.W. (1986). Stress-strain-strain-rate relation for the compressibility of sensitive natural clays (Discussion). *Géotechnique,* 36: 283-287.

Mesri, G. & Godlewski, P.M. (1977). Time- and stress- compressibility interrelationship. *J. Geotech. Engr. Div. ASCE*, 103, GT5, 417-430.

Mesri, G. (1986). Discussion on "Postconstruction settlement of an expressway built on peat by precompression". *Can. Geoecht. J.*, 23, 403-407.

Mesri, G. (1987) The fourth law of soil mechanics: the law of compressibility. *Proc. Int. Symp. on Geotech. Engr. of Soft Soils*, 2, 179-187.

Mesri, G. (1995). Compressibility parameters during primary consolidation. *Proc. Compression and Consolidation of Clayey Soils*, Hiroshima, 2, 1021-1037.

Mesri, G., (1973), Coefficient of secondary compression, *J. Soil Mech. Fnd. Div., ASCE*, 99, SM1, 123-137.

Mesri, G., Feng, T.W., & Benak, J.M. (1990). Postdensification penetration resistance of clean sands. *J. Geotech. Engr., ASCE*, 1, 8-56.

Mesri, G., Rokhsar, A. & Bohor, B.F. (1975). Composition and compressibility of typical samples of Mexico City clay. *Géotechnique*, 25, 3, 527-554.

Mesri, G., Stark, T.D. & Chen, C.S. (1994). Discussion of C_α/C_c concept applied to compression of peat. *J. Geotech. Engr., ASCE,* 120(4), 764-767.

Mesri, G., Stark, T.D., Ajlouni, M.A., & Chen, C.S. (1997). Secondary compression of peat with or without surcharging. *J. Geotech. Geoenv. Engr.,* 411-421.

Meyer, Z. & Dereczenik, M. (1994). Non-linear model of terminal settlement of peat. *Advances in understanding and modelling the mechanical behaviour of peat,* Balkema, Rotterdam, 89-94

Mitchell, (1969). Temperature effects on engineering properties and behaviour of soils. Highway Research Board Special Report, 103, 9-27.

Mitchell, K.J. (1976). Fundamentals of Soil Behaviour. John Wiley, New York.

Miyakawa, I. (1960). Some aspects of road construction over peaty or marshy areas in Hokkaido, with particular reference to filling methods. Civil Engineering Research Institute, Hokkaido Development Bureau, Sapporo.

Mochtar, N.E. (1985). Compression of peat soils. Ph.D. Thesis, University of Wisconsin, USA.

Nash, D.F.T. & Ryde, S.J. (2001). Modelling consolidation accelerated by vertical drains in soils subject to creep. *Géotechnique,* 51, 3, 257-273.

Nash, D.F.T., & Ryde S.J. (1999). Modelling the effects of surcharge to reduce the long term settlement of an embankment on soft alluvium. *Proc. 12th Eur. Conf. on Soil Mech. Geotech. Engr.*, Amsterdam, 3, 1555-1561.

Nash, D.F.T., & Ryde S.J. (2000). Modelling the effects of surcharge to reduce long term settlement of reclamations over soft clays. *Proc. Int. Symp. Coastal Geotech. Engr. in practice,* 1, 480-483.

Ng, S.Y., & Eischens, G.R. (1983). Repeated short-term consolidation of peats. *Testing of peats and organic soils*, ASTM STP 820, 192-206.

Nichol, D. & Farmer, I.W. (1998). Settlement over peat on the A5 at Pant Dedwydd near Cerrigydrudion, North Wales. *Engr. Geol.,* 50, 299-307.

Niemunis, A. & Krieg, S. (1996). Viscous behaviour of soil under oedometric conditions. *Can. Geotech. J.*, 33, 159-167.

O'Loughlin, C.D., & Lehane, B.M. (2001). Modelling one-dimensional compression of a fibrous peat. *Proc. 15th Int. Conf. Soil Mech. Geotech. Engr.*, Istanbul, 223-226.

O'Loughlin, C.D., & Lehane, B.M. (2001). Modelling the time-dependent compression of peat and organic soils. *Proc. 3rd Int. Conf. on Soft Soil Engr.*, Hong Kong, 369-375.

Oikawa, H. & Igarahi, M. (1997). A method for predicting *e*-log *p* curve and log c_v-log *p* curve of a peat from its natural water content. *Proc. Conf. on Recent Advances in Soft Soil Engr.*, Kuching, Sarawak, 201-209.

Orr, T.L.L. & McEnaney, T. (1994). Friction piles for a walkway on a peat bog. *Advances in Understanding and Modelling the Mechanical Behaviour of Peat,* Balkema, Rotterdam, 381-388.

Özişik, M.N. (1994). Finite difference methods in heat transfer. CRC Press., Boca Raton.

Perrin, J., (1973) Comportement des sols tourbeux et synthese des resultats, *Bulletion de liaison des Laboratoires des Ponts et Chaussees*, Paris, Special T, 241-257.

Powell, M. (1964). An efficient method for finding the minimum of a function of several variables, without calculating derivatives. *Comp. J.*, 7, 155-162.

Ripley, C.F. & Leonoff, C.E. (1961). Embankment settlement behaviour on deep peat. *Proc 7th Muskeg Research Conf., NRC*, 71.

Rodgers, M. (1997). Embankment construction on soft soil sites. *Road Embankments on Soft Ground in Ireland*, IEI, 72-80.

Rowe, R.K., MacLean, M.D., & Barsvary, A.K. (1984). The observed behaviour of a geotextile-reinforced embankment constructed on peat. *Can. Geotech J.*, 21, 563-576.

Rowe, R.K. & Mylleville, B.L.J. (1996). A geogrid reinforced embankment on peat over organic silt: a case history. *Can. Geotech J.*, 33, 106-122.

Royer, J.A., (1936) *Proc. 1st Int. Conf. Soil Mech. Fnd. Engr.*, Harvard University Press, Cambridge, Mass., Vol. I, 235-238.

Samson, L. (1985). Postconstruction settlement of an expressway built on peat by precompression. *Can. Geotech. J.*, 22, 2, 1-9.

Samson, L. & La Rochelle, P. (1972). Design and performance of an expressway constructed over peat by preloading. *Can. Geotech. J.*, 9, 447-466.

Samson, L., Leroueil, S., Morin, P., & Le Bihan, J.P. (1981). La pression de préconsolidation des argiles sensibles. *Report Terratech Limitée, NRCC.*

Samuels, H. (1992). Drainage and subsidence of a raised bog. M.Sc. Thesis, Imperial College London, England.

Sandroni, S.S, Silva, J.M.J., & Pinheiro, J.C.N. (1984). Site investigations for unretained excavations in a soft peaty deposit. *Can. Geotech. J.*, 9, 107-118.

Schmertmann, J.M. (1953). Estimating the true consolidation behaviour of clay from laboratory test results. *Proc. ASCE,* 79, 1-26.

Sheahan, T.C. & Watters, P.J. (1997). Experimental verification of CRS consolidation theory. *J. Geotech. Geoenv. Engr.*, 430-437.

Skempton, A.W. & Petley, D.J. (1970). Ignition losss and other properties of peats and clays from Avonmouth, King's Lynn and Cranberry Moss. *Géotechnique*, 20, 343-356.

Smith, R.E. & Wahls, H.E. (1969). Consolidation under constant rate of strain. *J. Soil Mech. Fdn. Div., ASCE*, 95(2), 519-539.

Smyth, M. (1993). Quaternary geology and geophysical studies of Clara and Raheenmore bogs, Co. Offaly, Ireland. Ph.D. Thesis, University College Galway, Ireland.

Stolle, D.F.E., Bonnier, P.G., & Vermeer, P.A. (1997). A soft soil model and experiences with two integration schemes. *Numerical Models in Geomechanics*, Balkema, Rotterdam, 123-128.

Stolle, D.F.E., Vermeer, P.A., & Bonnier, P.G. (1999). A consolidation model for creeping clay. *Can. Geotech. J.,* 36, 754-759.

Šuklje, L. (1957). The analysis of the consolidation process of the isotache method. *Proc. 4th Int. Conf. Soil Mech. Fdn. Engr.,* London, 1, 200-206.

Šuklje, L. (1969). Consolidation of viscous soils subjected to increasingly uniform load. *New advances in soil mechanics, Praha,* 1, 199-235.

Szavits-Nossan, V. (1988). Intrinsic time behaviour of cohesive soils during consolidation. Ph.D. Thesis, University of Colorado, Boulder, USA.

Szymanski, A. (1982). Deformation characteristics of selected kinds of organic soils. Ph.D. Thesis, Warsaw Agriculture University, Warsaw, Poland.

Tavenas, F., Leblond, P., Jean, P. & Leroueil, S. (1983). The permeability of natural soft clays. *Can Geotech. J., 20*, 3, 629-669.

Taylor, D.W. & Merchant, W. (1940). A theory of clay consolidation accounting for secondary compression. *J. Math & Phys.*, 19, 167-185.

Taylor, D.W. (1942). Research on consolidation of clays. *MIT. Pub. from Dept. Civil & Sanitary Engr.*, Serial 82.

Taylor, D.W. (1948). Fundamentals of soil mechanics. *John Wiley & Sons Inc.*, New York.

TC15 (1997). Construction on peat and organic soils. Draft (version 2.0), Delft Geotechnics, The Netherlands.

Termaat, R., & Topolnicki, M. (1994). Biaxial tests with natural and artificial peat. *Advances in understanding and modelling the mechanical behaviour of peat,* Balkema, Rotterdam, 241-251.

Terzaghi, K. (1923). Die Berechnung der Durchlassigkeitsziffer des Tones aus dem Verlang der Hydrodynamischen Spannungerscheinungen. *Sber. Wien. Akad. Wiss.*, 132, 3/4, 125-128.

Terzaghi, K. (1941). Undisturbed clay samples and undisturbed clays. *J. Boston Soc. Civ. Engrs.*, 28, 3, 211.

Thomas, L.H. (1949). Elliptic problems in linear difference equations over a network. *Sci. Comp. Lab. Rept.*, Columbia University, New York.

van der Burght, J.H. (1936). Long duration consolidation tests. *Proc. 1st Int. Conf. Soil Mech. Fnd. Engr.*, 1, 51.

van der Heijden, E., Bouman, F., & Boon, J.J. (1994). Anatomy of recent and peatified Calluna vulgaris stems: implications for coal maceral formation. *Int. J. Coal Geol.*, 25, 1-25.

van der Schaaf , S. (1999). Analysis of the hydrology of raised bogs in the Irish midlands: a case study of Raheenmore and Clara bog. Ph.D. Thesis, Wageningen Agricultural University, The Netherlands.

van Tatenhove, F. & van der Meer, J. (1990). The quaternary geology of Clara bog and Raheenmore, Co. Offaly, Ireland; preliminary mapping of superficial deposits. Fysisch Geografisch en Bodemkundig Laboratorium, Universiteit van Amsterdam, The Netherlands.

von Post, L. (1922). Sveriges Geologiska Undersoknings torvinventering och nogra as dess hittils vunna resultat (SGU peat inventory and some preliminary results). *Svenska MossKulturfor. Tidskr.* 36, 1-37.

Weber, W.G. (1969). Performance of embankments constructed over peat. *J. Geotech. Div. ASCE*, 95, SM1, 53-76.

Wissa, A.E.Z., Christian, J.T., Davis, E.H. & Heiberg, S. (1971). Analysis of consolidation at constant strain rate. *J. Soil Mech. Fdns Div. ASCE*, 97, SM10, 1393-1413.

Wolski, W., Baranski, T., Garbulewski. K., Lechowicz, Z., & Szymanski, A. (1985). Testing of anisotropic consolidation in organic soils. *Proc. 11th Int Conf. Soil Mech. Fnd. Engr.*, San Fransico, 699-702.

Yamaguchi, H. (1994). Changes in pore size distributions due to consolidation stress histories and dilatancy of peat. *Advances in understanding and modelling the mechanical behaviour of peat,* Balkema, Rotterdam, 275-288.

Yin, J.H. & Graham, J. (1989). Viscous-elastic-plastic modelling of one-dimensional time-dependent behaviour of clays. *Can. Geot. J.*, 26, 199-209.

Yin, J.-H. & Graham, J. (1990) Viscous-elastic-plastic modelling of one-dimensional time-dependant behaviour of clays: reply. *Can. Geotech. J.*, 27, 262-265.

Yin, J.-H. & Graham, J. (1994). Equivalent times and one-dimensional elastic visco-plastic modelling of time-dependent stress-strain behaviour of clays. *Can. Geotech. J.*, 31, 42-52.

Yin, J.-H. & Graham, J. (1996). Elastic visco-plastic modelling of one-dimensional consolidation. *Géotechnique*, 46, 3, 515-527.

Yin, J.-H. (1999). Non-linear creep of soils in oedometer tests. *Géotechnique*, 49, 5, 699-707.

Yu, Y. & Magnusson, O. (1995). Compressible properties of soft organic sulphide-rich soils. *Proc. Compression and Consolidation of Clayey Soils,* Hiroshima, 1, 239-244.

Zhu, G.F. & Yin, J.-H. (1999). Finite element analysis of consolidated layered soils using an elastic visco-plastic model. *Int. J. for Numer. Anal. Meth. Geomech.*, 23, 355-374.

Appendix A

Laboratory test data

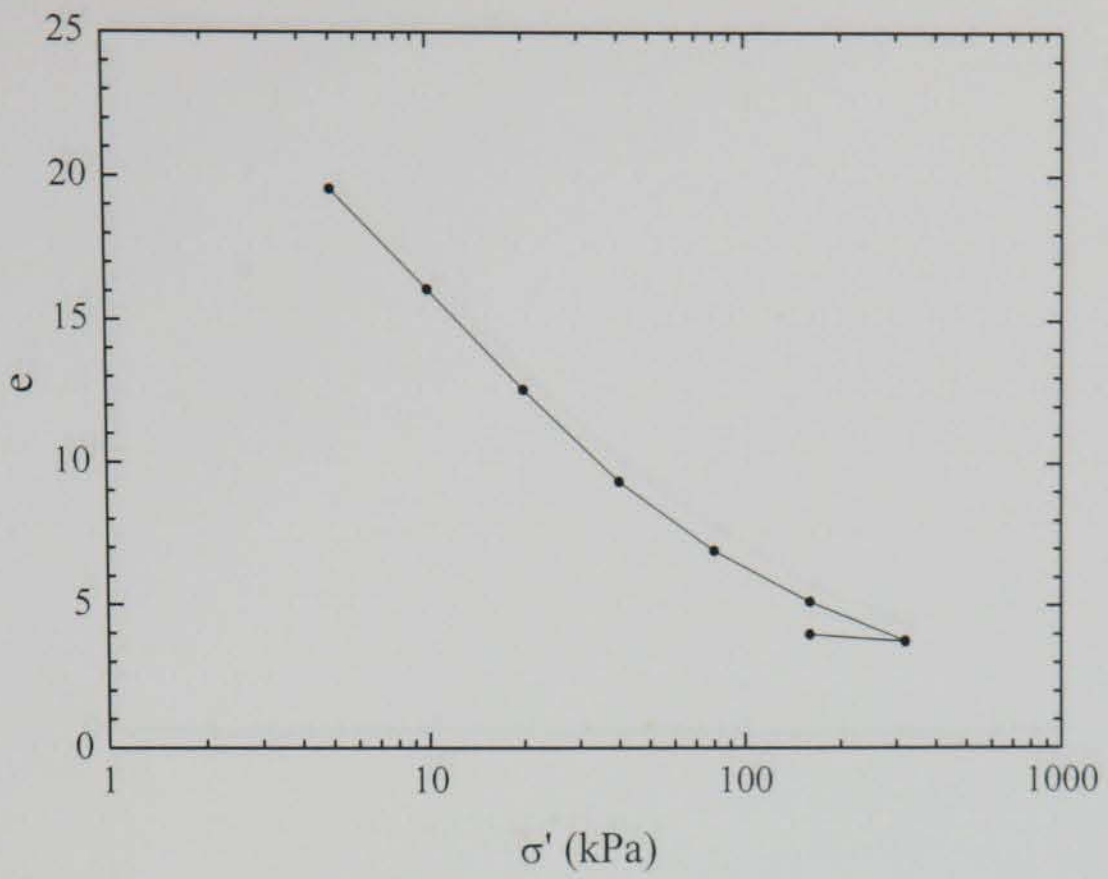

Figure A.1 e – log σ' data for CL_MSL_01

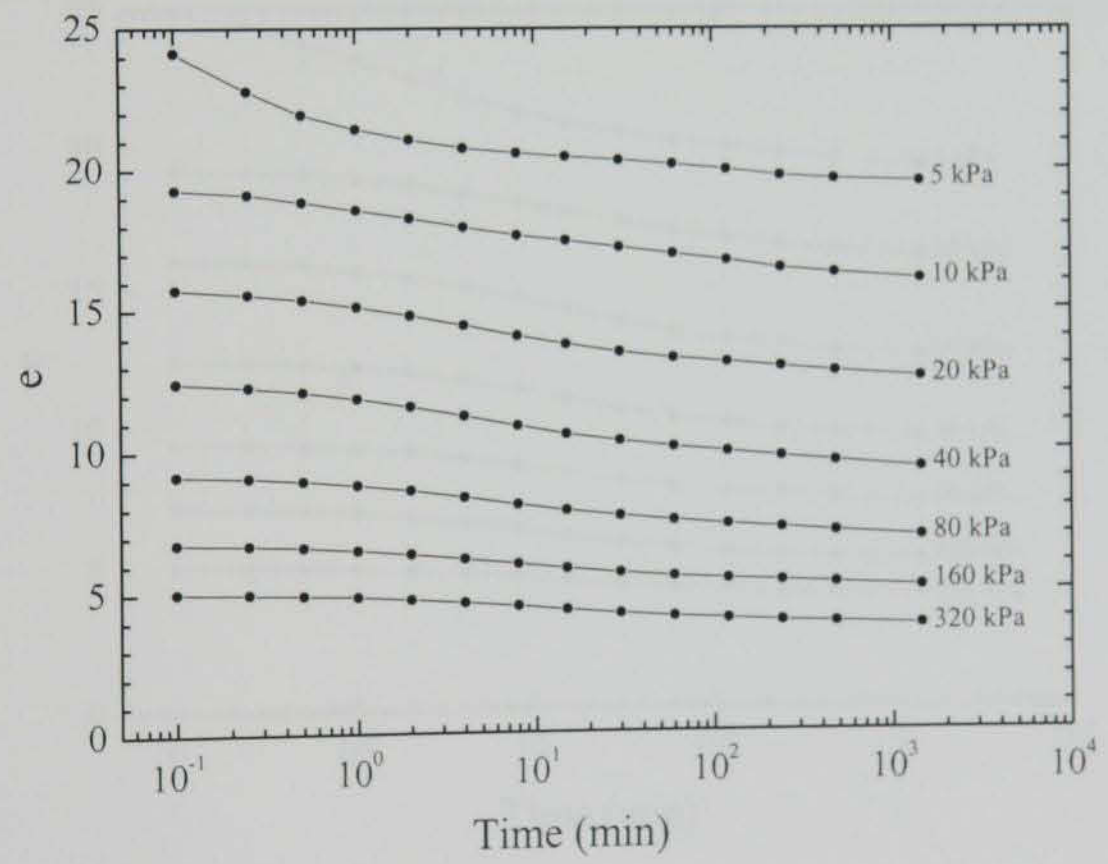

Figure A.2 e – log t data for CL_MSL_01

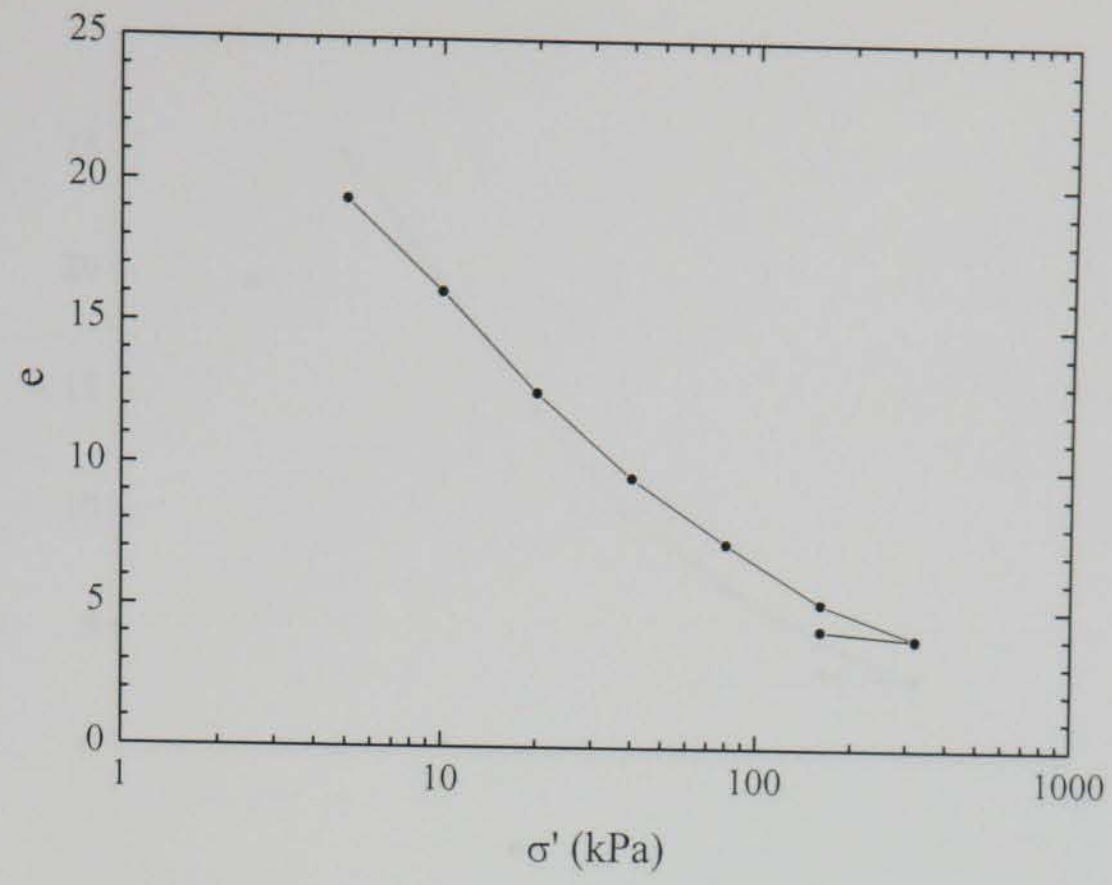

Figure A.3 e – log σ' data for CL_MSL_02

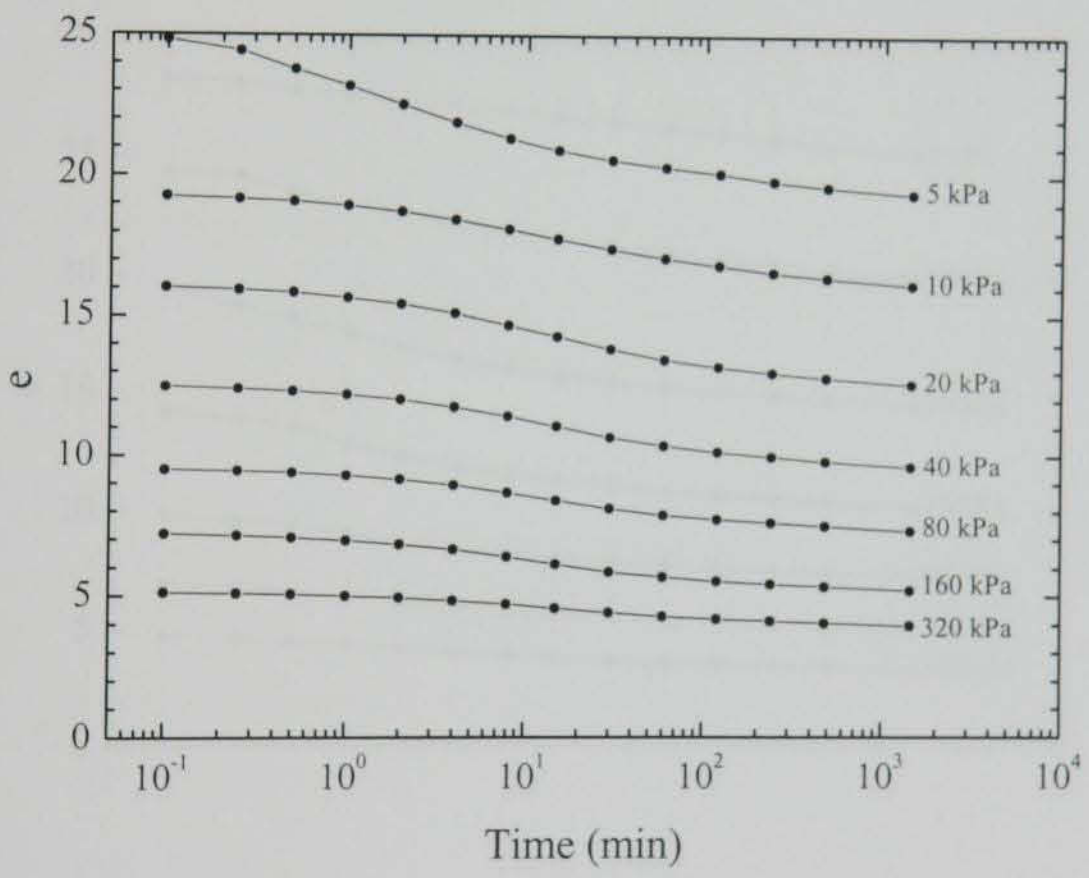

Figure A.4 e – log t data for CL_MSL_02

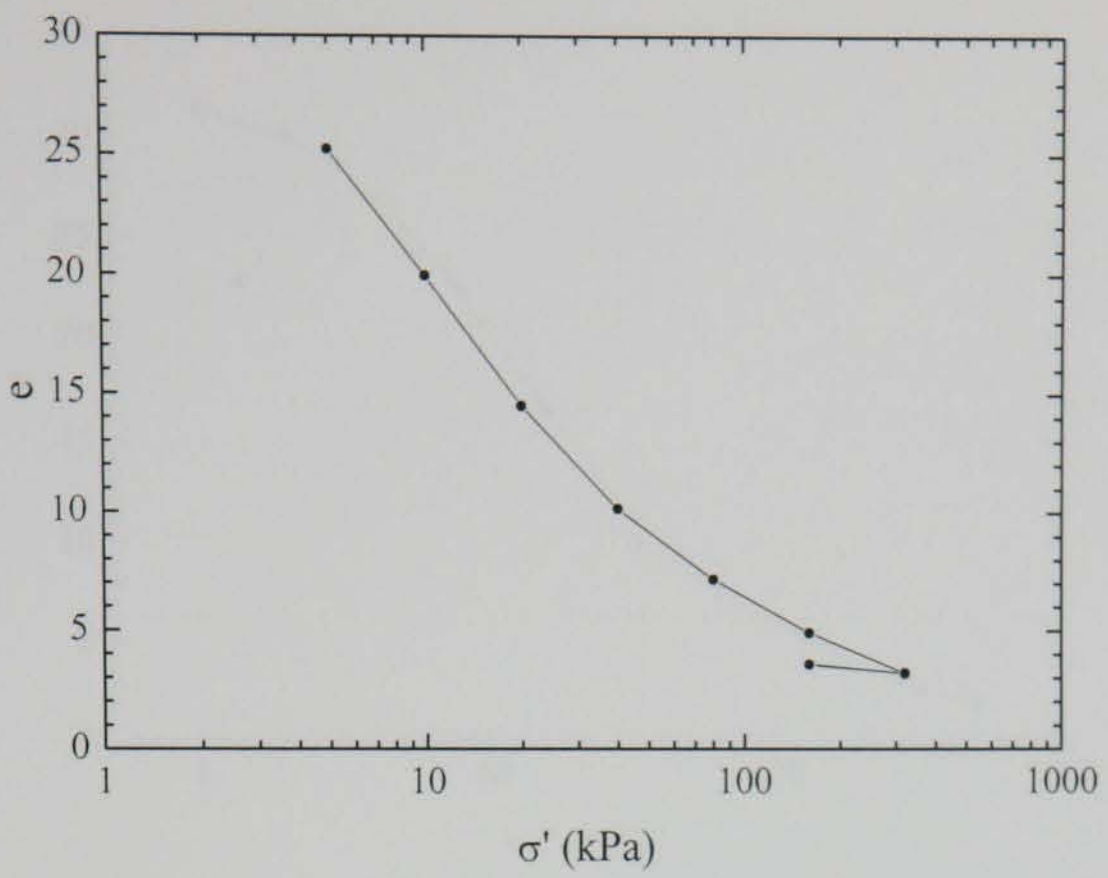

Figure A.5 e – log σ' data for CL_MSL_03

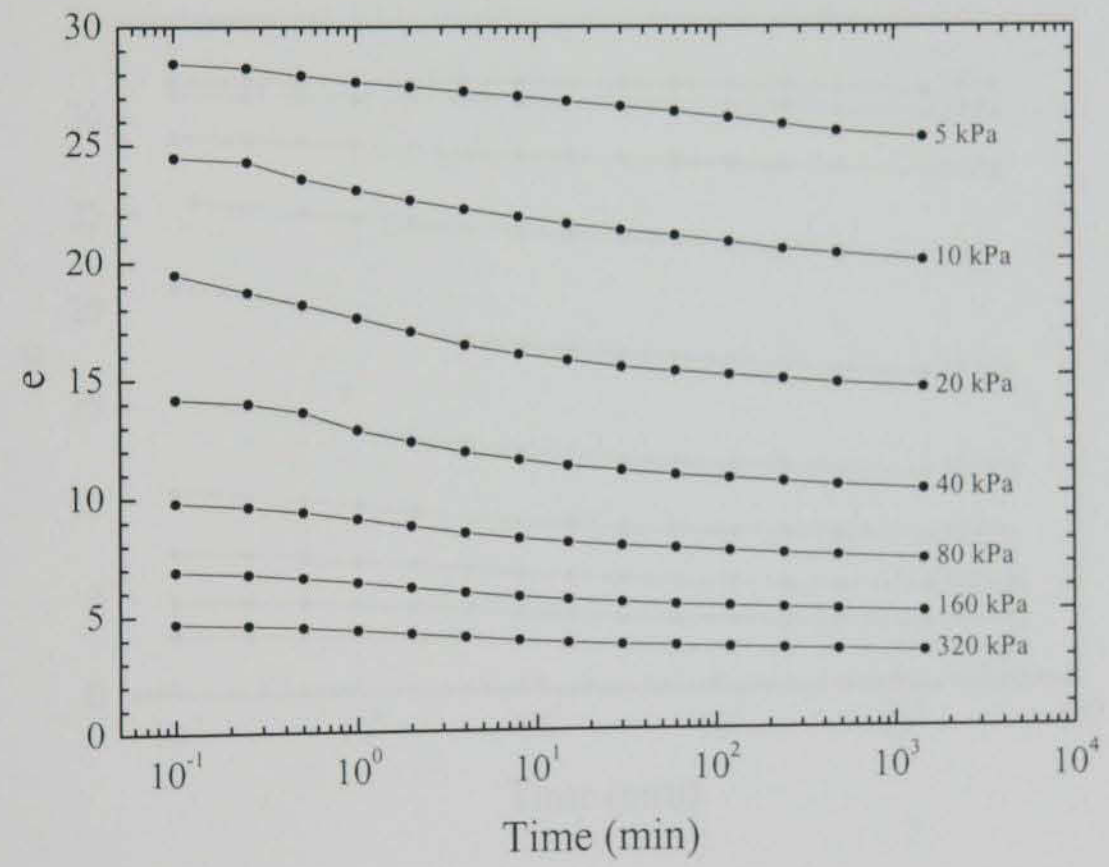

Figure A.6 e – log t data for CL_MSL_03

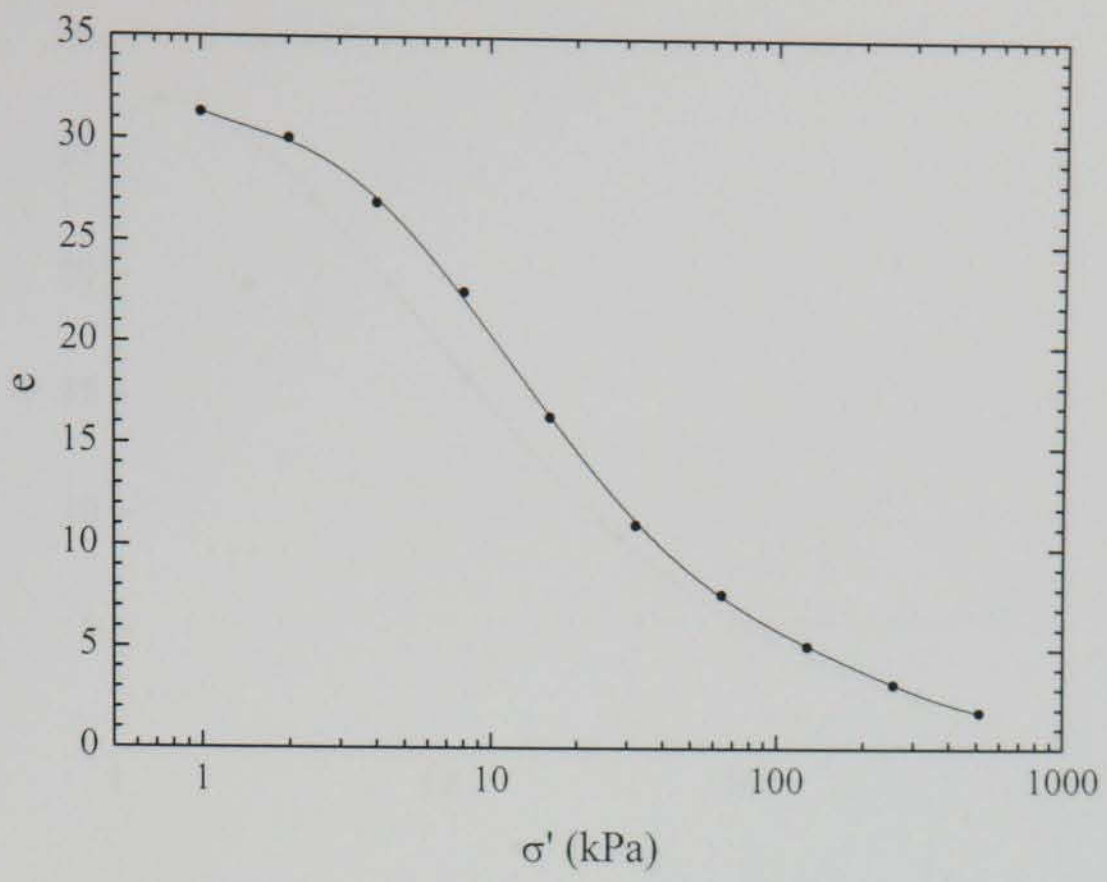

Figure A.7 e – log σ' data for CL_MSL_04

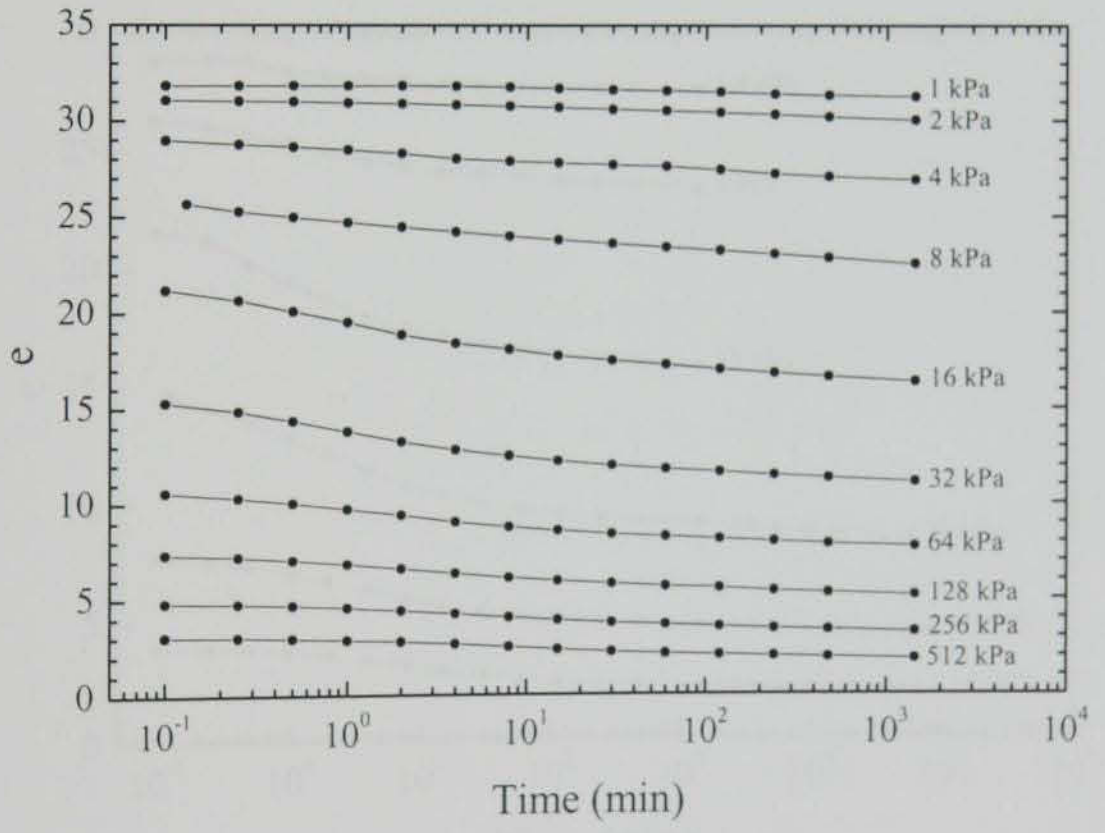

Figure A.8 e – log t data for CL_MSL_04

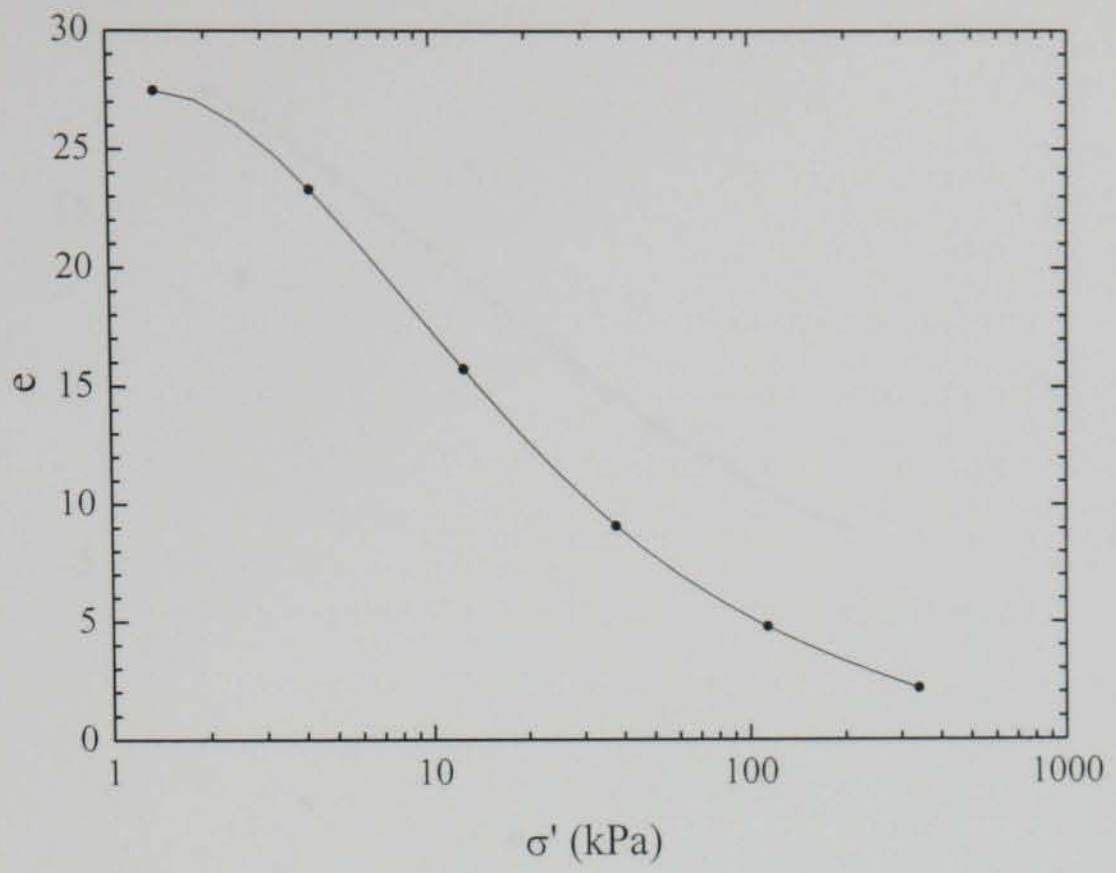

Figure A.9 e – log σ' data for CL_MSL_05

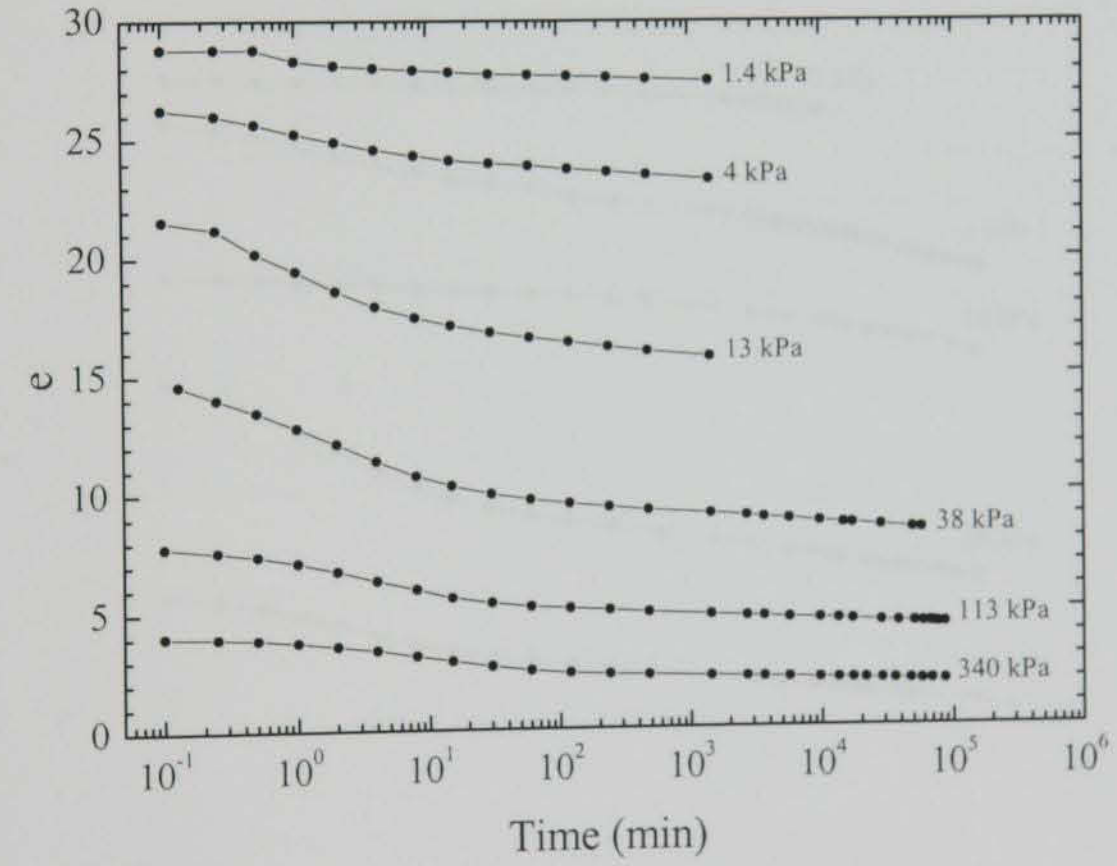

Figure A.10 e – log t data for CL_MSL_05

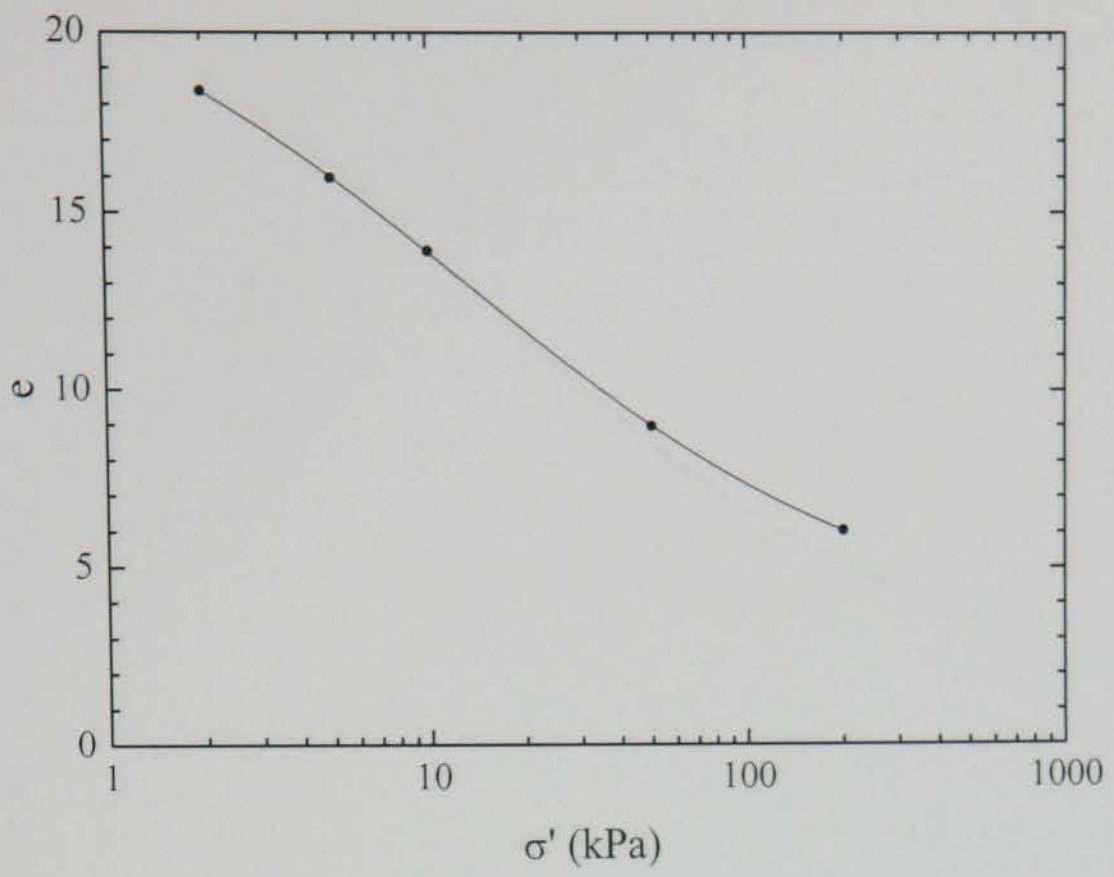

Figure A.11 e – log σ' data for CL_MSL_06

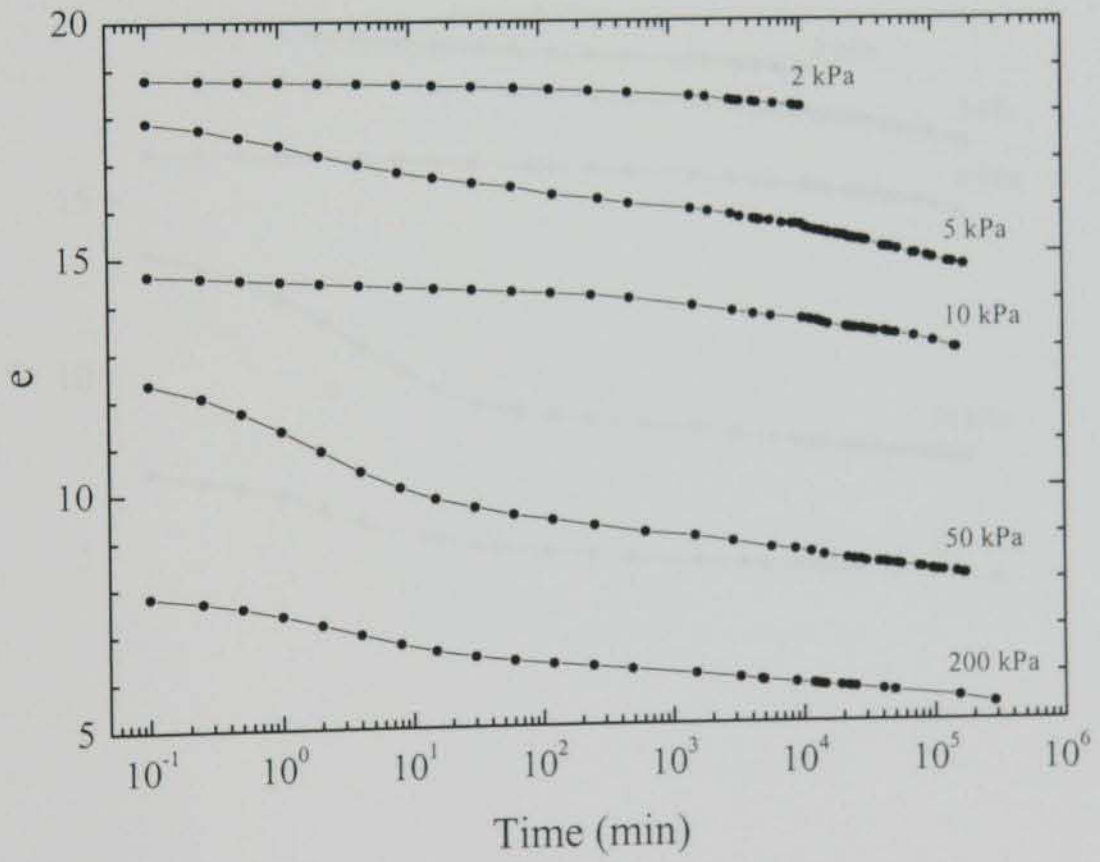

Figure A.12 e – log t data for CL_MSL_06

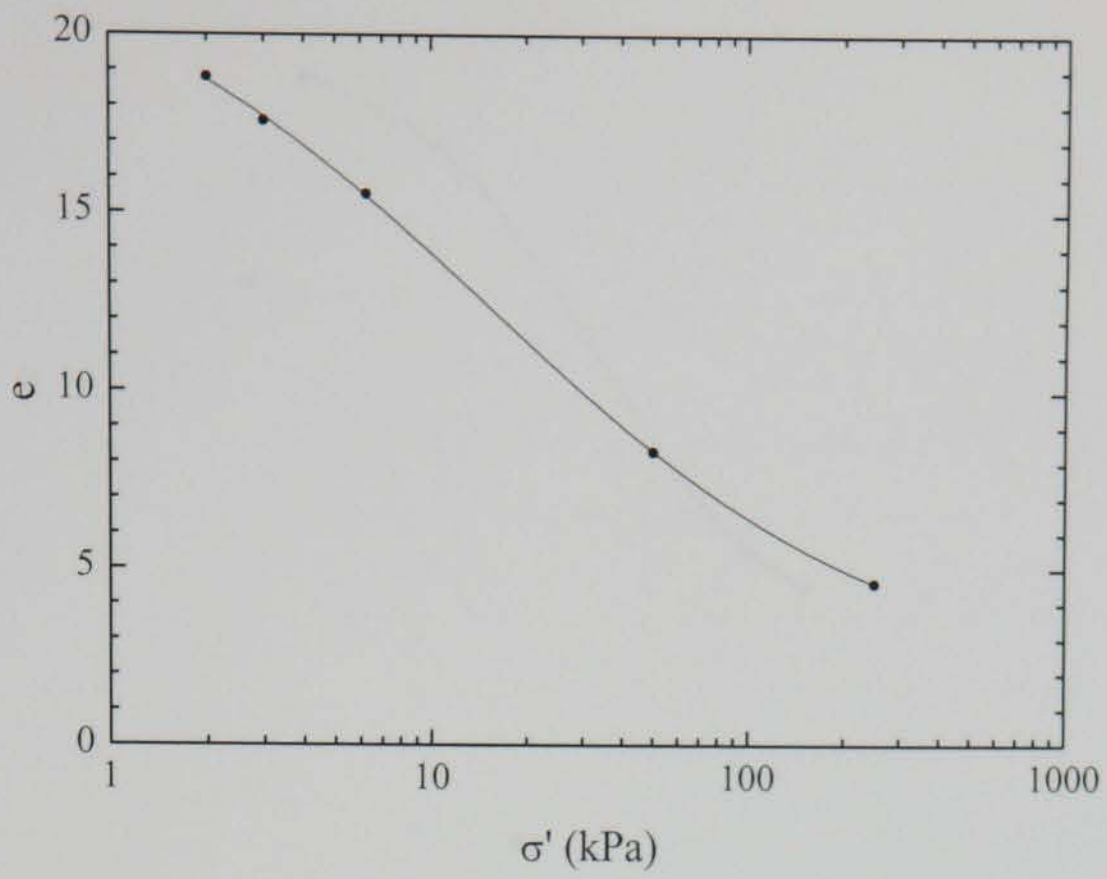

Figure A.13 e – log σ' data for CL_MSL_07

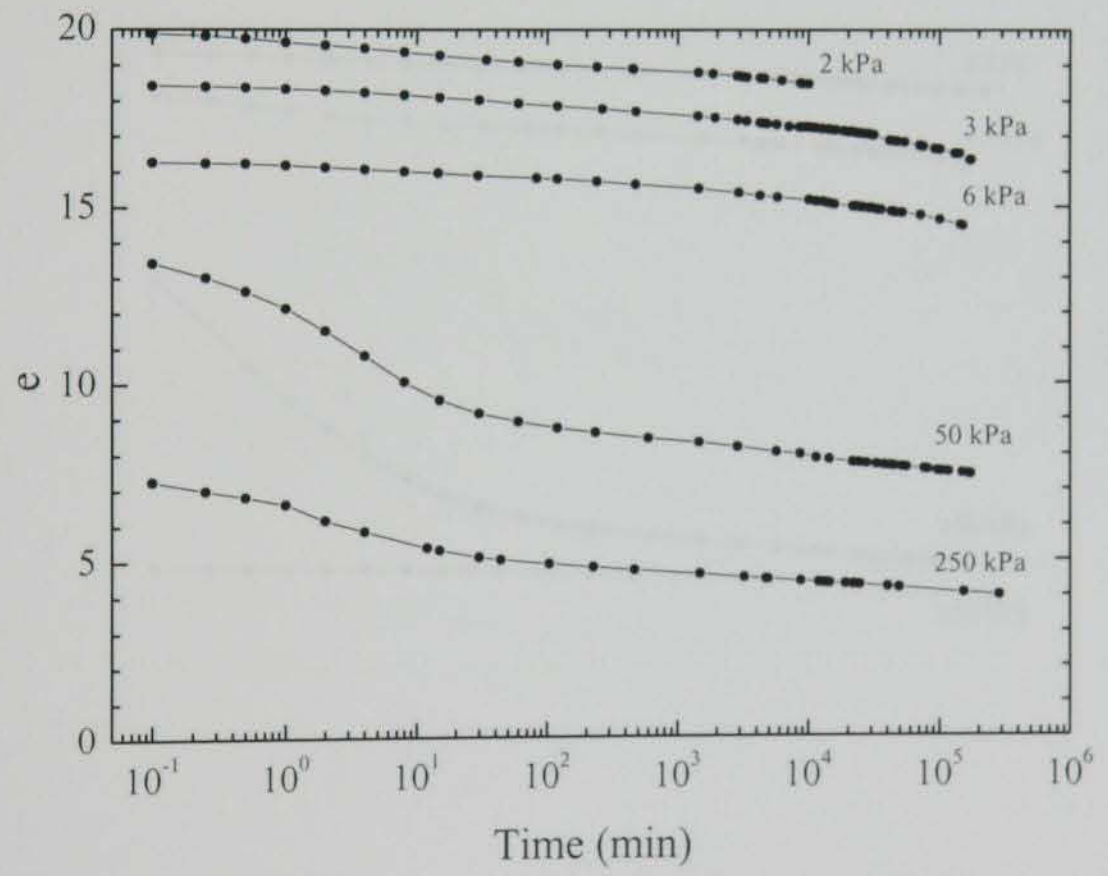

Figure A.14 e – log t data for CL_MSL_07

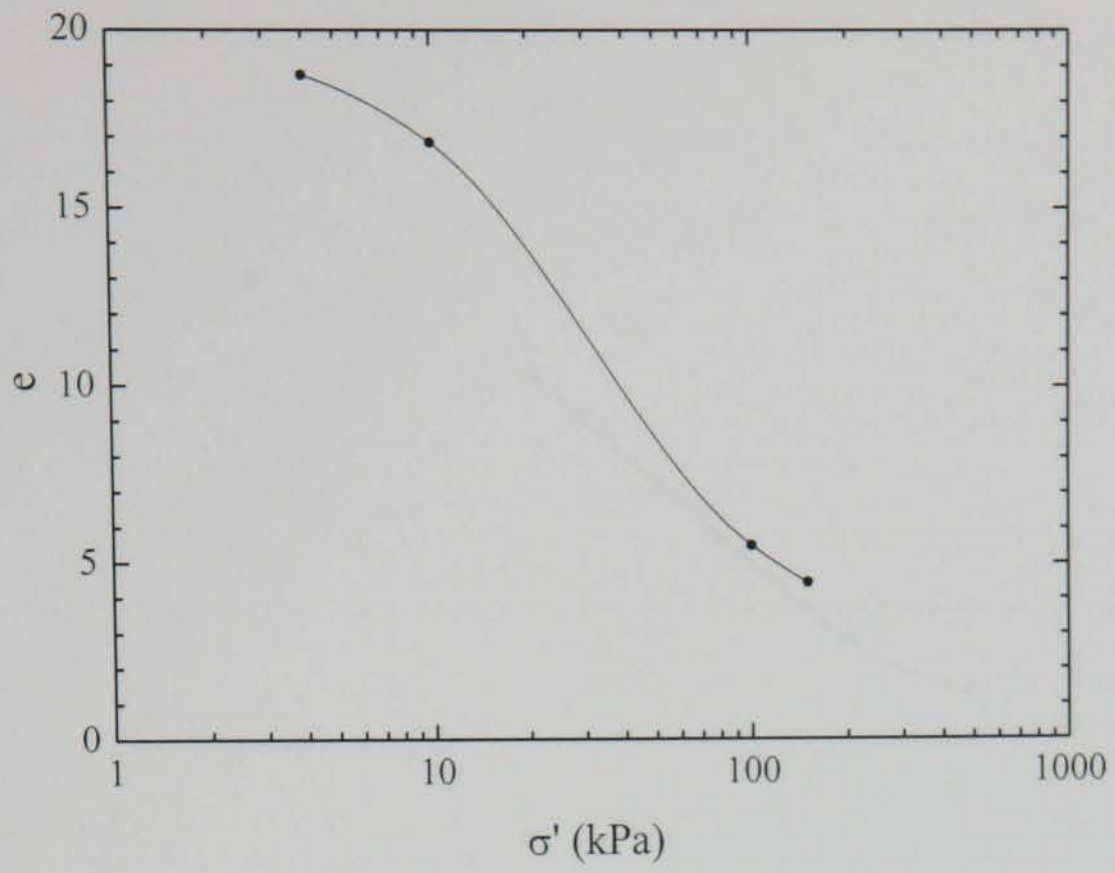

Figure A.15 e – log σ' data for CL_MSL_08

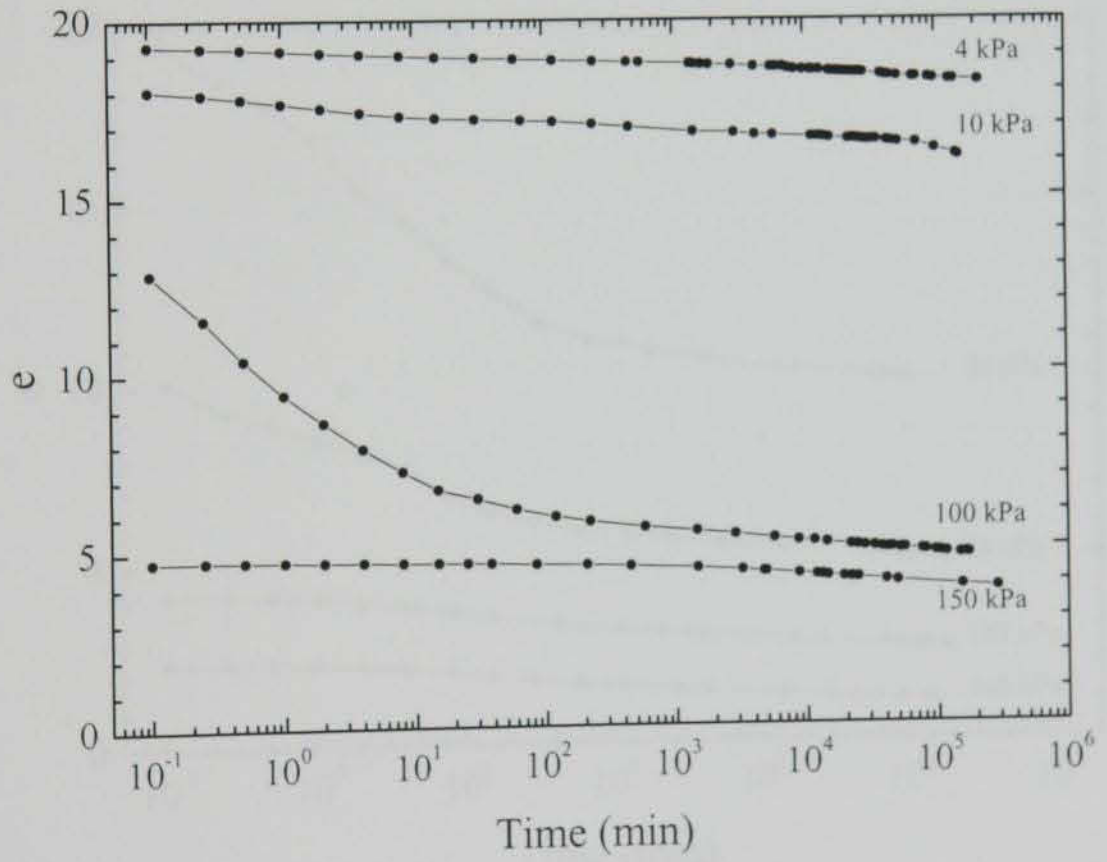

Figure A.16 e – log t data for CL_MSL_08

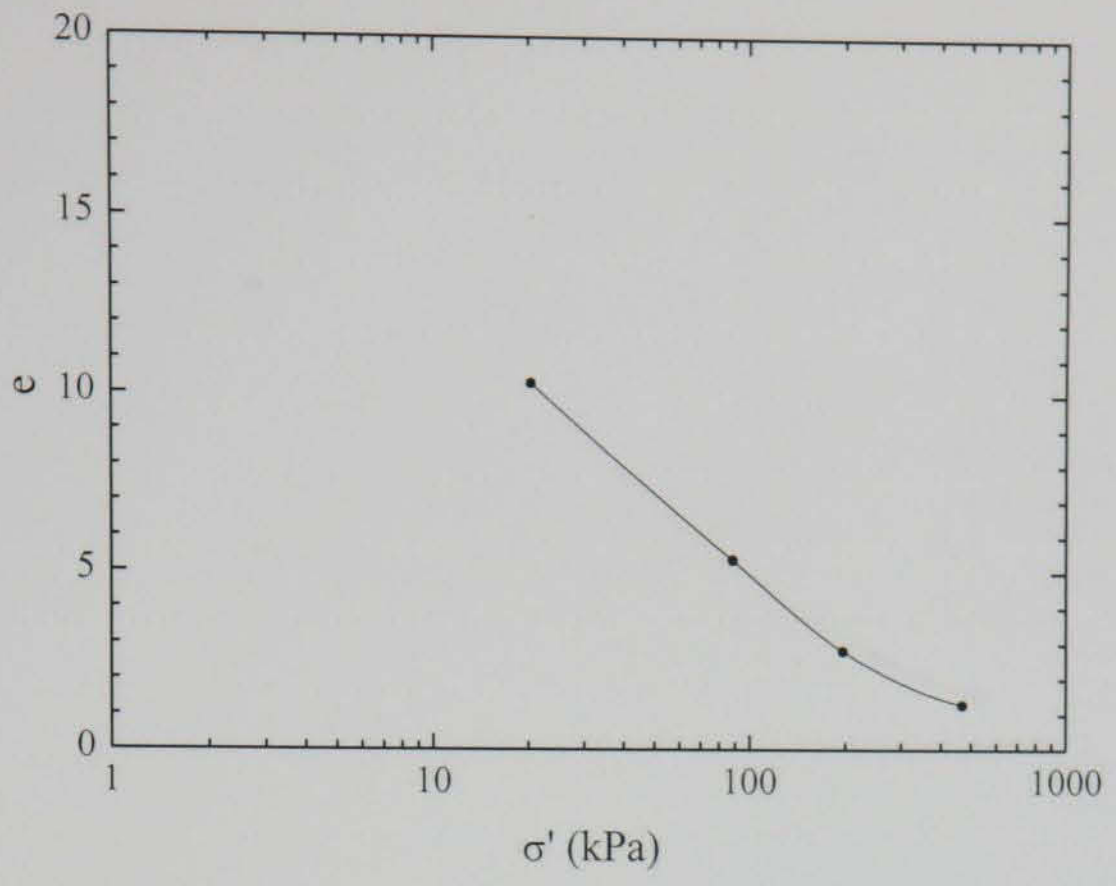

Figure A.17 e – log σ' data for CL_MSL_09

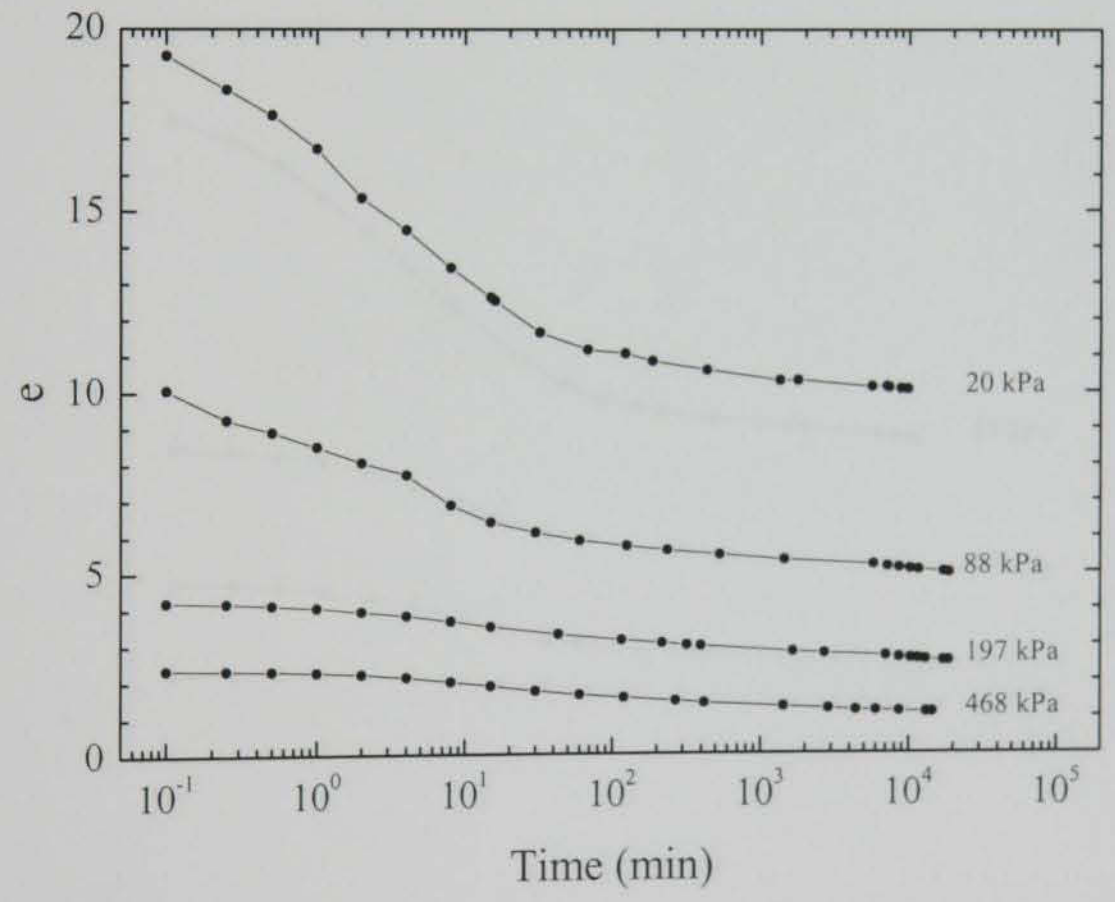

Figure A.18 e – log t data for CL_MSL_09

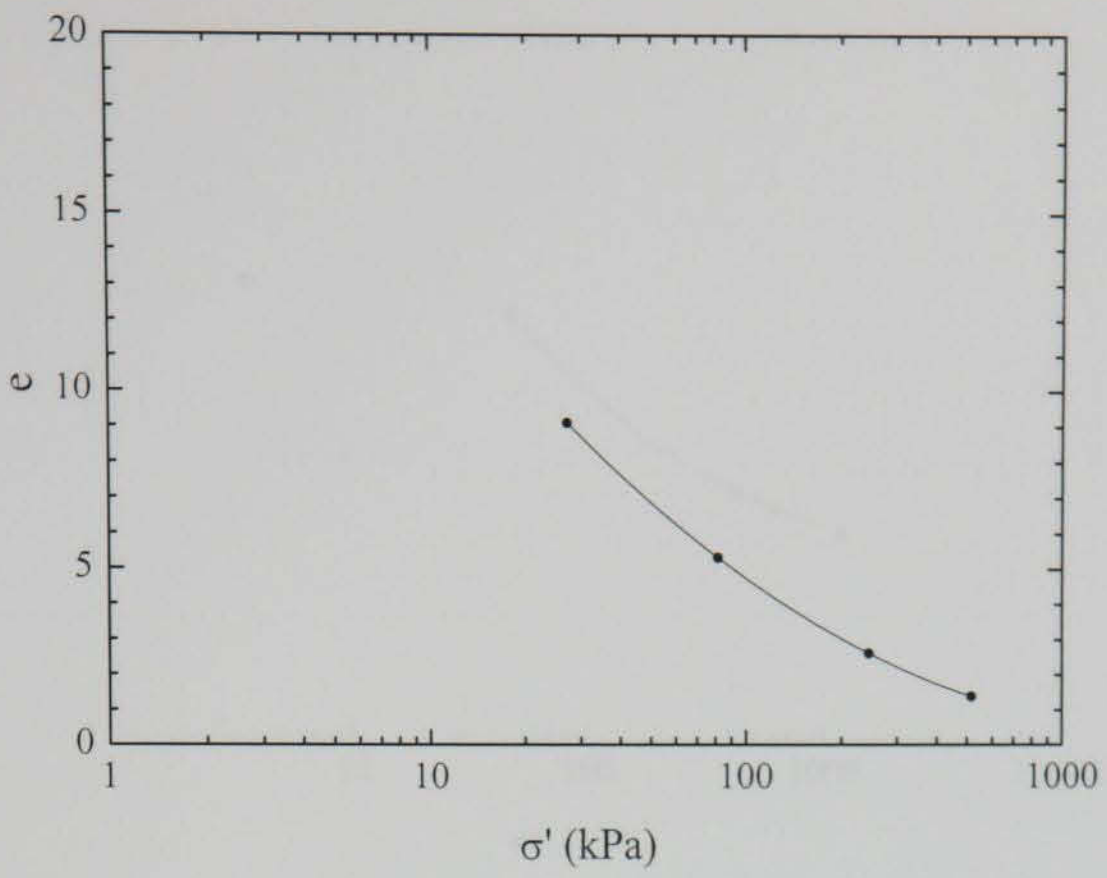

Figure A.19 e – log σ' data for CL_MSL_10

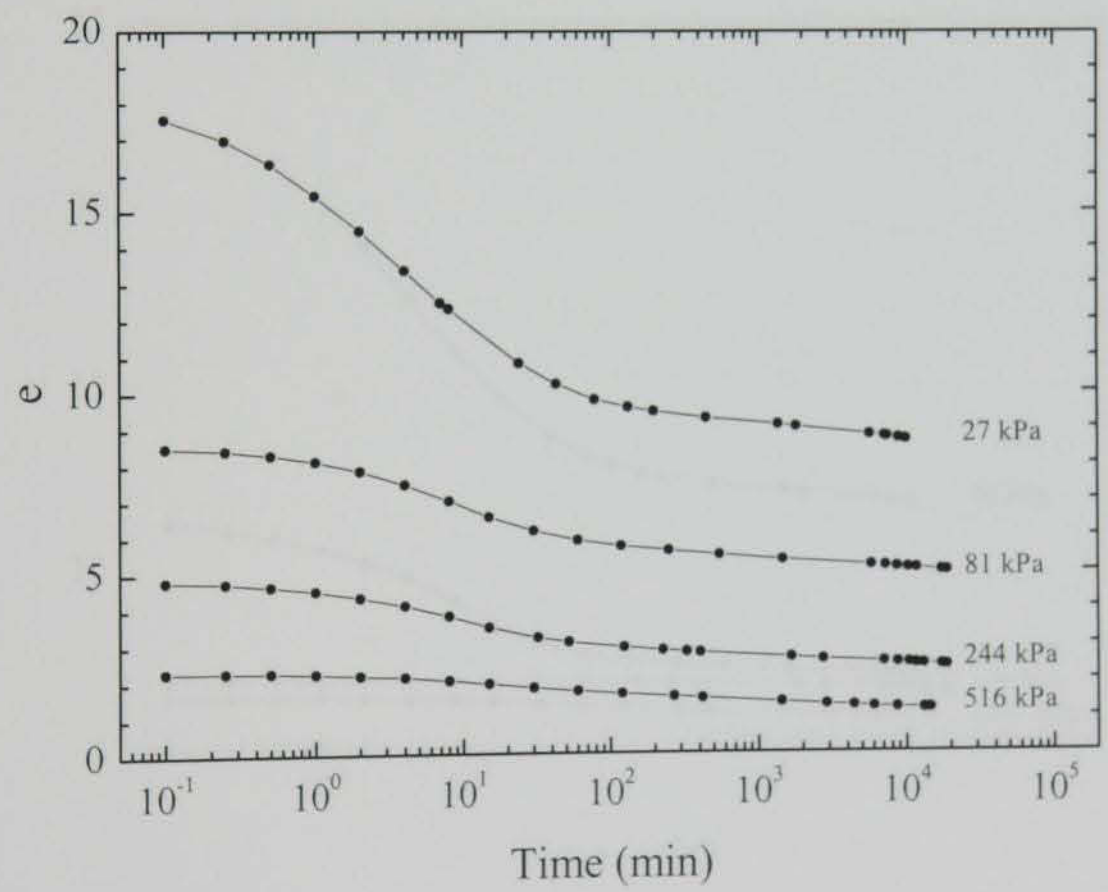

Figure A.20 e – log t data for CL_MSL_10

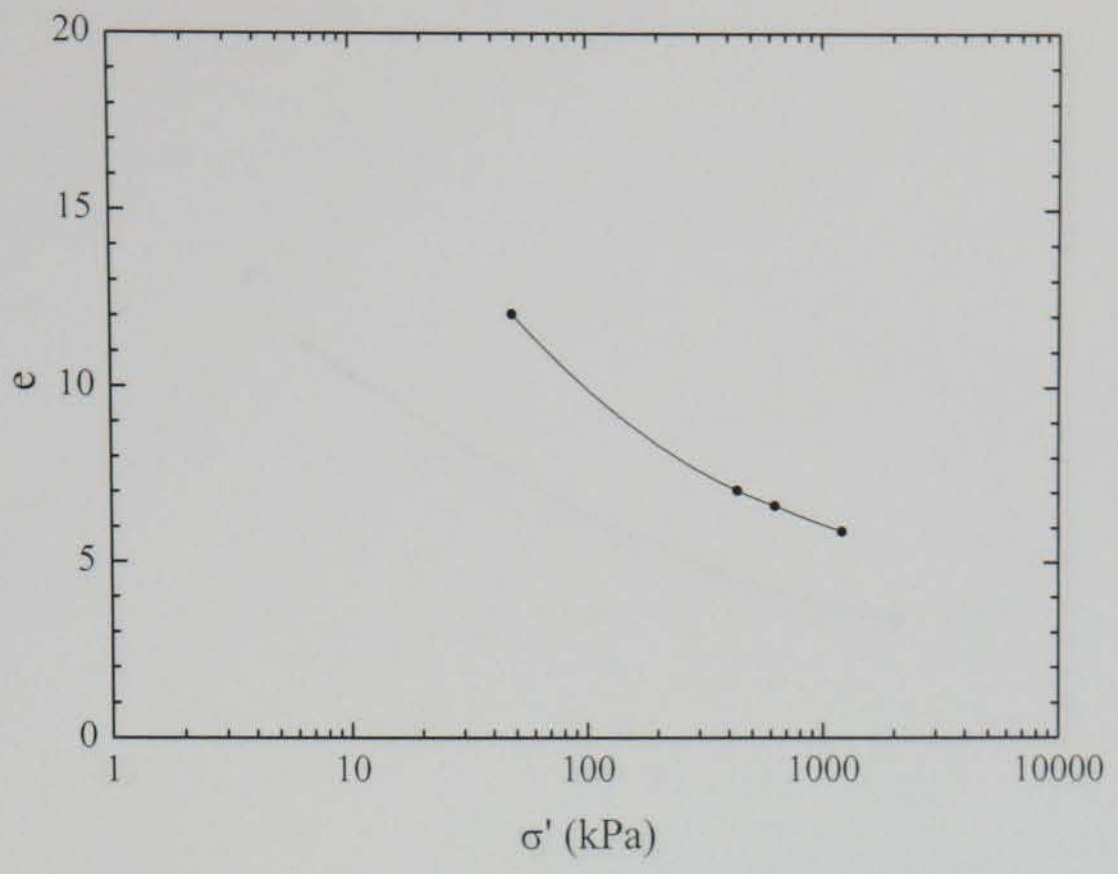

Figure A.21 e – log σ' data for CL_MSL_11

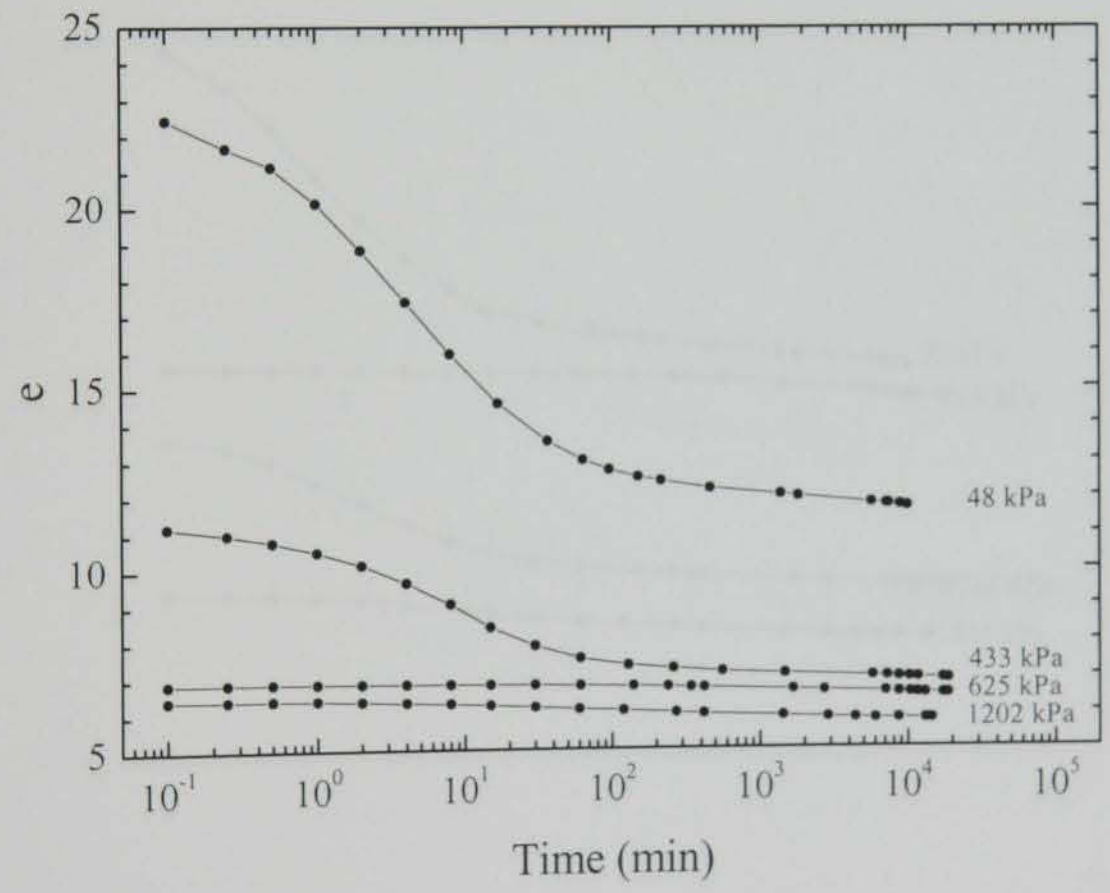

Figure A.22 e – log t data for CL_MSL_11

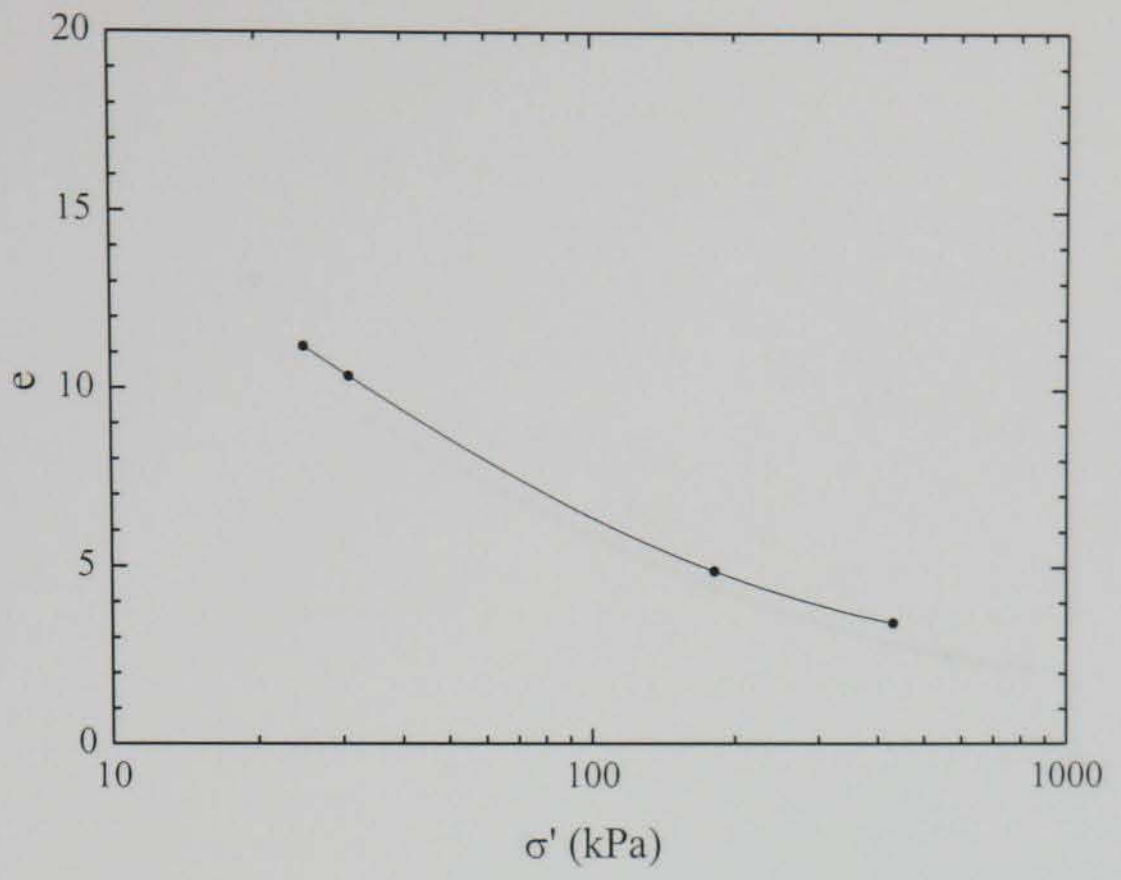

Figure A.23 e – log σ' data for CL_MSL_12

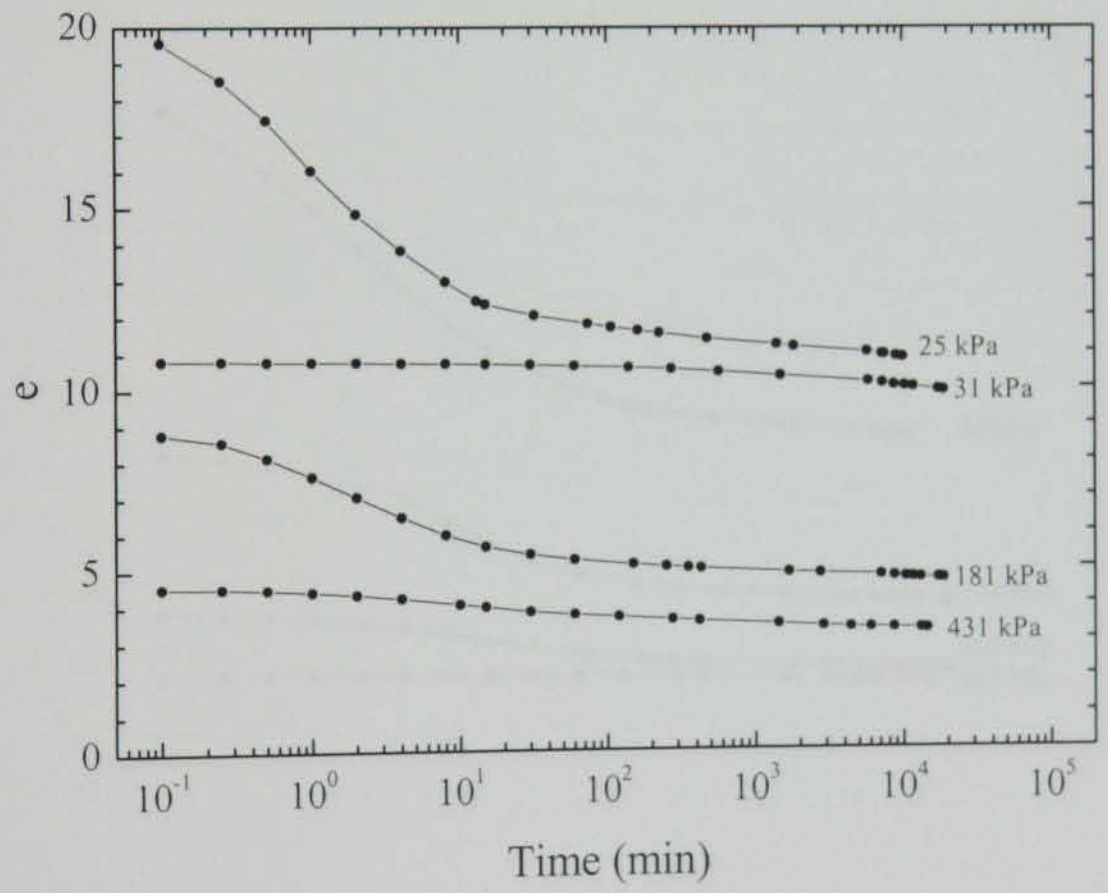

Figure A.24 e – log t data for CL_MSL_12

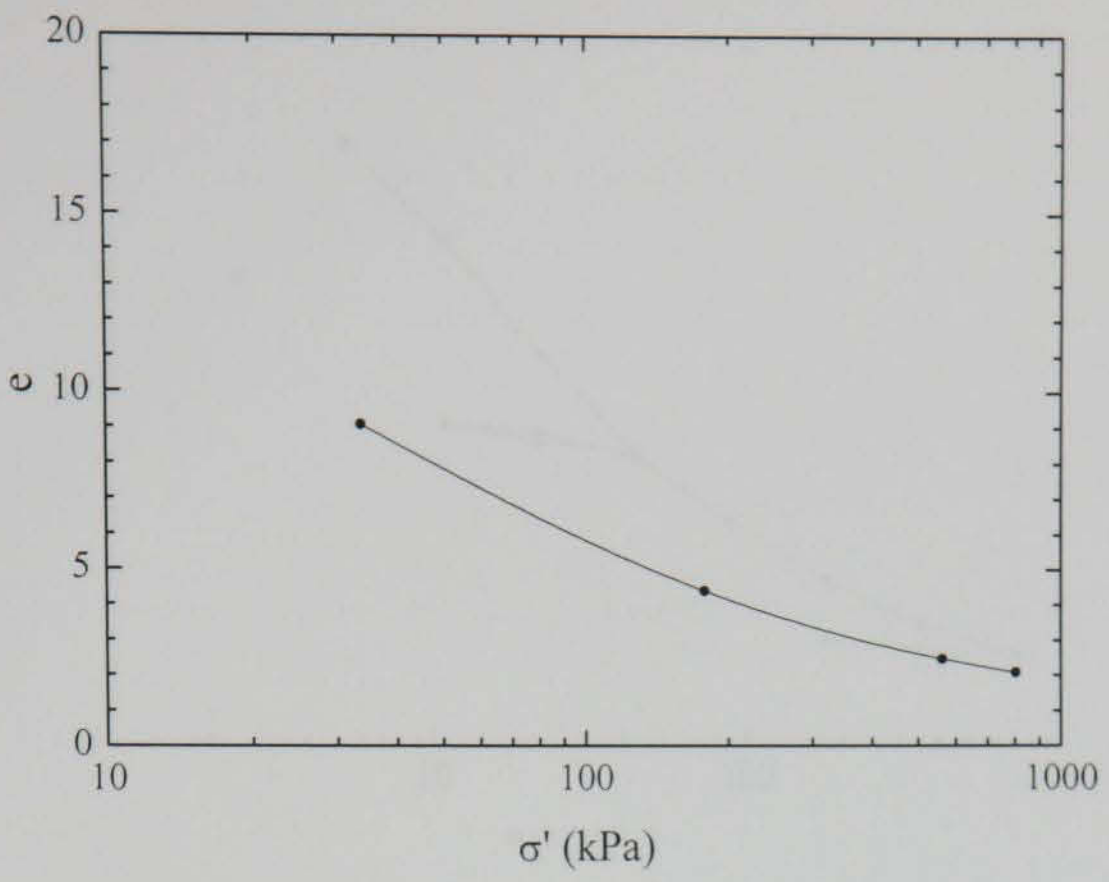

Figure A.25 e – log σ' data for CL_MSL_13

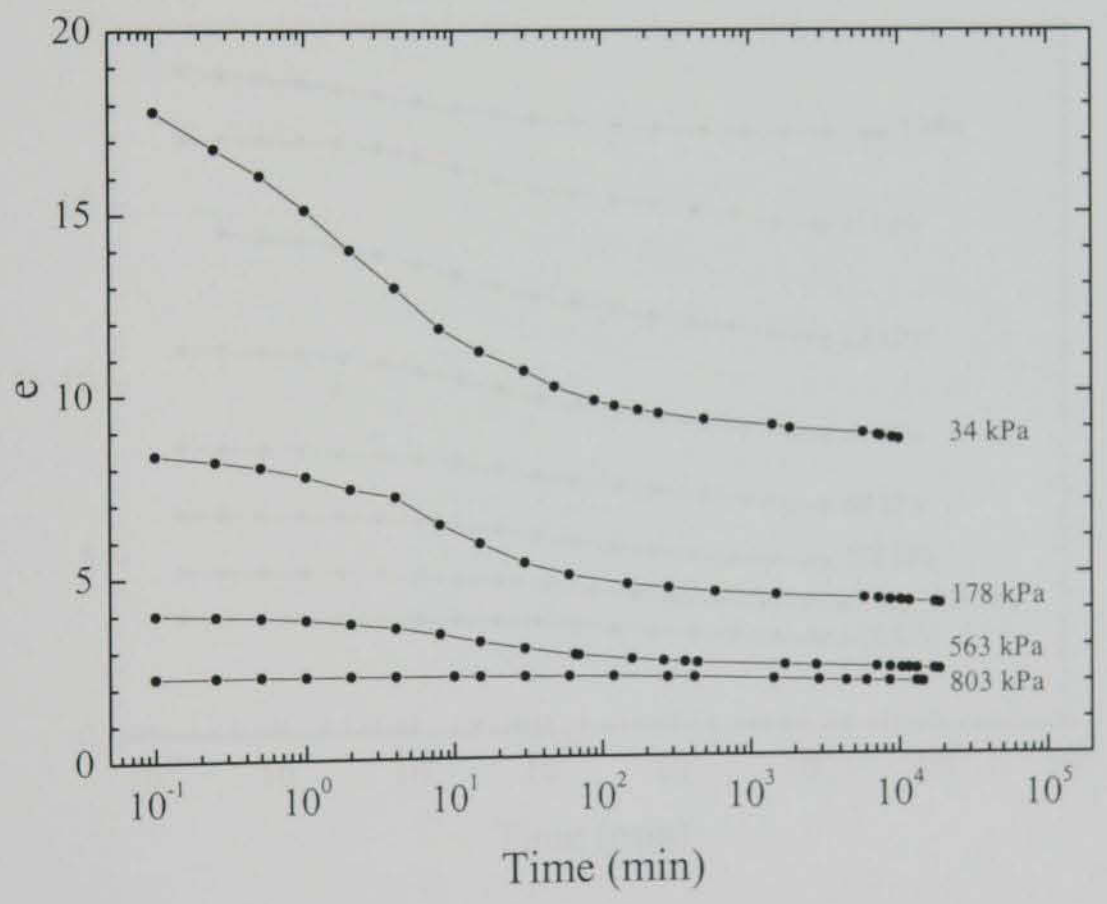

Figure A.26 e – log t data for CL_MSL_13

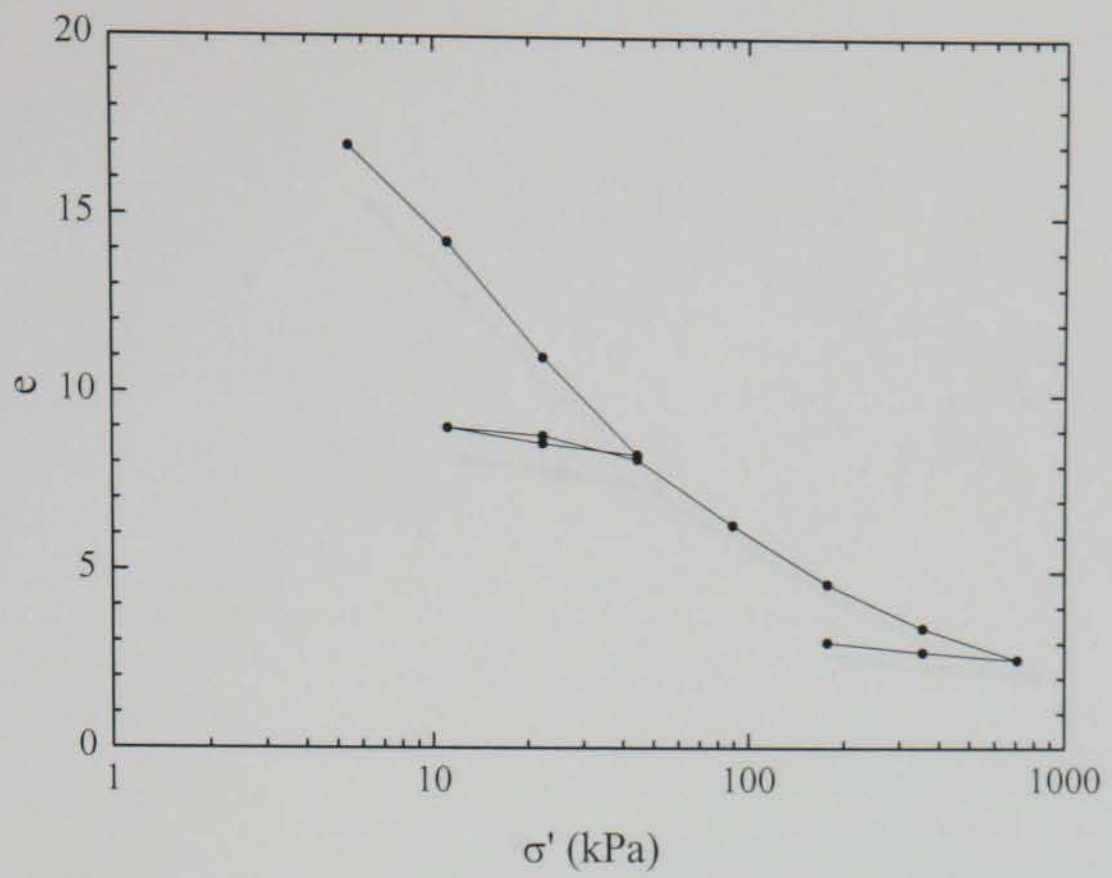

Figure A.27 e – log σ' data for CL_MSL_14

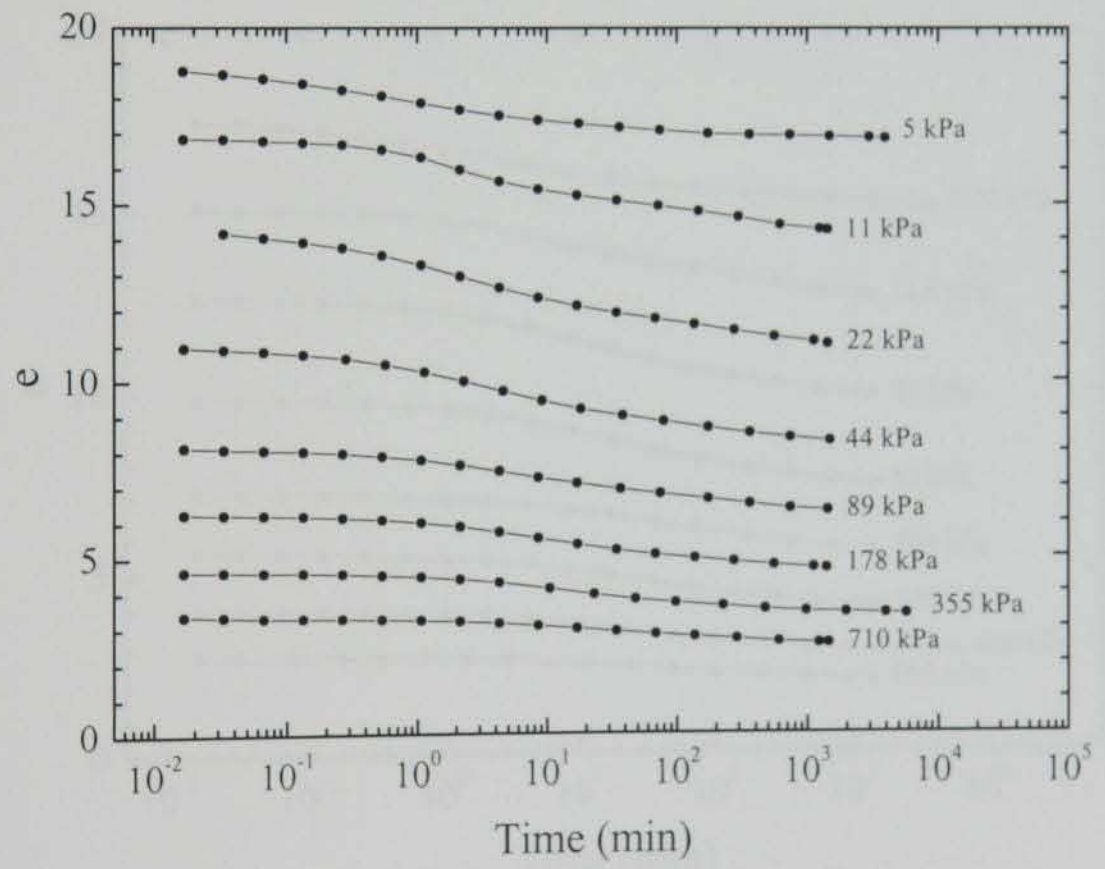

Figure A.28 e – log t data for CL_MSL_14

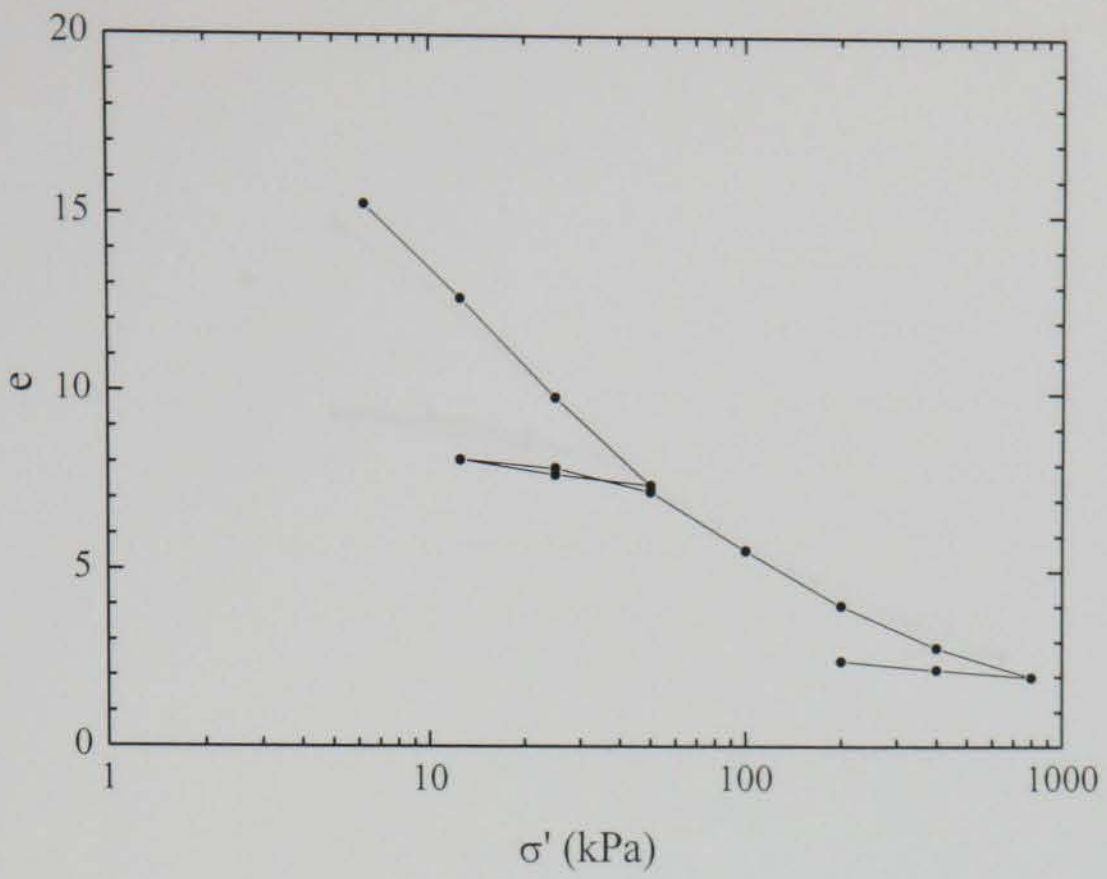

Figure A.29 e – log σ' data for CL_MSL_15

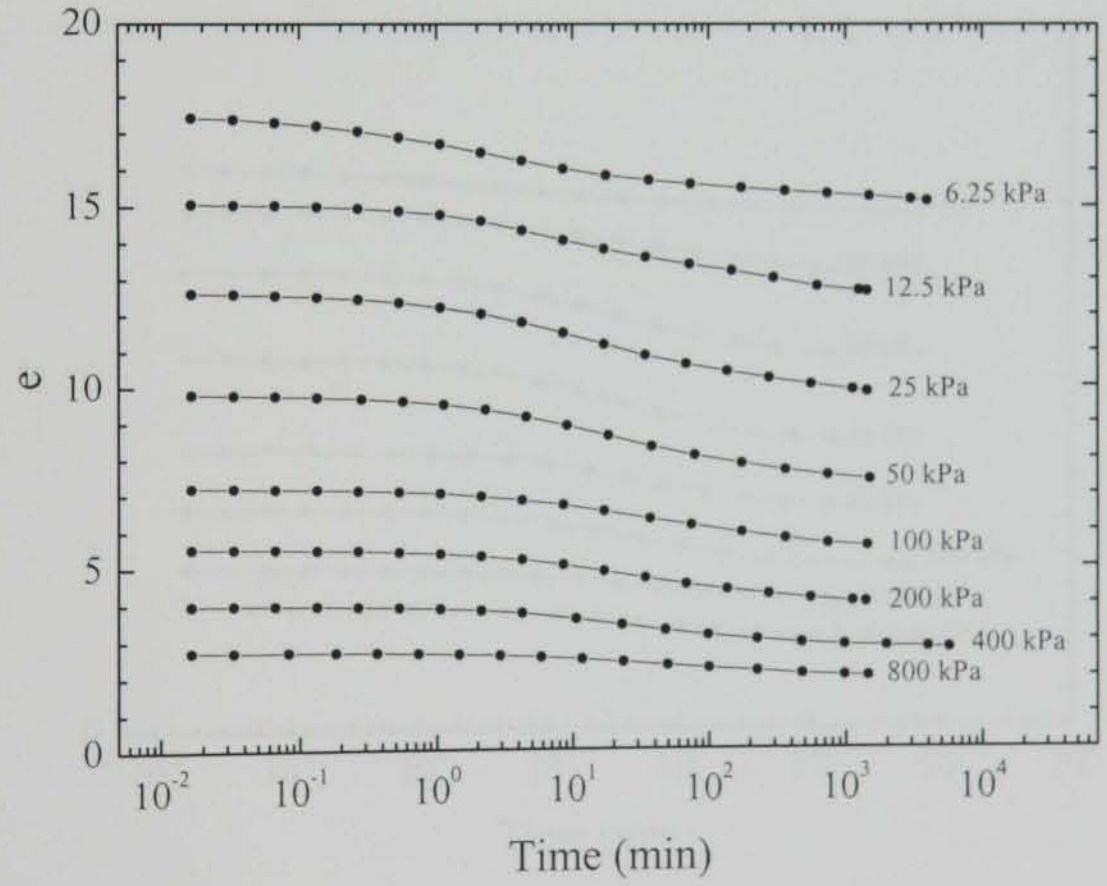

Figure A.30 e – log t data for CL_MSL_15

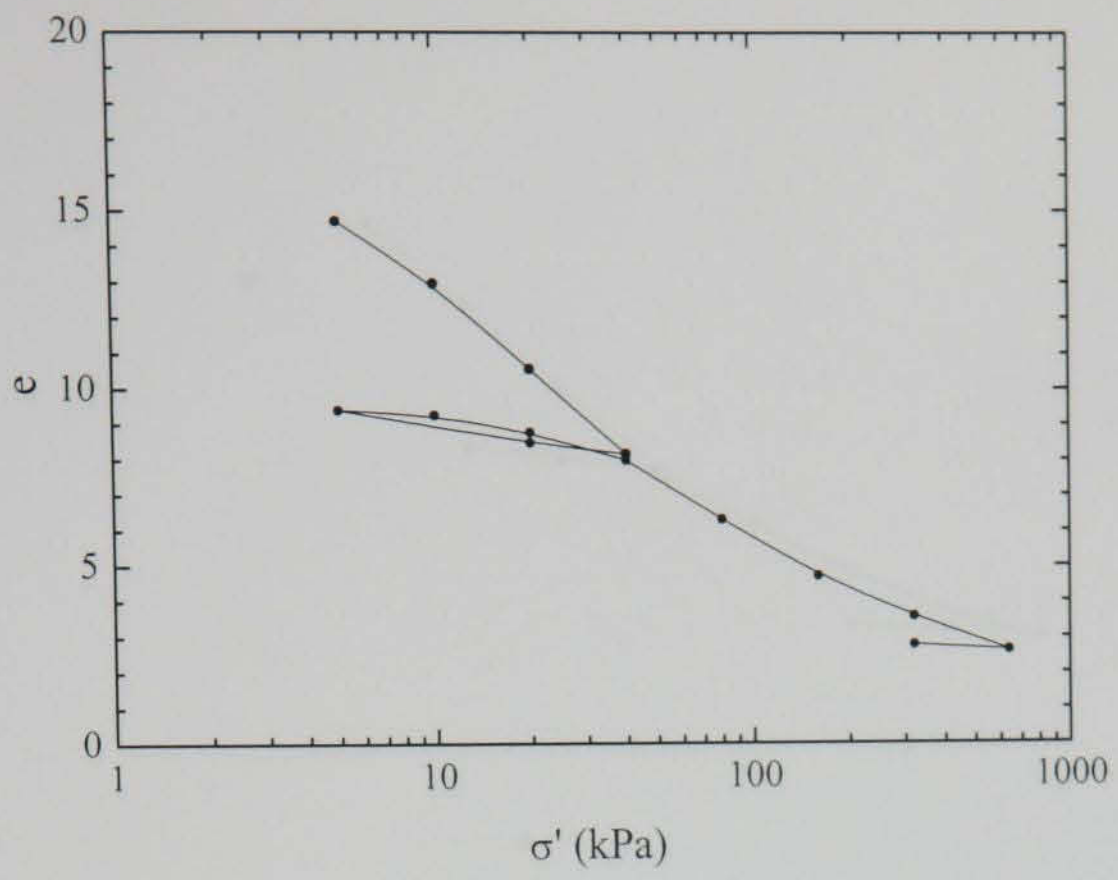

Figure A.31 e – log σ' data for CL_MSL_16

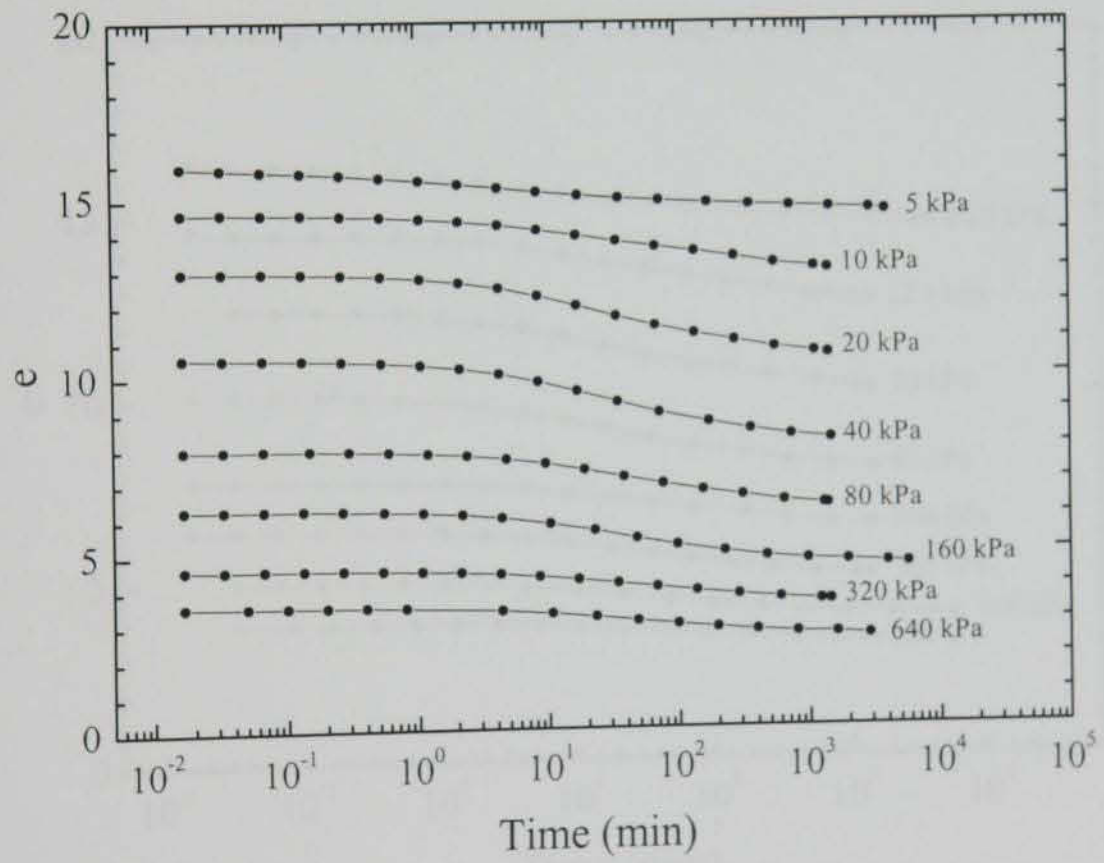

Figure A.32 e – log t data for CL_MSL_16

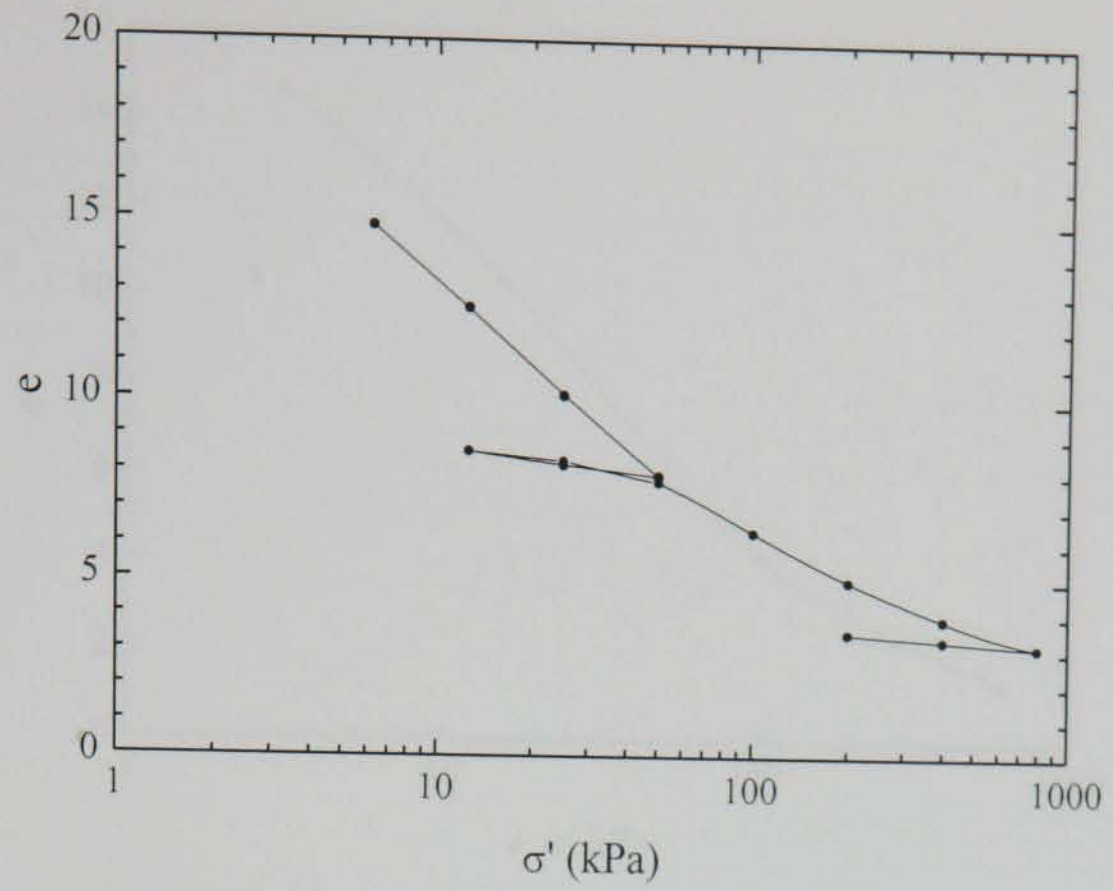

Figure A.33 e – log σ' data for CL_MSL_17

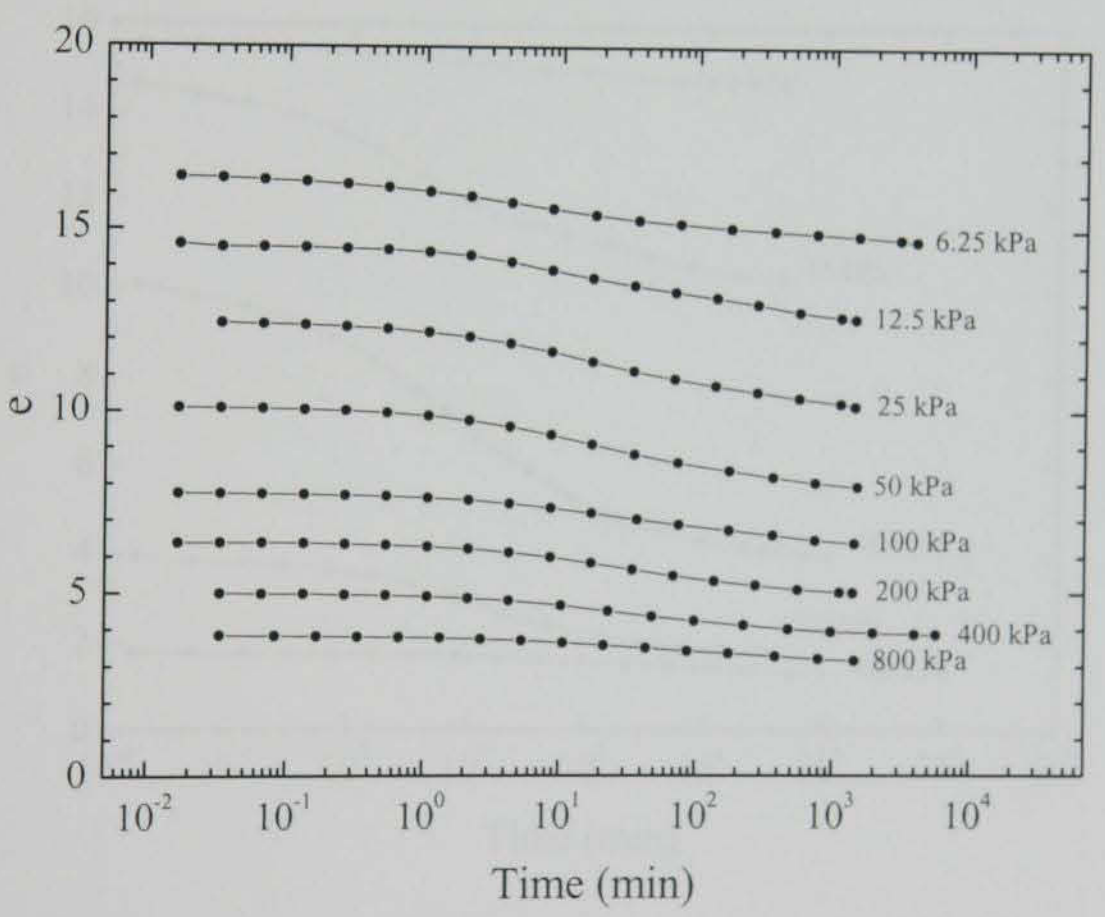

Figure A.34 e – log t data for CL_MSL_17

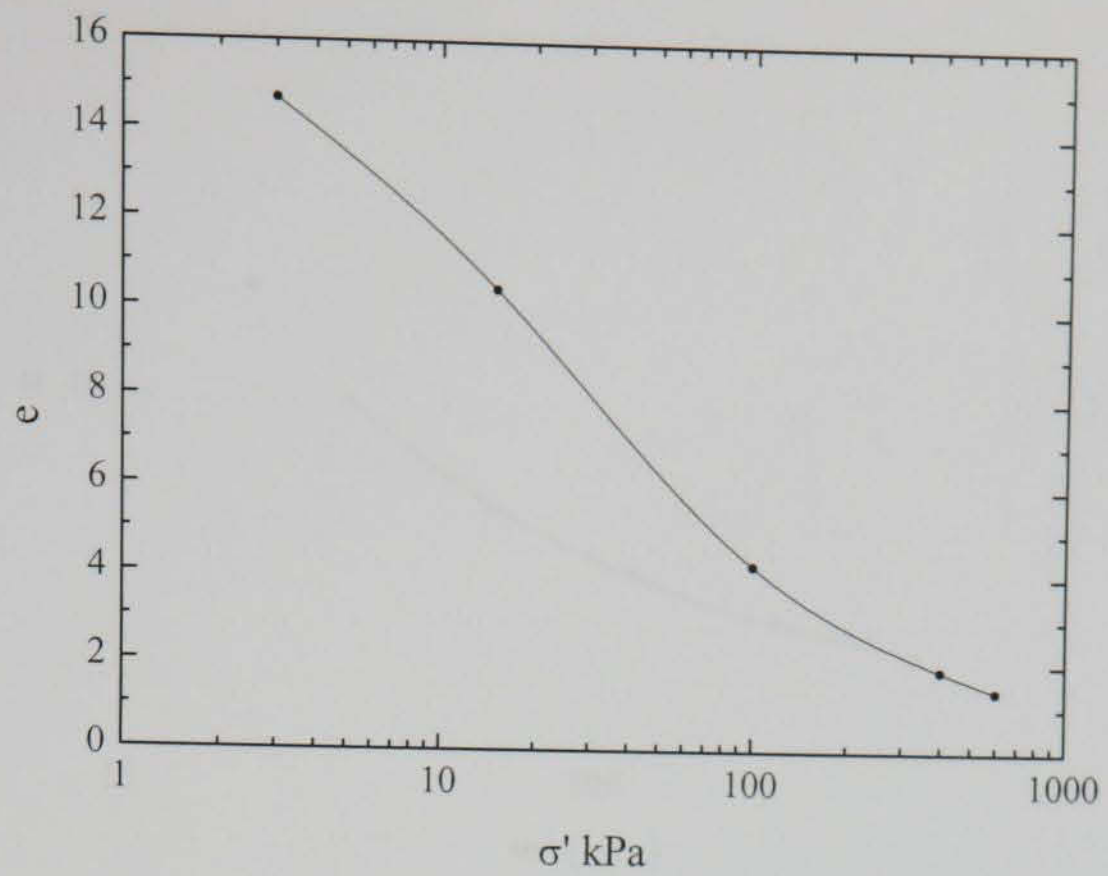

Figure A.35 e – log σ' data for CL_MSL_18

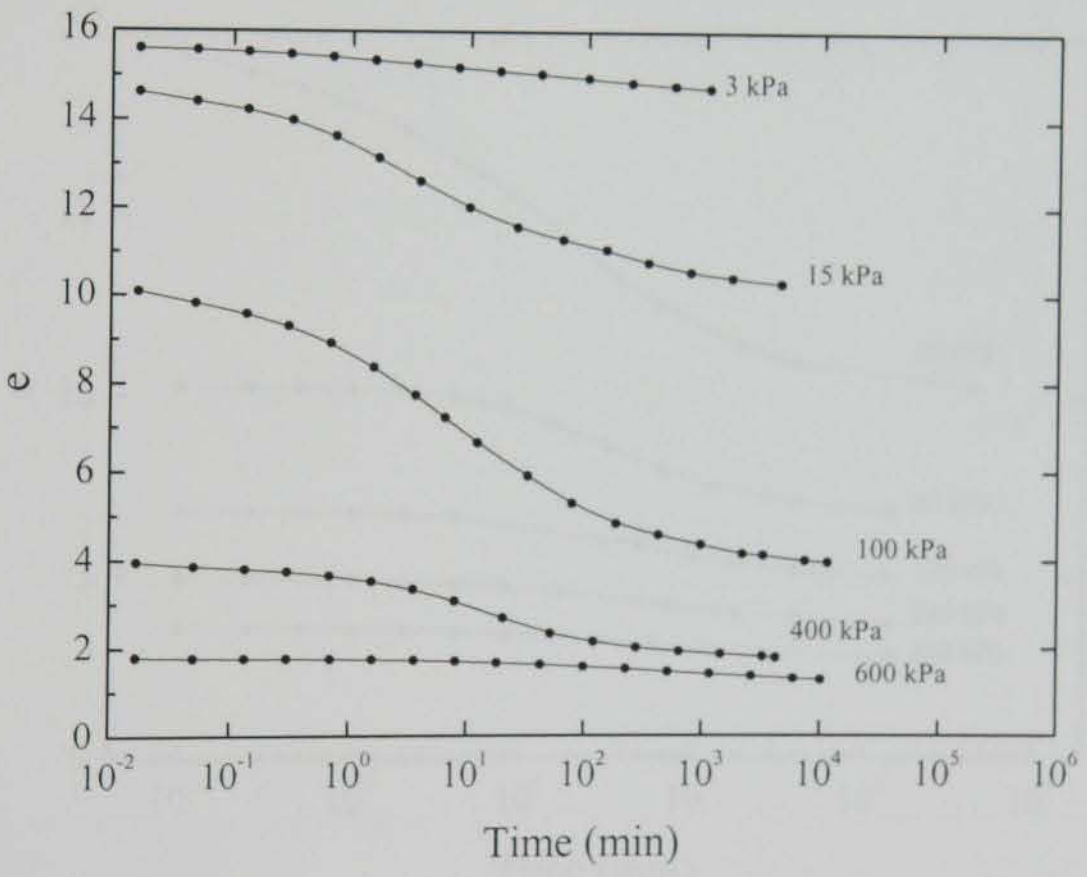

Figure A.36 e – log t data for CL_MSL_18

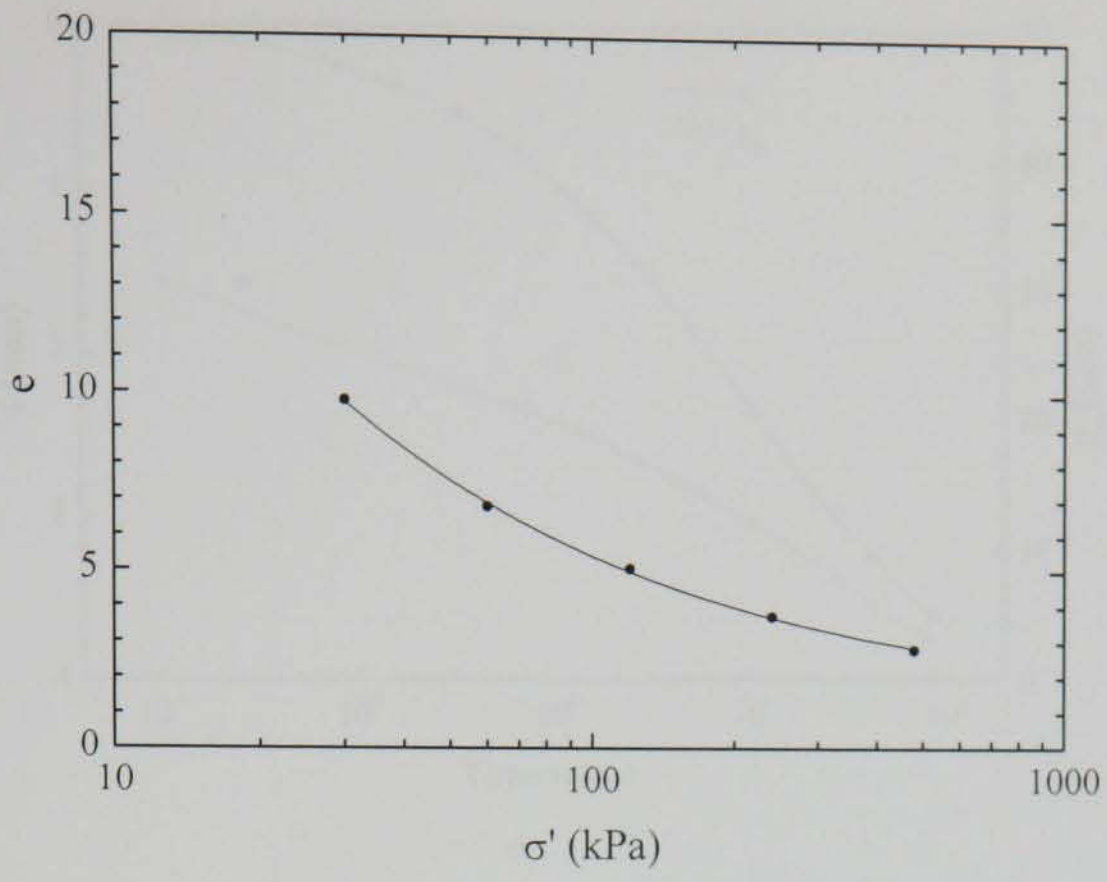

Figure A.37 e – log σ' data for CL_MSL_19

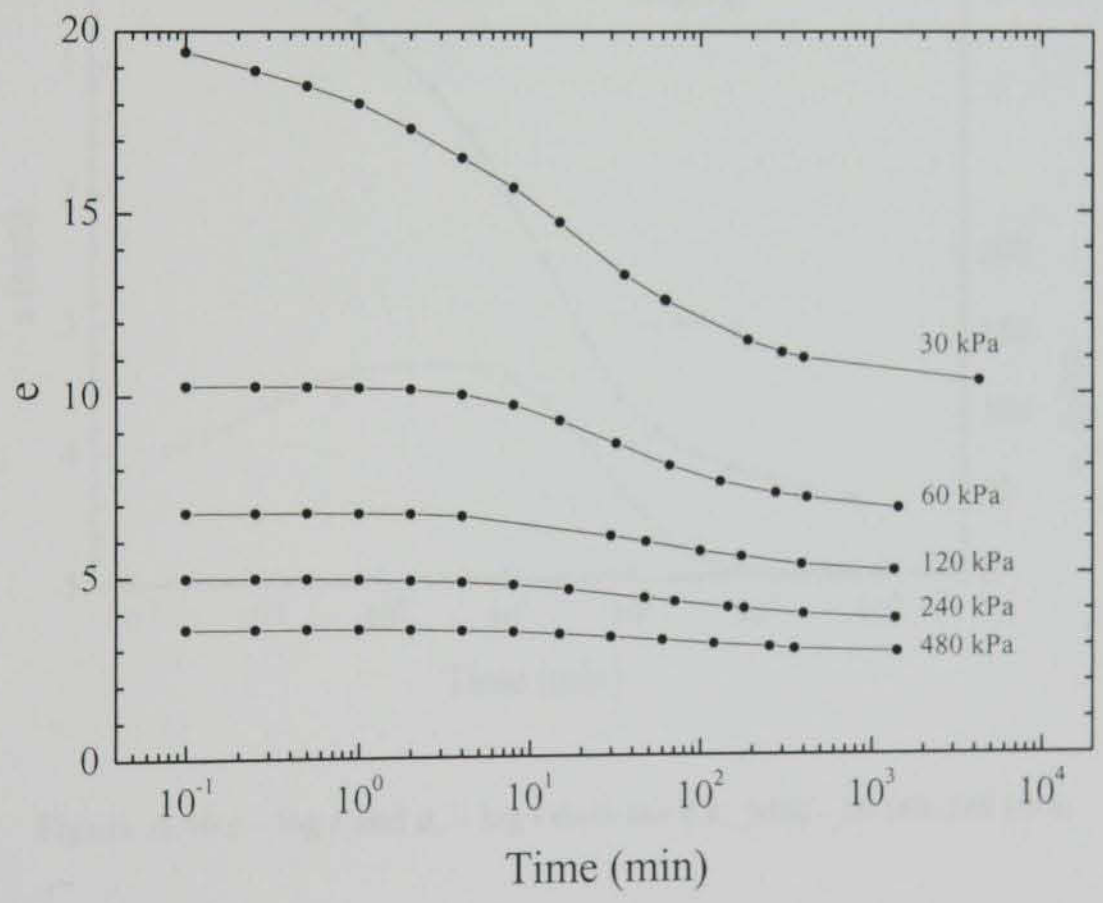

Figure A.38 e – log t data for CL_MSL_19

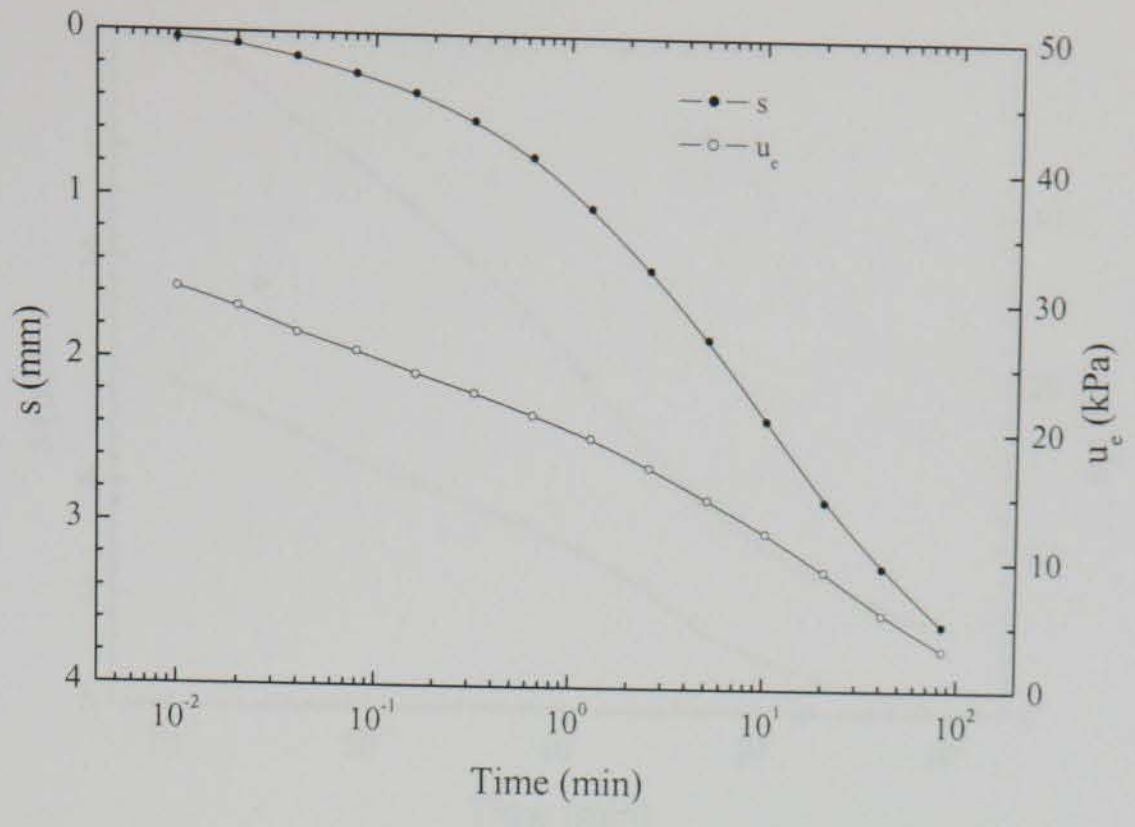

Figure A.39 s – log t and u_e – log t data for CL_MSL_20 (30-60 kPa)

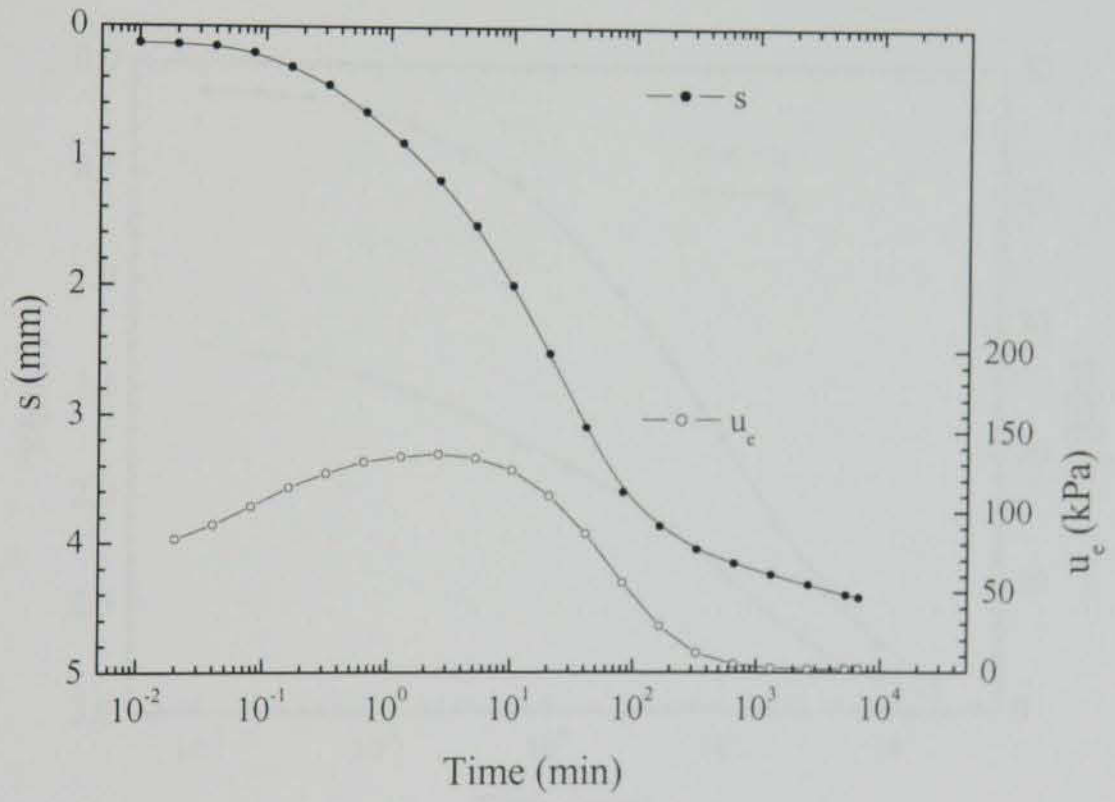

Figure A.40 s – log t and u_e – log t data for CL_MSL_20 (60-240 kPa)

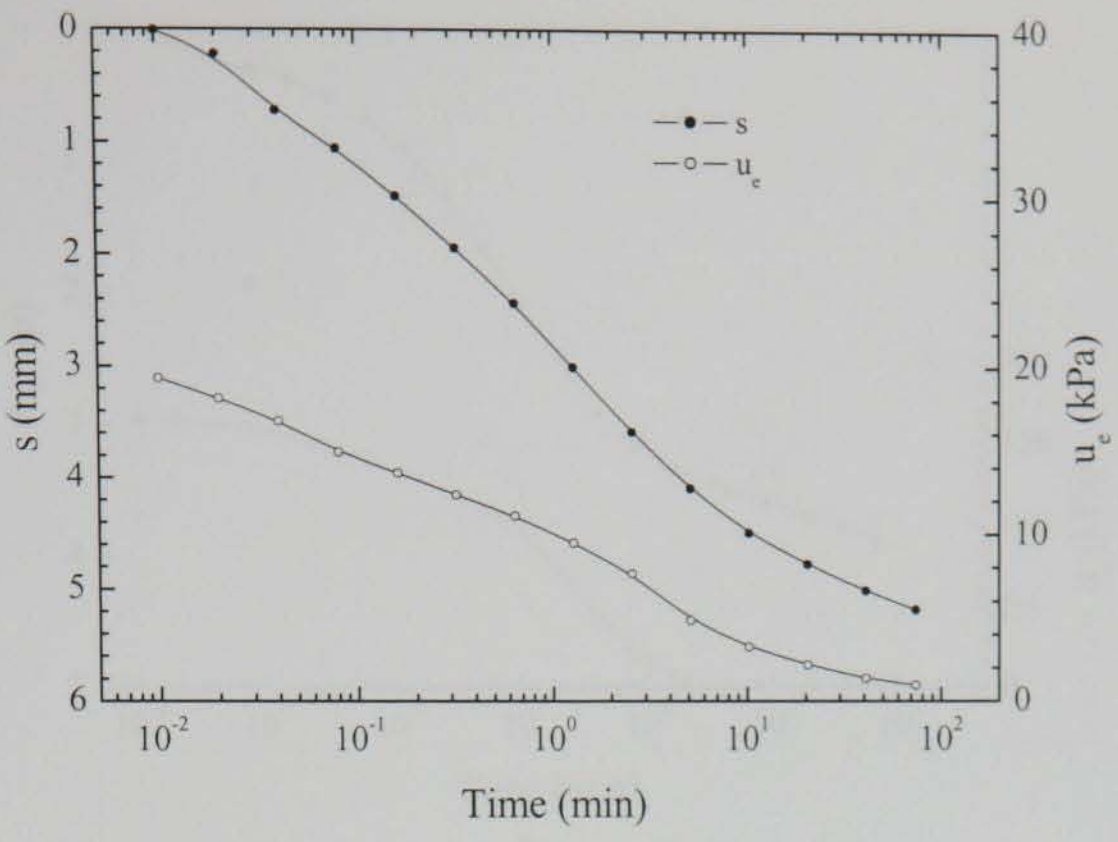

Figure A.41 s – log t and u_e – log t data for CL_MSL_21 (0-30 kPa)

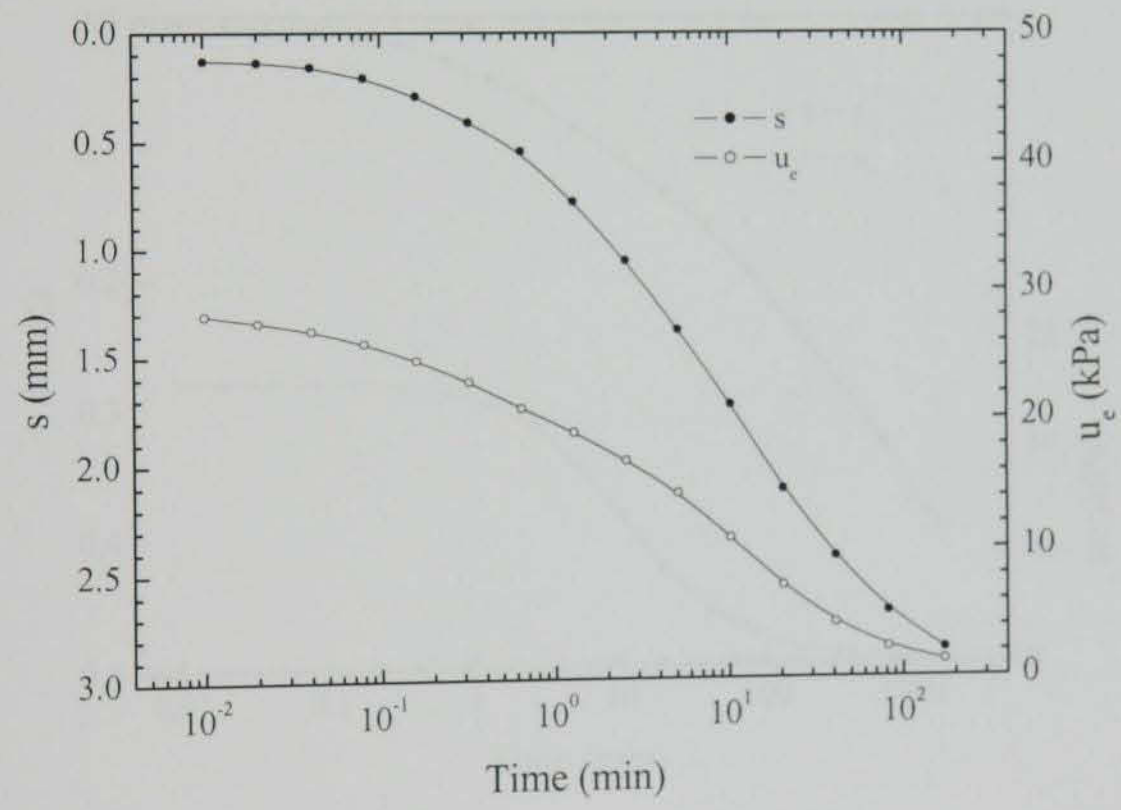

Figure A.42 s – log t and u_e – log t data for CL_MSL_21 (30-60 kPa)

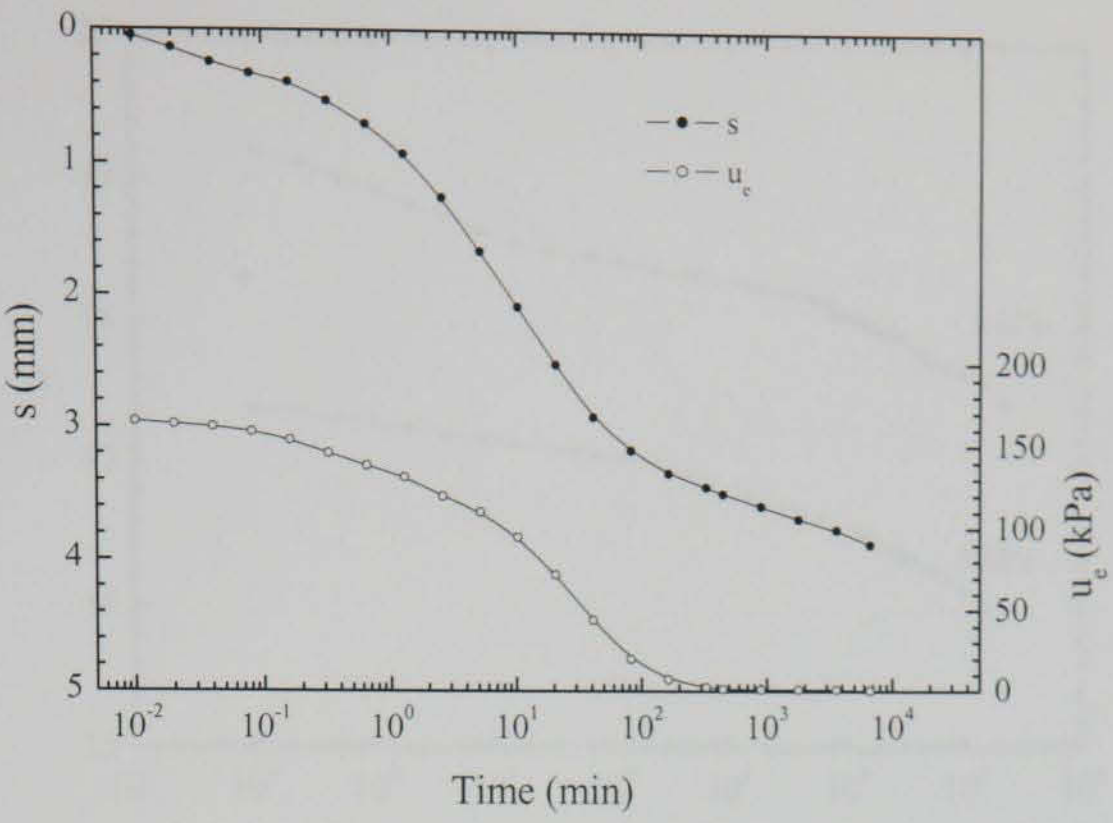

Figure A.43 s – log t and u_e – log t data for CL_MSL_21 (60-240 kPa)

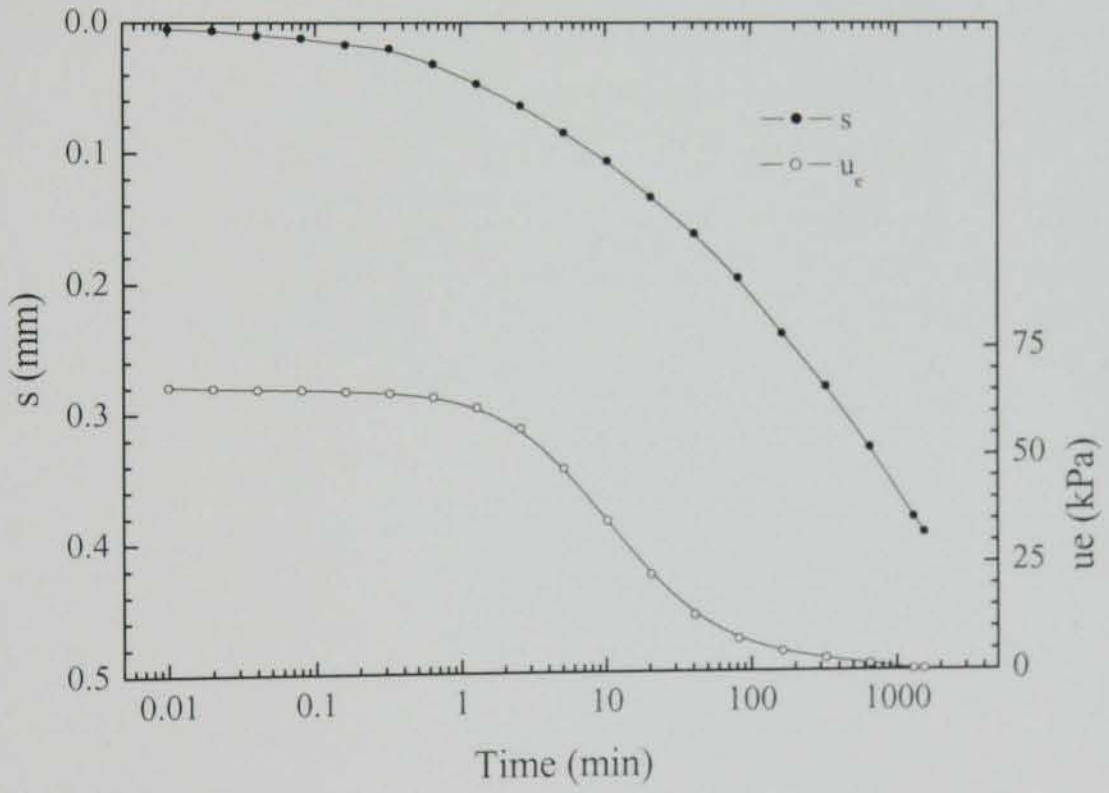

Figure A.44 s – log t and u_e – log t data for CL_MSL_21 (240-300 kPa)

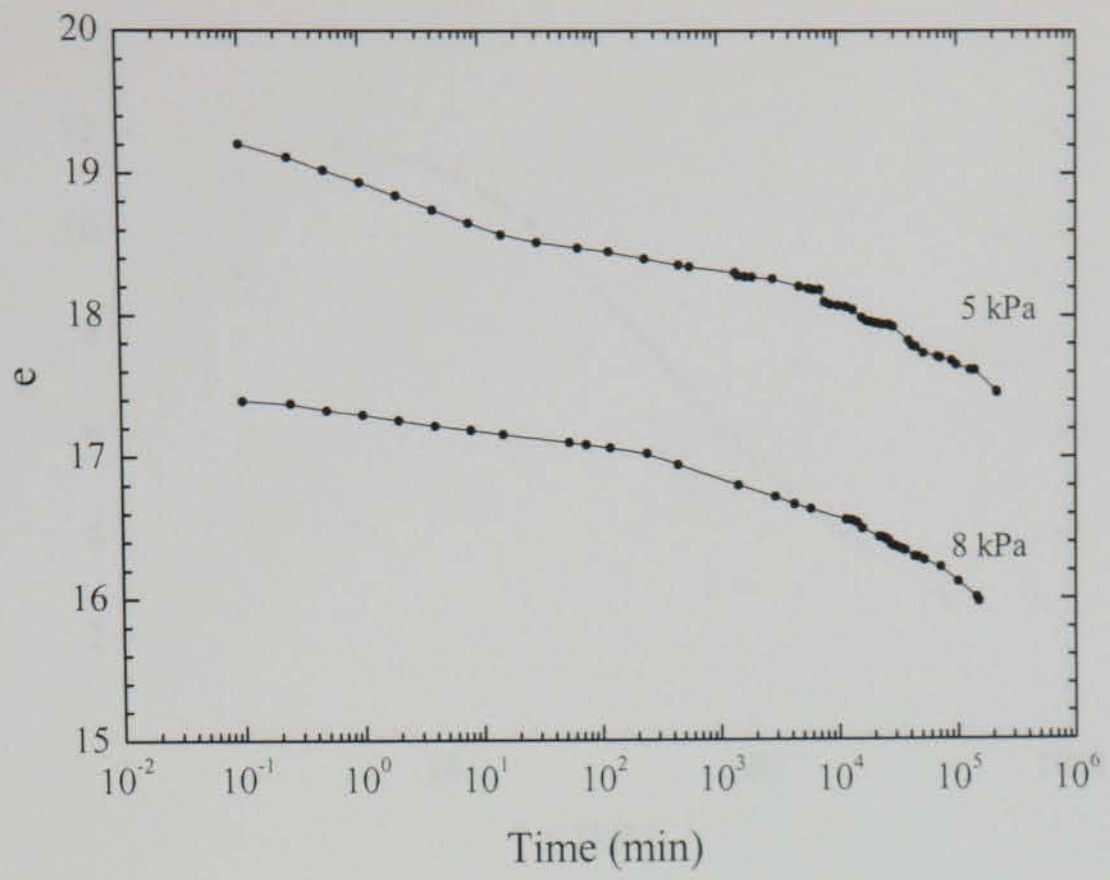

Figure A.45 e – log t data for CL_MSL_22

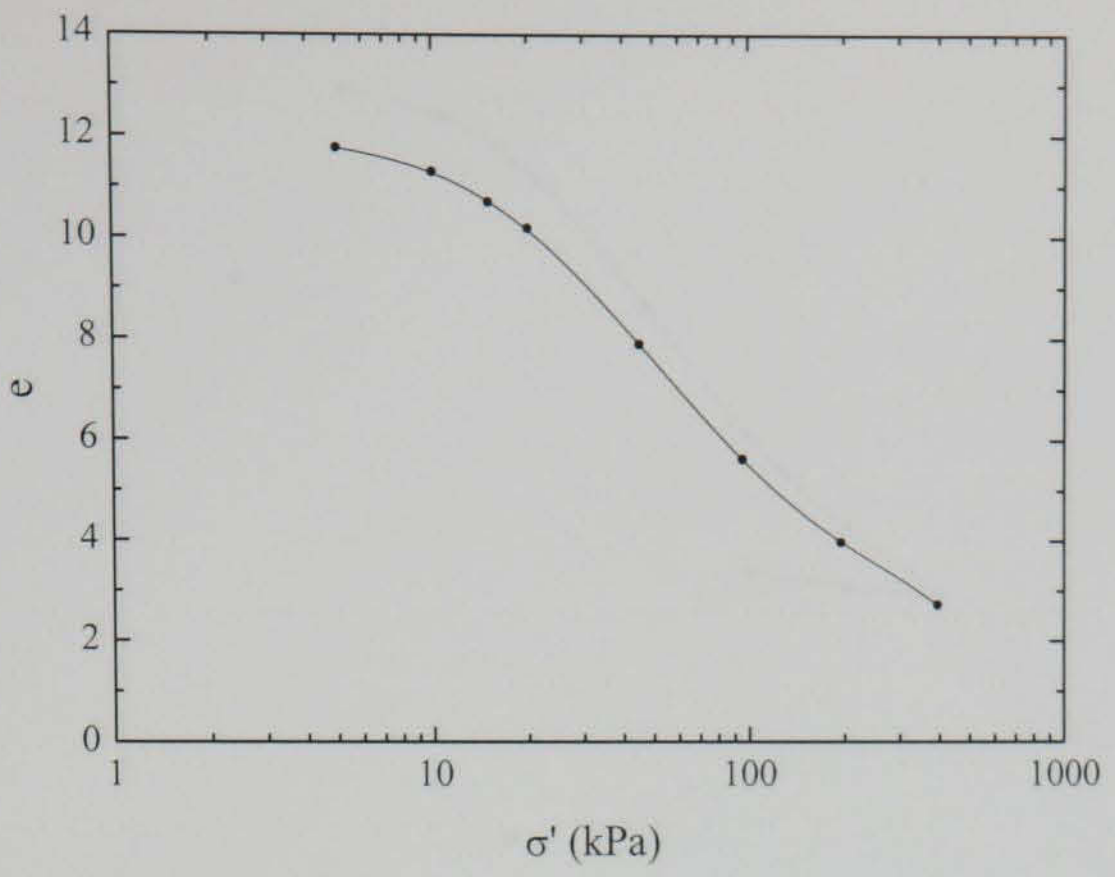

Figure A.46 e – log σ' data for BD_MSL_01

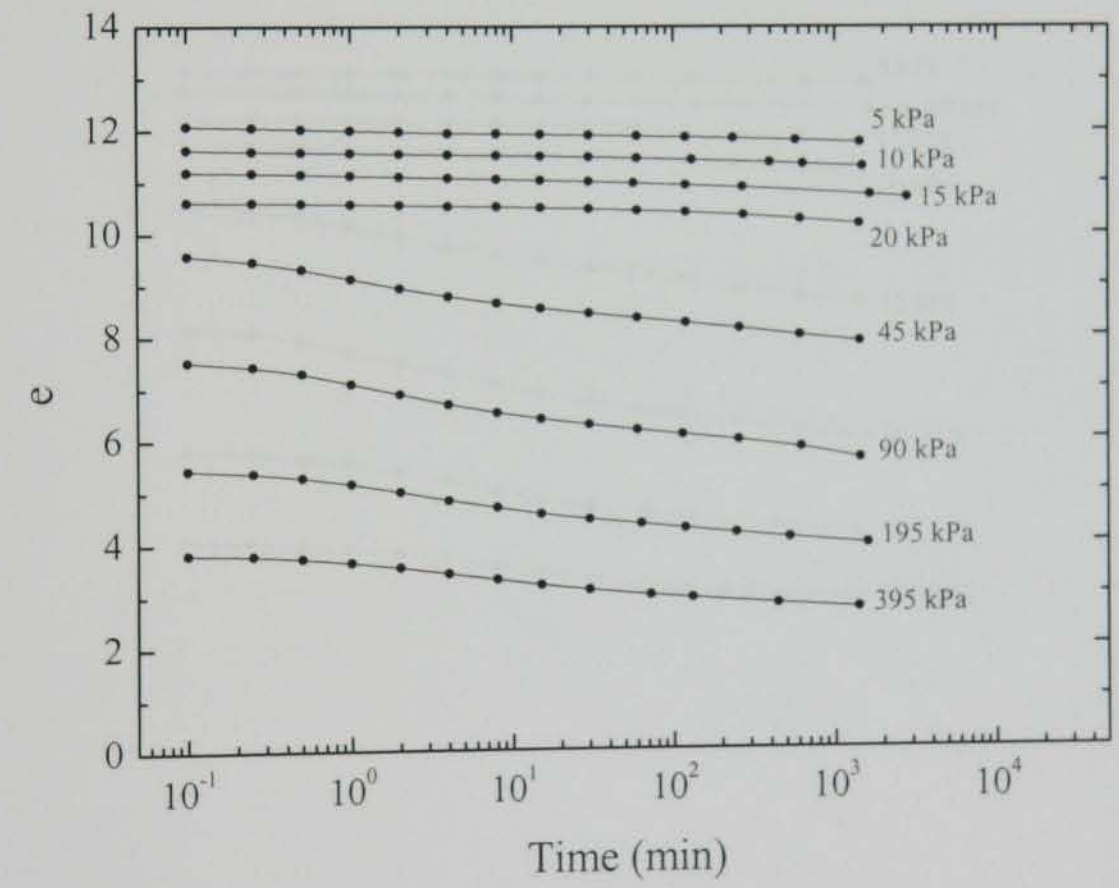

Figure A.47 e – log t data for BD_MSL_01

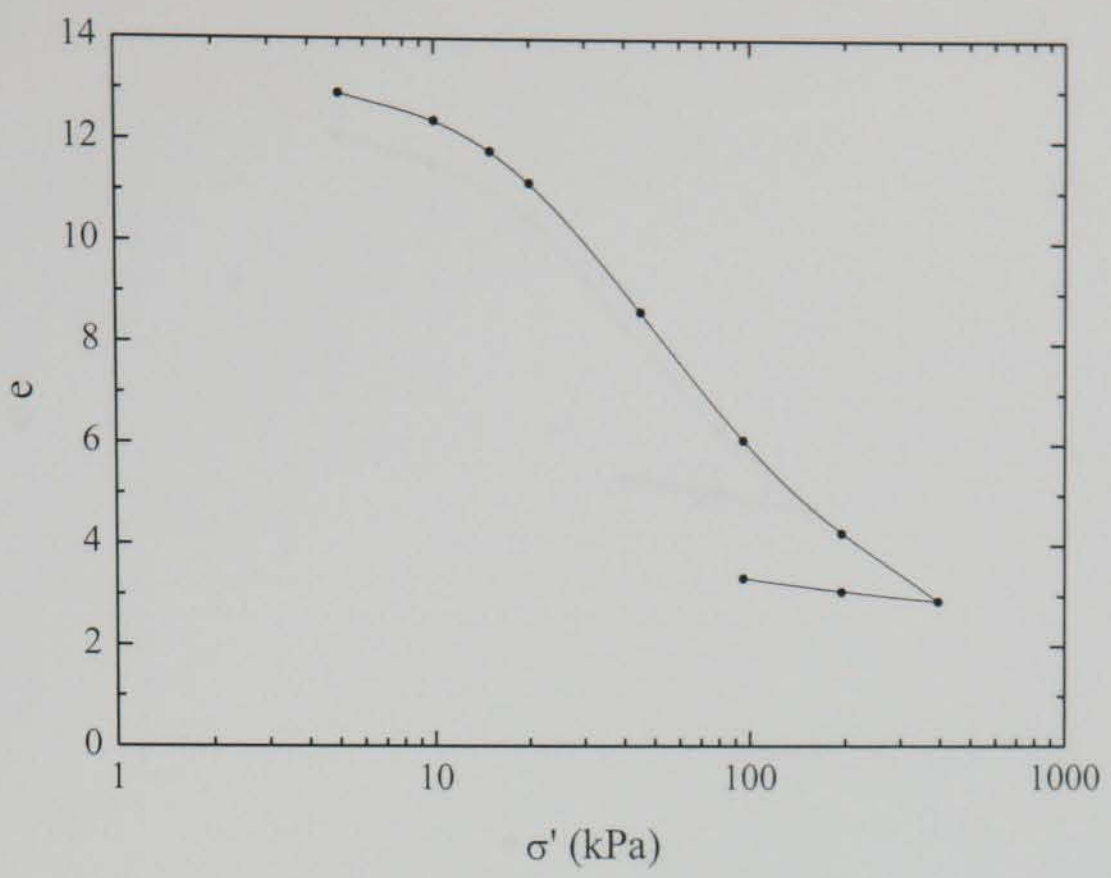

Figure A.48 e – log σ' data for BD_MSL_02

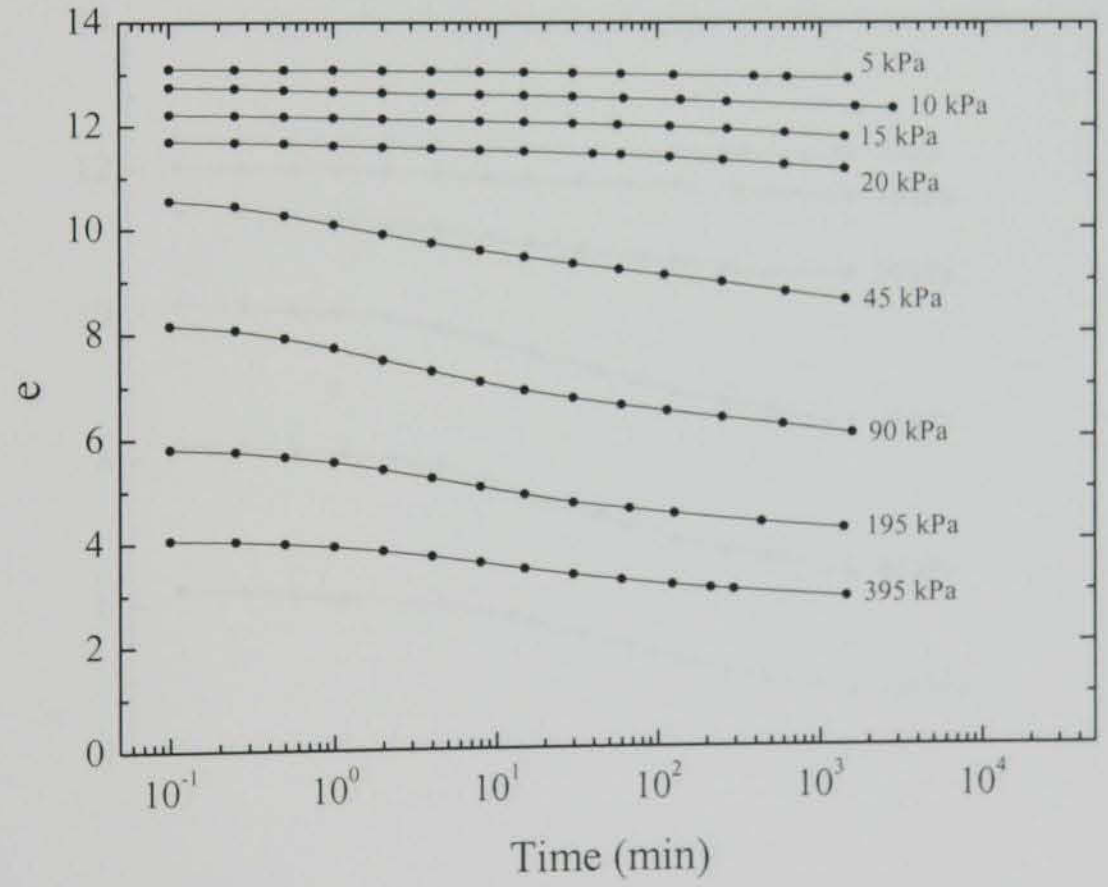

Figure A.49 e – log t data for BD_MSL_02

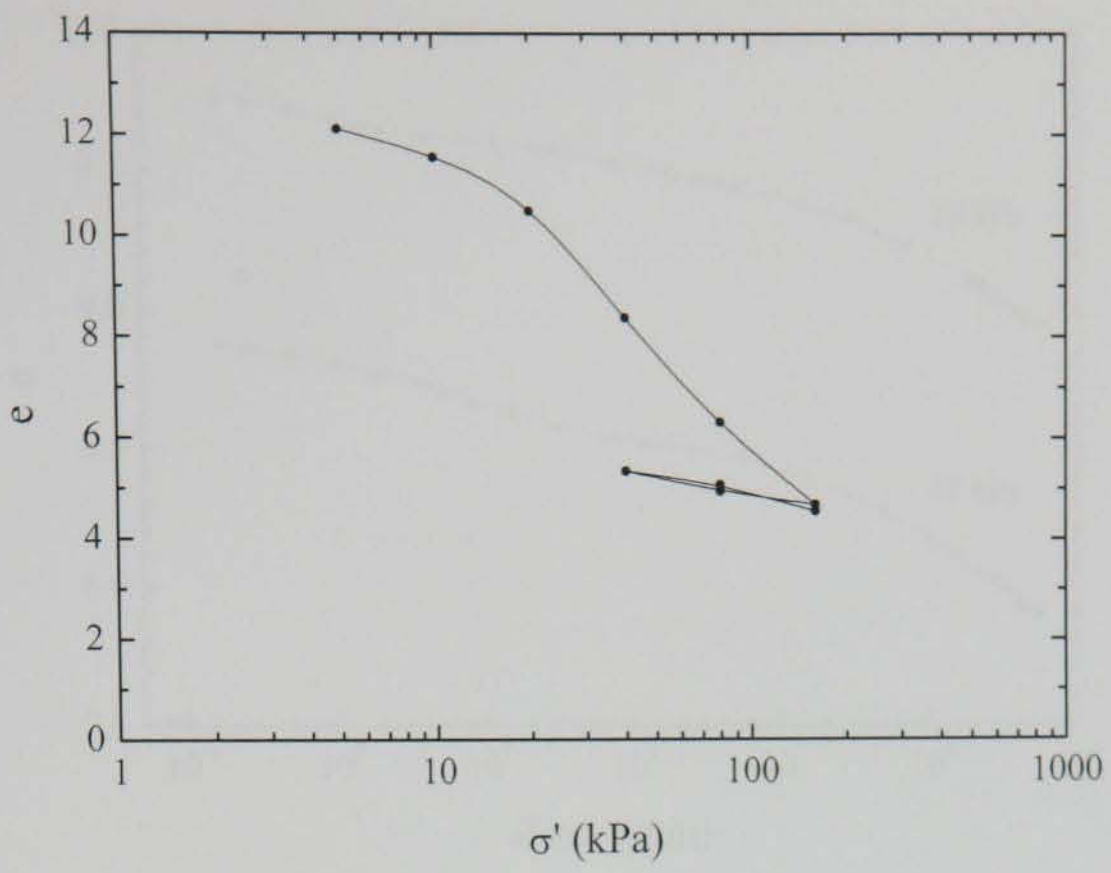

Figure A.50 e – log σ' data for BD_MSL_03

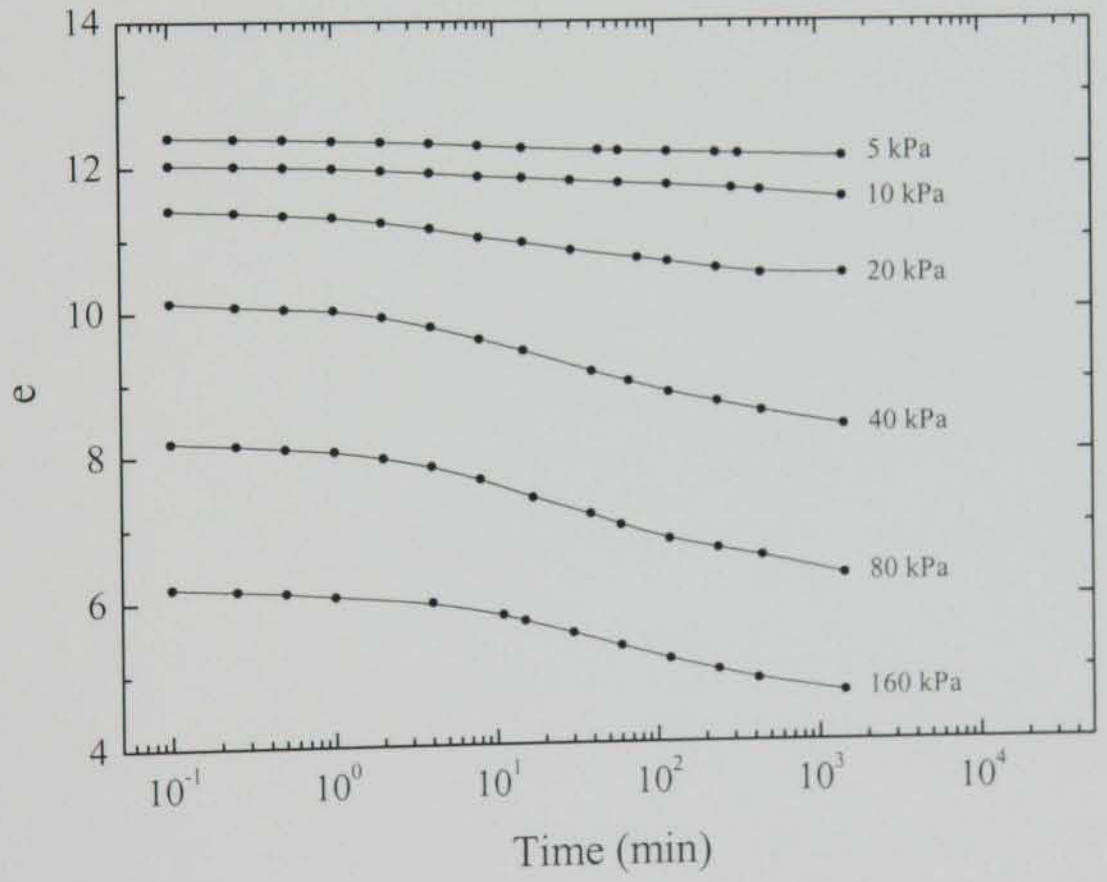

Figure A.51 e – log t data for BD_MSL_03

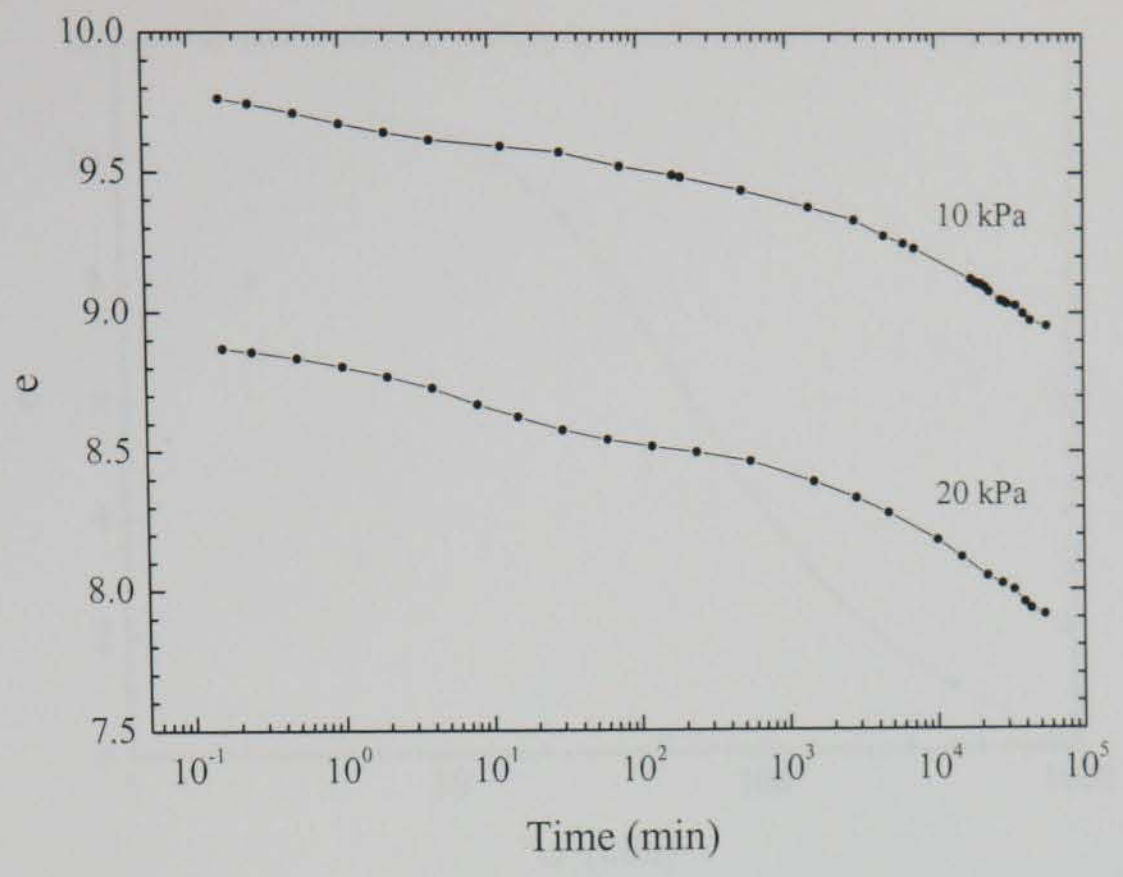

Figure A.52 e – log t data for BD_MSL_04

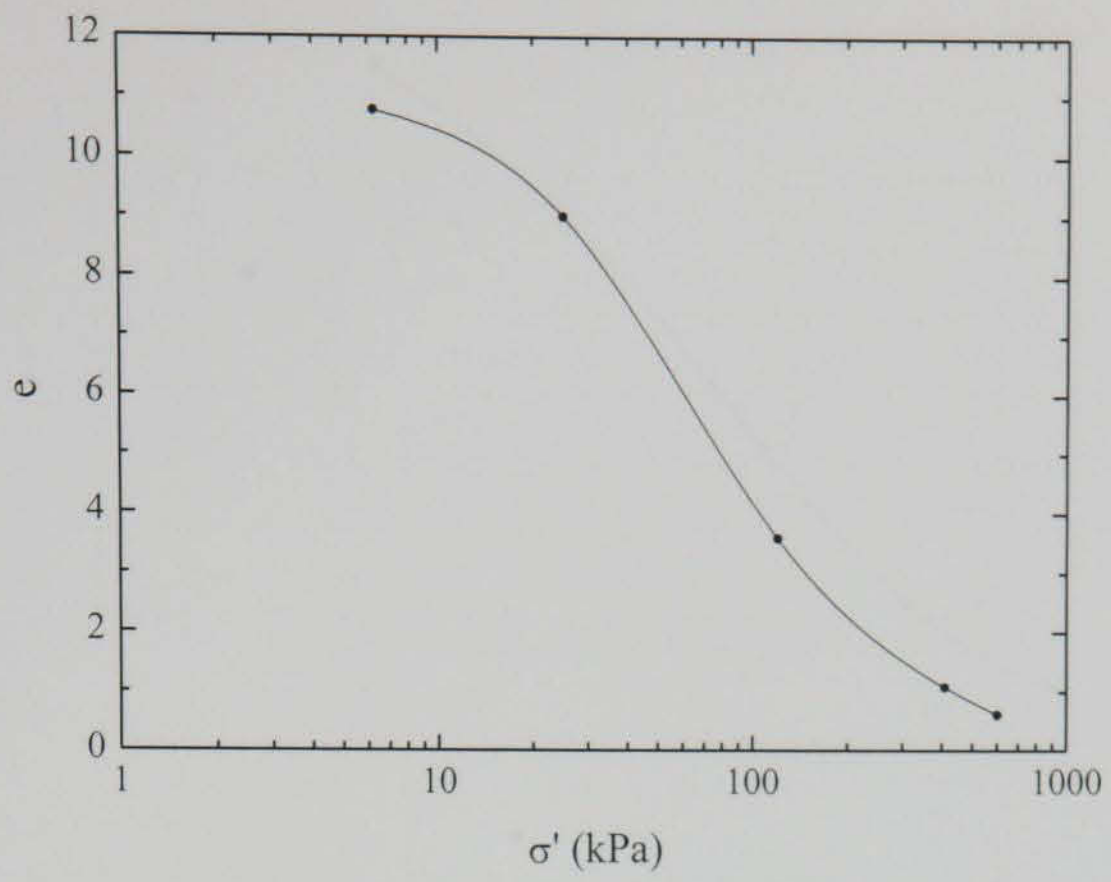

Figure A.53 e – log σ' data for BD_MSL_05

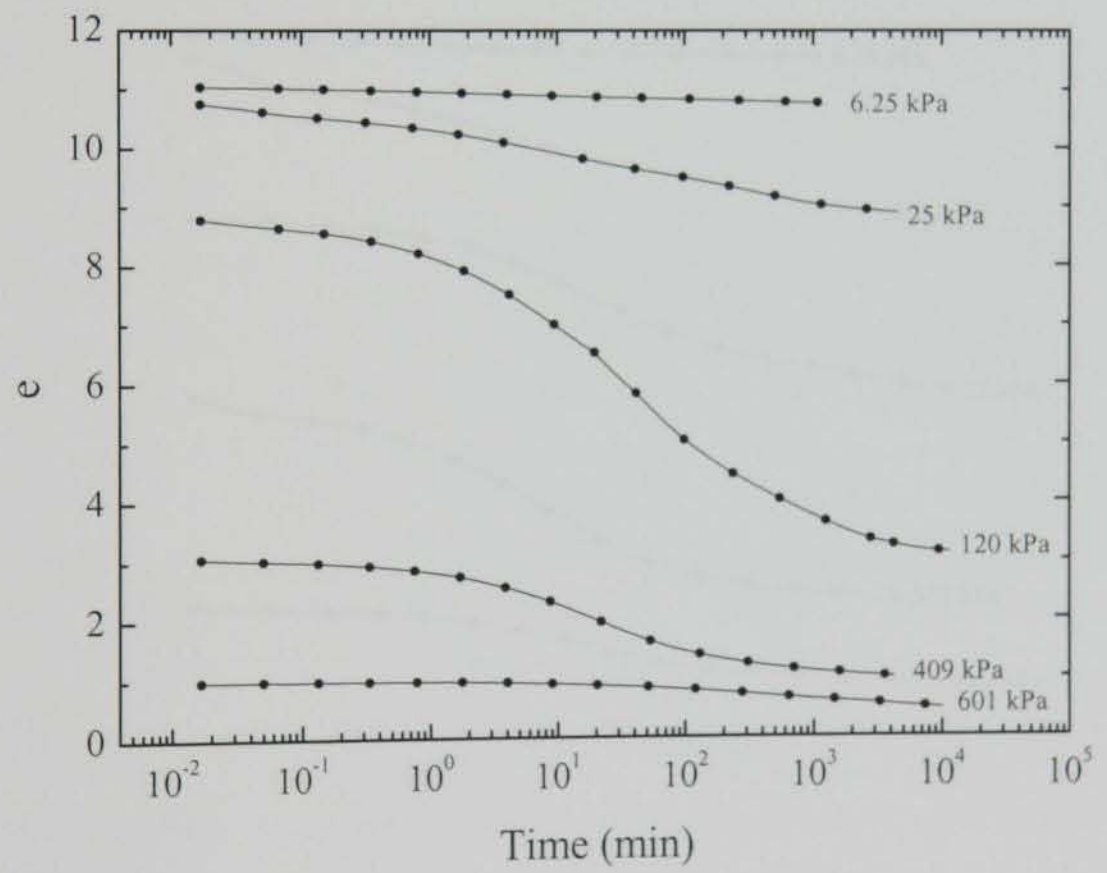

Figure A.54 e – log t data for BD_MSL_05

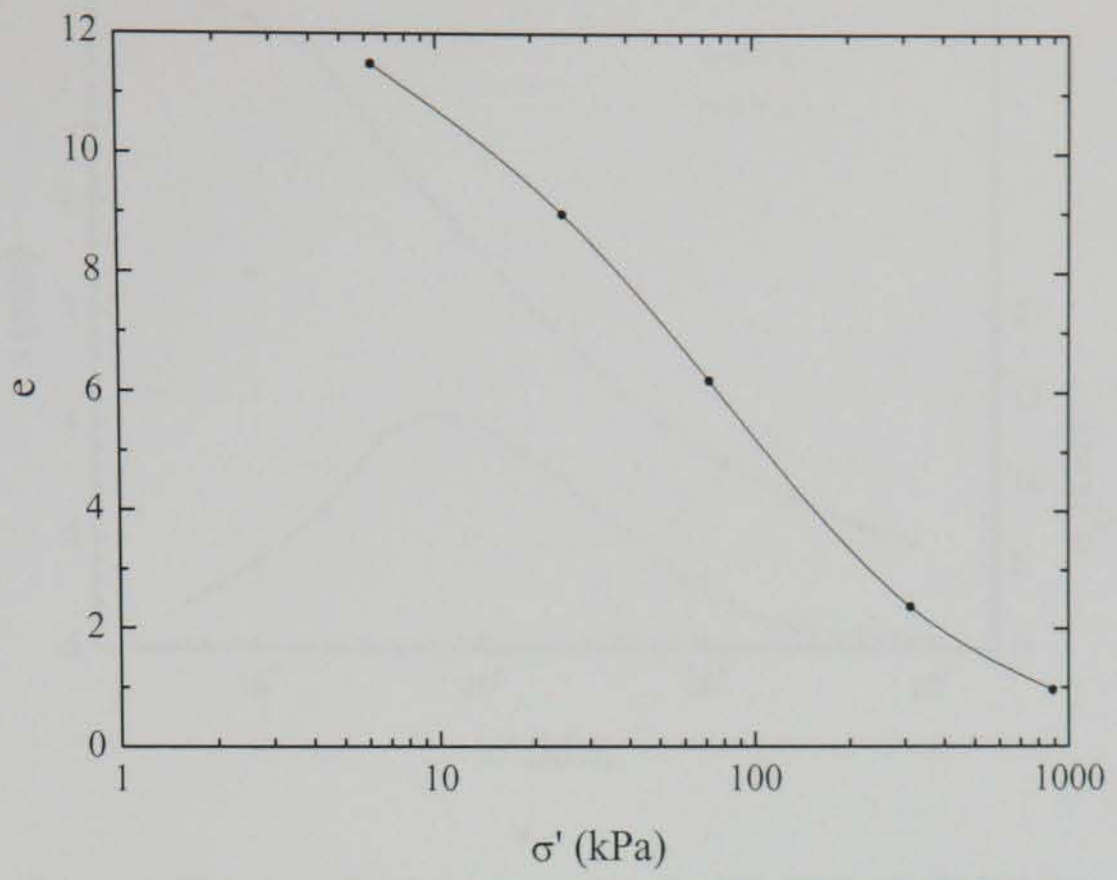

Figure A.55 e – log σ' data for BD_MSL_06

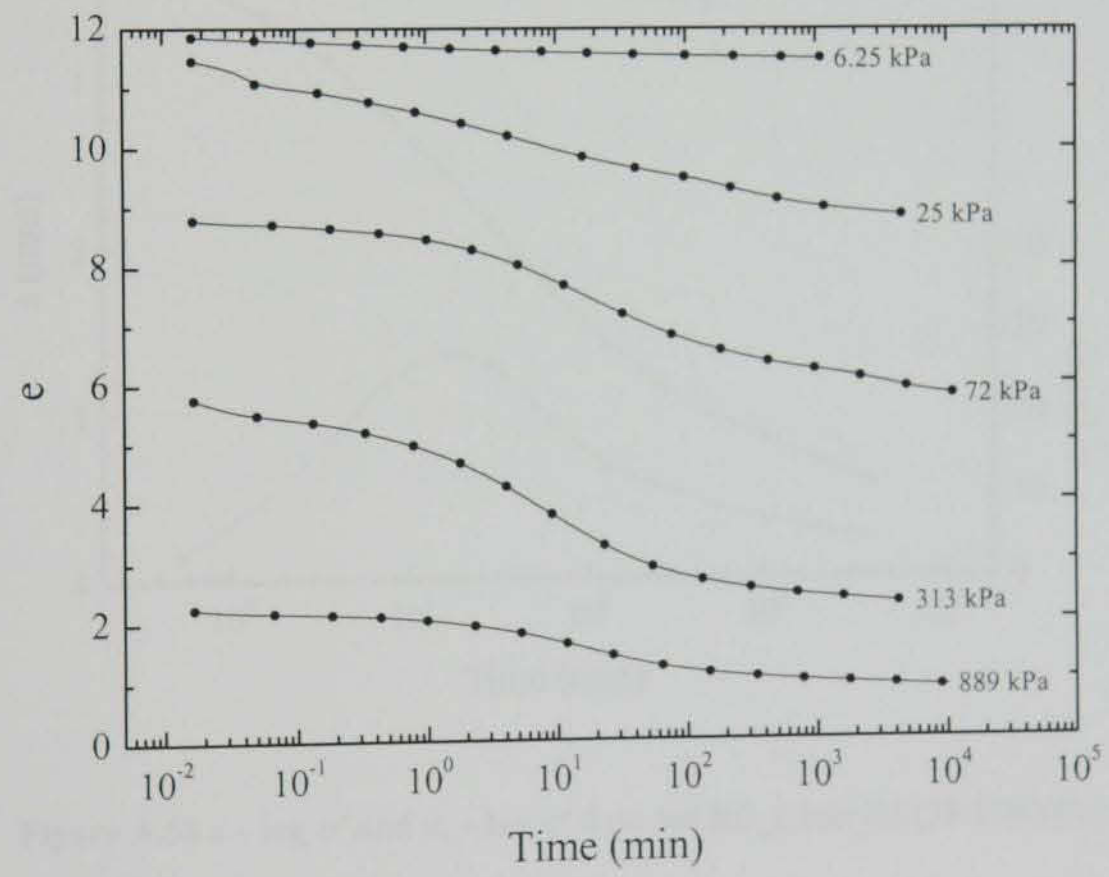

Figure A.56 e – log t data for BD_MSL_06

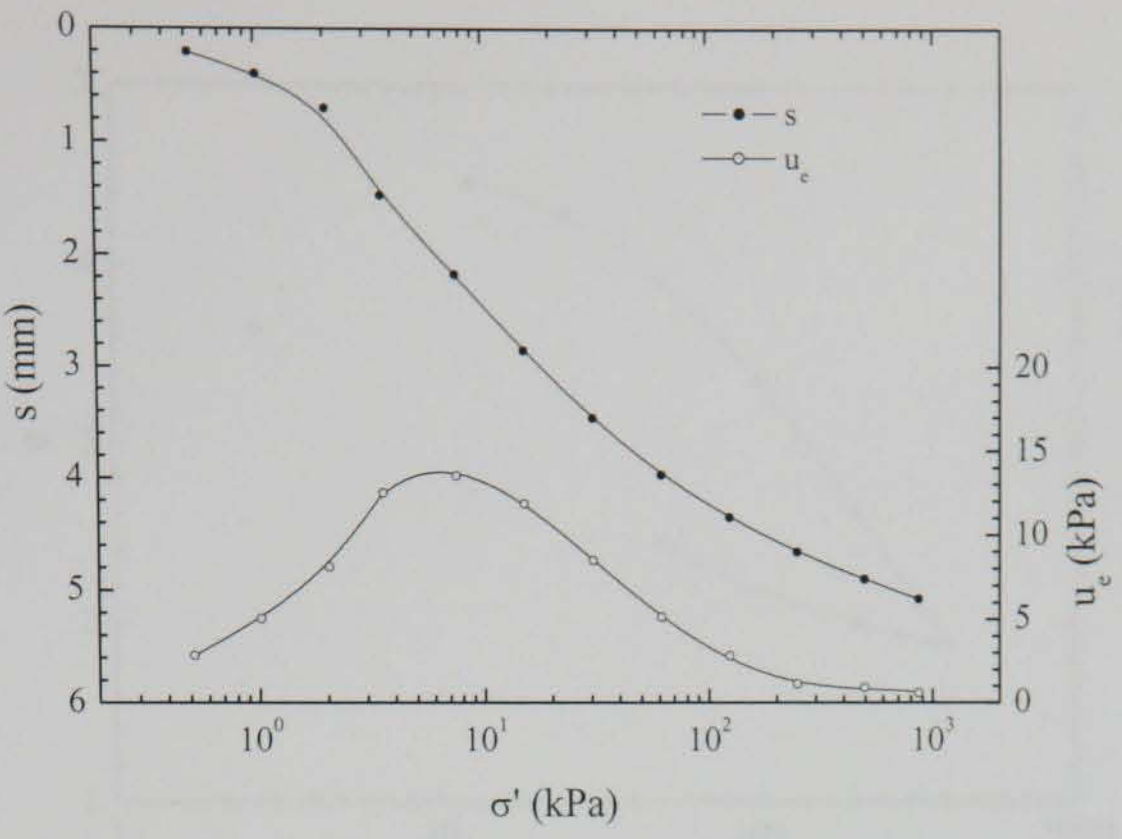

Figure A.57 s – log σ' and u_e – log σ' data for BD_CRD_01 (35-70 kPa)

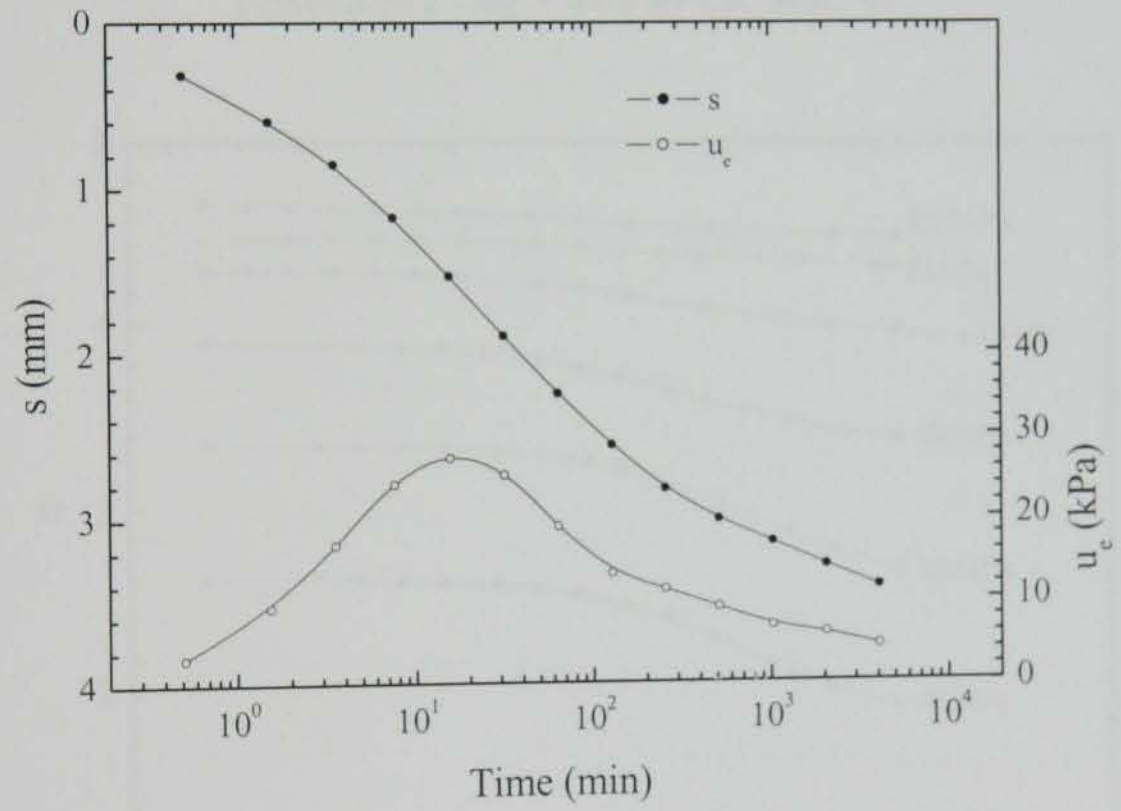

Figure A.58 s – log σ' and u_e – log σ' data for BD_CRD_01 (75-150 kPa)

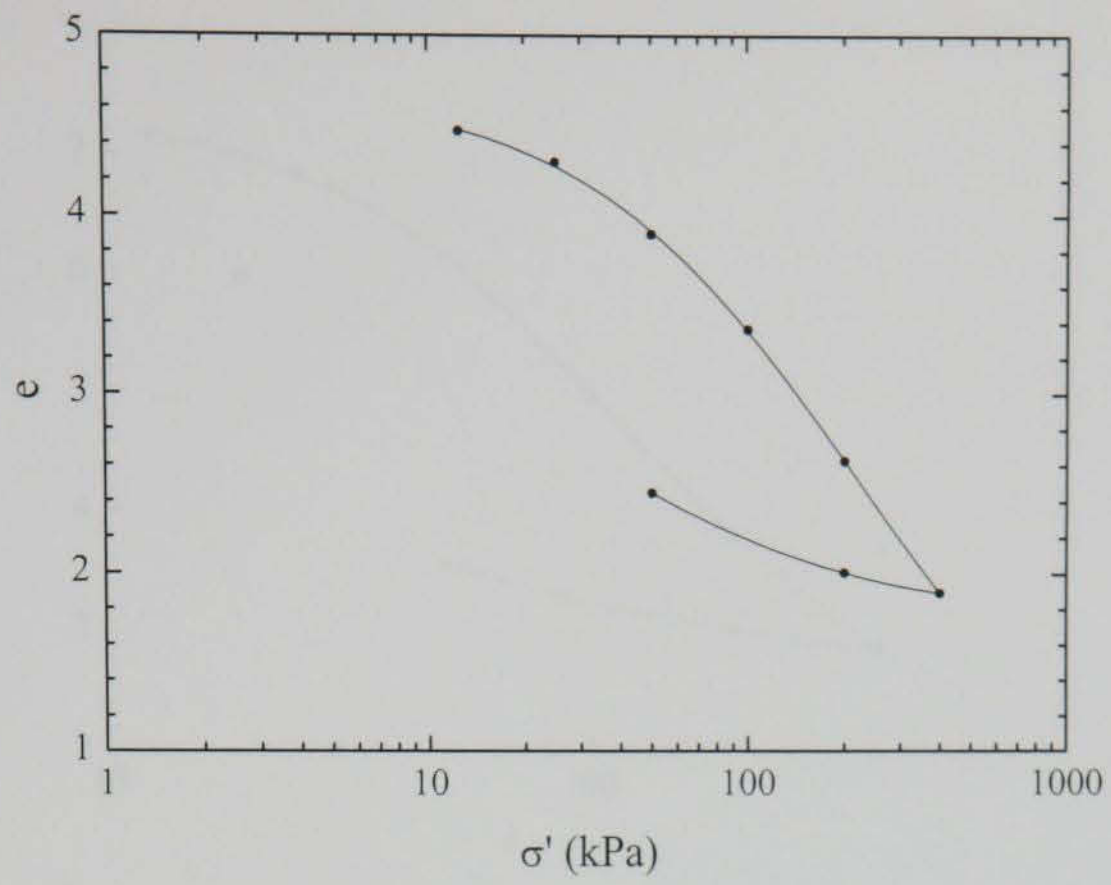

Figure A.59 e – log σ' data for CK_MSL_01

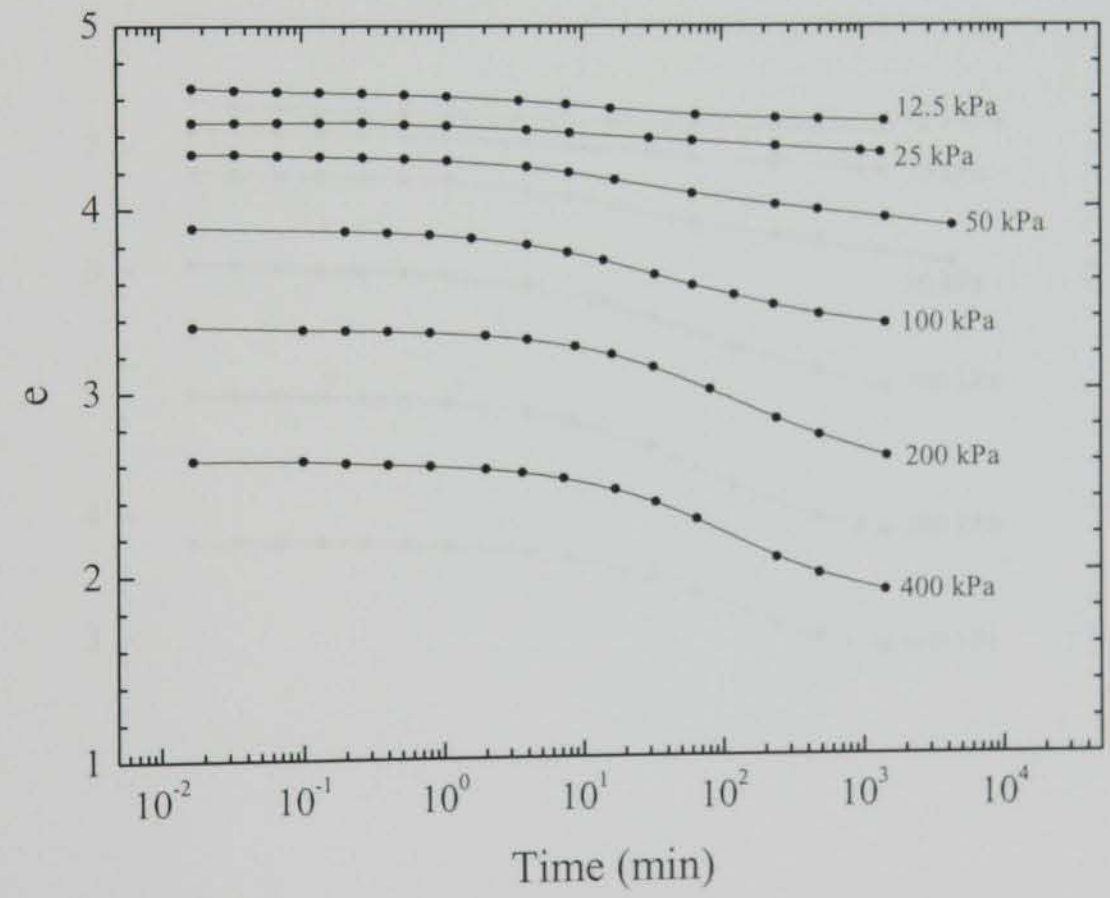

Figure A.60 e – log t data for CK_MSL_01

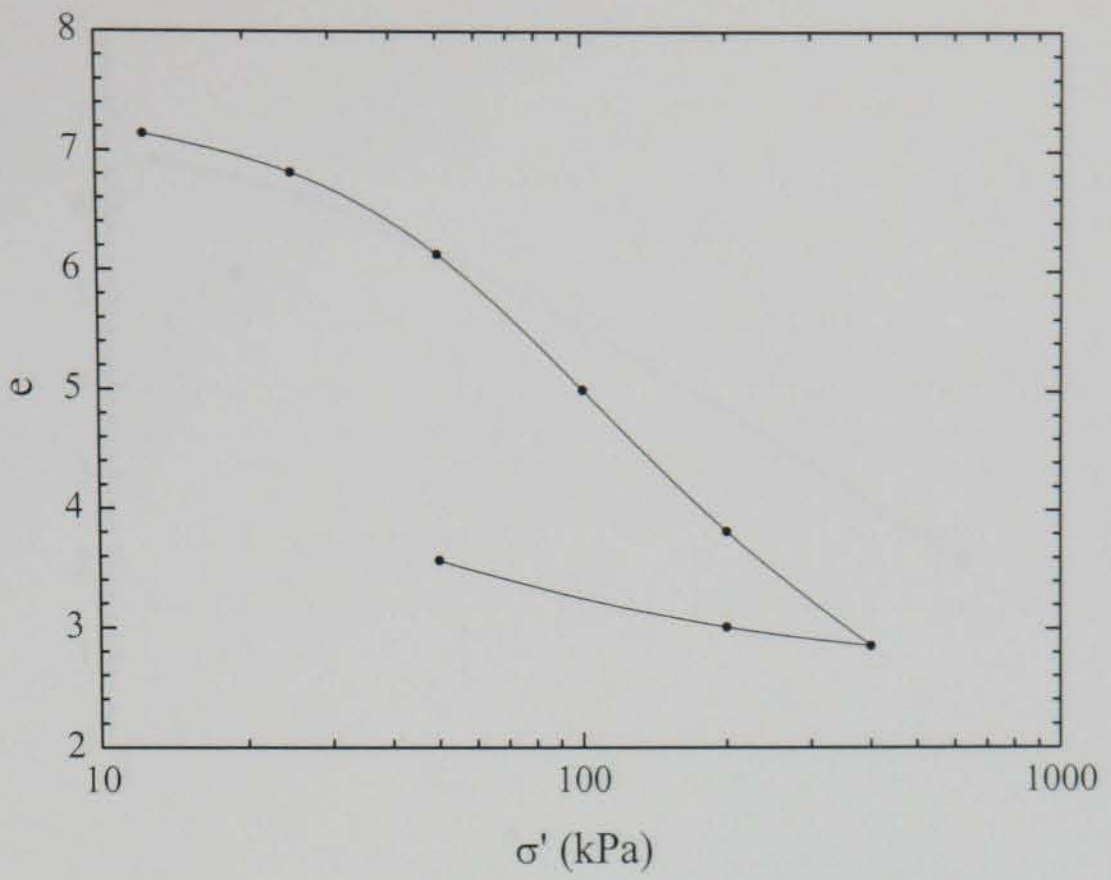

Figure A.61 e – log σ' data for CK_MSL_02

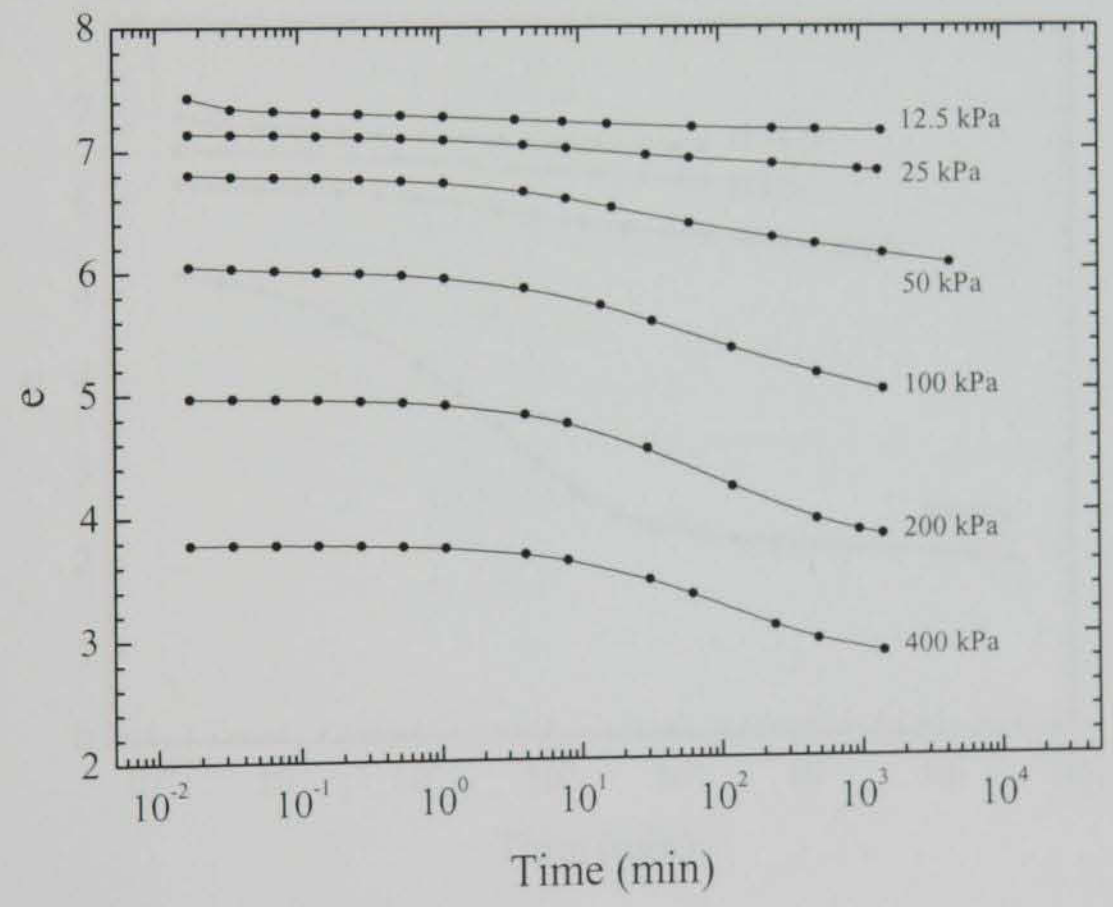

Figure A.62 e – log t data for CK_MSL_02

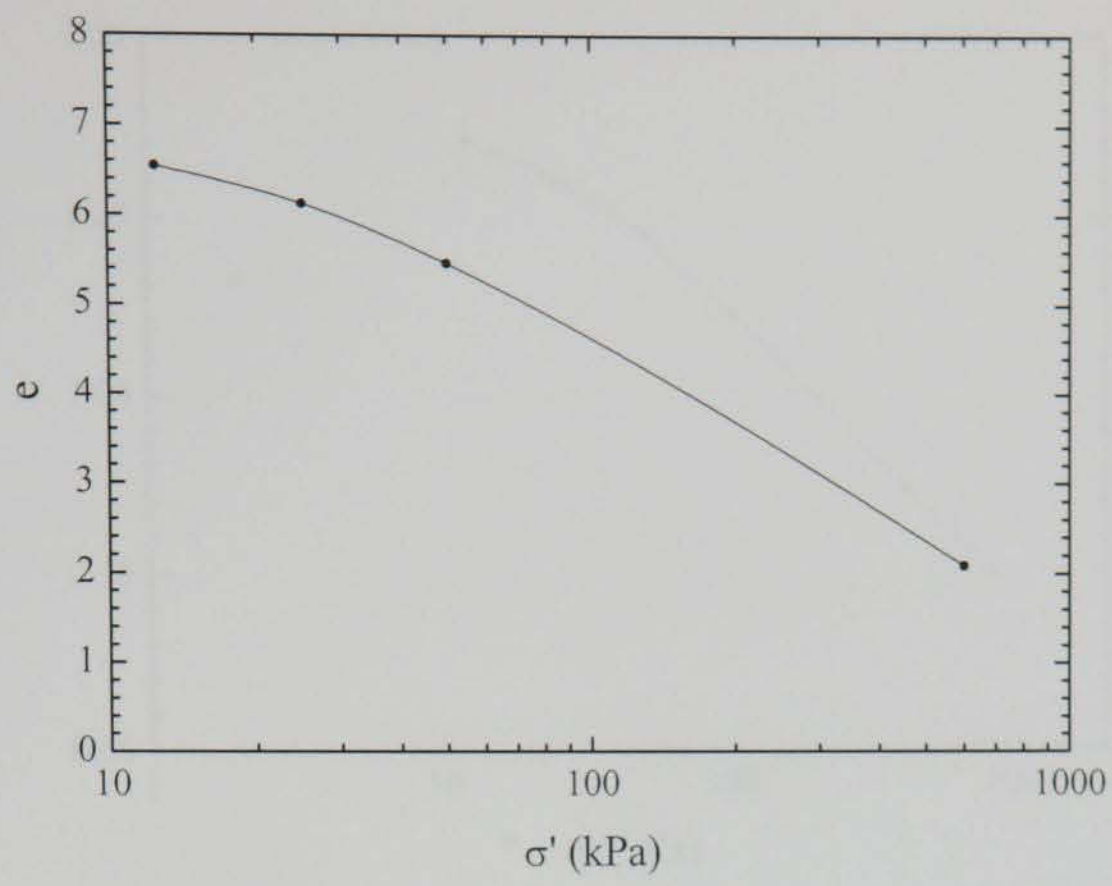

Figure A.63 e – log σ' data for CK_MSL_03

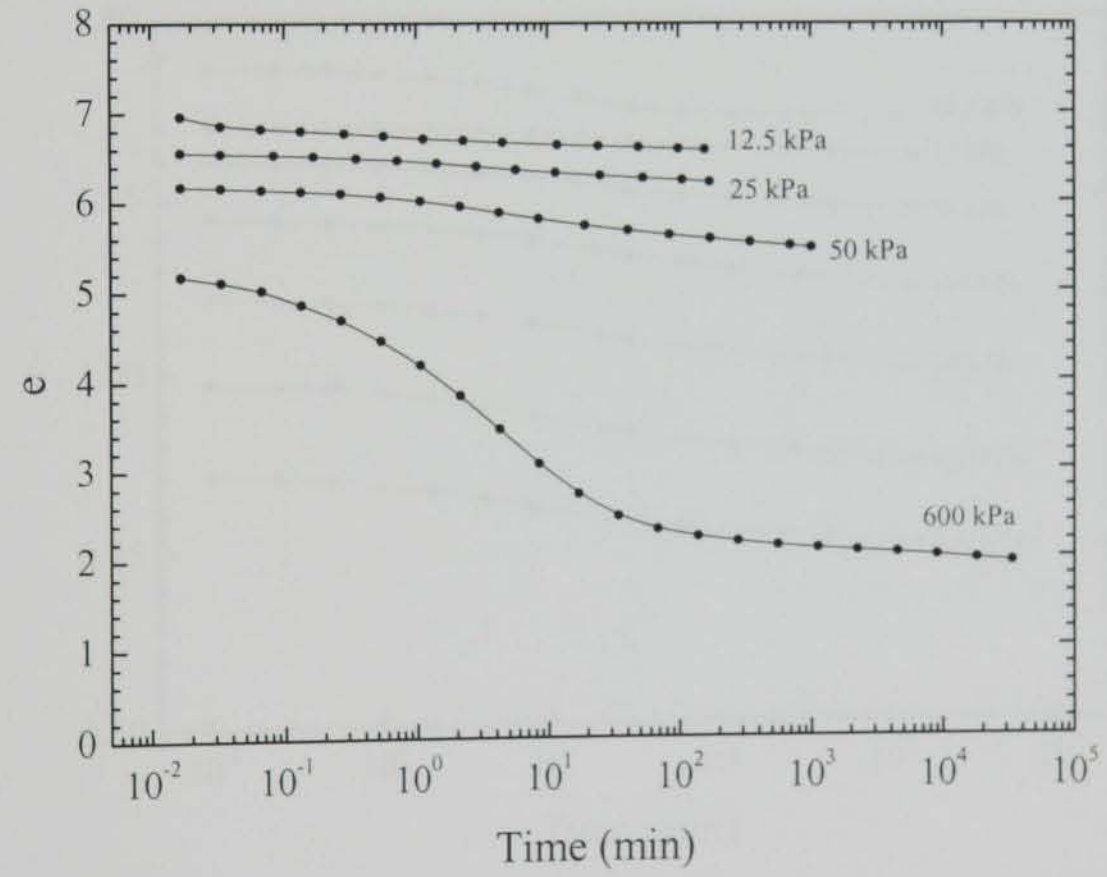

Figure A.64 e – log t data for CK_MSL_03

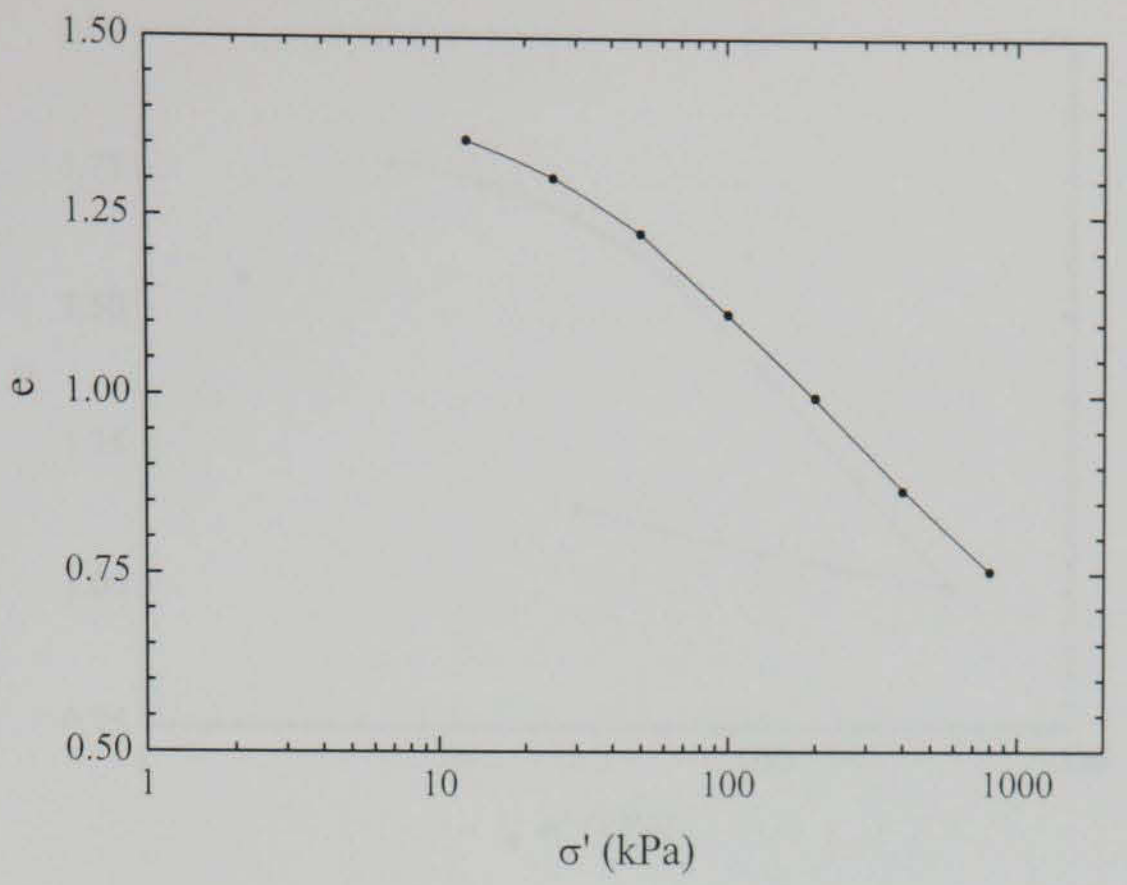

Figure A.65 e – log σ' data for BF_MSL_01

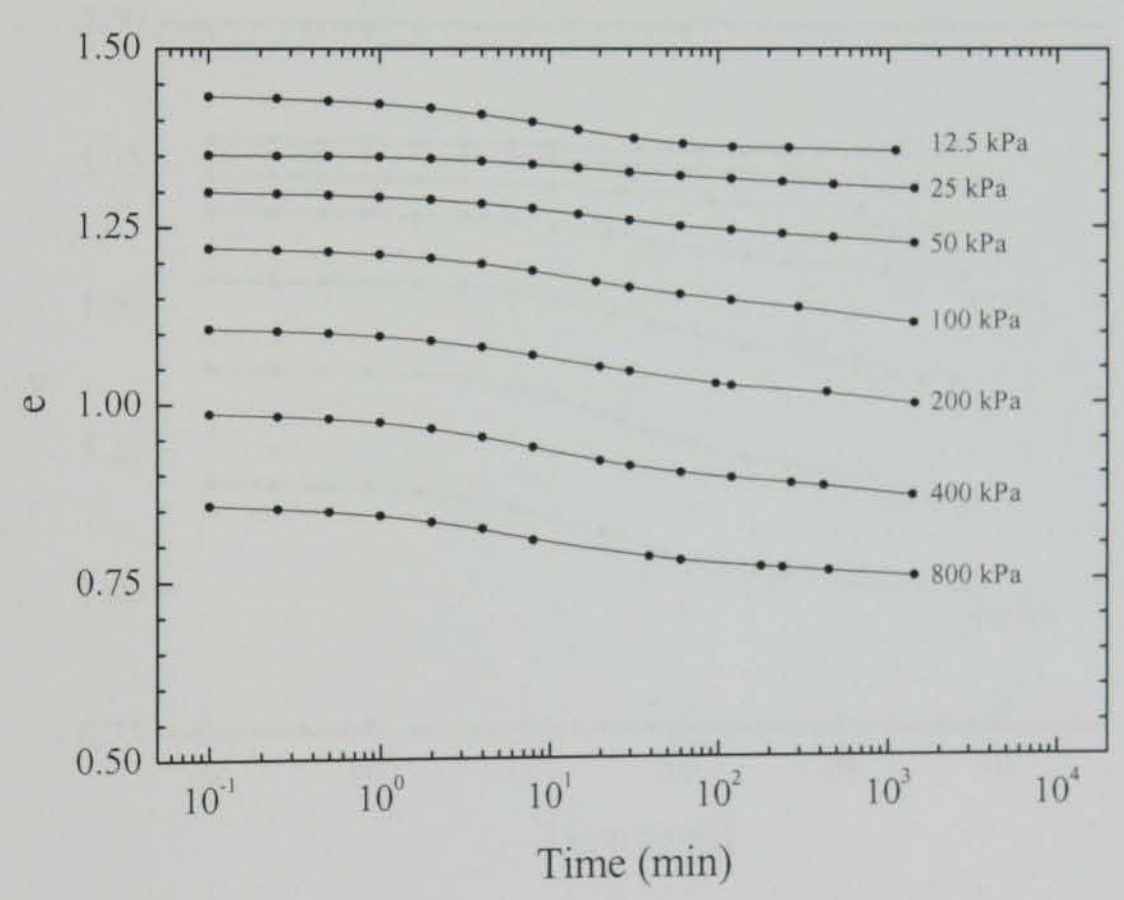

Figure A.66 e – log t data for BF_MSL_01

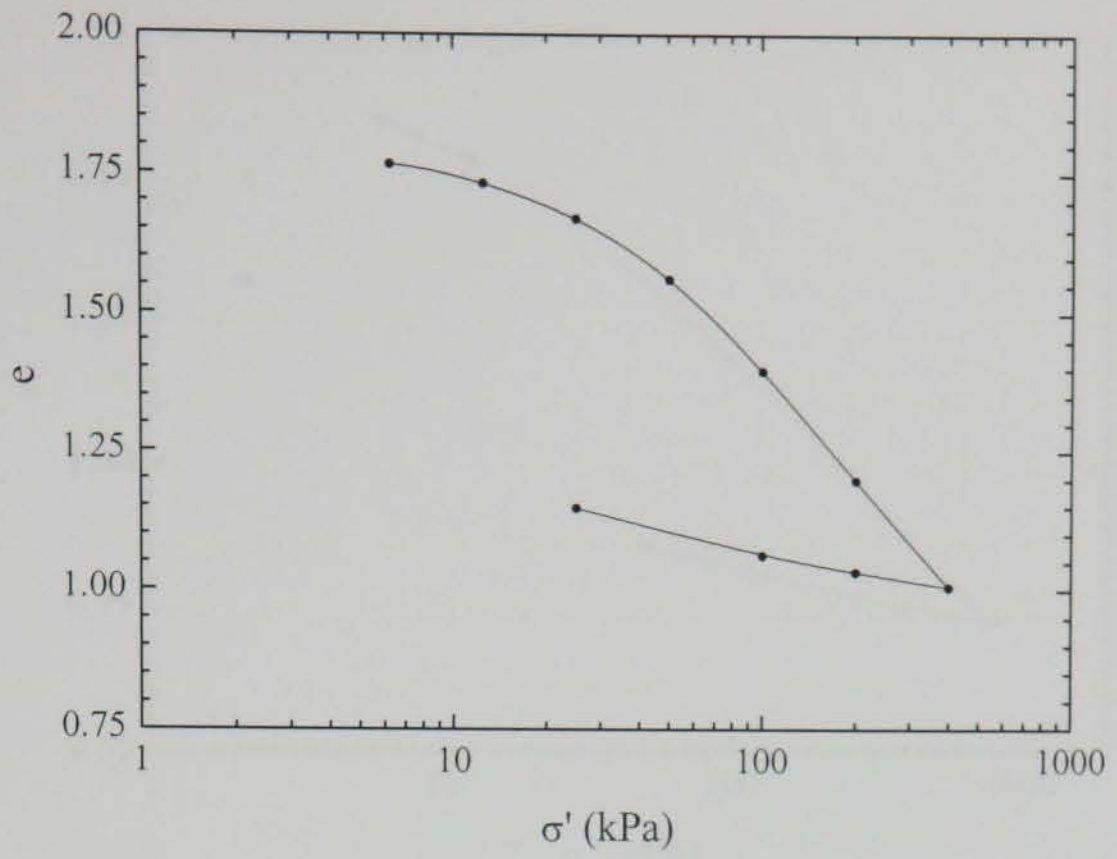

Figure A.67 e – log σ' data for BF_MSL_02

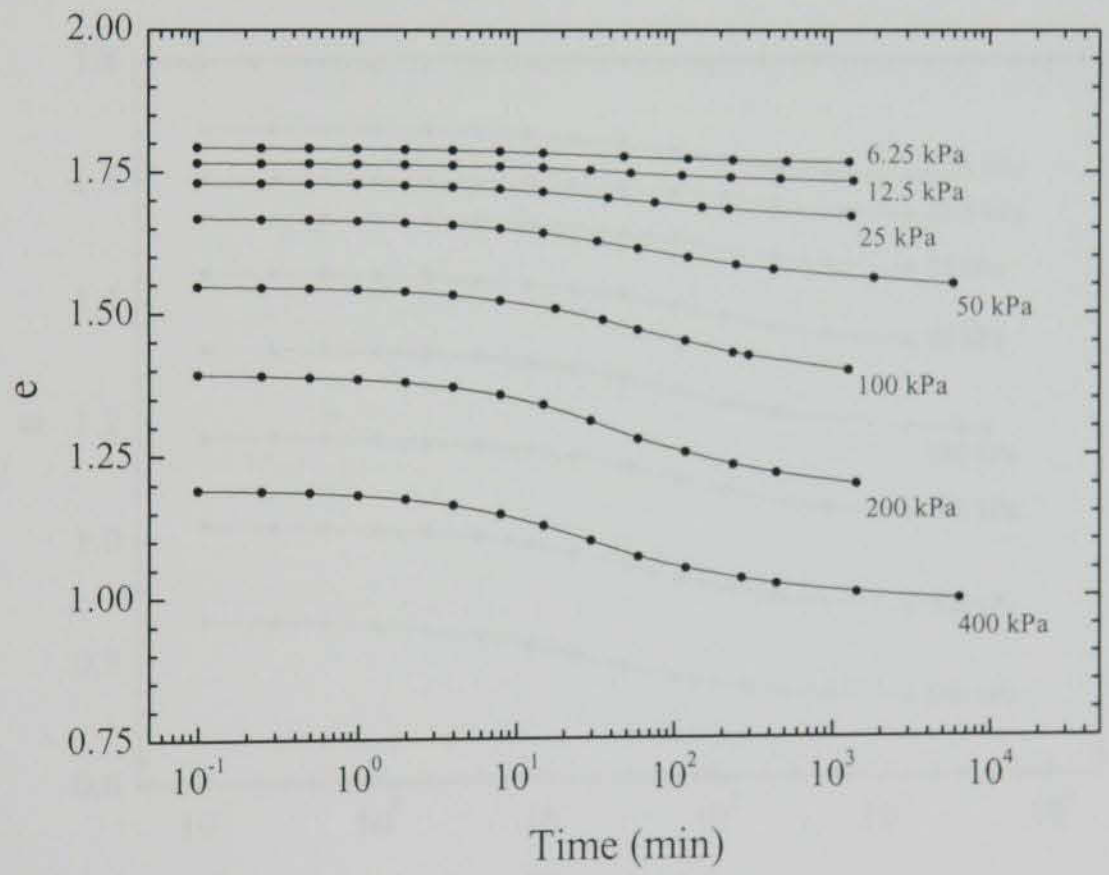

Figure A.68 e – log t data for BF_MSL_02

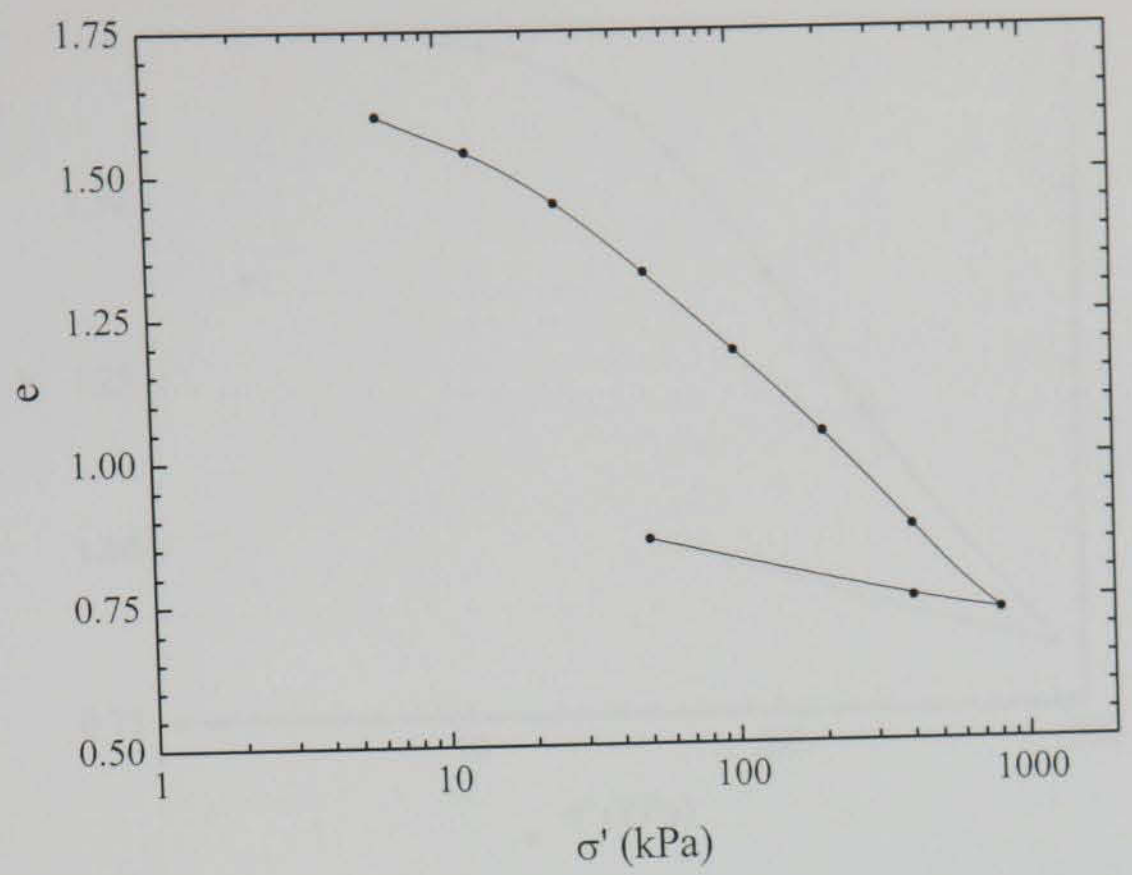

Figure A.69 e – log σ' data for BF_MSL_03

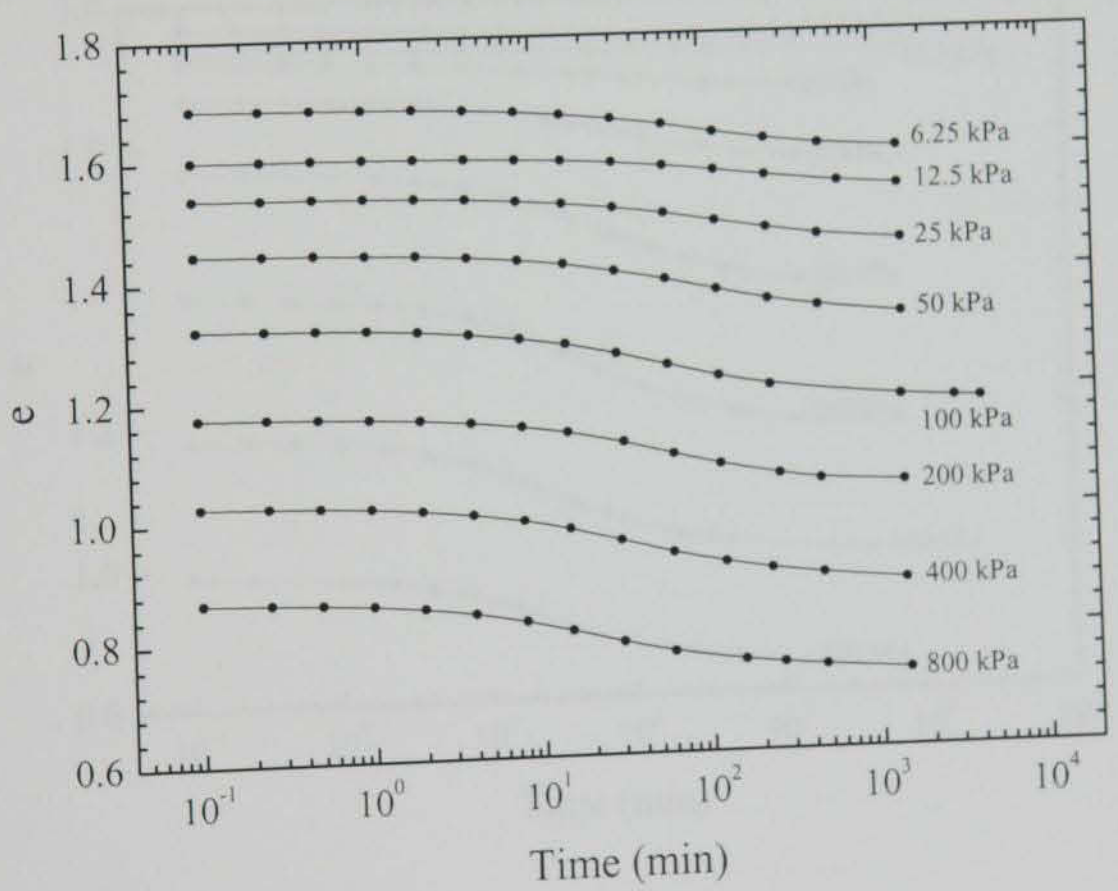

Figure A.70 e – log t data for BF_MSL_03

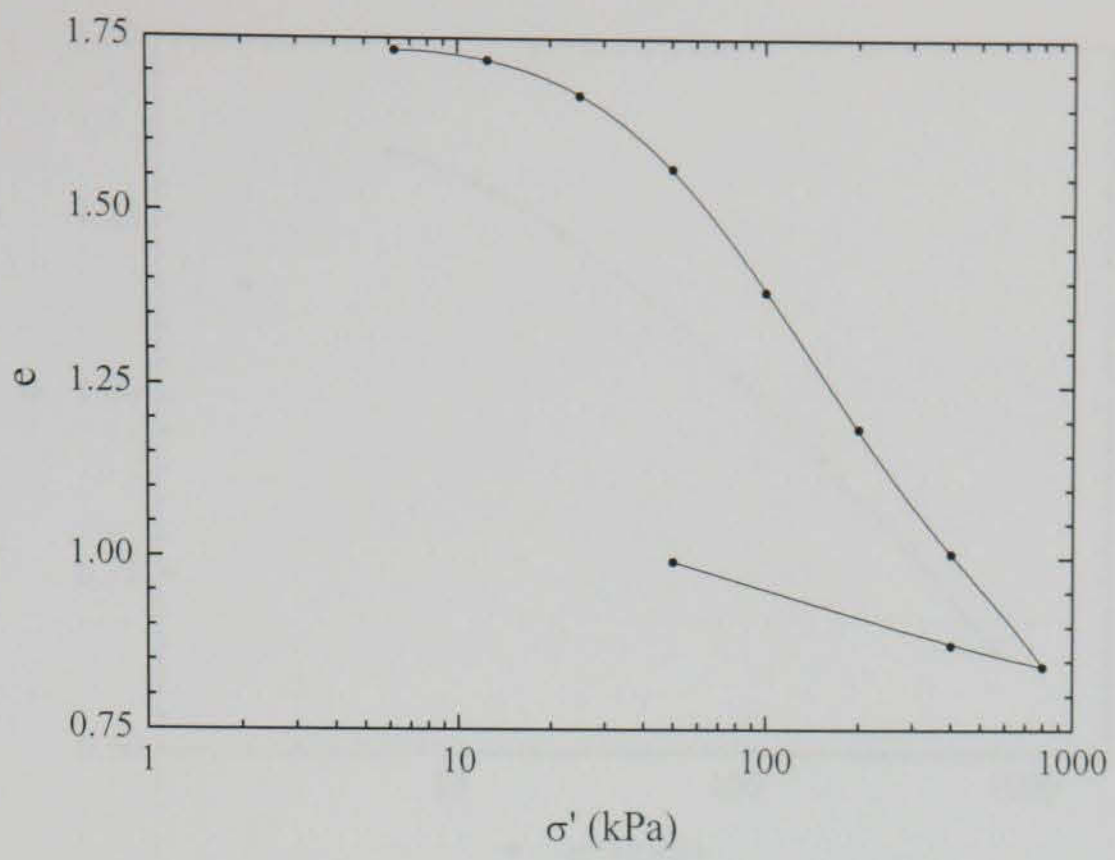

Figure A.71 e – log σ' data for BF_MSL_04

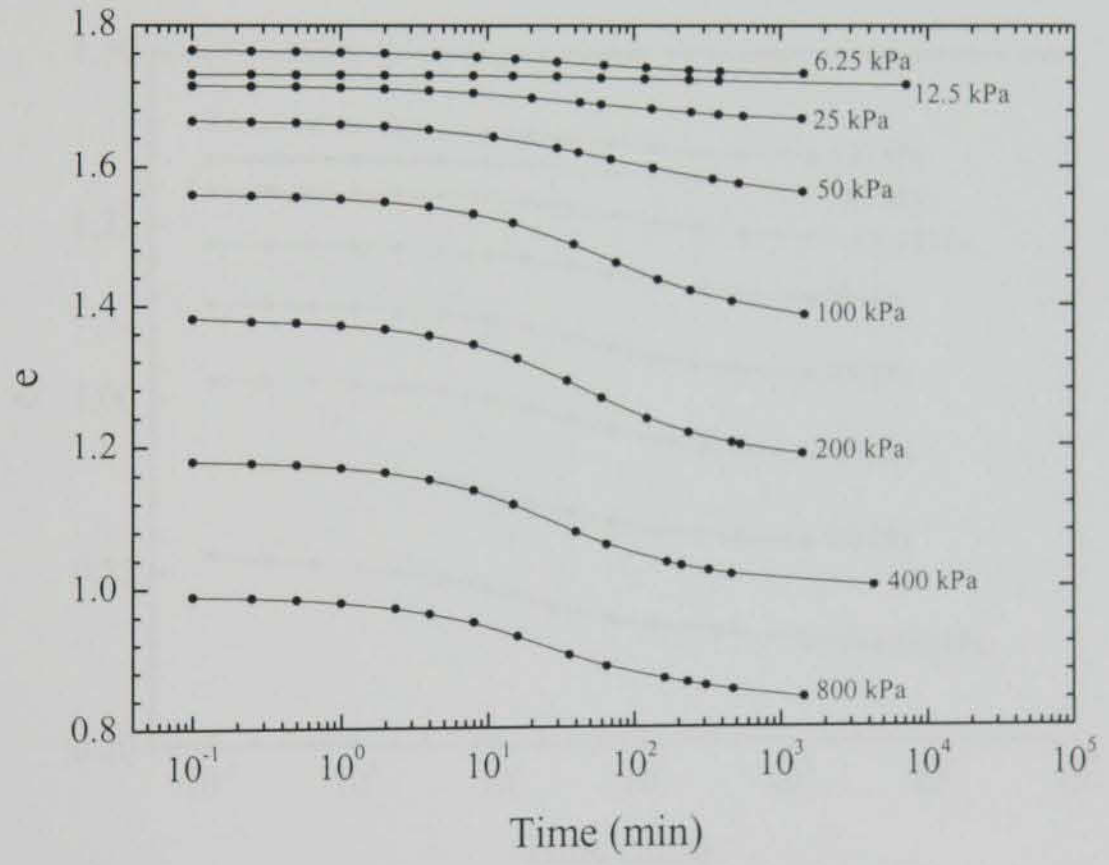

Figure A.72 e – log t data for BF_MSL_04

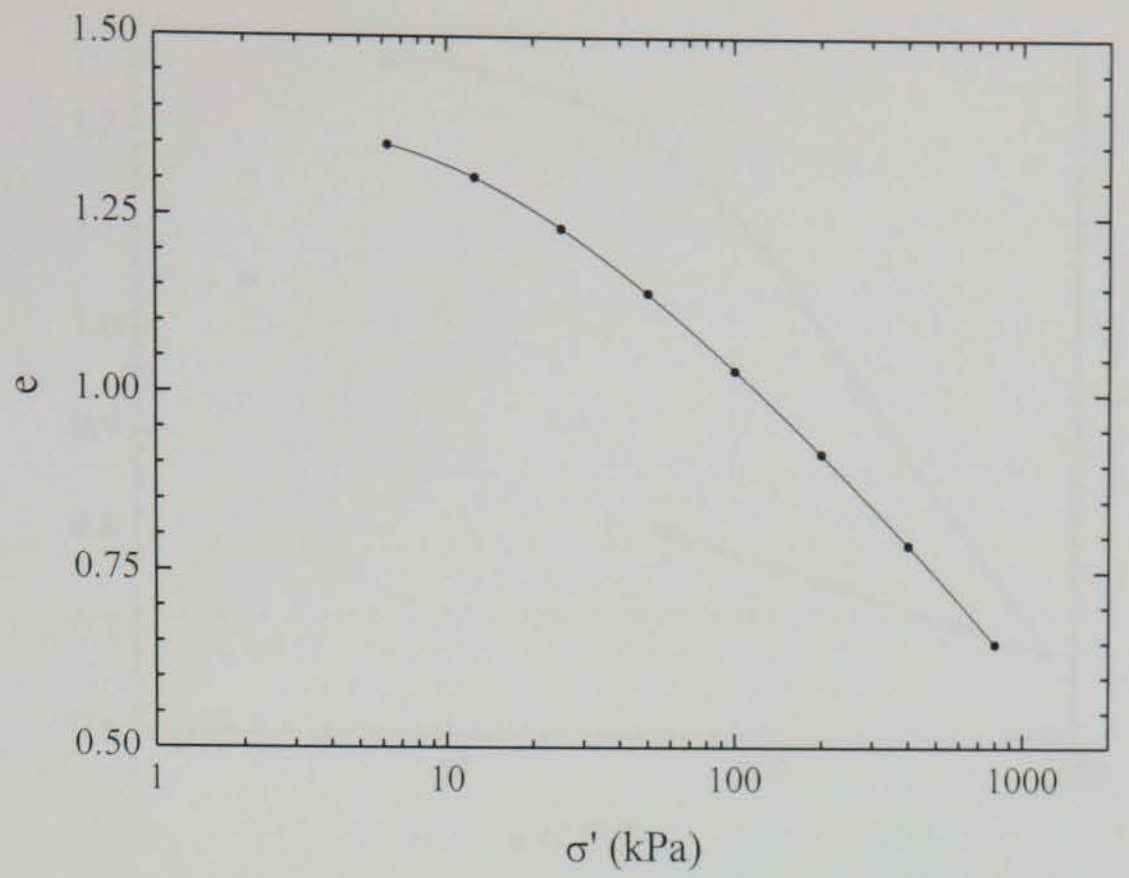

Figure A.73 e – log σ' data for BF_MSL_05

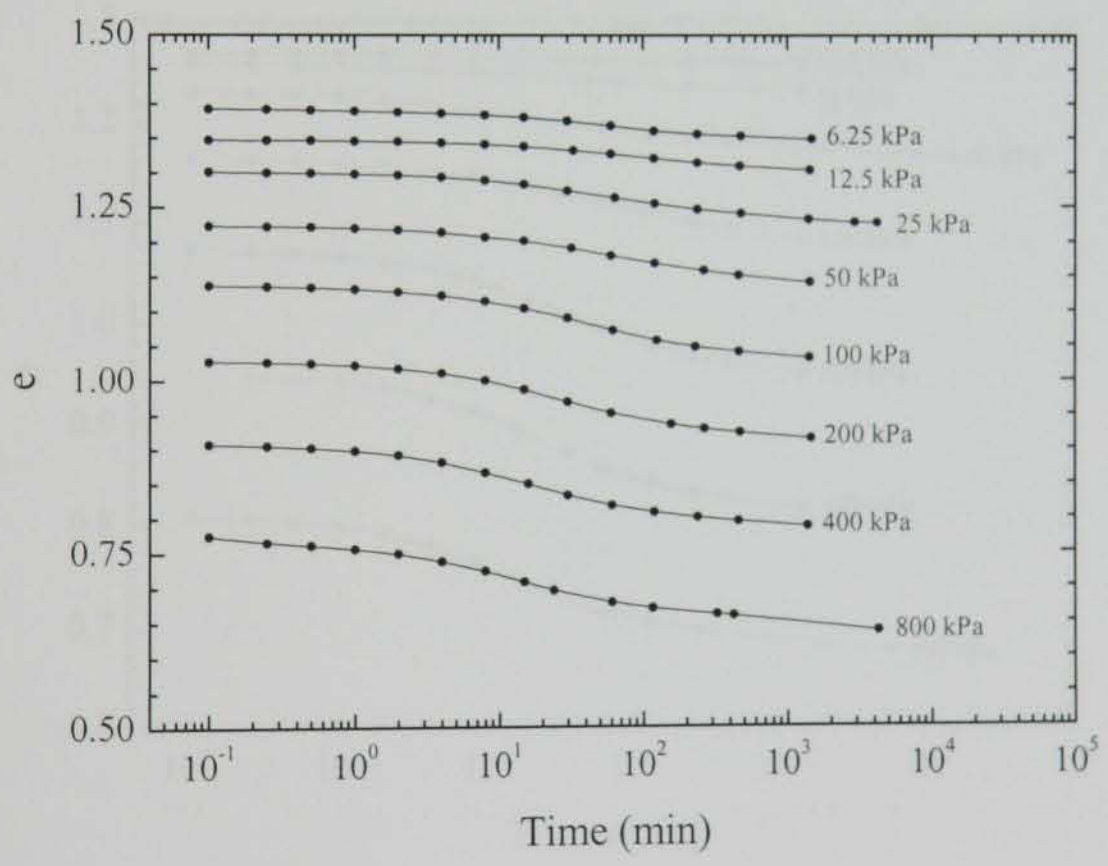

Figure A.74 e – log t data for BF_MSL_05

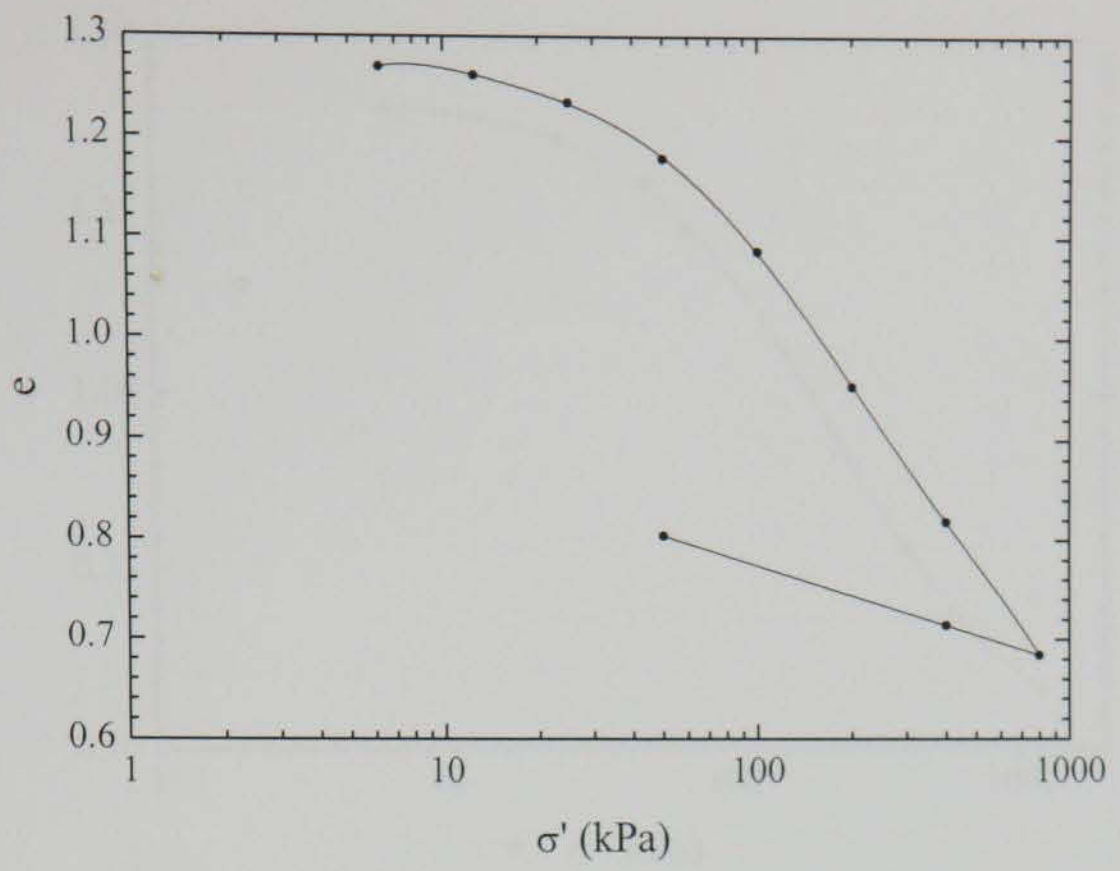

Figure A.75 e – log σ' data for BF_MSL_06

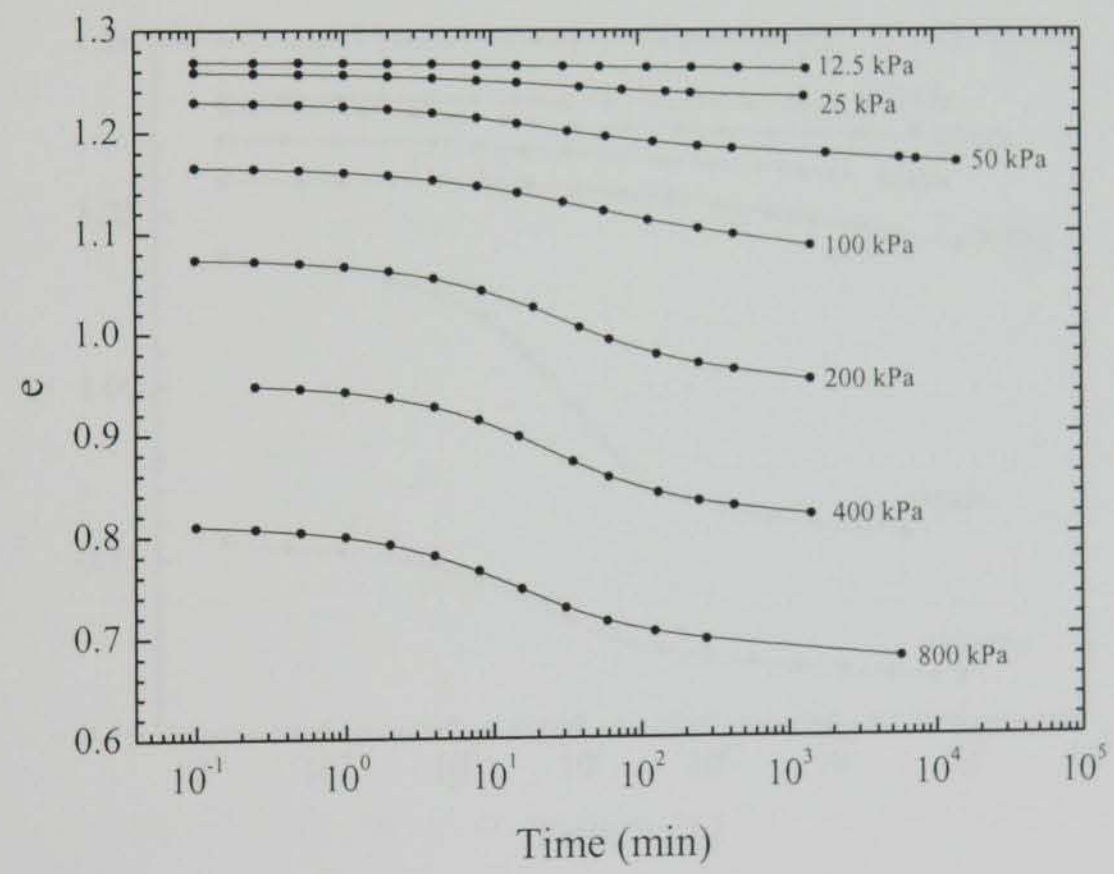

Figure A.76 e – log t data for BF_MSL_06

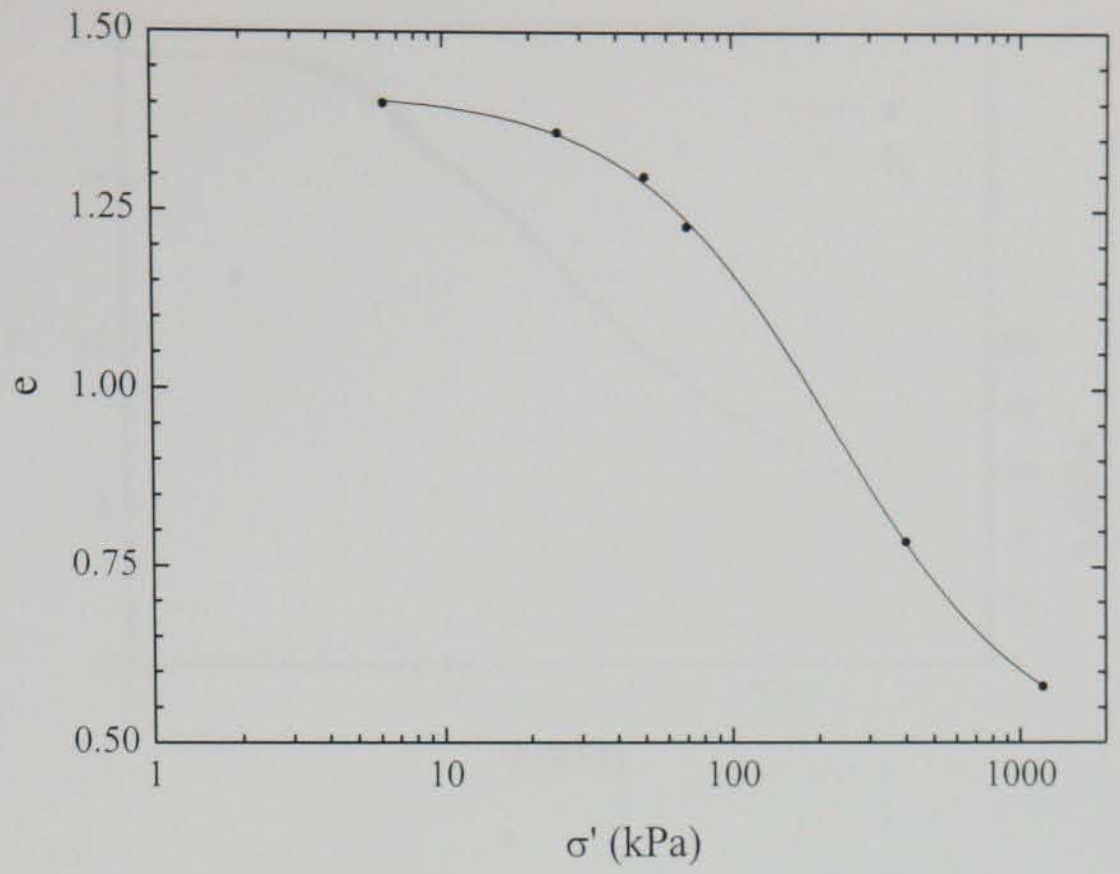

Figure A.77 e – log σ' data for BF_MSL_07

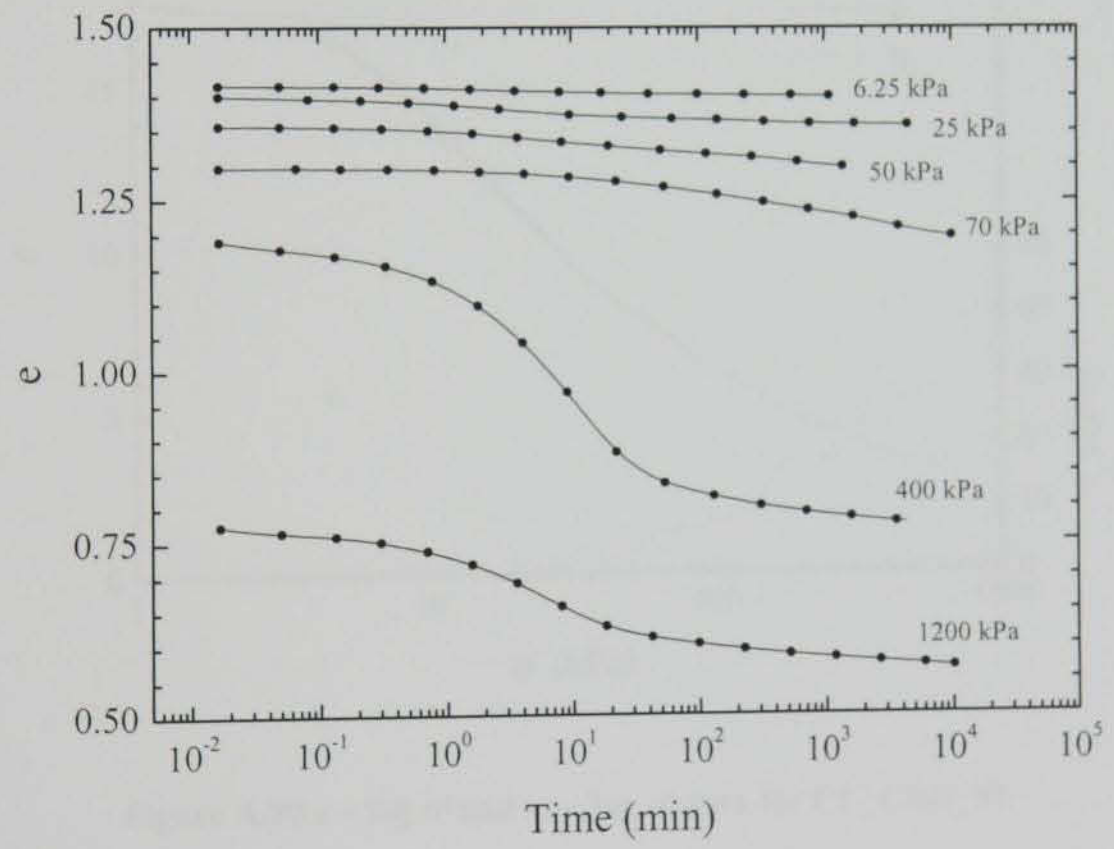

Figure A.78 e – log t data for BF_MSL_07

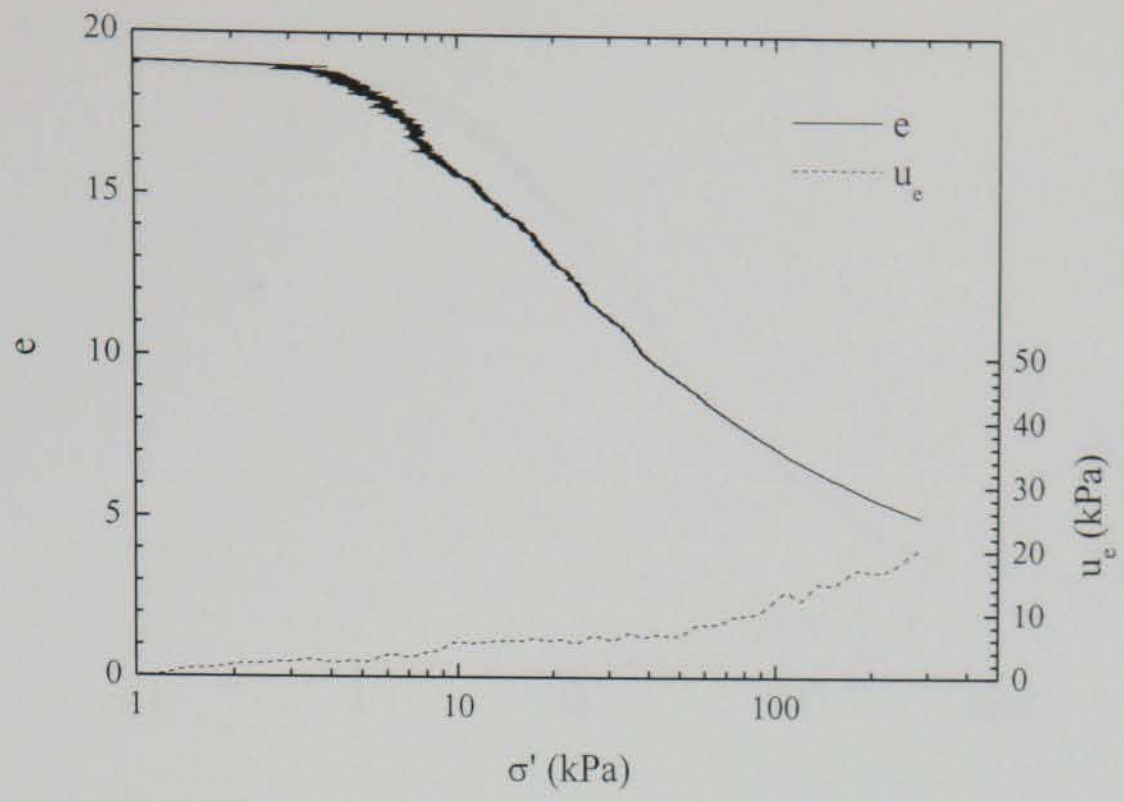

Figure A.79 e – log σ' and u_e – log σ' data for CL_CRD_01

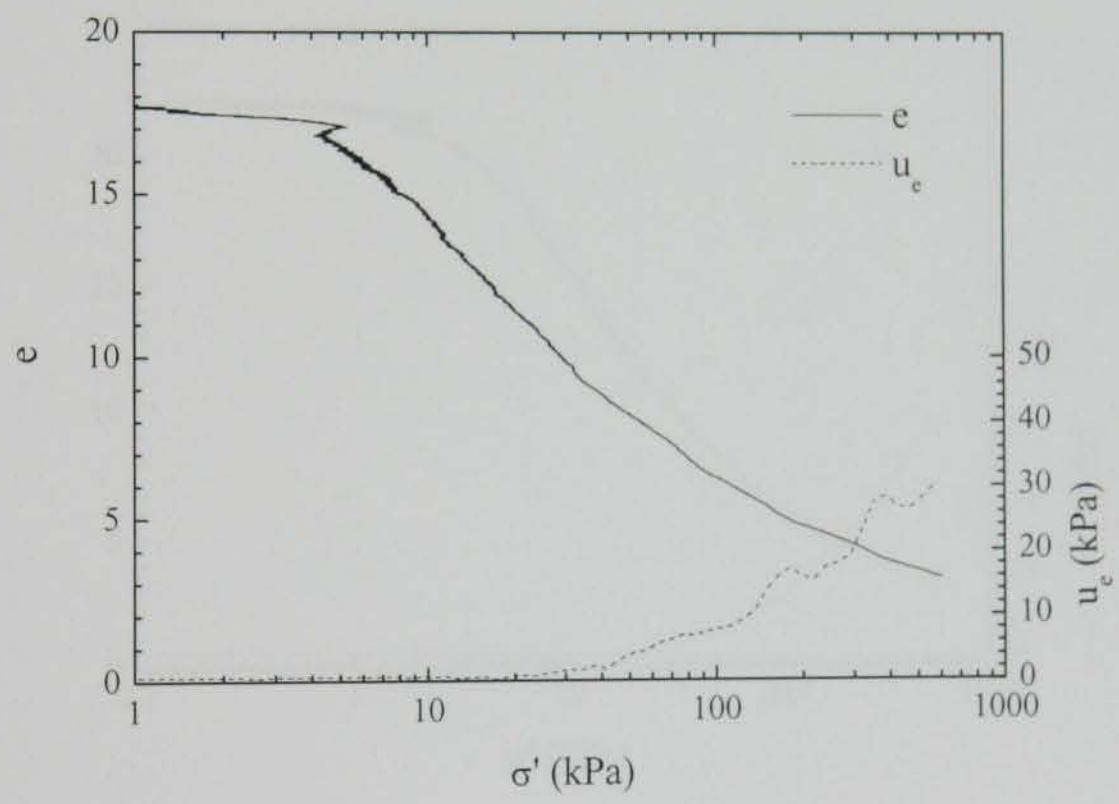

Figure A.80 e – log σ' and u_e – log σ' data for CL_CRD_02

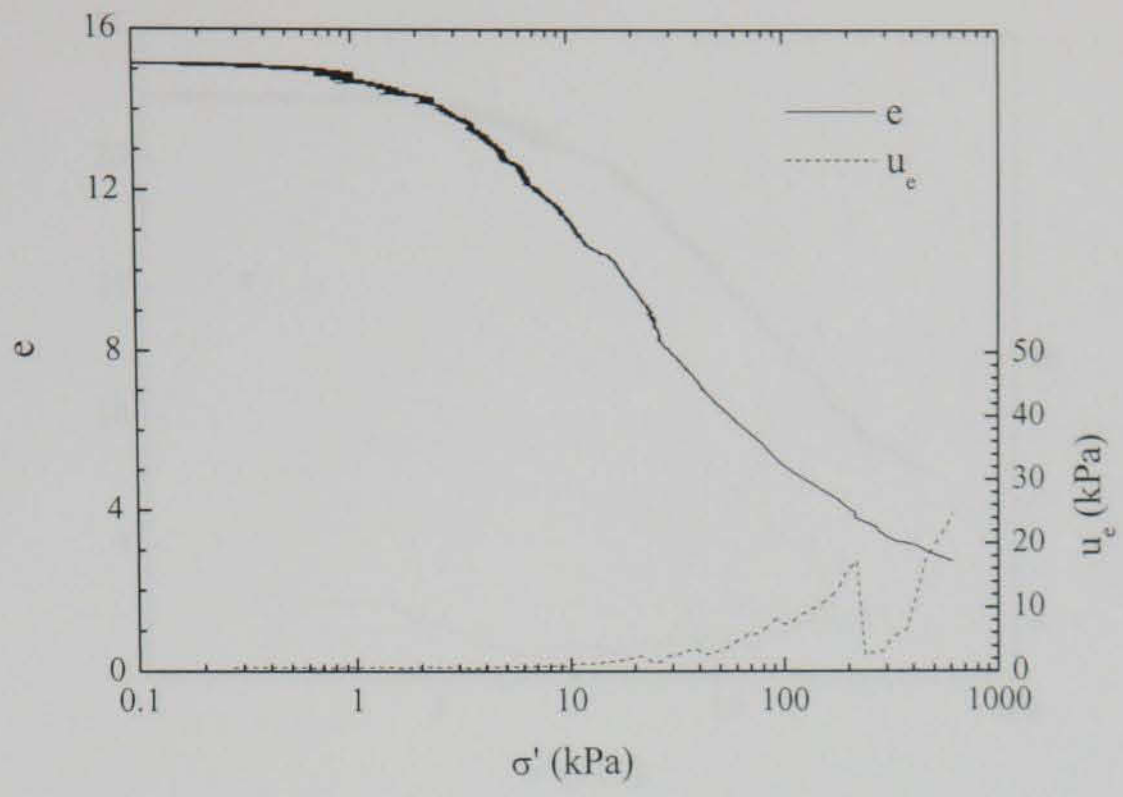

Figure A.81 e – log σ' and u_e – log σ' data for CL_CRD_03

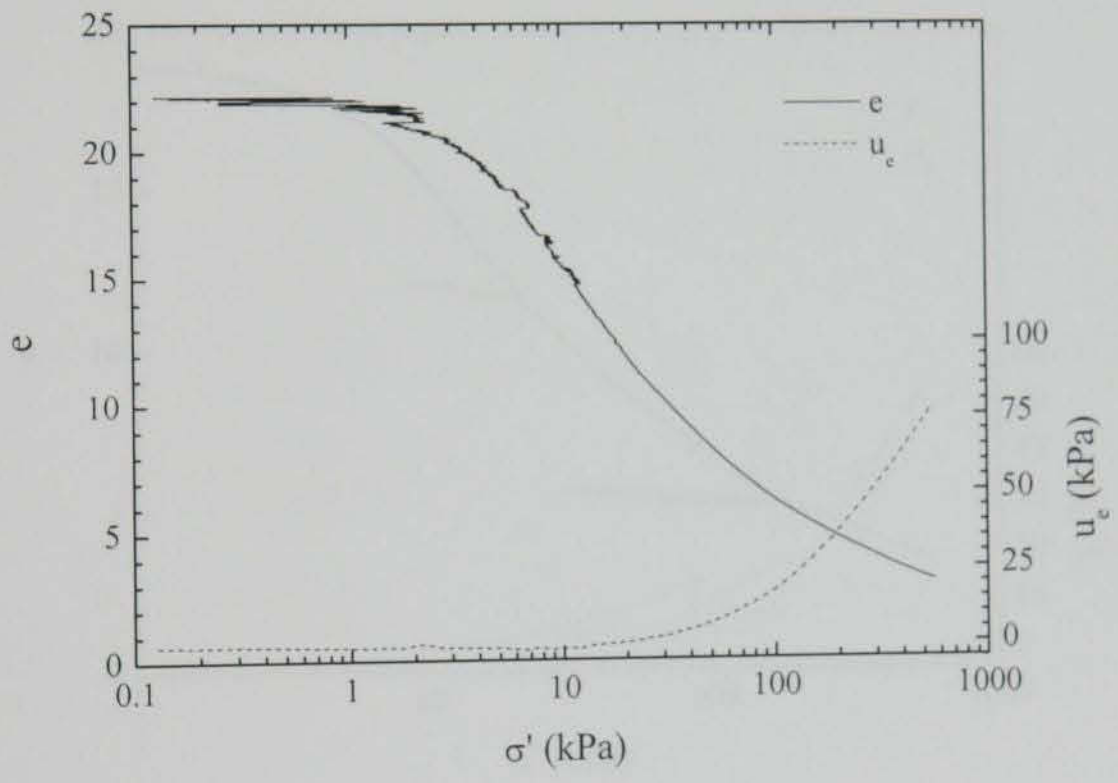

Figure A.82 e – log σ' and u_e – log σ' data for CL_CRD_04

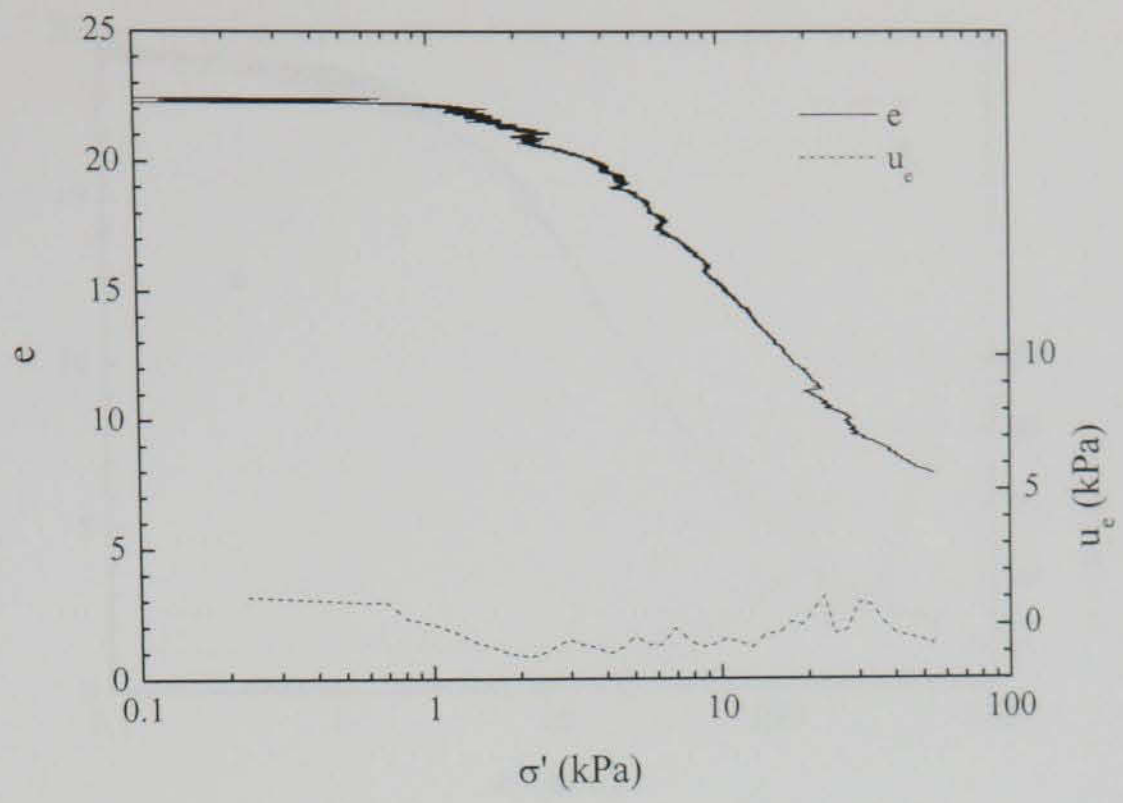

Figure A.83 e – log σ' and u_e – log σ' data for CL_CRD_05

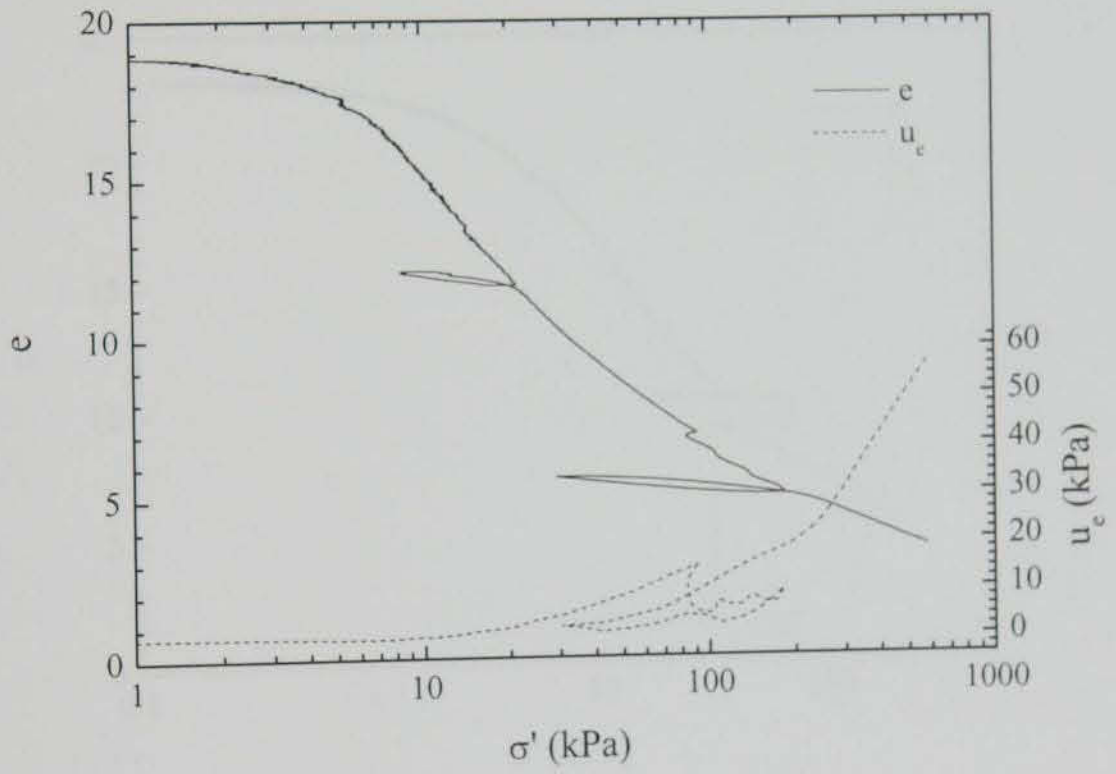

Figure A.84 e – log σ' and u_e – log σ' data for CL_CRD_06

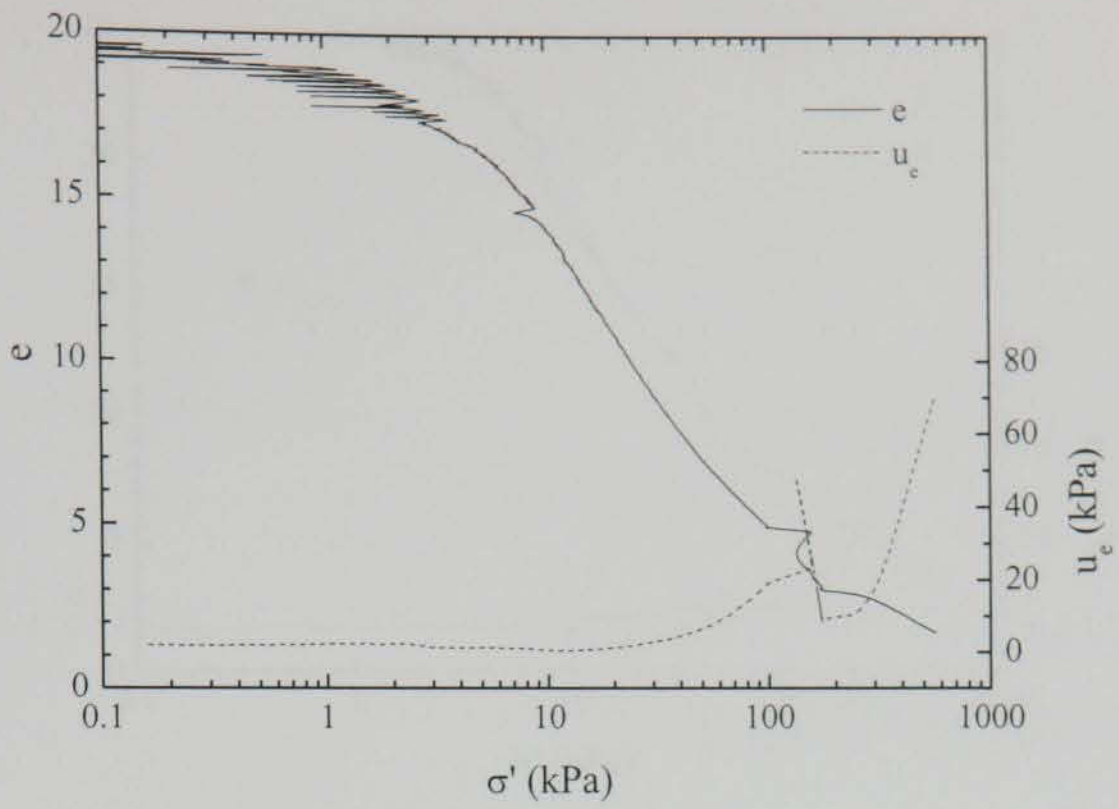

Figure A.85 e – log σ' and u_e – log σ' data for CL_CRD_07

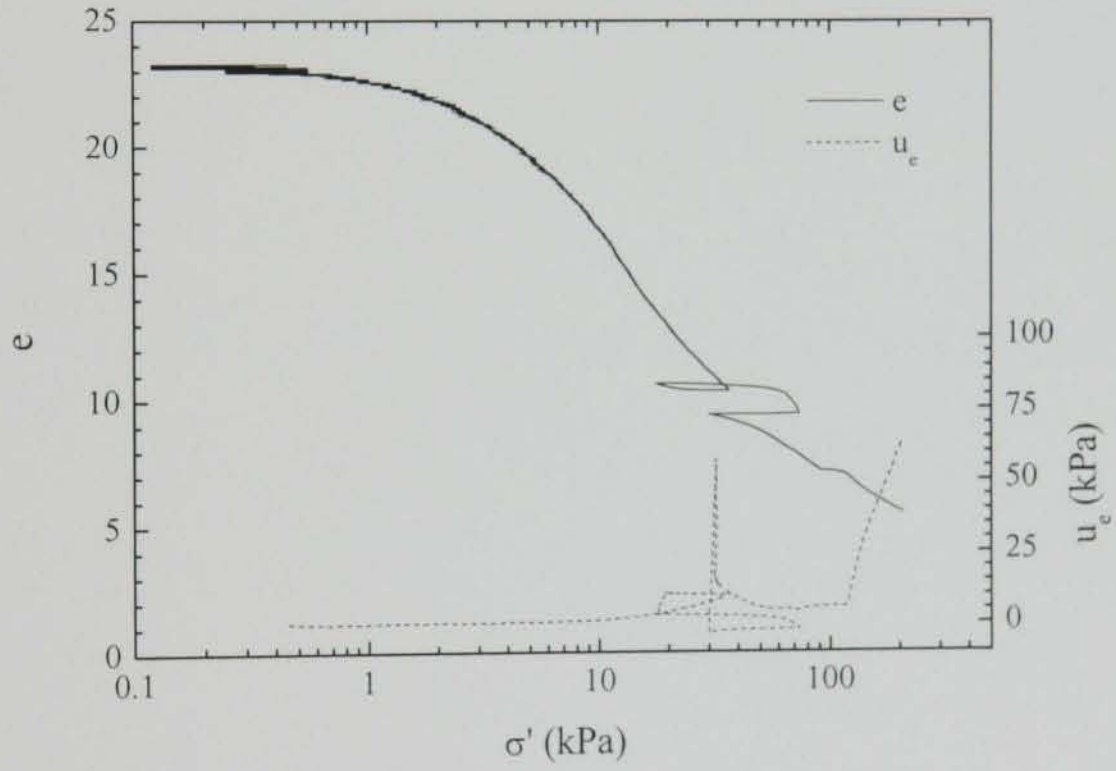

Figure A.86 e – log σ' and u_e – log σ' data for CL_CRD_08

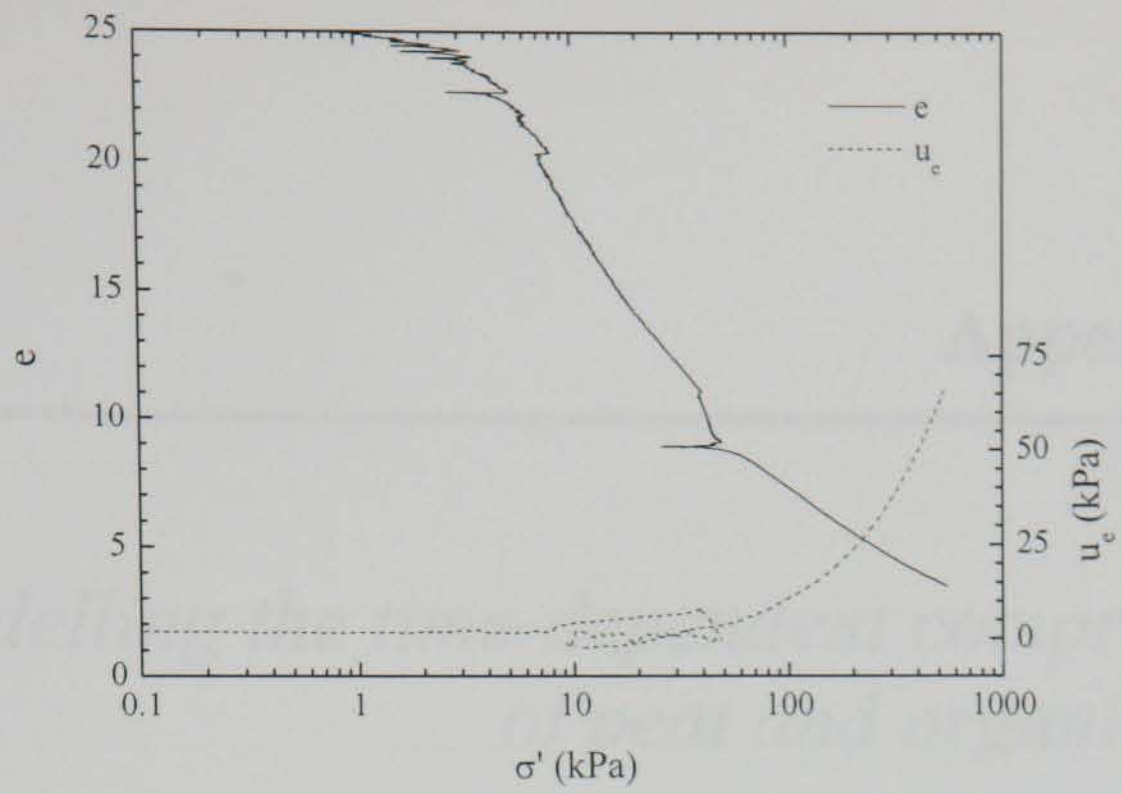

Figure A.87 e – log σ' and u_e – log σ' data for CL_CRD_09

Appendix B

Modelling the time-dependent compression of peat and organic soils

O'Loughlin, C.D. & Lehane, B.M. (2001). Modelling the time-dependent compression of peat and organic soils. *Proc. 3rd Int. Conf. Soft Soil Engr.*, Hong Kong, 369-375.

Modelling the time-dependent compression of peat and organic soils

Modélisation le compactage temps-dépendant de la tourbe et des sols organiques

O'Loughlin, C.D., Dept. of Civil Engineering, Trinity College, Dublin 2, Ireland
Lehane, B.M., Dept. of Civil Engineering, Trinity College, Dublin 2, Ireland

ABSTRACT: Creep (or secondary) settlement is well known to contribute significantly to the overall settlement of peats and organic soils. A number of constitutive models to predict one-dimensional creep behaviour have been proposed and have had mixed success. This paper examines the potential of the *elastic visco-plastic* model proposed by Yin and Graham (1996), and the C_α/C_c approach (Mesri and Godlewski 1977) to predict the response of an organic clay and a fibrous peat compressed under oedometric conditions. The effect of prolonged load increment durations and the application of load increment ratios considerably in excess of the value of unity applied in standard 24-hour oedometer tests is discussed as it has a direct bearing on conventional settlement predictions associated with pre-loading/surcharging techniques.

RÉSUMÉ: Le tassement de fluage (ou secondaire) est bien connu pour contribuer de manière significative au tassement global des tourbes et des sols organiques. Un certain nombre de modèles constitutifs pour prévoir le comportement unidimensionnel de fluage ont été proposés et ont eu un succès mitigé. Cet article examine le potentiel du modèle *élastique visco-plastique* proposé par Yin et Graham (1996), et l'approche de C_α/C_c (Mesri et Godlewski 1977) pour prévoir la réponse d'une argile organique et d'une tourbe fibreuse comprimées dans des conditions oedométriques. L'effet des durées prolongées d'incrément de chargement et de l'application des taux d'incrément de chargement considérablement au-dessus de la valeur unité appliquée dans les essais de 24-heures standard d'oedomètre est discuté car il a un effet direct sur les prévisions conventionnelles de tassement associées aux techniques de préchargement/surchargement.

1 INTRODUCTION

Although the consolidation process takes place over a finite time scale, the time dependent compression of soils is generally associated with the so-called *secondary* or *creep* compression. Traditional practice usually separates strains due to primary consolidation from those due to creep compression. However, it is now generally accepted that creep takes place during both consolidation and at constant effective stress. Soils with a high organic content very often have a high pore volume because of the open structure promoted by the organics. Such a structure leads to pronounced creep characteristics in addition to more rapid consolidation.

The dependence of creep on organic content is shown in Figure 1, which plots creep strain against time for soils which were loaded from 100 kPa to 200 kPa under oedometric conditions. The organic contents are shown to the right of each strain profile, and initial voids ratios, e_o, are shown in the legend text. The origin of strain and time in Figure 1 is that at end of primary (EOP) as estimated using Taylor's root time method. Although

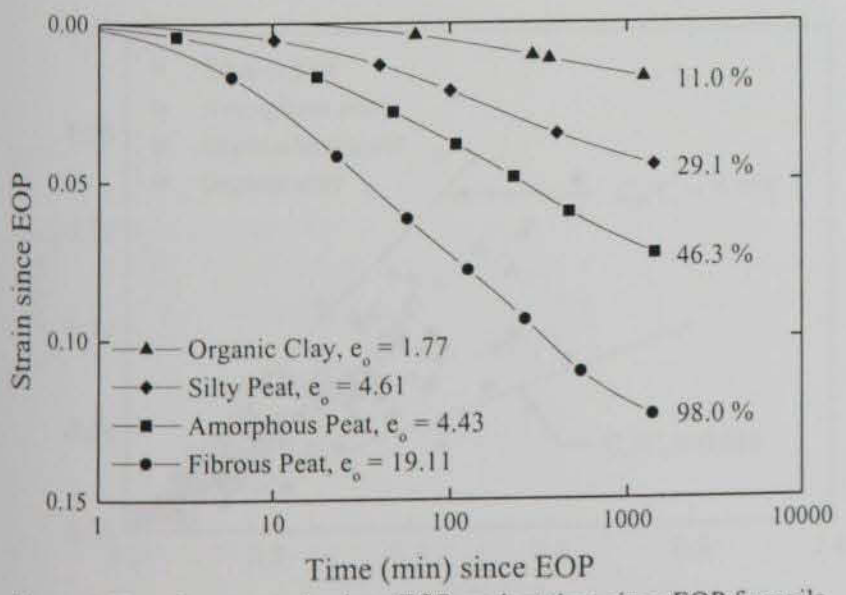

Figure 1 Plot of creep strain since EOP against time since EOP for soils of varying organic content and initial void ratios

such graphical methods are not particularly successful in estimating EOP for peat and organic soils (e.g. see Edil & den Haan 1994), they are sufficient to illustrate that:

(i) organic soils continue to creep by a considerable amount after primary consolidation ceases
(ii) the amount of creep compression is to some degree related to the organic content of the soil

Prompted by the significance of creep in organic soils, this paper examines procedures employed to predict time dependent settlements of organic soils in one-dimensional (1D) compression. In particular, the C_α/C_c procedure as described in Mesri and Godlewski (1977) and elasto-viscoplastic approaches (e.g. Yin and Graham 1996) are examined against a database of oedometer tests performed at Trinity College Dublin (TCD).

2 LABORATORY TESTS

The TCD database compiled for the purposes of this paper is summarized in Table 1. The majority of tests were carried out on a fibrous peat from the Irish midlands, while the remainder of the tests were performed on peats of varying degrees of decomposition; an organic clay and silt are also considered. The testing programme involved standard classification and identification tests, and oedometer tests of varying load increment ratio (LIR) and load increment duration (LID). All oedometer tests were performed on carefully sampled and prepared specimens which were either 19.05 mm or 20.00 mm in height, and had diameters of either 75.00 mm, 76.20 mm or 100.00 mm.

3 C_α/C_C CONCEPT

The C_α/C_c concept as described in Mesri and Godlewski (1977) suggests that "there is a unique relationship between $C_\alpha = \partial e/\partial \log t$ and $C_c = \partial e/\partial \log \sigma'$ that holds true at all combinations of time, effective stress, and void ratio." The correct interpreta-

Table 1 Average material properties of the soils tested

Soil origin	Soil classification	Organic content %	Water content %	v_0	Liquid limit %	Plastic limit %
Clara, County Offaly	Fibrous peat	98.0 – 98.5	1250.0 – 1750.0	19.8 – 33.0	-	-
Ballydermot, County Offaly	Amorphous peat	98.0	750.0 – 950.0	12.4 – 13.1	-	-
Arklow, County Wicklow	Amorphous peat	46.3	228.9 – 241.6	5.4 – 6.3	241 – 332	133 – 189
	Silty peat	23.2 – 29.1	105.8 – 174.1	3.6 – 5.6	153 – 159	83 – 86
	Organic silt	10.5	98.9	3.9	90	44
Belfast	Organic clay	11.0 – 12.0	35.0 – 70.0	1.9 – 2.8	25 – 35	58 – 77

tion of the C_α/C_c concept has been dealt with in various publications over the years by Mesri and his co-workers. Mesri and Godlewski (1977) propose that values of C_c should be determined from the EOP compression curve and paired with C_α values determined from the first log cycle of secondary compression. However, it is well recognized that the time taken for primary consolidation in compressible materials such as peat and organic soils is difficult to determine using conventional graphical techniques due to the absence of the 'inflection point', which distinguishes the EOP compression phase. The EOP can be determined accurately when excess pore pressures are measured, but this is seldom the case in standard oedometer tests. Mesri and Godlewski (1977) stated that although the EOP e – log σ' curve is usually used to define C_c, any e – log σ' curve during secondary compression, with the corresponding values of C_α, can be used to calculate the C_α/C_c ratios.

Mesri et al. (1997) and Lefebvre et. al (1984) showed that the uniqueness of C_α/C_c values are improved when normalized by the initial specific volume, v_o (v_o = 1+ e_o). Figure 2 shows the C_α/C_c relationship for the peats and organic soils listed in Table 1, where C_α and C_c are defined as:

$$C_\alpha = \frac{\Delta e}{\Delta \log t}, \quad C_c = \frac{\Delta e}{\Delta \log \sigma'} \tag{1}$$

In accordance with Mesri and Godlewski (1977), C_c is taken to apply to all effective stress levels, during both the over-consolidated and normally consolidated ranges. The data points in Figure 2 were determined from 24-hour compression data; C_c values were calculated at the tangent to the e – log σ' curve for each stress increment.

Figure 2 shows that the range of C_α/C_c values for the organic soils in question lie within the range 0.025 – 0.075. The mean values for the C_α/C_c values and the associated coefficients of determination (r^2) are summarized in Table 2 for each soil group.

It is evident from Table 2 that the spread of C_α/C_c ratios is lowest for the less compressible materials such as organic clays and highest for the very compressible soils such as peat. The C_α/C_c ratios obtained for the organic clay and silt are typically 0.05 ± 0.01 and within the range reported by Mesri and Castro (1987) and Ladd (1971). According to Mesri et al. (1994), reliable data suggests that C_α/C_c for peat lies within the range 0.06 ± 0.01. This range is compatible with the C_α/C_c ratio calculated for the amorphous peat in the present study, but not the fibrous peat. The somewhat lower C_α/C_c ratio of 0.044 derived for the fibrous peat is, however, consistent with the range of 0.028 to 0.062 reported for fibrous peat by Dhowian and Edil (1980).

Table 2 Mean C_α/C_c ratios for the soils in Table 1

Soil group	Number of data points used	C_α/C_c	r^2
Fibrous peat	72	0.044	0.579
Amorphous peat	34	0.060	0.607
Organic/Sandy silt	18	0.046	0.916
Organic clay	60	0.054	0.706

4 ELASTIC VISCO-PLASTIC MODELS

Current elastic visco-plastic models generally account for the time dependent straining of soils under 1D conditions by extending the classical Terzaghi theory of consolidation to include so called *time lines*, or lines of constant strain rate in the formulation. Bjerrum (1967) and Garlanger (1972) have proposed models in which void ratio or strain is assumed to be a function of effective stress and time. The difficulty with models such as these is in defining an appropriate origin of time, especially in situations when the applied load varies with time (Leroueil et al. 1985). Models, such as those proposed by Leroueil et al. (1985), Yin and Graham (1994) and den Haan (1996) overcome this problem by utilizing strain rate as a means of describing the viscous nature of the soil.

Figure 3 shows the stress, strain, strain-rate relationship for

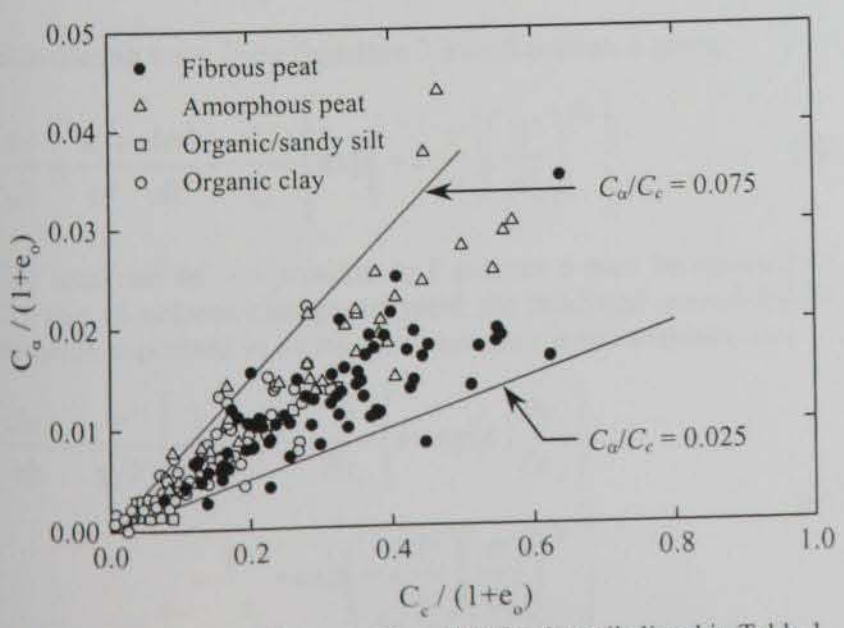

Figure 2 Relationship between C_α and C_c for the soils listed in Table 1

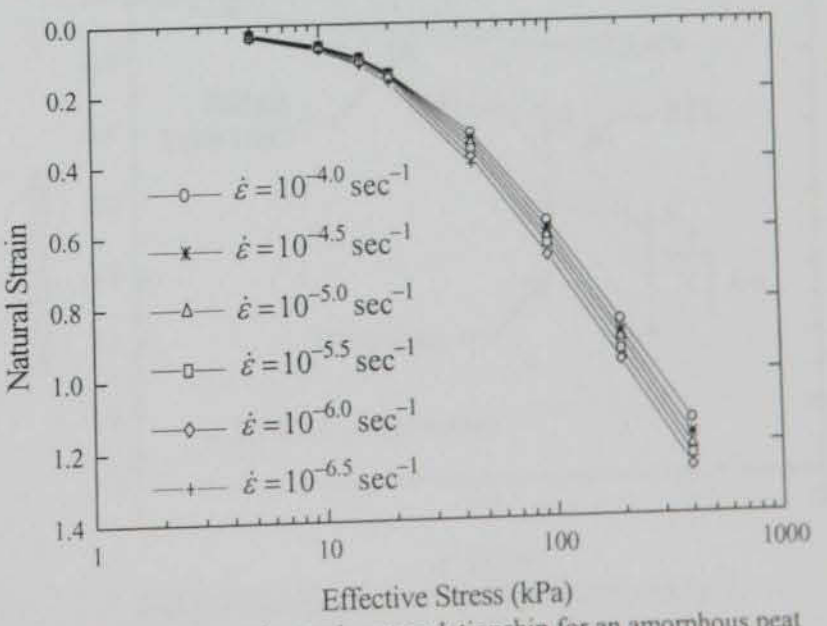

Figure 3 Stress, strain, strain-rate relationship for an amorphous peat

an oedometer test on an Irish amorphous peat. The lines of constant strain rate in Figure 3 may also be interpreted as lines of constant creep strain rate as the plotted strain rates vary between 10^{-4} and $10^{-6.5}$ sec^{-1}, which is typical of strain rates encountered in oedometer tests on peat after excess pore water pressures have dissipated. It is apparent from Figure 3 that a series of linear, parallel and equidistant lines only exist at stresses larger than approximately 25 kPa. The linearity between stress and strain in Figure 3 has been obtained by adopting *natural strain* as a measure of the deformation of the soil. Natural strain, ε^H, is related to traditional engineering strain, ε^C, by:

$$\varepsilon^H = -\ln\left(1-\varepsilon^C\right) \tag{2}$$

A number of workers such as Edil & den Haan (1994) and Lefebvre et al. (1984), have shown engineering strain to be inadequate in linearizing stress-strain data for peats over a wide stress range, and have successfully restored linearity through the use of natural strain.

5 *EVP* MODEL

The *EVP* model, as presented in Yin and Graham (1996), has been successfully applied to laboratory conditions by Yin and Graham (1996), and to field conditions by Nash & Ryde (1999). However, for more compressible materials such as peat, certain modifications need to be made. These modifications led to the *modified EVP model* as described in O'Loughlin and Lehane (2001) and in more detail in O'Loughlin (2001). The modifications and fundamental equations of the modified *EVP* model are now briefly described.

An Instant Time Line (Figure 4) is defined in stress-strain space along which strains are elastic and recoverable. The *EVP* model chooses to scale creep strain rates by introducing a term referred to as equivalent time, t_e. Time lines, which were defined by Bjerrum (1967) as lines equal to periods of sustained loading, are reinterpreted by the *EVP* model as lines with equal values of equivalent time, t_e, and constant creep strain rates. The relationship between strain, effective stress and equivalent time for the *EVP* model is given by:

$$\varepsilon = \lambda/v \ln\left(\sigma'/\sigma'_o\right) + \psi/v \ln\left(\left(t_o + t_e\right)/t_o\right) \tag{3}$$

where σ'_o is the effective stress at zero strain on the *EVP* model's Reference Time Line (RTL), λ/v is the slope of lines of constant creep strain rate, ψ is the coefficient of creep compression, v is the specific volume and t_o is a constant used to define the creep strain rate on the RTL. Total strain rate is equal to the sum of the elastic strain rate (denoted by subscript e) and creep strain rate (denoted by subscript c) and may be formulated as:

$$\dot{\varepsilon} = \dot{\varepsilon}_e + \dot{\varepsilon}_c = \frac{\kappa/v}{\sigma'}\frac{d\sigma'}{dt} + \frac{\psi/v}{t_o + t_e} \tag{4}$$

Substituting for t_e from Equation 3 into Equation 4 gives:

$$\frac{d\varepsilon}{dt} = \frac{\kappa/v}{\sigma'}\frac{d\sigma'}{dt} + \frac{\psi/v}{t_o}\left\{\exp\left(-\varepsilon\frac{v}{\psi}\right)\left(\frac{\sigma'}{\sigma'_o}\right)^{\lambda/\psi}\right\} \tag{5}$$

The total rate of compression in Equation 5 may be equated to the rate of volume change, to yield the modified consolidation equation expressed in terms of excess pore water pressure, u_e:

$$\frac{du_e}{dt} = \frac{\sigma'}{\kappa/V}\left[\frac{1}{\gamma_w}\exp(\varepsilon)\frac{\partial}{\partial z_o}\left\{k\exp(\varepsilon)\frac{\partial u_e}{\partial z_o}\right\} + \frac{\psi/V}{t_o}\exp\left(-\varepsilon\frac{V}{\psi}\right)\left(\frac{\sigma'}{\sigma'_o}\right)^{\lambda/\psi}\right] \tag{6}$$

Equation 6 differs from that published in Yin and Graham (1996), in that (a) the strain, ε, should be interpreted as natural strain, (b) the finite strain formulation used by Gibson et al. (1967) and den Haan (1996) has been adopted, and (c) the permeability, k, is allowed to vary with specific volume according to:

$$\ln v = c_k \ln\left(\frac{k}{k_o}\right) \tag{7}$$

where c_k is an empirical constant, and k_o is the extrapolated permeability at $e_o = 0$. Equation 6 can be used together with Equation 5 to solve problems for single-stage or multi-stage loading conditions.

5.1 *Determining model parameters*

The method of determining *EVP* model parameters as outlined in Yin & Graham (1994) shall be demonstrated using an oedometer test on fibrous peat from Clara in Ireland (Figure 4). Yin & Graham (1994) recommend that the elastic parameter, κ/v, be determined from ε - $\ln\sigma'$ data in the over-consolidated region, and that two typical load increments from the normally consolidated stress range be used to determine the remaining model parameters. In Figure 4, the instant time line is fitted to the first two load increments to yield the elastic parameter κ/v. The load increment from state point A to state point B is then used to determine the parameters ψ/v and t_o. The stress-strain path from A to B may be separated into an elastic component (A to a) and a visco-plastic component (a to B). The increase in strain from point A to a may be calculated from:

$$\varepsilon_a = \varepsilon_A + \kappa/v \ln\left(\sigma'_B/\sigma'_A\right) \tag{8}$$

The RTL in Figure 4 is positioned so that it passes through a, at which point t_e is zero. This means that t_e values are equal to actual loading durations as the soil state moves from point a to point B, allowing strain to be calculated by Equation 9.

$$\varepsilon = \varepsilon_a + \psi/v \ln\left(\left(t_o + \Delta t\right)/t_o\right) \tag{9}$$

Secondary compression ε - $\ln t$ data for the load increment between points A and B can then be fitted to Equation 9 where the term, ε_a may be calculated from Equation 8, to yield the parameters ψ/v and t_o. Parameters λ/v and σ'_o may be determined by considering a second loading increment from point B to point C in Figure 4. The strain at point b may be determined from:

$$\varepsilon_b = \varepsilon_B + \kappa/v \ln\left(\sigma'_C/\sigma'_B\right) \tag{10}$$

or from:

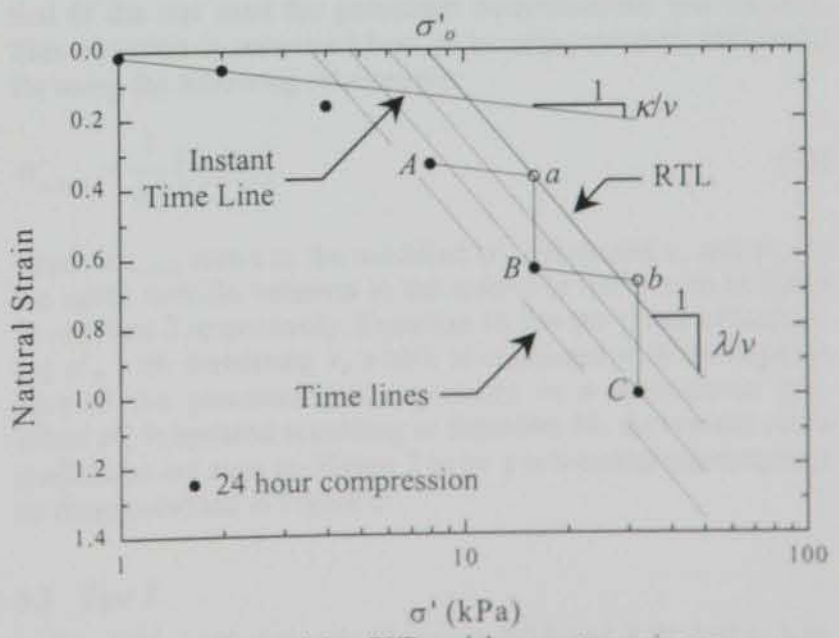

Figure 4 Determining *EVP* model parameters using an oedometer test on fibrous peat

Table 3 Typical modified *EVP* model parameters determined from standard 24-hour oedometer tests

Soil description	v_o	κ/v	λ/v	ψ/v	t_o : sec	σ'_o : kPa	k_o: m/sec	c_k
Clara fibrous peat	25.77	0.040	0.373	0.015	0.3	5.96	3.32×10^{-12}	0.16
Ballydermot amorphous peat	13.14	0.046	0.406	0.021	5.8	28.30	7.49×10^{-11}	0.17
Arklow amorphous peat	5.43	0.036	0.222	0.012	96.1	52.03	4.07×10^{-11}	0.12
Arklow silty peat	5.61	0.042	0.172	0.007	261.1	35.50	9.17×10^{-13}	0.10
Arklow organic silt	3.93	0.016	0.093	0.003	24.2	47.80	4.53×10^{-17}	0.05
Belfast organic clay	2.80	0.014	0.123	0.008	90.0	44.02	3.03×10^{-9}	0.18

$$\varepsilon_b = \frac{\lambda}{v}\ln\left(\frac{\sigma'_C}{\sigma'_o}\right) + \frac{\psi}{v}\ln\left(\frac{t_o + t_{e,b}}{t_o}\right) \tag{11}$$

The equivalent time at point b, $t_{e,b}$, may then be determined from Equations 10 and 11:

$$t_{e,b} = t_o\left\{\left[\exp\left(\frac{v}{\psi}\varepsilon_B\right)\left(\frac{\sigma'_B}{\sigma'_A}\right)^{\kappa/\psi}\left(\frac{\sigma'_B}{\sigma'_o}\right)^{-\lambda/\psi}\right] - 1\right\} \tag{12}$$

The equivalent time at point C may be calculated by adding the equivalent time at point b to the loading duration, t:

$$t_{e,C} = t_{e,b} + \Delta t \tag{13}$$

Substituting Equation 13 into Equation 3 allows the strain at point C to be calculated:

$$\varepsilon_C = \frac{\lambda}{v}\ln\left(\frac{\sigma'_C}{\sigma'_o}\right) + \frac{\psi}{v}\ln\left(\frac{t_o + t_{e,C}}{t_o}\right) \tag{14}$$

A direct relationship between λ/v and σ'_o may be obtained by considering the state point a in Figure 4. As a is on the RTL with $t_e = 0$, Equation 3 gives:

$$\varepsilon_a = \frac{\lambda}{v}\ln\left(\frac{\sigma'_B}{\sigma'_o}\right) \tag{15}$$

The parameters λ/v and σ'_o may now be uniquely determined from Equations 14 and 15. Permeability may be determined using graphical methods for each stress increment, and the empirical parameters c_k and k_o derived from Equation 8.

6 MODEL APPLICATION

The modified *EVP* model parameters were determined from all oedometer tests performed at TCD. Representative average parameters for each of the soil groups listed in Table 1 are listed in Table 3. These 'typical' parameters were derived from standard 24-hour tests and are used in the following in conjunction with programmed formulations of the modified *EVP* model to predict the settlements measured in oedometer tests on three independent samples:

(i) Test 1: Belfast organic clay, $v_o = 2.77$
(ii) Test 2: Clara fibrous peat, $v_o = 21.76$
(iii) Test 3: Clara fibrous peat, $v_o = 23.69$

6.1 *Test 1*

Figure 5 compares measured strains with that predicted using the modified *EVP* model for the normally consolidated stress increments of Test 1. This test involved a LIR of 1, with an initial stress of 6.25 kPa, up to a final stress of 800 kPa. The LID for all stress increments was 1 day, with the exception of the 400 kPa increment which was maintained for 3 days. The normally consolidated stress increments are shown to be well captured by the modified *EVP* model, although the 50 kPa stress increment shows evidence of recompression, which may be attributed to an apparent preconsolidation pressure at approximately 35 kPa.

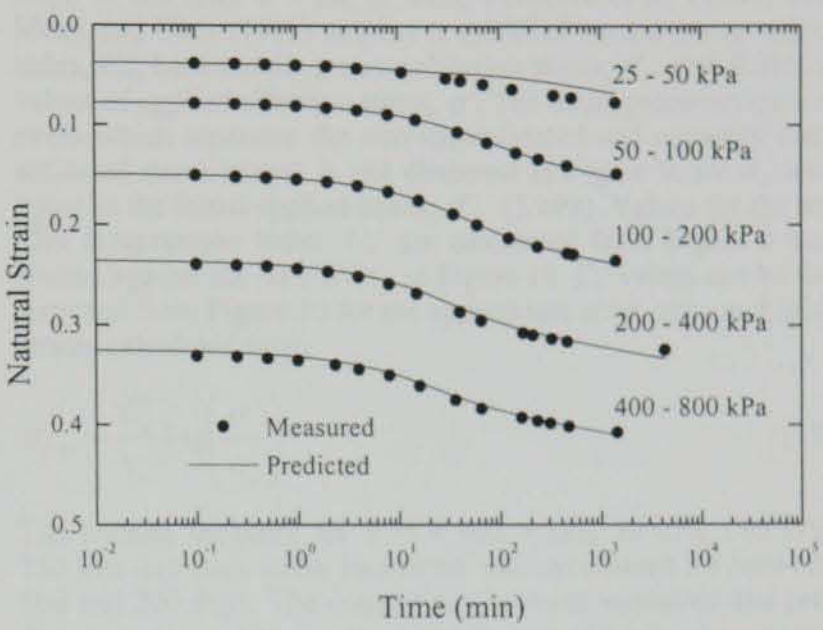

Figure 5 Comparison of measured results with those calculated using the modified *EVP* model for Test 1

6.2 *Test 2*

Figure 6 compares measured and predicted settlements for Test 2. This test involved LIRs varying between 0.43 and 4.24, and LIDs which were maintained for between 1 and 2 weeks. It is evident from Figure 6 that the modified *EVP* model overestimates the settlements for each stress increment. However, the initial specific volume of 21.76 for this test was different from that of the test used for parameter determination; see Table 3. This variation is presumed here to be approximately accounted for using the following relationship:

$$\sigma'_{o,\mathrm{mod}} = \frac{1}{\sigma'_o}\left(v'_o / v_o\right) \tag{16}$$

where $\sigma'_{o,\mathrm{mod}}$ refers to the modified σ'_o value, and v_o and v'_o are the initial specific volumes in the reference test (i.e. as in Table 3) and Test 2 respectively. Equation 16 has the effect of increasing σ'_o with decreasing v_o which is consistent with the dependence of the preconsolidation pressure in a non-viscous soil. When σ'_o is updated according to Equation 16, the revised strain predictions are seen on Figure 7 to be a substantial improvement on those provided in Figure 6.

6.3 *Test 3*

The LIRs in Test 3 varied between 0.24 and 4.84, and as was

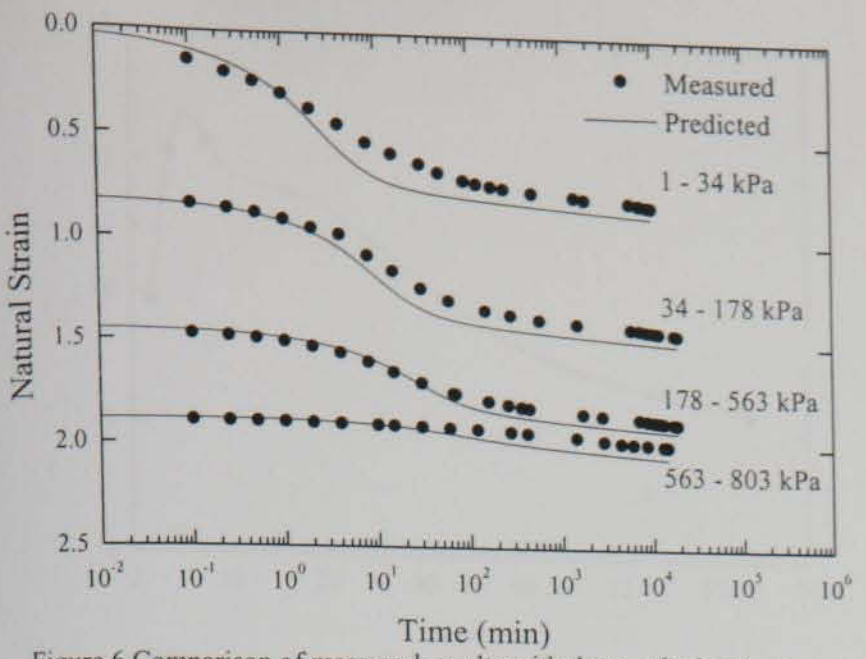

Figure 6 Comparison of measured results with those calculated using a constant σ'_o value in the modified *EVP* model for Test 2

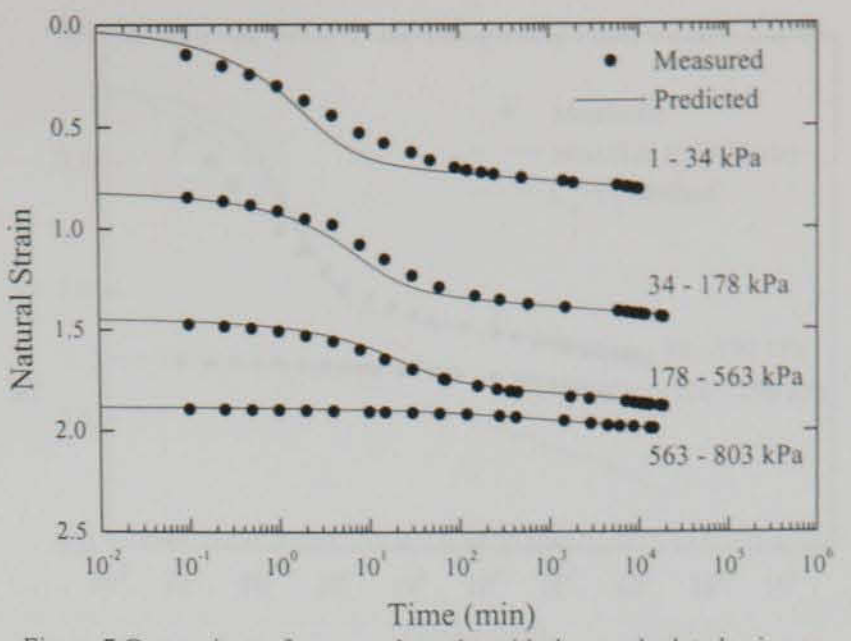

Figure 7 Comparison of measured results with those calculated using an updated σ'_o value in the modified *EVP* model for Test 2

the case with Test 2, LIDs ranging from 1 to 2 weeks were employed. The predictions in Test 3 were obtained using both the parameters given in Table 3 and using σ'_o adjusted according to Equation 16. Predicted and measured strain data are shown on Figure 8 where it is seen that employing an adjusted σ'_o value leads to slightly improved predictions. Although the modified *EVP* model captures the essential features of Test 3, it is evident that the agreement between measured and predicted data is not of the same level as that obtained for Test 2. This may be attributed to the inherent spatial variability of peat. The presence of fibres and other organic constituents leads to large variations in the compressibility characteristics, particularly in poorly humified peat where the length of fibres is often comparable to the diameter of the specimens (Magnan 1994, Edil 1994). The variability of peat is often so severe that it is almost impossible to obtain representative samples for testing, unless a very large number of samples are taken (Magnan 1994). Perrin (1973) showed that the recorded strains from 21 oedometer tests on a black peat from Borgoin, France under a stress of 57 kPa ranged from 5 to 40 %.

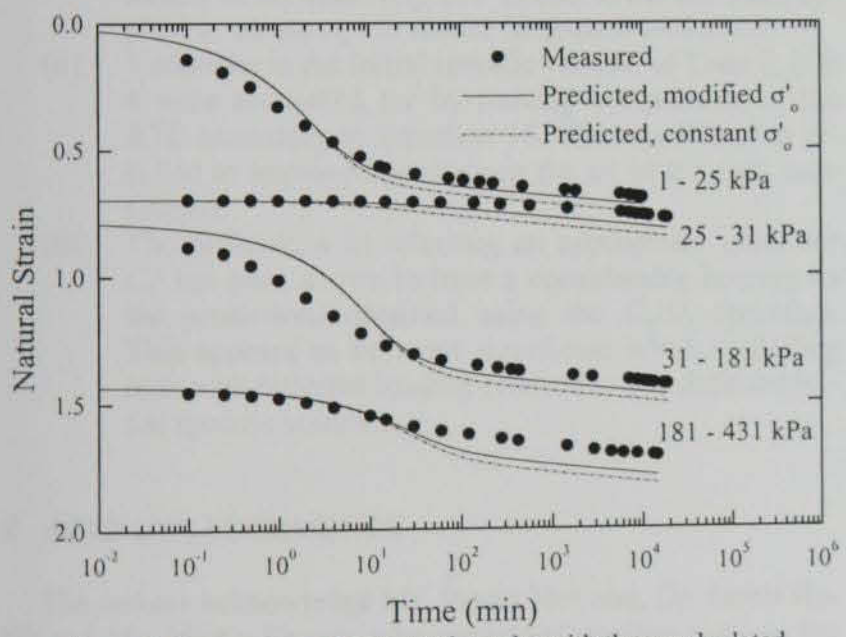

Figure 8 Comparison of measured results with those calculated using the modified *EVP* model for Test 3

7 COMPARISON OF MODIFIED EVP MODEL AND C_α/C_c APPROACH

The C_α/C_c approach remains in popular use and its application to a further test on Clara fibrous peat (referred to here as Test 4) is now compared with the predictions made by the modified *EVP* model. Figure 9 shows the EOP e – log σ' relationship for the test used for determining the modified *EVP* parameters for the fibrous peat in Table 3. As is often the case with peats, the e – log σ' curve is highly non-linear, even at comparatively low stresses. Rather than use a single value of C_c to describe the slope of the EOP e – log σ' data, Lefebvre et al. (1984) and Mesri and Choi (1985) employ a modified *secant* compression index, C_c', between the preconsolidation stress, σ'_p, and different values of applied effective stress, σ'. The usual preconsolidation stress which separates the over-consolidated and normally consolidated stress ranges is not observed in Figure 9, so σ'_p was taken as the initial applied stress, σ'_i, (5 kPa). Values for the secant compression index, C_c' are calculated from Figure 9 and plotted against the ratio σ'/σ'_i, in Figure 10. C_c' values can be determined from Figure 10 for the appropriate σ'/σ'_i ratio and EOP strains calculated using:

$$\varepsilon_{EOP} = \frac{C_c'}{v_o} \log\left(\frac{\sigma'}{\sigma'_i}\right) \tag{17}$$

The loading sequence for Test 4 was 4 kPa, 10 kPa, 100 kPa, 150 kPa and each stress increment was maintained for between 100 and 200 days. The comparison between measured and predicted strain profiles for the 100 kPa and 150 kPa stress increments are shown in Figure 11. The value of C_c' used in the C_α/C_c approach was estimated from Figure 10 as 10.65 for the 100 kPa increment, and 10.11 for the 150 kPa increment. The predicted strain profiles obtained using the C_α/C_c approach assumed a Terzaghi style solution for calculating strains during the consolidation phase. Secondary compression was assumed to start whenever primary consolidation was 95 % completed; C_α values were taken as $0.044 C_c'$ in accordance with Table 2.

For the modified *EVP* predictions, as was the case with Tests

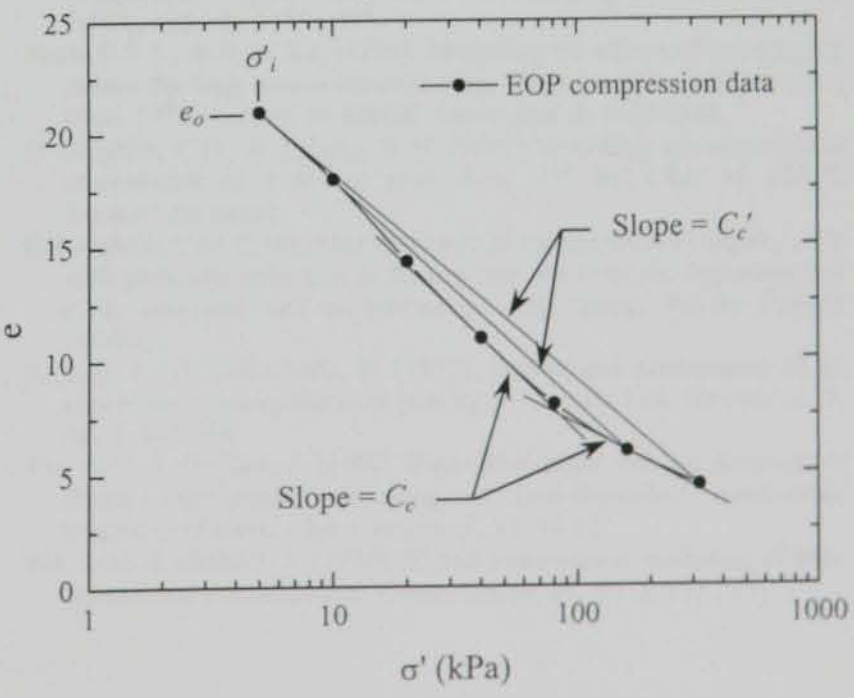

Figure 9 Definition of the secant compression index, C_c'

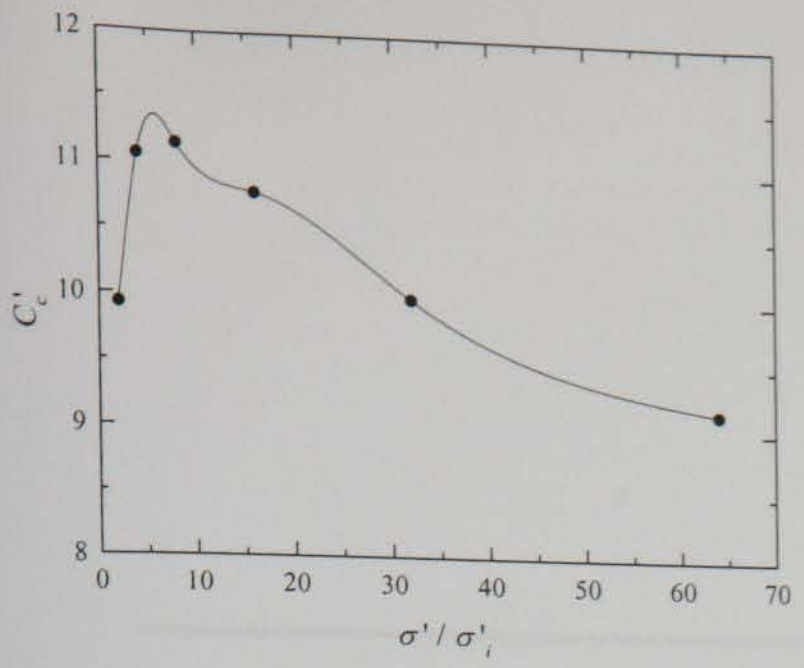

Figure 8 Relationship between C_c' and σ'/σ'_i for Clara fibrous peat

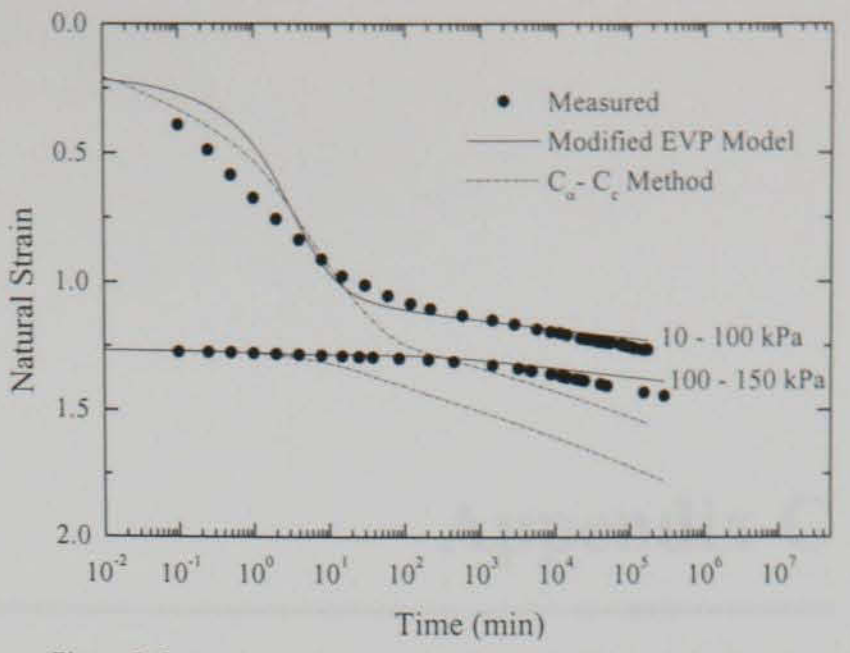

Figure 9 Comparison of measured and calculated strains for Test 4

2 & 3, σ'_o was modified according to Equation 16, in order to account for the different initial specific volume in Test 4 (v_o = 20.49). The modified *EVP* model predicts strains quite well while the C_α/C_c approach clearly predicts much larger strains than those which were observed. Such overpredictions reflect the difficulty in determining a suitable value of C_c' for tests with different loading conditions and different initial specific volumes.

8 CONCLUSIONS

The good agreement shown in Figure 5 between measured and predicted data for Test 1, suggests that the modified *EVP* model is valid for organic clays. The success of the modified *EVP* model and the C_α/C_c approach in describing the 1D compression of fibrous peat is summarized as follows:

(i) The modified EVP model has been demonstrated to be successful in predicting settlements for a wide range of LIR values. The relevance of LIR >> 1 is particularly relevant to peat deposits, as stress increments well in excess of the relatively low in-situ stress are often applied in an attempt to reduce long-term settlement.

(ii) Variations in the initial specific volume of Tests 2, 3 & 4 were accounted for by moving the position of the RTL according to Equation 16. This modification resulted in improved predictions for all of the tests considered.

(iii) The difficulties in selecting an appropriate value for C_c' has been shown to have a considerable bearing on the predictions obtained using the C_α/C_c approach. This appears to be most significant when modelling tests with different loading conditions and different initial specific volumes.

9 ACKNOWLEDGEMENTS

The authors acknowledge Mr. Bryan McCabe, Dr. Samir Hebib and Mr. Martin Carney who performed various tests on the peats, silts and organic clay.

10 REFERENCES

Bjerrum, L. (1967). Engineering geology of Norwegian normally-consolidated marine clays as related to settlements of buildings. *Géotechnique*, **17**, No. 2, 81-118.

Dhowian, A.W. & Edil, T. B. (1980). Consolidation behaviour of peats. *Geotech. Testing J.*, **3**, No. 2, 105-114.

Edil, T. B. (1994). General report session 3: Immediate issues in engineering practise. *Advances in understanding and modelling the mechanical behaviour of peat*, Balkema, Rotterdam, 403-413.

Edil, T. B., & den Haan, E. J. (1994). Settlement of peats and organic soils. *ASCE Geotech. Spec. Publ, No. 40*, **2**, 1543-1572.

Garlanger, J.E. (1972) The consolidation of soils exhibiting creep under constant effective stress. *Géotechnique*, **22**, No. 1, 71-78.

Gibson, R.E., England, G.L. & Hussey, M.J.L. (1967) Thetheory of one-dimensional consolidation of saturated clays. 1. Finite non-linear consolidation of thin homogeneous layers. *Géotechnique*, **17**, 261-273.

den Haan, E.J. (1996) A compression model for non-brittle soft clays and peat. *Géotechnique*, **46**, No. 1, 1-16.

Ladd, C. C. (1971) Settlement analysis for cohesive soils. *Research Report R71-2*, Massachusetts Institute of Technology, Cambridge, Massachusetts.

Lefebvre, G., Langlois, P., Lupien, C., & Lavallée, J.-G. (1984). Laboratory testing and *in situ* behaviour of peat as embankment foundation. *Can. Geotech. J.*, **21**, No. 2, 332-337.

Leroueil, S., Kabbaj, M., Tavenas, F. & Bouchard, R. (1986). Closure to stress-strain-strain rate relations for the compressibility of sensitive natural clays. *Géotechnique*, **36**, No. 2, 288-290.

Magnan, J.P. (1994) Construction on peat: State of the art in France. *Advances in understanding and modelling the mechanical behaviour of peat*, Balkema, Rotterdam, 369-379.

Mesri, G. & Castro, A. (1987). The C_α/C_c concept and K_o during secondary compression. *J. Geotech. Engrg.*, ASCE, **113**, No. 3, 230-247.

Mesri, G. & Choi, Y.K. (1985). Settlement analysis of embankments on soft clays. *J. Geotech. Engrg.*, ASCE, **111**, No. 4, 441-464.

Mesri, G. & Godlewski, P.M. (1977). Time- and stress-compressibility interrelationship. *J. Geotech. Engrg.*, ASCE, **103**, No. 5, 417-430.

Mesri, G., Stark, T. D. & Chen, C.S. (1994). Discussion of C_α/C_c concept applied to compression of peat. *J. Geotech. Engrg.*, ASCE, **120**, No. 4, 764-767.

Mesri, G., Stark, T. D., Ajlouni, M.A. & Chen, C.S. (1997). Secondary compression of peat with or without surcharging. *J. Geotech. Engrg.*, ASCE, **123**, No. 5, 411-421.

Nash, D.F.T., & Ryde S.J. (1999). Modelling the effects of surcharge to reduce the long term settlement of an embankment on soft alluvium. *Proc. 12th Eur. Conf. on SMGE, Amsterdam*, **3**, 1555-1561.

O'Loughlin, C.D., & Lehane, B.M. (2001) Modelling one-dimensional compression of a fibrous peat. *Proc. 15th Int. Conf. on SMGE, Istanbul*, (in press).

O'Loughlin, C.D. (2001) One-dimensional compression of organic soils with particular reference to fibrous peat. Ph.D thesis, Department of civil, structural and environmental engineering, Trinity College Dublin.

Samson, L., & LaRochelle, P. (1972). Design and performance of an expressway constructed over peat by preloading. *Can. Geotech. J.*, **9**, No. 4, 447-466.

Yin, J.-H. & Graham, J. (1994). Equivalent times and one-dimensional elastic visco-plastic modelling of time-dependent stress-strain behaviour of clays. *Can. Geotech. J.*, **31**, 42-52.

Yin, J.-H. & Graham, J. (1996). Elastic visco-plastic modelling of one-dimensional consolidation. *Géotechnique*, **46**, No. 3, 515-527.

Appendix C

Modelling one-dimensional compression of a fibrous peat

O'Loughlin, C.D. & Lehane, B.M. (2001). Modelling one-dimensional compression of a fibrous peat. *Proc. 15th Int. Conf. Soil Mech. Geotech. Engr.*, Istanbul, 223-226.

Modelling one-dimensional compression of a fibrous peat

Modélisation le compactage unidimensionnel d'une tourbe fibreuse

O'Loughlin, C.D., Dept. of Civil Engineering, Trinity College, Dublin 2, Ireland
Lehane, B.M., Dept. of Civil Engineering, Trinity College, Dublin 2, Ireland

ABSTRACT: Amongst the most widely used state-of-the art constitutive models for strain-rate dependant soils in one-dimensional compression are the *EVP* model proposed by Yin & Graham (1994, 1996) and the *abc* model developed by den Haan (1996). Although these models were developed independently, both assume an elastic visco-plastic type soil response. In the first section of this paper the fundamental differences between the models are clarified, whereas in the second section both models are applied to a poorly humified, fibrous peat from the Irish midlands. The relative merits of both approaches for modelling this peat are discussed.

RÉSUMÉ: Parmi le plus largement répandu des modèles constitutifs pour les sols dépendants de vitesse de deformation pour le compactage unidimensionnel sont les modéles *EVP* proposés par Yin et Graham (1989, 1996) et le modèle *abc* développé par den Haan (1996). Ces deux modèles ont été développés indépendamment, bien que tous les deux assument une réponse du sol de type élastique visco-plastique. Dans la première partie de cet article les différences fondamentales entre les modèles sont clarifiées, tandis que dans la deuxième partie les deux modèles sont appliqués à une tourbe fibreuse à partir des Midlands irlandais. Les mérites relatifs des deux modèles sont discutés par rapport à de tels matériaux complexes.

1 INTRODUCTION

Fibrous peat is encountered in the majority of raised bogs in central Ireland, and is an extremely compressible material with an extraordinarily high in-situ water content and initial voids ratio. Consolidation in peat occurs relatively quickly and settlement is dominated by the so-called *secondary* or *creep* compression. Conventional practice relies on methods similar to that suggested by Mesri & Choi (1985), whereby creep strains are measured relative to the end of primary (EOP) stress-strain curve. Such methods imply that EOP strains are unique irrespective of the drainage conditions, which is contrary to laboratory data reported by workers such as Edil et al. (1992), Berre & Iversen (1972) and Leroueil et al. (1986). Consequently, the focus over the past few decades has been to develop constitutive models that appropriately define the relationship between stress, strain and strain rate. The aim of this paper is to test the usefulness of the *abc* model of den Haan (1996) and the *EVP* model of Yin & Graham (1994, 1996) in describing the one-dimensional compression of an Irish fibrous peat under a variety of loading conditions.

2 ELASTIC VISCO-PLASTIC MODELS

Elastic visco-plastic models generally assume that, in the normally consolidated region, the creep strain rate for a given stress and strain state is unique and that, at a given creep strain rate, there is a linear relationship between strain (ε) and the logarithm of effective stress (σ') and a linear relationship between strain and the logarithm of creep strain rate ($d\varepsilon/dt$). The stress-strain-strain rate relationships assumed by the *abc* and *EVP* models are summarised in Figure 1 and particular characteristics of each of the models are now described briefly.

2.1 *EVP model*

The *EVP* model chooses to scale creep strain rates by introducing a term referred to as equivalent time, t_e. The relationship between strain, effective stress and creep strain rate for the *EVP* model is given by:

$$\varepsilon = \lambda/v \ln(\sigma'/\sigma'_o) + \psi/v \ln((t_o + t_e)/t_o) \quad (1)$$

where ε is the linear (or Cauchy) strain, σ'_o is the effective stress at zero strain on the *EVP* model's Reference Time Line (RTL), λ/v is the slope of lines of constant creep strain rate, ψ is the coefficient of creep compression, v is the specific volume and t_o is a constant used to define the creep strain rate on the RTL. Elastic strain rate (denoted by subscript e) is formulated as:

$$\dot{\varepsilon}_e = \kappa/v \frac{d\ln\sigma'}{dt} = \frac{\kappa/v}{\sigma'}\frac{d\sigma'}{dt} \quad (2)$$

The total rate of compression is taken as the sum of elastic strain rate and creep strain rate, which when equated to the rate of volume change, yields the modified consolidation equation expressed in terms of excess pore water pressure, u:

$$\frac{k}{\gamma_w}\frac{\partial^2 u}{\partial z^2} = \frac{\kappa/v}{\sigma'}\frac{\partial u}{\partial t} - \frac{\psi/v}{t_o}\exp\left\{-\varepsilon\frac{v}{\psi}\right\}\left(\frac{\sigma'}{\sigma'_o}\right)^{\lambda/\psi} \quad (3)$$

Equation 3 can be used together with Equation 1 to solve problems for single-stage or multi-stage loading conditions. A more suitable formulation for constant rate of strain (CRS) conditions may be written as:

$$\dot{\varepsilon} = \frac{\kappa/v}{\sigma'}\left(\frac{\partial\sigma'}{\partial t}\right) + \left(\frac{\psi/v}{t_o + t_e}\right) \quad (4)$$

where t_e may be determined from Equation 1.

Yin & Graham (1994) propose determination of the elastic parameter, κ/v, from ε - $\ln\sigma'$ data in the overconsolidated region, and the remaining *EVP* parameters from two load increments in the normally consolidated region. Firstly, the RTL is positioned so that it passes through a hypothetical stress-strain state, where the stress level is the total stress upon application of the first load increment, and the strain level is increased by the corresponding elastic component of strain. As t_e is taken as zero on the RTL, t_e values are equal to actual loading durations for this first load increment. Secondary compression ε – $\ln t$ data for the first load increment can then be fitted to the second term on the RHS of Eq-

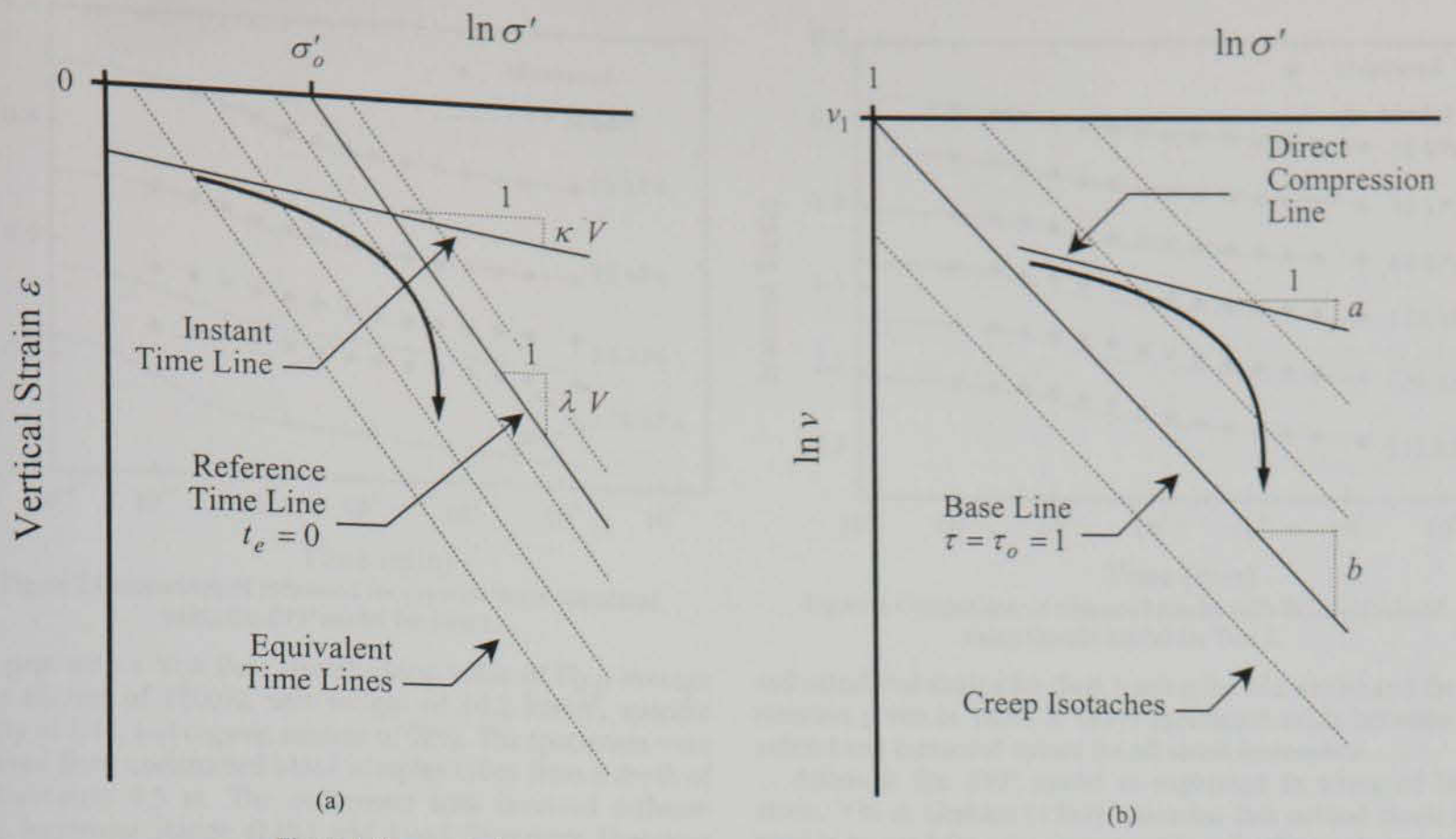

Figure 1 Stress - strain – creep strain rate relationship for (a) *EVP* model, (b) *abc* model

uation 1 to yield the parameters ψ/v and t_o. The magnitude of elastic strain due to the second load increment can be calculated either from Equation 1, or by moving along the instant line (Figure 1) from the previously known ε - σ' state. This allows the equivalent time for this stress-strain state to be calculated. As before, further creep straining from this point can be calculated from Equation 1, by considering that t_e at the end of loading is equal to t_e at the end of elastic straining plus the loading duration Δt. Enough information is now available to calculate the parameters λ/v and σ'_o uniquely using the end states of the two load increments.

2.2 *abc model*

In contrast to the *EVP* model, the *abc* model uses natural rather than linear strain as a measure of the soil compression, and adopts v_o as the specific volume at zero strain. Creep strain rates are linked to a term referred to as intrinsic time (τ) and defined as $c/\dot{\varepsilon}$, which relates $\dot{\varepsilon}$ uniquely to one value of intrinsic time. $\tau = \tau_o = 1$ day locates the base or reference line on which the strain rate is c/τ_o and v_1 is the specific volume at unit effective stress. The equivalent form of Equation 1 for the *abc* model is:

$$-\ln(v/v_1) = b\ln(\sigma') + c\ln(\tau/\tau_o) \tag{5}$$

The *abc* model introduces direct strain rate, which is defined as in Equation 2, but with the parameter a instead of κ/v; the model also uses the term direct as these strains are not assumed to be completely recoverable. The equivalent forms of Equations 3 and 4 for the *abc* model are:

$$\frac{d\sigma'}{dt} = \frac{\sigma'}{a}\left[-\frac{\gamma_s - \gamma_w}{\gamma_w}\frac{\partial}{\partial z}\left(\frac{k}{v}\right) + \frac{1}{\gamma_w}\frac{v_o}{v}\frac{\partial}{\partial z}\left\{k\frac{v_o}{v}\frac{\partial\sigma'}{\partial z}\right\} - \frac{c}{\tau}\right] \tag{6}$$

$$\dot{\varepsilon} = \frac{a}{\sigma_z}\frac{\partial\sigma'}{\partial t} + \frac{c}{\tau} \tag{7}$$

where γ_s and γ_w are the unit weights of soil and water respectively and the permeability, k, is allowed to vary with specific volume according to:

$$C_k \ln(k/k_o) = \ln(v/v_o) \tag{8}$$

Den Haan (1996) recommends that Equation 5 be fitted to the creep tails of $\varepsilon - \ln t$ data for all load increments in the normally consolidated stress range to give the creep parameter c and a constant equal to ($b\ln\sigma' - \ln v_1$). An average value of c is taken from these creep tails, and used to define the creep strain rate on the base line (c/τ_o). The interpolated strain at this creep strain rate is then determined for each normally consolidated stress increment and Equation 5 fitted to the interpolated values varying b and v_1 until an optimal fit is obtained. The parameter a may be estimated in much the same way as κ/v was for the *EVP* model. Permeability (k) is estimated for each load increment using Taylor's root time, and the empirical parameters C_k and k_o are derived from Equation 8.

2.3 *Differences between the abc and EVP formulations*

Despite differences in terminology, it is evident that the *abc* and *EVP* approaches are essentially very similar. There are, however, some notable differences in the detail published to date, which are summarised in Table 1.

Table 1 Differences in the *abc* and *EVP* models

***abc* model**	***EVP* model**
Natural strain	Linear Strain
Strain origin linked to soil's initial specific volume/stress history	Arbitrary strain origin
k dependant upon v	k assumed constant
Parameters derived from all data in normally consolidated region	Two load increments used as a basis for parameter selection
Finite strain formulation	Thickness of soil layer assumed constant throughout straining
Base line is related to 24-hour compression curves	RTL related to end of primary consolidation curves

3 LABORATORY TESTS

The performance of the *abc* and *EVP* models was assessed by comparing their predictions with oedometer and Constant Rate of Strain (CRS) tests carried out on a typical peat from the Irish midlands. This peat is a highly compressible, poorly humified fi-

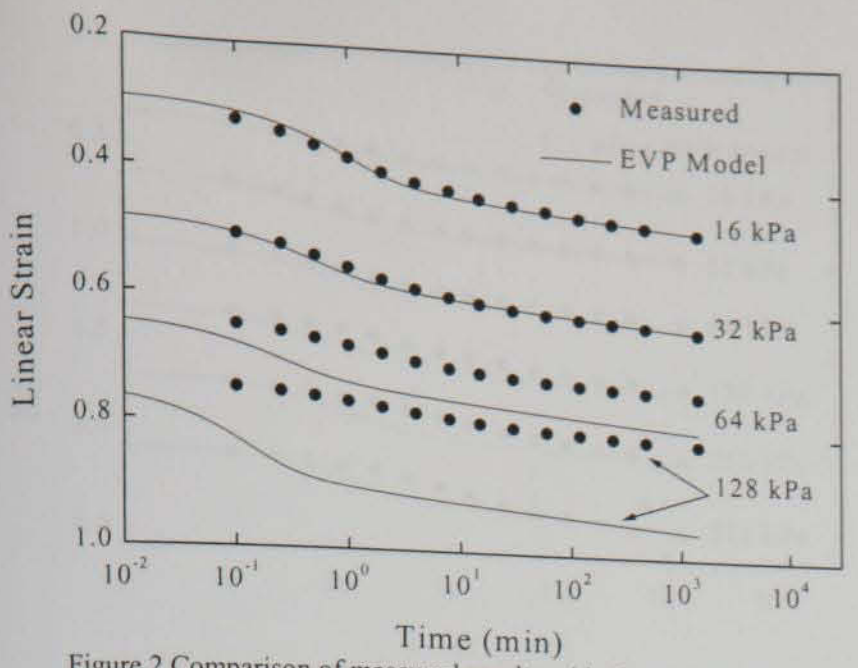

Figure 2 Comparison of measured results with those calculated using the *EVP* model for Test 1.

rous peat with a Von Post Humification value of H_{2-3}, average water content of 1800%, unit weight of 10.2 kN/m^3, specific gravity of 1.41, and organic content of 98%. The specimens were retrieved from undisturbed block samples taken from a depth of approximately 0.5 m. The oedometer tests involved different Load Increment Ratios (LIR) and Load Increment Durations (LID), and the CRS tests were performed at different strain rates. Two oedometer tests and one CRS test were selected for specific examination in this paper:

- Test 1: Standard 24 hour oedometer test with LIR=1
- Test 2: Oedometer test with high LID and LIR=2
- Test 3: CRS test performed at a nominal strain rate of 7.34×10^{-5} min^{-1}; negligible excess pore pressures were recorded at this relatively slow rate.

As the majority of reported 1-D compression data are from standard 24-hour oedometer tests (with LIR=1), Test 1 was selected to derive the model parameters. These parameters are then used to predict the response of Test 2 and Test 3.

4 PREDICTIONS

The model parameters were derived from Test 1 in accordance with the procedures recommended for the *abc* and *EVP* models and are listed in Tables 2 and 3. All load increments in the virgin stress range were used to determine the *abc* model parameters, whereas the 16 kPa and 32 kPa load increments were used to determine the *EVP* model parameters.

Table 2 *EVP* model parameters determined from Test 1

κ/v	λ/v	ψ/v	t_o : min	σ'_o : kPa	k : m/sec
0.052	0.234	0.007	1.28×10^{-6}	4.095	1.15×10^{-7}

Table 3 *abc* model parameters determined from Test 1

a	b	c	v_1	v_o	k_o: m/sec	C_k
0.056	0.519	0.018	73.886	32.833	1.77×10^{-6}	0.215

The parameters listed in Tables 2 and 3 have been used in conjunction with programmed formulations of the *abc* and *EVP* models to predict the settlements for Test 1. Figure 2 compares measured data with that predicted using the *EVP* model for selected normally consolidated load increments in Test 1. It is obvious from Figure 2 that the *EVP* model does not capture the entire normally consolidated stress-strain response. However, it is worth noting that the increments from which the parameters were determined, namely the 16 kPa and 32 kPa stress increments are quite well predicted. Figure 3 compares the measured

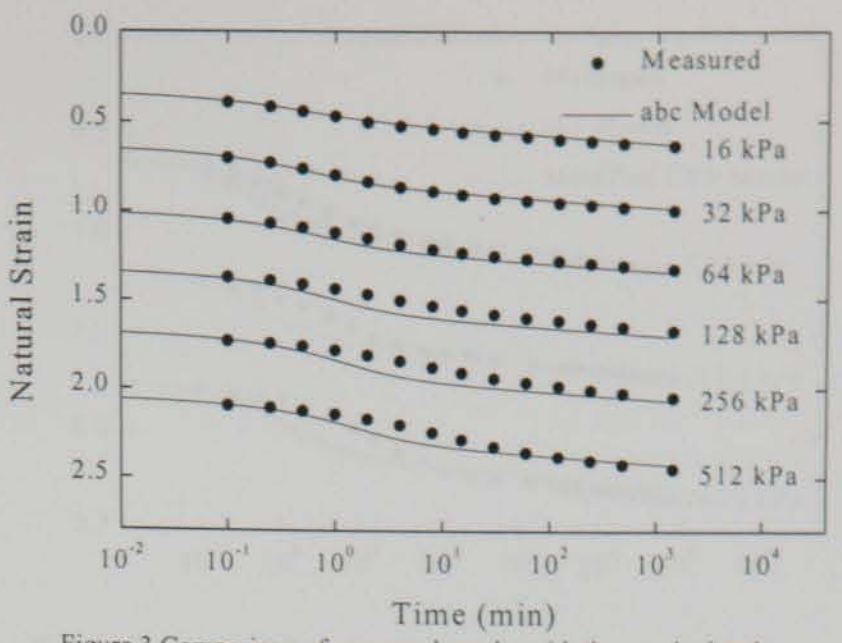

Figure 3 Comparison of measured results with those calculated using the *abc* model for Test 1.

and calculated strains for Test 1 using the *abc* model and the parameters given in Table 3. Good agreement exists between calculated and measured values for all stress increments.

Although the *EVP* model is expressed in terms of linear strain, Yin & Graham (1989) conceded that natural strain may need to be used for very compressible soils. Figure 4 shows Test 1 data plotted in stress-strain space at a strain rate of 10^{-6} sec^{-1} using both natural and linear strain as a measure of the compression. Strain data are normalized by the maximum strain in each case to allow for ease of comparison. It is evident from Figure 4 that the use of natural strain is much more successful in linearizing ε - log σ' data for this type of soil.

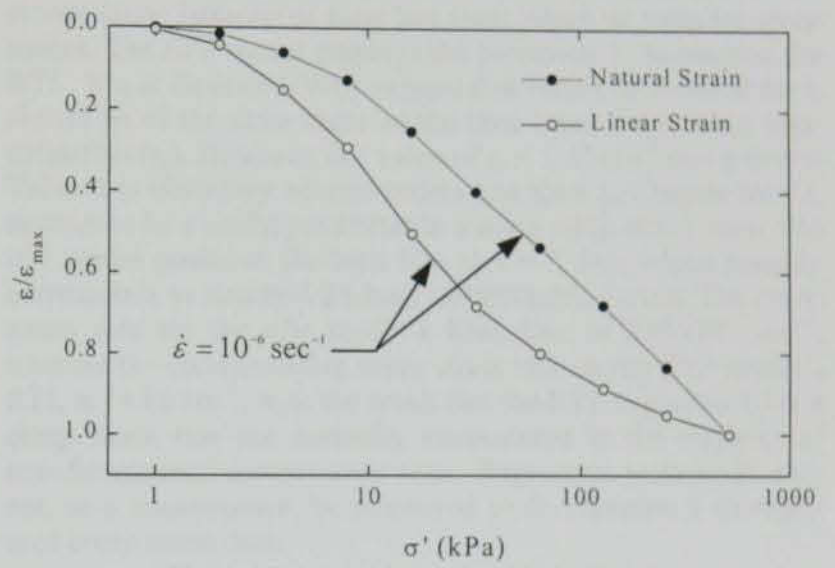

Figure 4 Stress-strain relationship for Test 1

The *EVP* model has been reformulated in terms of natural strain by the authors, with provision for varying permeability and changing dimensions of the soil layer during compression. Figure 5 compares the measured strains with those calculated using the re-assessed parameters given in Table 4 and the modified *EVP* model. There is an obvious marked improvement in the use of natural strain over linear strain in predicting the settlements over a wider stress range.

Both the *abc* model and the *modified EVP* model have been used in conjunction with the parameters in Tables 3 and 4 to predict settlements for Test 2. Measured and calculated data for selected load increments from Test 2 are shown in Figure 6. The 37.8 kPa increment was maintained for 40 days, whereas the 113.4 kPa and the 340.2 kPa increments were maintained for 60 days. The initial specific volume (v_o) for Test 1 was 32.8 where-

Table 4 Modified *EVP* model parameters determined from Test 1

κ/v	λ/v	ψ/v	t_o : min	σ'_o : kPa	k_o: m/sec	C_k
0.056	0.515	0.014	1.57×10^{-5}	7.775	1.77×10^{-6}	0.215

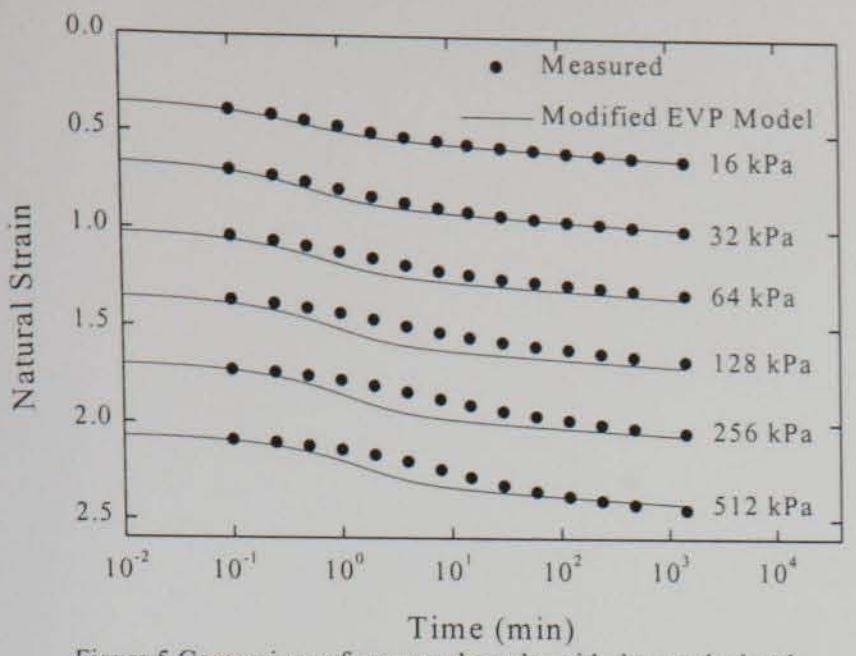

Figure 5 Comparison of measured results with those calculated using the modified *EVP* model for Test 1.

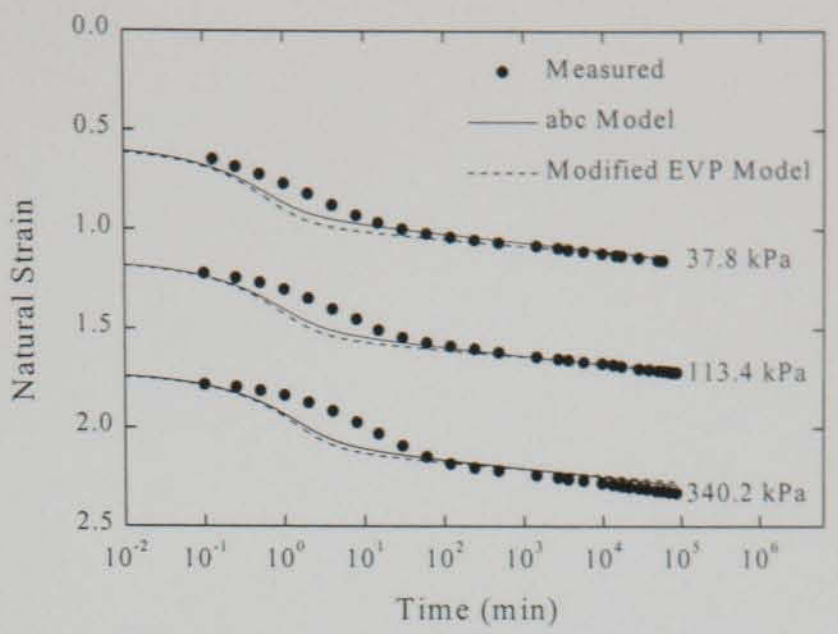

Figure 6 Comparison of measured results with those calculated using the *abc* and modified *EVP* models for Test 2.

as that in Test 2 was 29.8. This variation was taken into account in the *abc* prediction for Test 2 by employing v_o = 29.8 and a modified v_1 value derived from:

$$v_1' = v_o'(v_1/v_o) \tag{9}$$

where v'_1 and v'_o refer to the modified parameters in Test 2. In this case both models predict final settlements adequately, although settlements during consolidation are over-estimated.

The measured stress-strain relationship for the CRS test is shown in Figure 7. The apparent preconsolidation pressure for this test is approximately 6 kPa, at which point large fluctuations in the stress-strain readings were recorded. This may be attributed to the breakdown of large fibres in the peat sample, which could cause a sudden decrease in stress. Calculated stress-strain responses are also shown for each model in Figure 7. Both models capture the overall stress-strain relationship quite well, although the calculated stress-strain plots are shifted somewhat to the left of the measured results.

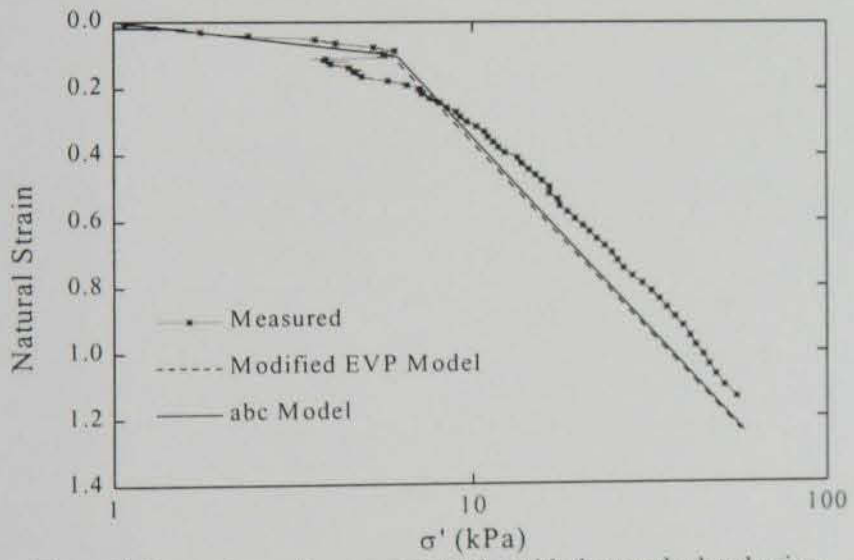

Figure 7 Comparison of measured results with those calculated using the *abc* and modified *EVP* models for Test 3.

5 DISCUSSION

The *abc* model is evidently adequate for predicting the overall settlement for all load increments in the virgin stress range, although certain modifications need to be made to the *EVP* model to describe the one-dimensional compression of fibrous peat. The most important of these modifications is the definition of strain. It is evident from Figures 2 and 4 that linear strain is not suitable for linearizing ε - log σ' data over a wide stress range. When the *EVP* parameters are determined from natural strain data, then the *EVP* model is much more successful in predicting settlements for all load increments (Figure 5). Good agreement has been obtained for both the *abc* and modified *EVP* models during the consolidation phase of Test 1, but strains for this phase were over-estimated for all load increments of Test 2. This is presumably due to the differences between the empirical parameters C_k and k_o (Equation 8) in the respective samples. However this is generally of little consequence for fibrous peat as the primary consolidation phase in such materials is typically short.

In Test 2, v_o was less than that in Test 1, and it was found that a best fit for the *abc* model required adjustment of the location of the base line (by modifying v_1) to keep it fixed in stress-strain space. This adjustment is consistent with the assumption of a constant σ'_o value employed in the *EVP* model.

The main difference in the models is the positioning of a reference creep isotache or time line from which to measure creep strains. The *EVP* model employs the parameter t_o, to position the RTL. Yin & Graham (1996) suggest that values determined for t_o should be of the same order as the time taken for primary consolidation (t_p). However, the value of $t_o = 1.57\text{x}10^{-5}$ min given in Table 4 is obviously several orders less than t_p. Despite this, t_o appears to be a useful parameter in scaling creep strain rates. The *abc* model positions the base line at τ = 1 day, which roughly corresponds to standard 24-hour compression curves. The creep strain rate on the *abc* model's base line is $2.08\text{x}10^{-7}$ sec^{-1}, whereas the corresponding creep strain rate on the *EVP* model's RTL is 14.86 sec^{-1}, with the result that the RTL is positioned at a creep strain rate not normally encountered in the majority of one-dimensional compression tests. Regression techniques cannot, as a consequence, be employed to fit Equation 1 to measured creep strain data.

6 REFERENCES

Berre, T. & Iversen K. (1972). Oedometer tests with different specimen heights on a clay exhibiting large secondary compression. *Géotechnique*, **22**, No. 1, 53-70.

Edil, T. B., Fox, P.J. & Lan, L. T. (1991). End of primary consolidation of peat. *Proc. 10th Eurpoean Conf. On Soil Mech. and Found. Engrg.*, Florence, Italy, **1**, 65-68.

den Haan, E.J. (1996) A compression model for non-brittle soft clays and peat, *Géotechnique*, **46**, No. 1, 1-16.

Leroueil, S., Kabbaj, M., Tavenas, F. & Bouchard, R. (1986). Closure to stress-strain-strain rate relations for the compressibility of sensitive natural clays. *Géotechnique*, **36**, No. 2, 288-290.

Mesri, G. & Choi, Y.K. (1985). Settlement analysis of embankments on soft clays, *J. Geotech. Engrg.*, ASCE, **111**, No. 4, 441-464.

Yin, J.-H. & Graham, J. (1989). Viscous-elastic-plastic modelling of one-dimensional time-dependant behaviour of clays. *Canadian Geotechnical Journal*, **26**, 199-209.

Yin, J.-H. & Graham, J. (1994). Equivalent times and one-dimensional elastic visco-plastic modelling of time-dependant stress-strain behaviour of clays. *Canadian Geotechnical Journal*, **31**, 42-52.

Yin, J.-H. & Graham, J. (1996). Elastic visco-plastic modelling of one-dimensional consolidation. *Géotechnique*, **46**, No. 3, 515-52.